A 40 SEC. OF ARC RADIO TELESCOPE

KELVIN WELLINGTON, B.Sc., B.E.

* * *

A thesis submitted in fulfilment of the
requirements for the degree of
Doctor of Philosophy

School of Electrical Engineering,
University of Sydney
1968

A 40 SEC. OF ARC RADIO TELESCOPE

PhD. Thesis, 1968 by Kelvin Wellington.

SUMMARY

This thesis outlines the design, construction and operation of a new type of high resolution radio telescope.

In its final form this telescope will 'map' an area of sky of one degree diameter with a pencil-beam resolution of 40 sec. of arc at a frequency of 1415 MHz during an observing period of approximately 8 hours. The total area of antenna structure is low, yet it is used extremely efficiently and provides a high sensitivity of 2 or 3.10^{-28} $Wm^{-2}Hz^{-1}$, sufficient for the telescope to be almost 'confusion' limited.

The antenna structure of the telescope consists of sixty-four 19 foot diameter and four 45 foot diameter paraboloid aerials, arranged in two lines to form a pair of compound grating interferometers, one in an east-west direction and one in a north-south direction.

These two linear arrays form high resolution fan beams at right angles. There is, however, no electrical interconnection between the arrays as in the normal 'cross-type' operation. Each linear array utilizes the rotation of the earth to synthesize an angular segment of a two-dimensional aperture. Use of the dual array enables a considerable reduction in the sky coverage requirements of the individual aerials.

The thesis is initially concerned with an investigation of the basic properties of the final telescope, both as an instantaneous fan beam instrument and as a synthesized pencil beam instrument. The particular problems next considered include determination of the necessary configuration, design of the antenna structure and a study of the expected telescope performance.

In the present stage of construction the high resolution capability has been developed and tested, and is now being used for solar observations. However, only the east-west telescope has been completed; the north-south telescope is under development with the antenna structure already finished.

Completion of this north-south array will allow high-resolution low-sensitivity pencil-beam observations over a one degree image plane.

The design of the present receiver system is described. Although this receiver system is being used for the preliminary fan beam observations only, many segments of it, such as local oscillator and intermediate frequency cabling, have been developed for the final system. Particular attention has been paid to the phase stability of the system.

Satisfactory adjustment of the antenna required the development of special methods which are detailed in the thesis, together with some of the preliminary observations.

C O N T E N T S

SUMMARY AND STATEMENT OF ORIGINALITY

General

This thesis outlines the design, construction and operation of a new type of high resolution radio telescope.

In its final form this telescope will 'map' an area of sky of one degree diameter with a pencil-beam resolution of 40 sec. of arc at a frequency of 1415 MHz during an observing period of approximately 8 hours. The total area of antenna structure is low, yet it is used extremely efficiently and provides a high sensitivity of 2 or $3.10^{-28}Wm^{-2}Hz^{-1}$, sufficient for the telescope to be almost 'confusion' limited.

The antenna structure of the telescope consists of sixty-four 19 foot diameter and four 45 foot diameter paraboloid aerials, arranged in two lines to form a pair of compound grating interferometers, one in an east-west direction and one in a north-south direction.

These two linear arrays form high resolution fan beams at right angles. There is, however, no electrical interconnection between the arrays as in the normal 'cross-type' operation. Each linear array utilizes the rotation of the earth to synthesize an angular segment of a two-dimensional aperture. Use of the dual array enables a considerable reduction in the sky coverage requirements of the individual aerials.

The thesis is initially concerned with an investigation of the basic properties of the final telescope, both as an instantaneous fan beam instrument and as a synthesized pencil beam instrument. The particular problems next considered include determination of the necessary configuration, design of the antenna structure and a study of the expected telescope performance.

In the present stage of construction the high resolution capability has been developed and tested, and is now being used for solar observations. However, only the east-west telescope has been

completed; the north-south telescope is under development with the antenna structure already finished.

Completion of this north-south array will allow high-resolution low-sensitivity pencil-beam observations over a one degree image plane.

The design of the present receiver system is described. Although this receiver system is being used for the preliminary fan beam observations only, many segments of it, such as local oscillator and intermediate frequency cabling, have been developed for the final system. Particular attention has been paid to the phase stability of the system.

Satisfactory adjustment of the antenna required the development of special methods which are detailed in the thesis, together with some of the preliminary observations.

Detailed Summary

Chapter 1 is a resumé of the developments in high resolution grating telescopes which led finally to the conception of the basic form of the present pencil beam radio telescope by Professor W.N. Christiansen while he was working with Dr. J.A. Högbom in Leiden.

The general performance requirements of the new telescope are described. The way in which an existing grating cross is utilised as the basis for the new telescope is summarised in Section 1.4 and described in more detail in a paper included as Appendix A.

Chapter 2 analyses the properties of linear grating arrays as applied to one dimensional (fan beam) observations. The first section assesses the generally known properties of the simple grating telescope and from these the author has compiled a list of advantages and disadvantages of this form of telescope.

Section 2.2 considers the use of this simple grating in one form of a correlation telescope, namely the compound grating interferometer. This antenna has all the advantages of the simple grating as well as the following important properties: (i) the multiple

responses of the simple grating are suppressed, and (ii) the resolution per unit area of antenna structure can be greatly increased. This type of antenna was originally proposed by Covington (1960) but its properties have not previously been fully investigated. This section concentrates in particular, on the ways in which the various configurations differ. The chapter concludes with a section describing the theoretical sensitivity of both total power and correlation telescopes.

Chapter 3 deals with the way in which the compound grating interferometer is used to synthesize a telescope with pencil beam resolution. The basic method uses the rotation of the earth to change the orientation of the linear array with respect to the source. The advantages consequent on the use of grating arrays with rotational synthesis are examined here briefly. A thorough examination by the author of the geometry of earth rotation synthesis follows in Section 3.3 and Appendix B. A combination of east-west and north-south baselines is demonstrated to be superior to other configurations.

Design parameters of the new telescopes are discussed in Chapter 4. The use of the existing grating cross was a considerable advantage, however it restricted the choice of the actual configurations previously evaluated in Chapter 2. The reasons for the final decisions are indicated and the effects of these on the performance of the telescope are considered. The necessary investigations and final details were the responsibility of the author. The work reported in Section 3.3 enabled the sky coverage requirements of the individual aerials to be determined. A number of problems relevant to the choice of configuration were investigated by the author and are presented in Appendix C. This enabled decisions to be made concerning the size and position of the additional antennae.

The additional antennae necessary to convert the grating cross into the new compound grating arrays were designed by the author and constructed under his supervision. These antennae are described in

Chapter 5. The particular aerial design was a conic approximation of the true paraboloid. The optimum shape is analysed in Appendix D.1. Section 5.6 summarises the final aerial specifications. A brief outline of structural details is included in Section 5.8 and the actual plans are presented in Appendix E. The principal merit of this design lies in its exceptional light weight construction, leading to considerable economy in manufacture.

Chapter 6 entails an analysis of the expected performance characteristics of the telescope, both as a fan beam instrument and as a pencil beam instrument.

Chapters 7 and 8 give details of the receiver system at present used to carry out the high resolution fan beam scans of the sun. This system combines the outputs of all the aerials so as to produce singular fan beam responses oriented in fixed directions relative to the earth. Chapter 7 describes in detail the radio frequency system in use. The phase stability of the distributed parts of the system is analysed in terms of the effects of temperature and frequency variations. A special method of temperature compensation has been developed which is vital to the present successful operation of the system.

Chapter 8 deals with the main receiver system used to correlate the signals of the large and small aerials. This system is constructed in the form of a number of separate modules in order to facilitate the operation of the receiver in several different configurations. The configurations are used for testing, alignment and special purpose observations besides the normal fan beam observations. The system design and the detailed specifications of the individual modules were the responsibility of the writer. The circuit design and the construction of the individual modules was carried out by Dr. R.H. Frater with the assistance of several other people from the Electronics Department.

From previous calculations of the theoretical performance of the telescope, it was apparent that the quality of observations depended critically upon the precision of adjustment of the individual aerials.

The methods used for this adjustment are outlined in Chapter 9. Because of the present low sensitivity a combination of methods was necessary. For phase adjustment of the widely spaced aerials none of the normal approaches was applicable. To overcome this problem the author developed a special observational method which involves slowing the fringes produced by a point source, while still preserving their phase with the necessary high degree of precision. Section 9.4 and Appendix F describe the equipment and procedure required for these observations.

Chapter 10 and a short paper in Appendix G present some of the preliminary solar observations and resulting conclusions obtained with the fan beam of the east-west compound grating interferometer.

Many of the Appendices are separate investigations containing original contributions and have been removed from the main thesis body to avoid interrupting the general development of the principal theme. Appendix J (relevant to Chapter 4) analyses a possible configuration for future compound grating interferometers; Appendix K presents an idea for increasing the survey sensitivity of image forming arrays. This last represents a worthwhile future development since it will take a minimum of 35 years to completely survey the available sky with the one degree image forming telescope.

The project was originated by Professor W.N. Christiansen, under whom the author has been directly working. The general continuity of development has been the responsibility of the author.

A project of the size and complexity of the complete telescope necessarily involves the efforts of numerous people. It is thus difficult to delineate the contributions of the various individuals. Acknowledgements have been made where appropriate throughout the text. Otherwise the work described is that of the author.

ACKNOWLEDGEMENTS

I gratefully acknowledge assistance received under the following scholarships: Raymond E. Purves - Clyde Industries Limited Research Studentship, a University Post-Graduate Studentship and a Norman I. Price Scholarship. The project itself has been made possible by grants from the Australian Research Grants Committee, the University of Sydney Research vote, the Nuffield Foundation and the Australian Electrical Research Board.

I would like to record my gratitude to my supervisor, Professor W.N. Christiansen, Head of the School of Electrical Engineering, for introducing me to the absorbing field of radio astronomy, for his continued guidance, support and encouragement throughout the period of development of the new telescope and for his suggestions during the final formulation of the thesis. His considerable experience and depth of insight have been invaluable.

I am indebted to Mr. K.R. McAlister of the Radiophysics division of the C.S.I.R.O. for his direction and helpful counsel during the design of the additional antennae. His many years of experience in building economical lightweight structures have been of great benefit. Mr. A. Watkinson, Officer in Charge of Fleurs Field Station, gave much assistance during the latter part of the project.

My thanks go to the individuals mentioned throughout the thesis who have assisted willingly in the various aspects of the project. In particular I would like to acknowledge the help of Professor R.E. Aitchison, Dr. R.H. Frater, Mr. I.G. Jones, Mr. N.A. Mackay and Mr. J. Jacobs. Special thanks are due to Mr. C. Peterson who, in addition to other assistance, developed the computer program used to draw the various interferometer responses, and also to Mr. J. Curdie, of the firm of Kent and Curdie, who surveyed the site. The staff of the School of Electrical Engineering (including those at Fleurs) are thanked for their continued support.

I am grateful to Mrs. Margaret McCann for her expert typing, and to the Department of Illustration for providing the excellent photographs.

My very warm thanks go to Miss Janet Builder and Miss Meredith Wallace for their assistance in the production of the manuscript. Meredith for her critical comments on the prose and her instant readiness to type late stencils, and Janet, for her excellently drawn diagrams and her continued encouragement from an early stage.

Finally, I wish to express my gratitude to my parents for their lasting interest and support, without which this thesis would not have been possible.

CHAPTER 1

CHAPTER 1: PROLOGUE

1.1 Introduction

The first grating interferometer was constructed by Christiansen and Warburton (1953a) at Potts Hill near Sydney during 1950-52. This consisted of an east-west line of steerable paraboloids about 1,000 wavelengths long. It produced a system of multiple fan beam responses which were used to scan the sun successively over a period of many hours. During this time the scanning angle changed appreciably with respect to the sun's axis. In order to achieve 180^{o} change in scanning angle, a second grating in a north-south direction was constructed. With these gratings, Christiansen and Warburton (1955) were able to synthesize the first two-dimensional picture of the sun using one dimensional strip scans.

The use of gratings, which measure instantaneously all the necessary Fourier components in one direction, overcame the difficult problems of phase measurement being experienced at Cambridge (Stanier, 1950) during the first application of two element aperture synthesis.

In 1957 Christiansen combined the Mills Cross concept with that of gratings to form the first Crossed Grating Interferometer. This instrument gave a 3 min. of arc pencil beam and was used to form two dimensional maps of the sun (Christiansen et al., 1957).

In 1963 the Fleurs field station, together with this Crossed Grating Interferometer, was acquired by the School of Electrical Engineering, University of Sydney. This made possible a plan, conceived by Christiansen, to utilize the Grating Cross as the basic structure of two new radio telescopes.

1.2 Astronomical and General Performance Requirements of the New Telescopes

A high resolution is the primary requirement of the new telescopes. This has always been the most sought-after quality in radio astronomy and has always led to new astronomical discoveries. At the time this project was begun, studies of bright radio galaxies showed the existence of a great deal of detailed structure. This has been reinforced more recently by the results of the long baseline interferometer work at Jodrell Bank (Adgie et al., 1965). The excellent maps of Ryle (1965) are also confirmation of the complexity of some radio sources and the need for higher resolution.

A similar situation existed with solar investigations. Observations at 21 cm wavelength had been carried out for several years at Fleurs using both the 3 min. of arc pencil beam of the crossed grating interferometer and the 2 min. of arc fan beam of the east-west arm of the same instrument. From these observations it was very apparent that a telescope with increased resolution was needed to evaluate the size, position and structure of the many radio emissive regions, associated with sunspots, which were not being resolved. The observations by Covington (1959) with a 1.2 min. of arc fan beam at 10 cm wavelength supported these conclusions. During the sunspot maximum these emissive regions are continually changing in structure and intensity so that it is also important to extend the observations over long periods.

High resolution is useless unless it has the necessary sensitivity to go with it. High sensitivity can be achieved by control over any or all of four parameters: collecting area, receiver noise factor, receiver bandwidth and integrating time. With unfilled aperture telescopes choice of these can generally be made independently of the resolution requirement. This allows optimization of the sensitivity such that the telescope is slightly confusion limited.

With the high resolution necessary, the return or efficiency of the instrument, in terms of steradians of sky examined in the lifetime

of the telescope, is likely to be low unless some method of image formation is used; i.e., simultaneous observation of many beamwidths of sky. This increase in information gathering ability can be considered, up to a point, as an increase in sensitivity (Christiansen et al., 1963). It is particularly necessary if the system sensitivity has been increased by lengthening the observing time.

Polarization and spectral flux variation provide important clues to the physical processes producing the incident radiation. The ability to measure these two quantities is an important requirement.

Previously a high resolution has led to the need for a still higher one. Thus a fourth desirable quality of high resolution radio-telescopes is the capability of being enlarged. This eliminates the lost time (about 5 years) taken to design and build a completely new system. Observational work and antenna growth can proceed side by side.

In all of these respects the new high resolution telescopes at Fleurs will be particularly suitable.

1.3 The Existing System

The existing Grating Cross consists of sixty-four paraboloids arranged in two lines, east-west and north-south, each 1240 feet long (Christiansen et al., 1961). The aerials, equatorially mounted at 40 foot intervals, are 19 feet (5.6 m) in diameter with a focal length of 6.25 feet (2.3 m). At the operating frequency of 1424 MHz (21 cm wavelength), the aerial beamwidth of about 2½ degrees, forms an envelope inside which is a grid of 3 min. of arc pencil beams at one degree intervals.

The feed on each aerial is a simple dipole and reflecting plate at the end of a metal tube mounted at the pole of the mirror. Each dipole is connected to a balanced open-wire branched feeder system. This forms an array with the beams in fixed directions relative to the earth.

1.4 Outline of the New System

Initially, the east-west and north-south arrays of the Grating Cross are converted into two separate high resolution telescopes. Each telescope is a Compound Grating Interferometer formed by adding two 45 foot (13.5 m) diameter paraboloids to each array of thirty-two aerial elements (Fig. 1.1). This arrangement provides the means of extending the resolution without large increases in the antenna structure and of suppressing the multiple responses of the simple gratings. These multiple responses create ambiguities when studying galactic sources.

Each telescope forms an instantaneous fan beam response, 35 sec. of arc by one degree. By observing continuously for up to nine hours the rotation of the earth can be employed, as in the early Potts Hill observations, to synthesize a pencil beam resolution of 40 sec. of arc.

Since the fan beams continuously scan the 'area' of sky seen by each aerial, this pencil beam resolution applies to a whole image plane of over one degree diameter. Thus the two compound grating interferometers are equivalent to a narrow pencil beam image forming telescope.

The following stage of development consists primarily of major changes in the receiver system enabling a very high sensitivity to be achieved. Individual receivers are placed on each aerial allowing each Fourier component of the sky distribution to be continuously recorded. The effective integration time for each picture point in the image plane is then between twelve and eighteen hours, increasing the sensitivity 300 to 450 times. Together with other improvements, the final sensitivity will be 2 or 3 x 10^{-28} $Wm^{-2}Hz^{-1}$. Extrapolation of the existing source surveys suggests that the telescope, with this sensitivity and resolution, will be sensitivity limited by a factor of 2.5.* This can be 'reduced' by combining 6 days' observations of the same region.

---

*This estimate assumes a static Euclidean universe and a signal to noise requirement of 5.

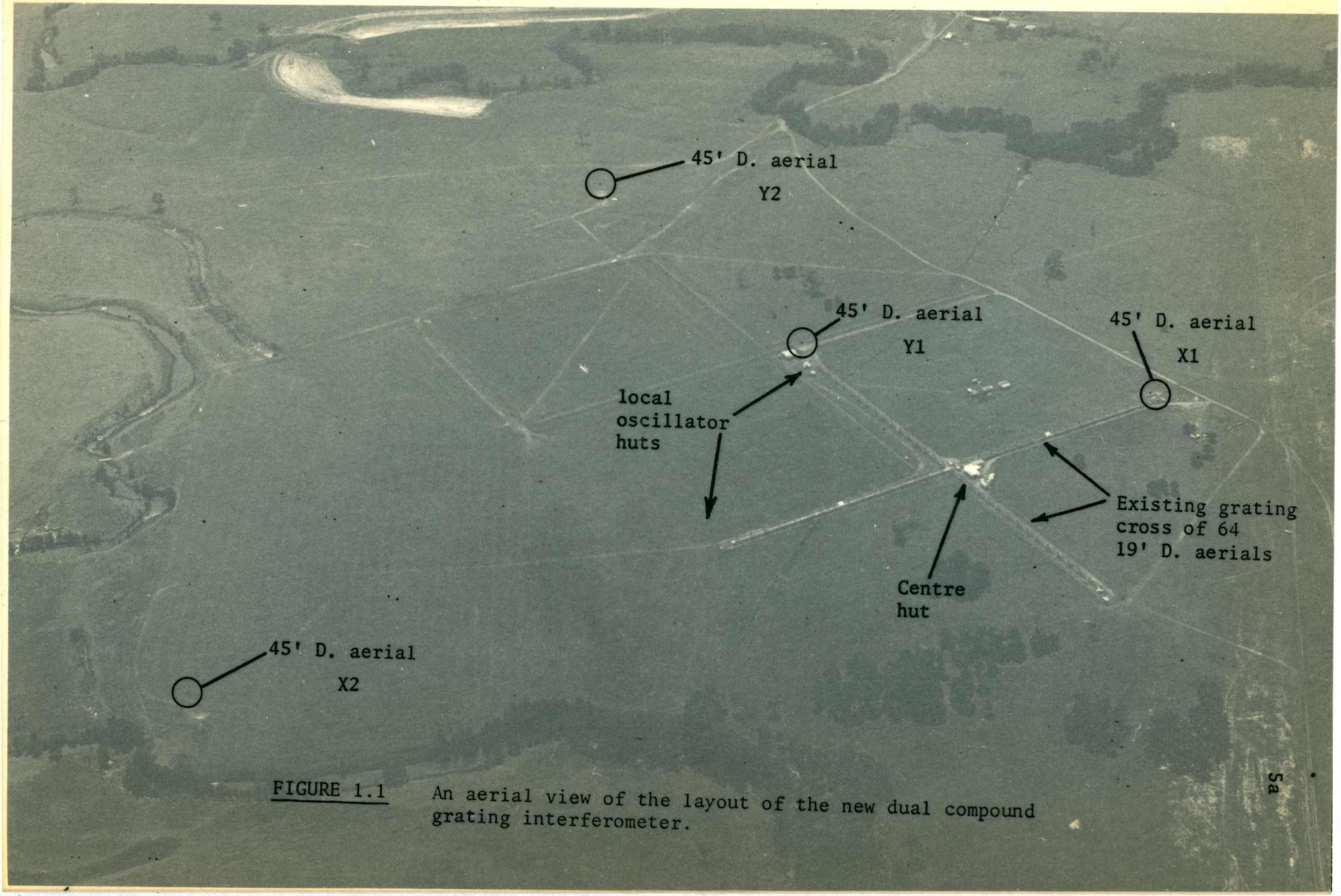

FIGURE 1.1 An aerial view of the layout of the new dual compound grating interferometer.

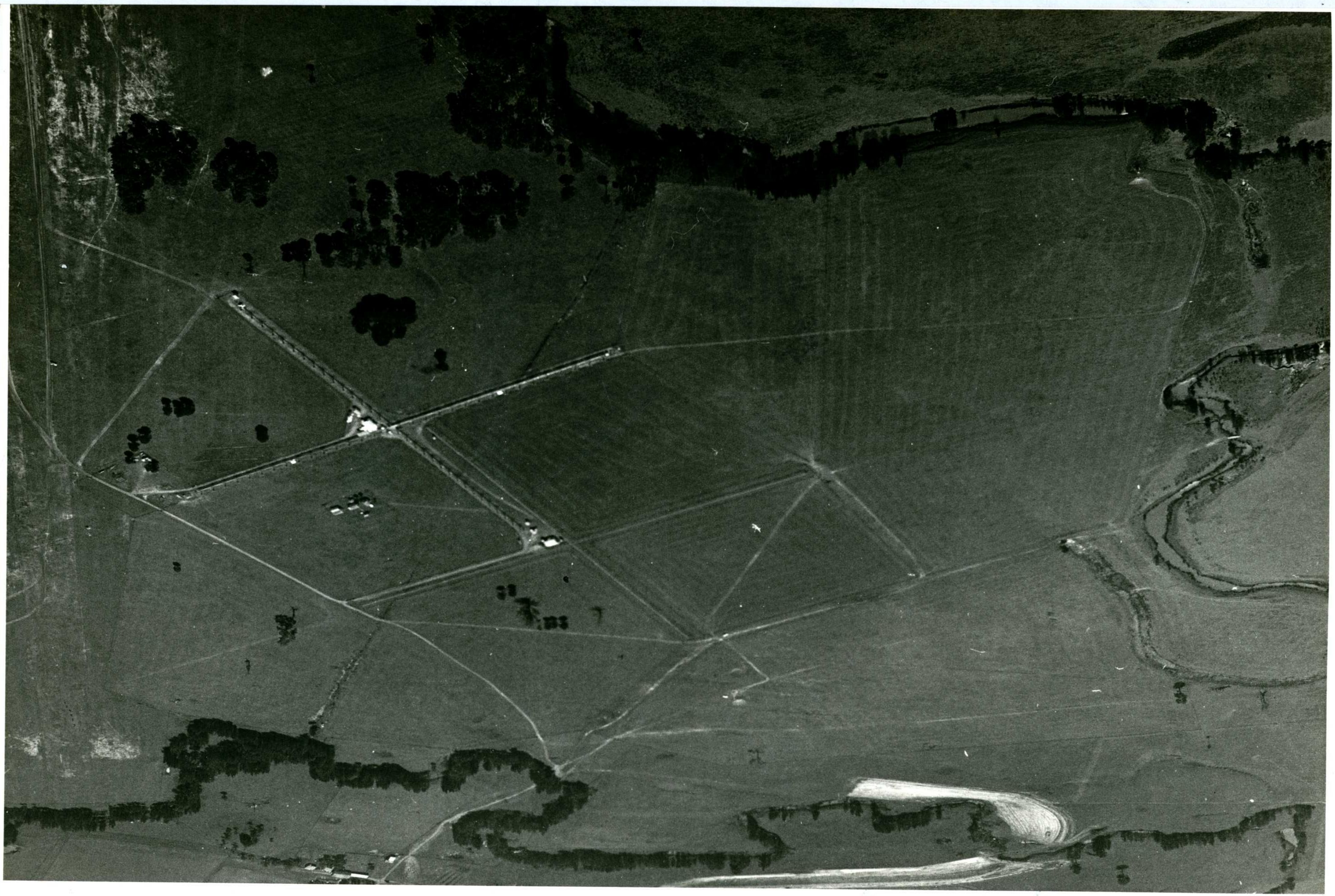

The fact that each telescope is a separate linear compound grating interferometer makes the system particularly suitable for economic increases in the resolving power. It is a relatively simple matter to add more large aerials at intervals of 1280 feet.

At present there are no other radio telescopes operating in the decimetre wavelength range capable of attaining such a high resolution with an instantaneous fan beam.

Extremely high resolution (<0.025 sec. of arc) has been achieved on isolated strong sources using long baseline two element interferometry (Palmer et al., 1967). However this method provides only isolated points on the visibility diagram.

The complete images of areas of sky produced by Ryle (1965) have a pencil beam resolution of about 23 sec. of arc. However these observations, using aperture synthesis principles, must generally be spread over a period of several months. This long time factor is unsuitable for many types of observing programs.

The final system at Fleurs overcomes this difficulty by synthesising an image having 40 sec. of arc pencil beam resolution from only six to nine hours' observations. This final system has been described in more detail in a publication included in Appendix A.

CHAPTER 2

GRATING TELESCOPES

CHAPTER 2: GRATING TELESCOPES

2.1 The Grating Interferometer

2.1.1 Introduction

The grating interferometer is an array of identical uniformly-spaced antennae. It is the radio analogue of the optical diffraction grating and provides a means of constructing large 'unfilled' apertures from combinations of mechanically small antennae. These large apertures are 'steered' by both electrical and mechanical means.

The positions of the individual antennae enable the angular spectrum of the sky distribution to be sampled at regular spatial intervals. The effect of this regular sampling is to create multiple, and hence ambiguous, responses. The first use of the grating was for observations of the sun (Christiansen and Warburton, 1953). In this case only one grating response fell on the sun at any one time thereby removing the ambiguity. However for general astronomical observations, these spurious responses must be eliminated.

In most of the high resolution gratings used for radio astronomy, the individual antennae have been moderately directive paraboloids. These are very useful 'building blocks' since each one can be mounted on a polar axis and can track a source for many hours by uniform rotation about one axis.

2.1.2 The Coordinate System

Two coordinate systems are used. One specifies the antenna system and the other specifies directions in space relative to this antenna system (Fig. 2.1). In Chapter 3, the relationship of these coordinate systems is investigated more fully for the particular telescope system under consideration.

The antenna is described by rectangular Cartesian coordinates (x,y,z). The orientation of the axes and the position of the origin do not alter the behaviour of the system. However careful choice of these can

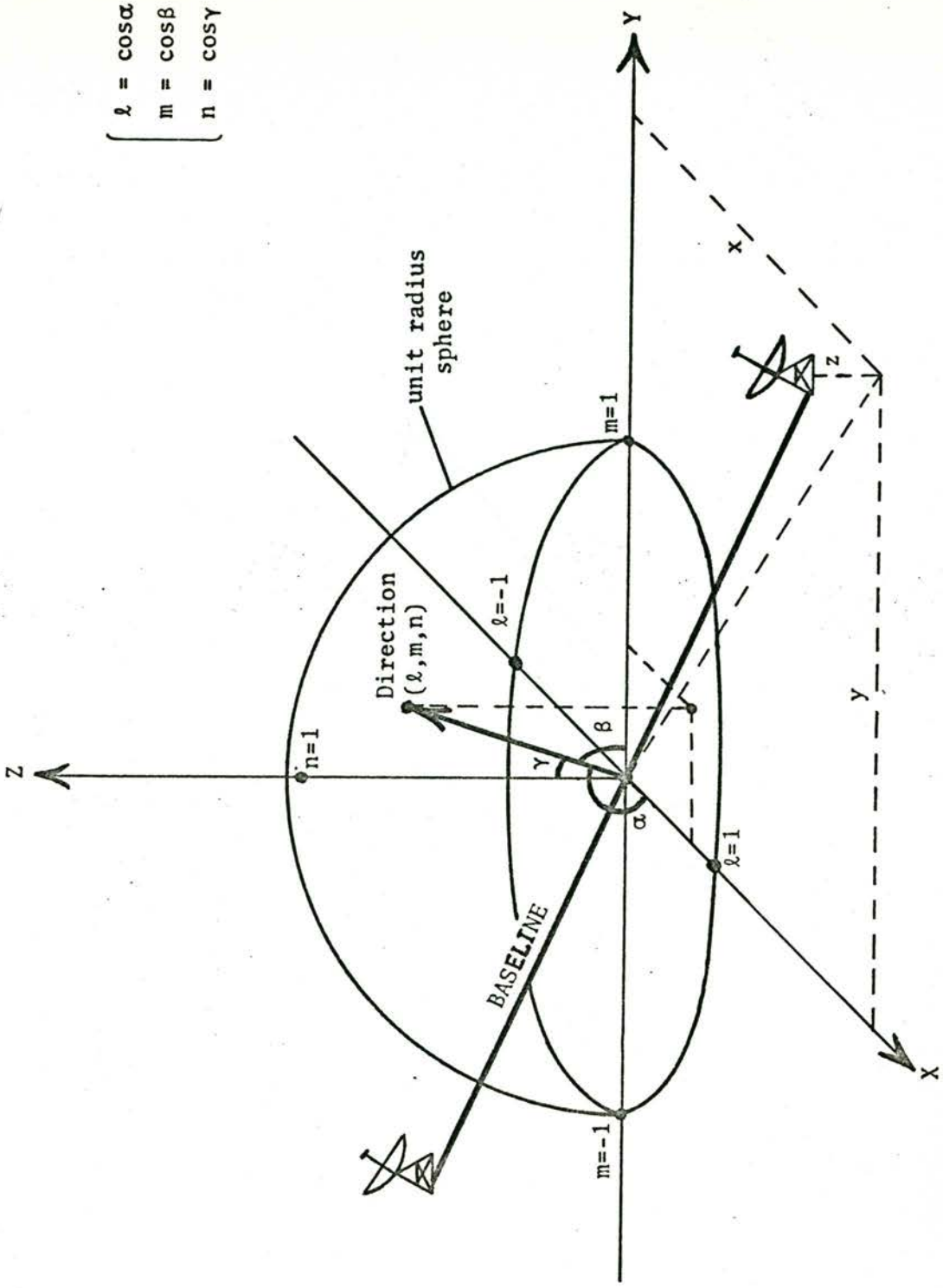

FIGURE 2.1 Illustrating the two coordinate systems in use.

simplify the descriptive equations. Generally, the (x,y) plane is regarded as the aperture plane and the Z axis as the direction of maximum response. In an interferometer the elements* are generally distributed in the (x,y) plane and in the following discussions concerning only linear arrays the elements are considered as being arranged along the X axis. Except where stated otherwise the unit of length in this (x,y,z) coordinate system is taken as one wavelength at the centre frequency of observation.

Directions are often specified in cylindrical coordinates (Chapter 3). However the direction cosines of spherical or polar coordinates are more convenient for mathematical usage. Trigonometric expressions which represent coordinate transformations only are then often removed.

The direction cosines (ℓ,m,n) are specified with respect to the (x,y,z) axes. ℓ and m can be considered as rectangular coordinates describing the projection of a direction on the (x,y) plane. In earth-bound radio astronomy only ℓ and m are necessary as only one hemisphere, n positive, is considered. (In addition as the grating arrays are oriented in the x direction, the response in the ℓ direction is the one of prime interest.)

A small solid angle of sky, $\Delta\Omega$, in the direction (l,m) has a projected area in the (l,m) plane of $\left((\Delta\ell),(\Delta m)\right)$

where $$\Delta\Omega = \frac{(\Delta\ell).(\Delta m)}{(1-\ell^2-m^2)^{\frac{1}{2}}} \qquad (2.1)$$

and $$\ell^2+m^2+n^2 = 1 \qquad (2.2)$$

This relates angular measure to the direction cosines.

---

*In the following text, the term 'element' refers to the individual components of the grating. In the present system these components are paraboloidal reflectors although in theory they can be any form of sensing element.

2.1.3 The Response of the Grating

An array of N identical paraboloids, evenly placed along the X axis with a spacing d, will have a grading function given by

$$g(x,y) = \sum_{i=0}^{N-1} g_f\left(x-id+(N-1)\frac{d}{2}\right) \qquad (2.1)$$

where the elements are equally weighted and have an individual grading of $g_f(x,y)$.

The Fourier transform, $G(\ell,m)$ of $g(x,y)$ is the sum of the Fourier transforms for the individual elements. Hence, using the shift theorem of Fourier theory,

$$G(\ell,m) = G_f(\ell,m) \sum_{i=0}^{N-1} \exp\left(2\pi j\ell d(i-\frac{N-1}{2})\right)$$

$$= N.G_f(\ell,m) \cdot \frac{\sin N\pi\ell d}{N \sin\pi\ell d} \qquad (2.2)$$

Thus the normalised field pattern for an array is given by

$$F(\ell,m) = F_f(\ell,m)\left(\frac{\sin(N\pi\ell d)}{N \sin(\pi\ell d)}\right) \qquad (2.3)$$

and the effective area by:

$$A(\ell,m) = N.A_f(\ell,m) \cdot \left(\frac{\sin(N\pi\ell d)}{N \sin(\pi\ell d)}\right)^2 \qquad (2.4)$$

where $G_f(\ell,m)$, $F_f(\ell,m)$ and $A_f(\ell,m)$ are the Fourier transforms of the grading function, the field pattern and the effective area of the individual elements.*

The response pattern (proportional to the effective area) repeats itself at intervals defined by

$$\ell = \frac{n}{d}$$

where n is an integer and d is expressed in wavelengths (Fig. 2.2).

---

*These are widely-used parameters describing antenna performance. Their derivations can be found in most texts containing the basic theory of radio astronomy antennae (Pawsey and Bracewell, 1954; Christiansen and Högbom, 1968; Bracewell, 1961b; Jasik, 1961).

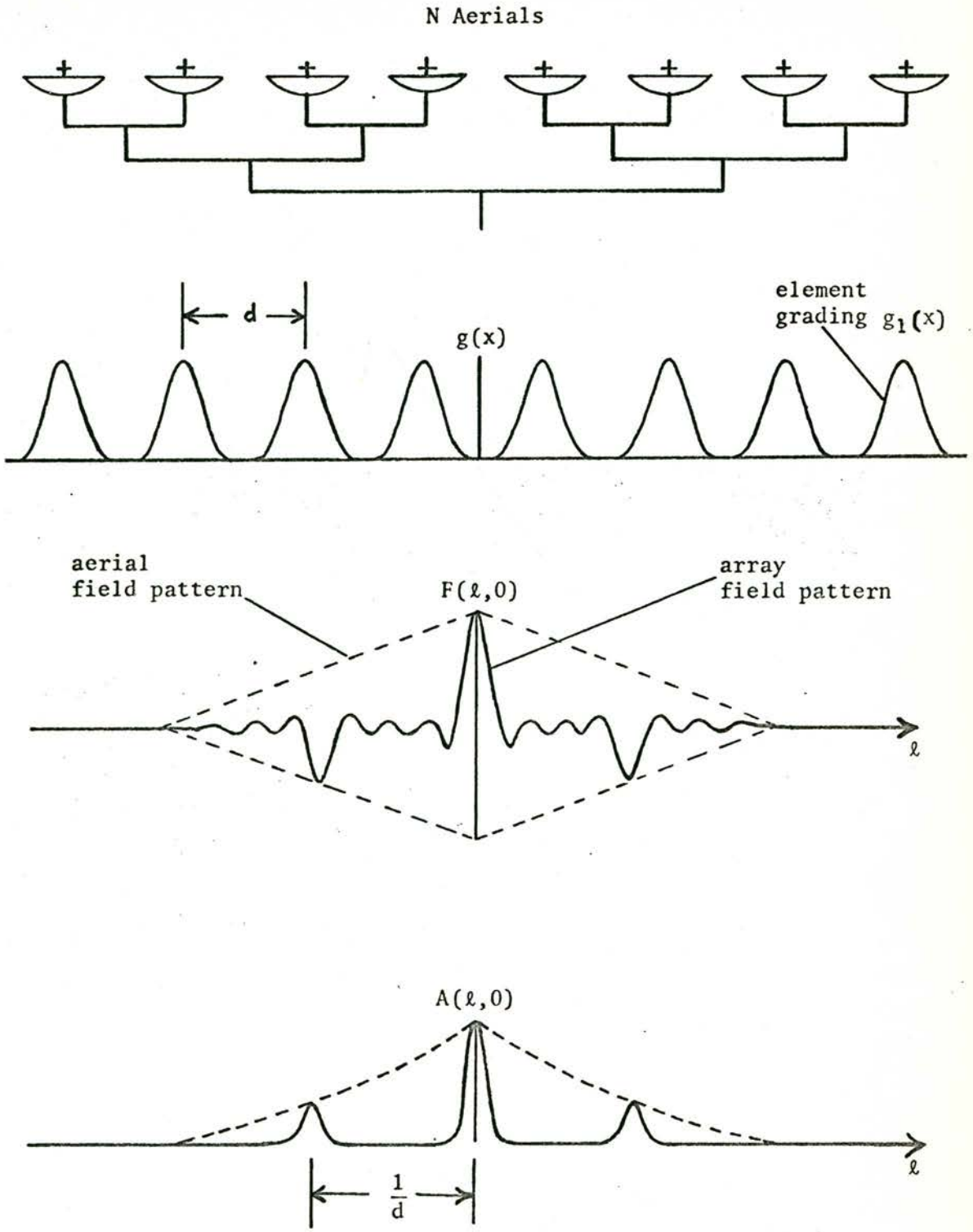

FIGURE 2.2 The response of a grating having uniform aperture illumination.

The field pattern can be considered as a series of spaced sinc(Nℓd) responses added together. Since sinc(Nℓd) is of finite size in directions away from the central maximum, the adjacent sinc(Nℓd) response becomes modified. In this way, the $\frac{\sin N\pi\ell d}{\sin \pi\ell d}$ pattern differs from a repetitive sinc(Nℓd). In most cases, provided $\underline{N}$ is large, this difference can be ignored.

The element field pattern, $F_i(\ell,m)$ attenuates all multiple responses except those in the axial direction of the elements. However complete suppression leaving a singular response is impossible. Gaps must be left between the elements to prevent interelement shadowing while tracking a source. As well as this, the illumination of the individual elements will be non-uniform, causing a broadening of $F_i(\ell,m)$ (considered in Section 2.2.8 in more detail). Thus, in general, at least three grating lobes remain, limiting the usefulness of the simple grating to observations of the sun and a few strong radio sources.

2.1.4 Variation of the Grating Parameters

The convolution theorem from Fourier theory provides a convenient means of quickly estimating the effects of variation of any of the parameters of an array. The array grading function, equation 2.1, is separable into an element grading function, a continuous sampling function and an aperture (or array grading) function.

(i) The element grading function, $g_i(x,y)$, is determined by the size and illumination of each element. These effect the width and shape of its Fourier transform, $G_i(\ell,m)$. The Fourier relationship is written:

$$G_i(\ell,m) \Longleftrightarrow g_i(x,y) \qquad (2.5)$$

$G_i(\ell,m)$ is the envelope factor of the array response.*

---

*If the element 'pointing' direction can be changed then $G_i(\ell,m)$ is not constant either in direction or shape. Instead $G_1\{(\alpha-\alpha_1),(\beta-\beta_1)\}$ is constant where (α,β) is the source direction ($\ell=\cos\alpha$ and $m=\cos\beta$) and (α',β') is the direction of pointing of the elements. The effect is discussed in Section 2.2.2.

(ii) The continuous sampling function, III, which involves only the element positions and spacing, d, takes one of two discrete forms. For an even number of elements in the grating,

$$\exp(-j\pi\ell d) \cdot \mathrm{III}(\ell d) \Longleftrightarrow \mathrm{III}\left(\frac{x+\frac{1}{2}}{d}\right) \tag{2.6}$$

and for an odd number of elements,

$$\mathrm{III}(\ell d) \Longleftrightarrow \mathrm{III}\left(\frac{x}{d}\right) \tag{2.7}$$

Variation of the element spacing, d, causes an inverse variation of the grating response separation (see Fig. 2.3).

(iii) The aperture function, $g_A(x,y)$, defines the linear extent of the array and the weighting which is placed on each element. If the array is uniformly weighted, this aperture function becomes rectangular having the Fourier transform,

$$\mathrm{sinc}(N\ell d) \Longleftrightarrow \mathrm{II}\left(\frac{x}{Nd}\right) \tag{2.8}$$

This gives the main response of the array determining the resolution and close sidelobes. In general a tapered* function is applied instead of uniform weighting in which case this main response shape is altered.

For a uniformly-illuminated grating, the grading function becomes

$$g(x) = \left[g_1(x)\right] \mathbb{X} \left[\mathrm{III}\left(\frac{x+\frac{m}{2}}{d}\right)\right] \cdot \left[\mathrm{II}\left(\frac{x}{Nd}\right)\right] \tag{2.9}$$

where $\mathbb{X}$ represents the convolution of two functions and m is an integer.

---

*Array 'taper' is the function which defines the relative amplitude weighting of the various elements in the array. In general the high spatial components have a reduced weighting or a 'taper' in order to reduce the sidelobe levels.

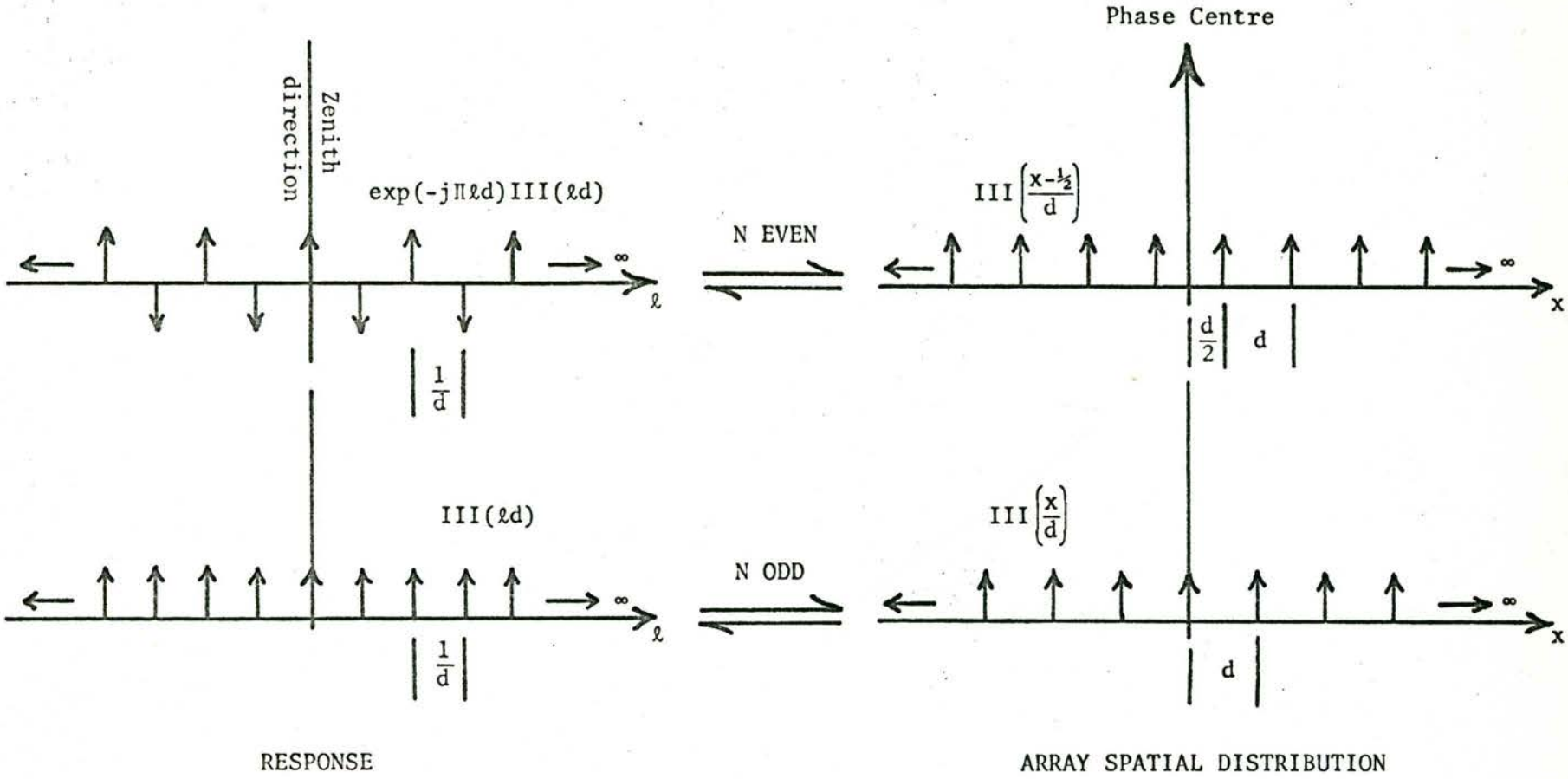

FIGURE 2.3 The two forms of the continuous sampling function illustrating the dependence of the field response of a grating upon the number of elements, N.

The Fourier transform, $G(\ell)$, of the grading function then becomes a combination of the separate Fourier transforms.

$$G(\ell) = \left[G_1(\ell)\right] . \left[\exp(-jm\pi\ell d)\right] . \left[III(\ell d)\right] \boxtimes \left[\operatorname{sinc}(N\ell d)\right] \quad (2.10)$$

This gives the same result for $F(\ell)$ as equation 2.3. However the separate Fourier transforms are better known and changes in them are more easily estimated (see Fig. 2.4).

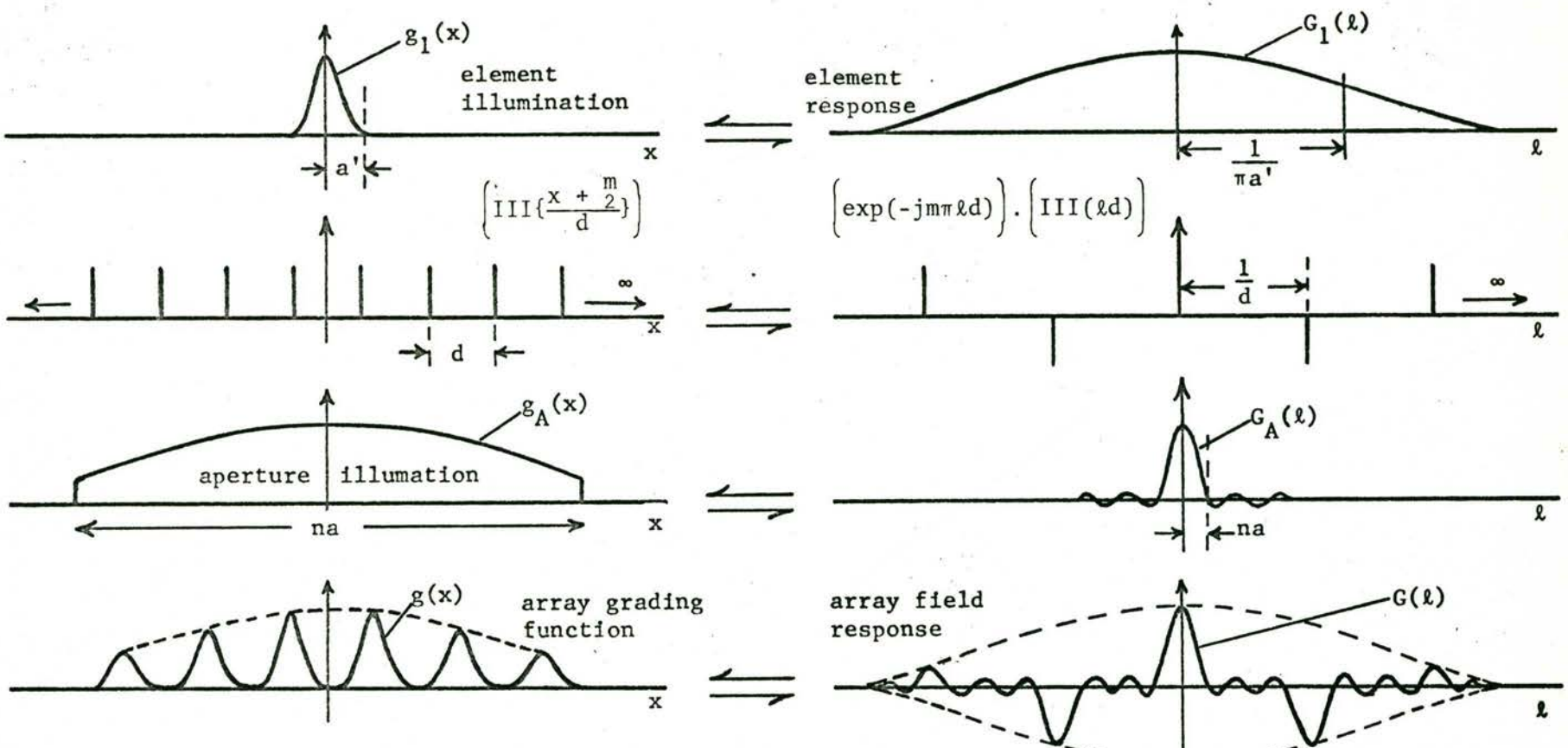

FIGURE 2.4 Illustrating the combination of the separate parameters which describe the configuration and response of a grating array.

$$g(x) = \left[g_1(x)\right] \circledast \left[III\{\frac{x + \frac{m}{2}}{d}\}\right] . \left[g_A(x)\right]$$

$$G(\ell) = \left[G_1(\ell)\right] . \left[\exp(-jm\pi\ell d)\right] . \left[III(\ell d)\right] \circledast \left[G_A(\ell)\right]$$

2.1.5 A Summary of the Advantages and Disadvantages of Gratings

Advantages

1. Gratings have the resolution of a continuous linear array but require considerably less antenna structure. Compared with the other extreme, gratings do not require the expensive rail tracks of moving-element aperture synthesis.
2. Combination of mechanical and electrical methods make feasible the beam steering of very large grating apertures.
3. The use of small individual units produces a lower overall cost.
4. Control of the grating aperture illumination is relatively easy.
5. Operation is frequency-independent. The changing of grating element feeds is relatively easy.
6. The application of an image-forming receiver system can lead to an optimum aperture efficiency and a high system sensitivity (Section 2.2.7).
7. Extension of the array for increased resolution is simple and economical.
8. The area of land required is small compared with a filled aperture.
9. The possibility exists of removing the multiple responses by wideband operation.

Disadvantages

1. Multiple responses can cause observational ambiguities.
2. Instantaneous sensitivity is relatively low.
3. Resolution is dependent upon zenith angle.

2.2 The Compound Grating Interferometer

2.2.1 Introduction

In the compound grating interferometer the response of a grating antenna is correlated or 'multiplied' with the response of another antenna. This second antenna is usually either a single element or another grating. The prime object is to form an economical high resolution linear aperture while suppressing the multiple responses of the grating. In this form it was first proposed and built by Covington (1959). Telescopes of similar type have also been built in Stanford, U.S.A. (Swarup et al, 1963), Japan (Kakinuma and Tanaka, 1963) and Sydney (Labrum et al, 1963).

The compound grating interferometer retains the advantages of the simple grating (Section 2.1.5). The resolution per unit area of antenna structure is even greater giving a high aperture economy. To provide continuous sampling of the spatial spectrum, the element spacing of the second grating is comparable with the overall length of the initial grating. Hence increases in resolution are achieved extremely economically. The highest efficiency, in terms of non-redundant Fourier components per element, is reached with equal numbers of elements in both gratings.

Suppression of the grating multiple responses, leaving a single fan beam, is achieved by making the size of the element or elements of the second grating comparable with the element separation of the first grating.

The compound grating interferometer can also achieve 32% higher directivity than the simple additive grating of the same overall length. This was pointed out by Covington and Harvey (1959) and is due to the spatial frequency 'tapers' attainable with the two systems. The simple grating, with elements uniformly weighted and feeding a square-law detector, will have a triangular spatial pass band. This pass band gives a response which is similar in shape to the function $(\text{sinc } x)^2$. The compound grating interferometer with uniformly weighted elements will have a rectangular pass band giving a response similar to (sinc 2x). The half-power beam widths of these responses are in the ratio 1·00 to 0·68.

However this gain in directivity is not always advantageous. The corresponding first sidelobe levels compared to the main response are 5% and 22% respectively. When this cannot be tolerated, removal by reweighting the spatial components broadens the beamwidth again. (Both systems measure the same spatial frequencies but in different amplitude ratios so that no new information is recorded.)

The compound grating interferometer, like the simple grating, is one form of unfilled aperture telescope. However, unlike the grating, the compound grating antenna must operate as a correlation telescope. Some of the advantages of this have been mentioned above. The basic theory of correlation telescopes is treated briefly in Appendix H and is assumed in the following sections.

2.2.2 The Basic Response

The basic configuration of a compound grating interferometer is that of Fig. 2.5. Here a regular grating of N elements is correlated with one larger element placed near one end.* The size of this single element is sufficient to suppress all but one grating response. The diameters of the small elements (or aerials) are generally less than half the separation, d.

The field response of the grating with the elements uniformly weighted is given by:

$$F(\ell,m) = F_1(\ell,m)\left\{\frac{\sin(N\pi\ell d)}{N\sin(\pi\ell d)}\right\} \qquad (2.3)$$

The field response of the single element at a distance, D, from the grating phase centre is given by:

$$F_2'(\ell,m) = F_2(\ell,m)\cdot\exp(-j2\pi\ell D) \qquad (2.11)$$

Thus the complex effective area (Appendix H) is:

$$\underset{\sim}{A}(\ell,m) = 2\left(N.A_1.A_2\right)^{\frac{1}{2}}\frac{\sin(N\pi\ell d)}{N\sin(\pi\ell d)}.\exp(-j2\pi\ell D) \qquad (2.12)$$

*See Footnote p.17.

With the large element a distance $\frac{d}{2}$ from the end of the grating*, such that $D = \frac{Nd}{2}$, the real and imaginary parts of equation 2.12 become:

$$\left.\begin{aligned} A_c(\ell,m) &= 2\left[N.A_1.A_2\right]^{\frac{1}{2}} \frac{\sin(2\pi N\ell d)}{2N\sin(\pi\ell d)} \\ \text{and} \\ A_s(\ell,m) &= 2\left[N.A_1.A_2\right]^{\frac{1}{2}} \frac{\sin^2(\pi N\ell d)}{N\sin(\pi\ell d)} \end{aligned}\right\} \qquad (2.13)$$

The response shapes of equation 2.13 have been calculated and plotted, using a computer routine, for the case of 16 grating elements (Figs. 2.6 and 2.7).

Equation 2.13 indicates that the power response when operating as a cosine telescope is similar to the field pattern of a simple grating of twice the length. This apparent increase in length, (although there is no increase in the spatial frequencies measured), occurs because of the presence of the interference term due to the displaced phase centres of the two component antennae. If the phase centres were coincident, only half the Fourier components would be measured and the cosine response would be proportional to $\frac{\sin(N\pi\ell d)}{N\sin(\pi\ell d)}$.

Since the sampling of the Fourier plane occurs at odd multiples of $\frac{d}{2}$, adjacent grating lobes are of opposite sign (Fig. 2.3).

A variation of this basic compound grating interferometer (Labrum et al, 1963), separates the phase centres by an even multiple of d; e.g. $D = (\frac{N+1}{2})d$, where the large element is one spacing from the end of the grating. In this case

$$A_c(\ell,m) = 2\left[N.A_1.A_2\right]^{\frac{1}{2}}\left\{\frac{\sin\{(2N+1)\pi\ell d\}}{2N\sin(\pi\ell d)} - 1\right\} \qquad (2.14)$$

and the response (Figs. 2.8 and 2.9) is very similar to that of equation 2.13 being slightly higher in directivity due to the additional spatial

---

*The subscript $_1$ refers to the (small) grating elements. The subscript $_2$ refers to the (large) 'multiplying' element(s). Where possible the dependent variables (ℓ,m) and/or (α,β) are omitted for clarity.

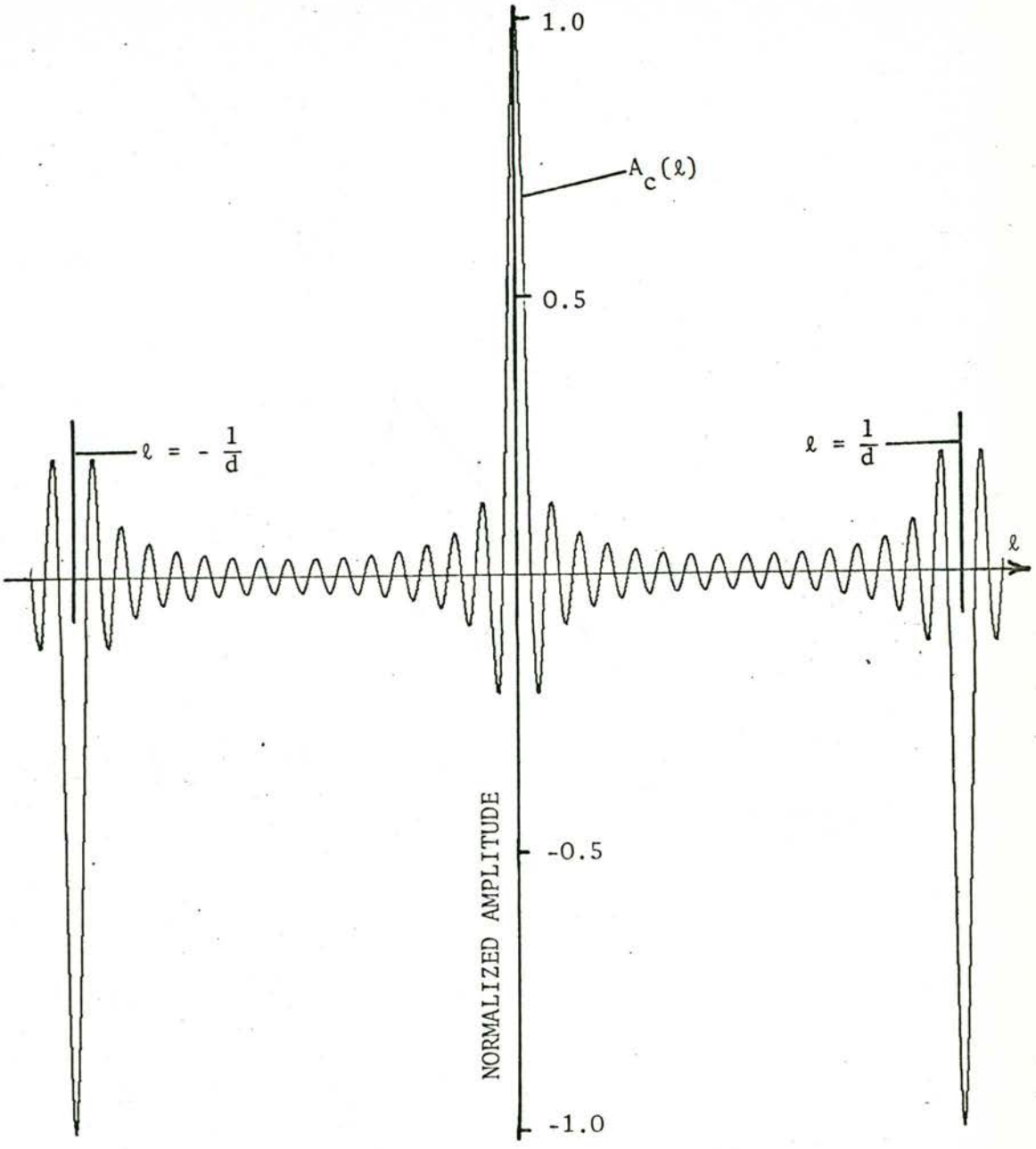

Harmonic spacing : d
Initial spacing : d/2
Spatial components: 16
(See equation 2.13 and Fig. 2.7)

FIGURE 2.6 The cosine response of a basic compound grating antenna.

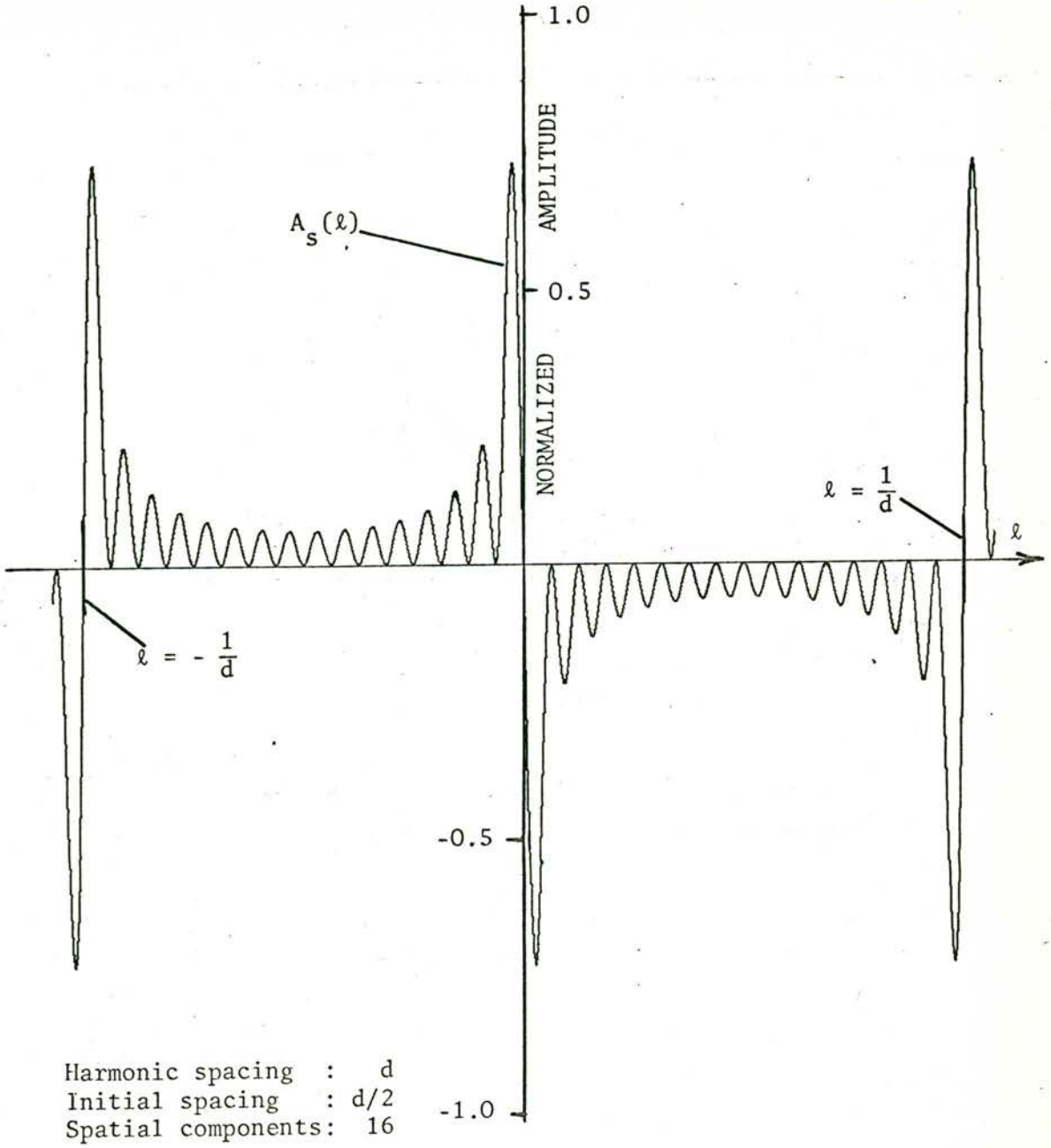

Harmonic spacing : d
Initial spacing : d/2
Spatial components: 16

(See equation 2.13 and Fig. 2.6)

FIGURE 2.7 The sine response of the basic compound grating antenna of Fig. 2.6

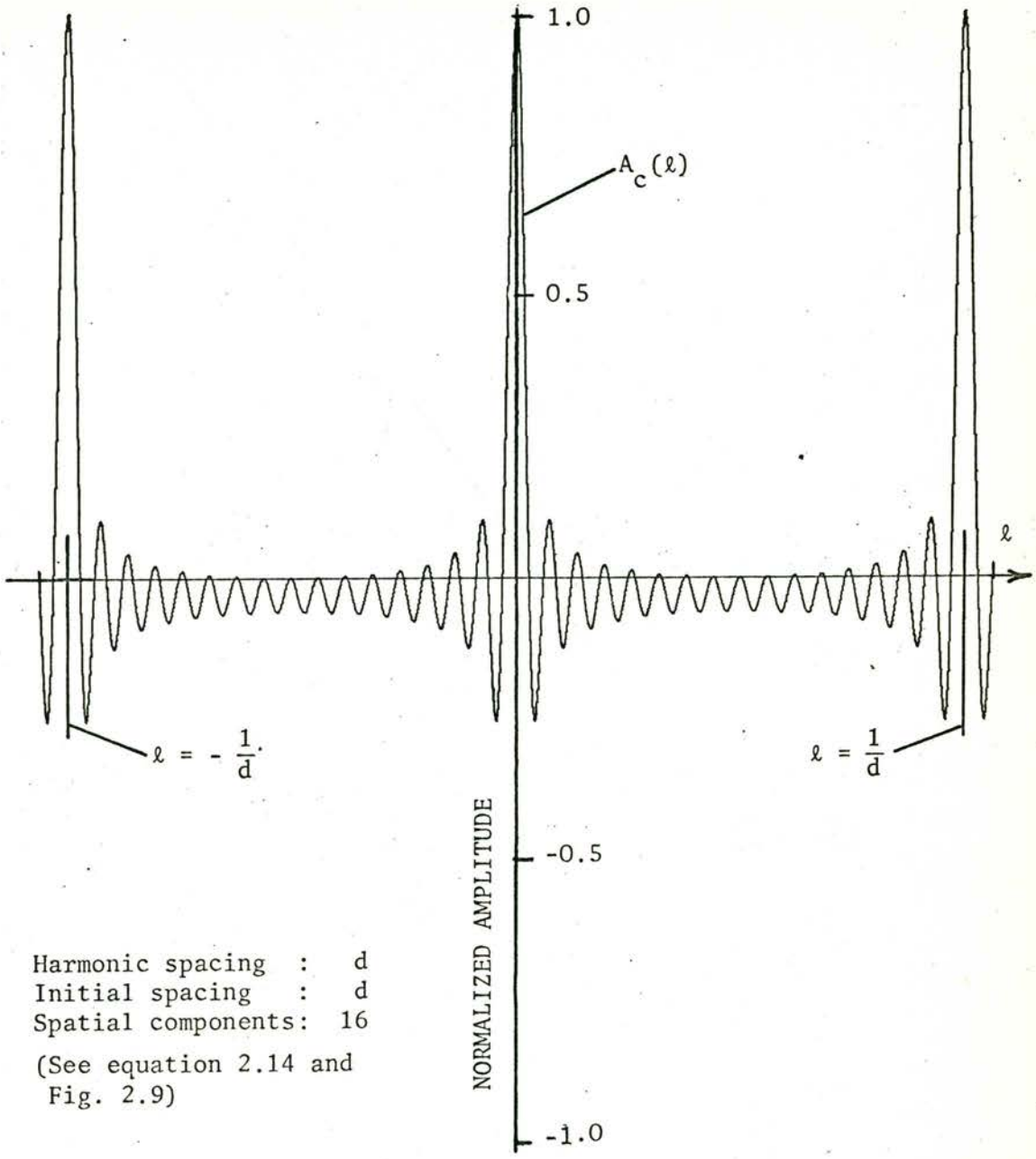

FIGURE 2.8 The cosine response of a basic compound grating antenna.

frequency. However the adjacent lobes are of the same sign and the -1 term indicates a negative D.C. baseline. Thus when this response is integrated over the whole sky the nett value is zero as for all correlation telescopes.

In the above equations 2.13 and 2.14 defining the complex effective area of the basic compound grating interferometer, the paraboloid elements are considered to be pointing in the zenith direction. In normal operation, these paraboloids follow a source away from the zenith. In angular coordinates, the element envelope is of constant size (Section 2.1.4). However expressed in direction cosines (ℓ,m) of the angular coordinates, this envelope becomes narrower away from the zenith. Restating equation 2.13 in angular coordinates,

$$A_c(\alpha,\beta) = 2\left[N.A_1\{(\alpha-\alpha^1)(\beta-\beta^1)\}A_2\{(\alpha-\alpha^1)(\beta-\beta^1)\}\right]^{\frac{1}{2}} \frac{\sin(N\pi d\cos\alpha)}{N\sin(\pi d\cos\alpha)} . \exp(-j2\pi D\cos\alpha) \qquad (2.15)$$

Here the angular size of A_1 and A_2 is constant. The other terms in equation 2.15 experience broadening as α increases and $\cos\alpha$ decreases.

2.2.3 The Sine Effective Area

Equation 2.13 and Fig. 2.7 show the sine effective areas of the basic compound grating interferometer. Although A_s is zero when A_c is a maximum, it increases rapidly on either side. If the receiver (normally cosine) has any phase error, ϕ_ε, between the correlated components, a portion of this sine response is added to the cosine response. This creates an undesirable asymmetric beam shape (Fig. 2.10).

Thus, this array configuration is very sensitive to this type of phase error which is also the most likely to occur in practice. Polarization measurements, in particular, depend upon the elimination of any sine response contribution.

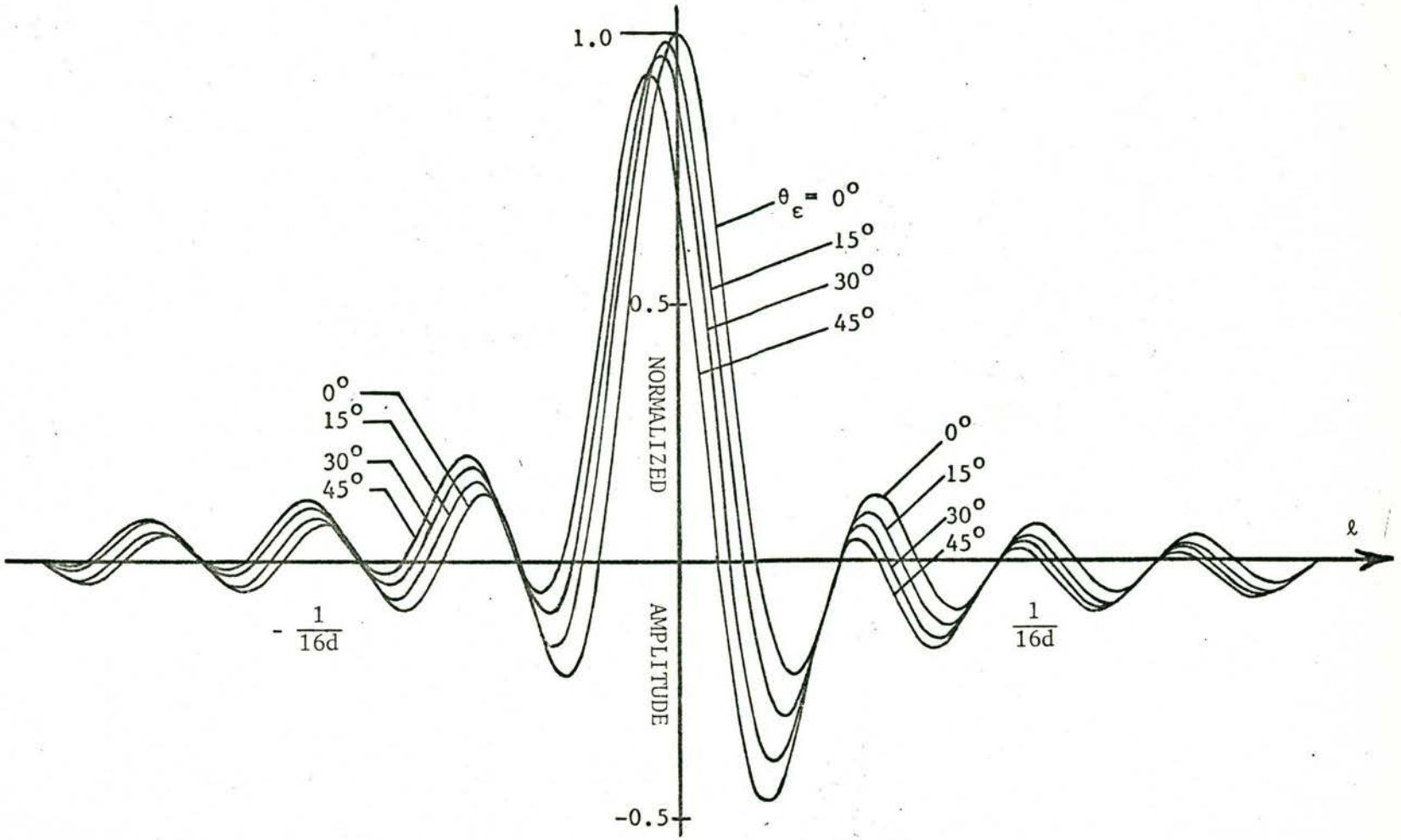

FIGURE 2.10 The main response of the compound grating antenna with phase errors (θ_ε) between the correlated components.

2.2.4 The Symmetrical and Quasi-symmetrical Compound Grating Interferometer

To eliminate this sine effective area, the phase centres of the two component antennae must be coincident, implying at the same time a symmetrical configuration.

The basic arrangement, Fig. 2.5, requires an additional large element as in Fig. 2.11a. The resulting response is

$$\underset{\sim}{A}(\ell,m) = 2\left(2N.A_1.A_2\right)^{\frac{1}{2}} \cdot \frac{\sin(2N\pi\ell d)}{2N\sin(\pi\ell d)} \qquad (2.16)$$

This has no imaginary part, hence $A_s = 0$. The cosine response is unchanged except for a sensitivity increase of $\sqrt{2}$ due to the presence of an additional element.

A symmetrical configuration is at present under construction by Covington et al., (1967) for polarization observations of the sun.

Quasi-symmetry

A slight modification to this symmetrical configuration, Fig. 2.11b, enables the large elements to be reduced to half their size. The phase centres of the two gratings are displaced by $\frac{d}{4}$. This gives

$$\underset{\sim}{A}(\ell,m) = 2\left(2N.A_1.A_2\right)^{\frac{1}{2}} \frac{\sin(2N\pi\ell d)}{2N\sin(\pi\ell d)} \cdot \exp\left(\frac{\pi\ell d}{2}\right) \qquad (2.17)$$

The response has the same directivity as before but the lobe period is doubled. (The spatial frequencies are being sampled twice as often.) For the same grating sidelobe suppression, the large element diameter can be halved.

The price paid for this is that A_s is no longer zero over all (ℓ,m). It has peaks midway between cosine responses (Fig. 2.12). However, it is small and slowly varying in the direction of the main response, which is the principal requirement for polarization investigations.

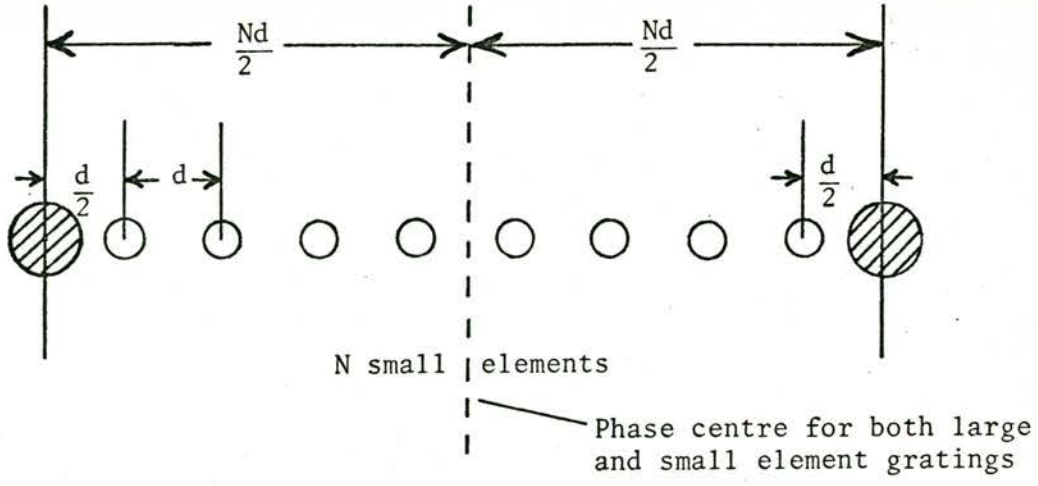

(a)

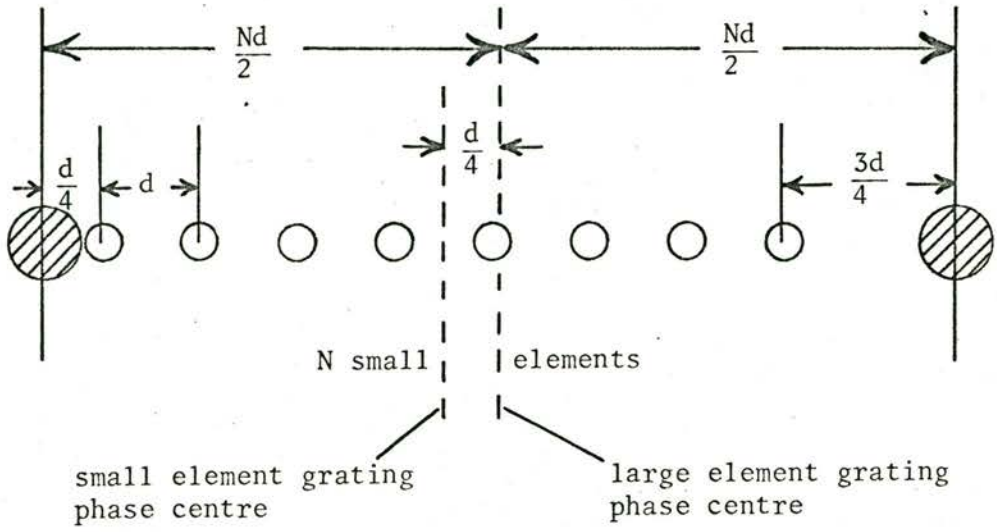

(b)

FIGURE 2.11 Two basic types of compound grating interferometer:
(a) the symmetrical configuration
(b) the quasi-symmetrical configuration.

2.2.5 The Missing Fourier Components

In all compound grating antennae there will be some Fourier components missing. These will generally be low spatial frequency components which are excluded because of the physical impossibility of placing a large element close enough to a small element. (Zero spatial frequency requires the coincidence of antennae.) This is often referred to as the 'centre problem' of correlation telescopes.

In the spectral sensitivity function C(x,y), this shows as a gap in the rectangular band-pass near zero (Fig. 2.5). The effect is to produce a wide negative sidelobe under the main response. This gap must always be present in the true correlation telescope so that the whole sky integral is zero. Any 'filling-in' of the gap turns the telescope into a partial total-power instrument (Mills, 1963).

If the array samples all the odd Fourier components, the adjacent grating lobes are of opposite sign and of the form $\frac{\sin Nx}{N \sin x}$. There is no zero spatial frequency sample missing. In practice usually only the first component at $\frac{d}{2}$ is missing.

If the array were to sample even Fourier components, all responses are positive and of the form $\frac{\sin Nx}{N \sin x}$. Without the zero frequency component, the response has a 'constant' negative baseline. Often the first spatial component is missing as well, creating a cosine variation upon this negative baseline. Both 'missing' components are modified by the element envelope.

In observations of point sources the total flux from the source can be considered as 'collected' by both main response and 'missing' components. Thus the amplitude effect on the main response of the missing spacings is small. However with extended sources, such as the sun or Magellanic clouds, the main response samples only a small portion of the total flux compared with the 'missing' spacing. Thus for broad sources any missing spacings create a very noticeable effect. In these cases it must be possible to measure the missing components in some other way and to add this information to the main response.

Compensation can be carried out in three ways:

(i) A single large element can be built which has a beam-shape identical with the negative response of the missing spacings. This was proposed by Christiansen et al., (1963). The large element does not need to be connected to the interferometer but can be separated geographically and run at different times. Generally the large element has sufficient sensitivity such that it need spend only a comparatively short time measuring the missing spacings.

(ii) A separate interferometer using smaller elements can be constructed specifically to measure the missing spacings. Again this instrument need not be connected in any way to the main interferometer. In this case the lower collecting area may cause a slight degradation in overall signal-to-noise ratio of the combined observations.

(iii) Sky maps of the desired image plane, produced by existing instruments having sufficiently high resolution, can be analysed for the required spatial components. These components can be reweighted and combined with the main system response.

Post-observational compensation on a fan beam response, although simple in concept, is tedious to apply. One form using (iii) above has been applied to the solar observations of the present compound grating interferometer. This is described in a later chapter.

In the final system at Fleurs (Christiansen and Wellington, 1966) the spatial components will be recorded separately and combined later in a computer. Under these circumstances compensation becomes easier to apply.

In many observations compensation can be omitted with the consequence of causing only a weak negative response (about 1.5% with the present system).

2.2.6 Steering the Response of an Array

With all the antenna elements in phase, an array forms a response in the zenith direction, in addition to responses (grating lobes) at periodic intervals away from the zenith. These responses can be steered electronically to any 'in-between' directions by applying a linear phase gradient across the array aperture. Christiansen (1961) used this technique to steer the north-south grating lobes of the crossed grating interferometer. This response steering, without physical movement, is the main advantage of an array.

Mathematically, it amounts to multiplying the aperture grading function by $\exp\{-j2\pi.x.(\Delta\ell)\}$ where $\{2\pi.x.(\Delta\ell)\}$ is the phase shift in radians added to the element at a distance $\underline{x}$ from an arbitrary origin. The Fourier transform of $\exp\{-j2\pi.x.(\Delta\ell)\}$ is a displaced impulse function. This function is convolved with the grating function, III(x). The nett effect is to shift the multiple grating responses by $(\Delta\ell)$, i.e. an angular distance $(\Delta\alpha)$, where $(\Delta\alpha) = -\frac{(\Delta\ell)}{(1-\ell^2)^{\frac{1}{2}}}$.

Steering can be extended to two dimensional movement but, due to the large number of separate elements which must usually be phased, it is seldom put into practice.

The linear phase function has no effect upon the amplitude of the grading function and the main response shape remains as before as long as the element envelope is now recentred on the shifted response. Otherwise, a general drop in gain of main beam and sidelobes will result.

This process is similar but not identical to tilting the whole array mechanically. If the array were tilted, the projected length in the direction of the response would remain constant. With electrical steering, the array appears foreshortened and the main response broadens (although expressed in the direction cosines, (ℓ,m), of the angular coordinates, it appears to remain constant).

The advantage of combining the two forms of beam steering lies in avoiding, on one hand, the impossibility of tilting the whole aperture mechanically and, on the other hand, the extreme complexity of electrically phasing each small segment of aperture.

Lobestopping

In some recently designed telescopes (Christiansen et al, 1963; Christiansen and Wellington, 1966), a continuous steering or 'lobe-stopping' is applied. This compensates for the rotation of the earth so that the interference patterns are brought to rest. The rate of change of the linear phase slope depends upon the direction of the source. It will not be constant but will vary with ($\cos\delta.\cos\alpha$) (Chapter 3).

2.2.7 Image Formation

Steering (both discrete and continuous) is necessary in both multibeam and synthesis image-forming arrays. In both systems the responses of the individual elements are returned separately to the array centre.

Multibeam image formation

For a multibeam system, the element responses are combined in a number of separate receivers, each placing a different phase gradient across the array. The result is the formation of many slightly-separated grating responses recording information over an area of sky and hence giving an image. Blum (1961) was the first to use this technique and has been followed by Mills et al (1963), Swarup (1967) and Wild (1967).

Image synthesis

In the more advanced image synthesizing system, the individual elements are correlated in pairs with steering applied to bring the fringes to rest. The spatial Fourier components thus produced are recombined later with varying phase relationships to produce an image of the whole area of sky inside the element response envelope. This element envelope is generally broad compared to the array directivity and hence defines a relatively large image plane. This process utilizes all the energy from this area of sky incident upon the individual elements.

Previously all grating arrays used the earth's rotation to scan a fixed beam across the sky distribution measuring different points in succession. This wastes a lot of the incident energy making the system less efficient. Image formation is and will be applied to many large correlation telescopes (e.g. Ryle, 1962; Christiansen and Wellington, 1966; McLean et al, 1967).

If the array is linear (large in one direction only, as for the compound grating interferometer), the image at any instant is a one-dimensional strip-integration of the true distribution. However, if these one-dimensional images are collected over a sufficiently large range of scanning angles a two-dimensional image can be synthesized. This is considered in the next chapter.

The application of any type of multi-beam or image forming system can be considered as an increase in the telescope sensitivity. Observations of separate picture points are simultaneous instead of successive.

The effective increase is $(n)^{\frac{1}{2}}$ where n is the number of separate picture points (or beamwidths) that are observed simultaneously. In the case of an image synthesizing telescope, the increase can be made quite large without the same increase in receiver complexity necessary for similar multi-beam observations. In the present compound interferometer using earth rotation synthesis (considered later) the ratio of resolution to image area is over 8000 giving a 'sensitivity' increase of about 90.

This apparent sensitivity increase is not the same as an increase in the normal system sensitivity. It is only real when observations of all picture points are necessary. For this reason it is called the survey sensitivity.

2.2.8 Array Element Sizes

In order to remove the multiple responses in the compound grating interferometer, the elements of the two gratings need to be of different sizes.

To avoid shadowing while tracking a source, the elements of the closely spaced grating generally require a diameter less than half the element spacing, d. If the elements were uniformly illuminated linear apertures of length d, then in the zenith direction the zeros of the element field pattern would fall on the grating sidelobes, suppressing them completely. As the elements are circular, the separation of zeros increases by 1.22 (and the beam-width by 1.17). Assuming a dipole feed and an $\frac{f}{d} \simeq 0{\cdot}4$ for the parabolic elements, the non-uniform illumination causes a further increase of zero separation from 1.22 to about 1.6. Since shadowing considerations require the spacing to be twice the element size, the resultant effective width of the small elements is unlikely to be greater than one third of the element spacing.

The larger elements, when paraboloids, also suffer the same loss of effective width. Their diameter needs to be approximately 1.6d in order that the zeros of the envelope suppress the grating sidelobes of the central main response. If the compound grating interferometer is used to form an image, the grating sidelobes need to be suppressed for the edges of the image plane (normally the beam width of the large element). This is illustrated in Fig. 2.13. The element size required is then about 2.3d. This compares with a small element size of <0.5d. However, the quasi-symmetrical compound grating interferometer of Fig. 2.11b allows halving of the large element size to 1.15d. This gives an element diameter ratio of about 2.3 to 2.5.

In practice complete suppression of the grating sidelobes over the whole image plane is not always necessary and the diameter requirement can be relaxed accordingly.

A system which uses elements of comparable size has several advantages:

(i) To form a fan beam response, the axes of all elements should be in line (see Appendix C.1). With different size elements, the small elements need to be on high towers in order that the large elements have sufficient ground clearance over the required sky coverage.

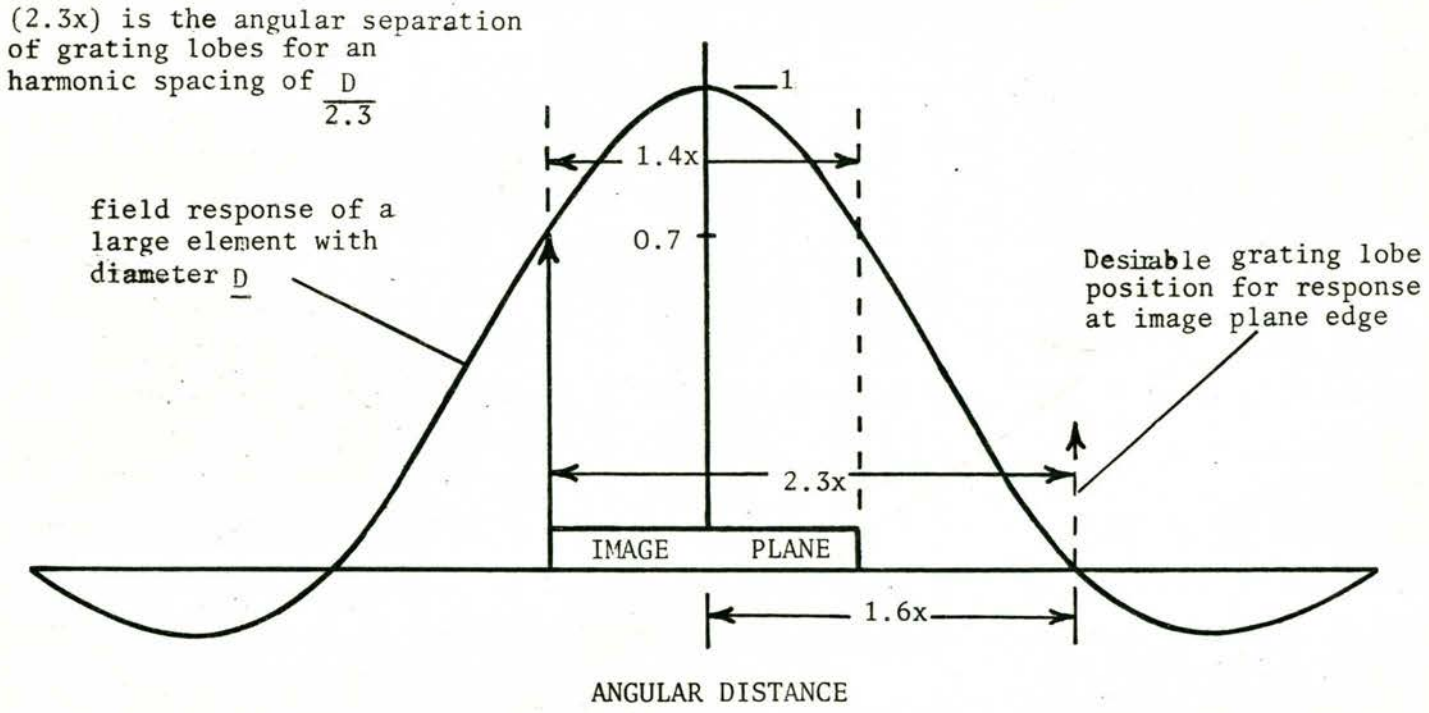

FIGURE 2.13 Illustrating the element size requirement for grating lobe suppression over the entire image plane.

(ii) With an image forming system, the image plane size is defined principally by the beamwidth of the larger element. The small element receives energy from a larger area of sky and much of this energy is wasted unless the elements are of similar size (or a system as in Appendix K is used).

(iii) Temperature and gravitational effects on the elements will be similar if the elements are of similar size.

(iv) Antenna cost is approximately proportional to the cube of the diameter. Thus the antenna structural costs are lowered in a system which doubles the number of elements in one of the gratings but halves their size. However, this structural cost saving is offset by the increase in receiver components some of which are proportional to the number of Fourier components measured.

2.2.9 Extension of the Compound Grating Antenna

The basic compound grating interferometers of Figs. 2.5 and 2.11 can be extended in both resolution and sensitivity by adding more large elements at intervals of Nd. These large elements form another grating which is correlated with the original closely spaced grating. Three versions having different characteristics are shown in Fig. 2.14. In each case the small-grating responses suppress the unwanted large-grating responses and the large-element envelope suppresses the unwanted responses of the small-grating.

(i) Fig. 2.14a is the normal extension of the basic compound grating antenna of Fig. 2.5. The response is given by:

$$\underline{A}(\ell,m) = 2\left[M.N.A_1.A_2\right]^{\frac{1}{2}}. \frac{\sin(MN\pi\ell d)}{MN \sin(\pi\ell d)} \cdot \exp(MN\pi\ell d) \qquad (2.18)$$

where $\underline{M}$ is the number of large elements.

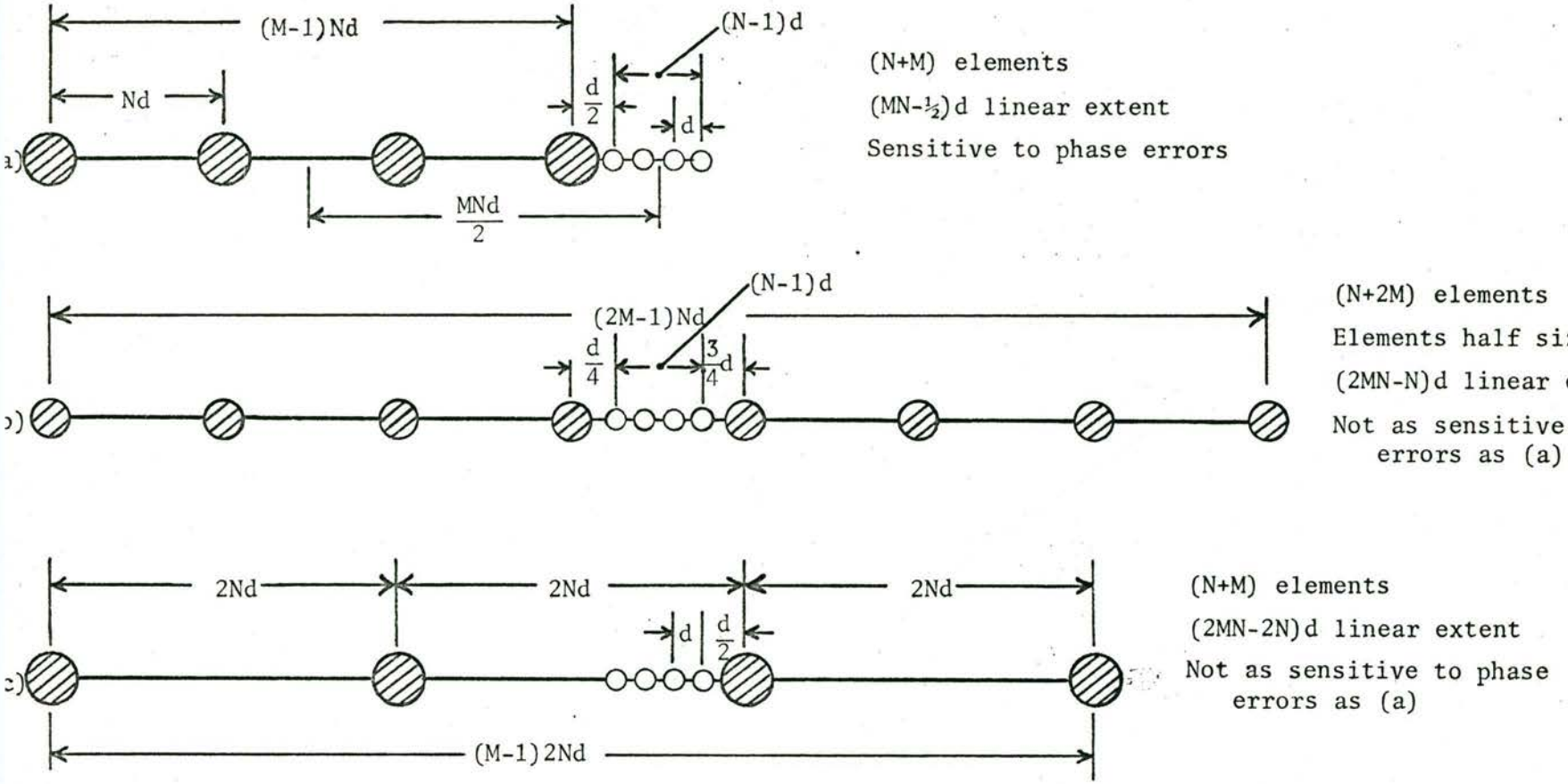

FIGURE 2.14 Three possible extensions to the basic compound grating interferometer.

This type has the highest possible resolution per linear extent, due to the large separation of phase centres. However, this separation creates a quickly varying and undesirable sine response.

(ii) To avoid this sine response the linear extent of the array and the number of elements in the large grating must be doubled. The size of these elements can then be halved provided a phase centre displacement of $\frac{d}{4}$ can be tolerated (Fig. 2.14b). (Extension of the quasi-symmetrical case of Fig. 2.11b.) The sine response is virtually eliminated over the main response region due to the slowly varying term, $\sin(\pi\frac{\ell d}{2})$. Thus,

$$\left.\begin{aligned} A_c(\ell,m) &= 2\left(2M.N.A_1.A_2\right)^{\frac{1}{2}}.\ \frac{\sin(2MN\pi\ell d)}{4MN\ \sin(\frac{\pi\ell d}{2})} \\ \text{and,} & \\ A_s(\ell,m) &= 2\left(2M.N.A_1.A_2\right)^{\frac{1}{2}}.\ \frac{\sin(2MN\pi\ell d)}{2MN\ \sin(\pi\ell d)}\ .\ \sin(\frac{\pi\ell d}{2}) \end{aligned}\right\} \quad (2.19)$$

(iii) The arrangement of Fig. 2.14c has the response:

$$\underset{\sim}{A}(\ell,m) = 2\left(M.N.A_1.A_2\right)^{\frac{1}{2}}.\frac{\sin(N\pi\ell d)}{N\ \sin(\pi\ell d)}.\frac{\sin(2MN\pi\ell d)}{M\ \sin(2N\pi\ell d)}.\exp(N\pi\ell d) \quad (2.20)$$

Hence,

$$\left.\begin{aligned} A_c(\ell,m) &= 2\left(M.N.A_1.A_2\right)^{\frac{1}{2}}.\ \frac{\sin(2MN\pi\ell d)}{2MN\ \sin(\pi\ell d)} \\ A_s(\ell,m) &= 2\left(M.N.A_1.A_2\right)^{\frac{1}{2}}.\ \frac{\sin(2MN\pi\ell d)}{NM\ \sin(\pi\ell d)}\ .\ \frac{\sin^2(N\pi\ell d)}{\sin(2N\pi\ell d)} \end{aligned}\right\} \quad (2.21)$$

The cosine response has the same resolution and grating lobe positions as that of Fig. 2.14a although the linear extent has been nearly doubled. However the sine response is now dependent on $\sin(N\pi\ell d)$. As in the quasi-symmetrical configuration, this sine response will vary slowly over the extent of the main beam (desirable). No additional large elements are

required and the only additional cost is the increased linear extent.

This is the form of the experimental arrangement at Fleurs.

2.3 Sensitivity

2.3.1 Total Power Telescopes

The theory pertaining to the sensitivity of the total power radio telescope is treated fully in several standard texts (e.g., Bracewell, 1961b; Christiansen and Högbom, 1968; Jasik, 1961; Pawsey and Bracewell, 1955, and Robinson, 1964). A brief outline follows.

A source in the antenna beam generates a temperature T_a at the antenna terminals. If this signal suffers a loss, ζ, before entering an amplifier of noise temperature, T_R, then the total amplifier input noise temperature, T_t, will be

$$T_t = (1-\zeta).T_a + \zeta.T_{300} + T_R \qquad (2.22)$$

This noise power creates error fluctuations in the output. The increase in antenna temperature $(\Delta T_a)_{rms}$, which would create the same output change, is given by:

$$\left(\Delta T_a\right)_{rms} = \frac{T_t}{(Bt)^{\frac{1}{2}}(1-\zeta)} \qquad (2.23)$$

where B and t are the receiver bandwidth and integration time.

The antenna temperature, T_a, due to a source must be significantly greater (say 5 times) than these error fluctuations in order to be detectable with reasonable certainty.

In determining the antenna temperature that a particular source generates, a radiotelescope has effectively two sensitivities.

One sensitivity applies to point sources when the antenna detects the entire flux* incident from the source. This sensitivity depends primarily on the antenna effective area. The minimum

---

* Entire flux having its polarization matched to the feed. With randomly polarized radiation this is half the total flux.

detectable flux density $(\Delta S)_{min}$ is then given by:

$$(\Delta S)_{min} = \frac{5M.k.T_t}{A_{mx}.(1-\zeta)(Bt)^{\frac{1}{2}}} \quad \text{(Watt Hz}^{-1}\text{ m}^{-2}\text{)} \qquad (2.24)$$

where ζ is the signal loss prior to amplification

A_{mx} is the maximum effective area of the telescope

$\underline{k}$ is Boltzman's constant ($+1.38 \cdot 10^{-23}$ joules degree^{-1}), and

$\underline{M}$ is a factor (≥ 1) depending upon receiver design (e.g. in a switched receiver M=2).

The other sensitivity applies to extended sources. In this case the sensitivity depends upon the angular extent and the brightness gradients across the source and also upon the size and shape of the antenna beam. In order to compute this sensitivity a simplification is made and the antenna beam is divided into two regions, one containing the main beam and the other the surrounding sidelobes, spillover, etc. The noise contribution from each region is evaluated separately by inte grating the sky brightness temperature over each region. Integration is facilitated by assuming that this brightness temperature is constant for each region. Sometimes the response pattern is divided into three regions: the main response, the forward sidelobes and the feed spillover (Yates, Wielebinski and Landecker, 1967).

Since the desired response is in the direction of the main beam, a beam efficiency factor η_b can be used where

$$\eta_b = \left(\iint_{\substack{\text{main} \\ \text{response}}} \underset{\sim}{A}(\ell,m).d\Omega \right) \div \left(\iint_{\substack{\text{all} \\ \text{sky}}} \underset{\sim}{A}(\ell,m).d\Omega \right)$$

$$= \lambda^{-2} \left(\iint_{\substack{\text{full} \\ \text{beam}}} \underset{\sim}{A}(\ell,m).d\Omega \right) \qquad (2.25)$$

It can then be shown that the minimum detectable brightness temperature $(\Delta T)_{min}$ of the telescope is given by:

$$\left(\Delta T_b\right)_{rms} = \frac{5M.T_t}{\eta_b.(1-\zeta)(Bt)^{\frac{1}{2}}} \quad (^oK) \qquad (2.26)$$

Equations 2.24 and 2.26 are standard sensitivity equations for single antenna radio telescopes but they also apply to the simple grating operating into a total power receiver.

2.3.2 Correlation Telescopes

In the case of a correlation telescope, i.e. the compound grating interferometer, the situation is somewhat different. The telescope output depends upon the correlation of signals from two often completely different antennae. The receivers on each of these antennae can also have differing noise temperatures, gains and signal input losses. Calculation of the resultant sensitivity, treated by Christiansen and Högbom (1968), is as follows:

The noise powers, P_1 and P_2, at the correlator inputs are:

$$\left.\begin{aligned} P_1 &= T_1G_1 = G_1\left(T_{a1}(1-\zeta_1) + \zeta_1 \,.\, T_{300} + T_{n1}\right) \\ P_2 &= T_2G_2 = G_2\left(T_{a2}(1-\zeta_2) + \zeta_2 \,.\, T_{300} + T_{n2}\right) \end{aligned}\right\} \qquad (2.27)$$

where the subscripts $_1$ and $_2$ refer to the component antennae.

T_1 and T_2 are the noise temperatures referred to the channel inputs,

G_1 and G_2 are the channel gains (preamplifiers etc.),

ζ_1 and ζ_2 are the channel losses prior to amplification, and

T_{n1} and T_{n2} are the preamplifier noise temperatures.

It is presumed that preamplifiers are present and that their gains are sufficiently large for the noise contribution of the correlation receiver to be insignificant.

If the total noise power of the receiver is large compared with the signal power then it can be regarded as constant and equal to $\frac{P_1+P_2}{2}$. The rms noise fluctuation in this power is then

$$(\Delta P)_{rms} = \frac{T_1G_1+T_2G_2}{2(B\mathfrak{t})^{\frac{1}{2}}} \tag{2.28}$$

Now the signal P_S from a correlation telescope operating with a phase switched receiver is given by:

$$\begin{aligned} P_S &= 2\ \underset{\sim}{V}_1 \cdot \underset{\sim}{V}_2{}^* \\ &= 2 \cdot \frac{(\Delta S)}{k} \cdot \left(A_1A_2(1-\zeta_1)(1-\zeta_2)\ G_1G_2\right)^{\frac{1}{2}} \exp(j\phi) \end{aligned} \tag{2.29}$$

where $\underset{\sim}{V}_1$ and $\underset{\sim}{V}_2$ are the voltage of the correlated signal components from the antennae of effective area A_1 and A_2 respectively.

Substituting the effective area $A(\ell,m)$ of the correlation telescope (given in Appendix H), equation 2.29 becomes:

$$P_S = \frac{2}{k}\ (\Delta S)\ \underset{\sim}{A}(\ell,m)\left((1-\zeta_1)(1-\zeta_2)\ G_1G_2\right)^{\frac{1}{2}} \tag{2.30}$$

From equations 2.28 and 2.30 and noting that a phase switched receiver is being used (which causes the signal to be measured for only half the total time), the flux $(\Delta S)_{rms}$ corresponding to the receiver noise power fluctuations is given by:

$$(\Delta S)_{rms} = \frac{k}{\underset{\sim}{A}(\ell,m)\left((1-\zeta_1)(1-\zeta_2)\right)^{\frac{1}{2}}(B\mathfrak{t})^{\frac{1}{2}}} \left(T_1\left(\frac{G_1}{G_2}\right)^{\frac{1}{2}}+T_2\left(\frac{G_2}{G_1}\right)^{\frac{1}{2}}\right) \tag{2.31}$$

This equation shows that $(\Delta S)_{rms}$ can be minimized by equalizing the noise powers P_1 and P_2. Under these circumstances the minimum detectable flux $(\Delta S)_{min}$ in the direction of maximum response {substituting A_{mx} for $\underset{\sim}{A}(\ell,m)$} is then:

$$(\Delta S)_{min} = \frac{10.k(T_1T_2)^{\frac{1}{2}}}{\left((1-\zeta_1)(1-\zeta_2)\right)^{\frac{1}{2}}(B\mathfrak{t})^{\frac{1}{2}}.A_{mx}} \quad \left(\text{Watts Hz}^{-1}\text{m}^{-2}\right) \tag{2.32}$$

This is identical with the single antenna sensitivity equation 2.24 provided that geometrical-means are used in place of the total noise power, T_t, and the loss factor, $(1-\zeta)$, and that a phase switched receiver is used.

As a true correlation telescope, the total power received (all-sky integral) must be zero. This makes it impossible to calculate a beam efficiency factor as in the case of a single total power antenna. Instead, a filling factor, F, is used (Erickson and Högbom, 1962) in which the collecting area is compared to an ideal filled-aperture telescope giving equivalent resolution. (This gives the ratio of signal powers due to the flux incident from identical areas of sky.) For the correlation telescope, equation 2.26 for the minimum detectable brightness temperature $(\Delta T_b)_{min}$ then becomes:

$$(\Delta T_b)_{min} = \frac{5(T_1 T_2)^{\frac{1}{2}}}{(1-\zeta_1)(1-\zeta_2)^{\frac{1}{2}}(B\tau)^{\frac{1}{2}}F} \quad (^oK) \qquad (2.33)$$

Equations 2.32 and 2.33 become the standard sensitivity equations for correlation telescopes. They can be applied to either the full compound grating antenna or just a two aerial interferometer.

In all these sensitivity equations, a detection ratio (signal output to receiver noise output fluctuation) of 5 has been assumed.

CHAPTER 3

GRATING TELESCOPES FOR TWO DIMENSIONAL OBSERVATIONS

CHAPTER 3: GRATING TELESCOPES FOR TWO DIMENSIONAL OBSERVATIONS

3.1 Introduction

Grating telescopes were designed initially for observations with a high resolution in one direction only. These observations are termed 'one dimensional' since they integrate the sky brightness distribution along a strip perpendicular to the direction of high resolution. Two dimensional observations entail the use of a narrow pencil beam having high resolution in all directions.

There are two methods by which gratings can be used to form a narrow pencil beam. The first is to combine two simple gratings at right angles in the manner of a Mills-cross antenna. This was done originally by Christiansen et al. (1957) and repeated at several other centres (Bracewell and Swarup, 1961; Blum, 1961; Covington et al, 1967; Hatanaka, 1963). The second method, applied initially by Christiansen and Warburton (1955) is to use the earth's rotation to form a two dimensional antenna from a one dimensional grating. This is called rotational synthesis.

Both of these methods, as applied in the past, form spurious pencil beam grating lobes in directions away from the main response. This has limited their usefulness to observations of the sun and of a few strong radio sources.

In the present telescope the earth's rotation is used again to form a two dimensional antenna but this time from a one dimensional compound grating antenna. By so doing, a pencil beam response is formed without the limitation caused by spurious grating lobes.

3.2 Rotational Synthesis

3.2.1 Introduction

The feasibility of rotational synthesis depends primarily upon the geometrical relationships associated with the rotation of the earth. During this rotation, the length and orientation of the interferometer baseline appear to change when viewed from a point in outer space. These changes are considered in detail in Section 3.3, particularly in relation to the present telescope.

For some time, Ryle (1962) has been using rotational synthesis However in this case, the one dimensional aperture has been a two (or three) aerial interferometer so that to completely synthesize (or 'fill') a two dimensional aperture, it has also been necessary to synthesize a 'filled' linear aperture by varying the spacing between the separate aerials. This method, although being exceptionally economical in terms of antenna structure, and achieving exceedingly high sensitivity, is very lengthy in terms of time per completed observation.

The compound grating antenna measures all the spatial components along a line by combining the observations of many 'pairings' of individual aerials. There is no need to physically relocate the aerials to synthesize the one dimensional antenna.

For simplicity the compound grating interferometer can be thought of as operating like Ryle's 'super-synthesis' but with all the two-aerial interferometer positions being taken simultaneously instead of serially. This enables the operation to be considered in terms of two aerial interferometers and the length and orientation of the baseline joining them.

3.2.2 The Basic Two Aerial Interferometer

A two aerial interferometer is the simplest form of correlation telescope and measures one spatial Fourier component of the sky brightness distribution within the beamwidth of the individual aerials. This aspect is the basis of the general application of Fourier transform theory to antennas. It is discussed in a number of texts* and is outlined here

---

* See Footnote p.10.

from the aperture synthesis point of view.

The complex effective area of the two aerial interferometer is given by:

$$\underset{\sim}{A}(\ell,m) = A_o(\ell,m).\exp(j\phi) \tag{3.1}$$

where $A_o(\ell,m)$ is the correlation effective area of the two antennae with zero spacing between them, and ϕ is the phase difference of arrival of the signals at the antennae.

If (u',v') represents the spacing between the centroids of the two antennae relative to the (x,y) coordinate system, then:

$$\phi = 2\pi(u'.\ell + v'.m) \tag{3.2}$$

Thus the complex antenna temperature, $\underset{\sim}{T}_a(u'.v')$ generated by the sky brightness distribution $T_b(\ell,m)$ is given (Christiansen and Högbom, 1968) by:

$$\underset{\sim}{T}_a(u',v') = \frac{1}{\lambda^2} \cdot \frac{T_b(\ell,m)}{(1-\ell^2-m^2)^{\frac{1}{2}}} .A_o(\ell,m).\exp\{j2\pi(u'\ell+v'm)\}d\ell.dm \tag{3.3}$$

This equation has the form of a Fourier integral and represents the sampling of $T_b(\ell,m)$ by the interferometer pattern to give the antenna temperature $\underset{\sim}{T}_a(u',v')$ for that aerial separation:

$$\underset{\sim}{T}_a(u',v') \rightleftharpoons \frac{T_b(\ell,m).A_o(\ell,m)}{\lambda^2(1-\ell^2-m^2)^{\frac{1}{2}}} \tag{3.4}$$

Synthesis

If the separation is varied in magnitude or orientation, a different spatial component of the sky brightness temperature is measured and a spatial Fourier 'map' can be built up. If this 'map' is extended to infinite separations, then the inverse transformation will give the true sky brightness distribution over a region limited by the interferometer envelope, $A_o(\ell,m)$. This is the basis of all aperture synthesis systems, including rotational synthesis as employed by the new telescope at Fleurs.

In practice the spatial components are generally not measured with uniform weighting and are certainly not taken to infinity. To account for this, a synthesized aperture grading function, $g_s(u,v)$, is used to define the weighting applied to the measurement of each spatial component. This grading function becomes a multiplication factor applied to:

(i) the two aerial interferometer grading to give an overall spectral sensitivity function, $\underset{\sim}{C}_s(x,y)$.

$$\underset{\sim}{A}_s(\ell,m) \rightleftharpoons \underset{\sim}{C}_s(u,v) \tag{H.4}$$

(ii) the 'true' antenna temperature distribution, $\underset{\sim}{T}_a(u,v)$, such that the measured distribution, $\underset{\sim}{T}_a'(u,v)$, is given by:

$$\underset{\sim}{T}_a'(u,v) = \underset{\sim}{T}_a(u,v).g_s(u,v) \tag{3.5}$$

then

$$\underset{\sim}{T}_a'(u,v) \rightleftharpoons \left\{\frac{1}{\lambda^2}.\frac{T_b(\ell,m).A_o(\ell,m)}{(1-\ell^2-m^2)^{\frac{1}{2}}}\right\} \otimes \{G_s(\ell,m)\} \tag{3.6}$$

where $G_s(\ell,m)$ is the Fourier transform of the aperture grading function:

$$G_s(\ell,m) \rightleftharpoons g_s(u,v) \tag{3.7}$$

As in Sections 2.1.3 and 2.1.4., $G_s(\ell,m)$ can be considered as defining the beam shape, in this case of the synthesized aperture. This beamshape is to all intents and purposes, the same as that of a large solid aerial having the same grading function.

The result is that the 'true' sky brightness distribution inside the element 'envelope' is smoothed by the synthesized beam shape, $G_s(\ell,m)$.

Information is actually lost in this smoothing process and cannot be recovered in the ensuing inverse transformation. Bracewell and Roberts (1964) and Bracewell (1964) have considered smoothing in some detail in so much as it applies to any form of antenna.

The object in synthesizing an aperture is to measure as completely as possible the spatial Fourier components over as large an area as

possible. This gives the highest resolution of the sky brightness distribution with the minimum of spurious effects (grating lobes, etc.).

3.2.3. Strip Integration

Christiansen and Warburton (1955) did not measure all the Fourier components separately but combined those measured at any particular instant to form a fan beam (or strip integrated) response. The fan beam then scans the source many times as it rotates relative to the source. This form of operation is interesting because, although there is a drop in sensitivity, no spatial information is lost.

The strip scans, giving a one dimensional brightness distribution, are analysed into the separate Fourier spatial components and with sufficient angular source rotation, used to fill the spatial 'map'. By this means the instrument is used to carry out the Fourier transformation from the sky brightness distribution to the spatial distribution using only one dimensional operations.

In the same manner the one dimensional operations of strip scan, Fourier transform and line-plot can be repeated to reconvert the spatial distribution to the measured sky brightness distribution. The full sequence of operations is shown diagramatically in Fig. 2 of Appendix A. The theory has been treated extensively by Bracewell (1956) and Smerd and Wild (1957a and 1957b).

Recently Bracewell and Riddle (1967) proposed a method of analysing these strip scans which does not involve going directly through the Fourier operations.

The telescope described in this thesis is operating at present in the fan beam mode. As such it can produce two dimensional pictures by the above operations. In the final mode of operation the spatial components will be recorded separately, thus eliminating the initial Fourier transformation.

3.2.4 Sampling Intervals

In practice the spatial plane can only be sampled at a finite number of points. Equation 3.3 will then appear as a Fourier series instead of a Fourier integral. The resultant effect is that the derived sky brightness becomes periodic as in the case of the grating (p.10). The repetition rate is inversely proportional to the spatial step length.

If the zero-separation envelope, $A_o(\ell,m)$, is narrow enough, then all but one periodic response will be suppressed. This is the parallel of the grating lobe suppression in the linear compound grating antenna.

Rotational synthesis with a linear grating array will have sampling intervals in both radial and rotational directions:

Radial sampling intervals are caused by the finite spacing between grating elements. Each element pair traces out an ellipse during rotation, so that the Fourier plane is sampled on a series of ellipses. These ellipses create grating lobes on the sky distribution at an angular distance from the main lobe which is inversely proportional to the projection of the harmonic element separation. This projected separation is proportional to the array length, determined in Section 3.3. The grating lobe positions for the telescope configurations of Chapter 4 have been computed and are shown for particular declinations in Chapter 6.

Rotational sampling intervals are determined by the receiver integration time. This is generally the time between the recording of data points. Since reduction operations must be carried out on each data point it is desirable to space these points as widely as possible.

This spacing is determined by the size of the required image plane (assuming lobestopping occurs for the centre of the image plane). As the image region 'rotates', points at the edge will experience a differential fringe rate which is proportional to their distance from the centre point. Unless the output is sampled at greater than twice the frequency of these differential 'fringes', information will be lost which is relevant to the higher spatial frequencies of picture points at the edge of the image plane (the fringes will be 'smeared').

In the same manner as radial sampling, rotational sampling creates periodic responses. In this case the responses are periodic in both radial and rotational directions and are somewhat analagous to the far-out antenna response of the Culgoora heliograph (Wild, 1961 and 1967).

Again, the distance of the response from the main response (not necessarily at the centre point of the image plane) is inversely proportional to the sampling interval and the spatial component being sampled.

3.2.5 Image Plane Envelopes

Section 2.2.7 considered the synthesis of an image plane and the way in which this synthesis gives an effective increase in sensitivity of the instrument (survey sensitivity). The size of this plane is limited by a number of envelopes. The first three of these envelopes are due to - and can occur in - the linear fan beam instrument. The remaining one is the consequence of rotational synthesis.

Although they restrict the size of the image plane, the envelopes have the advantage of attenuating the far-out sidelobe responses, in particular, the grating lobes caused by the radial sampling of the spatial plane. The degree of attenuation can be large, as was pointed out by Ryle and Neville (1962).

The different envelopes are considered briefly here and their effects estimated in Chapter 6 for the specific configuration outlined in Chapter 4.

1. Zero-separation element envelope

This envelope, $A_o(\ell,m)$, has been discussed in Section 2.2.8. The larger the grating elements are, the smaller is this envelope and the more effectively it reduces the grating lobes. In most systems built or planned up to the present this has been the narrowest of the envelopes and usually defines the image plane size.

2. Bandwidth envelope

The receiver system always has a finite bandwidth. When the path lengths of the signal from the source to the receiver differ a loss

of correlation* occurs. (Signals at different frequencies in the pass band will have different phase relation.) This correlation loss forms an envelope whose angular size is proportional to the receiver bandwidth and to the element separation. (The envelope shape is the Fourier transform of the frequency response.)

In the future, with large bandwidths and element separations, this envelope will be used to define the image plane size. The envelope is centred in the direction of zero path error and may be moved by inserting delay lines in the signal paths from the individual elements. Scheuer et at (1963) used this bandwidth envelope to form multiple beams with a long baseline interferometer.

3. Lobestopping envelope

In a correlation telescope employing lobestopping, the receiver integration time can be increased. As mentioned in Section 3.2.4, a differential fringe movement occurs for image points away from the centre 'lobestopped' point and a long integration time will 'smear' these fringes out. This forms an envelope over the centre point whose size is inversely proportional to the integration time (sampling interval) and to the spatial frequency being measured. The effect on the picture points is to cause a loss in resolution and sensitivity towards the image plane edge.

4. Rotational envelope

This envelope occurs only during the synthesis of a two dimensional distribution from one dimensional observations and is important in that it gives significant added protection from grating sidelobe effects when compared to the beam observations. The envelope is centred on each picture point and attenuates the sidelobe responses of other sources in proportion to their angular distance from the picture point.

---

*This will be discussed in Section 8.3

It can be visualized by considering a grating array of omni-directional elements so that the instantaneous signal ratio of main response to grating sidelobe response is unity. After rotational synthesis, the main response is equal to the signal integrated over the whole observing period while the grating sidelobe signal is spread over an extended lobe (2^{o} diameter circle at $\delta = -90^{o}$ with the present array). The lobe to main response ratio thus has a lower value when compared with the fan beam observations.

To derive the actual reduction ratio, the array is considered as a collection of separate two aerial interferometers. At any instant the response of a two aerial interferometer, sited along the X axis and operating with a cosine receiver, is proportional to $\cos(2\pi \ell id)$, where id is the separation (i being an integer). After synthesis, in which the two aerial interferometer traces out a circle in the spatial plane, the response is proportional to $J_o(2\pi \ell id)$ in the ℓ direction (it is also circularly symmetrical). The response of the synthesized aperture is then proportional to :

$$\sum_{i=k_1}^{k_2} J_o(2\pi \ell id) \qquad (3.8)$$

when a uniform weighting function is applied over the synthesized aperture. (k_1 and k_2 are the lower and upper spatial harmonic numbers measured by the array.)

This expression can be evaluated by numerical computation to give the envelope response at any particular angular distance from the main response.

3.2.6 Rotational Weighting Function

The synthesized aperture weighting function, $g_s(u,v)$, introduced in Section 3.2.2, defines the final weighting applied to each spatial frequency. As such, it is the combination of several separate factors:

(i) The linear array has an instantaneous weighting or grading function, $g_A(id)$, as described in Section 2.1.4.

(ii) The effect of 'rotating' the array yields a weighting function of $\left(\frac{1}{id}\right)$, where (id) is the particular spatial component magnitude $\{id = (u^2+v^2)^{\frac{1}{2}}\}$. (The larger the separation the shorter the time spent on recording any particular spatial component.)

(iii) During computation a weighting can be applied to modify (i) and (ii) to give the optimum $g_s(u,v)$ for the particular observation.

The final weighting function determines the 'picture-point' beam shape. For some observations, low sidelobes will be desirable; the higher spatial frequencies are then given reduced weighting, causing some resolution to be sacrificed as a consequence. However on other occasions, say for the positions of point sources, the maximum resolution will be required.

$g_s(u,v)$ can be decided after the observation by varying the weighting in (iii). This is preferable, even though it involves further computer time, since a uniform array illumination can then be used. Operations such as calibration become easier if all element responses are equal.

3.2.7 Sensitivity

Equations 2.32 and 2.33, the standard sensitivity equations for a correlation telescope, still apply in the case of rotational synthesis. The integration time, t, is extended to cover the whole observing time. This causes an enormous increase in sensitivity over that of the instantaneous response of the linear array (between 300 and 400 times in the present instrument).

However, the effect of a change in $g_s(u,v)$ on the sensitivity is not immediately obvious (it affects the computation of A_{mx}). It is easier to consider the telescope as a collection of NM separate two aerial interferometers run simultaneously, each with an effective

collecting area of $2\left[A_1.A_2\right]^{\frac{1}{2}}$. A factor $\underline{R}$ is introduced to cater for the reduction in sensitivity due to $g_s(u,v)$. Equation 2.32 becomes:

$$(\Delta S)_{min} = \frac{5k(T_1T_2)^{\frac{1}{2}}R}{\left[(1-\zeta_1)(1-\zeta_2)(A_1A_2)(B\mathbf{t})(NM)\right]^{\frac{1}{2}}} \quad (\text{Watts } m^{-2}Hz^{-1}) \qquad (3.9)$$

Because of the effective shorter integration time on the higher spatial frequencies, the full sensitivity (R=1) is achieved when the data samples are weighted inversely proportional to the separation, (id). This does not give a good response shape.

Högbom (1963) has computed values for this reduction factor, $\underline{R}$, for a truncated triangular weighting:

$$g(id) = \left[1 - p\frac{i}{k_2}\right] \qquad (3.10)$$

where k_2 is the maximum spatial harmonic and

p is a parameter defining the truncation.

This type of weighting yields a maximum value of $\underline{R}$ of about 0.94 when $p = \frac{5}{6}$. (R = 0.87 for a uniform weighting of samples, i.e. p = 1.)

This variation in sensitivity is not a major factor and the final weighting function used will depend on the required synthesized beamshape.

3.3 The Geometry of Earth Rotation Synthesis

3.3.1 Introduction

In radio-astronomy there are three commonly-used cylindrical coordinate systems:

(i) Altitude-azimuth at a particular place on the earth's surface (generally centred on the telescope with an axis in the zenith direction).

(ii) Right ascension-declination, giving the relative directions of celestial objects (origin at the centre of the earth and one axis parallel to the earth's polar axis).

(iii) Galactic latitude-longitude, (a system fixed in relation to the galaxy).

These coordinate systems are interrelated with the relationships varying with time due (principally) to the rotation of the earth (Fig. 3.1).

With a parabolic dish on an equatorial mounting, this rotation of the earth can be compensated for by rotation of the dish at a constant rate about its polar axis. The aperture of the dish has both a constant projection and a constant orientation relative to the source. This means the antenna beam angular-size and polarization vector direction are constant during observations, making the equatorial mounting very suitable for the individual antennae in an array.

On the other hand, large arrays are laid out on the surface of the earth. Beam steering is no longer simple because of the changing relationship between the source direction and the telescope aperture. However this changing relationship proves very useful. It enables a linear array to synthesize a two-dimensional aperture (thus giving pencil-beam resolution) without changing the relative positions of the components of the linear antenna.

To synthesize a pencil-beam resolution of the sky in a particular direction, it is necessary to measure the Fourier components in that direction over a large range of magnitudes and orientations so as to

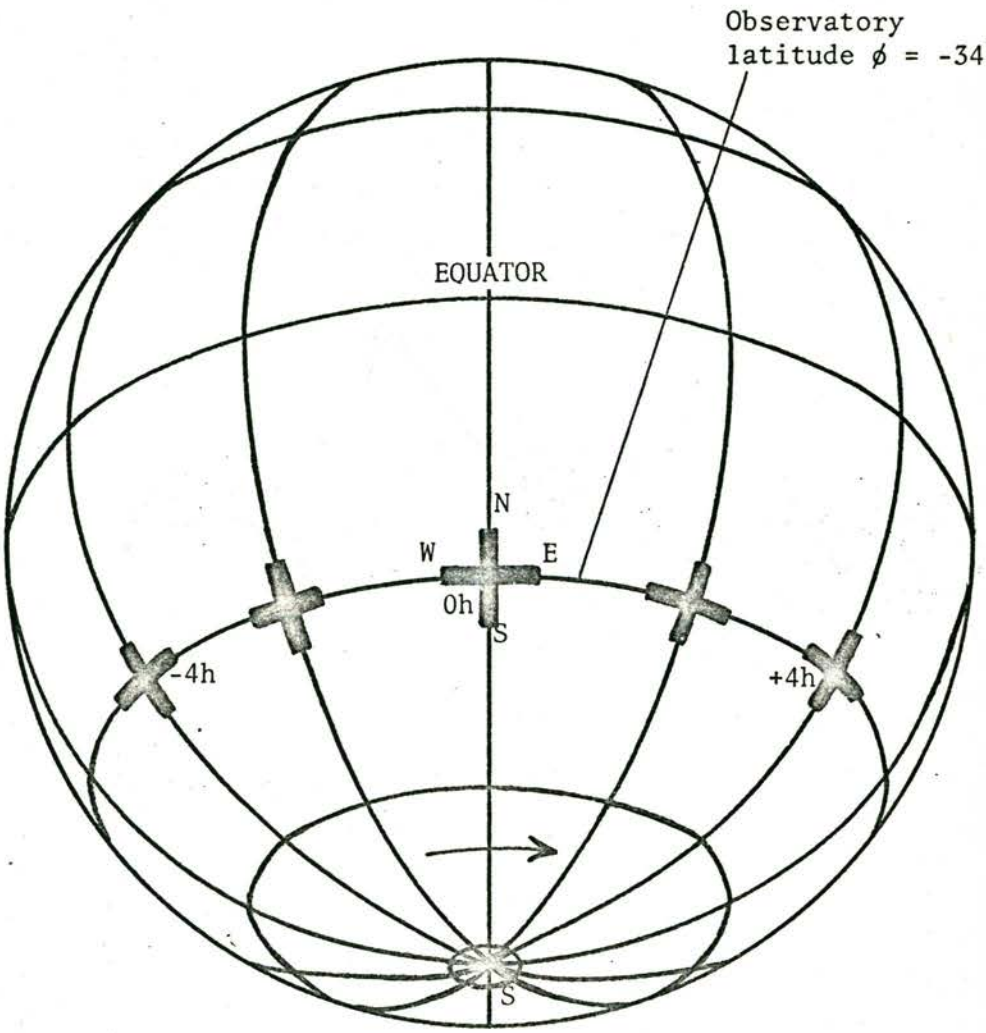

FIGURE 3.1 Illustrating the variation in appearance, during an observing period of 8 hours, of an EW and a NS line antenna on the earth's surface as seen from a fixed point in outer space ($\delta = -30^{\circ}$).

cover an essentially circular area, centred on the origin, of the Fourier diagram. (The beam shape is the two dimensional Fourier transformation of this synthesized area.)

Christiansen and Warburton (1955) used earth rotation (and solar rotation) to synthesize the first two dimensional picture of the quiet sun by using the one dimensional strip scans from a linear grating. This overcame the problems of phase stability experienced by O'Brien (1953) in his attempt to synthesize a two dimensional grating using two moveable aerials. Högbom (1960) demonstrated the feasibility of using rotational synthesis to form a single beam instrument, again using only two elements with variable spacing. This method is being used by Ryle (1962).

The present system being developed in Sydney is the first in which linear (fan beam) arrays are combined with earth rotation synthesis to form a single pencil-beam response. No moveable elements are used. In the following sections the geometrical relationships of earth-rotation synthesis are investigated with particular reference to the present system at Fleurs, Sydney.

These relationships between the array baseline and the source coordinates determine:

(i) the aperture that can be synthesized by a line antenna with a certain ground orientation,

(ii) the equations specifying the control functions of the receiver system for observing with such an array and,

(iii) some of the computations necessary during reduction of the observations.

3.3.2 The Conic Projection

Consider the baseline joining the elements as fixed at one end at the centre of the earth* and making some angle σ with the north-south

---

*The earth's diameter can be considered negligible when compared with stellar distances so that the array can be 'moved' to the earth's centre.

axis of the earth. As the earth rotates, this line traces out a cone in space. Thus, when observations continue for 24 hours, a continuous line antenna* would synthesize a three-dimensional conic aperture.

There are two exceptions to this:

(i) a baseline oriented in the east-west direction ($\sigma = 90^{o}$) traces out a circular plane parallel to the equatorial plane of the earth,

(ii) a baseline parallel to the north-south axis of the earth ($\sigma = 0^{o}$) stays as a straight line.

However these two cases can be considered as degenerate cones.

This conic aperture is relatively stationary in space so that when it is phased to 'look' at a certain declination, the effective aperture is the projection of the cone onto a plane at right angles to the desired declination direction. These conic projections have shapes which depend upon the declination of the source, δ, and upon the cone half angle, σ. Fig. 3.2 shows a range of these projections.

The equations describing this dependence of the conic projections upon δ and σ are derived in Appendix B for the general case of a baseline L, with arbitrary direction.

Note that the effective apertures generated in this manner cannot be equated directly with filled apertures. Instead the synthesis telescope power response is the field response of a physical aperture of this shape.

---

*In the initial analysis a continuous line antenna can be assumed. However the results are quite general. In the case of a two element interferometer the equations describe both the motion of the baseline joining the elements and the single Fourier component being sampled at any instant. A linear grating array is a collection of two element interferometers. As such the effective aperture becomes a series of concentric rings.

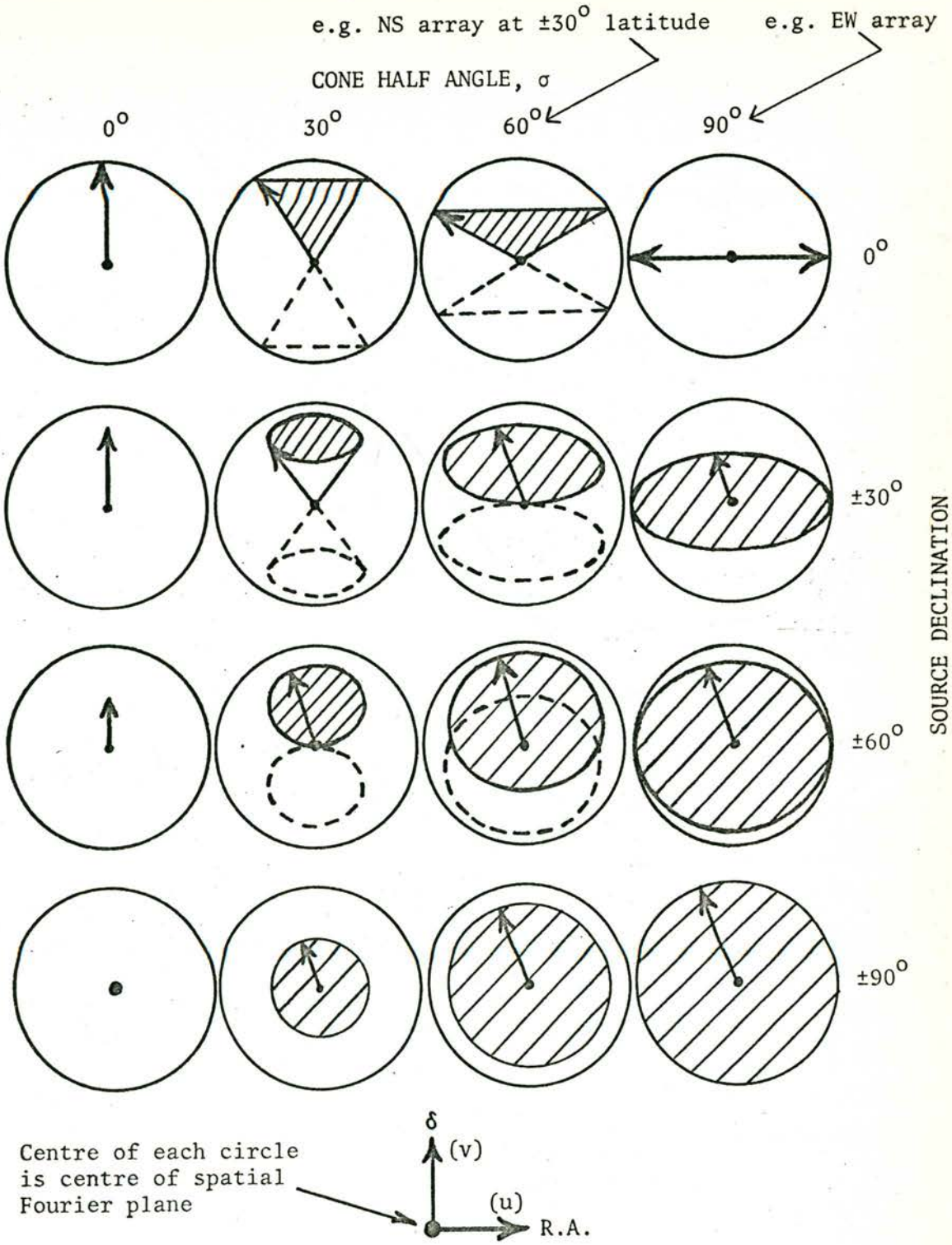

FIGURE 3.2 The above diagrams illustrate the projections (hatched areas) of conic apertures of various half angles seen from different declinations. The projections include the period when the source is below the horizon.
Symmetry considerations cause the synthesized aperture to include the area inside the broken curve .

3.3.3 The Synthesized Effective Aperture

The effective aperture of the telescope is the extent over which the Fourier spatial plane is sampled (Christiansen et al, 1963). This coverage is given by (u,v) in equation B.4.

If the baseline, instead of being specified by the angle that it makes with the north-south axis, is resolved into two components, L_1 and L_2, parallel and perpendicular to the north-south earth axis, then equation B.4 describing the normalized projected lengths becomes:

$$\left.\begin{aligned} u &= \frac{L_2}{L}.\sin(\alpha-h) \\ v &= \frac{L_1}{L}.\cos\delta - \frac{L_2}{L}.\sin\delta.\cos(\alpha-h) \\ w &= \frac{L_1}{L}.\sin\delta + \frac{L_2}{L}.\cos\delta.\cos(\alpha-h) \end{aligned}\right\} \qquad (B.6)$$

where

(i) (α,δ) are the source coordinates and h is the hour-angle of intersection of the baseline with the celestial sphere,

(ii) u and v are the right ascension and declination projections, and

(iii) w is the projection in the direction of the source.

From the above equations it is apparent that the effective aperture, (u,v), has a constant dimension in the right ascension direction irrespective of the source declination. (u is independent of δ.) However the dimension in the declination direction, v, is dependent upon the declination*. This variation of effective aperture with declination is a factor common to all large telescopes which are not mechanically steerable.

---

*The end point of the generating vector traces out an ellipse (degenerating on occasions to a circle or a straight line) which always has its major axis, u, in the right ascension direction. The minor axis of this ellipse ($\frac{L_1}{L}.\cos\delta - v$) is in the declination direction and the ratio of major to minor axes is $1:\sin\delta$. The centre of the ellipse $(0, \frac{L_1}{L}\cos\delta)$ is displaced from the origin of the spatial plane in the declination direction, unless the array is east-west ($L_1 = 0$).

This is a disadvantage which must be tolerated for high resolution observations.

Synthesis of the effective aperture fortunately does not require a full 360^{o} rotation of the baseline with respect to the source. Only 180^{o} rotation is necessary, filling half the Fourier plane. The other half is identical*.

Even so, for sources in the other hemisphere from the antenna, 12 hours coverage is not possible due to horizon limits. These limits (Smart, 1962, p.47) are given by: $\cos \alpha_h = - \tan \delta \cdot \tan \phi$, and computed for a latitude of -34^{o} in Fig. 3.3. $2\alpha_h$ is the period during which the source is visible from the aerial.

When the following of a source is limited in hour-angle to less than 12 hours, either by the horizon or by limitations of the antenna design, then only a portion of the conic projection is synthesized and some orientations are missing. These gaps must be filled by an array in another direction. Such was the situation at Fleurs. The existing east-west and north-south grating arrays were limited in hour-angle coverage and hence it was necessary to use both to achieve full Fourier plane coverage. This has certain other advantages as indicated in Section 3.3.7.

3.3.4 Data Reduction

The equations for (u,v) are required during the data reduction. The information for a particular declination is collected in terms of hour-angle (time) increments. During the observation the spatial Fourier plane is gradually filled. In order to carry out the inverse Fourier transform, the knowledge of the spatial component being measured at a

---

*The sky distribution is real, thus $T_b(u,v) = T_b^*(u,-v)$ where $T_b(u,v)$ is the Fourier map of the sky brightness distribution. One may consider this also a consequence of the antenna baseline having a direction but not a positive or negative sense.

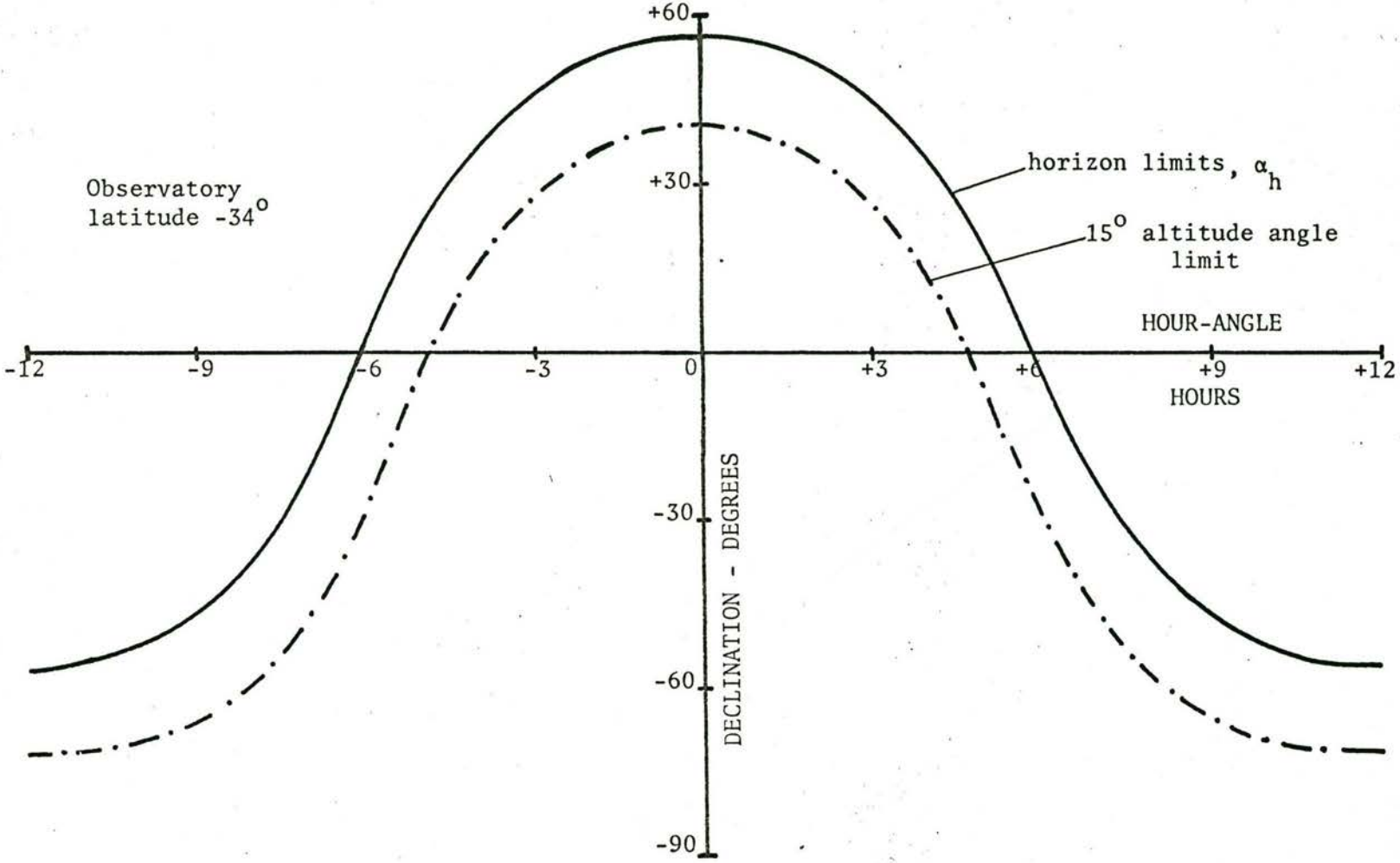

FIGURE 3.3 Hour-angle observing limits created either by the horizon or by the refraction effects at low altitude angles (<15° approx.).

particular instant is a necessity.

In addition, it is desirable to carry out the Fourier transformation using a Cartesian coordinate lattice (Ryle and Neville, 1962). In this way the (u,v) components are separable and the computer time for transformation is reduced by a factor of $N^{\frac{1}{2}}$ where N is the total number of data points. (The equations for (u,v) give the actual Cartesian spatial point being measured. These data points are then interpolated to form a regular lattice.)

3.3.5 Evaluation for the Particular Case of East-West and North-South Baselines

With baselines east-west (EW) and north-south(NS) and a latitude of -34°, equations B.4 for the normalized baseline projections become:

(i) For the east-west array:

$$\left.\begin{aligned} u &= \cos\alpha \\ v &= \sin\delta.\sin\alpha \\ w &= -\cos\delta.\sin\alpha \end{aligned}\right\} \qquad (3.11)$$

(ii) For the north-south array:

$$\left.\begin{aligned} u &= \sin 34^{\circ}.\sin\alpha \\ v &= \cos 34^{\circ}.\cos\delta - \sin 34^{\circ}.\sin\delta.\cos\alpha \\ w &= \cos 34^{\circ}.\sin\delta + \sin 34^{\circ}.\cos\delta.\cos\alpha \end{aligned}\right\} \qquad (3.12)$$

To plot the effective aperture and to derive some of the control functions, the cylindrical projections (ℓ,ψ,μ) are more convenient. Let ℓ be the projected array length, ψ be the angle this projected length makes with the source declination axis ($\underline{V}$ axis) and μ the angle between the array and its (u,v) projection. Then,

$$\left.\begin{aligned} \ell &= (u^2+v^2)^{\frac{1}{2}} \\ \psi &= \tan^{-1}\left(\frac{u}{v}\right) \\ \mu &= \cos^{-1}(\ell) = \sin^{-1}(w) \end{aligned}\right\} \qquad (3.13)$$

A computer program was written by the author to evaluate these projections together with some of the derivatives.

In Appendix B, Figs. B.4 and B.5 show the dependence of the synthesized effective aperture of an EW and a NS array (at a latitude of -34^{o}) upon source declination. Hour-angle coverage in these figures is for 12 hours.

The east-west array gives an elliptical effective aperture, with right-ascension and declination resolutions in the ratio $1:\sin\delta$. The declination resolution is highest at the pole and zero in the equatorial direction.

The north-south array gives an aperture roughly similar to a two dimensional array on the ground. The resolution is highest in the zenith direction but is still considerable in both the polar and equatorial directions. On its own a north-south array would be useless for forming a pencil-beam except near the polar direction.

In Fig. 3.4 the effective apertures of the NS arrays are combined with those of the EW array. The observing limits imposed by the individual antennae have been applied. In this figure the radius vector in a particular direction represents the relative spatial frequency magnitude in that direction across the source. It can be seen that coverage is good up to $\delta = -30^{o}$. At $\delta = -15^{o}$ there are four angular gaps of about 20^{o} each. At $\delta = 0^{o}$, the NS array still provides good declination resolution while the EW array has maximum resolution but no angular coverage. Thus, between $\delta = -30^{o}$ and $\delta = 0^{o}$, the instrument will still give valuable information.

3.3.6 Observing Time Required

In Appendix B the variation of ψ (rotational coverage) with hour-angle has been evaluated and plotted in Figs. B.6, B.7, B.8 and B.9. This is for an hour-angle coverage of 12 hours. For longer periods the EW array gives symmetrical curves; the NS array does not.

Fig. 3.5 is the result of combination of EW and NS arrays, each having the same (symmetrical) antenna hour-angle coverage. This shows the hour-angle coverage required at a particular declination for complete

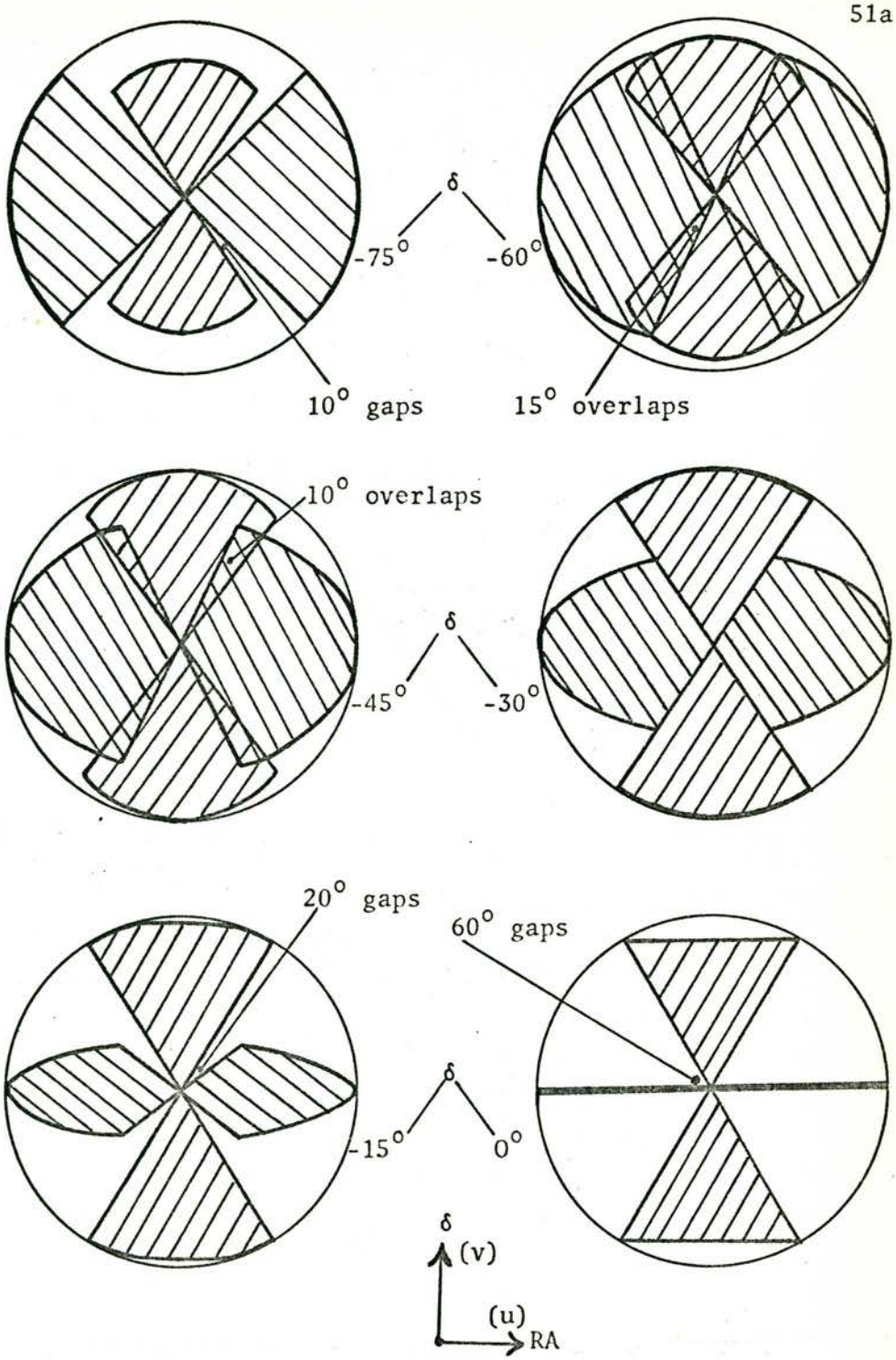

FIGURE 3.4 The effective apertures for various source declinations with the new telescope at Fleurs (Lat.-34°). (EW and NS array rotational coverages combined with the aerial sky coverage {curve A of Fig. 5.2}.) The outer circle represents an aperture of 3709 wavelengths at 1415 MHz.

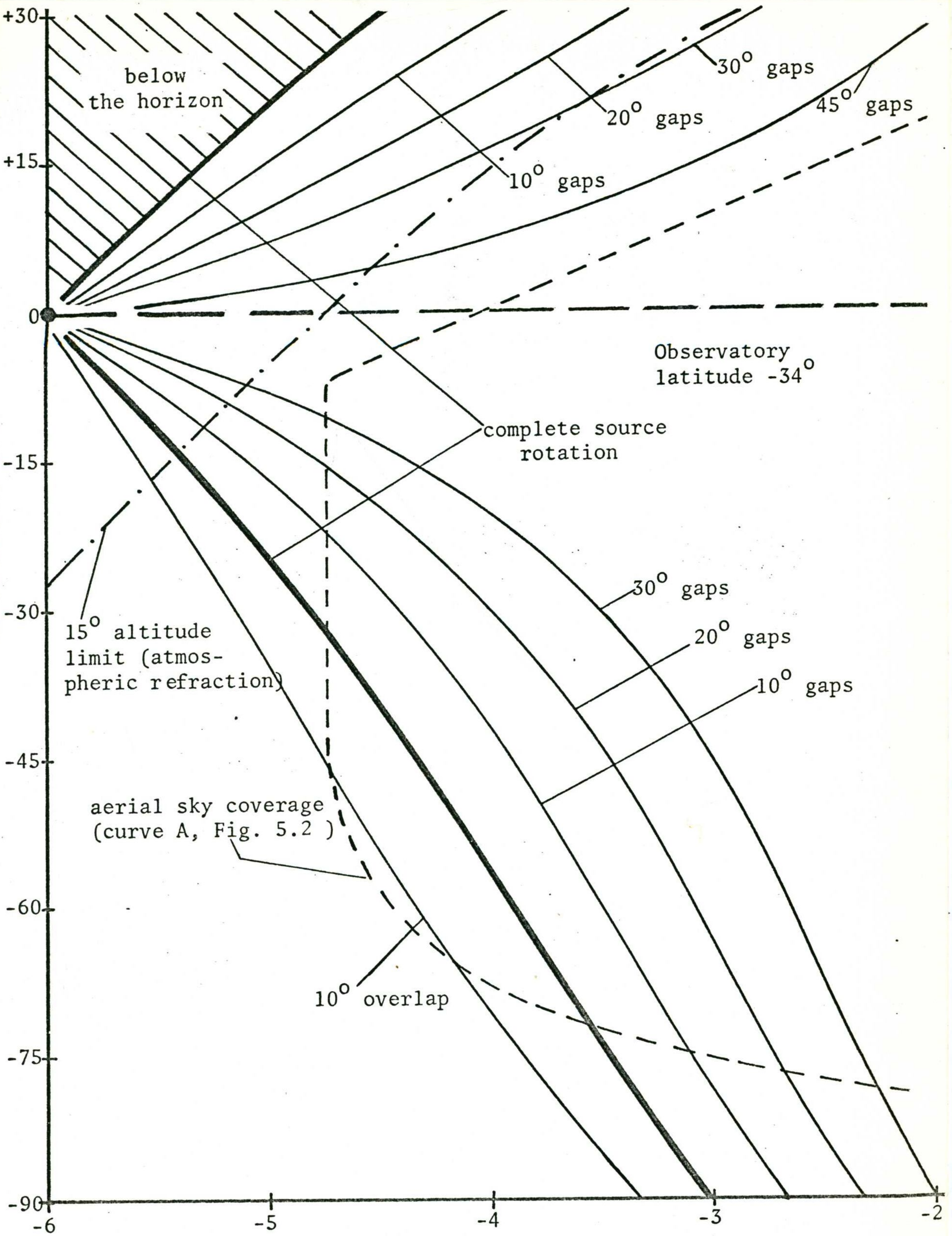

FIGURE 3.5 Showing hour-angle observing requirements vs. source declination for various amounts of rotational coverage using both NS and EW linear antennae.

rotational coverage (and also for different gaps and overlaps in the synthesized aperture). In Fig. 3.5 the horizon limit is indicated by the hatched area.

When critical observations are being conducted it is desirable to remain above 15^{o} altitude to avoid atmospheric refractions. This presents no worry at Fleurs as the present antennae will not reach 15^{o} altitude. (This is apparent from the aerial coverage curve and the 15^{o} altitude line in Fig. 3.5.)

3.3.7 The Advantages of using both an East-West and a North-South Baseline

In rotational synthesis using a linear array, the choice of baseline orientation has a marked effect upon the Fourier plane coverage. Different arrangements have been investigated by Swenson and Mathur (1967) and Högbom (1963).

The most efficient arrangement, in terms of antennae required to achieve a certain resolution/image-size ratio, has all baselines close to the east-west orientation. However this configuration has certain disadvantages:

(i) 12 hours sky coverage is required from each aerial for all the declinations to be observed.

(ii) Declination resolution deteriorates towards the equatorial plane.

(iii) Inter-element shadowing occurs for these lower declinations at the extremes of hour-angle.

(iv) Horizon limits preclude synthesis in the other hemisphere (Fig. 3.3).

(v) A continuous 12 hour observing period will generally include sunrise and/or sunset*.

---

*Critical observations need to be broken into two observing periods some months apart to avoid the dawn and/or dusk. At these times the conditions change rapidly, introducing ionospheric phase errors.

(vi) For lower declinations ionospheric refractions are likely to affect observations*.

With the aerials all collinear, an instantaneous fan beam can be used over the full hour-angle coverage. This has considerable merit, especially for the initial observing periods. However Högbom (1963) has proposed an interesting configuration in which a vernier compound grating interferometer is formed by correlating the responses of two gratings with baselines parallel and east-west, but slightly displaced in the north-south direction. The resultant synthesized aperture (with 12 hour observing) is almost the same as that of an east-west linear array but the shadowing and centre problems are reduced, although the fan beam response is limited to the meridian plane.

With a baseline oriented in any direction other than east-west, the Fourier plane coverage is less, even with 12 hours observations. As a symmetrical beam shape is desired, the spatial frequencies in some orientations will need to be attenuated, resulting in a lower aperture efficiency and signal-to-noise ratio.

However, duplicating the spacings with different orientations, for example east-west and north-south lines, results in a number of advantages:

(i) Following the source for the full 12 hours is not necessary. This leads to cheaper antenna mountings, lower observing time requirements and the avoidance of sunrise and sunset observing times.

(ii) Observations are not made at low altitude angles thus lowering the atmospheric refraction effects.

(iii) Element shadowing can be avoided completely over the main region

---

*Synthesis at low declinations requires the combination of high and low altitude observations. Horizontal stratification of the ionosphere produces deviations in zenith angle which are dependent on zenith angle magnitude. The effect does not appear to be serious with the present resolution of 40 sec. of arc unless altitude angles are less than about 15° (Williams, 1963).

of observations.

(iv) The collecting area and hence the signal-to-noise ratio is increased.

(v) The linear array which is not east-west will provide some higher resolution at lower declinations.

(vi) Fan beam observations at right angles are available over a large range of hour-angles.

(vii) With antennae that reach the horizon, synthesis would be possible for some declinations in the other hemisphere.

These advantages are offset to some degree by the increase in system cost due to the larger number of aerials and associated receivers that are required. However a large section (the 'rear-end') of the receiver system can be used successively on both arrays.

The synthesized aperture using two separate arrays can have some odd shapes and gaps which depend upon declination (Fig. 3.4). These increase the sidelobes in certain directions but over the intended range of observations do not prove to be a serious disadvantage.

3.3.8 Differential Signal Path Length

In equation B.6 the expression for $\underline{w}$ represents the normalized differential path length of the signals. When multiplied by the particular element separation, this gives the length which must be compensated using delay cable. The rate at which this delay cable length should be varied to keep the signal paths equal for a particular (α,δ) coordinate is given by (again normalized):

$$\frac{dw}{dt} = \frac{L_2}{L}.\cos\delta.\sin(\alpha-h).\frac{d\alpha}{dt} \qquad (3.14)$$

In practice the delay cables will be switched in steps so that at times a path length error will be present. The rate of switching depends on the bandwidth used and the allowable correlation loss for a particular spatial harmonic.

Equation 3.14 also gives the rate at which the signal phase must be varied to 'stop' the fringes. This 'lobestopping' is desirable if the required data sampling rate is to be minimized.

For the particular cases of east-west and north-south arrays, the expressions for $\underline{w}$ and $\frac{dw}{dt}$ are stated, in a slightly different form, in equations B.7 and B.8 (note: $\underline{w} = \sin\mu$).

3.3.9 Information Frequency

Assuming that 'lobestopping' is applied in the receiver system, the information rate and hence the data sampling interval is determined by the differential fringe rate for the points in the image plane most distant from the centre, or 'lobestopped', point. This rate is determined by $\frac{d\psi}{dt}$, the rate of change of the source rotation angle, ψ. Equations B.7 and B.8 give $\frac{d\psi}{d\alpha}$ for an east-west and a north-south array (note: $\frac{d\alpha}{dt}$ = constant).

Differential fringe rate variation has been used recently by Elsmore et al (1966) to determine the errors in the assumed positions of small radio sources.

CHAPTER 4

DESIGN PARAMETERS OF THE NEW TELESCOPES

CHAPTER 4: DESIGN PARAMETERS OF THE NEW TELESCOPES

4.1 Introduction

The acquisition of the Fleurs Field Station with its large Grating Cross made possible the plan, outlined in Chapter 1, to construct two high-resolution fan-beam telescopes and use them for two-dimensional high sensitivity observations of radio sources and for high resolution fan-beam scans of the sun.

In order to eliminate the multiple responses of the simple gratings and to increase the resolution, it was necessary to use a compound grating arrangement of the type discussed in Chapter 2. This forms an instantaneous fan beam.

Pencil beam resolution is achieved by using the change in scanning angle (of the fan beams) which occurs over many hours of observations. A rotation of 180° is required and an east-west array can achieve this only if observations can be continued for 12 hours. This was impossible with the existing grating elements. Thus two separate compound grating interferometers are necessary, one in an east-west direction and the other in a north-south direction, each observing for up to nine hours.

4.2 Choice of the Basic Configuration

Many factors governed the choice of configuration of the two compound grating interferometers. They were all interrelated and largely dependant upon the existing gratings of thirty-two aerials each.

A resolution of the order of 35 sec. of arc was considered a necessary advance in the state-of-the-art. To achieve this at 21 cm wavelength, spatial components up to twice the grating length are required. Thus compound gratings with at least two large multiplying aerials each were necessary. This narrowed the choice to the three

'basic' types, (a), (b) and (c) illustrated in Fig. 4.1 and considered in Chapter 2.

For complete suppression of the grating sidelobes, the size of the additional aerials in Fig. 4.1(a) and Fig. 4.1(b) should be twice that of Fig. 4.1(c). This is a consequence of 4.1(c) measuring spatial frequencies twice as often as 4.1(a) and 4.1(b), and thus causing the grating sidelobes to have twice the separation.

The configuration chosen for the east-west compound grating antenna was that of Fig. 4.1(b). The two additional large aerials are termed X1 and X2. These are situated on the eastern and western extensions respectively of the grating baseline. X1 is close to the eastern end of the grating while X2 is a grating length from the western end.

The size of these additional aerials was limited by the ground clearance and the sky coverage requirements to about half the size required for complete suppression of the grating sidelobes over the whole image plane. However the smaller aerial size carries the advantage of increasing the image plane area. If the presence of these grating sidelobes proves troublesome, two more aerials will be added at a later date to form the configuration of Fig. 4.1(d) which is similar to Fig. 4.1(c).

The configuration of Fig. 4.1(c) would have been desirable from the point of view of reducing the sine response, A_s. However besides the unwanted expense of doubling the number of large aerials (and hence correlators), it is physically impossible because of ground slope which causes difficulties with the aerial ground clearances. Of configurations 4.1(a) and 4.1(b), the sine response of the latter is preferable (Section 2.2.4).

In addition to these factors, the east-west grating has one foot more ground clearance on the eastern end than on the western end. This again gives preference to configuration 4.1(b).

The configuration chosen for the north-south compound grating interferometer was that of Fig.4.1(a). The two additional large

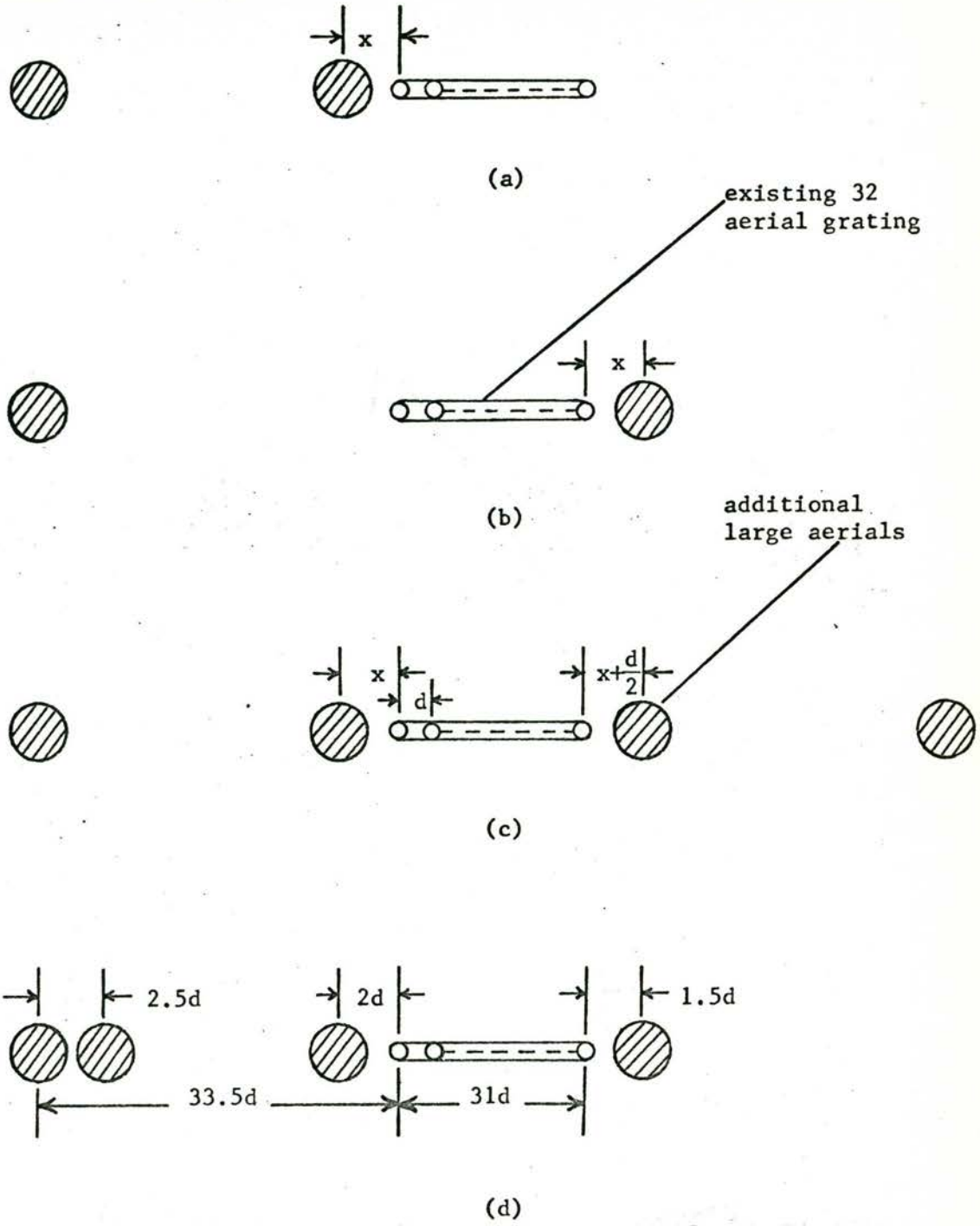

FIGURE 4.1 The configurations considered for the new telescope.

aerials, called Y1 and Y2, are both on the northern extension of the grating baseline. Y1 is close to the north end of the grating and Y2 is a grating length further away. Lack of sufficient ground clearance at the southern end of the existing grating precluded configuration 4.1(b). The aerial sizes had to be limited for the same reasons as for the east-west system.

4.3 The Sky Coverage Requirement

Section 3.3.6 discussed the relationship between the aerial sky coverage and the resulting declination range over which pencil beam synthesis is possible. A maximum variation in pointing direction about the hour-angle axis is naturally desirable as it allows full synthesis observations at declinations closer to the equatorial plane. However the extremes of hour-angle coverage become increasingly difficult and expensive to achieve and the return, in terms of (i) declination coverage gained and (ii) the lowered declination resolution at these declinations, is increasingly small. (This is assuming both east-west and north-south systems are used, removing the necessity of 12 hrs following for declinations towards the poles.)

The result is that the following sky coverage was considered a reasonable minimum requirement at which to aim:

Declination: -80° to $+23^{\circ}$

Hour angle : $\pm 3\frac{1}{3}$ hrs at $-80^{\circ}\delta$
to $\pm 4\frac{2}{3}$ hrs at $-30^{\circ}\delta$, with
reduced H.A. coverage to $+23^{\circ}\delta$.

These specifications enable image synthesis south of $-30^{\circ}\delta$, partial synthesis north of $-30^{\circ}\delta$ and daily high resolution observations of the sun with perpendicular fan beams throughout the year. Where possible during design, the hour-angle coverage was to be extended.

To achieve this coverage with the already existing small aerials, it was necessary to lower the mechanical drive cable by 2½ feet and to

reshape two of the ribs on each small aerial.

Interelement shadowing (Appendix C.2) is also dependent upon the sky coverage and was another reason for limiting the requirements in both the hour-angle and declination directions. Shadowing between the aerials has been completely avoided. In the case of the large aerials to be constructed a certain flexibility was available in the choice of their size and spacing.

4.4 The Size of the Additional Aerials

It was decided that the additional aerials should be placed so as to enable each linear array to form an instantaneous fan beam (see Appendix C.1). This is not a prerequisite of the final earth-rotation synthesis system, although it does facilitate the phase and delay control operations and the data reduction. However it has enabled low sensitivity observations to be carried out at an early stage in the construction of the system.

This decision, in addition to other considerations, imposed the restriction of axis collinearity between the additional aerials and the existing grating aerials. The existing grating aerials have a maximum ground-to-axis height of 12½ feet. This, when combined with the required sky coverage, limits the size of the aerial which will clear the ground. Appendix C.3 analyses this relationship taking into account the possibility of: (i) varying the paraboloid design, in particular the vertex-to-axis distance, (ii) digging a trench to give added clearance under the reflector edge and (iii) raising all the existing 64 small aerials.

The large aerial diameter is crucial for the atten uation of the grating sidelobes (Section 2.2.8). Analysis of these sidelobe levels showed the need for a diameter of at least 40 to 60 feet. Clearly a compromise was necessary and a large aerial diameter of 45 feet was finally decided upon.

4.5 The Positions of the Additional Aerials

The previous sections 4.2., 4.3 and 4.4 have indicated the general layout of the east-west and north-south arrays, the required sky coverage and the size of the additional aerials. All aerials had to have collinear axes. The object of these configurations is to sample the spatial Fourier transform of the sky distribution at sixty-four regular intervals (40 foot spacings) from the lowest possible spacing up to a maximum value. It was necessary to ascertain the actual aerial positions which were most suitable.

A number of alternatives existed. They are given by the following equation for the spacing, s, of the added aerial from the nearest grating aerial:

$$s = n.d + x \qquad (4.1)$$

where d is the sampling interval of 40 feet

n is an integer, 0,1,...

x is a fraction of d, in particular

either 0, $\frac{d}{4}$, $\frac{d}{2}$ or $\frac{3d}{4}$.

In-between values of x were investigated but they cause no thinning-out of the grating lobes since this is determined by the sampling interval of d. The grating lobes formed in these cases are only occasionally of the desired shape. Phase effects distort the intermediate lobes in a manner similar to the $\frac{d}{4}$ configuration in Appendix J. This made such values for x undesirable.

In choosing values for n and x it was necessary to consider minimizing: (i) the missing low spatial components and (ii) the inter-element shadowing, and to keep in mind the possibility of later extension to: (a) still higher resolutions by using additional large aerials and (b) a symmetrical or nearly symmetrical configuration.

Shadowing prevented the initial separation being less than 50 feet (Appendix C.2). This narrowed the choice to 50 feet, 60 feet, 70 feet or 80 feet. The various merits of these spacings have been

considered in general terms in Sections 2.2.2 and 2.2.4 and Appendix J However, briefly:

1. The $\frac{d}{4}$ or $\frac{3d}{4}$ (50 feet or 70 feet) initial spacing, is only satisfactory if a quasi-symmetrical configuration with the sampling interval at $\frac{d}{2}$ (20 feet) is constructed immediately. 50 feet and 70 feet are then the initial spacings leaving only spacings of 10 feet and 30 feet missing. These are easily compensated and grating lobes have twice the separation. With the sampling interval at $\underline{d}$, every second grating lobe is useless as a main response. (See Appendix J.) As a grating sidelobe it responds only to small sources, but this usefulness is debatable.

2. There are primarily two distinctions between the choice of 60 feet and 80 feet ($\underline{x}$ equals $\frac{d}{2}$ and zero respectively) for the initial spacing:
   (i) the 60 foot initial spacing has fewer lower spacings missing (only 20 feet) and hence is easier to compensate than the 80 foot initial spacing (zero and 40 feet missing).
   (ii) a 60 foot initial spacing causes sampling of only the odd Fourier components so that adjacent grating lobes are of opposite sign. This might make the grating sidelobes more recognisable in the synthesis observations.

   The first of these reasons decided the <u>initial spacing at 60 feet</u> (aerials X1 and Y1).*

---

*If a 40 foot spacing were possible, it would have been preferable for the reason that the missing spacing then causes only a D.C. baseline shift (modified by the aerial beam shape). However this is not greatly different from the present baseline shape created by the 20 foot spacing interference pattern (modified by the aerial beamshape).

If each system is made 'symmetrical' by the addition of two more aerials, both the 60 foot and 80 foot cases will result in the same configuration having a 60 foot initial spacing and a sampling interval of 20 feet. Grating lobes will all be positive and twice the separation. The missing spacings will be zero, 20 and 40 feet.

The choice of a 60 foot initial spacing for X1 and Y1 also determined the positions of X2 and Y2. These are positioned at 1340 feet, (32.d + 60), from the nearest small aerial. This means the largest spatial component sampled is 2580 feet.

Configurations in which X2 and Y2 did not carry on the regular sampling (alternative values for x) were explored. As might be expected, these formed many spuriously shaped grating lobes giving the desired response at infrequent angular intervals.

The final aerial positions are indicated in Figs. 4.2 and 4.3. The theoretical responses of both the east-west and the north-south configurations are considered in Chapter 6.

4.6 Array Survey

Existing aerial positions

The existing east-west and north-south grating arrays were surveyed in order to determine:

(i) the 'best-fit' baselines on which the new 45 foot diameter aerials were to be positioned, and

(ii) the errors in the positions and orientations of the small aerials. (These aerials had not been checked for movement of their foundations since 1957.)

This survey was initiated by Professor Christiansen and carried out very competently by Mr. J. Curdie, of the surveying firm of Kent & Curdie, under the direction of the author. The plan of Fig. 4.4 is the result of this survey.

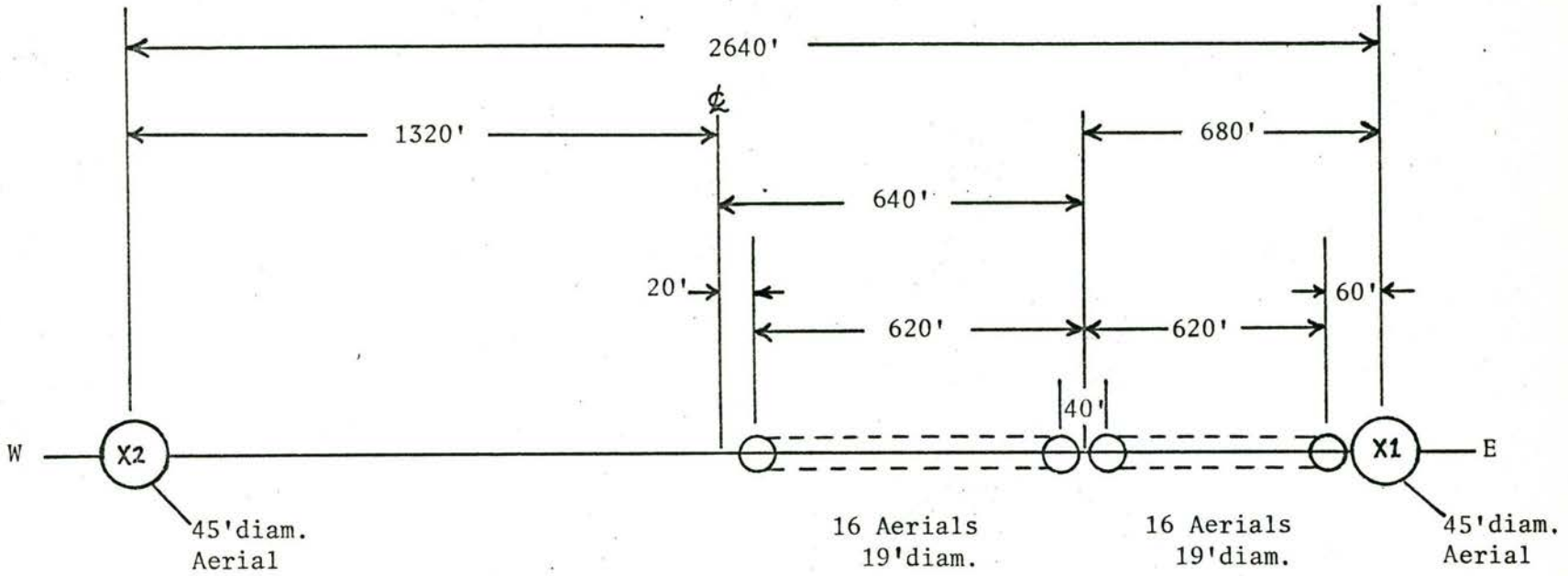

FIGURE 4.2 EAST-WEST BASIC COMPOUND INTERFEROMETER DIMENSIONS.

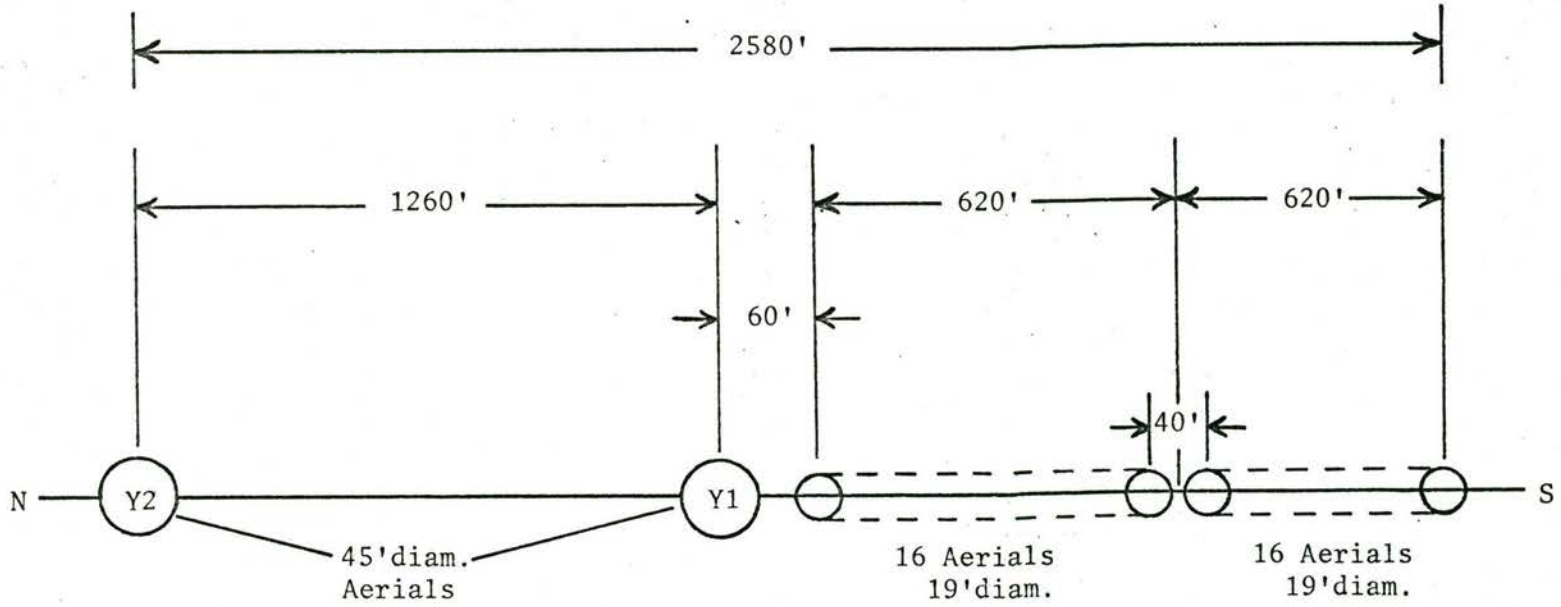

FIGURE 4.3 NORTH-SOUTH BASIC COMPOUND INTERFEROMETER DIMENSIONS.

FIGURE 4.4

Plan view of the survey of the aerial positions (drg. B-F45-53). Position errors (in decimals of a foot) are given in the four corner tables.

PLAN

OF SURVEY OF RADIO TELESCOPE AT FLEURS
SHOWING LOCATION OF PERMANENT MARKS
(CONCRETE BLOCKS) AND POSITIONS OF AERIALS
FOR THE SCHOOL OF ELECTRICAL ENGINEERING
UNIVERSITY OF SYDNEY

NOT TO SCALE

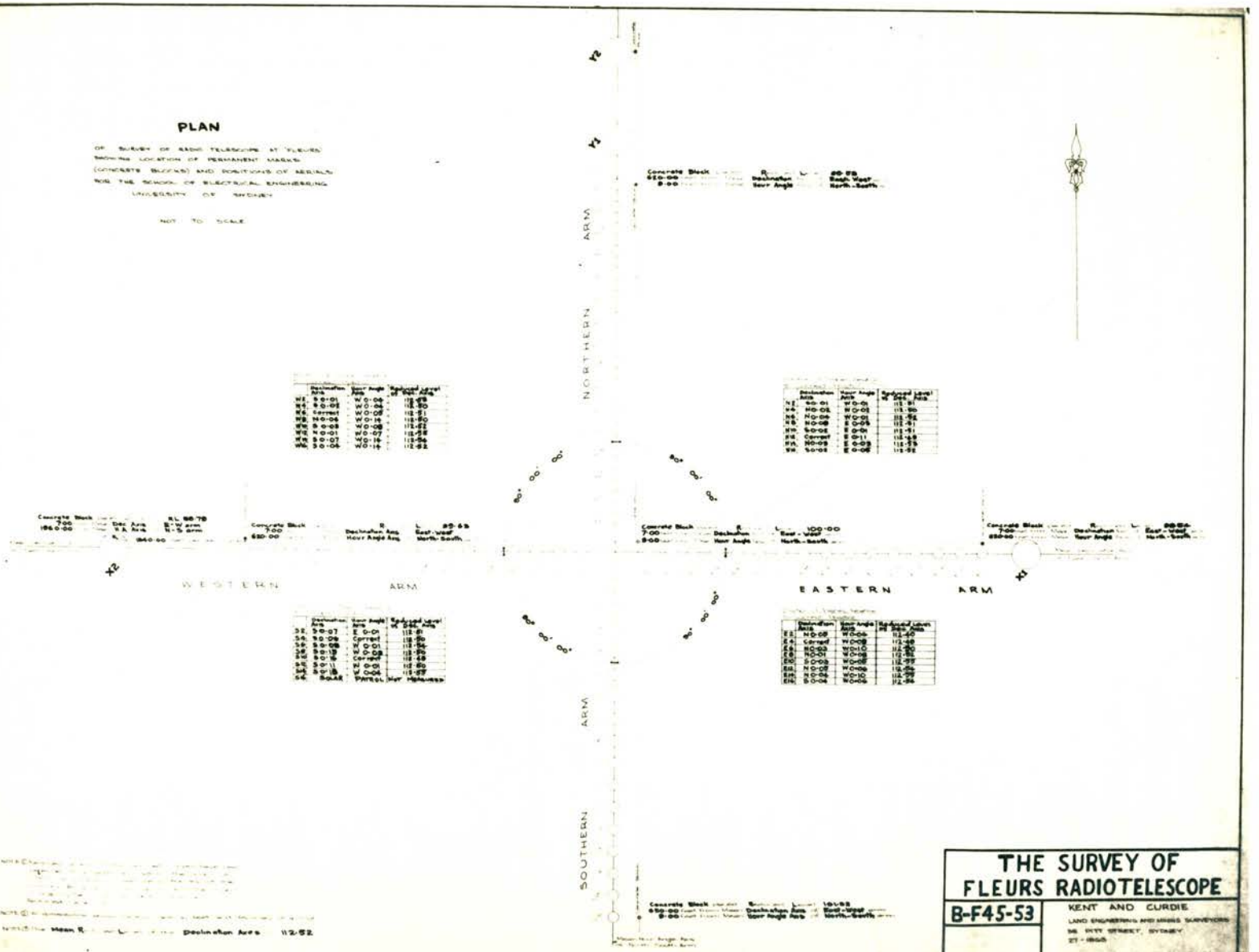

Mean R ... Declination Axes 112-52

THE SURVEY OF FLEURS RADIOTELESCOPE

B-F45-53

KENT AND CURDIE
LAND ENGINEERING AND MINING SURVEYORS
98 PITT STREET, SYDNEY
27 - 1955

K.F. WELLINGTON

The east-west baseline is taken as the mean line through the declination axes of the east-west aerials. The north-south baseline is taken initially as the mean line through the hour-angle axes of the north-south aerials. These two baselines are at right angles. Permanent marks, in the form of concrete blocks underground, were placed as indicated in Fig.4.4 to facilitate the recovery of these baselines at a later date.

These baselines are used to define a level surface placed, arbitrarily, 100 feet below the concrete block at the intersection of the two arrays. This surface is the datum for vertical position measurement. The mean declination axis of the array then has a height of 112.52 feet. The positions of the aerials along the baselines are measured from the intersection of the two arrays.

To reduce the work involved, only every second aerial was surveyed. The positions of these aerials relative to the mean axes and to the datum surface are tabulated in Fig. 4.4. Dimensions are in feet.

This survey gives only the relative positions of the individual elements. Several quantities remain to be determined accurately. These are:

(i) the latitude and longitude of the centre point,

(ii) the absolute azimuth orientation of the baselines relative to the true north-south direction and

(iii) the deflection of the vertical (due to gravitation anomalies) over the datum plane.

Approaches are at present being made to external organizations capable of carrying out this work with the necessary accuracy.

New aerial positions

The baselines, defined by the survey of the existing aerial positions, were extended beyond the grating array ends in order to define positions for the new aerials.

A correction for the curvature of the earth was applied using the (approximate) formula:

$$C \simeq 0.67M^2 \qquad (4.2)$$

where C is the correction in feet and

M is the distance in miles.

The vertical aerial positions relative to the 'level' surface (actually spheroidal) are corrected to a plane horizontal with respect to the array centre. For aerials X1 and Y1 this correction is only 1/8" but for aerials X2 and Y2 it becomes a significant $2\frac{1}{8}$".

The aerials of the grating were all measured within ±1/16" so that the new aerials could be positioned with an accuracy better than 1 in 67,000. This amounts to an accuracy of 3 sec. of arc in baseline direction, or $\frac{3}{8}''$ in position, for the distant aerials.

CHAPTER 5

DESIGN OF THE ADDITIONAL ANTENNAE

CHAPTER 5: DESIGN OF THE ADDITIONAL ANTENNAE

5.1 Introduction

The previous chapter considered the configuration of the two new compound grating interferometers. To construct these, four additional antennae were required in specific positions relative to the existing gratings. The diameter of each of these antennae is 45 feet. This was determined by the requirements of (i) grating sidelobe suppression and (ii) sky coverage coupled with the ground clearance at the desired antenna position (Section 4.4 and Appendix C.3).

The design and construction of these additional antennae, outlined in this chapter, affects many aspects of the final system performance. Particularly influenced are the sidelobe and grating sidelobe levels, the stability of measurement throughout the observing period, the useable image plane size, the system sensitivity and the range of declinations over which synthesis can be completed.

Section 5.6 sets out the actual antenna specifications. Appendix E.2 contains the detailed plans of the antennae.

5.2 General Considerations

At frequencies over 200 MHz, the individual aerials of grating arrays are usually equatorially-mounted paraboloids. These are by far the most convenient type of aerial (Sections 2.1.1 and 3.3.1). At these frequencies, even small paraboloids will have diameters of tens of wavelengths contributing useful gain and directivity. Some additional advantages of using paraboloids are:

(a) the system operating frequency can be changed easily by replacing the primary feed,

(b) the distortions of the surface are greatest at the outer edge

where their effect is reduced due to the tapered primary feed illumination, and

(c) polarization measurements can be made by simply rotating the primary feed.

As the existing grating aerials are equatorially-mounted paraboloids, it was natural that the additional antennae should also be paraboloids.

These existing aerials with their associated transmission lines were initially designed for operation at 1424 MHz. This was chosen as the operating frequency for the present system (Stage 1). In the next stage of system development this main observing frequency will be shifted to 1415 MHz in order to centre it in the frequency band of 1400 to 1427 MHz, which is protected for radio astronomy applications. This will allow a wider bandwidth to be employed without suffering from interference problems.

Operation is also planned at the lower frequency of about 700 MHz. It is unlikely that the system will be required to operate at a frequency higher than 1424 MHz, where the performance of the existing aerials would begin to deteriorate. This maximum operating frequency sets the limit to both the surface transparency (and hence the wind loading) and the allowable deviations of the surface from the true paraboloid.

It was apparent that considerable economy would be required in both the design and the construction of the new aerials. As in most large radio telescopes, the mechanical cost of the aerials represents a large portion of the total budget. The finance available at the time set a limit on the capital cost of about $6000 per aerial. This is small compared with the 'normal' cost of paraboloids of this size. For this reason, surface tolerances and mesh opacity were reduced as much as possible, without sacrificing system performance, in order to keep the reflector structure simple, light and inexpensive. This reflector structure forms the most expensive part of the paraboloid.

Steel has approximately a three times lower cost and a three

times higher modulus of elasticity than aluminium. In view of this, steel has been used throughout, the only exception being the aluminium rings supporting the mesh. As these rings predominate at the edges of the aerial, it was most important to minimise their weight.

In Appendix C.1, the delineation of the array baseline is discussed and the resulting conclusions impose the following restrictions on the aerial design:

1. The mountings must be equatorial.
2. The hour-angle and declination axes must be separated by 15½ inches.
3. With the aerials pointing along the meridian plane, the declination axes must be collinear.

Due to the lack of counterweights it was necessary to keep the vertex to declination axis distance at a minimum (three feet). This is considered in Appendix C.3 together with the ground clearance details.

One of the new aerials, X1, is shown in Fig. 5.1. The dipole feed, D, at the prime focus illuminates the paraboloid reflector, R. This reflector is supported on the tower, by the shaft framework, S. The gears and drive motors are mounted on this shaft framework. The box, B, at the tower base contains the equipment for controlling the drive motors. The portions of the receiver system at the aerial are housed in a box, G, at the paraboloid vertex. The low-loss local oscillator line, C, together with the other receiver signal lines, can be seen emerging from the ground beside the foundations. The trench nearly surrounding the tower allows the aerial edge to go below the ground level. An automatic pump keeps this trench free of water. Limit switches, L, prevent the aerial driving too far.. Mechanical scales and potentiometric indicators, K, are affixed to both the hour-angle axis and the declination axis.

FIGURE 5.1

The additional 45 foot diameter antenna (X1) on the east end of the existing 32 element grating. A description is included at the end of Section 5.2.

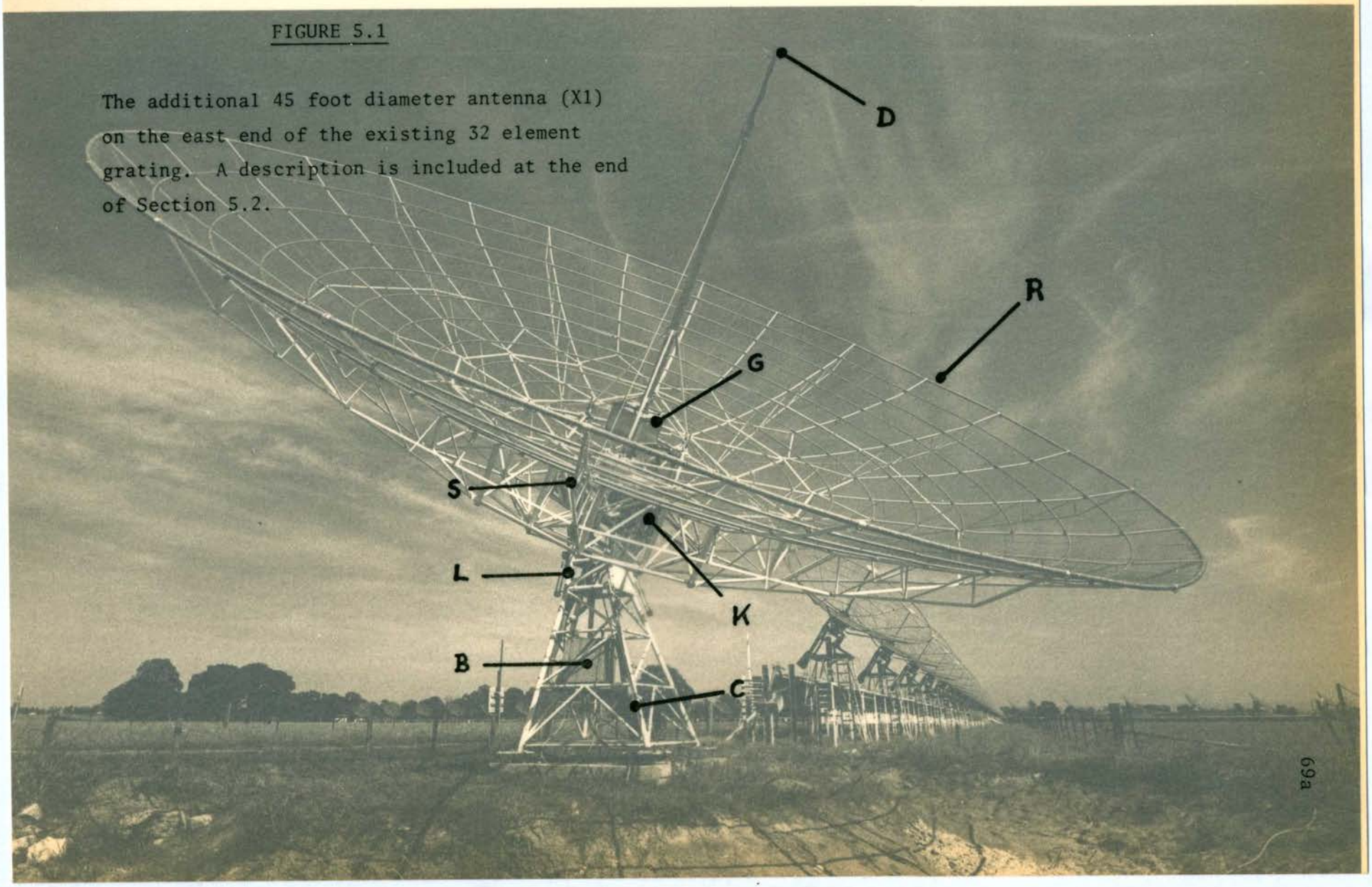

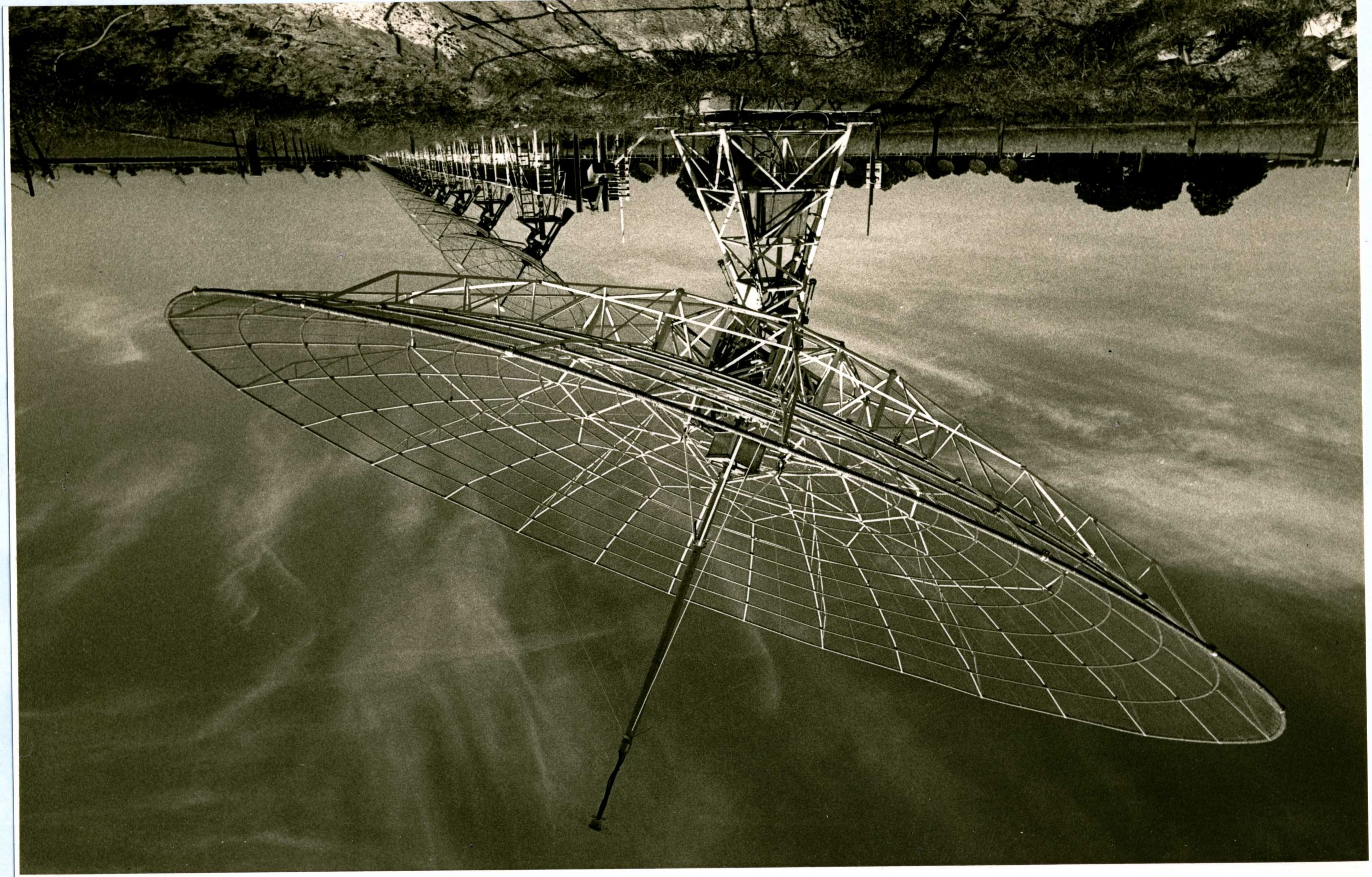

5.3 Sky Coverage

The details of the required sky coverage were discussed in Section 4.3. In some directions the ground clearance for this sky coverage is negative so that a trench is necessary to accommodate the edge of the aerial. This lack of ground clearance was the main reason why the sky coverage could not be enlarged much above the minimum requirement. (Extended coverage is desirable because it allows pencil beam observations at declinations closer to the equatorial plane.) However, there was also little point in increasing the coverage of the new aerials beyond that of the existing aerials.

Fig. 5.2 indicates the actual sky coverage achieved on both the large and the small aerials. Curves B and C show the present sky coverage of aerials X1 and X2 respectively while curve D shows the coverage of the small aerials.

Curve A gives the coverage which will be achieved with the large aerials when the limit switches are repositioned. It is also planned to redesign the limit switches on the southern side of the tower to give increased hour-angle coverage for declinations near the south pole.

Curve E shows the sky coverage that is necessary to achieve full source rotation coverage (Chapter 3).

The hour-angle coverage is symmetrical about the meridian. Coverage is identical for both east-west and north-south arrays.

5.4 Focal Length

The focal length of the new aerials can be chosen independently of the existing aerials (Appendix C.1). The important decision lies with the value of the f/d ratio. This has several consequences:

(a) It governs the size and complexity of the feeds required.

(b) In conjunction with the feed, it determines the excess antenna noise temperature.

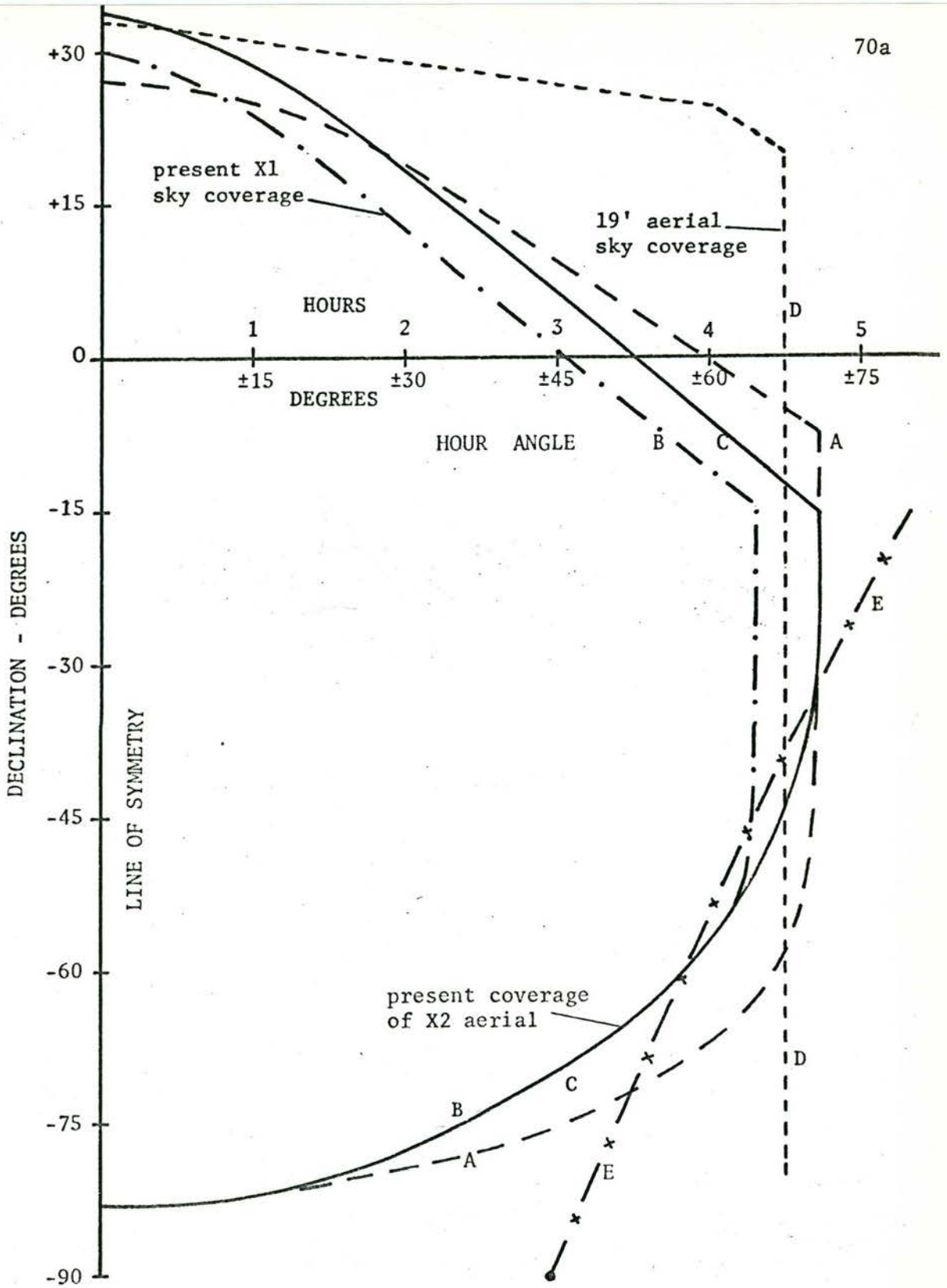

FIGURE 5.2 Sky coverage chart showing present and future sky coverage of both large (curves A, B and C) and small (D) aerials and also the sky coverage necessary to achieve full source rotation (E). (See Section 5.3 for details.)

FIGURE 5.3 Composite photographs of the 45 foot diameter aerial (X2) at the western end of the east-west compound interferometer showing the extremes of sky coverage available.

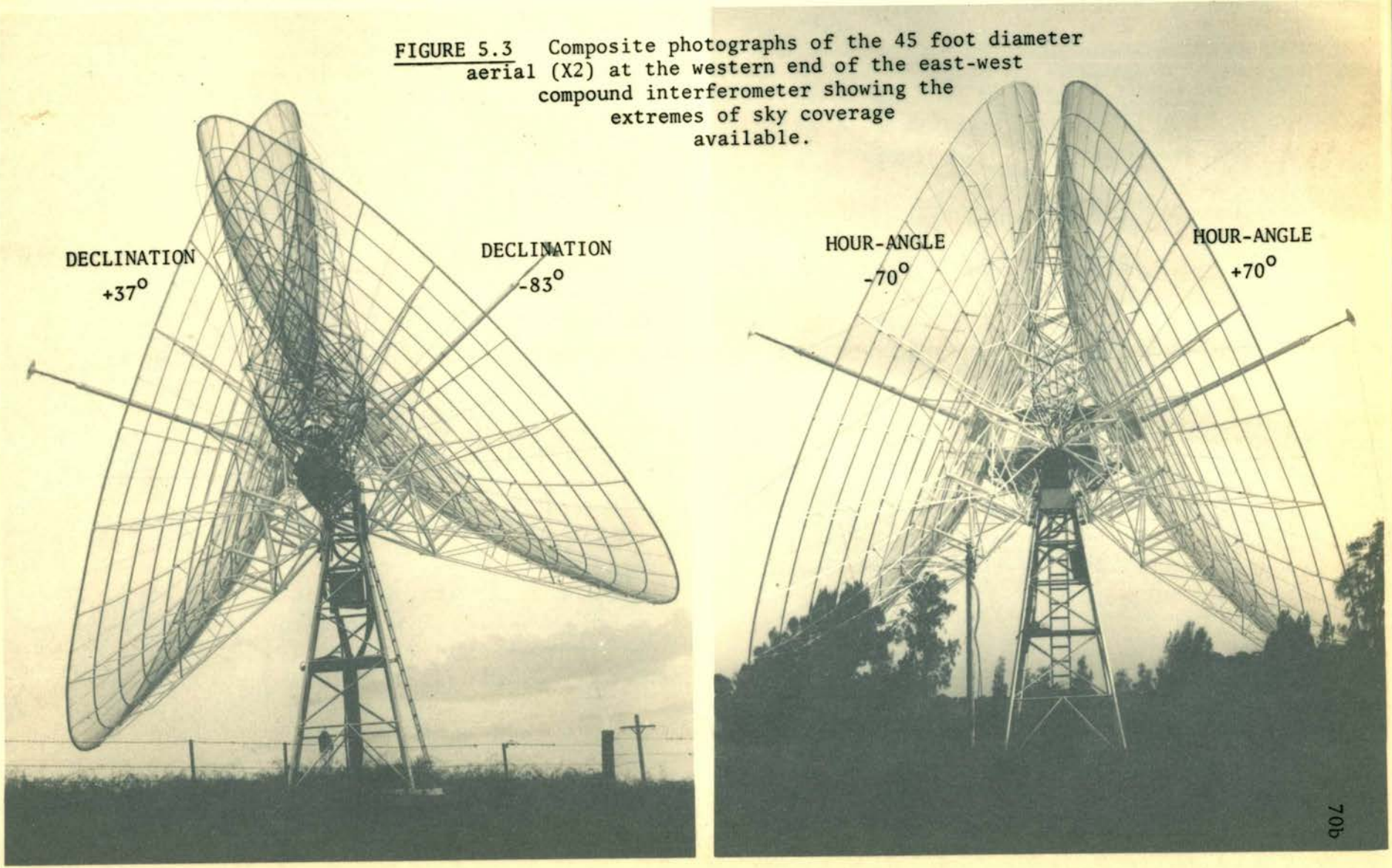

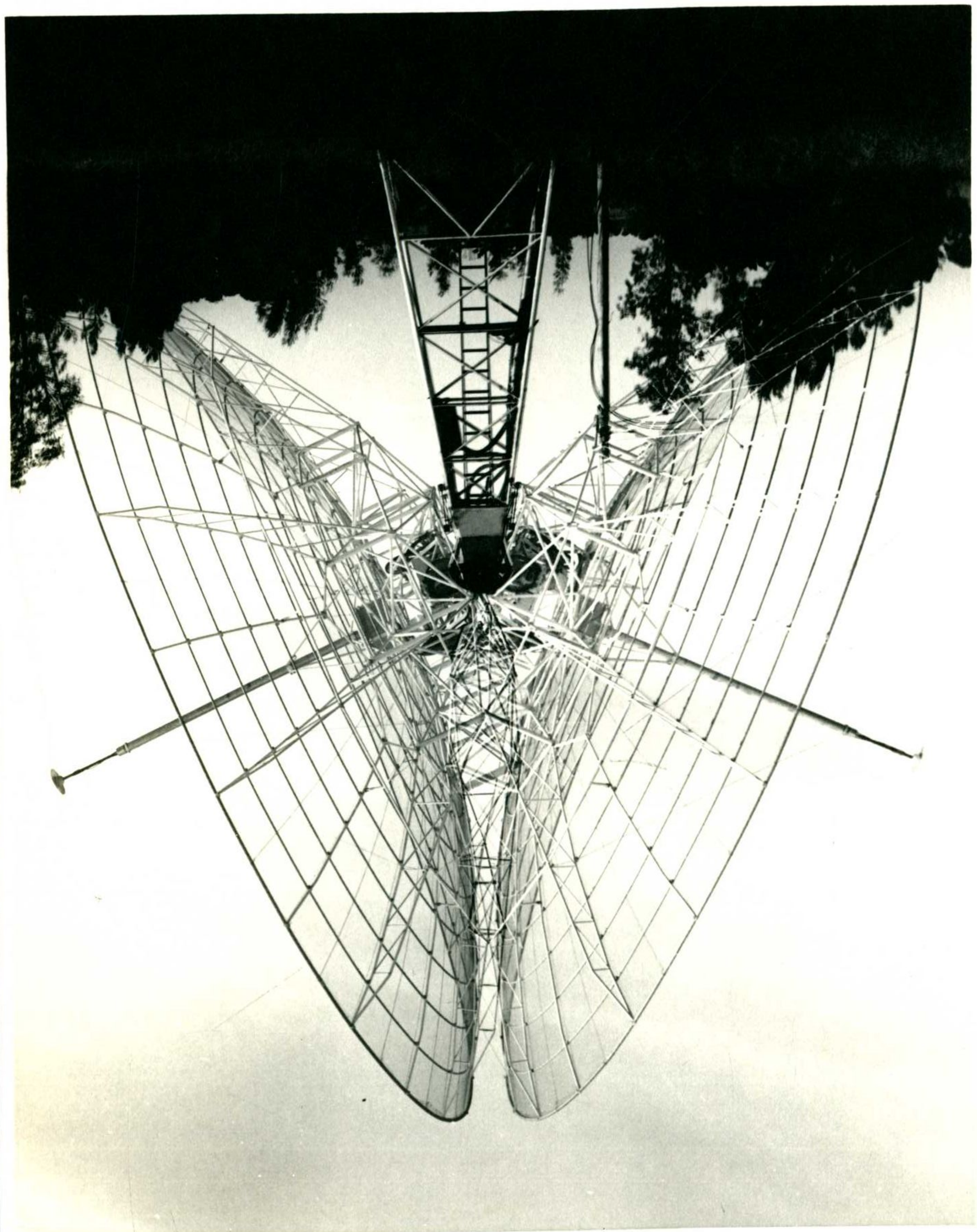

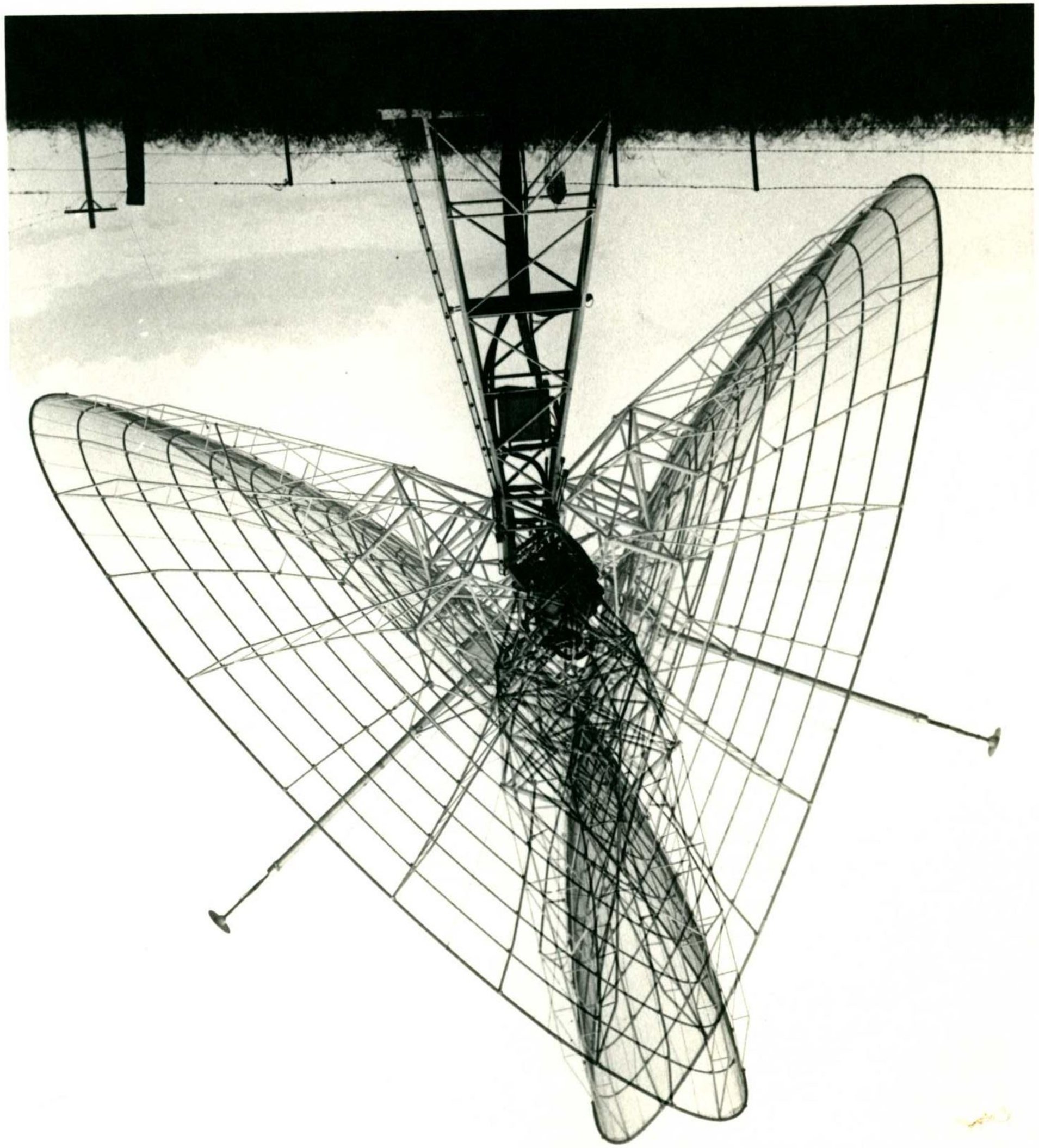

(c) A small f/d will give a greater focal point stability than a large f/d.

(d) Focal point shielding will be better with a small f/d.

(e) Polarization performance will be more satisfactory with a large f/d as cross polarization is lower.*

The possibility of using a Cassegrain system of primary illumination was considered. This has the advantages of (i) minimising antenna spillover noise, (ii) keeping the feed and front end receiver equipment together at the vertex where weight is not critical and (iii) minimising feed-receiver transmission losses thereby improving the system noise figure.

However, there are disadvantages: (i) A larger, more directional feed and a hyperbolic subreflector are required. (ii) As there are two reflecting surfaces, surface tolerances of both are more severe.

In the light of these facts, the feed system chosen for the present operation is a single dipole and reflector at the primary focus. However if low noise operation becomes vital this feed system can be changed into a Cassegrain one.

To optimise the illumination of the paraboloid, a moderate f/d of 0.41 was used. This gives a peripheral illumination which is 10 to 12 db below the central illumination. With a paraboloid diameter of 45 feet the focal length becomes 18½ feet.

5.5 Antenna Pointing Accuracy

In any radio telescope a pointing accuracy of 1/10 to 1/20 of the half-power beamwidth is desirable. A beamwidth of 40 sec. of arc for the compound grating system implies a pointing accuracy of 2 to 4 sec. of arc. However, this pointing depends primarily on the

---

*For single aerial polarization measurements, the improved shielding of a small f/d is often preferred.

electrical phase stability of the receiver system. Incorrect pointing of the individual aerials only moves the pattern envelope, changing the signal amplitude.

If a single grating response were being used, this would be positioned in the envelope central direction. In this region the envelope amplitude is relatively constant so that the element pointing needs to be only 1/3 to 1/5 of the aerial beamwidth.*

However the present system is designed to observe simultaneously the whole region inside the antenna beam (1^{o} diameter). The amplitude of the signal from the edge of this region needs to be stable. Because the envelope has a much steeper amplitude slope here, higher element pointing accuracies are required (see Fig. 5.4). A pointing accuracy of ± 1/10 of the beamwidth, i.e. ± 6 min. of arc, was considered satisfactory for the new aerials.

This pointing error creates an amplitude error of ± 0.02db at the envelope centre increasing to ± 0.5db at the 1^{o} diameter image plane edge. In cases where this edge amplitude-variation is too great, the image plane size will be restricted to $\frac{1}{2}^{o}$ diameter (± 0.2db amplitude error) and the observations repeated for the adjacent regions.

The aerial pointing error is caused by gear backlash, feed pole deflection, gear and structural deflections, tracking precision and pointing indicator inaccuracies. Considerable care in design was necessary to minimize these effects.

---

*For the centre of the envelope, 1/3 to 1/5 pointing error causes an amplitude variation of about ± 0.2 db.

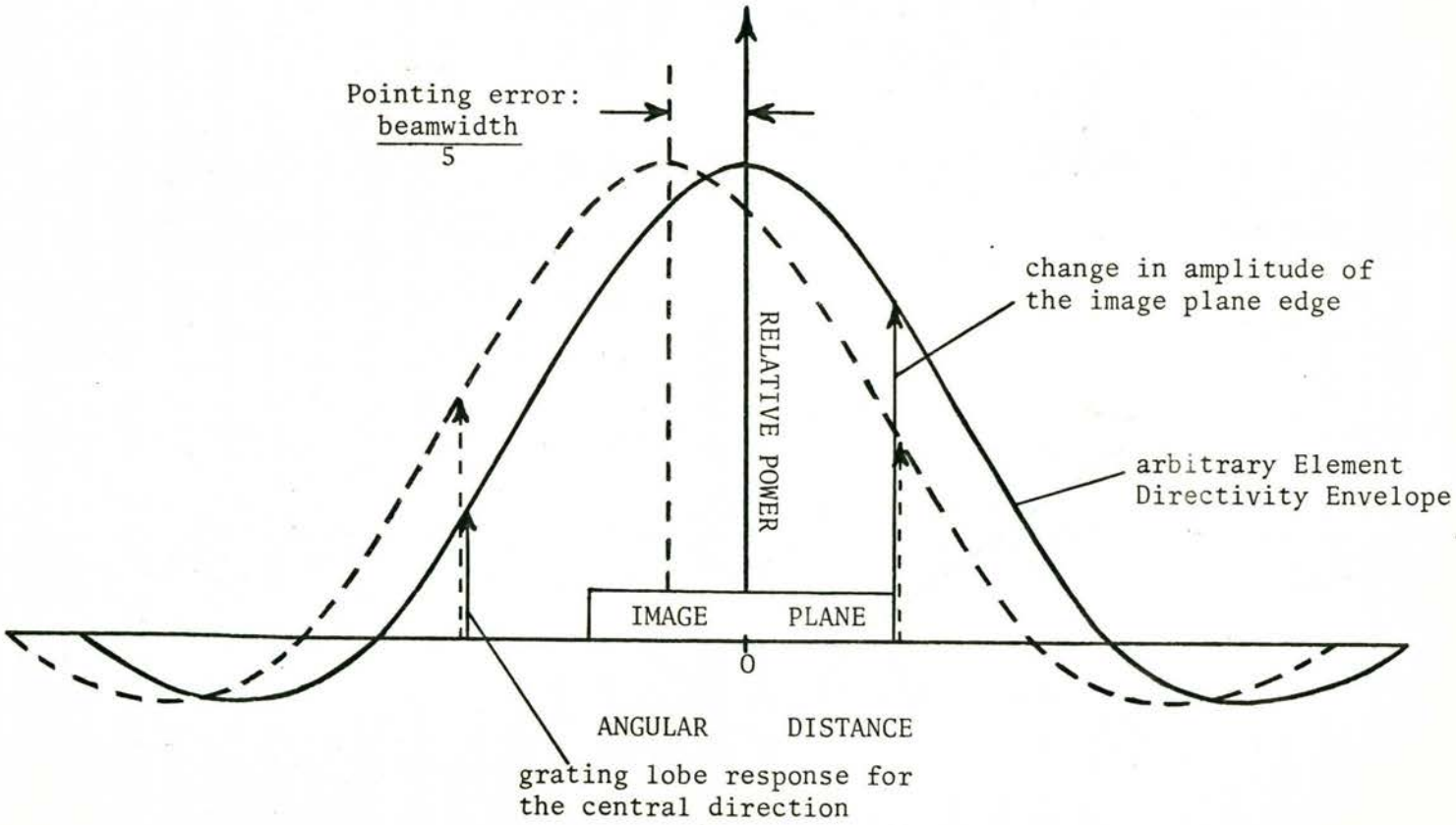

FIGURE 5.4 Illustrating the effect of an aerial pointing error upon the image plane edge and grating lobe responses.

5.6 SUMMARY OF ANTENNA SPECIFICATIONS

Diameter	45 ft (13.7 m)
Focal length	18.5 ft (5.6 m)
f/d ratio	0.411
Normal operating wavelength	21 cm
Reflecting surface	22 gauge galvanised steel hex. mesh (½ inch between centres)
Energy reflected from surface	97% at 21 cm
Beamwidth, E and H planes	1.1^{o} and 1.0^{o} at 21 cm
Equatorial mounting	Latitude $33^{o}51'.5$
Sky coverage	Down to 70^{o} zenith angle. Hence $\pm 4\frac{2}{3}$ hours hour-angle coverage and -83^{o} to $+35^{o}$ declination coverage with limited hour-angle coverage for the northerly declinations.
Surface accuracy	Weighted r.m.s. error: <0.35 inches.
Feed support	Centre pole (self-supporting). Provision for alternative tripod or quadrapod. Receiver box at dish vertex.
Drive rates	
Declination and hour-angle	$7\frac{1}{2}^{o}$ per min.
Hour-angle tracking	Sidereal or solar rates (15^{o} per hour).
Weights	
Reflector	3400 lb.
Shaft and drive system	800 lb.
Foundations	20,000 lb. reinforced concrete.
Structural materials	Galvanised steel mesh. Light steel tubing (outer reflector). Aluminium tubing for mesh support rings and feedpole. Heavy gauge steel tube for remainder of structure.
Capital Cost	$6000 approximately.

5.7 The Reflecting Surface

The choice of material for the relecting surface is important to the basic design. It can be solid and self-supporting and contribute to the strength of the backup structure or it can be an open mesh, present merely to reflect the incident radiation. For wavelengths less than 10 cm, the surface is best made from solid-sheet or expanded-sheet metal. With an operating wavelength of 21 cm, a very light and open galvanized steel mesh is best and this has been used here. This mesh is constrained to the required shape by concentric aluminium rings. The unsupported sections of mesh are held flat by pretensioning, applied during assembly. They form a series of intersecting conic surfaces which approximate the desired parabolic shape with a minimum of error (Appendix D.1). The aluminium rings are supported by radial ribs emanating from a central space-framed 'hub'. The mesh and rings are attached to the ribs so that they provide torsional rigidity to the outer structure. The steel parts in contact with the aluminium are galvanized to avoid corrosion.

The precise paraboloid shape and the method of adjustment are set out in Appendix E.

Mesh reflectivity

The mesh used has a 0.5 inch hexagonal grid and is made from 22 gauge wire. At 21 cm wavelength about 3% of the incident radiation is lost by transmission through the mesh. This corresponds to a gain loss of less than 0.15 db and a mesh leakage down by 15 db. Since the reflector gain is of the order of 45 db, the leakage suffers a loss of approximately 60 db, compared with the incident signal.

This mesh transparency increases rapidly with any increase in mesh size or decrease in wire gauge or wavelength. At 10 cm wavelength, the loss is about 10%.

The resistivity of the mesh is not important so that a galvanized steel is adequate. Christiansen and Högbom (1968) have pointed out that

even a stainless steel mesh (high resistivity) can be used without affecting the efficiency of reflection.

Wind forces

The mesh has a porosity factor of 0.1 solid in the normal direction. With the supporting rings and backup structure this factor remains less than 0.2 solid (in the normal direction) for the overall paraboloid.

The direct wind force F can be calculated using the formula (Brown and McKee, 1964):

$$F = \left(\frac{p.A.V^2}{400}\right) \text{ lbs} \qquad (5.1)$$

where p is the porosity factor

A is the cross sectional area in square feet (reduced by 0.6 for cylindrical members and by $\frac{2}{3}$ because the area is >100 sq. feet)

and V is the wind velocity in miles per hr.

The maximum wind velocity was set at 100 miles per hr. although in the vicinity of Sydney gusts seldom rise above 70 miles per hr. This gives a maximum loading of about 6000 lb with the antenna face-on to the wind and about 4500 lb with it side-on. Although the cross-sectional area is lower when side-on, the opacity factor is higher.

These wind forces can be considered to act through the centroid of area which is about 5½ feet above the declination axis. With such low opacity factors aerodynamic lift due to the antenna shape is almost non-existent.

To confirm these calculations, a scale model (½" to the foot) was constructed and tested in the wind tunnel of the School of Aeronautical Engineering. The resultant forces were 30% lower but of the same ratio.

Mesh tension

The mesh surface used is not self-supporting between attachment points. It is necessary to assemble it under tension so that the deflection under gravity or wind is minimized. In this design, it is sufficient to consider the mesh as a catenary. Hence we find the deflection (Δs), between support points, ($\Delta \ell$) apart, is given by:

$$(\Delta s) = 2C \sinh^2 \left(\frac{\Delta \ell}{4c}\right) \qquad (5.2)$$

and hence $(\Delta s) \simeq \frac{(\Delta \ell)^2}{8C}$ provided $\frac{(\Delta \ell)}{4C} > 100$

where $C \simeq \frac{\text{mesh tension}}{(\text{mesh wt.} + \text{windforce}) \text{ per unit length}}$

Hence for a given mesh and deflection, doubling the panel width requires the mesh tension to be quadrupled. The mesh in use has a weight of 0.12 psf and a porosity factor of 0.1 solid. Thus with a 45 mph wind and a panel width between rings of three wavelengths (2.1 feet), 15 lb per foot tension is necessary to keep the deflection below $\frac{\lambda}{32}$.*

The mesh is the lightest and most porous that it is feasible to use. The required tension is easy to apply and maintain. The contributions of the mesh and support rings to the paraboloid surface weight are nearly equal (about 200 lb.) and the wind area contribution of the rings is only 25% that of the mesh.

The mesh is put on in rose-petal fashion in order to maintain electrical symmetry. Large triangular panels, each 24 feet in length, are attached at the vertex and outer rings and partially tensioned. They are then pulled down to the shape of the parabola and attached to the intermediate rings by steel bag-ties. The petals (48 per aerial) are seamed together and soldered so that the surface is electrically continuous.

---

*As the principal frequency is 1415 MHz, the wavelength (λ) referred to here and in the following text is 21 cm.

Surface tolerance considerations

A number of analyses have been conducted into the effects of surface errors on the electrical performance of paraboloids (e.g. Ruze, 1952; Cheng, 1955; Bracewell, 1961a). Basically there are four sources of surface error:

1. Periodic errors due to approximations in design. In the present paraboloid, these occur because the surface mesh is supported by concentric rings at discrete radial intervals. Since the mesh is drawn tight between these rings, the surface becomes a series of intersecting cones approximating the desired parabola of revolution. Appendix D.1 derives the support ring positions necessary to limit the errors to a given figure, in this case to $\pm \frac{1}{16}$ inches axial.

2. Random or periodic constructional errors. These occur during surface alignment. With diameters of 40 wavelengths and over (65 wavelengths in this case), it is preferable to adjust the surface after construction. As the adjustment points are not independent of one another, it is necessary to define a realistic tolerance so that the assembly time is not excessive.

3. Deformation errors due to gravity, wind and temperature. These occur over large areas of the surface in a regular fashion and also change the position of the focus, often distorting it from a point to a line-segment or an area. A further disadvantage is that the errors are not stable but change with orientation and environment. (Temperature effects can be disregarded unless one is trying to hold dimensional accuracies over 1 in 10,000.)

4. Surface roughness errors. These are irregularities (bolt heads, mesh seaming or small dents) which have correlation intervals which are small compared to the wavelength. They can be ignored in terms of the far field pattern as they produce only evanescent waves which fade quickly with distance.

Measurement of surface error usually entails measurement of the axial displacement, dx, of a point of known radial position. Appendix E.1 describes the method used here. The relation between dx and the actual signal path error, ε, is given by

$$\varepsilon = dx\ (1 + \cos\theta) \tag{5.3}$$

where θ is the angle between axial and focal directions.

Since the equation of the parabola in two dimensions is

$$y^2 = 4fx, \text{ where } f \text{ is the focal length,}$$

$$\text{then} \quad dx = \frac{\varepsilon}{2}\left[1 + \left(\frac{y}{2f}\right)^2\right] \tag{5.4}$$

Thus the axial displacement accuracy may be relaxed towards the edge without increasing the signal path error.

Another factor allowing relaxation of the tolerances is the aerial aperture illumination. This is tapered radially such that the edge illumination is down approximately 10 db on the centre. When this is coupled with an area factor, we have the relationship of Fig. D.2.1 showing that the greatest power contribution comes from the intermediate radii. This relationship was applied as a radial weighting factor during assembly. The derivation is treated in Appendix D.2 in more detail.

The nett effect of the above factors was to allow an axial surface deviation after assembly of $\frac{\lambda}{32}$ rms and $\pm\frac{\lambda}{16}$ maximum over the middle half of the reflector tapering to $\frac{\lambda}{16}$ rms and $\pm\frac{\lambda}{8}$ maximum at the outer edge. This tolerance includes errors (types 1 and 2 above) due to design approximation and mesh deflection contribution. Under normal operating conditions, structural deformation errors (type 3 above) do not increase these errors beyond $\frac{\lambda}{16}$ rms for the centre and $\frac{\lambda}{8}$ rms for the outer edge. The constructional errors are mostly random in nature and swamp any periodic effects of the design approximation and mesh deflection.

After construction the aerials X1 and X2 were resurveyed and the weighted rms errors computed as less than 0.2 inches ($\frac{\lambda}{40}$). From relationships computed by Ruze (1952), these errors appear principally as a drop in aerial gain of 0.7 db.

Structural deformations generally occur over large areas (large

correlation interval) thus raising the sidelobe level significantly as well as reducing the gain. As these effects change with orientation, the aim has been to keep the deformation errors smaller than the constructional errors. Assuming the combined error does not exceed $\frac{\lambda}{24}$ (0.35 inches) rms (weighted), the element gain loss due to these errors will be less than 1.2 db (i.e., 0.6 db system gain loss).

5.8 Structural Details

5.8.1 Reflector Structure

The reflector structure (Fig. 5.5) consists of a strong centre section, 18 feet in diameter and 4 feet deep, supporting twelve light-weight radial ribs 13½ feet long, tapering to the outer edge of the paraboloid. These ribs provide strength in an axial direction. The concentric aluminium support rings are clamped with U-bolts to the top chord of the ribs forming rigid joints. The rigidity of the joints combined with the tensioned mesh surface provides resistance to torsional forces in the outer section.

The centre section (Drg. B-F45-25, Appendix E.2) is a rigid space frame welded from heavy gauge pipe. A six-pointed "Star of David" configuration forms the basis of an annulus with a hexagon inner ring and a twelve-sided outer ring. The twelve vertices provide attachment points for the ribs. The inner hexagon provides support points for the declination axis and is sufficiently large to allow this axis to be positioned inside the structure without unduly restricting the sky coverage. Deformation of this centre section under normal operating conditions is negligible. This type of structure reduces the outer radial weight to a minimum. Lower total weight and lower drive torques are the final result.

No counterweights are used for two reasons: (i) counterweights on this type of design restrict the sky coverage unless on very short radius arms when the additional weight must be several times the dish weight, and (ii) a stronger and more expensive reflector structure is necessary to support the counterweights. Instead, the axis-to-vertex distance (3 feet) is as short as the sky coverage requirement will permit. This reduces the dish-weight moment arm to about 3½ feet from the declination axis. The disadvantage is that the drive gears have to withstand the load of the unbalanced reflector as well as any wind forces (see Section 5.8.4).

FIGURE 5.5

This assembly drawing, B-F45-00, shows the reflector framework. The strong 'star' configuration in the centre can be seen in heavy outline. Lightweight ribs emanate from this centre section with torsional rigidity being supplied by the concentric aluminium rings and the mesh reflector surface.

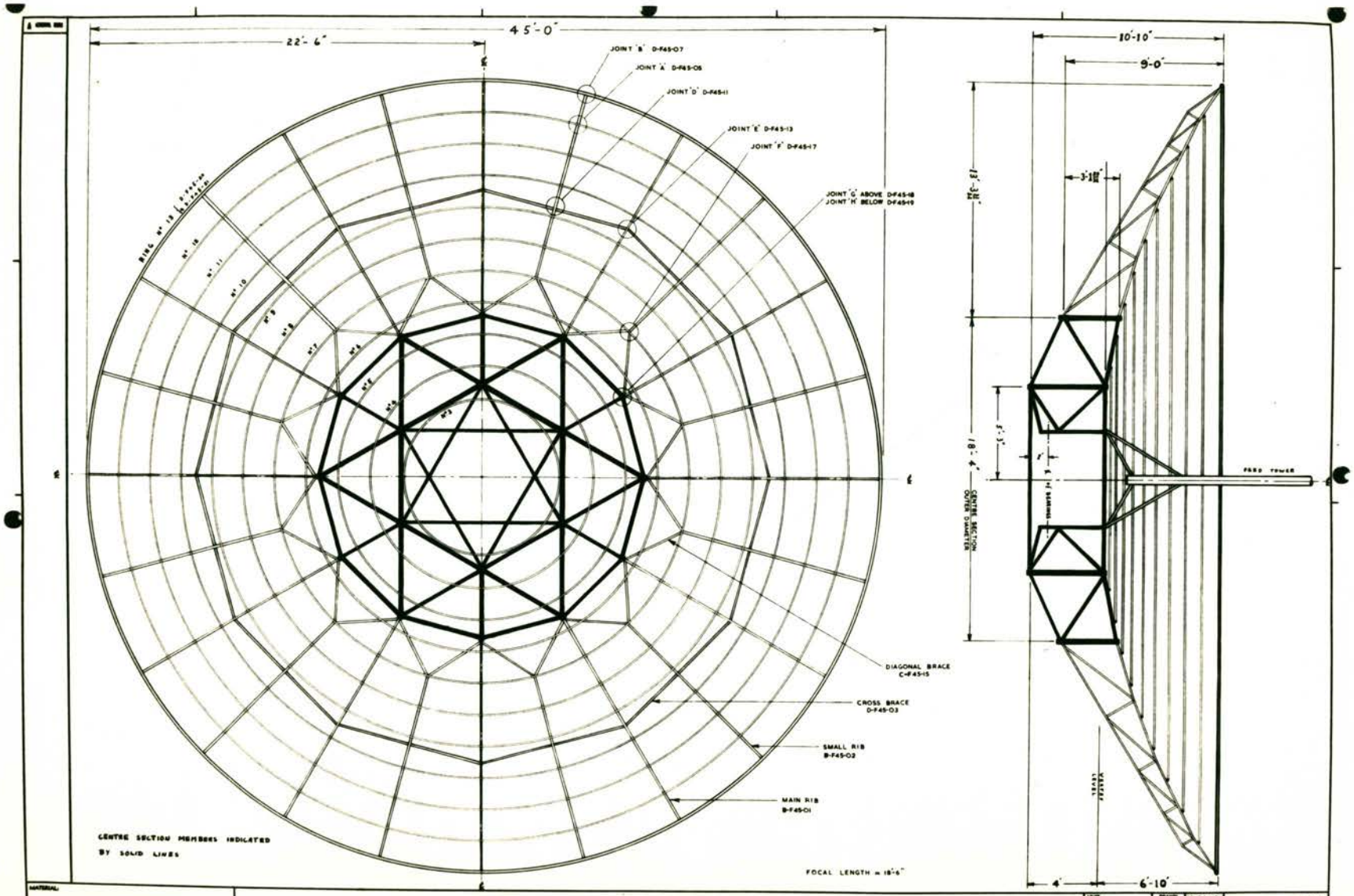

MATERIAL

FINISH

FLEURS 45 FT. DIA. AERIAL - REFLECTOR ASSEMBLY

SCALE ¼" = 1 Foot

UNIT

ASSY.

C.P.L.

DRAWN

TRACED

CHECKED

PASSED

APPROVED

B-F45-00

5.8.2 Tower and Foundations

The supporting tower (Drgs. B-F45-40 and 41, Appendix E.2) is a welded steel tubular framework of square cross section. It tapers from a 6 foot or 8 foot base to a narrow neck just below the top. This narrow neck is necessary to allow the reflector structure to clear the tower at the extremes of zenith angle. The top section of the tower above the neck is heavily plated and tilted over to the north. It provides support points for the bearings which hold the hour-angle or polar axis.

On the top of the north face of the tower is welded a heavy mild steel bar, machined for accurate mounting of the hour-angle main segment. This segment and the main bearings are bolted and pinned in position after the alignment and meshing of the gears is carefully checked.

The soil at the field station is a clay mixture. During summer it becomes rock hard and is inclined to shrink. During the wet season it can be completely covered with water and becomes soft and mobile.*

Because of the nature of this soil, the foundations were made primarily of the dead-weight type. They are sufficiently heavy to counteract the overturning moments due to wind loading (6000 lb at 100 mph) and the unbalanced weight of the aerial (3400 lbs) and of sufficient area so that the direct load causes no subsidence. Pillars, 2 feet square and over 5 feet deep, at each corner are joined by sections also 2 feet square. The complete foundations (15,000 and 20,000 lb wt.) were cast in concrete and reinforced with ½" diameter steel rods. To provide additional resistance to the overturning moments, the corner pillars are 'belled' out at the bottom.

Each of the four tower feet rests upon a 14 inch square steel plate which is supported on 1 inch diameter studs cast in the corner

---

*Stability tests are being carried out on the survey bench marks set in concrete blocks at the centre and ends of the array.

pillars. These plates allow vertical and lateral movement of the tower feet so that the paraboloid position and orientation can be accurately set.

The shape of the tower is such that, when the antenna is pointing in the zenith direction, the centre of gravity of the whole structure lies over the centre point of the foundations. When not in use the aerials are stowed, pointing in this direction.

5.8.3 Shaft Framework

The reflector structure is supported on the tower by the shaft framework so that rotation of the aerial about the two perpendicular axes is possible. The shaft framework must be (i) small enough to fit into the available space, (ii) sufficiently strong to support the dish and to provide drive torques without significant distortion and (iii) large enough to leave room for mounting the gearboxes and motors. Appendix E.2 (Drg. B-F45-44) shows the final design.

A tetrahedron structure is used in which the hour-angle axis, 2½ feet long, and the declination axis, 5 feet long, form two sides at right angles separated by 15½ inches. Three inch diameter heavy gauge pipe is used for the axes with solid 2½ inch diameter sections set into the ends to take the main bearings. These stub sections were accurately welded into place using heavy jigs.

The bearings which fit on the ends of these stub sections are self-aligning spherical roller bearings in flange-type housings. These make for easy alignment during assembly. During operation the bearings are expected to rotate twice a day through 135° at a speed of $7\frac{1}{2}^{\circ}$ per minute with those on the hour-angle shafts rotating twice an additional 135° at 15° per hour. As slow speeds tend to cause permanent deformations of the rolling surfaces, it was necessary to reduce the load factor of the bearings.

During welding of the framework, the main axes (declination and hour-angle) were accurately set so they were (a) at right angles to each other and (b) 15½ inches apart. It was inconvenient to build-in

facilities in order to adjust these later.*

With the tetrahedron as a starting point, the structure is further triangulated to form a platform parallel to the hour-angle axis and containing the declination axis. This platform is used to mount two more tetrahedrons, one at each end of the declination axis, to provide support points for the main declination drive pinions. The declination drive is applied symmetrically, either side of the hour-angle axis, in order to reduce twisting forces which could distort the reflector surface.

Resistance to distortion is important since moments due to the dish structure weight are high and are balanced by large forces with small moment arms (Section 5.8.4). Distortion in the gear mounts had to be minimized to avoid backlash and tracking errors. Pointing accuracy depends almost entirely on the accuracy of the primary drive gears and the strength of the shaft structure. This structure with its six tetrahedrons linked face to face, forms a strong space frame.

5.8.4 Drive System

The primary drive gears (segment and pinion) for both axes were made as large as was feasible in order to minimize angular backlash and tooth loading. A pitch circle diameter of 37.5 inches was chosen for the segment.

Angular backlash is caused principally by machining and assembly inaccuracies. An involute tooth shape is used so that the gears can be meshed as close as the indexing error permits. The best to be expected from this is 1 min. of arc backlash.

Tooth loading is high due to the possible wind forces (Section 5.7) and to the unbalanced weight of the reflector of 3400 lb (no

---

*An error in the 15½ inch dimension causes the phasing of the array to change with the angle of viewing. If the axes are not perpendicular, then pointing of the antenna, although correct at zero declination, will be in error at the pole. In fact, it would be impossible to point directly at the pole.

counterweights). The worst combination of these forces could create a maximum torque load of 31,000 lb ft. However under normal operating conditions this should rarely rise above 20,000 lb ft.

Two segments, with face widths of 1½ inches, are bolted and pinned to the centre section at opposite ends of the declination axis. The hour-angle drive uses one segment with a 3 inch face width mounted on the north side of the tower top.

The remainder of the drive system is situated on the platform provided by the shaft structure (Fig. 5.6). The main driving pinions are combined with large diameter second gears. These second gears are driven by large ratio gearboxes.

The planned operation of the antenna requires two driving speeds. First, for 'setting-up', the dish has to be moveable from the zenith to any point in the sky in 15 minutes or less. Secondly, it has to track a source accurately throughout nine hours of observations. For the fast rate, both declination and hour-angle drives use 1500 r.p.m. ¼ H.P. sliding-rotor brake motors to move the antenna at thirty times the tracking rate ($7\frac{1}{2}^{o}$ per minute). The slow speed (15^{o} per hour), on the hour-angle drive only, uses a 1500 r.p.m. 1/6th H.P. synchronous motor driving a 30 to 1 worm gearbox. This worm gearbox is connected by a clutch onto the input of the main hour-angle gearbox.

The gear ratios in the system are 150 to 17 for the main segment and pinion, 180 to 16 for the second gear and pinion and 2176 to 3 for the gearbox, giving an overall ratio of 72,000 to 1. Except for the 30 to 1 worm drive, spur gears have been used throughout because of their high efficiency.

All open gear teeth are treated and greased with a molybdenum disulphide lubricant. Besides providing lubrication and rust resistance, this treatment reduces the possibility of cold welding of the gear teeth. As a further precaution against cold welding, all the main pinions are formed from Durax steel and pressed and keyed into the second gears.

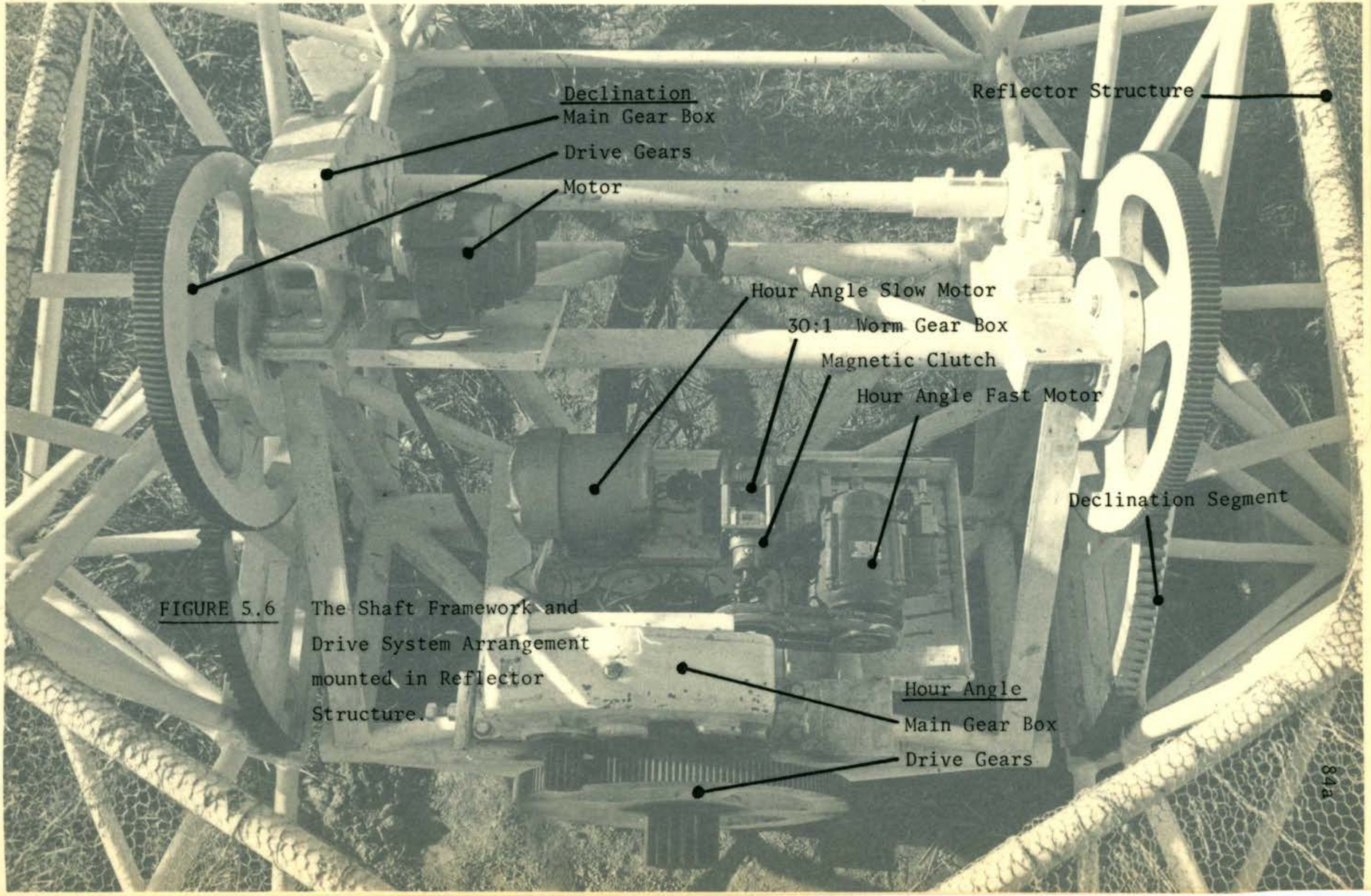

FIGURE 5.6 The Shaft Framework and Drive System Arrangement mounted in Reflector Structure.

5.9 Control System and Position Indicators

A block diagram of the complete control system is shown in Fig. 5.7. This is a closed loop system and is necessary when the complete interferometer is operating as an image forming telescope. The closed loop will be used to compensate for:

(i) variations in the mains frequency used to drive the synchronous motor,

(ii) the difference between solar and sidereal time,

(iii) any slip in the clutch drive,

(iv) backlash and indexing error in the drive gears* and

(v) any gravitational deflections causing a change in pointing of the electrical axis.*

The closed loop will also simplify observational procedure.

The system will not compensate for pointing errors caused by wind. With velocities below 20 knots, wind forces, proportional roughly to the square of the velocity, are a small fraction of the forces due to gravity.

Briefly the system operation is as follows: The required right ascension coordinates are set, via rotary switches, in a binary counter. Digital time is subtracted serially every second to produce the required hour-angle. This is then converted to an analog signal. A correction factor, depending upon the aerial hour-angle, is added ((iii) and (iv) above). This signal is then compared with the indicated hour-angle and the resultant error signal used to control a variable frequency oscillator. The oscillator has a centre frequency of 50 Hz and ± 15% frequency variation. A 200 watt power amplifier then drives the synchronous tracking motor. The fast motor is permanently connected to the gearbox input shaft so that at tracking speed it rotates at only 50 r.p.m.

---

*(iv) and (v) depend upon the addition of an experimentally-measured correction factor. This may prove to be unnecessary.

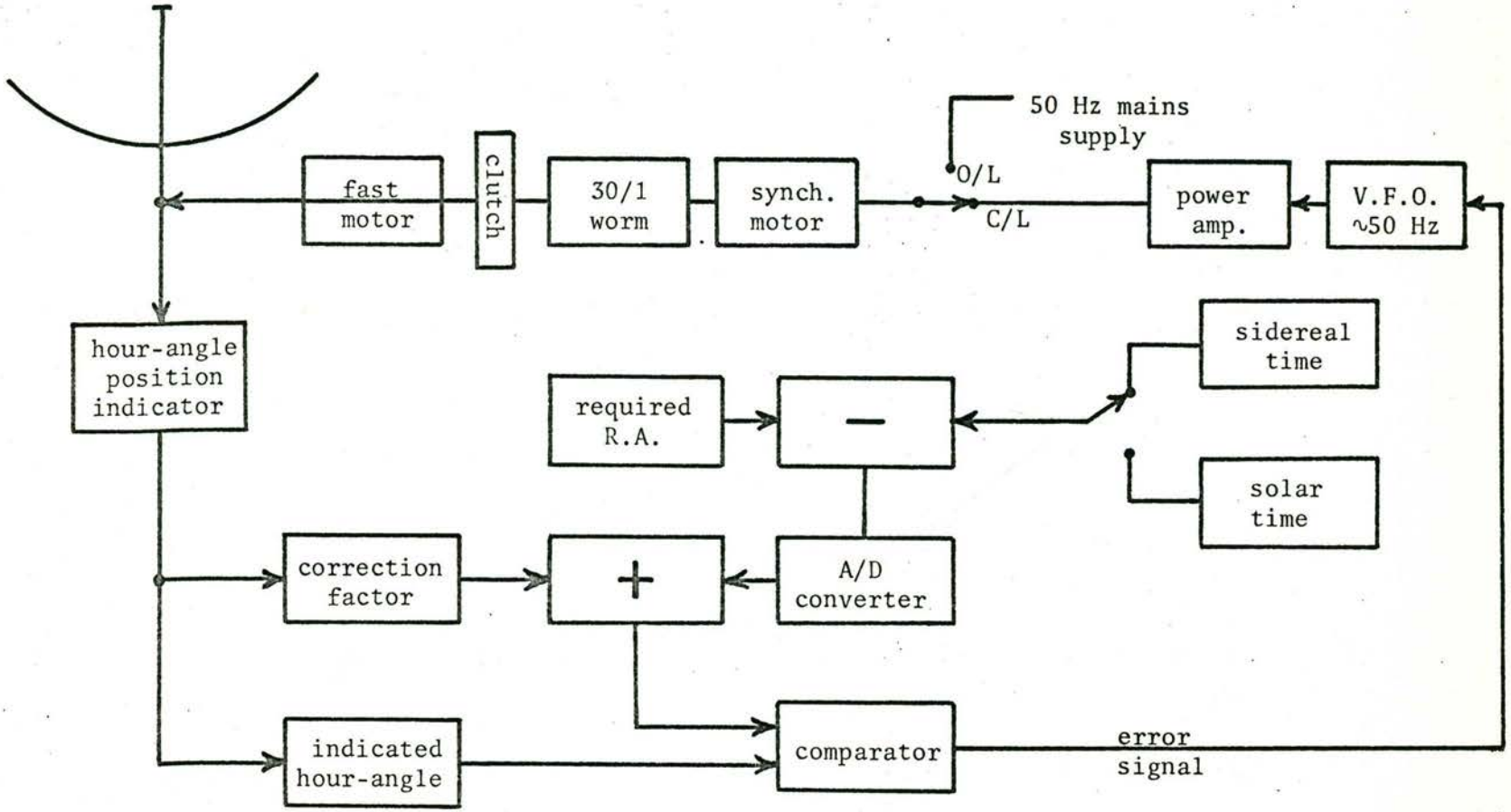

FIGURE 5.7 Block digram of the closed loop hour-angle control system for each 45 foot antenna.

This control system has the advantage that it can be switched to an open loop system when high pointing accuracy is not required. The synchronous motor is then driven from the 50 Hz mains supply. At present this is the normal mode of operation.

Fig 5.8 shows the electrical circuit for operating each antenna both at the antenna and remotely at the centre hut. There are electrical interlocks preventing:

(i) both motors operating together,

(ii) the brake being held off when the clutch is not engaged,

(iii) the telescope being driven beyond the limits of sky coverage and

(iv) operation at the aerial when it is being controlled remotely and vice versa.

The limit switches are placed on the tower corners where a striker bar around the inner hexagon of the reflector structure touches at the extremes of zenith angle. The limit switch circuit is so arranged that a particular limit switch will only prevent the dish being driven further into the limit, but will not prevent it being driven in the opposite direction. Two additional switches are sited on the hour-angle axis. One is accurately set to stop the aerial at the starting point of each period of observation. The other is arranged to facilitate parking of the aerial in the vertical position.

Aerial positions are indicated at present by a system of potentiometers connected directly to the drive shafts. A regulated voltage is applied to the potentiometers and the voltage ratios, linearly proportional to the shaft positions, are indicated on a system of meters in the central hut. These meters are calibrated so that each aerial can be pointed with an accuracy of a couple of minutes of arc.

FIGURE 5.8

The electrical control system used for pointing the aerials.

(a) Drawing B-F45-52 shows the electrical circuits used to control each 45 foot diameter aerial. The aerial control box and central control aerial panel are duplicated for each aerial.

(b) The two control racks in the centre hut. The right hand one controls the 32 small aerials while the left hand one controls the 45 foot aerials. This second rack contains two controller panels which can be switched separately to control any or all of the 45 foot aerials.

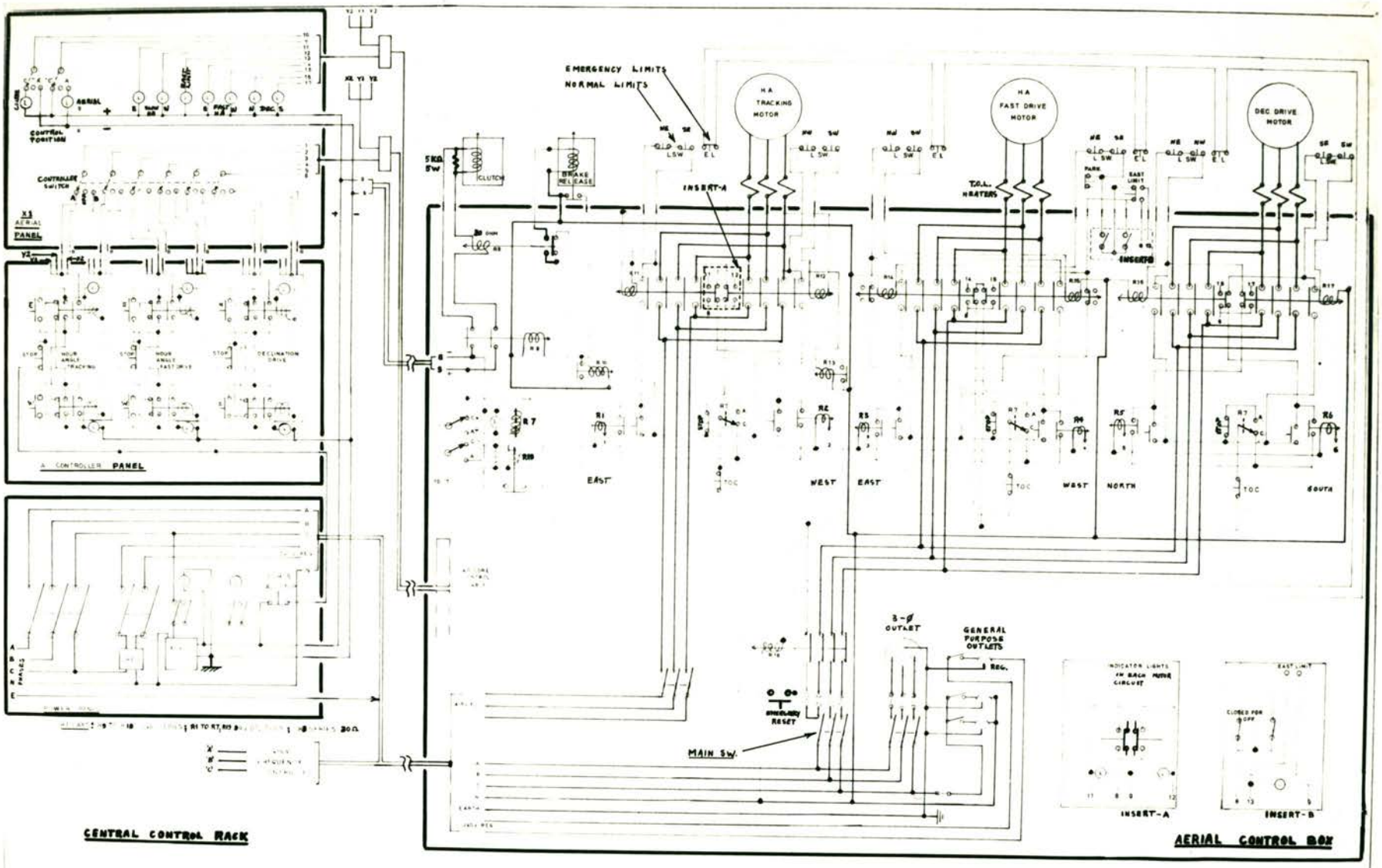

CONTROL CIRCUIT 45 FT DIA. AERIAL

UNIT	DRAWN		S.U.E.E.S.
ASSY.	TRACED		B-F45-52
C.P.L.	CHECKED		
	PASSED		
	APPROVED		

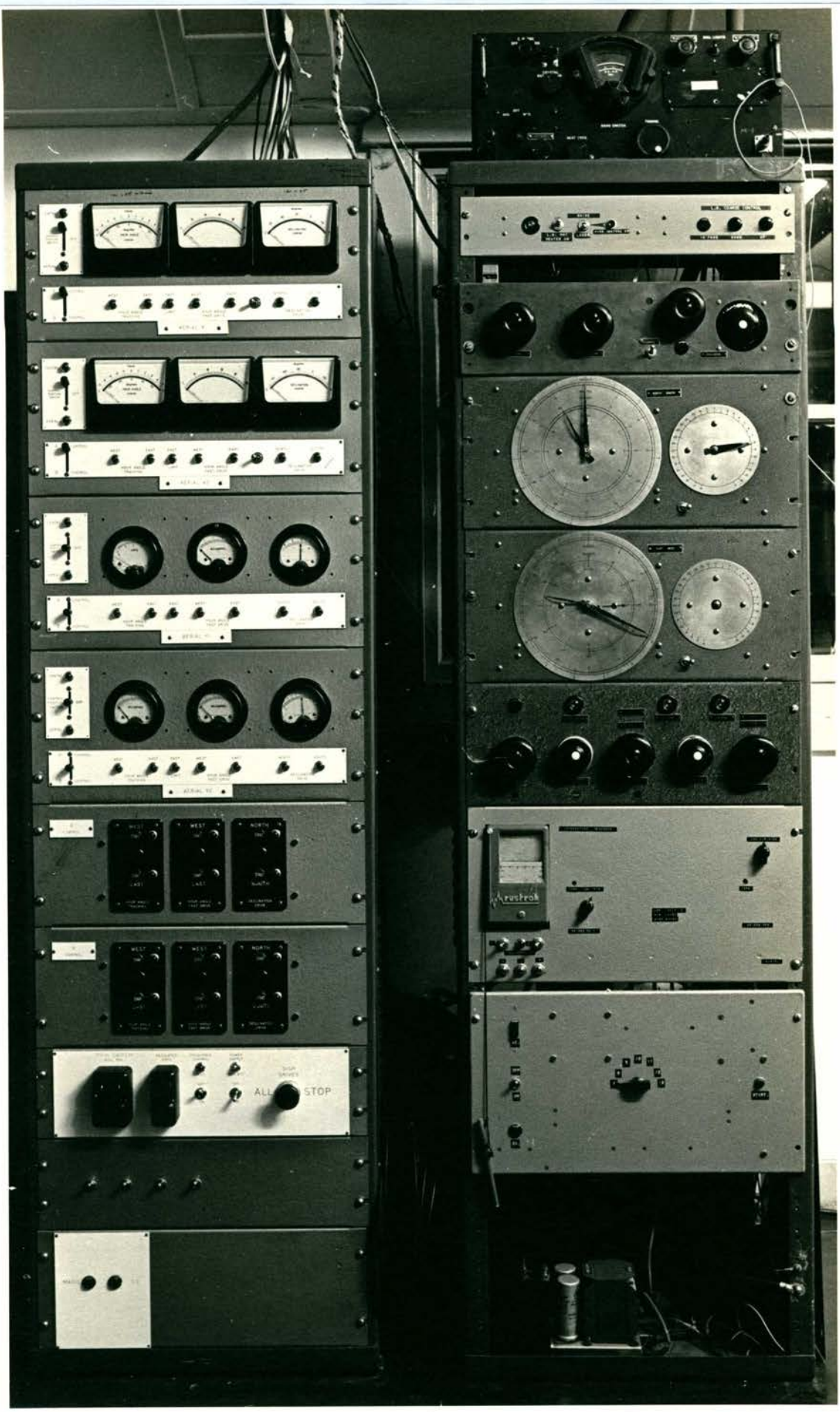
ALL
STOP
rustrak

5.10 Primary Feed and Support Mast

The primary feed for use in the initial observations consists of a half wavelength dipole for 21 cm operation and a folded dipole for 42 cm operation set below a 16 inch (2λ at 21 cm) diameter aluminium reflecting plate (Fig. 5.9). These dipoles are set mutually orthogonal to reduce interaction.

Two methods of support are possible, a single central mast and a tripod or quadrapod arrangement. A central mast is used at present. This type of support is simple, cheap and light, and is convenient for adjusting the position and orientation of the dipoles. However, it has the disadvantage of limiting the type of feed that can be used and the weight of front-end receiver equipment that can be installed at the focus. At present, mixers and preamplifiers are installed in an insulated box at the vertex and the 21 cm dipole is fed through 18 feet of low loss coaxial line. The measured loss in this line is 0.9 db.* For the present observations this is not significant but at a later stage low noise receivers are planned. Then it may be necessary either to place the receiver equipment at the focus or to use a Cassegrain secondary mirror system. To facilitate this, mounting points for either a tripod or a quadrapod are set at the edge of the 18 foot diameter centre section.

The central mast is a 5 inch diameter aluminium pipe extending to within 30 inches of the dipole and supported at the vertex by a small framed tripod. A 1½ inch diameter brass pipe extends from the dipole down to the vertex and is supported at the ends of the aluminium pipe. The whole arrangement weighs 80 lb and is self supporting.

By correct choice of the weights and rigidities of the pipes and the position of the support points, the dipole is kept at the focus irrespective of the zenith angle. The centre sag of the inner brass

---

*This causes a signal loss of 19% and 10% for the single aerial and correlation system respectively.

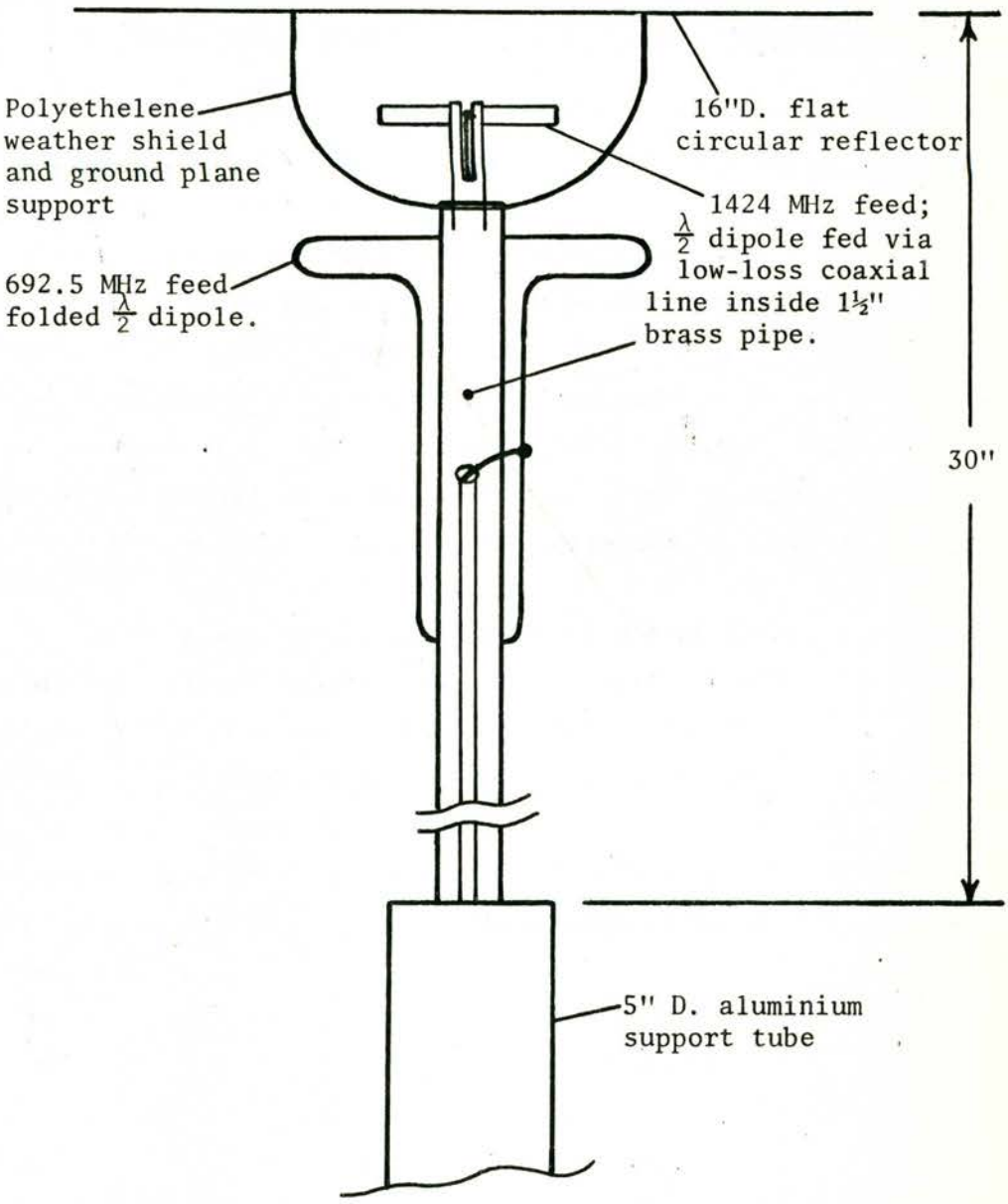

FIGURE 5.9 The two-frequency feed for the large antennae. The 1424 MHz and 692.5 MHz dipoles lie in orthogonal planes.

pipe and the consequent rise of the feed compensates for the drop in the cantilevered sections due to the weight of the feed, support pipes and receiver cables. Heavier feeds can be compensated for by adding a sliding weight to the inner brass pipe. A similar arrangement was used by Hooghoudt et al (1957).

Wind forces on the mast cannot be balanced out. However the effect is small. A 20 mph wind causes a pointing error of less than one fortieth of the beam width at 21 cm.

Small adjustments to feed can all be made at the base or vertex. These include repositioning, 6 inches in any direction, and rotation through 360° for polarization measurements. To change the feed, the mast is pivoted down to the edge of the reflector by removing one anchor bolt.

Fig. 5.10 gives the field pattern of one of the primary feeds. These feeds were assembled and adjusted in their support tubes prior to installation in the reflector. Field patterns and impedances are sensitive both to separation of the dipole from its ground plane and to length of the dipole arms (Fig. 5.10). The v.s.w.r. of feed and cables was also rechecked after installation. The presence of the antenna reflector surface degraded, slightly, the impedance match but this match always remained < 1.1.

The resultant secondary pattern of a single large aerial is shown in Chapter 6.

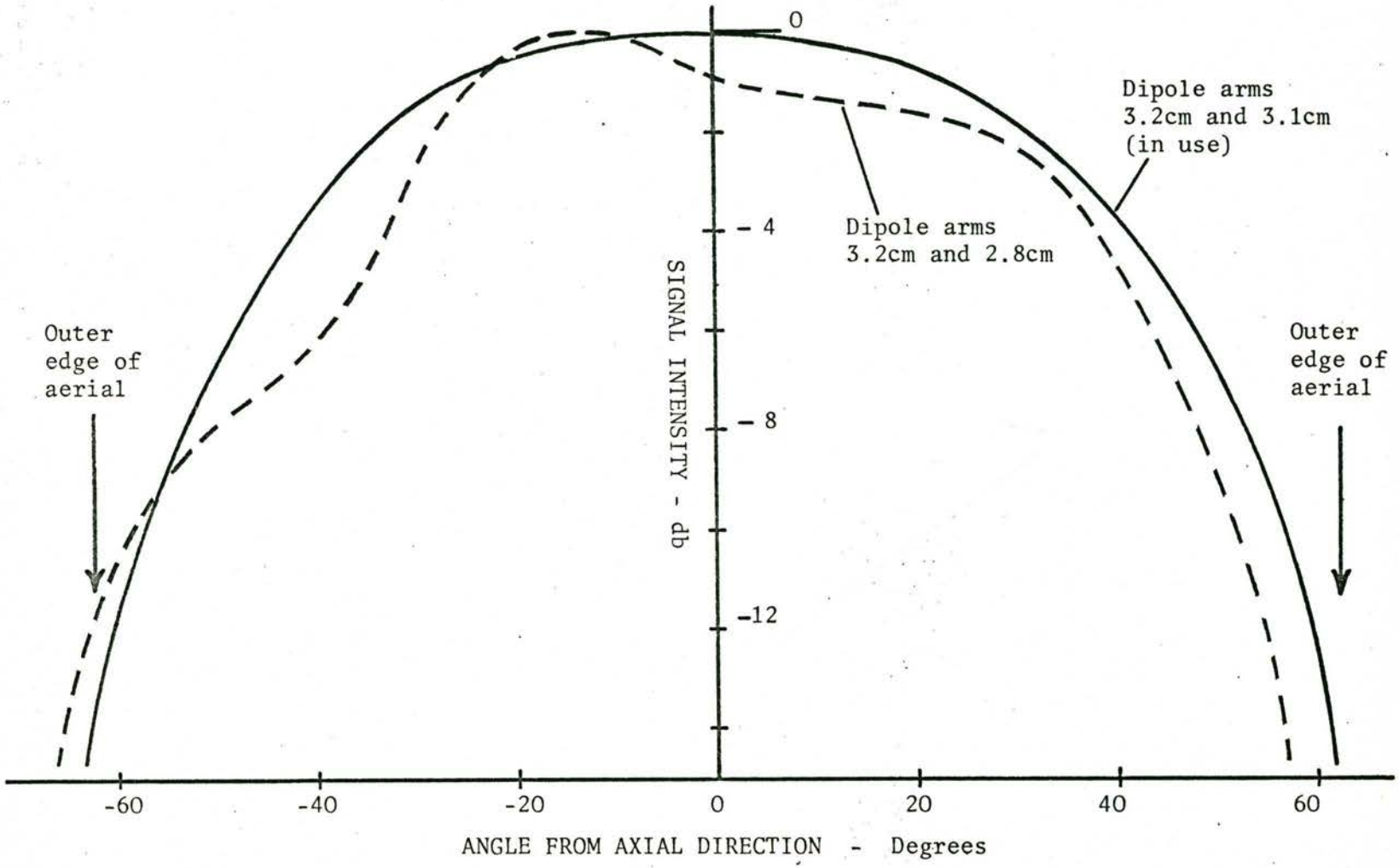

FIGURE 5.10 Radiation pattern of one of the dipole-reflector feeds used on the large aerials showing the effect of varying one of the dipole arms.

5.11 Adjustment of the Antenna Position

Antenna position and orientation

The new antennae are positioned over points defined by the survey described in Section 4.6. With the antennae set at zero hour-angle the tower position was adjusted so that both the hour-angle axis and the declination axis pass vertically over the survey point.

The antennae are oriented so that their polar axes are parallel to the earth's axis with an accuracy better than ± 2 min. of arc. This was done in two operations. First, a special $33^{\circ}51'.5$ angle jig and a level were used to set the axes at the right inclination. Secondly, two theodolites on a north-south line were used to sight at the same time on both ends of the hour-angle axes and to ensure that the azimuth directions were north-south.

Checks were made on the alignment of the polar axes by observing radio source positions, in particular that of the sun, at an hour-angle of zero and ± 4 hours. For a source near $0^{\circ}\delta$, incorrect alignment shows up as small declination errors at the extremes of hour-angle when compared with the meridian plane direction:

(i) If these errors are of the same sign, the polar axis has an error in the latitude setting.

(ii) If the errors are of opposite sign, the polar axis has an error in the azimuth setting.

Care was necessary to ensure the errors being corrected were not caused by other effects such as reflector and feed pole deflections.

Pointing of the new antennae

The pointing, or alignment of the scales with the radio axis, was carried out (1) by survey methods and (2) by observations of the positions of several strong radio sources.

(1) Survey methods

With the aerial pointing roughly in the zenith direction, a theodolite was mounted above the vertex of the reflector. The theodolite was adjusted so

that its 'normally vertical' axis was perpendicular to a plane containing the outer ring. The aerial direction was then 'moved' to level the theodolite 'bubble'. The scales were set to 0^{o} hour-angle and $-33^{o}51'.5$ declination. With the reflector pointing in the zenith direction, the feed pole was installed and set vertical, again using a theodolite, this time from outside the reflector. Declination scale settings were checked using the method described by Payten (1967).

(2) Radio source methods

For pointing, using radio source observations, the receiver was converted to the total power configuration described in Section 8.2.3. In the arrangement used here, a low noise RF power switch was also placed before the mixer unit in order to stabilize the observations against receiver gain variations. The wide system bandwidth as well as both sidebands were used to increase the system sensitivity.

With the aerial tracking the sun according to the scale positions, the feed pole position and direction were adjusted to maximize the receiver response.

Two measurements showed the reflector to be very close to the theoretical shape. A measurement of the focal length of the antenna showed that the focal position lay between the dipole and its ground plane, being, as expected, closer to the ground plane. The position of the shadow thrown by this circular ground plane on the antenna vertex served as a check on the symmetry of the radio reflecting surface. 6 min. of arc deviation of the radio axis from the theoretical axis is equivalent to 1 cm of movement of the shadow.

Drift scans of sources at several declinations were taken at many hour-angle positions. Reduction of these scans provided numerous scale calibration points. The sources used were the sun, Taurus, Virgo, Orion, Hydra, 3C273, Sagittarius and Centaurus. These sources are all smaller than the primary beamwidth.

5.12 Conclusion

The successful design for a low cost 45 foot diameter antenna has been described in this Chapter. The design was constrained by a number of requirements imposed by the present compound interferometer system. However the antenna evolved is well suited to use either as a single moderately sized antenna or as a 'building block' for future large arrays.*

In 1966, one of the antennae was used separately by members of the School of Electrical Engineering for scaled aerial measurements (Yates et al., 1967 and Yates, 1967).

The University of Tasmania also has one of these antennae under construction for use in galactic and solar work.

The design was carried out by the author under the guidance of Mr. K.R. McAlister of the C.S.I.R.O. Radiophysics Laboratory, Sydney. Considerable experience in lightweight structure was derived from the 85 MHz aerials designed for the Culgoora Heliograph (McAlister and Labrum, 1967).

Where possible commercial firms were contracted to fabricate sections of the antenna structure. The assembly of these sections at the field station was carried out by the author with the assistance of Workshop and Field Station personnel, in particular, Messrs. J. Jacobs, R. Shepherd and R. Taplin.

---

*Drake (1964) has estimated the optimum size of the antennae in an array at between 38 and 76 feet diameter. This is based on the relative costs of antenna and receiver. As low noise receivers become more readily available these sizes will be reduced.
For much the same reason the Soviet Union has been constructing deep space tracking antennae as arrays of 50 foot aerials rather than as single large antennae (Lovell, 1963).

CHAPTER 6

Page

PERFORMANCE OF THE TELESCOPE

CHAPTER 6: PERFORMANCE OF THE TELESCOPE

6.1 The Main Response

For the telescope configurations outlined in Chapter 4, the theoretical fan-beam responses are calculated from equations 2.18 and 2.20. M and N are the numbers of large and small antennae (2 and 32 respectively for each grating array). The harmonic spacing, d, is 40 feet, being equivalent to 57.9 wavelengths at 1415 MHz and 28.3 wavelengths at 692.5 MHz. This spacing creates grating lobe responses which, in the zenith direction, are separated by 1^{o}.

A_1 and A_2 are the effective areas of the small and large aerials respectively. The directivity of these aerials, considered in Section 6.3.1, creates an envelope over the main response of about 1^{o} half-power width. This limits the fan beam response to a half-power length of 1^{o}.

The lowest and highest spatial frequencies measured by each array are 60 feet and 2580 feet respectively. The east-west array has an additional spacing of 2640 feet between the large aerials but this is not used in forming the array response.

6.1.1 Uniform Aperture Illumination

When the signals from the individual aerials are all weighted equally, the main fan-beam responses are given by:

East-West System

$$\underset{\sim}{A}(\ell) = 2\left(64A_1A_2\right)^{\frac{1}{2}}\left(\frac{\sin 32\pi\ell d}{32\sin\pi\ell d} \cdot \cos 66\pi\ell d \cdot \exp(j32\pi\ell d)\right) \tag{6.1}$$

giving

$$A_c = 16\left(A_1A_2\right)^{\frac{1}{2}}\left(\frac{\sin 130\pi\ell d}{128\sin\pi\ell d} - \frac{2\cos\pi\ell d}{128}\right) \tag{6.2}$$

and

$$A_s = 16\left(A_1A_2\right)^{\frac{1}{2}}\left(\frac{\sin^2 32\pi\ell d}{32\sin\pi\ell d} \cdot \cos 66\pi\ell d\right) \tag{6.3}$$

North-South System

$$\underset{\sim}{A}(\ell) = 2\left(64A_1A_2\right)^{\frac{1}{2}}\left(\frac{\sin 32\pi\ell d}{32\sin\pi\ell d} \cdot \cos 32\pi\ell d \cdot \exp(j66\pi\ell d)\right) \tag{6.4}$$

giving

$$A_c = 16\left(A_1A_2\right)^{\frac{1}{2}}\left(\frac{\sin 130\pi\ell d}{128\sin\pi\ell d} - \frac{2\cos\pi\ell d}{128}\right) \tag{6.5}$$

and

$$A_s = 16\left(A_1A_2\right)^{\frac{1}{2}}\left(\frac{\sin 64\pi\ell d}{64\sin\pi\ell d} \cdot \sin 66\pi\ell d\right) \tag{6.6}$$

These two arrays have identical cosine responses. At 1415 MHz, the half power beamwidth is 33½ sec. of arc by 1 degree. The missing 20 foot component creates a slowly varying negative baseline with a magnitude of about 1.5% of the main response. The first sidelobes are 22% of the main response measured below this negative baseline. Fig. 6.1 gives the normalized cosine response for both arrays assuming omnidirectional aerials.

The sine responses of the two arrays are different due to the dissimilar configurations. As indicated in Chapter 4, the sine response of the east-west array is preferable to that of the north-south array since it does not vary as quickly over the region of the main response. The sine response shapes of the east-west and north-south arrays are illustrated in Figs. 6.2 and 2.7 respectively.

6.1.2 Tapered Aperture Illumination

For most observations, it is desirable to reduce the 22% sidelobes created by uniformly weighting the aerials. This can be done either experimentally, by tapering the aperture illumination in the receiver, or during data processing by (i) tapering the separately measured spatial components or (ii) convolving the observations with a suitable correction function. The object in both cases is to attenuate the higher spatial frequencies thereby reducing the sharp cut-off in the spatial band-pass (array function).

Hand correction

For many years observations have been corrected by hand. However convolution in this manner is tedious for all except a few simple functions. Most of these 'popular' hand-convolving functions are of the impulse form where the labour involved is considerably reduced (Labrum et al, 1964; Christiansen and Högbom, 1968). Hand tapering of this form has been used on the solar observations with the present fan beam telescope (Section 9.2.3).

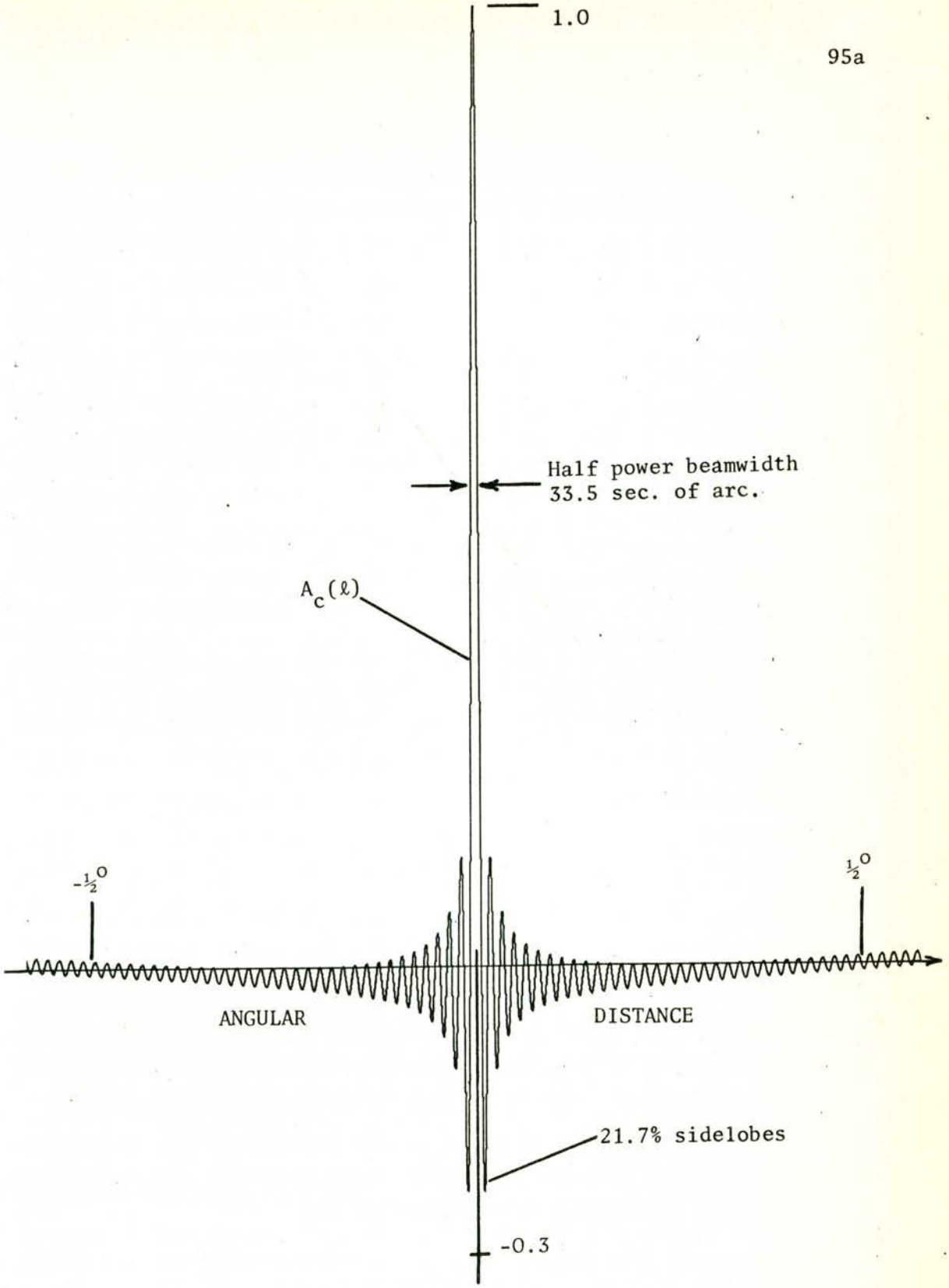

FIGURE 6.1 The normalized fan beam cosine response for both the east-west and north-south compound interferometers in the zenith direction with uniform aperture illumination and omnidirectional aerials.

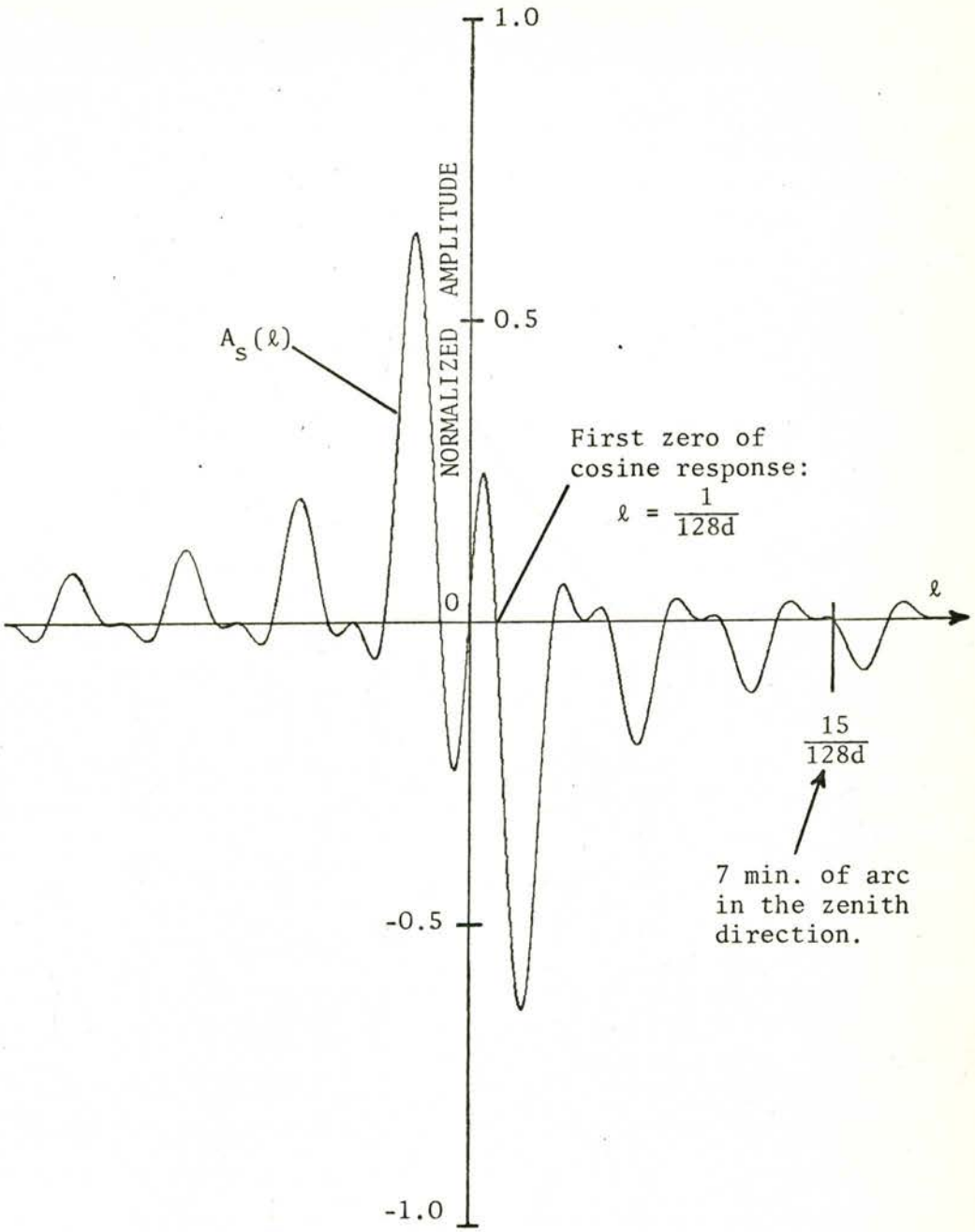

FIGURE 6.2 The sine response of the east-west compound grating interferometer with uniform aperture illumination and omnidirectional aerials.

Receiver taper

If the output from each small aerial is returned to the receiving hut and correlated separately with each large aerial, then all the Fourier components are measured individually. In this case, a taper of any shape can be applied easily by controlling the magnitude of each component before summation. This method of tapering is possible with the final receiver system.

Optimum taper

To determine the optimum taper, a survey was undertaken of the different types of taper frequently used on both linear and circular apertures. For each taper the levels of the first and second sidelobes were compared with the beamwidth.

Most aperture tapers fit the equation:

$$(BW) = (0.1)\left[\{^{\text{1st S/L}}_{\text{in db}}\} + 4\right] \qquad (6.7)$$

One linear aperture exception is the $(\text{cosine})^2$-on-10 db-pedestal taper. This taper broadens the fan beam to 40 sec. of arc and reduces the first sidelobe to 3% of the main response. The theoretical cosine and sine responses of the east-west array, with this taper, are shown in Fig. 6.3. In this figure, the element envelope (Section 6.3.1) has also been applied, resulting in a reduction of the distant sidelobe and grating sidelobe magnitudes.

A second linear aperture exception is the Hamming taper which is a $(\text{cosine})^2$-on-a-very-low-pedestal. This taper increases the beamwidth to 50 sec. of arc and reduces the first sidelobe to less than 1%. Both of these tapers are characterized by a comparatively high sidelobe-reduction to beamwidth-increase ratio.

6.1.3 Pencil Beam Response

The final pencil beam response of the telescope is calculated by taking the Fourier transform of the synthesized effective aperture. The shapes of these apertures depend considerably upon the source declination

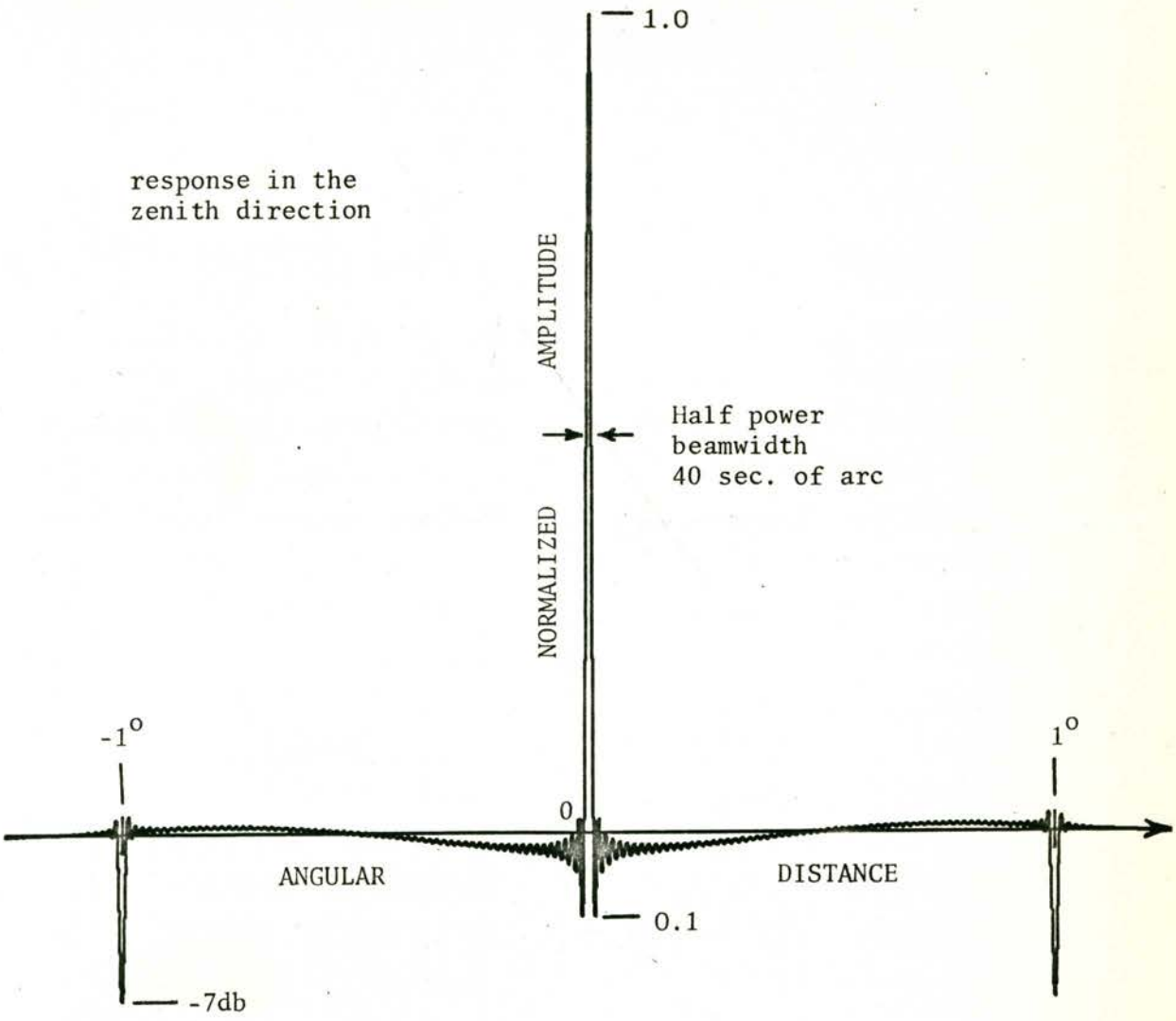

FIGURE 6.3a The theoretical cosine response of both east-west and north-south compound grating interferometers. A (cosine) -on-a-10db-pedestal taper has been applied to the array aperture; the element directivity envelope used is that of Fig. 6.5.

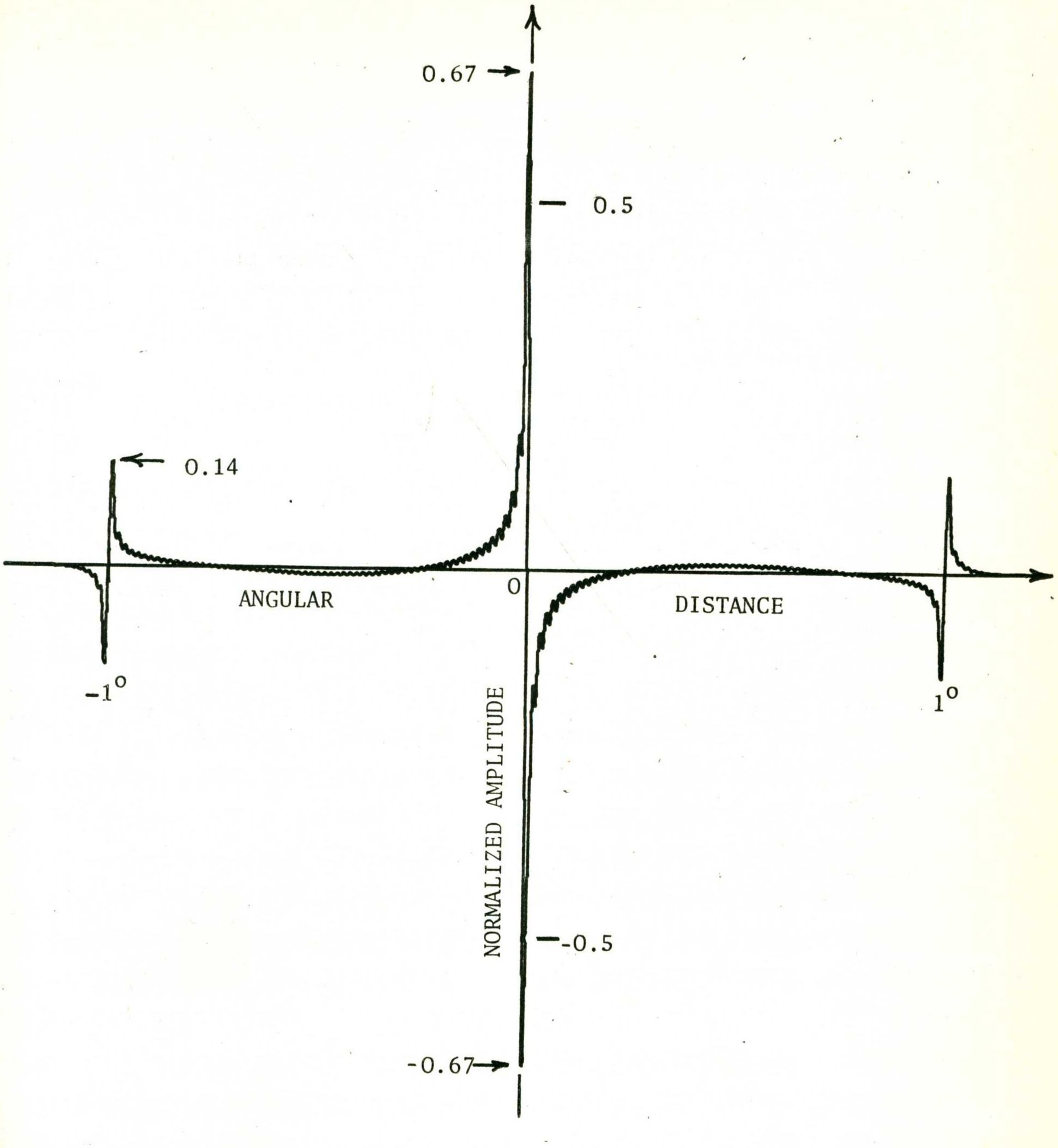

FIGURE 6.3b The theoretical sine response of the north-south compound grating interferometer. A (cosine) -on-a-pedestal taper has been applied to the array aperture; the element directivity envelope used is that of Fig. 6.5.

and were considered in Section 3.3.5.

For a declination of -60^{o}, the synthesized aperture is nearly circular and as such the pencil beam response is almost symmetrical. With uniform weighting over the synthesized aperture, the half power beam width is 38½ sec. of arc and the first sidelobe level is 13% of the main beam.

The two dimensional aperture taper used on these synthesized observations will depend upon the information required. In some cases the sidelobe level produced by uniform weighting will be too high and a taper will be necessary to reduce it. This taper will cause a broadening of the beamwidth. However, the extreme case - a reduction to 3% sidelobe level - causes only a broadening to 43 sec. of arc.

In the final system the observations are stored on magnetic tape in the form of spatial component samples so that the synthesis can be carried out several times if necessary, each time using a different aperture taper.

6.2 The Grating-Lobe Positions

The multiple responses of a grating telescope, aligned along the X axis, occur at intervals defined by

$$\ell = \frac{n}{d} \qquad \text{(Section 2.1.3)}$$

From this expression the grating lobe angular separation ($\Delta\alpha$) is given by:

$$\Delta\alpha \simeq \frac{1}{(d \sin\alpha)} \qquad (6.8)$$

provided $\alpha >> \Delta\alpha$. The expression ($d \sin\alpha$) is the projected harmonic separation and is proportional to the projected array length, ℓ, derived in Chapter 3.

This projected separation, and hence the grating lobe separation, changes throughout the observing period for all declinations except $\pm 90^{o}$. Combination of the lobe separation and the rotation angle, ψ, gives

Fig. 6.4, which shows the grating lobe patterns from a strong point source at the centre of the diagram.

With a harmonic distance of 40 feet and a frequency of 1415 MHz, the minimum angular separation of lobes is almost exactly 1^{o}. This minimum separation occurs when either array is observing in the zenith direction. For Fig. 6.4, the north-south and east-west array have been combined with the element sky coverage limits.

6.3 Image Plane Envelopes

6.3.1 Element Directivity Envelope

The element directivity or zero-separation envelope determines the attenuation over the image plane occasioned by the directivity of the individual aerials. Fig. 6.5 shows the envelope for the present configuration.

Total power scans of the sun, using the aerials separately, were combined to produce this figure. In the case of the 45 foot diameter aerial, the angular diameter of the sun produced a slight amount of beam broadening (~3%) so that the actual envelope is slightly narrower than in Fig. 6.5.

This envelope defines the image plane of the two dimensional synthesis. For the present telescope this has been arbitrarily chosen as the beam-width of the large aerials (~1 degree diameter). The main pencil beam response to sources at the edge of this region is then 1.5 db below the response to sources at the centre of the region. The final choice of size of the image plane depends upon the type of observation being carried out. If it is necessary to avoid the grating lobe effects, the image will be reduced to 0.5^{o} diameter. For other observations it will be possible to use a 2 degree diameter region. In this case the edge attenuation is 7 db.

The attenuation of the grating lobes created by a source at the image plane centre point is $\geq$ 7 db. This is due principally to the directivity of the large aerials. For a picture point at the 1^{o} image

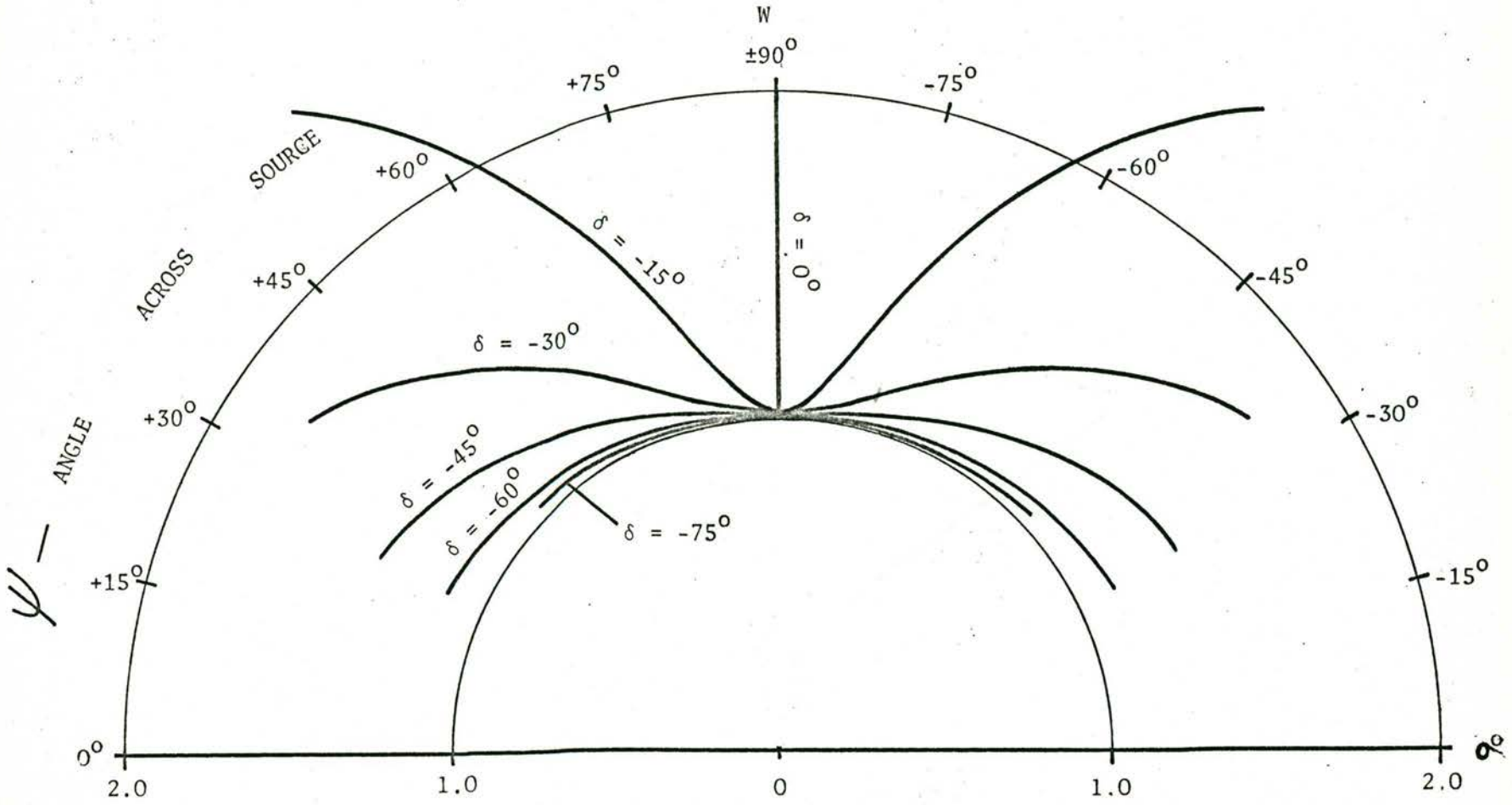

ANGULAR DISTANCE OF GRATING RESPONSE FROM SOURCE AT CENTRE

(Angular distance units are degrees for a harmonic spacing of $\frac{180}{\pi}$ wavelength)

FIGURE 6.4a East-West Array Grating Lobe Patterns Created by Sources at Various Declinations. The patterns are symmetrical; aerial limits have been applied.

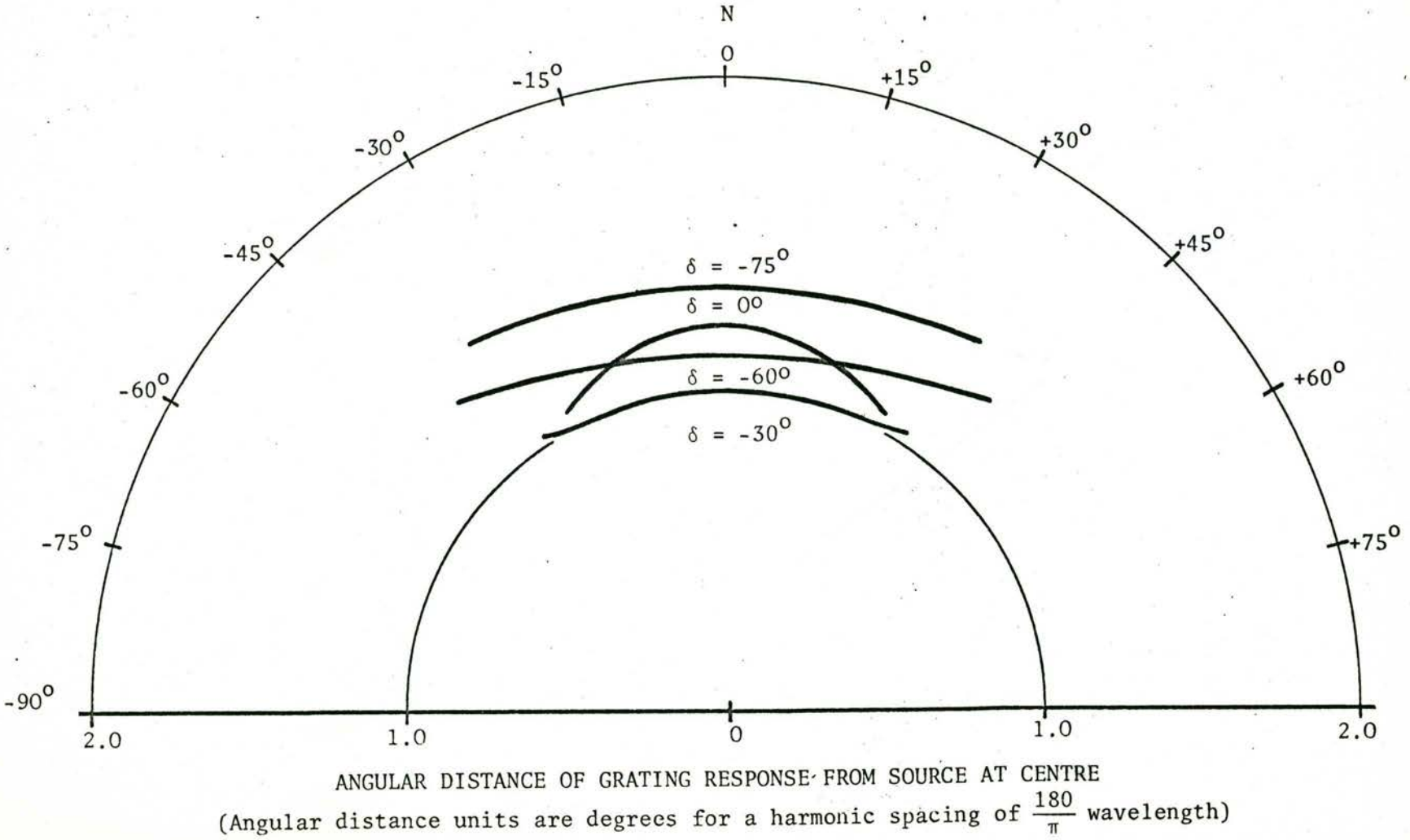

ANGULAR DISTANCE OF GRATING RESPONSE FROM SOURCE AT CENTRE

(Angular distance units are degrees for a harmonic spacing of $\frac{180}{\pi}$ wavelength)

FIGURE 6.4b North-South Array Grating Lobe Patterns created by sources at various declinations
The patterns are symmetrical; aerial limits have been applied.

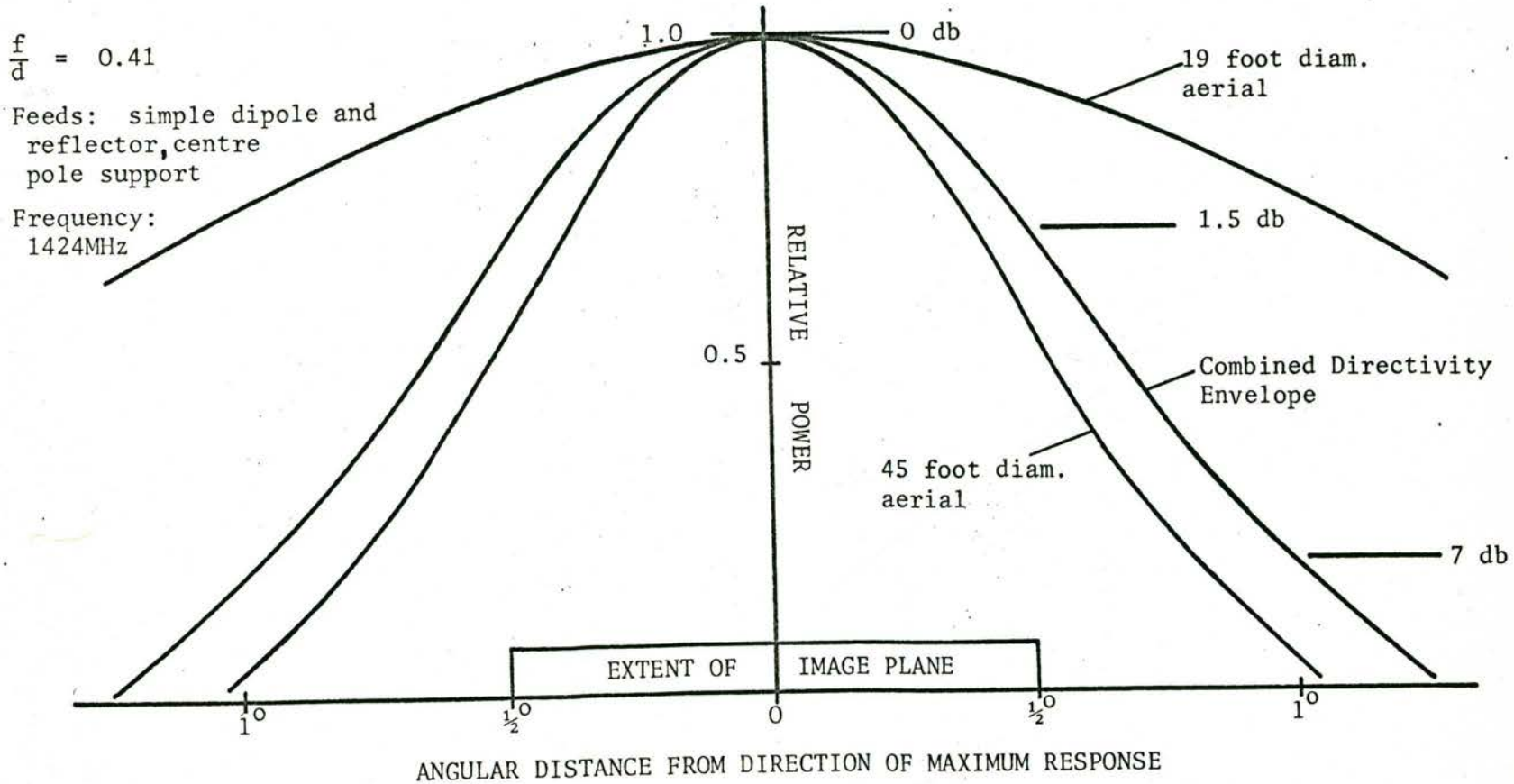

FIGURE 6.5 The Element Directivity Envelope and the Individual Aerial Polar Diagrams for the Compound Grating Interferometers at Fleurs

plane edge, the largest grating lobe is equal to the main response.

The envelope response is >13 db below the centre for ang. distances > 1.25^{o} and drops to > 25 db for distances > $3\frac{1}{2}^{o}$ where the small aerial response also becomes low.

6.3.2 Bandwidth Envelope

Each spatial frequency has a correlation-loss envelope centred about the direction of zero path difference and lying in the direction of high resolution. For a given bandwidth the angular width of this envelope is inversely proportional to the aerial separation. Thus the grating array response has an envelope which is the sum of these separate envelopes.

If the bandwidth, B, is rectangular (which it will tend towards in the final system), the individual envelopes are proportional to sinc(nBt) where n is the spatial harmonic number and t is the time difference of the two signals. The array bandwidth envelope then approximates a $\text{sinc}^2\left(\frac{nBt}{2}\right)$ shape.

With the full 8 MHz bandwidth planned for the final system, the half power angular width of this envelope is about 5^{o}. At the 1^{o} image plane edge the correlation loss is about 3% and for angular distances $>5^{o}$ from the image plane centre the attenuation is >13 db.

With the present pass band of 400 KHz, the bandwidth envelope is only about 3 db down at 60^{o} from the meridian. This removes the necessity of compensating for the signal path length difference in this case.

6.3.3 Rotation Envelope

Section 3.2.5 considered briefly the attenuation envelope imposed over each picture point during the derivation of a two-dimensional brightness distribution from one-dimensional observations. This envelope is important as it reduces the magnitude of the distant sidelobes after synthesis.

The new telescope measures 64 spatial components. The attenuation of the rotation envelope is computed by a summation of $J_o(2\pi \ell id)$ over these 64 spatial components. (i is an integer and in the present

UNIVERSITY OF SYDNEY LIBRARY

configuration {i = 2m + 1} where m is an integer such that $1 \leq m \leq 64$.) This summation has been carried out for the lower six spatial components of the array and the attenuation at the nearest grating lobe position in this case was 8 db. This is already a significant reduction. Computation for the full 64 components was hampered by the lack of tables of Bessel functions extending to high values of the argument. An estimate based on incident power considerations indicates a reduction, with the full array, of >13 db at the grating lobe positions.

6.4 Sensitivity

Estimates of the system sensitivity can be made using equations 2.32, 2.33 and 3.9. To make these calculations, details of the receiver system are required. Chapters 7 and 8 give these details for the present system but assumptions are necessary in the case of the final system.

1. Sensitivity of the final receiver system after two dimensional synthesis:

$T_1 = T_2 = 600^{\circ}K$	$(A_1A_2)^{\frac{1}{2}} = 35$ sq.m
$\zeta_1 = \zeta_2 = 0.15$	B = 8 MHz
t = 12 to 18 hours	R = 1
N = 32 aerials	M = 2 aerials

A sine-cosine phase-switched receiver (R = 1) is used together with lobestopping and delay compensation.

These figures give a point source sensitivity of 2 or $3.10^{-28}Wm^{-2}Hz^{-1}$ (assuming a detection ratio of 5). If low noise receivers ($T_2 = 100^{\circ}K$) are used on the four large aerials and ζ is reduced to <0.1, the minimum flux which can be detected reliably will be $<1.10^{-28}Wm^{-2}Hz^{-1}$.

2. The instantaneous fan beam has a much lower sensitivity due to the lower value of time constant necessary. In the final system, provided that lobe-stopping is applied, a variable time constant can be used up to a maximum value of about 3 minutes. However, for fast varying sources on the sun, a time constant of about ¼ sec. is necessary, giving a sensitivity of $8.10^{-27}Wm^{-2}Hz^{-1}$.

3. The present receiver system differs from the final system principally in the following parameters:

$T_1 = T_2 = 700^0K$ B = 0.4 MHz

$\zeta_1 = 0.78$ and $\zeta_2 = 0.28$ R = 2

t = ½ sec.

In this case the fan beam sensitivity is 1 or $2.10^{-25}Wm^{-2}Hz^{-1}$, the main drop from the above (2) value being caused by the smaller bandwidth.

4. With the two large aerials as an interferometer, as described in Chapter 9, the sensitivity is $4.10^{-25}Wm^{-2}Hz^{-1}$, with B = 2.2 MHz and t = 32 sec. This sensitivity was achieved in observations of the quasar 3C273.

CHAPTER 7

THE RECEIVER SYSTEM : PART I

7.1 The Receiver System Outline

The basic system in use at present is illustrated in the block diagram of Fig. 7.1 and in greater detail in Figs. 7.2 and 8.1. The single correlator is fed on one side by the output from the thirty-two aerial grating and on the other side by the output from the long baseline two aerial interferometer.

The output of the thirty-two aerial grating is formed as follows: The signals from sixteen aerials (east arm) are added at signal frequency (1424 MHz), filtered to remove the image frequency and then converted to an intermediate frequency, (I.F.)*, of 30 MHz. This I.F. is amplified and returned to the central receiving hut where it is added to the I.F. signal from the other sixteen aerials (west arm) similarly processed. This gives, at I.F., the voltage pattern of an instantaneous fan beam which is stationary relative to the earth, and about 1.8 min. of arc wide.

The signal from each 45 foot aerial is image-filtered, converted to 30 MHz I.F. and amplified at the antenna before being returned to the central hut. At the centre it is added to the I.F. signal from the other 45 foot aerial.

For observations away from the meridian with a wide receiver bandwidth, delay lines (extra lengths of I.F. cable) are added to each of the four I.F. signals after they enter the central hut. This compensates for the differing times of arrival of the R.F. signal* at various parts of the linear antenna.

In the main receiver following the delay lines, the 30 MHz I.F. signals are converted to 5.5 MHz. This enables easy phase adjustment of the signals through phase control of the 35.5 MHz second-local-

---

*In this and the following chapter, intermediate frequency (≈30 MHz) has frequently been abbreviated to I.F. and radio frequency (≈1400 MHz) to R.F.

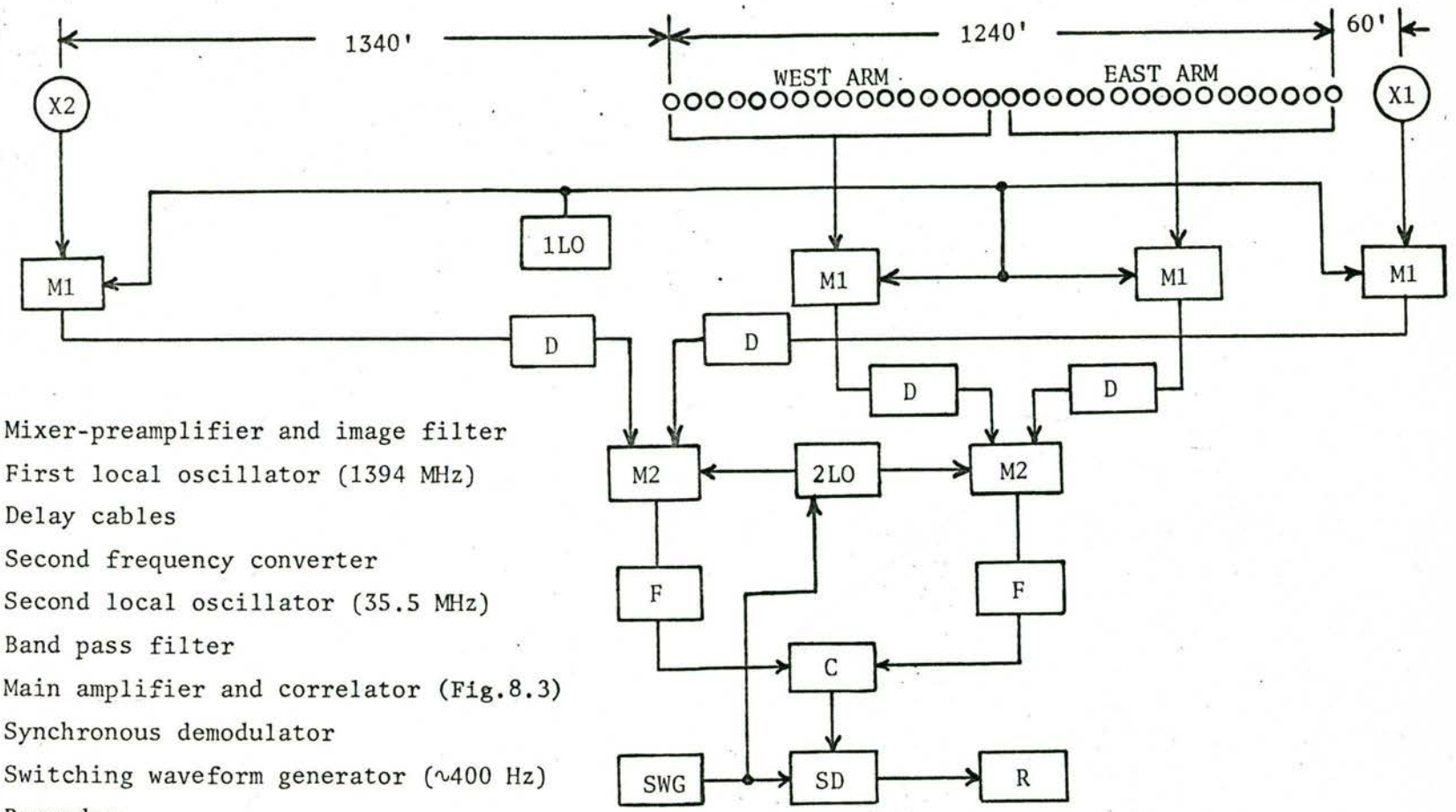

M1 Mixer-preamplifier and image filter
1LO First local oscillator (1394 MHz)
D Delay cables
M2 Second frequency converter
2LO Second local oscillator (35.5 MHz)
F Band pass filter
C Main amplifier and correlator (Fig.8.3)
SD Synchronous demodulator
SWG Switching waveform generator (~400 Hz)
R Recorder

FIGURE 7.1 Schematic diagram of the present receiver system for the compound grating interferometer.

oscillator (2.L.O.).* A calibrated digital phase controller is inserted in one second-local-oscillator line. Using this, the relative phase of the two signals to be correlated can be adjusted to within $\pm 1^{o}$ electrical. The phase and gain of each of the four signal inputs can be trimmed (60^{o} and 3 db range) by controls on these second converters. One of the converters also has its second-local-oscillator phase-switched in half wavelength steps at approximately 400 Hz in order to code the correlated signal for detection by the synchronous-demodulator unit.

Band-pass filters are inserted in the signal lines following the converter units. These define the width of the passband when it needs to be reduced. This is necessary when the observing direction is away from the zenith and no delay lines are in use. (A narrow bandwidth broadens the correlation envelope.)

The system operates on a single sideband (upper) at 1424 MHz. With the simple delay system used in this early stage, the maximum bandwidth of the signal is 2.2 MHz, determined in the final correlating stage. For solar observations away from the meridian, this bandwidth is reduced to 400 KHz.

The local (or heterodyne) oscillator signals (at 1394 MHz), which are necessary for the first frequency conversion from 1424 MHz to 30 MHz, are distributed with phase coherence to the six mixers (including two on the north-south grating) from a common oscillator at the geometric centre of the east-west array. A special method of distribution, described in Section 7.2.6, involves the combination of cables and open-wire transmission lines. This was developed by the writer in order to make the operation of the receiver system insensitive to the daily temperature variations.

---

*The second-local-oscillator (35.5 MHz), referred to occasionally by 2.L.O., is distinct from the main local-oscillator, termed L.O., at a frequency of 1394 MHz.

Apart from the first local oscillator unit, the receiver system is entirely solid state. This contributes greatly to its present successful operation.

Observations with the system include the sun during the day and radio sources at night. For radio sources, the highest sensitivity possible is desirable. The strongest visible radio source (Taurus) creates a mixer input of about $16^{o}K$ for each 45 foot aerial and about $45^{o}K$ for each 16 aerial grating. The quiet sun creates input temperatures of about $12,500^{o}K$ and $5,400^{o}K$ respectively (assuming a flux density of $7.10^{-21}Wm^{-2}Hz^{-1}$). With a large solar outburst these input temperatures can rise to $180,000^{o}K$. *

From the above it is obvious that the receiver must have a large dynamic range. The gain of the main receiver in the hut can be varied by the use of attenuator pads thus relaxing somewhat its dynamic range requirements. However this cannot be done conveniently with the distributed mixer-preamplifier modules so that a linearity better than 5% is desirable up to about 50 μv input.

In the final receiver system each mixer-preamplifier will handle only the signal from one aerial and each correlator channel will handle only one interferometer fringe pattern. Thus, dynamic range requirements will not be so severe. Instead, the emphasis is shifted to long term output stability.

---

*(i) With a bandwidth of 2.2 MHz and an input impedance of 50Ω this input temperature is equivalent to an rms input of about 16 μv.

(ii) The average receiver noise temperature is $700^{o}K$.

7.2 The Radio Frequency System

7.2.1 Introduction

The radio frequency (R.F.) system used in Stage 1 (the present form of operation) is illustrated in the block diagram of Fig. 7.2

The thirty-two aerials of the existing east-west grating are divided into two groups of sixteen. The outputs of the aerials in each group are added together in phase using an open-wire branched feeder system at the signal frequency (1424 MHz). At the final branch junctions, in the centre of the east and west arms, the signals are fed into image filters and then into crystal mixers which convert the signals to an intermediate frequency (I.F.) of 30 MHz. The path lengths from all aerials to the mixers are equal and about 100 m long.

Placement of these mixers on each arm, instead of at the grating centre, has two significant advantages: (i) the signal loss in the open-wire lines is reduced by about 4 db and (ii) a method of temperature compensation (Section 7.2.6 and 7.3.2) of the remaining open-wire lines becomes possible, thus improving the phase stability of the system considerably.

The signal dipole on each 45 foot aerial is connected to an image filter and a crystal mixer at the vertex by about six metres of helical membrane coaxial cable. This keeps the signal loss to a minimum. (Cable loss 0.9 db.)

Heterodyne (or local) oscillator power is distributed at 1394 MHz to each crystal mixer unit from an oscillator situated at the geometric centre of the system baseline. Buried low-loss coaxial cables are used for the long runs to each 45 foot aerial. A combination of buried cables and open-wire transmission lines are used in supplying local oscillator power to the mixers on the grating arms.

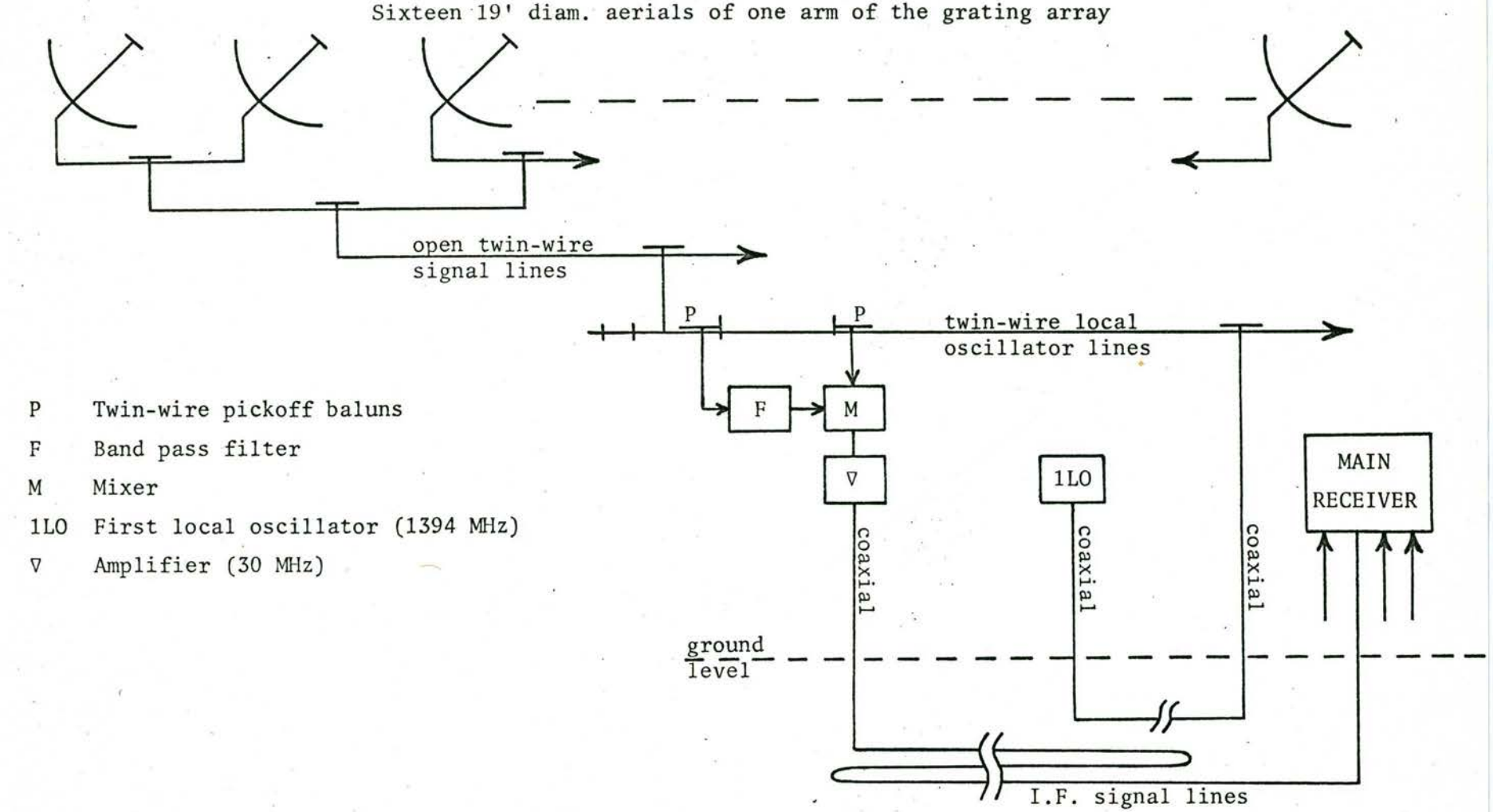

FIGURE 7.2 Schematic diagram of one channel of the radio frequency receiver system.

7.2.2 The small aerial signal lines

In Stage 1 it was impossible to make all channels identical as some of the existing open-wire lines had to be used as signal returns from the small aerials.

These open-wire lines have been described in detail by Christiansen et al (1963). The conductors are hard-drawn copper wires 0.16 inches in diameter and separated 0.75 inches apart by polythene spacers at 6 foot intervals. The spacers are mounted in pairs, $\frac{\lambda}{4}$ apart, in order to minimize reflections. The characteristic impedance with this diameter and spacing ratio is 270 ohms and the measured attenuation at 1424 MHz is about 1 db per 100 feet.

The branching system is made up from five lines, each running the full grating length and separated vertically about 6 inches. The aerial dipoles are connected in pairs to sections of the top line by a vertical twin line. Each section is joined at its midpoint to the line below using T-junctions (described in Section 7.2.6). Pairs of short circuits ($\frac{\lambda}{4}$ apart) block off the unused sections of line at each branch point. This branching continues down to the midpoints of the second bottom line. At these points, a T-junction coupled with a 'balun' feeds the signal (from 16 aerials) into the image filter in front of a mixer.

The length of twin line from each aerial dipole to the image filter is about 100 metres. Together with the five junction points this length causes a signal loss of about 6 db.

7.2.3 The image filters

The present method of tied array operation* precludes the use of the image band automatically generated in the mixer conversion process. Thus image filters are necessary.

---

*'Tied-array' refers to the recombination of the signals from the grating aerials using the R.F. branched-feeder transmission lines. The lengths of these lines are not changed during the course of observations. The result is that the fan beam responses created by the 'block' of aerials are fixed in direction relative to the earth.

Single cavity bandpass image filters, which pass 1424 MHz and reject 1364 MHz, are placed in front of every mixer. These give an image rejection of 19.7 db with a signal loss of 0.5 db. Band width of the filters is 12 MHz. Fig. 7.3 shows the frequency response of one of the filter units.

It is possible to apply image filtering to the signals on only one side of the correlator. This is inadvisable for two reasons:

(i) The image rejection is halved, using the same type of filter,

(ii) The filters apply a phase slope to the signal pass band on only one side of the correlator. Unless matched on the other side, some loss of correlation will occur.

7.2.4 The mixer-preamplifier unit

The performance of a sensitive distributed receiver system depends to a large extent on the initial or 'front-end' units. Cost and availability prohibited the use of any low noise R.F. preamplifiers.

In the present system, the image filter is followed by a conventional balanced mixer using a matched reverse pair of 1N21FMR (Microwave Associates) diodes in a stripline hybrid ring circuit. This hybrid ring was a modified version of the one used by Labrum et al (1963). The diodes are self biased using a local oscillator power of 2 mW (although they operate satisfactorily at ½ mW). All mixers were adjusted for input matching to give an SWR $\leq$ 1.6 (5% reflected power). The line length between image filter and mixer was trimmed to a length which minimized the noise figure of the combination.

The mixer is capacitively coupled to a three stage stagger-damped transistor amplifier designed by Dr. R.H. Frater (1966a). The stages are inductively coupled cascode circuits centred on 30 MHz and using AFZ12 and AF114 transistors. Output impedance of the complete unit is 75 Ω to match the I.F. signal return lines.

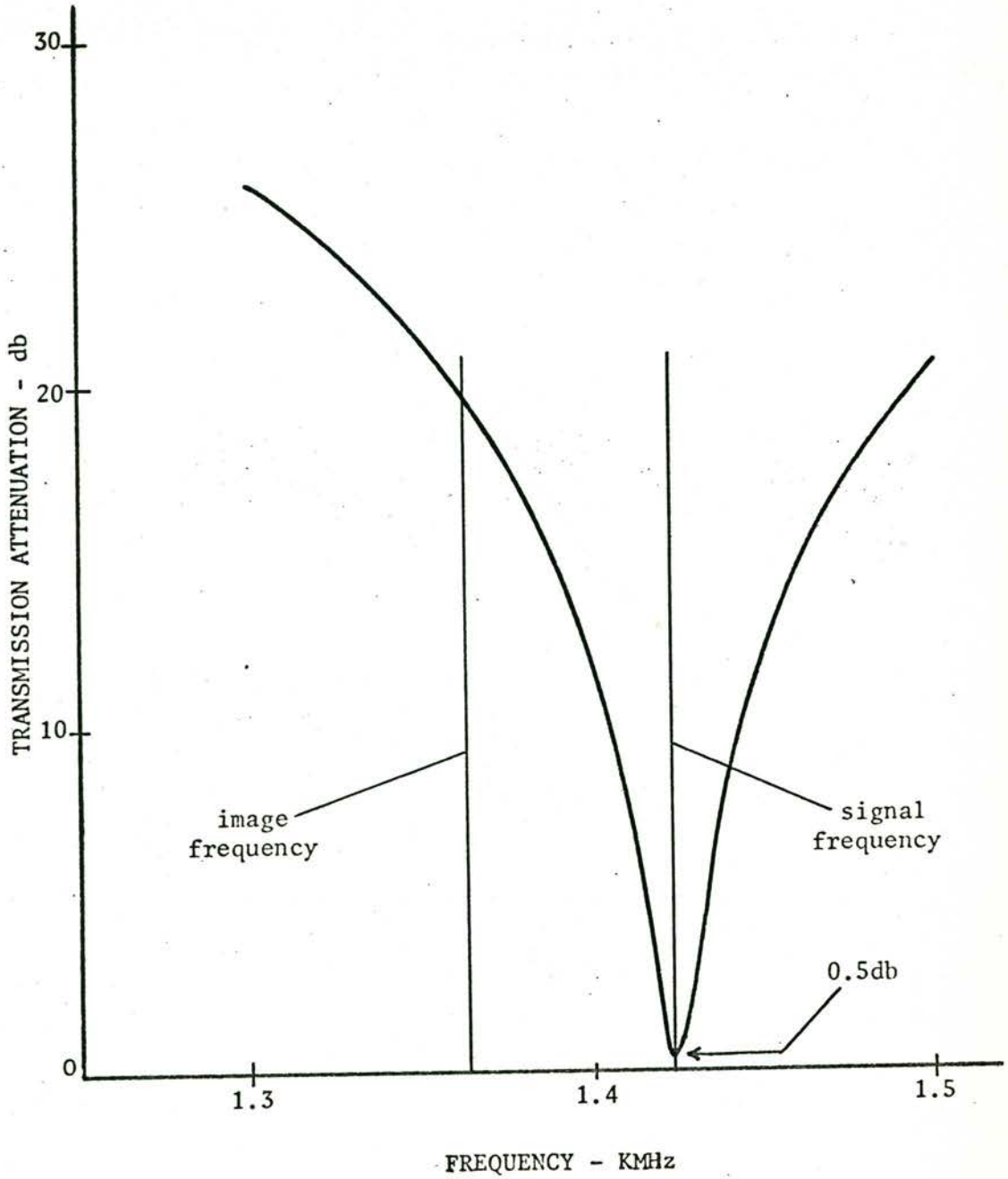

FIGURE 7.3 Image Filter Frequency Response.

A total of eight mixer-preamplifier units were built. Overall gains (including mixer conversion loss) vary between 50 db and 55 db. Each mixer is matched to an image filter so that the combined unit has a bandwidth of over 3 MHz centred on 1424 MHz. However this 3 MHz bandwidth is reduced in the main correlator unit to 2.2 MHz or 400 KHz, to avoid using the edges of the preamplifier pass bands since large and erratic variations are likely to occur from one unit to another.

Noise figures for the mixer-preamplifier units, with image-suppressed operation, vary between 4.7 db (570^{o} K) and 5.5 db (740^{o} K) ±0.5 db. This variation is due partly to the spread of mixer diode properties and partly to the spread of input transistor noise figures.

The mixer and preamplifier are housed in an airtight container (Fig. 7.4) and operate in an open, but shaded environment. Hence during observations they are likely to experience temperature differentials of up to 2^{o}C and gross temperature changes over a day of 20^{o}C. However stability tests on a pair of units showed these conditions cause negligible effects in terms of relative gain (<0.1 db) and phase shift ($<1^{o}$ elec).

Also included in the mixer box is a protective circuit shielding the preamplifier from transients in the ±12 V power supply lines. The supply currents (6 mA at +12 V and 8 mA at -12 V) for each unit can be monitored from the central hut together with the mixer diode currents.

7.2.5 The local oscillator unit

As a temporary measure, pending the completion of a crystal controlled oscillator, a Rohde and Schwarz variable-frequency high-power unit has been used. This is based on a disc-seal triode in tunable coaxial cavities. It can develop an output power up to 25 watts and is tunable over the wide frequency range of 275 MHz to 2750 MHz.

The frequency stability of the unit is inadequate, the variations being principally due to temperature changes. A change from

FIGURE 7.4

One of the Mixer-Preamplifier Units.

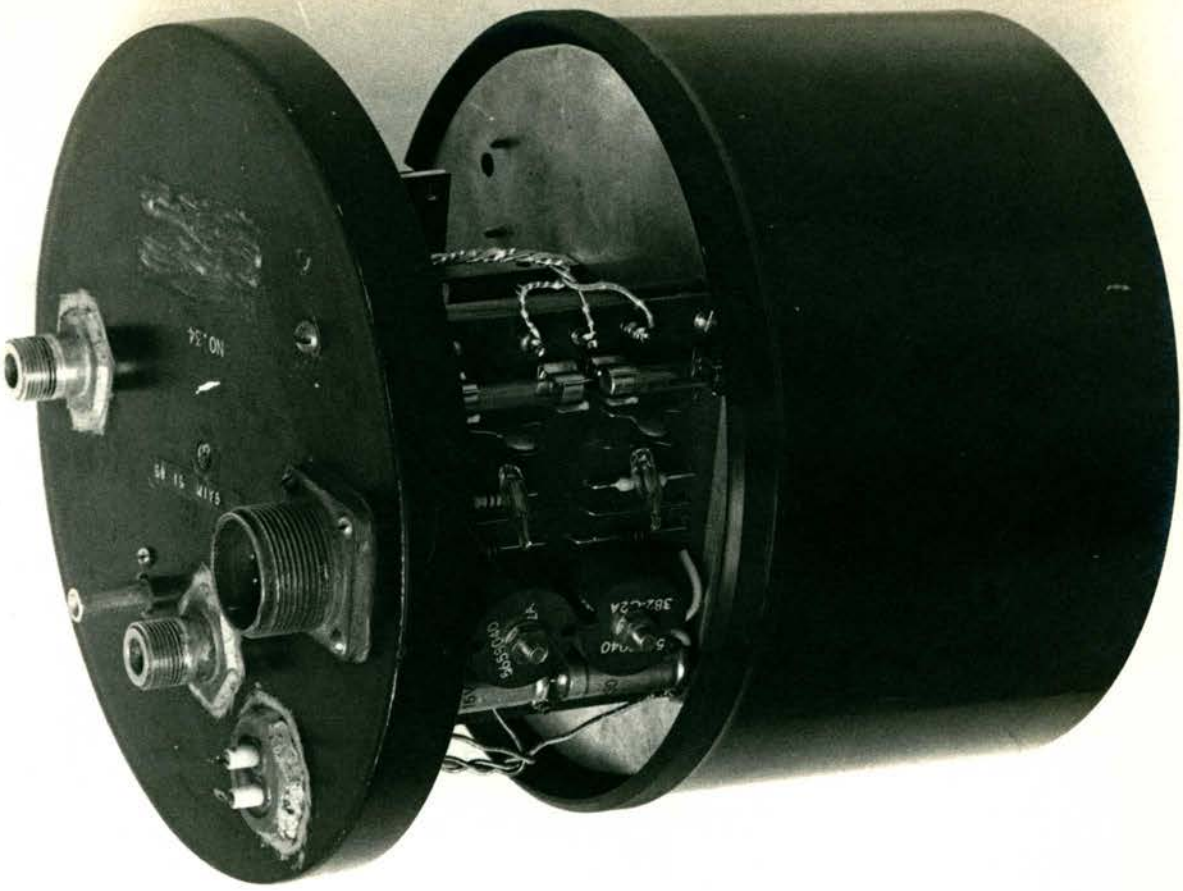

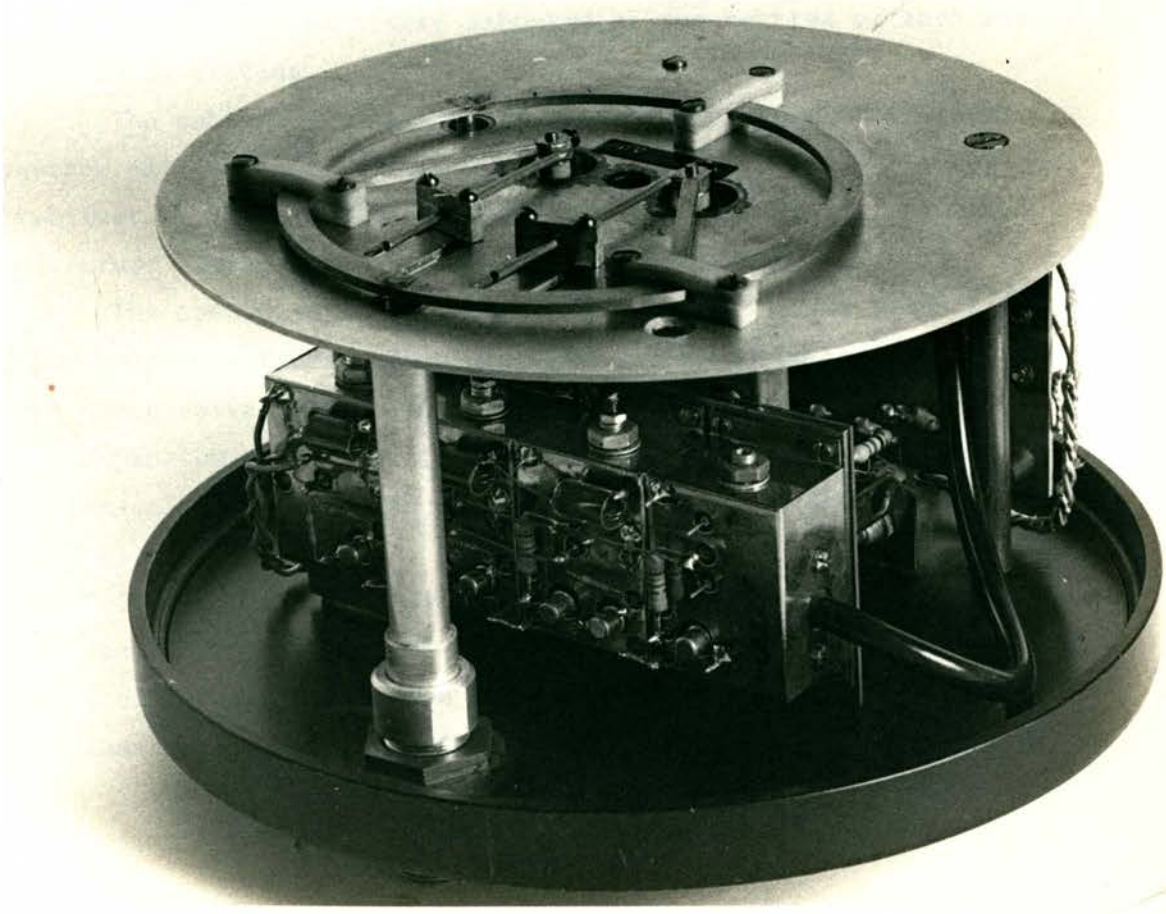

27°C to 32°C in environment produced a 600KHz drop in the output frequency at 1394 MHz. (Temperature and frequency can be monitored and recorded continuously.) In order to reduce these frequency variations it was necessary to stabilize partially the temperature of the hut containing the local oscillator. A remotely controlled vernier frequency adjustment was also added. The result is that the frequency needed to be checked every 15 to 30 minutes while observing. This Rohde and Schwarz unit is now being replaced by a crystal-controlled single-frequency oscillator.

7.2.6 The local oscillator distribution

Fig. 7.5 shows the distribution system in use for the present Stage 1 observations. The heterodyne signal power is split and distributed by a branched feeder system. Buried cables take some of the power to each of the 45 foot aerials. The remaining oscillator power is transmitted by buried cable to the grating centre and then via open-wire lines to the mixers situated at the centres of each arm of the small aerial grating.

The cables used have a low phase-temperature coefficient. Together with the I.F. signal returns, they are buried at a depth of three feet. This reduces considerably the nett and differential temperature variations to which they are subjected.

The open-wire lines in the small aerial signal paths are very temperature sensitive. They are also subjected to the nett daily temperature variations making them a source of large phase error. Their expansion over a day (say 20°C temperature change) amounts to approximately 3.5 cm length change (60° electrical phase change at 1424 MHz).

To eliminate this error and make the system phase stable, this expansion is compensated for by using similar open-wire lines in the local oscillator distribution system to the same mixers. These open-wire lines have similar length (identical number of wavelengths but at

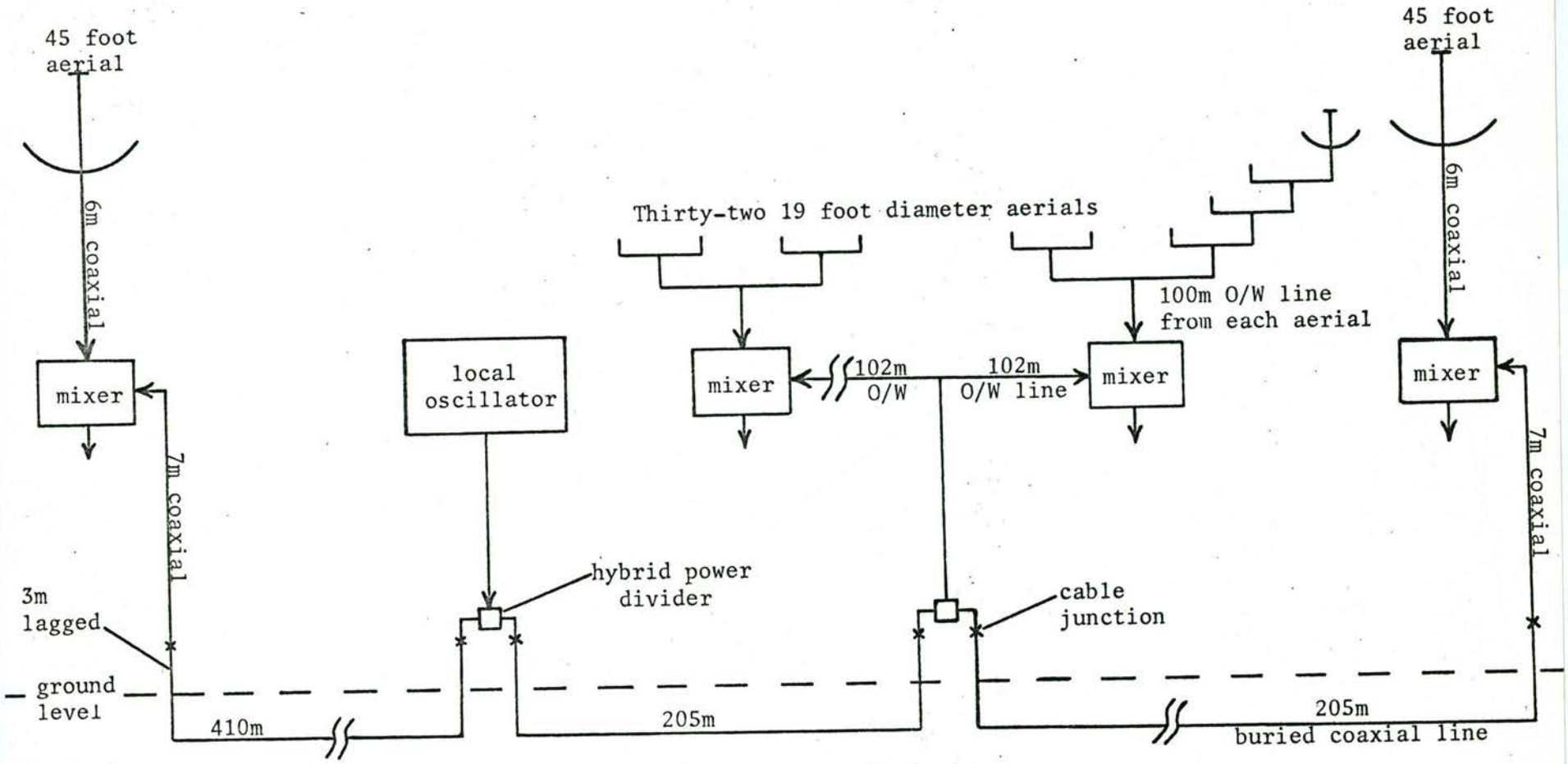

FIGURE 7.5 Local oscillator distribution of the present distributed receiver system.

slightly different frequencies) and are subject to the same temperature variations as the signal open-wire lines. Expansion in the signal side is balanced by expansion in the local oscillator side, thus making each channel temperature-insensitive. The theory of this is given in Section 7.3.2.

In Stage 2 of the system the open-wire branched feeder system will be removed. In its place the buried cable system of Fig. 7.6 will come into operation to distribute local oscillator power to the mixer units sited on each aerial. This branched feeder system has equal length arms ensuring that the relative phase of each signal depends only upon the small differential temperature variation.

Cables

Each mixer unit requires 2 mW of local oscillator signal (1394 MHz) supplied from a common oscillator at the array centre (a distance of up to 1320 feet away). At this frequency cable attenuation is high. To minimize this, efforts were made to choose cable sizes with the lowest attenuation factor.

The pressurized cable used has a helical membrane dielectric and is made by Hackethal, Germany. It was chosen primarily for its relatively low temperature-phase coefficient ($<+1.10^{-5}$ per degree C). Experience gained with this cable type in the Netherlands (Watkinson, 1963) has shown the performance figures to be reliable. The cables of other manufacturers with similar performance figures all proved to be more expensive.

For a given type, cable attenuation is inversely proportional to size and hence cost. The problem becomes one of deciding between a costly cable system, which conserves local oscillator power, and a cheaper cable system which consequently requires a more powerful (and expensive) local oscillator.

The present cable in use is a 7/8" diameter (Hackethal) Flexwell cable. This has an attenuation of only 5.4 db per 100 m at 1394 MHz. Even so, a local oscillator power of about 3 watts is necessary.

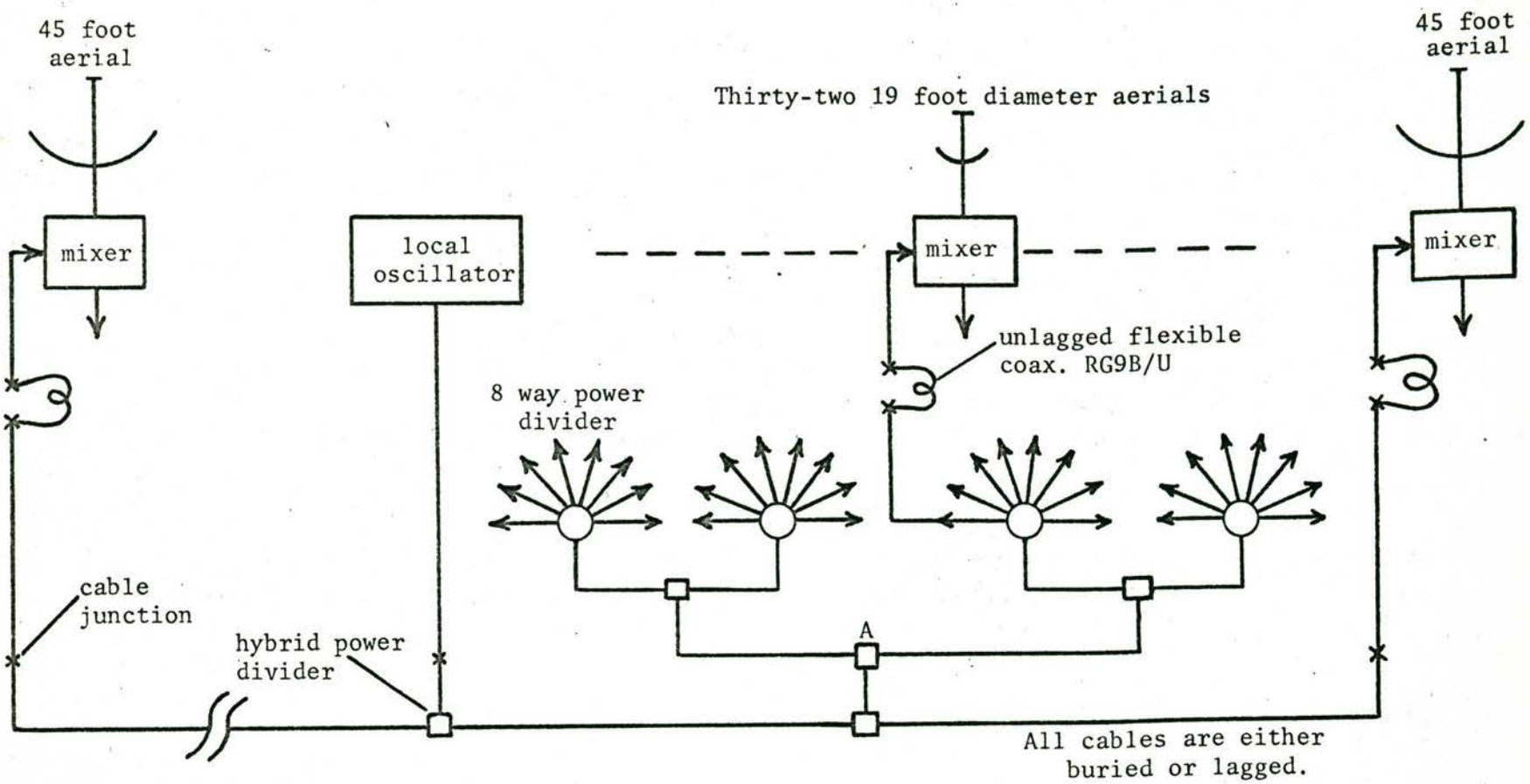

FIGURE 7.6 The Final Local Oscillator Distribution System.

This is the system for the east-west compound grating antenna. A similar system applies to the north-south antenna. There is provision at A for joining the north-south and east-west distribution systems to a common local oscillator for operation of the gratings as a crossed grating interferometer.

In Stage 2 the local oscillator will be distributed at 700 MHz and doubled in frequency at each mixer. Cable attenuation at 700 MHz is lower (3.8 db per 100 m) conserving local oscillator power and allowing a less expensive cable to be used in the short runs of the branched feeder system. In addition some of the 700 MHz oscillator signal will be used to drive mixers operating at the second observing frequency (692.5 MHz).

The Hackethal local oscillator cables are buried with the I.F. signal returns and power and control cables (Fig. 7.7). An enveloping layer of sand prevents the surrounding ground from causing sharp pressures on the outer conductors. These pressures would restrict uniform expansion from taking place. The exposed cable ends are insulated with a layer of polyurethane foam in order to reduce the effects of air temperature fluctuations.

The extra cable, added at each 45 foot diameter aerial in order to take local oscillator power up to the mixer at the vertex, is approximately the same length (6 m) as the coaxial line bringing the signal down from the feed to the mixer. If subjected to the same temperature variations, mutual compensation of expansion occurs so that the receiver channel phase does not vary. (This is similar to the compensation used with the open-wire lines.) For this reason, neither is insulated. Instead, the local oscillator coaxial line is placed in close contact with the tower which has a large thermal capacity similar to the feed pole which encloses the signal coaxial line.

Twin wire junctions

Christiansen et al (1961) developed a special type of T-junction for use with the twin wire transmission lines. These junctions have an arrangement of choke flanges such that the electrical properties are not dependent upon the quality of mechanical contact between the junctions and the twin wire conductors. This fact also allows easy movement of the junctions along the lines facilitating phase adjustment of the system. These T-junctions are used on both the signal and the local oscillator twin-wire branched feeder system.

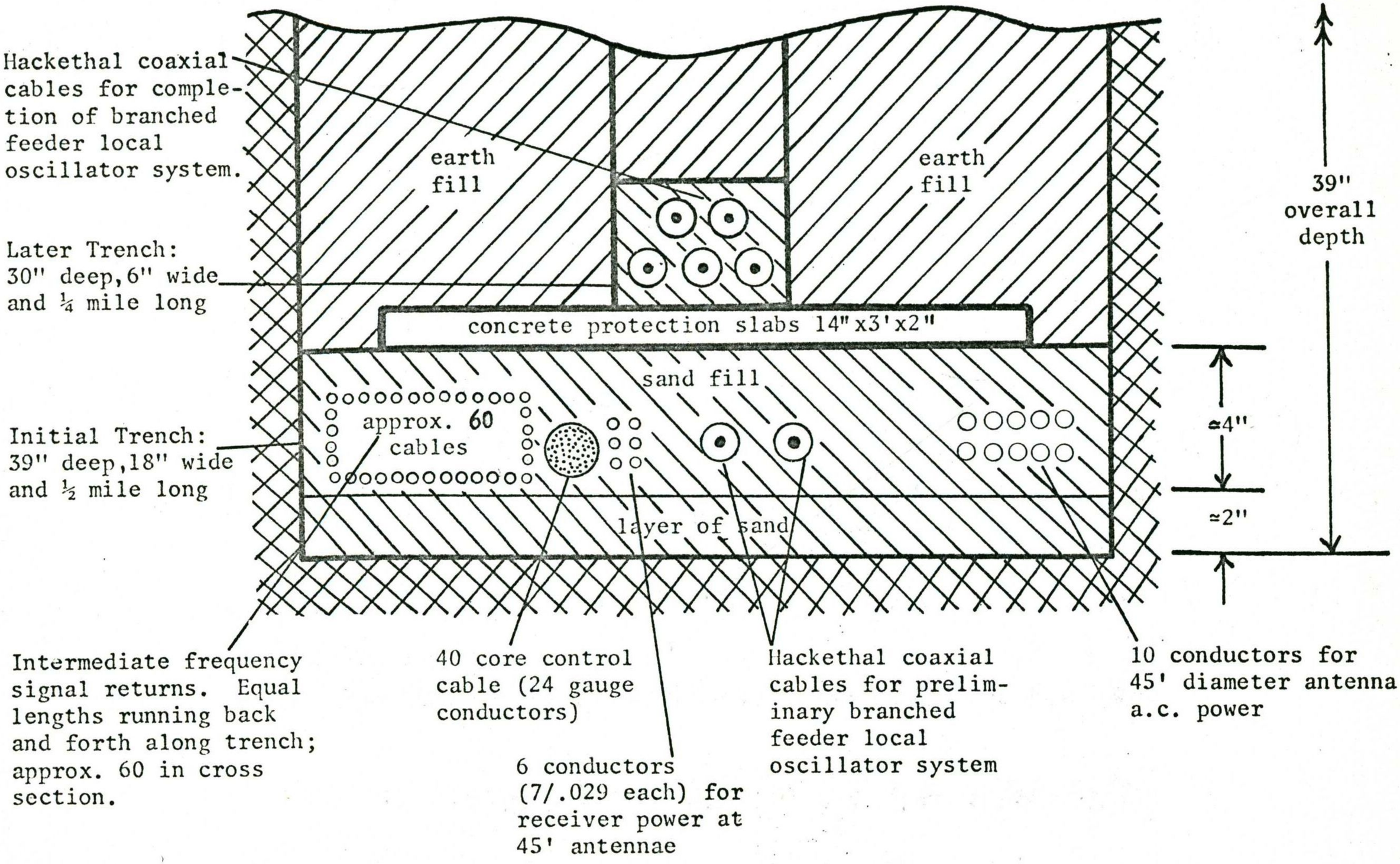

FIGURE 7.7 Schematic diagram of cable layout in trench.

To transfer power from the twin wire lines to coaxial cables and vice versa, additional T-junctions are combined with balance-to-unbalance transformers. Two T-junction-balun arrangements 'couple' local oscillator power from the buried cable system onto the 'bottom' open-wire lines of the east-west and north-south arrays. At each mixer another two T-junction-balun arrangements are used, one to 'pick-off' local oscillator power from the 'bottom' line and feed it to the mixer and the other to 'pick-off' the signal from sixteen small aerials collected by the branched-feeder system. These T-junctions are made 'one-sided' by blocking off one arm of the 'T' using short-circuiting plates (Fig. 7.8).

Power dividers and line-stretchers

The local oscillator power is divided in the present branched cable system (Fig. 7.5) using hybrid-ring directional couplers with the fourth port terminated. Three dividers are used (one 6 db and two 3 db).

Coaxial line 'stretchers' are inserted in the local oscillator lines after each of these power dividers. These line-stretchers, together with the sliding T-junctions on the open-wire lines, allow the R.F. phase of any channel to be varied independently of the remainder.

7.2.7 The north-south grating

At present only the east-west compound grating interferometer has been completed. In order to continue the regular pencil beam solar observations, a receiver system was added to the thirty-two aerials of the north-south grating to make it compatible with that of the east-west grating in its new form.

At first, one image filter and a mixer were added to the centre junction of the open-wire branched feeder system. This system collected the signals from all thirty-two north-south aerials. Local oscillator power was tapped off from the east-west buried cable system. This arrangement proved unsatisfactory during observations as phase

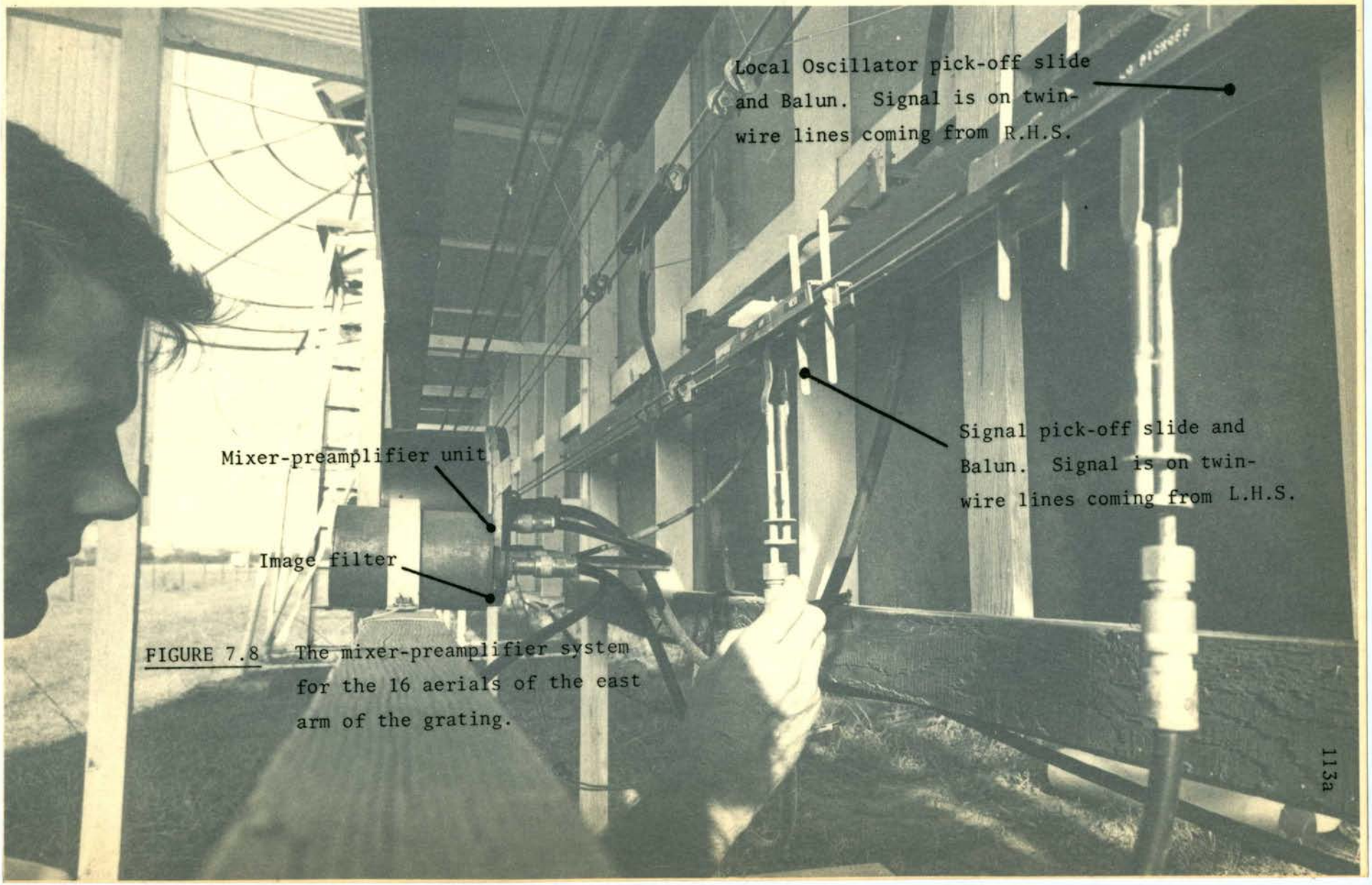

FIGURE 7.8 The mixer-preamplifier system for the 16 aerials of the east arm of the grating.

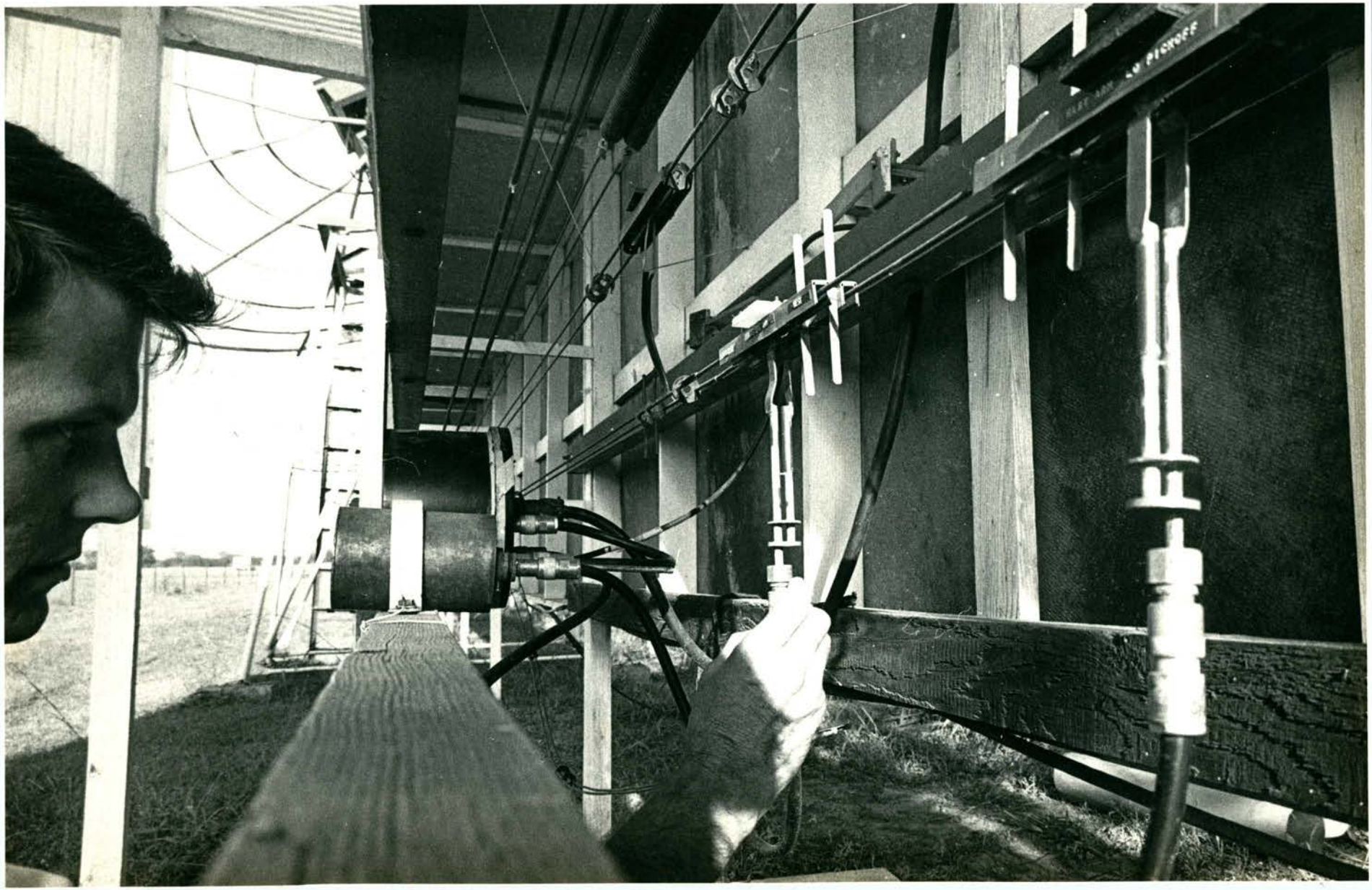

variations between the east-west and north-south gratings occurred due to the uncompensated open-wire lines (200 m) in the north-south grating.

This difficulty was eliminated by converting the north-south grating receiver system to be identical with that of the east-west grating. Two image filter-mixer combinations were installed in the middle of the north and the south arms. An open-wire temperature compensating system feeds local oscillator power to these mixers. The outputs of these mixers are returned to the centre hut.

Pencil beam observations are carried out using the same receiver system as for the compound grating observations. The east-west grating output is correlated with the north-south grating output instead of with the output from the 45 foot aerials.

7.3 Phase Stability of the Distributed Parts of the System

Stability requirements make the R.F. system the most critical part of the whole telescope. The disturbing influences are principally temperature and frequency variations. In Stage 1 a phase stability of ± 10 degrees electrical has been required*. In Stage 2 it is hoped to reduce this to ± 3 degrees electrical.

7.3.1 Theory

Fig. 7.9 depicts one receiver channel. This represents a superheterodyne front-end fed by a remote local oscillator, accepting a signal from an antenna some distance away and returning the signal to a central hut at a lower intermediate frequency. The three transmission lines are at different temperatures and experience differing changes of temperature.

The electrical lengths of the signal, local oscillator (L.O.) and intermediate frequency (I.F.) transmission lines are x, y and z. These lengths increase by dx, dy and dz when the temperatures rise. The signal magnitudes can be ignored for the present, considering only the phase terms. The angular frequencies of the local oscillator, I.F. amplifier and signal response are represented by ω_0, ω_1 and $(\omega_0+\omega_1)$ respectively. This assumes that only the upper frequency sideband of the conversion process is received. (For the lower sideband put $-\omega_1$ for $+\omega_1$ throughout.) ω_1 is fixed and any change in observing frequency is caused by a change in ω_0.

The signals at the various points of Fig. 7.9 , designated by letters, may be expressed as follows:

---

*A phase change of 10^{o} elec. causes (i) an amplitude increase in one sidelobe of 5% of the main beam and (ii) a pointing error change of 3 sec. of arc (8% of the beamwidth).

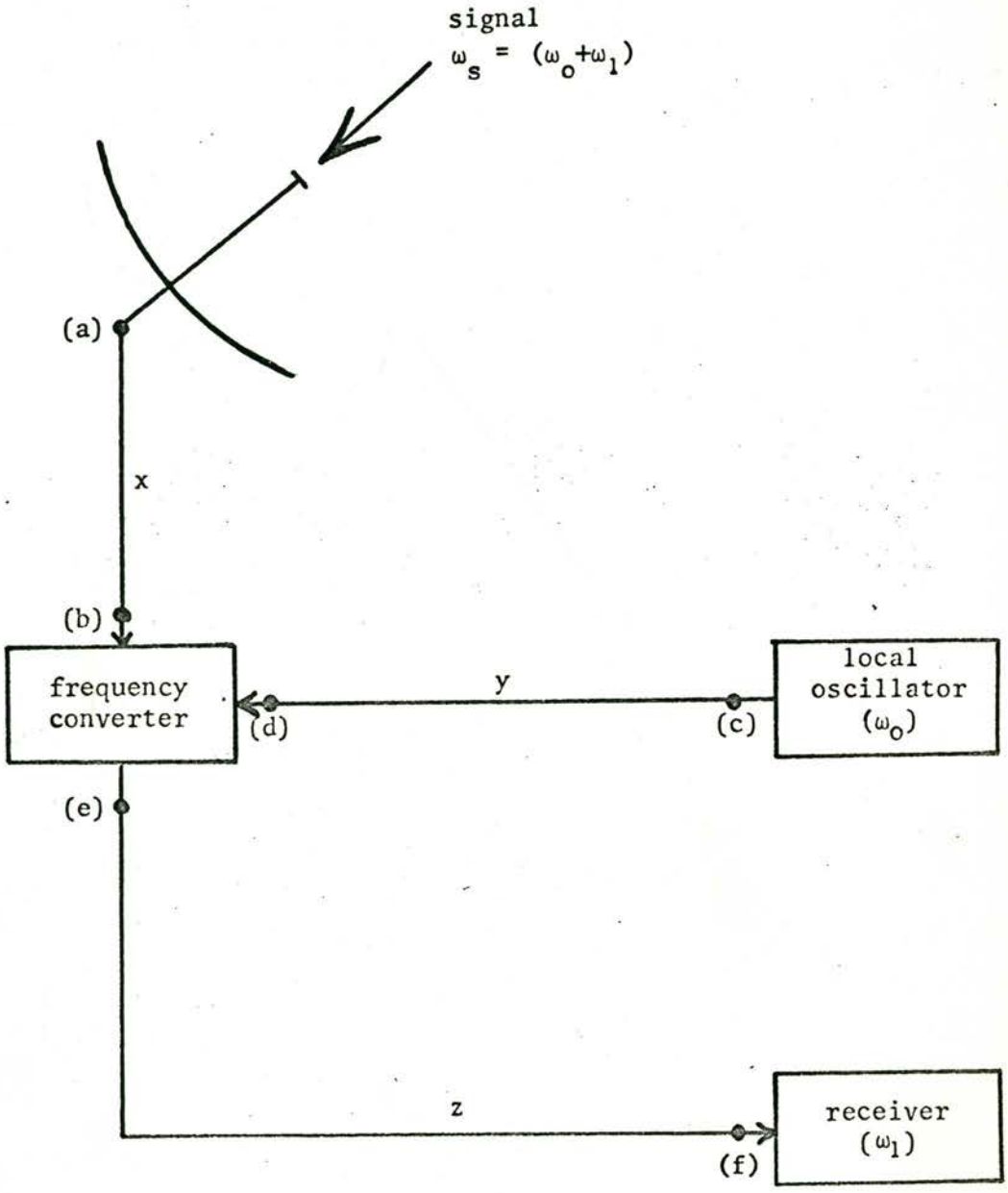

FIGURE 7.9 Schematic Diagram of One Receiver Channel.

(i) Before a temperature change:

At (b) we have:

$$\cos\left((\omega_0+\omega_1)(t-\frac{x}{c}) + \theta_s\right) \tag{7.2}$$

where θ_s is the phase of the signal relative to the local oscillator and c represents the velocity of propagation of light.

At (d)

$$\cos\left(\omega_0(t-\frac{y}{c})\right) \tag{7.3}$$

Thus at (f), rejecting the upper conversion sideband $(2\omega_0+\omega_1)$, we have:

$$\text{Output} \propto \cos\left(\omega_1 t-\frac{\omega_1}{c}(x+z) - \frac{\omega_0}{c}(x-y) + \theta_s\right) \tag{7.4}$$

(ii) After a temperature change:

Expression (7.4) becomes:

$$\text{Output} \propto \cos\left(\omega_1 t-\frac{\omega_1}{c}(x+z) - \frac{\omega_0}{c}(x-y) + \theta_s-\frac{\omega_1}{c}(dx+dz) - \frac{\omega_0}{c}(dx-dy)\right) \tag{7.5}$$

(iii) At a different local oscillator frequency, $(\omega_0+d\omega_0)$:

Expression (7.4) becomes:

$$\text{Output} \propto \cos\left(\omega_1 t-\frac{\omega_1}{c}(x+z) - \frac{\omega_0}{c}(x-y) + \theta_s-\frac{d\omega_0}{c}(x-y)\right) \tag{7.6}$$

Expression (7.4), (7.5) and (7.6) give the phases of the output of one channel relative to an arbitrary reference.

We have two requirements to make of any distributed phase-critical system:

(i) phase should be insensitive to temperature changes and

(ii) phase should be insensitive to frequency changes.

From expression (7.5) the phase change due to temperature variation is:

$$-\left[\frac{\omega_1}{c}(dx+dz) + \frac{\omega_0}{c}(dx-dy)\right] \text{ radians} \qquad (7.7)$$

while that due to frequency variation is:

$$-\frac{d\omega_0}{c}(x-y) \quad \text{radians} \qquad (7.8)$$

The distributed receiver system will have several channels, each with different phase variations. These will be caused (i) by different $\underline{x}$, $\underline{y}$ and $\underline{z}$ (implying also different $\underline{dx}$, $\underline{dy}$ and $\underline{dz}$ under similar temperature changes), or (ii) by differential temperature variations (implying again different $\underline{dx}$, $\underline{dy}$ and $\underline{dz}$).

7.3.2 Compensation for temperature variations

Section 7.2.6 has described how the expansion of the twin-wire signal lines from the grating aerials is compensated by the expansion of a similar length in the particular local oscillator distribution feeder.

The effect is to make expression (7.7) close to zero.

i.e. $\left[\frac{\omega_1}{c}(dx+dz) + \frac{\omega_0}{c}(dx-dy)\right] \simeq 0$

Here $dz = 0$ since all I.F. return lines are equal. (The effect of the differential ground temperature on the I.F. returns can be ignored here.) Let $\underline{dx}$ and $\underline{dy}$ be the expansion of the signal and L.O. open-wire lines respectively. Suppose the expansion coefficient (of both) is ρ and the temperature rise (of both) is (ΔT), then

$dx = \rho.x.(\Delta T)$ and $dy = \rho.y.(\Delta T)$

Expression (7.7) becomes

$$(\omega_1+\omega_0) \cdot \frac{\rho.x.(\Delta T)}{c} - \omega_0 \cdot \frac{\rho.y.(\Delta T)}{c}$$

and this can be made zero by choosing x and y (the open-wire lengths (elec.) in the signal and local oscillator feeders) such that

$$x.(\omega_1+\omega_0) = y.\omega_0$$

This compensates for the effects of nett temperature variations and leaves the system subject only to phase variations caused by temperature differentials across the system length.

If the 100 m open-wire signal lines are not compensated then temperature changes can create a large phase differential between the correlated aerials. This is a 'gross' effect where the grating as a whole changes phase relative to the two aerial interferometer. As the two systems do not have coincident phase centres an imaginary (or 'sine') component is added to the beam shape (Fig. 2.10). This effect was noticed during observations of the sun when the compensating system was not in use*.

*During these observations the temperature change between 1200 and 1530 hours caused considerable distortion which was corrected by manually inserting phase into the two element signal path.

7.3.3 Estimate of phase errors caused by temperature variations

Assume the following:

	T	ΔT	Coeff. Expansion/^{o}C.
Cable below ground			
Hackethal Flexwell 7/8"	½^{o}C	<½^{o}C	+ 1.10^{-5}
Cable above ground			
Telcon HM8	20^{o}C	2^{o}C	+ 1.10^{-5}
Open-wire lines above ground	20^{o}C	2^{o}C	+ $(1.7).10^{-5}$
I.F. cable below ground Reliance CD.6122	½^{o}C	<½^{o}C	- 8.10^{-5}

The temperatures above and below ground have a large time lag so they cannot be made to balance in any practical manner.

1. T is the maximum nett temperature change experienced over the observing period.
ΔT is the maximum differential temperature change at any time between different receiver channels.
Values for T and ΔT are derived from experiments conducted by Erickson and Watkinson (1962) and confirmed by Mackay (1966).

2. The coefficients of expansion of the Hackethal and Telcon cables are manufacturers' figures, checked against various experimental references. The coefficient for the open-wire lines is that of copper. The coefficient for the I.F. cable is an experimental one and checks closely with the manufacturer's figure of -6.10^{-5}.

Using expression (7.7), and comparing two channels in three specific cases below, the maximum phase-differential due to nett and differential temperature changes is estimated for the least favourable situation:

(i) Comparing two small aerials

100 m open-wire signal line	(1^{o}C)	$+3^{o}$ elec.
100 m open-wire local oscillator line	($\frac{1}{2}^{o}$C)	$-1\frac{1}{2}^{o}$ elec.
600 m I.F. return ($<\frac{1}{2}^{o}$C differential)		$\pm\ \frac{1}{2}^{o}$ elec.

Thus provided the lines are free to expand, the differential phase between small elements should be limited to 2^{o} electrical.

(ii) Comparing the two 45 foot aerials

410 m buried coaxial local oscillator line	($\frac{1}{2}^{o}$C)	$\mp\ 3\frac{1}{2}^{o}$ elec.
6 m in air coaxial signal line	(2^{o}C)	$< +\frac{1}{2}^{o}$ elec.
7 m in air coaxial local oscillator line	(2^{o}C)	$<-\ \frac{1}{2}^{o}$ elec.
600 m I.F. return ($<\frac{1}{2}^{o}$C differential)		$\pm\ \frac{1}{2}^{o}$ elec.

Thus total phase differential of cables should be $<4^{o}$ electrical.

(iii) Comparing one small aerial with one 45 foot aerial

205 m buried local oscillator coaxial line	($\frac{1}{2}^{o}$C)	$\mp\ 2^{o}$ elec.
7 m in air local oscillator coaxial line	(20^{o}C)	$+\ 2\frac{1}{2}^{o}$ elec.
6 m in air signal coaxial line	(20^{o}C)	$-\ 2^{o}$ elec.
100 m open-wire signal line	(20^{o}C)	$+\ 60^{o}$ elec.
102 m open-wire local oscillator line	(20^{o}C)	$-\ 60^{o}$ elec
100 m open-wire line @ differential temp.	(1^{o}C)	$\pm\ 3^{o}$ elec.
600 m I.F. return ($<\frac{1}{2}^{o}$C differential)		$\pm\ \frac{1}{2}^{o}$ elec.

Thus in this case the maximum phase differential should be $<6^{o}$ electrical.

The phase errors considered in the above table do not include those due to:

1. bending of the double screened flexible cables (RG9B/U) during changes in the antenna pointing direction (this error was found to be negligible from laboratory experiments.
2. initial adjustments (Chapter 9),
3. phase differentials (due to temperature differentials) of the filters, mixers, preamplifiers, delay dables (if used) and main receiver, (Sections 7.2.4 and 7.3.5), and
4. frequency variations in the local oscillator.

The last of these, the effect of frequency variations, will now be considered.

7.3.4 Dependence of relative phase upon frequency stability

From expression (7.8), the phase relationship between channels will be frequency insensitive if either

$$(x-y) = 0 \qquad (7.9)$$

or

$$(x_1-x_2) - (y_1-y_2) = 0 \qquad (7.10)$$

For the present Stage 1 neither of these conditions is possible. The small aerials have identical systems so that their relative phases are insensitive to frequency variations. This also applies to the two large aerials. However, when the phase of the signal from a small aerial is compared with that from a large aerial, equation (7.10) becomes

$$(100\text{m}-6\text{m}) - (100\text{m}+205\text{m}-417\text{m}) = 206\text{m} \neq 0$$

This unbalanced cable gives a phase-frequency dependence of approximately 5 degrees electrical for 20 KHz frequency charge. Again, the variation is between the correlated signals, causing distortion of the beam as in Fig. 2.10.

To compensate the system, 206 m of buried cable could be inserted into the local oscillator path of the small aerials. This is not available. However the frequency of observation must be stable for other reasons. These are:

(i) the bandwidth of the image filters,

(ii) the narrow-band effects on the open-wire lines, and

(iii) the stability of the beam positions in the sky.*

A frequency counter is permanently connected to the local oscillator during observations and any frequency drifts are corrected by a remote-controlled frequency adjustment. Generally a check is necessary every 15-30 minutes.

In Stage 2, a crystal controlled oscillator will be used which has a stability of <1 in 10^7 per degree C. (This stability amounts to <3 KHz variation in a signal frequency of 1415 MHz for an environmental temperature change of 20° C.)

The whole system will also be relatively phase insensitive to frequency variations (apart from bandwidth-limiting tuned circuits) because:

(i) the local oscillator branched-feeder cable system will have almost equal length paths,

(ii) the I.F. returns are all equal, and

(iii) I.F. signal delay cables will be inserted continuously so that all signal paths will be equal. (The telescope will be continually 'looking' in the direction of the 'white-fringe'.)

---

*At 45° hour-angle the beams shift by approximately 1/15th of their width for 20 KHz frequency shift.

7.3.5 Phase Stability Test

The test arrangement described here is used for two purposes:

(i) to test the phase stability of various segments of the distributed receiver system, particularly that of the temperature compensating arrangement, and

(ii) to enable comparative phase-length measurements of different image-filter-mixer-preamplifier combinations.

The arrangement uses the main receiver, described in Chapter 8, operating in the normal correlating mode. The two converter channels are fed from widely-separated and well-isolated mixer-preamplifier units. A 1424 MHz signal is distributed to both mixers so that the receiver output gives a measure of relative channel phase. The object, either a signal path or a mixer unit whose phase length is to be measured, is incorporated into one channel.

For stability measurements, the system is generally set to run overnight with recorders measuring the relative phase, the frequencies of both R.F. oscillators, and ground and air temperatures. When possible the path lengths (signal, L.O. and I.F.) of both channels are equalized to avoid any frequency-phase effects (Section 7.3.4). Temperature-phase changes are then easily determined. If the path lengths are not identical (as during comparison of X1 and the east arm) then a phase vs. frequency calibration is carried out beforehand and appropriate corrections made to the results.

Fig. 7.10 shows the receiver arrangement used to test the stability of the open-wire lines. One grating arm is temperature compensated and its phase variation compared with that of an uncompensated arm. Figure 7.11 shows this phase comparison together with the comparison of two compensated channels.

The measurements of channel phase-temperature stability all proved satisfactorily within the estimates.

Comparative phase-length measurements on the mixers are carried out by inserting different mixers in one channel of the arrangement of Fig. 7.10 (see Section 9.3.2).

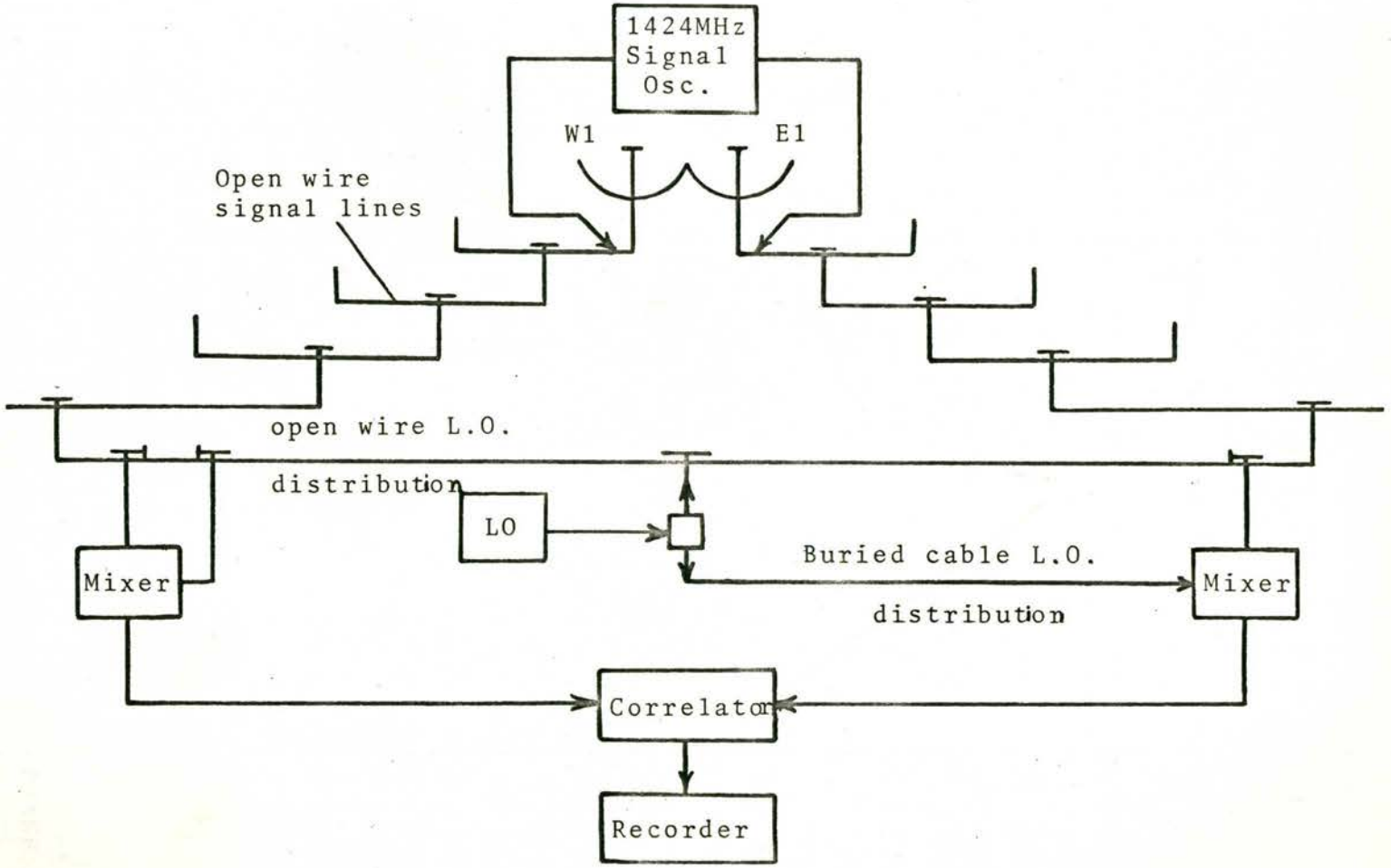

FIGURE 7.10 The Receiver Configuration used to test the relative phase stability of the two small aerial receiver channels.

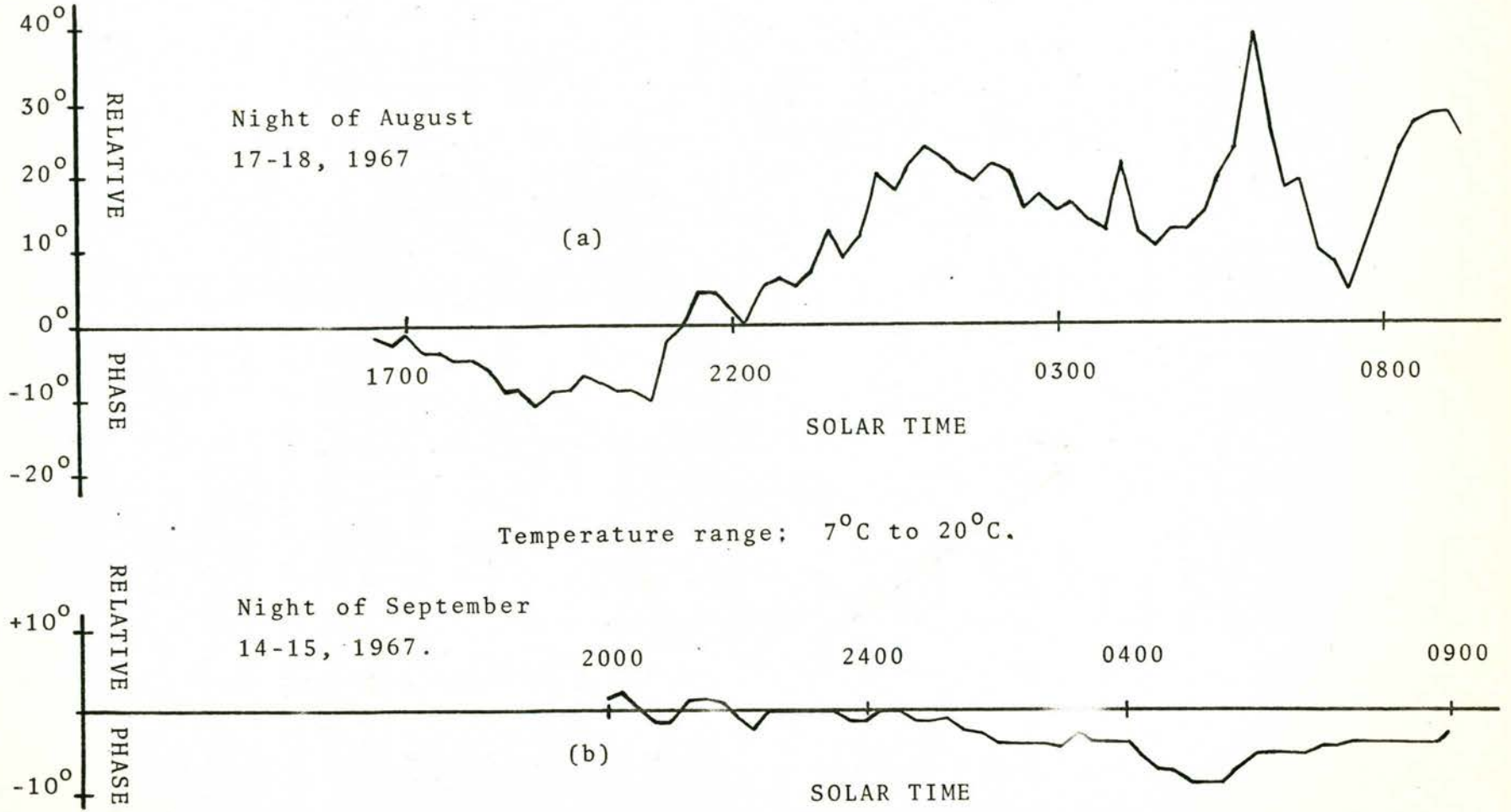

FIGURE 7.11 The effect of temperature variations upon the aerial receiver channels.

(a) Comparison of compensated and uncompensated channels.

(b) Comparison of two compensated channels.

7.4 Intermediate Frequency Transmission Lines

7.4.1 Cable details

The output of each preamplifier is returned individually to the central receiver hut through equal lengths, 2150 feet (660 m), of Reliance foam-dielectric coaxial cable. Equalization of the cable lengths avoids unwanted phase variations over the bandwidth. Although only four lines are required for the present system, the total number for the Stage 2 receiver system (39 lengths in all) were laid at the same time.

The cables are buried with the local oscillator distribution cables at a depth of three feet. This keeps nett and differential temperature variations at $\frac{1}{2}^{o}$C and $<\frac{1}{2}^{o}$C respectively (over the half mile extent). The temperature-phase coefficient of this cable is -8.10^{-5} per degree C. This coefficient is not as low as that of the local oscillator cables but the lower signal frequency (30 MHz I.F.) keeps the phase error contribution down to about $\frac{1}{2}^{o}$ electrical. The use of equal lengths allows the small nett temperature changes to be ignored.

The cable attenuation at 30 MHz is 1.2 db/100 ft (instead of the expected 1.05 db/100 ft) which gives a channel attenuation of 26 db. The temperature-attenuation coefficient (stated by the manufacturer) of 0.2% per degree C means that gain variations due to nett temperature changes are negligible.

The attenuation vs. frequency of the 660 m lengths is about 13.5 db/octave. Thus the two receiver pass bands (400 KHz and 2.2 MHz wide) in use at present have slopes of only 0.12 db and 1.4 db so that equalization is unnecessary. However, with a bandwidth of 8 MHz in Stage 2, the slope of 5.5 db will need equalizing.

This cable was chosen because (i) continuous lengths could be produced under electronic control (ensuring consistent properties), (ii) it is relatively inexpensive (important considering approximately 46 miles will be used in the complete telescope).

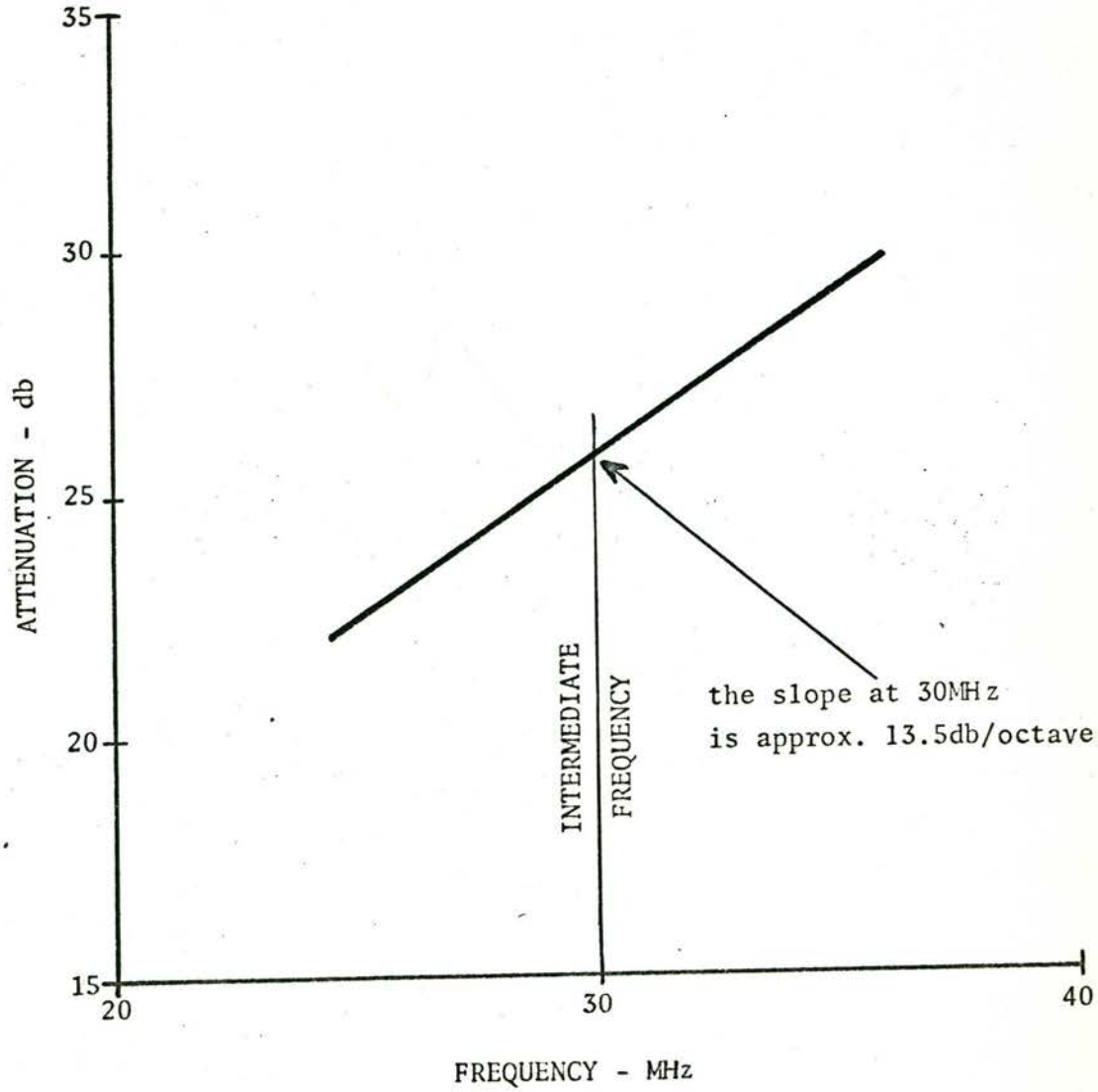

FIGURE 7.12 The Frequency Response of the 660m lengths of Intermediate Frequency Return Cables.

The characteristic impedance is 75 Ω and the velocity of propagation is 0.80 to 0.82 which implies a relatively low percentage of solid dielectric.

7.4.2 I.F. cable layout and channel isolation

The I.F. cables from aerial X2 (the furthest aerial) run straight to the centre hut. All other I.F. cables (of the same length) are folded back and forth along the trench to use up the extra length (Fig. 7. 13). Cables to the east and to the west of the central hut are completely separated, although cables on either side are bunched closely together.

The outer conductor of the I.F. cables is only a single braided shield (allowing some signal leakage). This leakage and the close physical contact between the cables of some channels means that the instantaneous channel isolation is not high.

In the final system each channel will have phase rotators (in the hut) rotating at different rates in order to bring to rest the fringes from the required sky direction. Each correlator output will be integrated over many fringe periods. This will give the system a certain amount of inbuilt interference protection. All stray signals, originating either from sources away from the image plane, from coupling between antennae, from channel crosstalk or from interference picked up before the phase rotators, will almost always have a phase modulation applied by the phase rotators, causing suppression after integration.

However the fringe rate from a pair of antennae (Section 3.3.8) is proportional to:

$n.d. \cos\delta.\cos\alpha$ for an east-west baseline, or

$n.d. \sin 34^{o}.\cos\delta.\sin\alpha$ for a north-south baseline,

where n is the spacing number and

d is the harmonic separation.

Thus the fringe rate and the difference fringe rate tend to zero in the polar regions and also change with hour-angle so that this form of

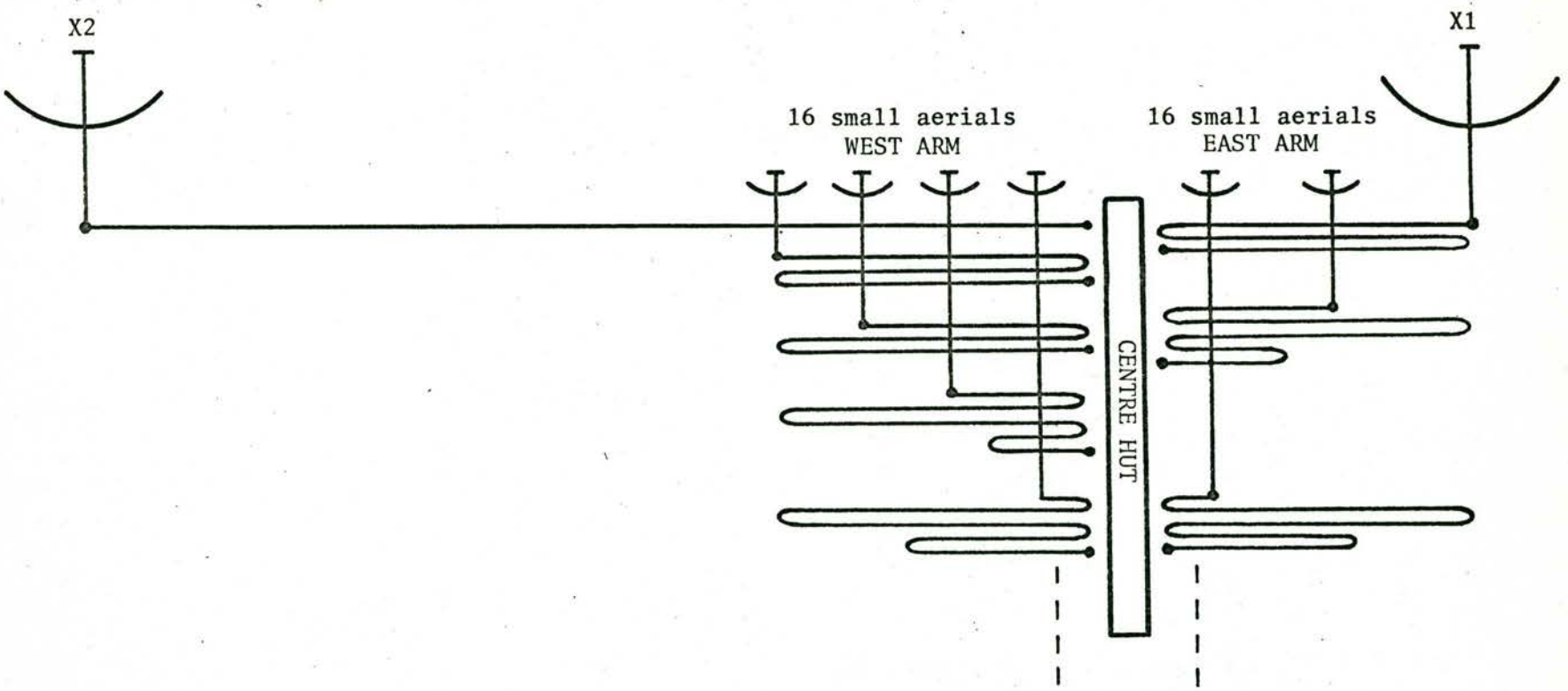

FIGURE 7.13 Schematic diagram of the layout of I.F. signal return cables.

protection varies considerably in degree.* Some additional protection in the future will be given by phase switching the signals from the large aerials at the aerial positions (or phase switching the local oscillator for the mixers at these aerials).

In the present system, no phase rotators are used and phase switching of the large aerials is done in the main receiver. Thus channel crosstalk could have occurred between the west arm and aerial X2 and between the east arm and aerial X1. This would have appeared as a total power component in the output, either as a D.C. baseline shift or as a small total-power fan-beam scan always in the positive direction. (Adjacent desired responses are positive and negative.) Neither of these crosstalk effects was apparent in observations but would be cured if necessary by phase switching aerials X1 and X2 at the mixer-preamplifiers.

---

*1. This form of protection is lower for the north-south array than for the east-west array.

2. Protection is dependent upon the differential fringe rate, which is smallest for adjacent spatial components {n and (n + 1)}. This is advantageous as it causes the least distortion in the spatial visibility function of the sky.

CHAPTER 8

THE RECEIVER SYSTEM : PART II

CHAPTER 8: THE RECEIVER SYSTEM : PART II

8.1 Introduction

The intermediate frequency (I.F.) signals from the distributed portions of the receiver system come together in the centre hut. The main or 'rear-end' receiver system modifies and combines these weak signals to give the desired high-level output.

The basic design of this system is the heterodyne arrangement illustrated in Fig. 8.1. This has been constructed in the form of a number of separate modules, facilitating the operation of the receiver in several different configurations. These configurations are used for testing, alignment and special purpose observations besides the normal fan beam observations.

This chapter describes the system design and the detailed specifications of the individual modules. These were the responsibility of the writer. The circuit design and the construction of the principal modules was carried out by Dr. R.H. Frater with the assistance of several people from the Electronics Department.

The complete main receiver, with the exception of the delay lines, is contained in one 19" rack (Fig. 8.2). Interconnections between these modules are made with detachable shielded cables. These cables must be of constant length as the relative phases of the different channels are critical to the system operation.

Following an initial period of operation, several additions and modifications were made by the writer to this basis system:

1. A variable time constant facility (¼ sec to 32 sec) was added to the main synchronous demodulator unit.

2. The fringe rate converter module (Section 9.4 and Appendix F) was designed and constructed.

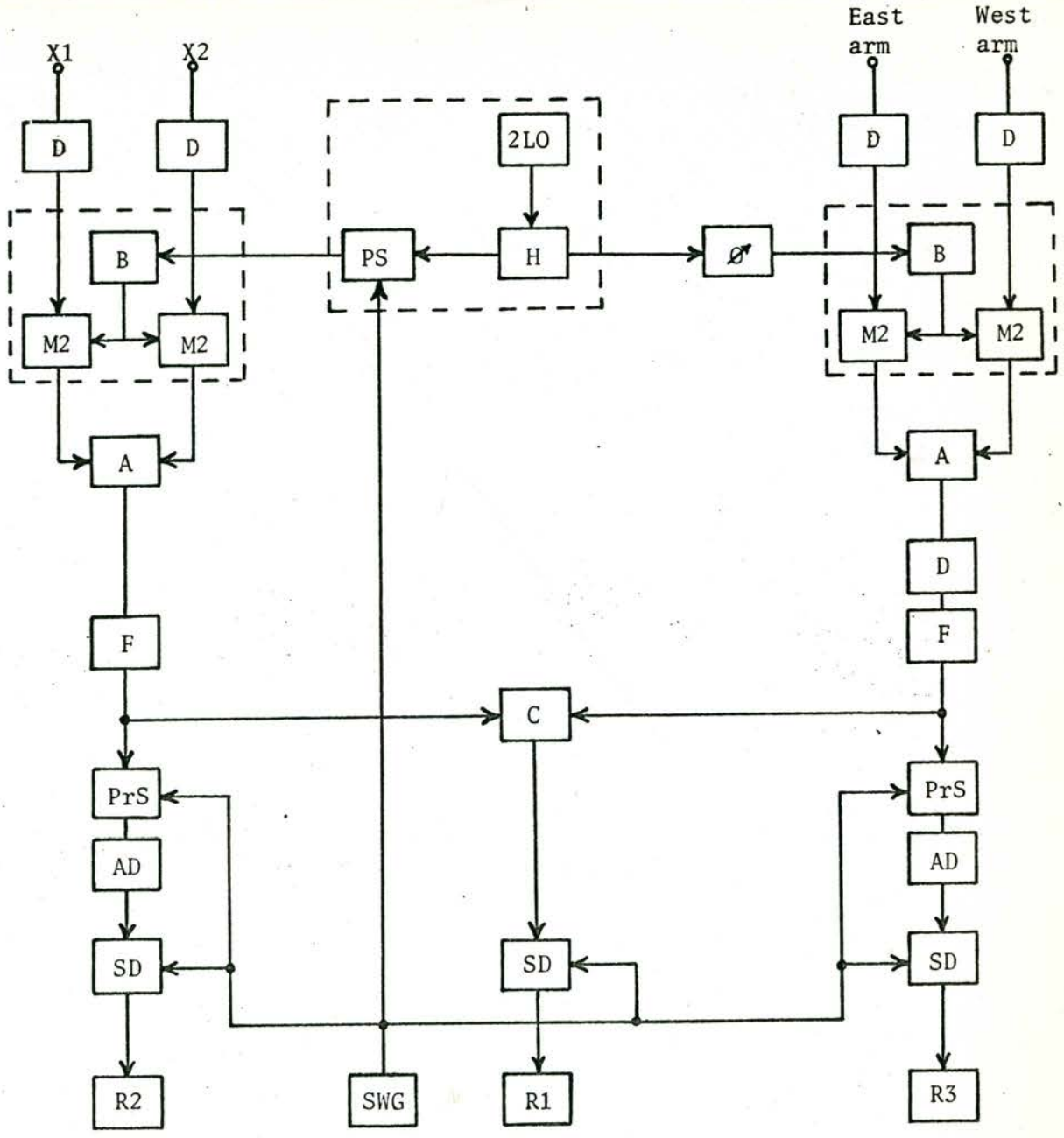

D	Delay cables	M2	Second frequency converter
A	Signal adder	F	Band pass filters
B	Buffer amplifier	2LO	Second local oscillator
H	Hybrid	C	Main amplifier and correlator (see fig.8.3)
PS	Phase switch	SWG	Switching waveform generator (∿400 Hz)
PrS	Power switch	AD	Amplifier and detector
R	Recorder	Ø	Digital phase control

FIGURE 8.1 Schematic representation of the main receiver system.

FIGURE 8.2

The Main Receiver System

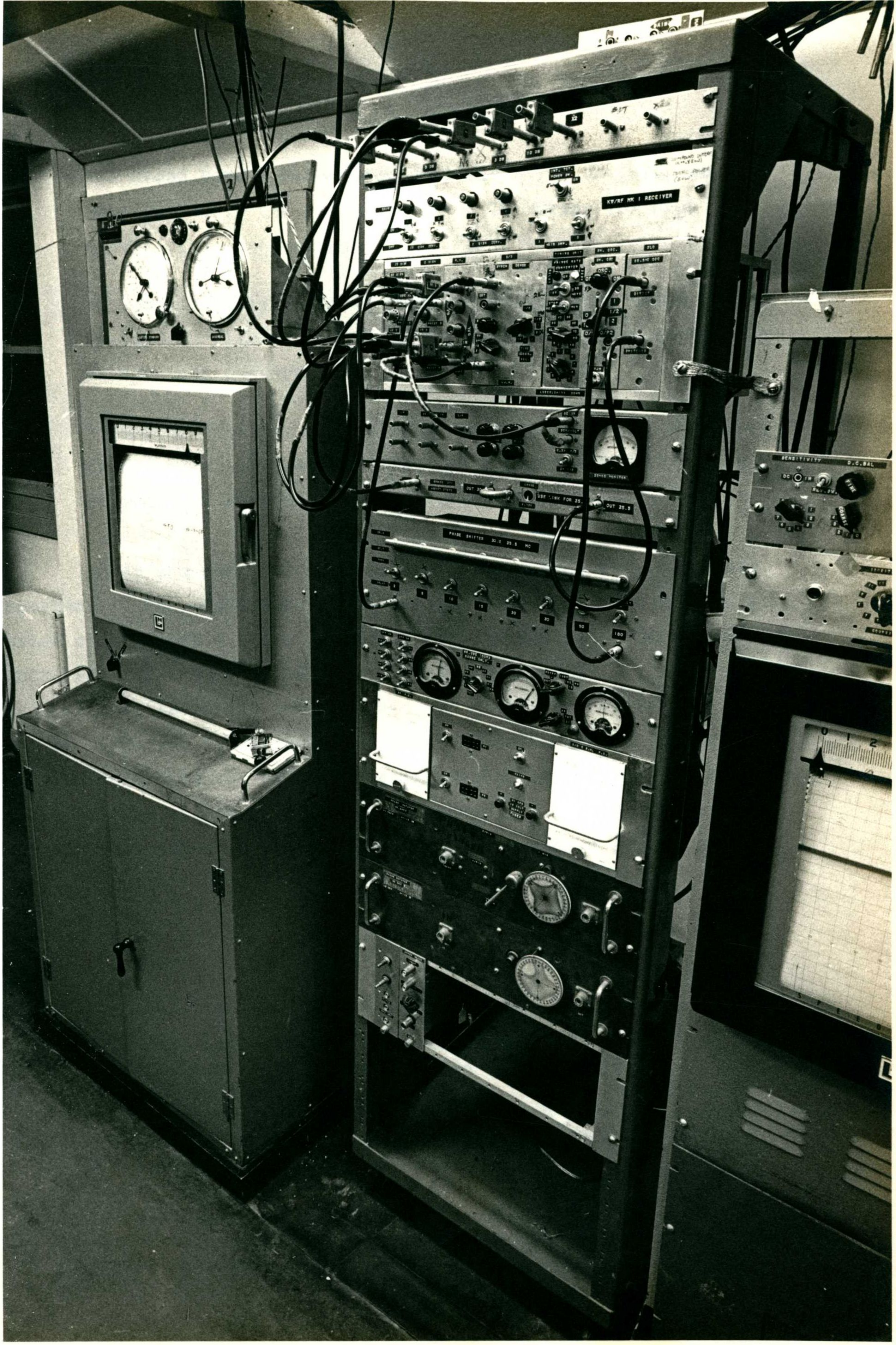
KY/RF MK I RECEIVER
SENSITIVITY
D.C. BAL
PHASE SHIFTER
OUT 25.5

3. Two broad band I.F. booster amplifiers (20 db gain) were constructed to the design by Mr. C.T. Murray for high sensitivity observations.

4. Two continuously variable phase rotators* were added to the system for 'lobestopping' of the fringes and for testing the fringe rate converter.

5. A monitor facility was built to measure the radio frequency (R.F.) mixer crystal currents and the preamplifier supply currents of each mixer-preamplifier module.

Phase and gain stabilities of the main receiver system are important. The requirements are for $\pm 2^{o}$ elec. and ±0.5 db over a period of at least 9 hours. During this period the receiver in the centre hut can undergo a temperature variation of $\pm 5^{o}$.

These stability requirements, although strict, are not as long term as those for the mixer-preamplifier modules and the associated distribution cables. Phase and gain calibration of the main receiver can be carried out in about fifteen minutes.** Calibration of the distributed modules is a much more lengthy procedure (Chapter 9).

---

*These are goniometer type rotators designed by Goddard (1961). One of these rotators is tuned to 35.5 MHz for use in the second local oscillator line and the other is tuned to 30 MHz for use in the I.F. signal lines. The rotation rate is made continuously variable by using a combination of gears, a synchronous motor and a variable frequency power supply.

**If necessary main receiver calibration can be done before and after an observing period. However, during operation a check proved necessary only about once per week.

8.2 The Main Receiver System

8.2.1 The Second Frequency Converter Module

Two of these modules are used, each one processing two preamplifier signals. Their positions in the receiver system are indicated in the block diagrams of Fig. 7.1 and 8.1.

During most solar observations the I.F. return lines plug directly into these converter units. When higher sensitivity is desired (requiring a wider bandwidth), the delay module is interposed between the I.F. lines and the converter modules.

Although called a 'converter' module these units fulfil several functions in addition to that of frequency conversion:

(a) They provide essential phase and gain control of each of the four incoming intermediate frequency signals.

(b) Two of the four incoming signals (one side of the correlator) are coded (phase switched at 400 Hz) for detection by the synchronous-demodulator unit.

(c) Each module sums a pair of signals after frequency conversion to 5.5 MHz. The signals of aerials X1 and X2 are combined in one module while the other module combines the signals from the two blocks of 16 aerials of the east-west grating array.

Down conversion from 30 MHz to 5.5 MHz was chosen in order to benefit from the availability of a 5.5 MHz input main amplifier-correlator module.

A 35.5 MHz high-side local oscillator signal is injected into each converter module via a 10 db attenuator and a buffer stage. In each module there is a separate conversion stage for each input. This consists of a longtail pair of AFZ12 transistors which is balanced against the input signal and driven in phase opposition by the 35.5 MHz signal. The phase of each input signal can be 'trimmed' about 60° elec. by a phase shift network in the 35.5 MHz signal line. Gain control

(about 3 db range) of each input signal is made possible by control of the emitter current of the signal input transistor in the tail of the longtail pair. This gain variation creates a small phase variation ($<10^{o}$) so that phase alignment is carried out after gain equalization. A switch in the +12 V supply gives on-off control of the signal channel.

The attenuator and buffer stage in the local oscillator input to each converter provide the necessary isolation between the two correlator channels thus preventing cross modulation.*

With mixer-preamplifier gains of 50 to 55 db and an intermediate frequency cable return loss of about 26 db, the signal level at the input to the converter modules is high enough such that the noise figure of these converter modules is negligible when compared with that of the mixer-preamplifier units.

The total gain of the converter module is about 20 db while the bandwidth is sufficiently broad not to affect the signal band shape. Up to this point in the system the bandshape is determined by the image filter, the mixer-preamplifier and the cable amplitude dispersion.

For a 400 KHz bandwidth, a filter 'pad' (consisting of a single tuned circuit) is interposed between each converter module output and the corresponding correlator input. These 'pads' (two), being in different channels, must be carefully aligned to have the same passband and avoid any differential phase shift across the band.

For the maximum bandwidth of 2.2 MHz these 'pads' are removed and the bandwidth is determined by tuned circuits in the main amplifier-correlator module.

---

*In some early high sensitivity two aerial interferometer observations, involving the two large aerials and using the fringe rate converter, cross modulation from this cause proved troublesome until it was traced.

8.2.2 The Second Local Oscillator

The second local (or heterodyne) oscillator module, designed by Mr. W.S. Lamond, supplies about 800 mV of 35.5 MHz signal to the converter stages. The required frequency stability of 1 in 10^5 over $5^{\circ}C$ is easily achieved using a crystal controlled transistor oscillator. A hybrid splits the output into two channels (one for each converter module), one of which is switched in phase between 0° and 180° by the 400 Hz square wave. The phase error between these channels is less than 0.5° elec. This local oscillator phase switching causes the converter output signal to be phase switched. The desired output of the correlator is then a 400 Hz square wave. This is detected by the synchronous demodulator which then gives a d.c. output proportional to the signal power.

8.2.3 The Main Amplifier-Correlator Module

As mentioned in Section 8.2.1, this unit was already available in the Department. It is of the same type as those used on the Mills Cross by the School of Physics. The dynamic range, the gain stability and the phase stability of this unit are adequate for use in the compound interferometer system. The I.F. input is 5.5 MHz. Fig. 8.3 is a schematic representation of its operation demonstrating the sum and difference method of multiplication.

This sum and different method of multiplication has considerable advantage when defining the bandwidth. Band-pass filters, 2.2 MHz wide and with a sharp cutoff, are placed in each channel after the hybrid where both signals are present. As each of these channels is detected separately, absolute phase alignment and phase stability of the amplifiers and filters are not critical. However their amplitude responses, the differential gain stability and the detector phase characteristics are important and care is necessary during construction (Blum, 1959; Robinson, 1964).

A zero bias control and a gain control in one channel only are

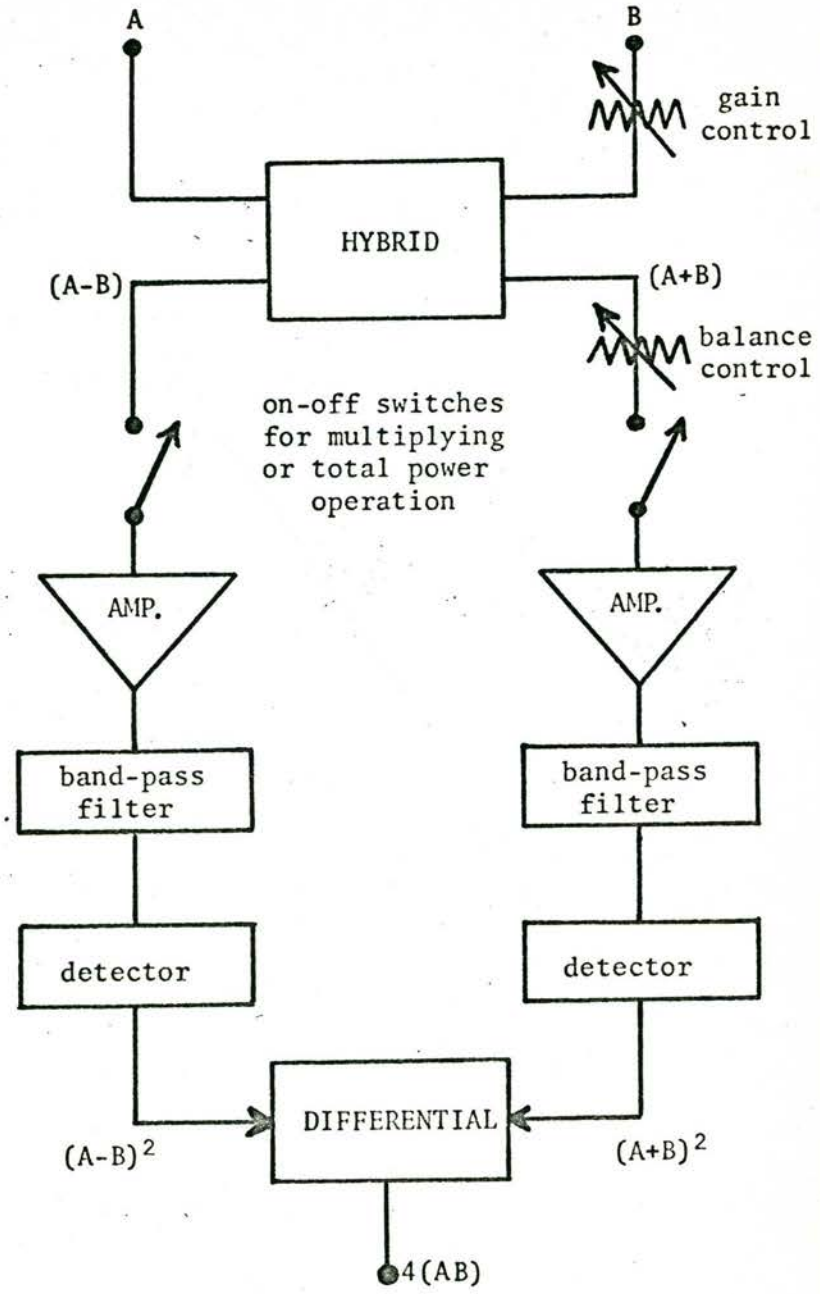

FIGURE 8.3a Schematic diagram of the main amplifier correlator module.

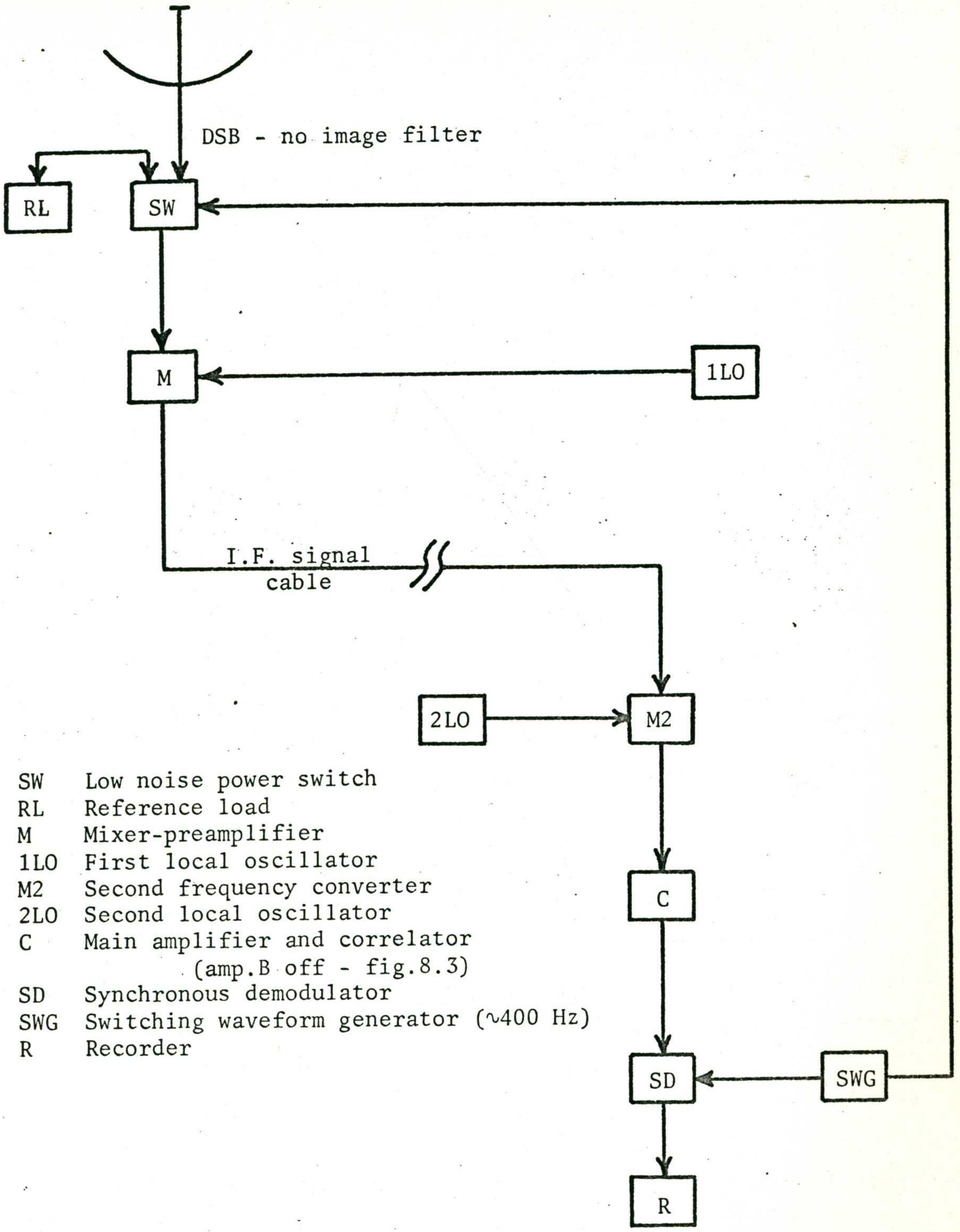

SW Low noise power switch
RL Reference load
M Mixer-preamplifier
1LO First local oscillator
M2 Second frequency converter
2LO Second local oscillator
C Main amplifier and correlator (amp.B off - fig.8.3)
SD Synchronous demodulator
SWG Switching waveform generator (∿400 Hz)
R Recorder

FIGURE 8.3b Schematic diagram of the receiver arrangement for total power observations using one aerial.

necessary for alignment. A facility for turning off either channel, (A + B) or (A - B), as well as A or B, proves very useful. The correlator then becomes a total power detector.

8.2.4 The Synchronous Demodulator and Square Wave Generator Modules

The synchronous (or phase-sensitive) demodulator is sensitive only to signals modulated at a particular switching frequency (≃ 400 Hz), and its odd harmonics. The desired signal is modulated at this frequency by half wavelength phase-switching the 35.5 MHz second local oscillator signal to the channel on one side only of the correlator. This phase modulates the desired output signal. The demodulator is insensitive to voltages which are in quadrature with this modulation.

The unit used in the present receiver system is one which was designed originally for use on the Mills Cross (Frater, 1965). This unit has an input matching the output of the main amplifier-correlator module, a high level output and a variable sensitivity. The output is fed via a gain and offset control to a Speedomax chart recorder and to an analogue-to-digital converter and paper tape punch.

The dynamic range of the unit is between 40 and 50 db. The zero drift is only about 50μv/^{o}C and the gain stability about 0.02%^{o}C.

Three of these units were built. One is used on the output of the correlator while the other two are used as total power monitors of the two signals being correlated. Thus, these three outputs give:

(i) the response of the 35 sec. of arc fan beam,

(ii) the output of a two aerial long baseline (3822λ) interferometer (observing only small diameter sunspots) and

(iii) the response of a two min. of arc fan beam (total power of the EW grating).

The main output synchronous demodulator was modified to take a variable time constant. The pair of integrating capacitors were relocated in another module where large amounts of low-leakage capacitance could be switched in parallel. The time constant, normally

¼ sec., can be varied between ¼ sec. and 32 sec., and will be extended to 128 sec. The large time constants are necessary for the fringe integrating method of phasing (Section 9.4).

The synchronous demodulator is driven by the square wave generator which supplies a ±12V square wave at a frequency of about 400 Hz. The square wave is also used:

(i) to drive the $\frac{\lambda}{2}$ phase switch in the 35.5 MHz local oscillator (via the fringe rate converter),

(ii) to drive the power switches in the monitor channels,

(iii) to drive the I.F. power switch used for receiver calibration,

(iv) to provide 'backing-off' control at the input to the synchronous-demodulator and,

(v) to drive an R.F. power switch used on the 45 foot aerials for pointing calibration of the individual aerials.

Power supplies

Both the synchronous demodulator and the square wave generator modules share a common power supply. A second power supply is used for the remainder of the receiver including the distributed preamplifier units. Separate power supplies prevent leakage of any 400 Hz square wave into the signal channels. This leakage would create an erroneous output.

A third power supply is used exclusively for the fringe rate converter unit. This is desirable in order to isolate the counter from any stray pulses in the system.

8.3 The Delay System Unit

In the delay unit various lengths of cable are inserted in each of the four incoming signal channels. These cables delay the signals when the direction of observation is away from the zenith so that the differential path length between the signals is minimized. This reduces the phase dispersion (and hence loss of correlation*) across the pass-band. As a consequence a wider bandwidth can be employed leading to an increased sensitivity.

With a 400 KHz bandwidth and a time constant of ¼ sec the receiver system has adequate sensitivity for solar observations and no need for delay lines. However for radio source observations a wider bandwidth is necessary and delay lines are then required for observations away from the zenith.

The present delay line module was designed and built by Mr.N.A. Mackay at the instigation of the author.

Figure 8.5 shows the complete unit. Reed relays switch the I.F. signals between two paths, one having delay and attenuation and the other having no delay but identical attenuation. Four amplifiers before the delays boost the incoming signals so that the whole unit has zero gain and contributes very little to the channel noise factor. The amplitude and phase differential dispersion of the cable paths have not been compensated.

The cable type used is identical with the I.F. return lines. It was cut to length (an even number of wavelengths at 30 MHz) with an error of less than $\pm 1^{o}$ elec. using the phase meter of Dr. R.H. Frater (1966). However the expansion coefficient of this cable is -8.10^{-5} per degree C and the possible temperature variation is $\pm 5^{o}$C (since reduced

---

*The loss of correlation between two signals depends on the time delay error, t, and the system bandwidth and shape. Quantitatively, it is given by the envelope of the normalized autocorrelation function $C(t)$ (Sheridan and Sparks, 1967). For a rectangular band of width B,

$$C(t) = \text{sinc}\,(B.t) \qquad (8.1)$$

FIGURE 8.5 THE DELAY SYSTEM UNIT

The complete unit. Manual control uses the push buttons at the top. Automatic control is via the tape reader on the front. Amplifiers and reed relays are situated in the top section above the cables.

to $\pm 2^{o}$C by air conditioning). This can cause phase errors in the delay module lengths of up to 10^{o} elec.

A system now being developed for the final receiver (Frater and Mackay, 1967) uses a phase-locked pilot signal to eliminate these phase errors. An alternative solution (Read, 1963 and Wesseling, 1967) is to pass both signal sidebands of a frequency converted signal through the delay lines. The signals are then phase insensitive and suffer only slight losses of correlation.

Switching of the delay lengths was initially done with push buttons. At a later date this operation was automated by the author using punched paper tape for the control function (Section 9.4.5).

Because of the 'tied-array' form of operation*, observations away from the zenith experience delay errors along the 16 aerial grating blocks. These errors (up to 0.175 μs) cannot be corrected. Thus there is little point in using cable lengths shorter than this error length. The lengths indicated in Fig. 8.4 allow observations with a 1.8 MHz bandwidth to ±4 hrs hour-angle at $0^{o}\delta$ for the same correlation loss (up to 16% or 0.1 db for some of the spatial frequencies) as a 400 KHz bandwidth without delay lines.

Shorter lengths are being cut so that the full 2.2 MHz bandwidth can be used over ±1½ hrs hour-angle with an even lower correlation loss. This correlation loss applied to a linear instrument generally has the effect, similar to an aperture taper, of attenuating the higher spatial frequencies. The result is a broadening of the beamwidth, a lowering of the sidelobes and a slight drop in the overall gain.

In the final receiver system delay errors will amount to about half an I.F. wavelength ($\frac{1}{60}$ μs) which, with an 8 MHz rectangular bandwidth, will cause only 3% correlation loss.

To utilize the delay system in the two element radio source observations (Section 9.4), the four channels are placed in series and

---

*See Footnote in Section 7.2.3.

different delay cable lengths inserted so that path length error is held to within one I.F. wavelength (10 m). This arrangement proves very successful allowing observations up to 3 hrs from the meridian with 2.2 MHz bandwidth. The sensitivity drop is immediately apparent when a few delay steps are missed.

CHAPTER 9

ADJUSTMENT OF THE TELESCOPE

CHAPTER 9: ADJUSTMENT OF THE TELESCOPE

9.1 Introduction

The theoretical performance of the compound grating antenna has been considered in detail in the previous chapters. From these deliberationsit is apparent that the quality of performance depends critically upon the adjustment of the individual aerials.

Broadly speaking there are two approaches to the adjustment of the system. One is terrestrial and the other is celestial.

In the terrestrial approach the response of the system is adjusted to have the desired shape and direction of pointing relative to an earth-bound framework. A variety of separate techniques, including precision surveys and accurate electrical measurements, are necessary. All of these techniques are independent of the radio observations carried out by the telescope. Sutton (1967) has investigated these methods as applied to the Molonglo Radio Telescope.

The celestial approach is basically an observational one. It relies on the use of one or more calibrating sources. These are radio sources of known size and position, determined previously by other means, such as lunar occultations or optical identifications. The telescope performance, position and orientation are determined relative to these sources and the observations of other sources are related to a framework based on their positions.

These two approaches are, of course, tied intimately together by the earth's relation to the celestial sphere. In practice neither approach is applied exclusively and generally one approach is used to check the other.

In the present system the location of the individual aerials (defining the length and direction of the baselines) has been carried out using precision survey methods. This was discussed in Chapter 4.

This chapter is concerned primarily with the methods used to adjust the relative amplitude and phase of the signals from the individual aerials. For this, a combination of both terrestrial and celestial approaches has been necessary due to the low instantaneous sensitivity.

9.2 Amplitude Adjustments

9.2.1 Amplitude Adjustments for the Required Aperture Illumination

The amplitudes of the signals from the aerials in both gratings were measured by pointing the aerials, one at a time, at the sun. The receiver was operated in the total power mode and connected to the relevant mixer-preamplifier channel.

Because of the quasi-symmetrical configuration and the present 'tied-array' form of operation, it is necessary to apply a uniform amplitude taper to the grating arrays of 16 aerials each. The signals from each small aerial were equalized by trimming the current transformer flaps on the open wire T-junctions (Christiansen et al, 1961).

This equality was checked during phasing of the grating array elements by measuring the amplitude of interference fringes formed, using adjacent aerials (40 foot spacing) as an interferometer.

Pointing calibration of the small aerials was carried out at the same time by comparing scale readings of the direction of maximum response with the known position of the sun.

The signals from the aerials of the different grating arms were equalized by comparing fan beam scans of the sun taken separately using each arm operating into the total power receiver. In this case both the gain and receiver noise of each channel differed due to the use of separate mixer-preamplifier units. Signal gains were equalized by inserting attenuator pads in the intermediate frequency return lines.

In the same manner, the separate signals from the two large aerials were equalized using the sun as a source.

These amplitude adjustments give the linear aperture of the whole array a uniform illumination. However it is an easy matter to vary the

relative amplitudes of the four receiver channels by inserting attenuator pads in the intermediate frequency lines. This has the effect of placing a staircase illumination taper across the aperture. Observations are carried out with uniform illumination and with various staircase tapers.

9.2.2 Amplitude Adjustments for Maximum Sensitivity

An amplitude adjustment is necessary to optimize the sensitivity (Section 2.3). In this case the signal plus noise power of each correlator channel is equalized using the total power receiver.

During galactic observations the signals into any of the mixer-preamplifier units are very small in comparison with the channel noise. Under these circumstances the receiver channel noise powers are equalized.

During solar observations the signal powers into the mixer-preamplifier units are always greater than the channel noise power. In this case the signal-plus-noise powers are equalized.

Means of further refinement can be gleaned from considering Equation 2.27 . The noise temperatures, T_n, of some mixer-preamplifier units are lower than others (present range: $570^{o}K$ to $740^{o}K$). Careful choice of the location of these low noise units can give a sensitivity improvement.

In the present system ζ_1 and ζ_2 are 0.78 and 0.28 for the grating and the large aerial respectively. Hence $\zeta_1 . T_{300} > \zeta_2 . T_{300}$. For galactic observations, the system noise $\left\{\propto (T_1 T_2)^{\frac{1}{2}}\right\}$ is minimized by placing the low noise units on the large aerials.

For solar observations where the signal powers of all channels are greater than the receiver noise power, the sensitivity improvement by this method is not so significant. However, since the large aerial signal is much greater than the grating signal, a slight sensitivity improvement is achieved by placing the low noise units on the grating arrays.

In the final receiver system arrangement, with mixer units on each aerial, ζ will be < 0.2 for all aerials. In this case only two mixer units contribute to T_2 while 32 units contribute to T_1 . A large improvement in system sensitivity is achieved at relatively low cost by placing two low noise parametric amplifiers on the large aerials. This reduced T_2 and hence the system noise.

9.2.3 Experimental Aperture Tapers

'Running-mean' taper

For most observations the compound grating interferometer is used with a uniform illumination taper across the aperture. The response with this taper has a minimum beamwidth and 22% sidelobes.

During reduction of these observations a cosine-on-pedestal or 'running-mean' taper is applied. This taper amounts to convolution of the observed distribution with a 'three-point' impulse function. This is easy to apply as the distribution is displaced to either side and added to the original distribution in the correct ratio. (The Fourier transform of a symmetrical impulse pair is a cosine function (Bracewell, 1965) so that convolution with a symmetrical three point impulse function is the same as multiplying the aperture grading by a cosine-on-a-pedestal taper.)

Staircase tapers

During some solar observations, weak sources of small diameter appear in the vicinity of strong sources. In order to distinguish between these weak sources and possible sidelobe effects, a 'staircase' illumination taper is occasionally used.

This staircase taper is applied by changing the gains of the four receiver channels. Two such staircase tapers tried experimentally are shown in Fig. 9.1.

1. The first taper, Fig. 9.1a, lies between a cosine-on-10db-pedestal and a $(\text{cosine})^2$-on-10db-pedestal taper. (These are frequently used linear aperture tapers which give 37 and 40 sec. of arc beamwidth and 10% and 3% sidelobes respectively.) For this staircase taper the

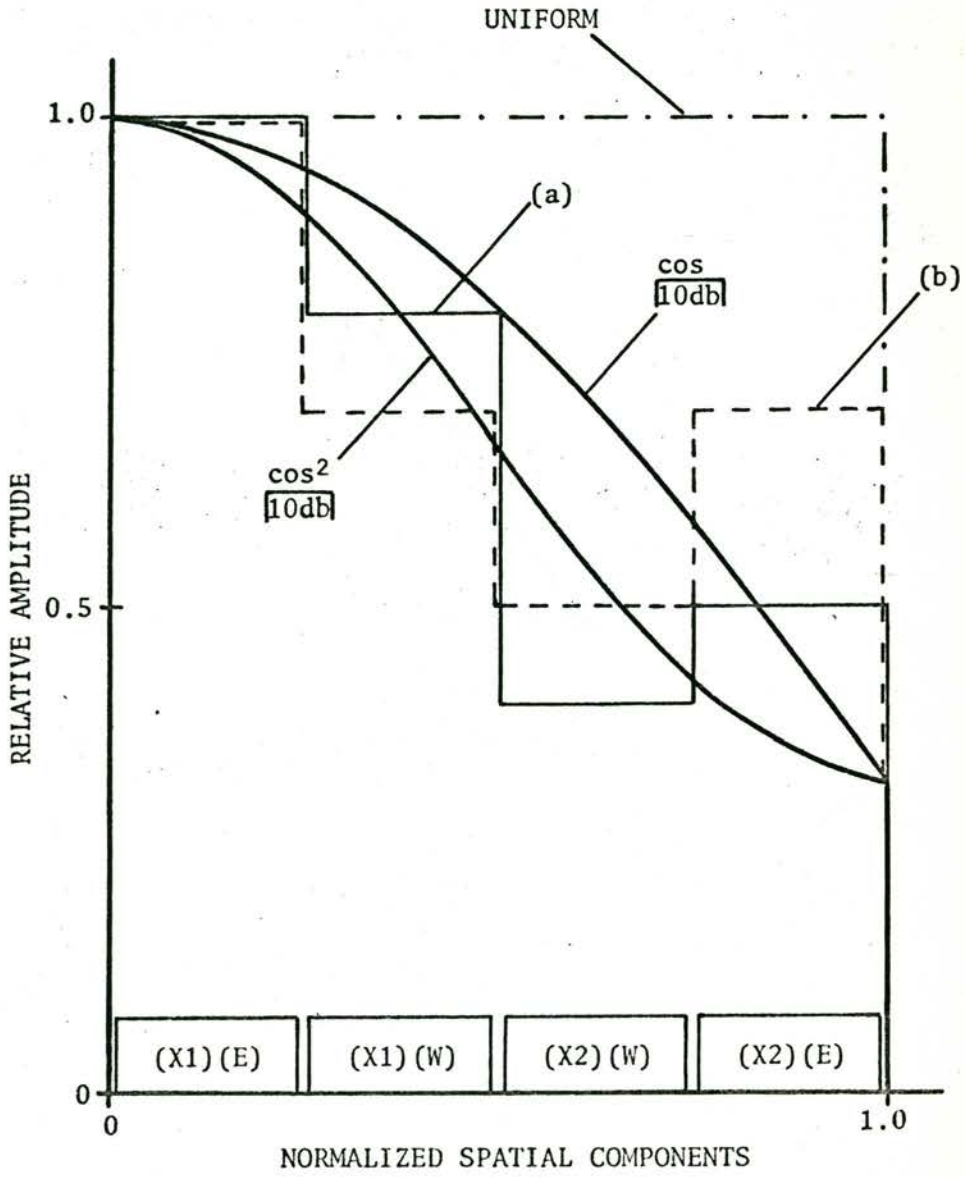

FIGURE 9.1 Aperture Tapers for the Compound Grating Interferometer.

the total power responses of the four channels are arranged approximately in the ratios:

$$(X1) : (X2) = 4:1$$
$$(E) : (W) = 3:2$$

2. The second taper, Fig.9.1b, reduces the sidelobes close to that of a $(\text{cosine})^2$-on-10db-pedestal. The total power ratios in this case are:

$$(X1) : (X2) = 2:1$$
$$(E) : (W) = 2:1$$

Removal of 'reverse' taper

In both of these staircase tapers, a slight 'reverse' taper is present for the higher spatial components. The effect of this on the response is small. However two methods of avoiding it are as follows:

1. The east and west gratings are equally weighted and tapering is applied to the large aerials only.

2. The signals from the (N1) and (S1) aerials* of the north-south arm of the crossed grating interferometer are added together to form an interferometer with a 40 foot spacing. The signal from this interferometer is added to the (X1+X2) side of the correlator receiver. This adds a component to the aperture taper corresponding to the spatial frequencies generated by (X1).(E). The complete aperture illumination taper can then be adjusted to have no reverse taper effects. This method was tested but with the present receiver arrangements it was difficult to keep the (N1+S1) interferometer lobe maximized on the sun.

An important advantage of this second method is that it provides a measurement of the 20 foot spatial component which is missing from the response of the full compound grating interferometer. In the final

---

*The existing 64 aerials of the crossed grating interferometer are numbered from the intersection out along each arm. Thus N1 is the first aerial from the centre along the north arm.

system it will be a relatively easy matter to correlate the (N1+S1) aerials with the (E1+W1) aerials. This combination measures the 20 foot components for both the east-west and north-south compound grating interferometers.

9.3 The Methods of Phase Adjustment

Phase adjustment of the compound grating antenna is an important part of its operation. Errors can easily degrade the beamshape as seen from the example of Fig. 2.10. This figure shows the theoretical response expected (in this case, from the north-south system) when phase errors are introduced between the correlating channels.

Adjustment of the relative phases was carried out in three stages.

(i) The phases of all the small aerials were equalized.

(ii) The phase difference between the two large aerials was reduced to zero.

(iii) The phase of the large aerials was equalized with the phase of the small aerials.

9.3.1. The Relative Phase of the Small Grating Aerials

The 32 small aerials are divided into two groups of 16. The 16 aerials in each group are interconnected by R.F. open wire transmission lines, as described in Section 7.2.2. The relative phase of these small aerials is adjusted by moving the sliding T-junctions on these open wire lines.

(a) Reflection technique

Phase measurement of the aerials in each block was carried out using the modulated load reflection technique proposed by Swarup and Yang (1961). In this method a signal is sent out along the line under test and reflected from the other end. At the input end the reflected

wave interferes with the forward wave producing standing waves. The position of the minima of these standing waves, detected by a slotted line probe, is a measure of the length of the line under test. At the reflection end of the line some form of modulated load is used. This modulated load causes the reflected wave, and hence the standing wave, to exhibit a small audio frequency modulation. A phase-sensitive detector enables this modulated signal to be separated from all other stray reflected signals.

Since the test signal travels in both directions along the line, the phase measurement by this method suffers a half-wavelength ambiguity. This ambiguity is removed either by physical measurement of the line length or by repeating the length measurement at another (usually half) frequency.

In the case of these small aerials, the modulated load is a 1424 MHz dipole which is short-circuited at a rate of 400 Hz. This modulated dipole is held close to the normal signal dipole of each small aerial in turn.

By this method, using a signal frequency of 1424 MHz, the 16 aerials in each arm were phase equalized.

(b) Injection method

Because of the presence of mixer-preamplifier units on the output of each arm, the reflection technique could not be extended to equalized the phases between the two 16 aerial blocks. Instead an injection method was used. In this method a 1424 MHz signal is injected into each small aerial in turn using a probe dipole placed close to the aerial dipole. The main receiver is used in the correlating mode to compare the phase of this injected signal with the signal from a reference channel, after both signals have passed through mixer-preamplifier units. Care must be taken when moving the probe dipole that the connecting cable is not flexed unduly causing its phase length to change. For this reason the cable length was kept short and the injection method was applied only to the four small aerials close to the

grating centre. This enabled the two arms (east and west) to be phase equalized.

(c) Observational method

Neither of the above two methods measures any inequality in path length of the paraboloid reflectors or any errors in their positions. These differences are small due to the similar construction of all 32 small aerials and to the precision survey of their locations. However any errors and inequalities were removed in a final phase adjustment by using an observational method.

In this method adjacent small aerials are pointed at the sun, two at a time. The receiver records the interference fringes of each of these two aerial interferometers as the sun drifts through the lobes. The position of the fringes in the sky relative to the known position of the sun gives the phase relationship of each pair of aerials. This thenprovides the corrections necessary to equalize the phases of all the small aerials.

The corrections to the aerials using this observational method are carried out twice. For the first correction the known optical position of the centre of the sun is used in the phase computations. Use of this position can create a phase error in the expected lobe position since disturbances on the sun can cause the centroid of the radio emission to differ from the optical centre. The effect of this error is to impose a linear phase slope across the grating. The 32 small aerials will still form a correctly shaped grating response but this could have a collimation error up to 2 min. of arc from the transit position.

To remove the possibility of this pointing error, the 32 aerials are used as a total power fan beam array to plot the one dimensional brightness distribution of the sun. This brightness distribution is Fourier analysed to determine the phase of the 40 foot spatial component relative to the assumed optical position. This phase is then applied as a correction along the grating to reorient the fan beam

response to the transit position.

In order to check the phase relation between the two arms, two compound grating interferometers were formed from the 32 aerials of the grating. In the first arrangement, the (E1) aerial of the east arm was correlated with the 16 aerial west arm grating. In the second arrangement the (W1) aerial of the west arm was correlated with the 16 aerial east arm grating. These two configurations were used successively to observe the sun. They both form fan beam responses having a 2.5 min. of arc beamwidth. When all the aerials are in phase these two configurations give identical scans.

9.3.2 The Relative Phase of the Two Large Aerials

Two methods were used to adjust the relative phase of the large aerials. In the first method a combination of reflection and injection methods was applied to all the cables and receiver units in the system. The combined phase difference was reduced to zero. In the second method, an observational one, the fringes of the source 3C273 were used to trim the phase difference of the signals from the two aerials.

(a) Reflection and injection methods

The large aerials each have mixer-preamplifier units close to the feed dipole. These units prevented the reflection technique from being applied directly. Thompson and Krishnan (1965) experienced a similar difficulty due to the presence of travelling-wave amplifiers in their signal lines. They overcame this problem by the use of circulators. This was not applicable here because of the frequency conversion in the mixer.

Instead, the receiving channels were each separated into the following components:

(i) The signal lines from dipole to image filter.

(ii) The local oscillator distribution system.

(iii) The intermediate frequency signal return lines.

(iv) The image filter and mixer-preamplifier combination.

Comparative phase measurements were carried out separately on all these components.

The reflection technique described in Section 9.3.1 was applied to the first three categories. The modulated loads in this case were constructed as small coaxial diode switches which could be plugged into the ends of the cables to be measured.

The half wavelength ambiguity was eliminated by physical measurement in the case of the signal lines and by repetition of the reflection measurements at half frequency in the case of the local oscillator and intermediate frequency cables. This half frequency measurement on the local oscillator cables was complicated by the presence of the frequency-sensitive power dividers. These dividers were temporarily removed and measured separately.

Comparative phase measurements of the image filters and mixer-preamplifiers were carried out by injection methods using the phase stability test setup described in Section 7.3.5. One image-filter mixer combination was used as a reference. The remaining combinations were compared successively with this reference.

The phase differences of all the separate components were added and the combined figure reduced to zero by adjusting the coaxial line stretchers (Section 7.2,6).

(b) Observational method

As in the case of the small aerials, the above phase difference measurements do not allow for inequalities in path length of the paraboloid reflectors or errors in aerial positions. These inequalities and errors were corrected, as before, by observing the interference fringes of a radio source. However in this case, the source used was the quasar 3C273 since the angular diameter of the sun was too great to create fringes(of known position) with the large spacing that exists between the large aerials.

Because of the low intensity of the radiation from 3C273 and the high fringe frequency (approximately 16 per min.) it was necessary to

develop a special method of slowing the fringes while still preserving their phase with the necessary high degree of accuracy. This method and the associated equipment are described in Section 9.4 and Appendix F.

9.3.3 The Relative Phase of the Large and Small Aerials

This relative phase was measured using observational methods. Other methods are unsuitable due to the different signal path lengths of the reflectors (Appendix C.4) and to the different arrangement of receiver components.

The minimum spatial component measured by the compound grating antenna is 60 feet. The two aerials which measure this component (X1 and E16) are used as an interferometer to observe the sun. The position in the sky of the resulting fringe pattern is used to indicate the relative phase of the two aerials.

As before, a total power fan beam scan of the sun is made using the 32 small elements as a simple grating. This scan is Fourier analysed to determine the phase of the 60 foot spatial component relative to the optical centre of the sun. The relative phase between the two aerials is then adjusted to position the fringe maxima in the expected directions.

9.4 Relative Phase Adjustment using the Fringe Rate Converter

9.4.1 Introduction

As mentioned previously one method of phasing two aerials is to use them as an interferometer to observe a point source which has an accurately known position. Such a source will produce sinusoidal output fluctuations (fringes) as the earth rotates and provided both time and the longitude of the observing site are known accurately, the phase can be adjusted to produce a fringe-maximum at the zenith.

This method has been used to phase the adjacent small aerials of the grating array (40 foot spacing) using the sun as a source. For this spacing of aerials, the sun can be used as a 'point' source provided the assumed position is modified by a correction factor which depends upon the distribution of emissive regions. This method was discussed in Section 9.3.1.

For larger aerial spacings it becomes impossible to use the sun as a point source. The spatial Fourier component being measured by the two aerials begins to depend considerably upon the time-varying radio plages and not so much upon the quiet sun component. The fluctuations of these plages cause the spatial Fourier component being measured to vary in magnitude and phase,making accurate phase measurements difficult. The result is that a small diameter radio source must be used instead of the sun.

The two aerials X1 and X2 have a separation of 3822 wavelengths at 1424 MHz producing fringes with a period of 54 sec. of arc. The quasar 3C273 is the most suitable radio source for use in phasing these two aerials. This source has an overall dimension of 19 sec. of arc and is approximately 40 flux units in strength at 1424 MHz. The position is known accurately from lunar occultations. All other accurately known sources of comparable size are either significantly weaker in intensity or outside the available declination range.

9.4.2 Sensitivity

Connected as an interferometer with a bandwidth of 400 KHz and a time constant of ¼ sec., the two aerials X1 and X2 do not have sufficient sensitivity to observe the 3C273 fringes. The signal is about half the noise level. A gain in sensitivity of 2.5 times can be obtained by increasing the bandwidth from 400 KHz to about 2.2 MHz, but this is still not sufficient to enable reliable positioning of the fringes. Short of replacing the mixer front-ends with low noise receivers, the only method of increasing sensitivity is to increase the integrating time. However an increased integrating time 'smears' the fringes out unless some means of slowing or stopping the fringes is employed (first used by Hanbury Brown et al, 1955). It was primarily for this purpose that the fringe rate converter was built.

An additional advantage of the fringe rate converter method is that the accuracy of measurement of phase depends upon the stability of a precision digital clock and not upon the accuracy of measurement of the chart records. This is important since normally the fringes have a period as short as 4 sec., making measurement difficult.

9.4.3 The Fringe Rate Converter

Le Roux first suggested (Lequex, 1962) that lobestopping could be achieved by phase switching the receiver at the fringe rate, thus rectifying the fringes. Since the fringe rate and phase are dependent upon source declination and hour-angle, it is difficult to derive the synchronized switching waveform necessary in this method.

However, in the fringe rate converter, a switching wave is generated at a fixed, closely-controlled frequency set slightly off the fringe frequency. This switching wave controls the phase switch in the second local oscillator line. The result is a form of frequency conversion (or quasi-synchronous rectification) applied to the source fringe rate so that the output fringes are slowed from a period of about

4 sec. to 4 min. or longer. This slower fringe rate is the difference frequency between the actual fringe rate and the generated switching wave.

A disadvantage of this rectification procedure is a resultant drop in sensitivity of 36%. However the slow output rate enables the time constant of the receiver to be increased considerably. Initially an eight fold increase in sensitivity ($t = \frac{1}{2}$ sec. increased to $t = 32$ sec.) brought the signal well out of the noise.

As the source fringe frequency changes, so does the output fringe frequency. When this rate reaches about one cycle per 4 minutes, the fixed switching frequency is reset to another value closer to the source fringe frequency.

Fig. 9.2 is a block diagram of the fringe rate converter unit. The design of the switching unit and other factors concerning the system operation are considered in more detail in Appendix F. Fig. 9.3 is a schematic representation of the two element interferometer receiver system using the fringe rate converter.

9.4.4 Preservation of Phase

The primary aim of this fringe rate converter system is the measurement of relative phase between two aerials, in particular X1 and X2. To do this successfully the phase of the fringes must be preserved. This is ensured by controlling the operation with a precision sidereal digital clock. This clock supplies:

(i) 10 Hz and 50 Hz square waves, one of which is used to drive the counter, and

(ii) a one minute square wave which is used for
   (a) starting the fringe rate converter
   (b) placing markers on the chart records, and
   (c) controlling the delay lines.

The phase of the source fringes can be derived accurately from a knowledge of the phase of both the general switching wave and the rate-converted fringes. A considerable advantage of the system is that the

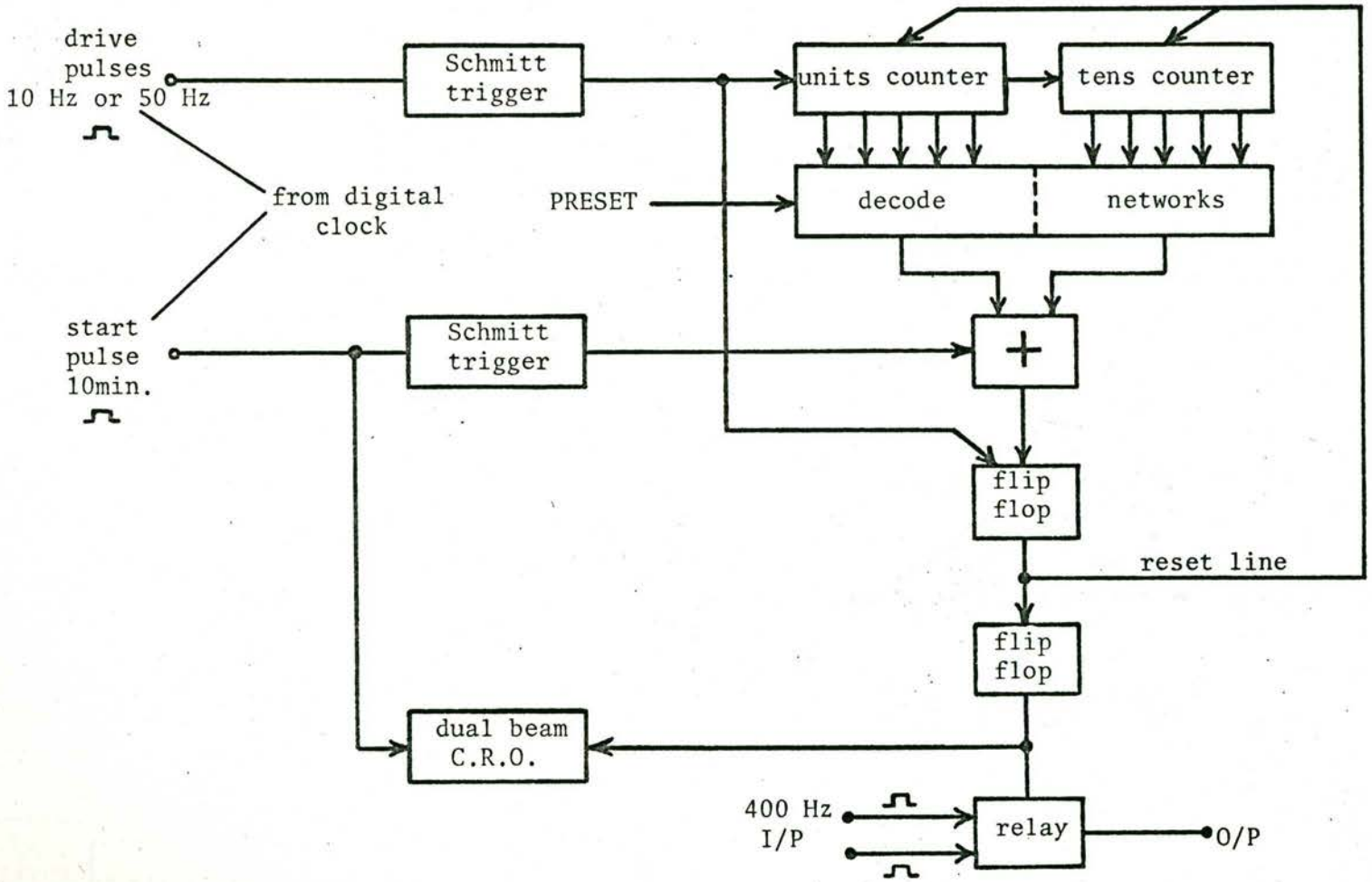

FIGURE 9.2 Block diagram of the fringe rate converter.

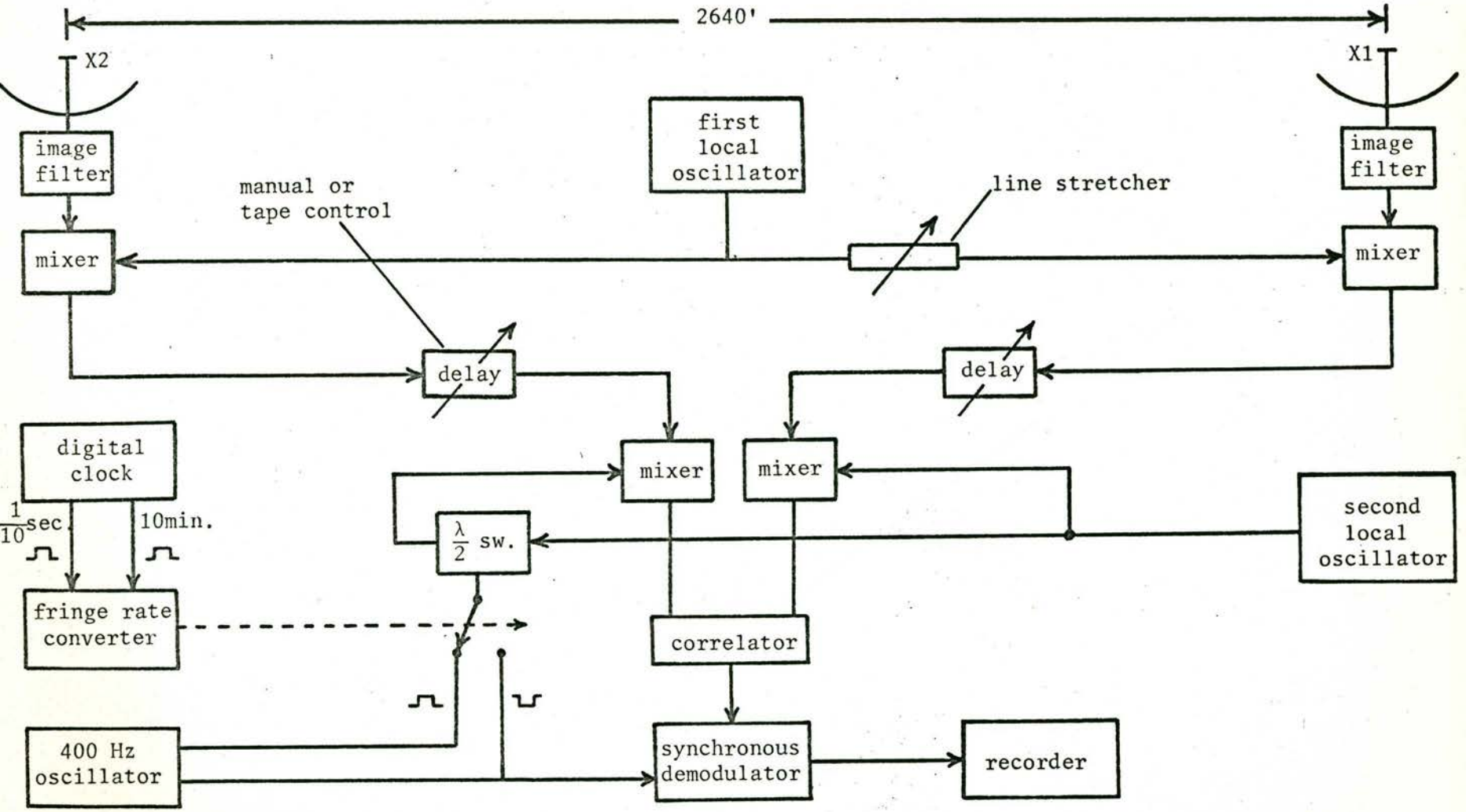

FIGURE 9.3 Schematic diagram of the receiver system for two element interferometer observations using the fringe rate converter.

output wave phase does not need to be read from the chart with high precision.

9.4.5 Signal Delay Unit

In order to attain the maximum sensitivity the receiver is operated with a bandwidth of 2.2 MHz. Aerials X1 and X2 have a baseline length of 3822 wavelengths. To avoid correlation loss (Equation 8.1) as the source moves away from transit (75% loss at ½ hr hour-angle with the quasar 3C273) it is necessary to use delay cables to equalize the signal path lengths.

As there are only two signal paths to be compensated, the Stage 1 delay unit was used in a modified form (see Section 8.3) resulting in a binary delay system in which the shortest length is 20 m (or two wavelengths at 30 MHz). Thus path lengths are kept equal to within ± 10 m. This causes negligible (1%) correlation loss.

The delay unit is not temperature compensated and as a result, phase errors of up to 10^{o} can occur during switching. These errors are measured after each observation period and corrections made in computing the fringe phases.

With the ½ mile baseline, delay switching occurs every 3 to 6 minutes. To avoid this task and the associated human errors (3 steps missed cause ~40% correlation loss), the delay switching was automated using punched tapes to indicate the required delays. These tapes are advanced by the digital clock once a minute. Parity and continuity check systems are incorporated into the tape reader. A different tape is used for different declinations. The tape reader can be seen on the front of the delay rack in Fig. 8.5.

9.4.6 Observations

The following checks are carried out during observations:

(i) The digital clock is checked against the transmission of standard time from station VNG.

(ii) The timing of the fringe rate converter is checked by noting, on a dual beam oscilloscope, the coincidence of one second pulses with the output square wave.

(iii) The local oscillator frequency is continually monitored and kept within 20 KHz of 1394 MHz.

(iv) Before and after observations the relative phases of the two correlator channels (including all delay length combinations) are calibrated.

To date the fringe rate converter system has been used to observe 3C273, Hydra and the sun using the aerials X1 and X2. Sample records of the observations are shown in Fig. 9.4.

The position of Hydra is not known with sufficient accuracy to be of use in phasing the system. However with further observations it will be possible to determine its right ascension position in relation to 3C273. Although Hydra has an intensity greater than 3C273, the signal-to-noise ratio of the observations (Fig.9.4b) is not as good due to the larger size of Hydra.

The sun record, Fig. 9.4c, is one of interest. There is fine detail present of sufficient intensity to produce fringes visible with the simple interferometer of X1 and X2. These fringes are shown for two periods about eighty minutes apart indicating the gradual drop in intensity of this source. The fringe rate converter record of the same region demonstrates the simplification of phase measurement and some of the available increase in sensitivity. The time constant was only 13.1 sec. and the bandwidth only 400 KHz. No delays were used.

3C273 has been observed on many occasions for periods between two and three hours either side of transit. The records have been reduced, using a computer program written by Mr. I.G. Jones. This program accepts the time of the peaks of the output fringe wave, the starting time of the switching unit and the receiver time constant and then computes the relative phase of the receiver channels. Fig. 9.5 shows the results of one such observation.

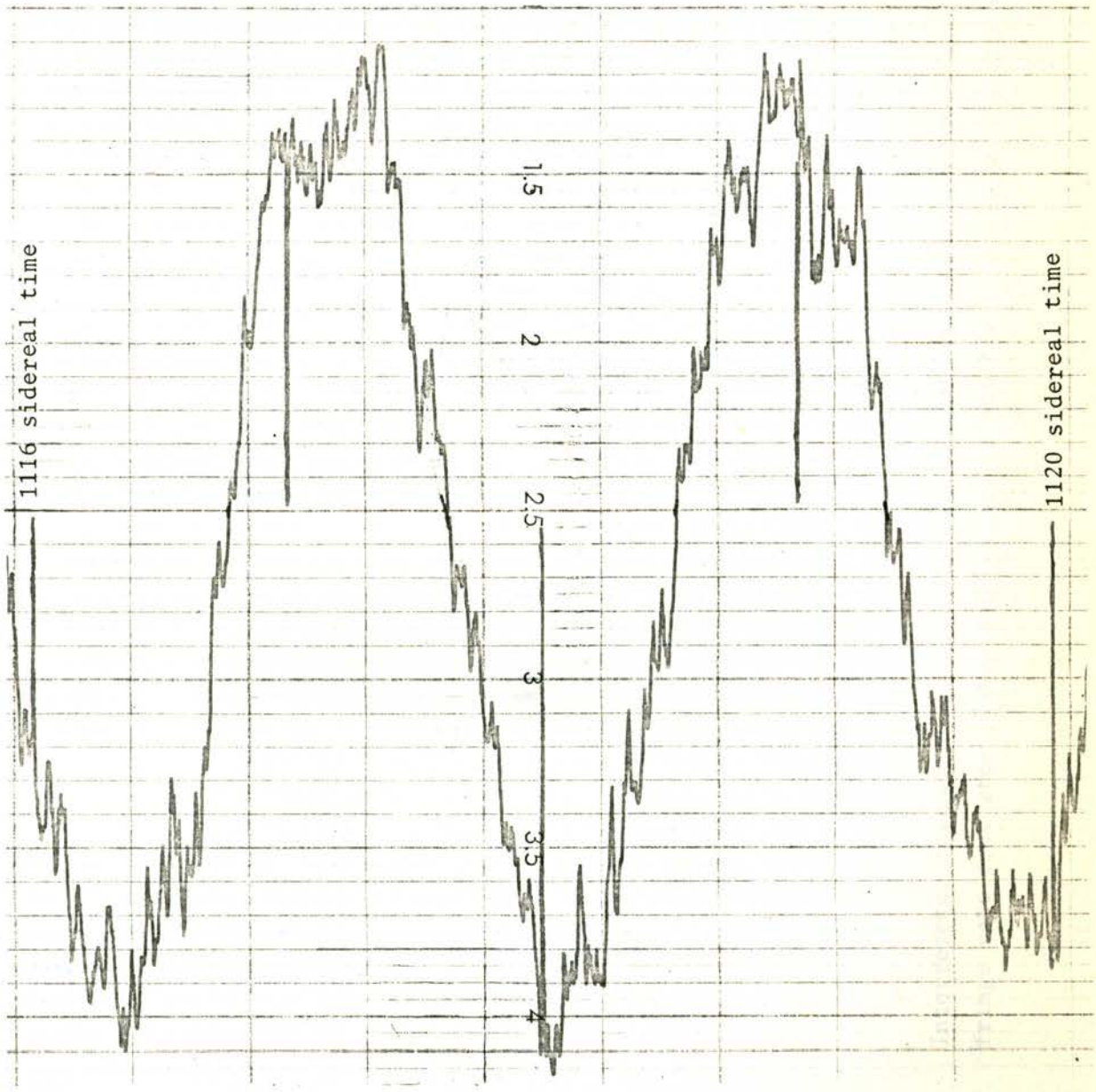

FIGURE 9.4a Interference fringes from the quasar 3C273 observed on August 2nd, 1967 using the fringe rate converter system and aerials X1 and X2.

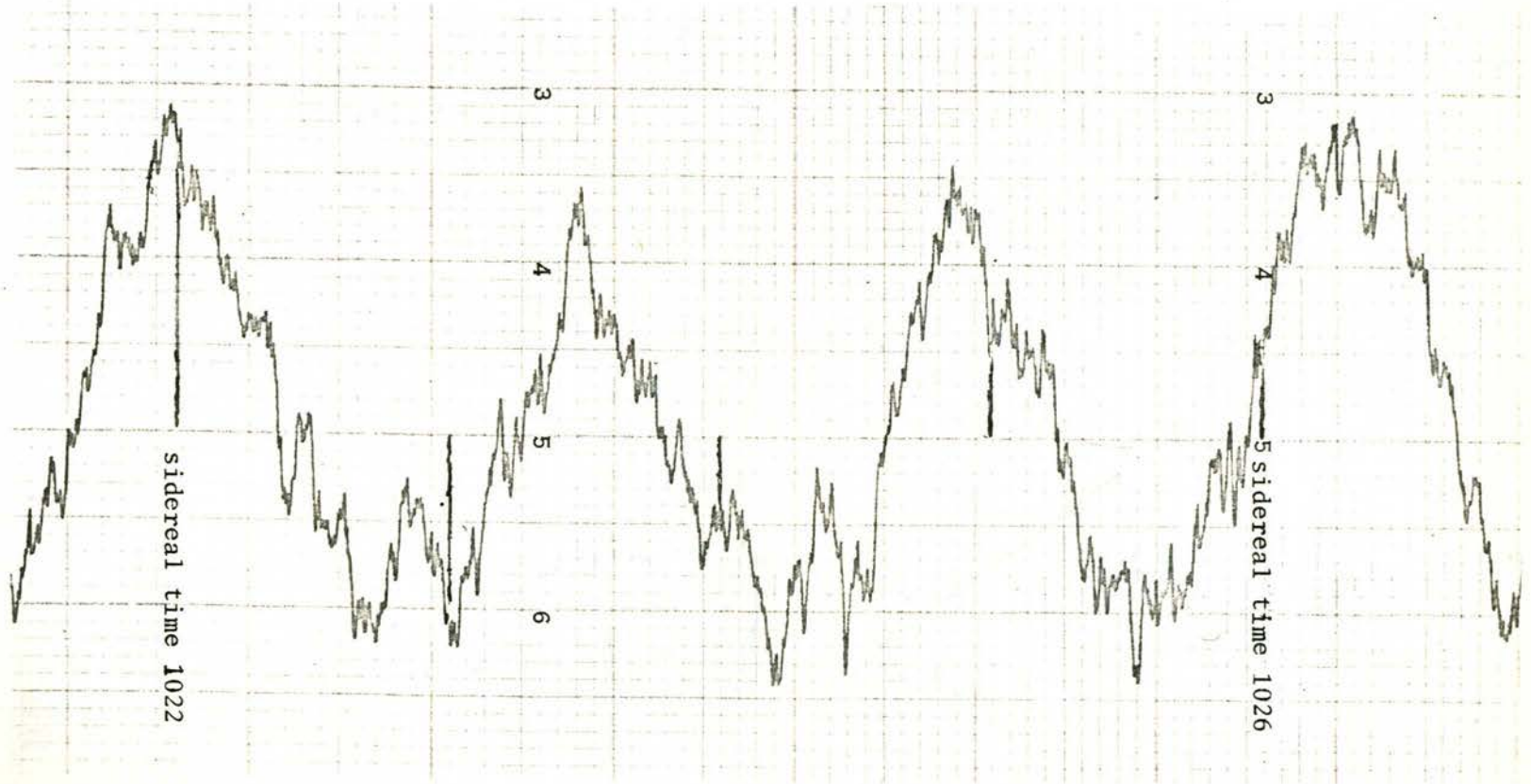

FIGURE 9.4b

Interference fringes from the radio source Hydra observed with the fringe rate converter system and aerials X1 and X2.

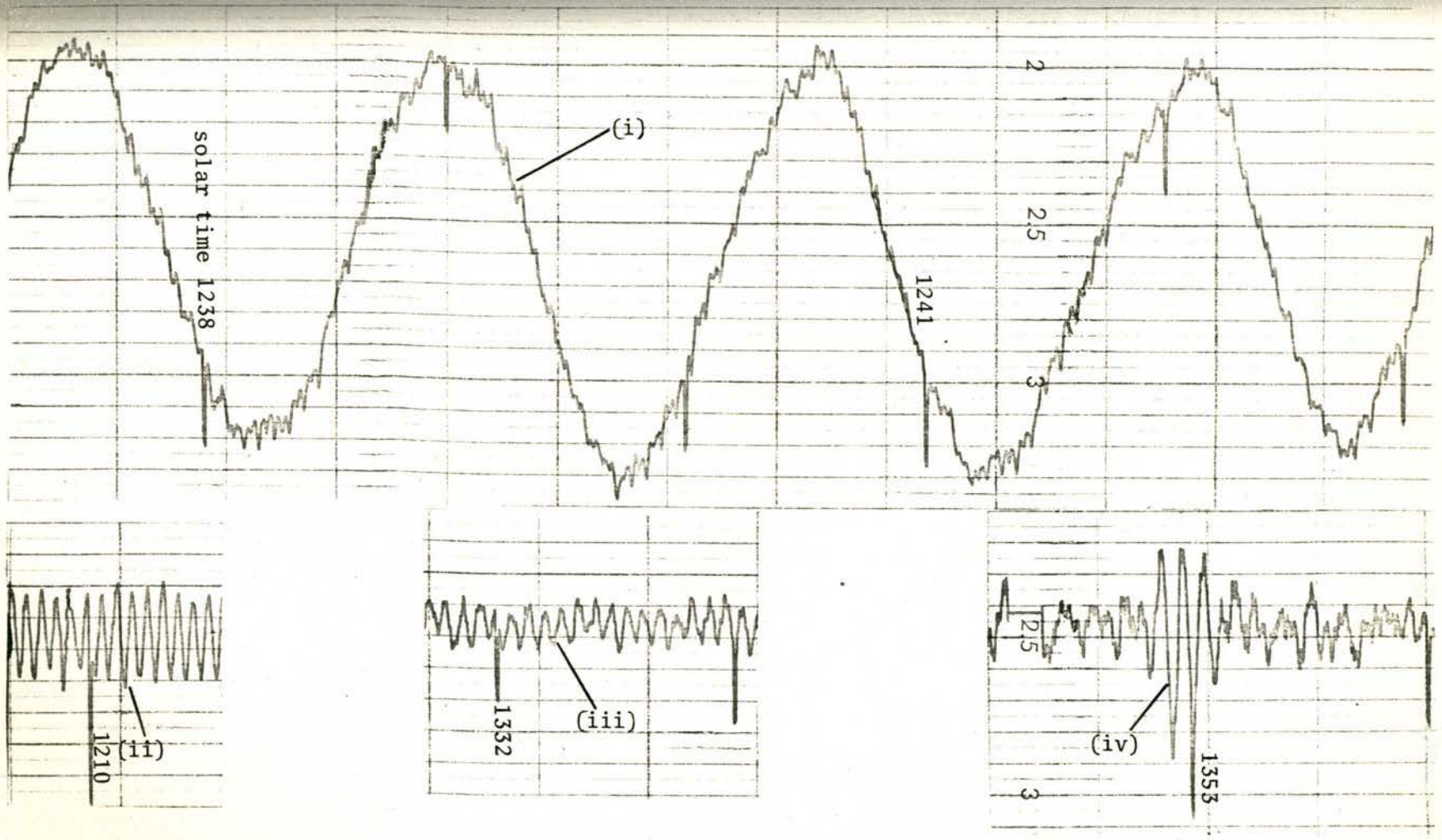

FIGURE 9.4c

Interferometer records of the solar outburst on July 26, 1967; chart speed of 1½ inches per min.
(i): Aerials (X1) and (X2) using the fringe rate converter system.
(ii) and (iii): Aerials (X1) and (X2) giving simple fringes.
(iv): (X2)(E+W) filter mode response.

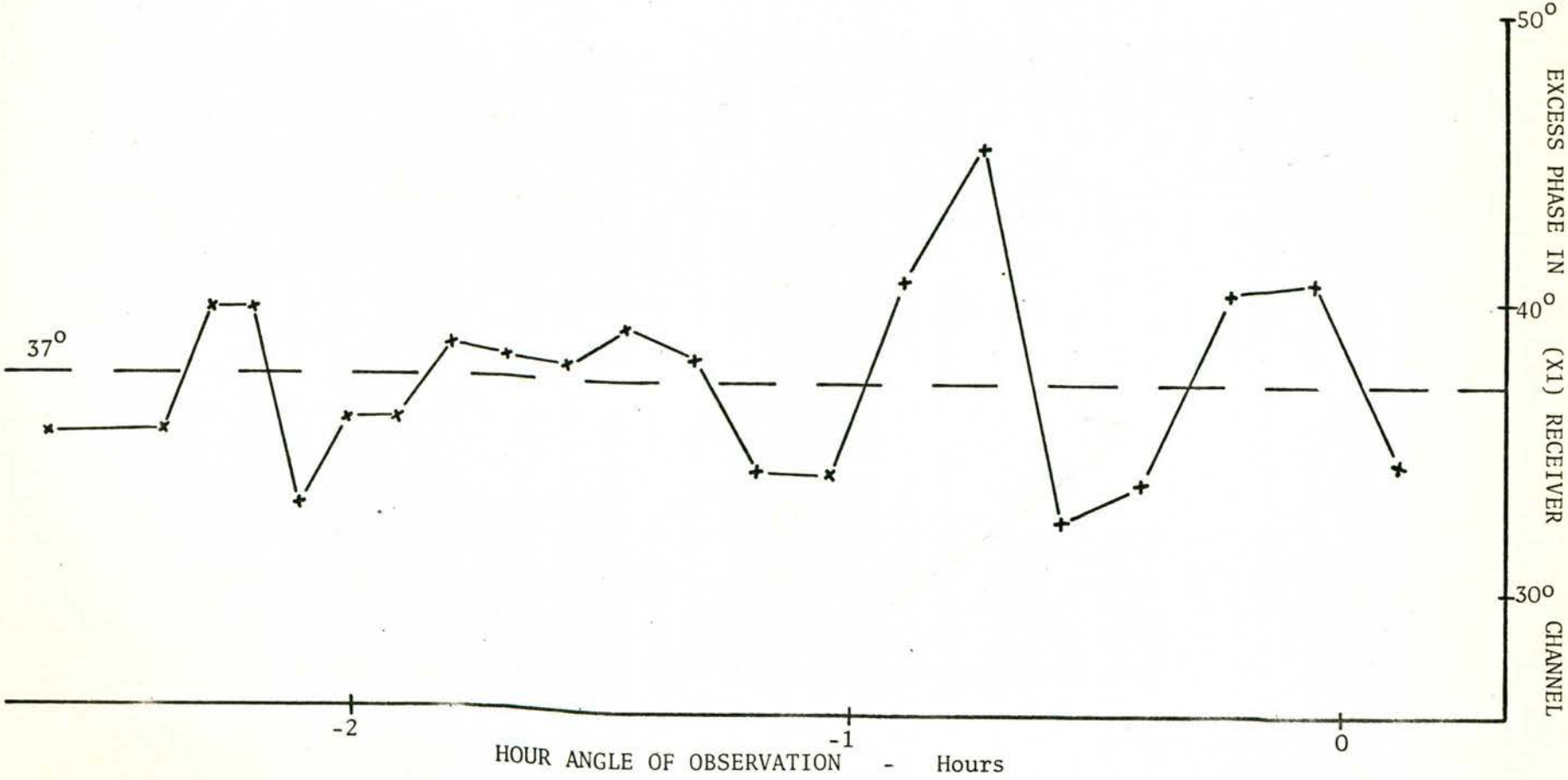

FIGURE 9.5 Results of an observation of 3C273 on July 26, 1967, with aerials (X1) and (X2) using the fringe rate converter system.
On this occasion the average phase error is 37° elec. in the X1 receiver channel.

9.4.7 Extension of Fringe Rate Converter Observations

1. Installation of both a sine and cosine receiver on the fringe rate converter system will allow continuous measurement of the relative phase of aerial channels. This effectively increases the sensitivity, and hence accuracy, of measurement because the average can be taken over a larger number of samples. Observations will be possible on many weaker sources.

2. Observations can be continued over increased hour-angle coverage and the phase variation plotted over the whole period. This variation can be used to determine temperature effects on the receiver system and effects of flexure in the aerial signal cables.

3. If observations are carried out with calibration sources at different declinations, the length and orientation of the baseline between the aerials can be established.

4. As soon as the installation of the preamplifiers on the small aerials is finished, the fringe rate converter system will be applied to completely phase all aerials using the one source (3C273).

Lack of time has prevented these lines of investigation from being developed. However the principal aim, that of ascertaining the phase relationship of the aerials X1 and X2, has been successfully completed.

9.5 Phase and Amplitude Adjustment Using a Fourier Analysis Technique

This method of adjustment is similar to those used in Sections 9.3 and 9.4 in that they are all based on the observations of sources. However here the observation is made with the complete telescope. The procedure is simple in principle: The resultant distribution is analysed into its spatial components and the relative phases and amplitudes of these components are compared with the expected values. Suitable corrections are then made to the aerials which sample the particular components that are in error.

This technique was first proposed by Blum et al (1961) who applied it to observations of the radio source Hydra with the east-west and north-south grating arrays of the Nançay Station. Hydra, when observed with the resolution of these gratings, appears as a point source. Under these conditions an array of correctly adjusted aerials will show equal amplitude and zero phase for all the spatial components.

The present compound grating antenna at Fleurs has a higher resolution than the Nançay grating so that Hydra no longer appears as a point source since smaller diameter sources are too weak to be observed with the sensitivity of the instantaneous fanbeam, this method cannot be applied directly to adjust all of the spatial components. The writer proposed a modified form in order to check some of the lower spatial components. The methods used are described in the following Sections 9.5.1 and 9.5.2.

9.5.1 Solar Observations

In this case solar observations are used and the method takes advantage of the redundancy of spatial components which occur in the total-power response of the simple grating.

The 32 small aerials form a simple grating which samples half the number of spatial components measured by the full compound interferometer. These spatial components are measured by the grating with varying degrees of redundancy, reducing the effects of random phase errors. (It does not affect any phase errors which are either periodic or cumulative.) The compound grating antenna has no redundancy in its spatial measurements making the response sensitive to individual phase errors.

Sections 9.2 and 9.3 have described the methods by which the grating array and the compound grating interferometer are adjusted to have uniform aperture illumination and zero aperture phase gradient. To check this adjustment, observations of the sun are made successively using both of these systems and the resultant scans are Fourier analysed into spatial components. After being normalized and corrected for antenna taper, comparison of the spatial distributions indicates which aerials of the compound grating antenna need correction.

Fig. 9.6 shows the amplitude results from one such observation*. This result is of particular interest because on this occasion the evident low intensity of the smallest spacing of the compound interferometer enabled the diagnosis of a faulty electrical connection in the feeder line to the (E16) aerial.

This method is only applied over the lower 16 spatial components since the higher ones are either not measured by the grating or have a low redundancy.

---

*Mr. C. Peterson assisted in the observations and developed the computer program used to carry out the Fourier analysis.

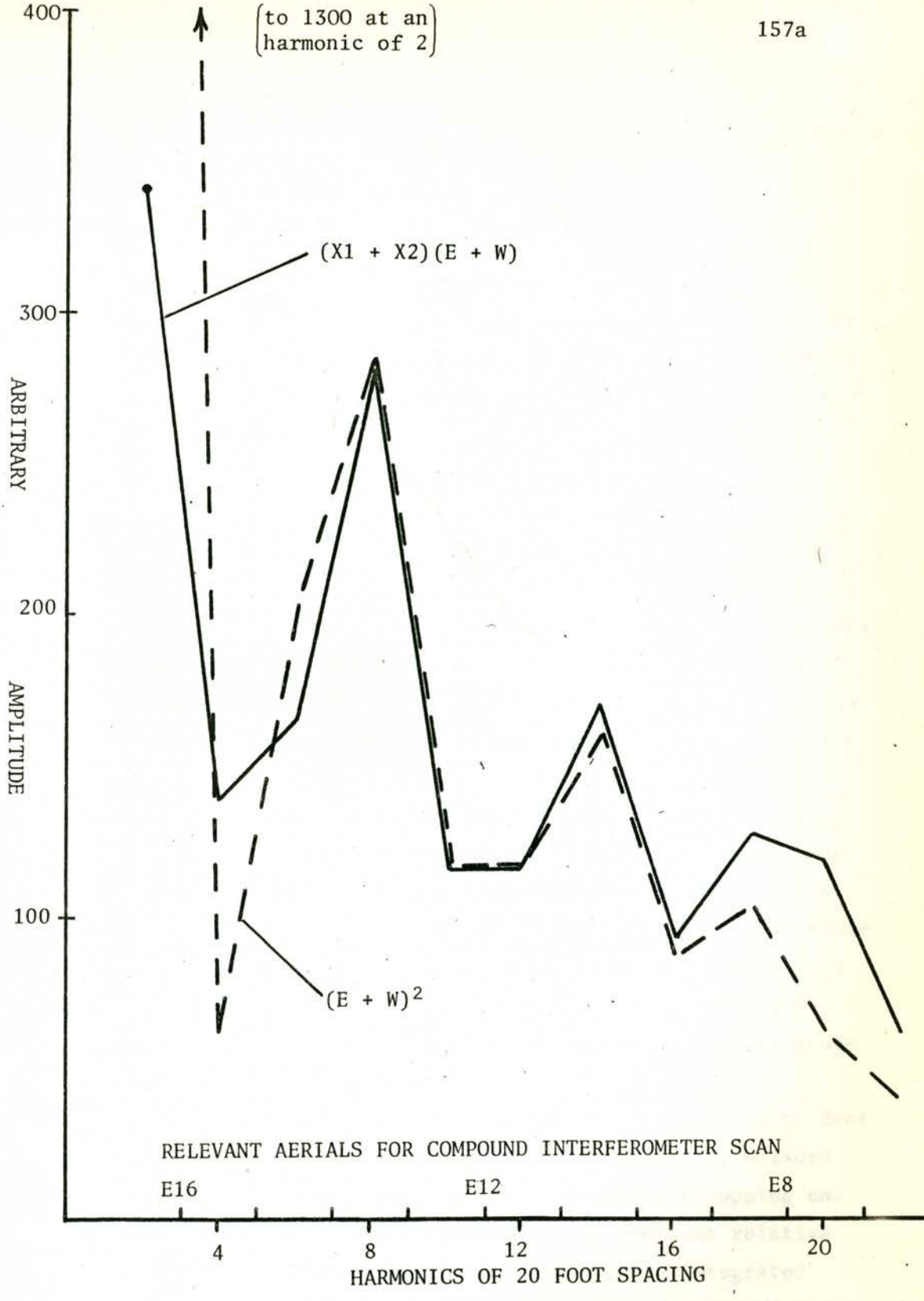

FIGURE 9.6 Amplitude comparison of the spatial components of an observation of the sun with the compound interferometer and the east-west total power grating.

9.5.2 Radio Source Observations

The method of Section 9.5.1 relies on the spatial redundancy present in a total power grating array and on the short term stability of the solar radiation. To avoid this dependence, the radio source Taurus was observed using only the lower eight spatial components of the compound grating antenna. These components form a 5.3 min. of arc fan beam response while Taurus has a half width of 3.6 min. of arc (Labrum et al, 1964).

Twiss et al (1962) have shown Taurus to have an approximately Gaussian spatial brightness distribution with only small spatial phase variations. This makes it suitable for use in adjustment of the lower eight spacings of the system.

Fig. 9.7(a) shows an observation of Taurus. Several records were combined to improve the signal-to-noise ratio. The smoothed scan was Fourier analysed and the results compared with the expected distribution (Fig. 9.7(b)). This gives phase and amplitude corrections for the lower 8 spatial components.

At present digital recording equipment is being added to the receiver system. This will make it possible to integrate reliably many scans of a source in a manner similar to that of Thompson and Krishnan (1965). This integration can be used to raise the signal above the noise level. An accurate measurement of the full array beamshape can also be made using the 'point' source 3C273. The Fourier analysis technique described in this Section can then be applied to determine the amplitude and phase adjustments over the whole array.

In the final telescope system the Fourier analysis (as such) does not need to be carried out since the receiver arrangement will measure all the spatial components separately. Application of lobestopping ensures that the phase of these components will remain constant relative to the source. The output of each correlator can then be integrated until sufficient sensitivity is achieved to give reliable measurement of the phase and amplitude of each spatial component.

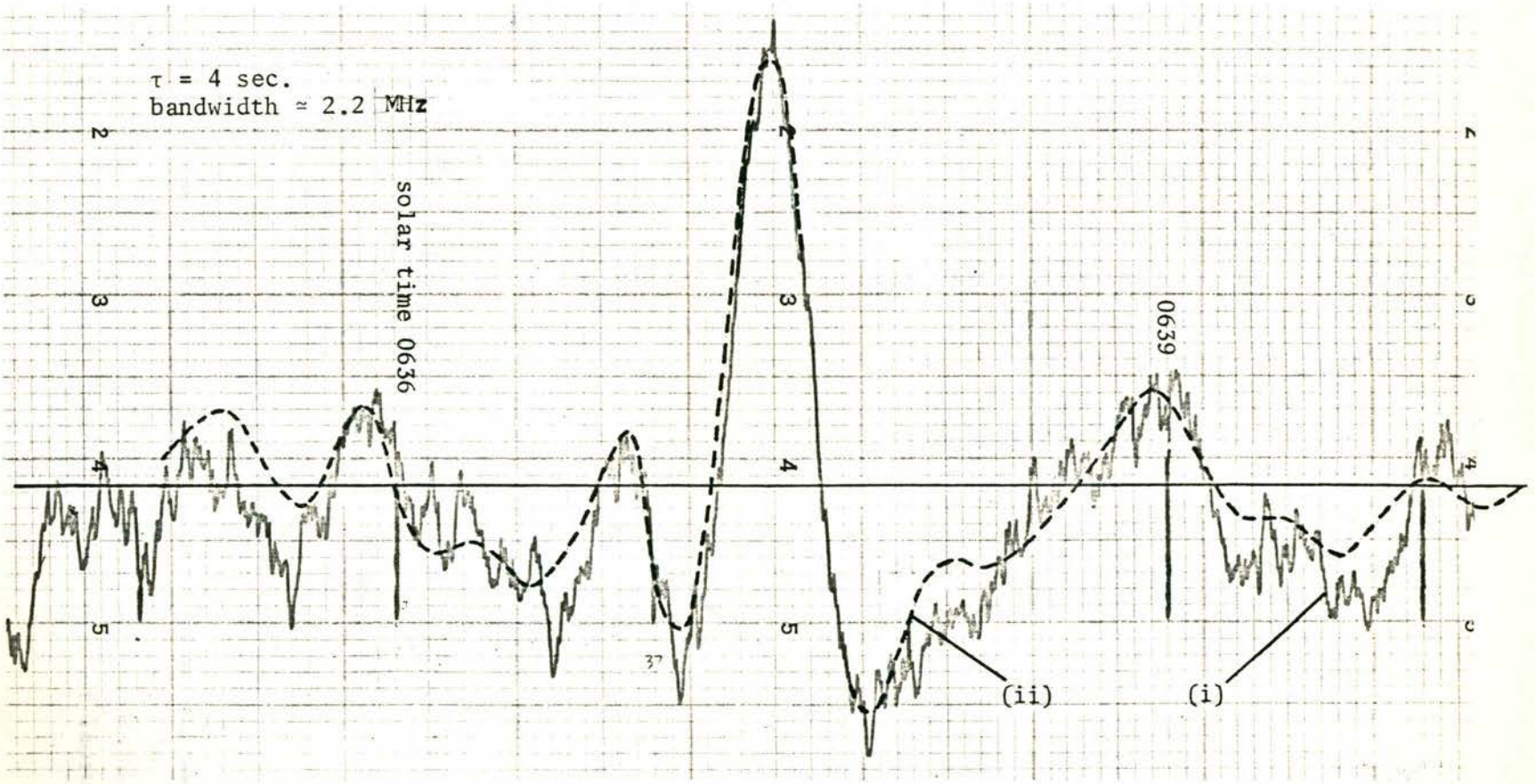

FIGURE 9.7a

An observation of the radiosource Taurus on July 31, 1967 using the compound grating interferometer (X1)(E16→E9).
(i) Portion of the record at about +1 hour H.A.
(ii) A smoothed record formed by combining six scans.

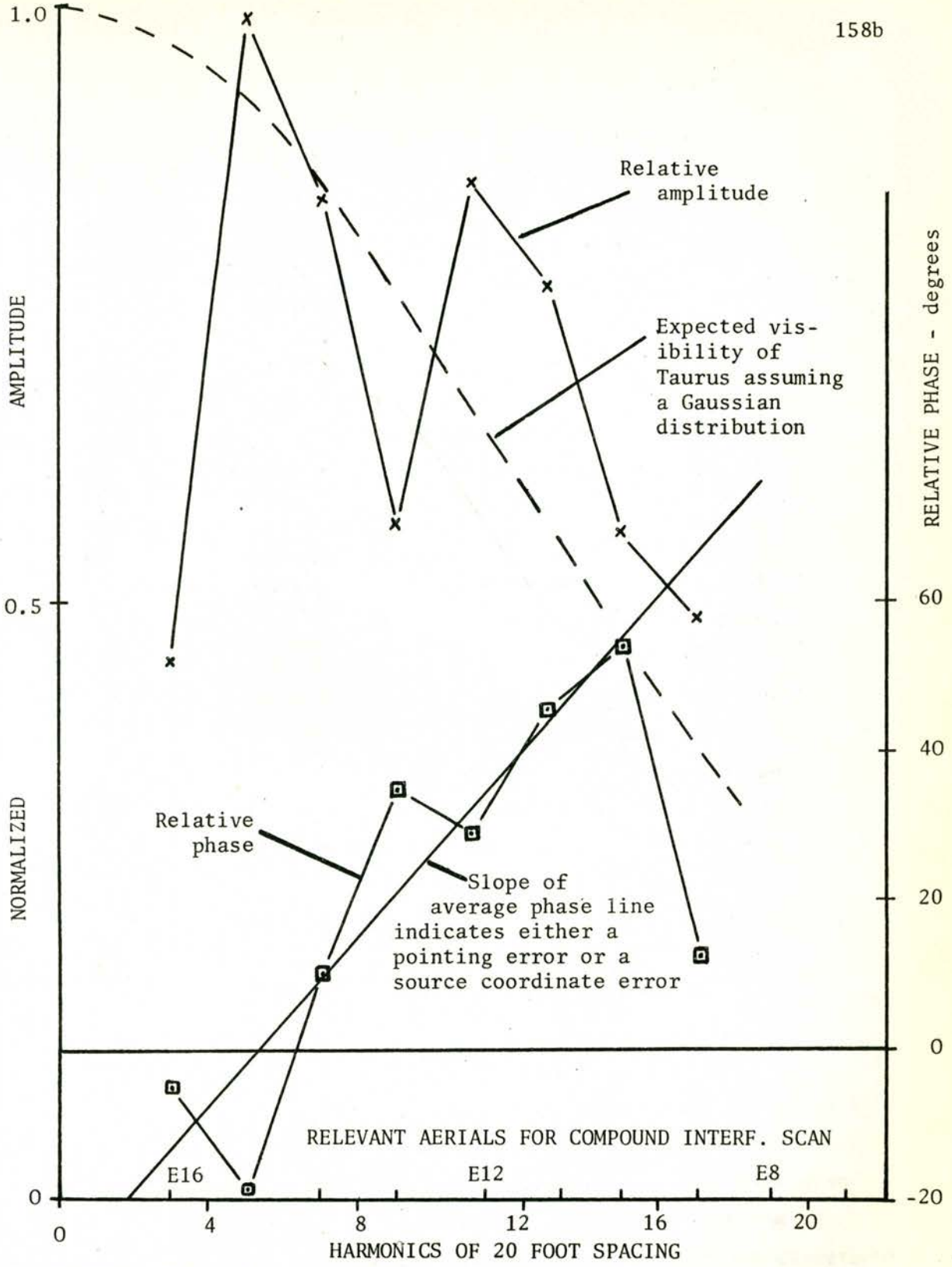

FIGURE 9.7b Results of Fourier analysis of Taurus scans of Fig. 9.7a

CHAPTER 10: OBSERVATIONS

The east-west telescope was first operated as a high resolution fan beam instrument in April, 1967. During the first few months, observations were irregular being disturbed by the various tests and adjustments discussed in Chapter 9.

The observations to date have been largely restricted to the sun because of the present low sensitivity. Exceptions were some observations of Taurus and Virgo carried out during the phasing operations described in Section 9.5.2.

Following the adjustment period, regular solar observations were carried out from July to September, 1967. Some preliminary results from this period are described in a paper (Appendix G) presented at the Solar Research Conference at Culgoora, N.S.W. Attention is directed to the conclusions drawn from these observations. The most important inference is that there is significant fine structure on the sun having an angular size comparable to the 35 sec. of arc beamwidth. Fine structure of this angular size has not been observed previously at this wavelength.

No attempt is made here to interpret these conclusions in terms of solar physics.

As described in Appendix G, the filtering modes of operation prove extremely useful in detecting the presence of this fine structure. Operation in these modes is carried out by deliberately omitting from the telescope response some of the lower spatial components. Fig 10.1 gives the theoretical responses for two such configurations. An experimental response having the same shape is seen in Fig. 3 of Appendix G. This agreement between the theoretical and experimental responses also provides an indication of the accuracy of phase adjustment of the distant aerial, X2, compared with the grating array. Incorrect adjustment causes an easily detectable asymmetry in the response shape.

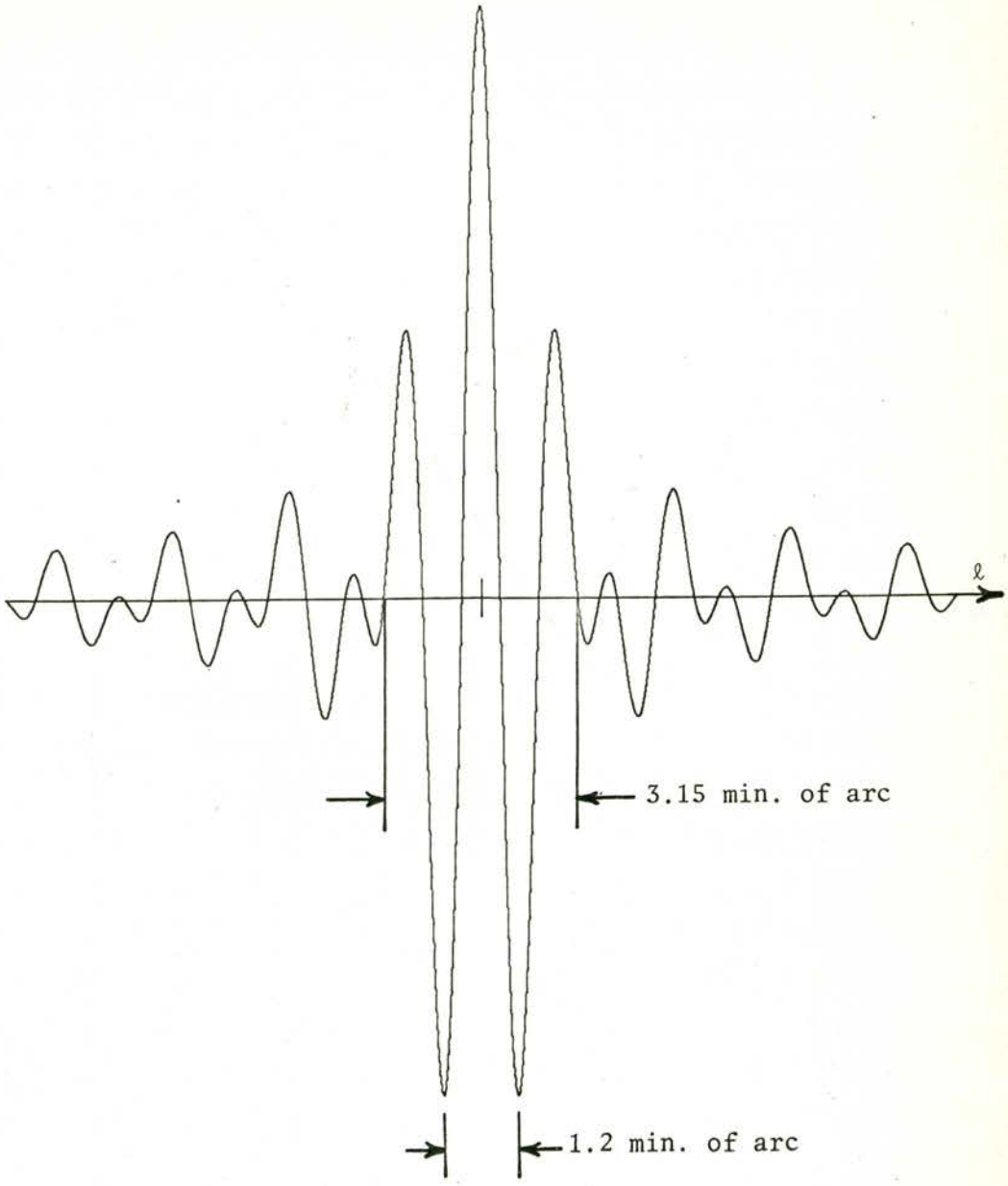

FIGURE 10.1a The response of the compound grating interferometer operating in the filtering mode: (X2)(E+W).

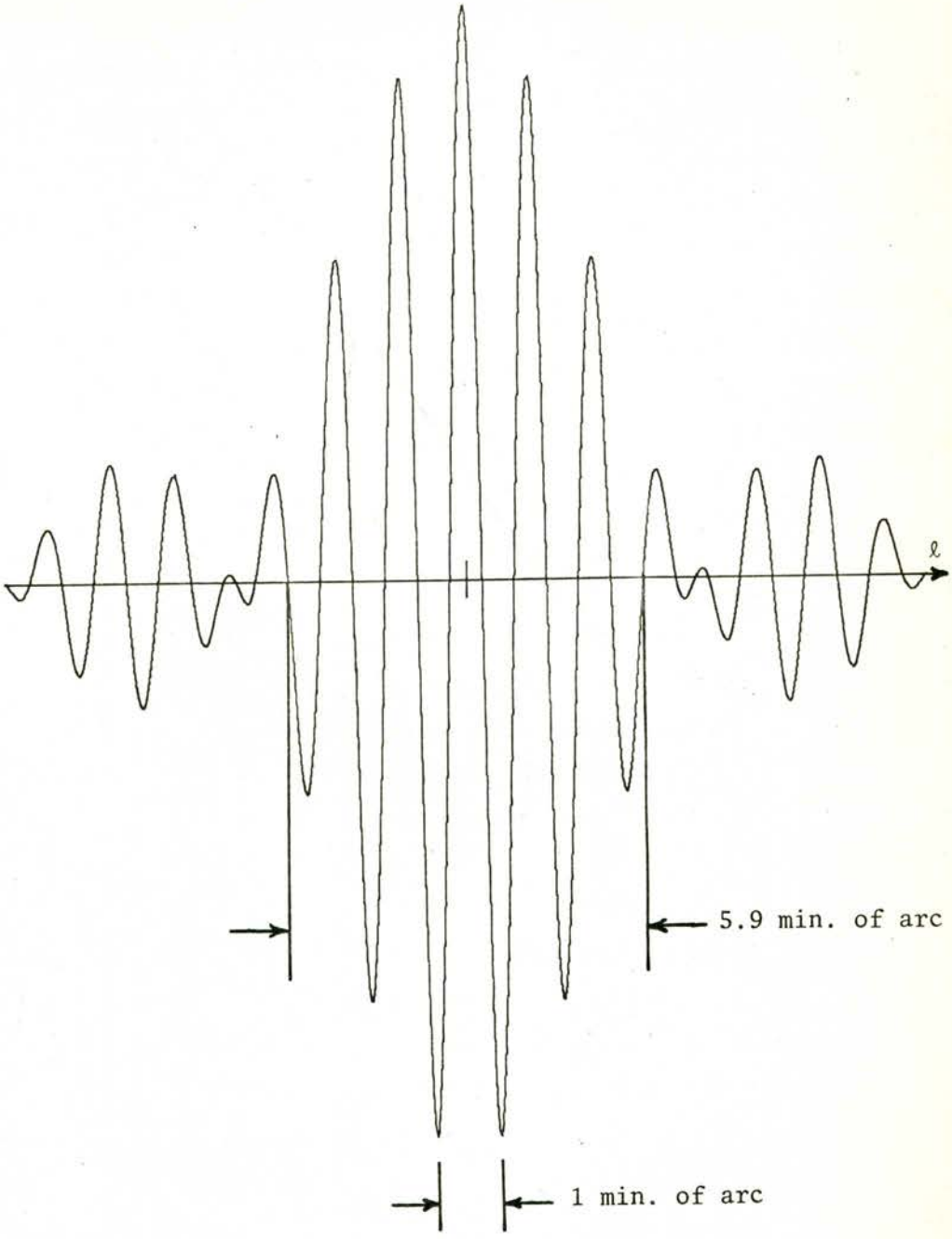

FIGURE 10.1b The response of the compound grating interferometer operating in the filtering mode: (X2)(E).

The sun is at present undergoing a period of increasing activity. As mentioned in Section 9.4.6, some of the bursts have been observed with the long baseline two element interferometer consisting of aerials X1 and X2. Fig. 10.2 shows a record of portion of the declining phase of one such burst. On this occasion both signal and image sidebands of the receiver system were used, creating a clearly visible modulation envelope over the 4 sec. period fringes. Comparison of the decay rate of these fringes with that of the total power record indicates that the active region was increasing in angular size as it was dropping in intensity.

Fig. 10.3 shows a section of a 35 sec. of arc compound interferometer record of the sun obtained on Sept 10,1967. For comparison, a total power east-west grating scan of the sun has also been included. This east-west grating previously provided the highest resolution available at this frequency (1424 MHz). The two records were taken about ½ hour apart so that some scan angle rotation had occurred between the scans. In spite of this, the effect of the increased resolution of the compound grating interferometer can be clearly seen. The baseline of the compound interferometer scan is a broad negative cosine curve caused by the absence of the 20' spatial component.

As a further demonstration of the improvement in visible detail on the sun now available as a consequence of higher resolution, the telescope was operated with different resolutions by omitting some of the higher spatial components. Consecutive drift scans of the sun taken with progressively increasing resolution are presented in Fig. 10.4. These curves are tracings of the original records.

Frequency 1424 MHz + 1364 MHz
Double side band receiver; 400 KHz Bandwidth
1 sec. time constant
Aerials X1 and X2 on a baseline of 2640 feet
Hour angle about -5^{o}.

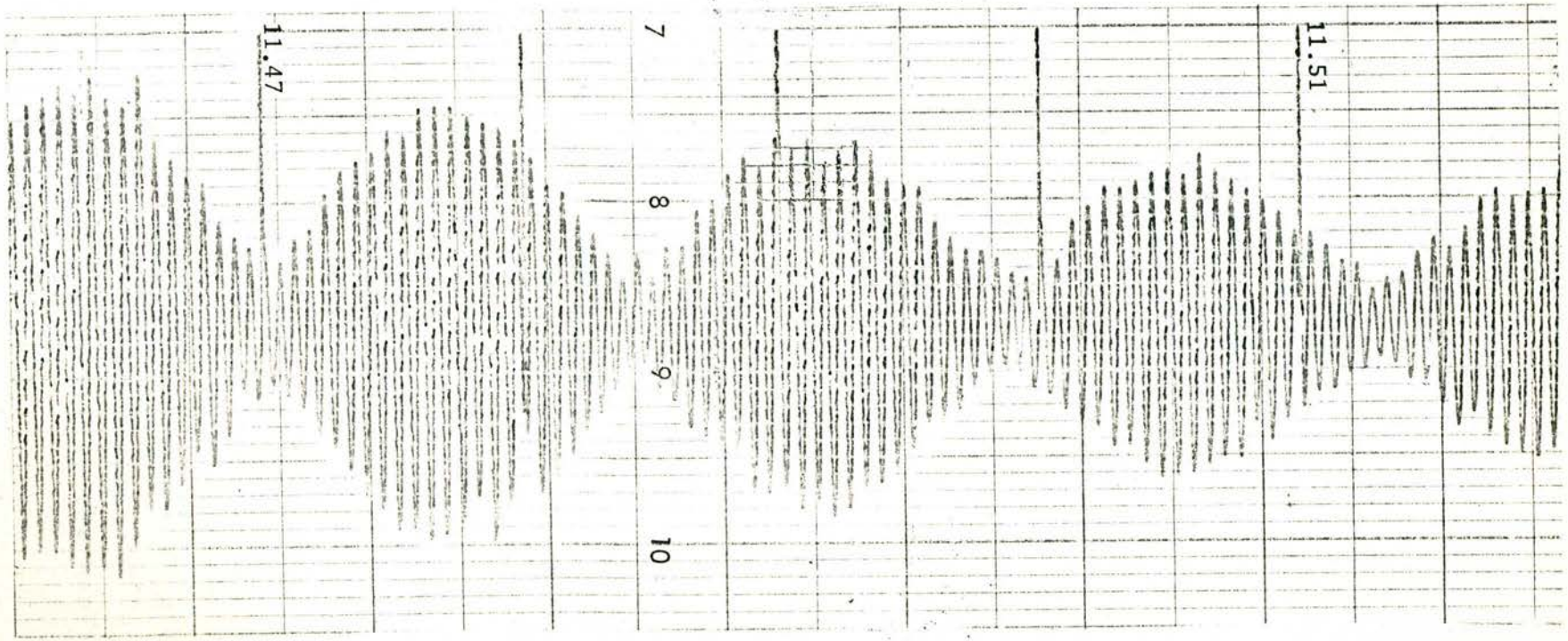

FIGURE 10.2 Portion of the interferometer record of the large solar outburst on March 22, 1967.

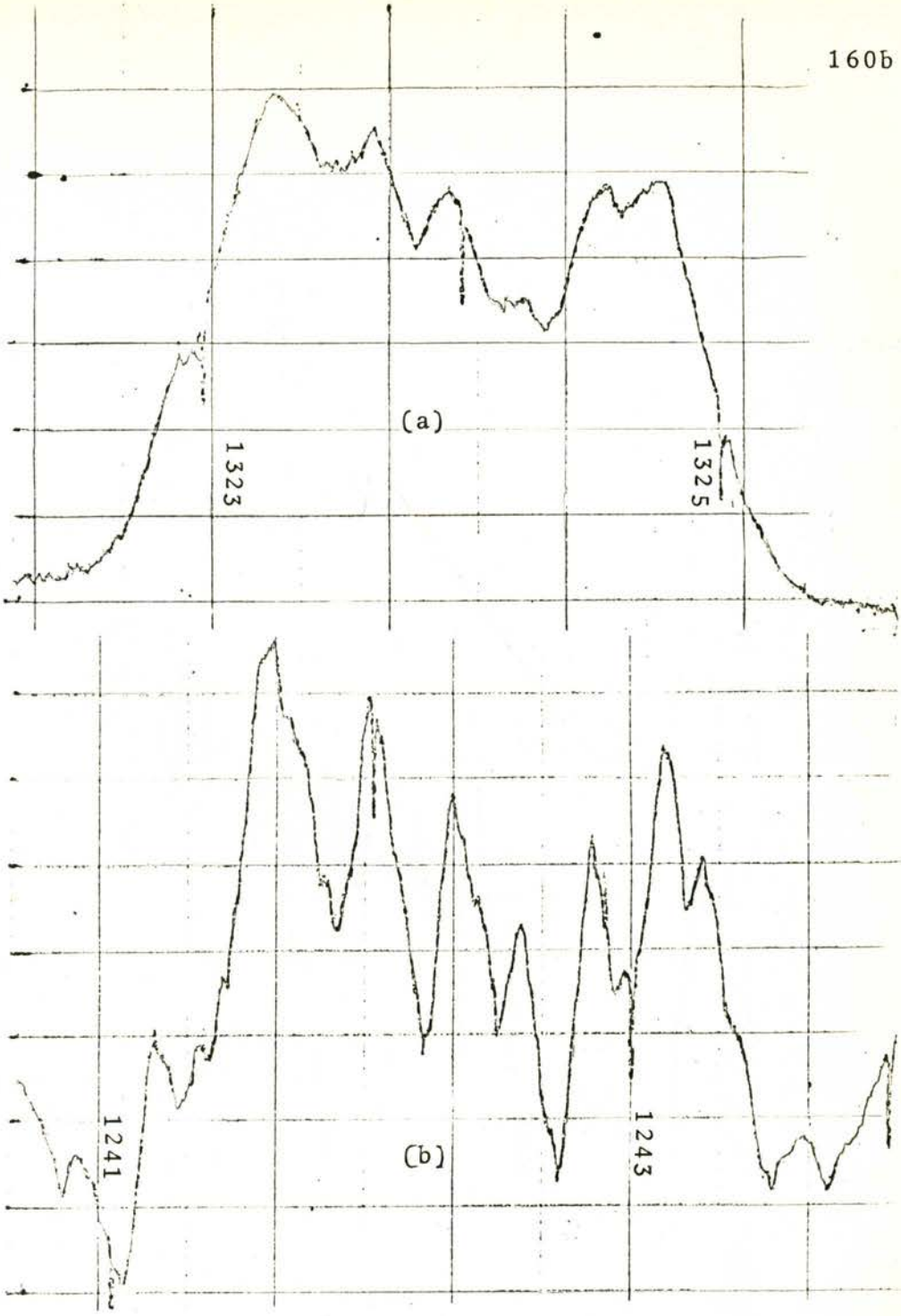

FIGURE 10.3 Comparison of fan beam scans of the sun, taken on Sept 10, 1967, with (a) the east-west grating (2 min. of arc) and (b) the east-west compound interferometer (35 sec. of arc) demonstrating the benefits of the higher resolution.

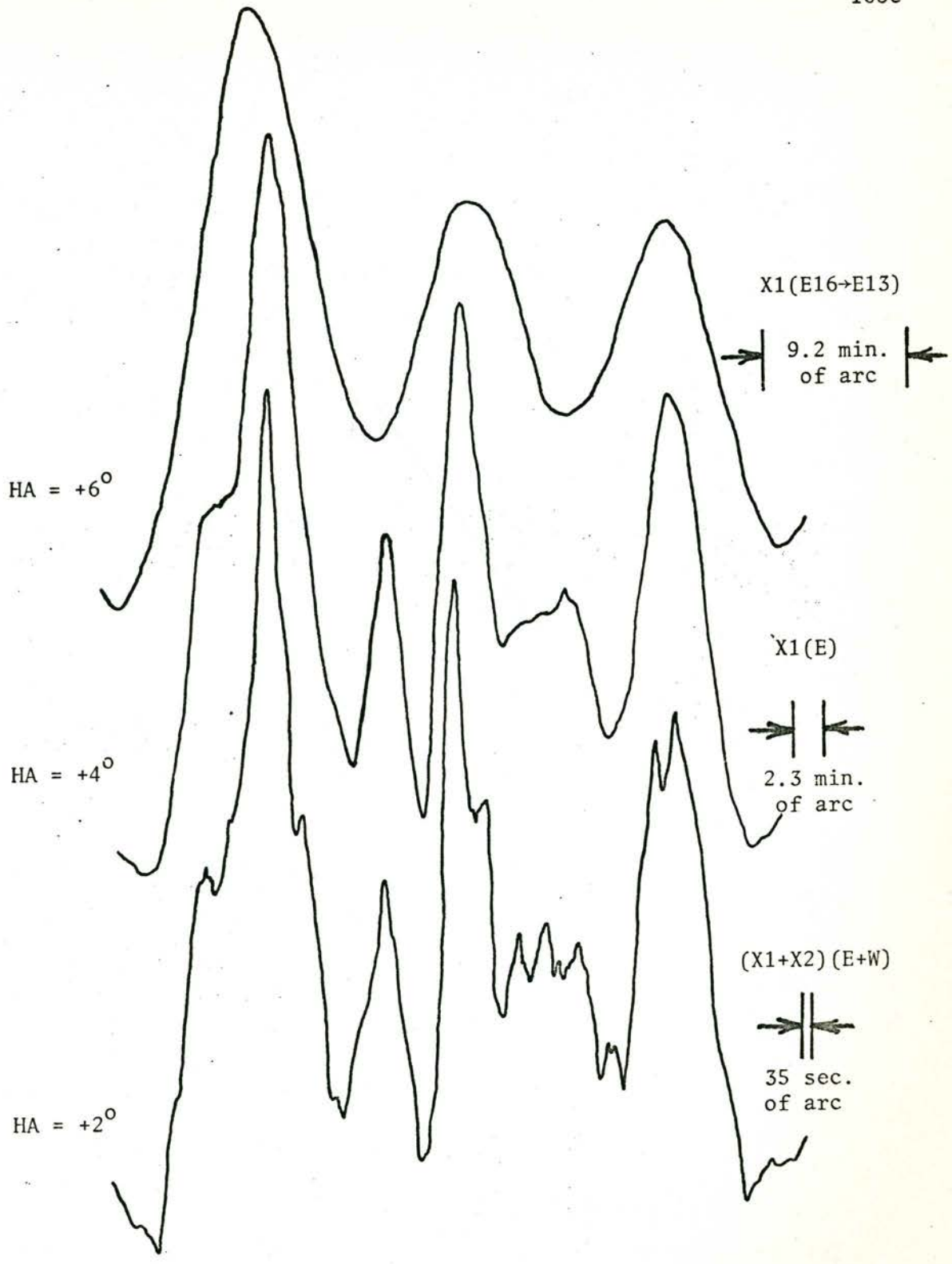

FIGURE 10.4 Tracings of scans of the sun on September 14, 1967 using the east-west compound interferometer with different resolutions.

BIBLIOGRAPHY

ADGIE, R.L., GENT, H., SLEE, O.B., FROST, A.D., PALMER, H.P. and ROWSON, B. 1965, *Nature, 208,* 275.

ANDERSON, L.J. and GROTH, L.H., 1963, *Trans IEEE, AP-11,* 148.

ARSAC, J. 1955, *Optica Acta, 2,* 112.

ARSAC, J. 1956, *Optica Acta, 3,* 55.

BARBER, N.F., 1958, *Proc. Instn. Radio Engrs., 46.*

BLUM, E.J., DENISSE, J.F., and STEINBERG, J.L. 1958, *Proc.I.R.E. 46,* 39.

BLUM, E.J., 1959, *Annls. Astrophys., 22,* 140.

BLUM, E.J., 1961, *Annls. Astrophys., 24,* 359.

BLUM, E.J., DELANNOY, J. and JOSHI, M., 1961, *Seance du 24 Avril,* 2517.

BOOKER, H.G., and CLEMMOW, P.C., 1950, *Proc. Instn. elect. Engrs. (III), 97,* 11.

BORN, M. and WOLF, E., 1959, *Principles of optics.* New York: Pergamon Press.

BOWEN, E.G. and MINNETT, H.C., 1962, *J. Br. Instn. Radio Engrs. 23,* 49.

BRACEWELL, R.N. and ROBERTS, J.A., 1954, *Aust. J. Phys. 7,* 615.

BRACEWELL, R.N. 1956a, *Aust. J. Phys., 9,* 198.

BRACEWELL, R.N. 1956b, *Aust. J. Phys., 9,* 297.

BRACEWELL, R.N., 1959, 'Radio Astronomy Techniques' in *Handbuch der Physik,* Flugge, S. (Ed.), Berlin: Springer.

BRACEWELL, R.N., 1961a, *Trans. I.R.E., AP-9,* 49.

BRACEWELL, R.N., 1961b, *Trans. I.R.E., AP-9,* 59.

BRACEWELL, R.N. and SWARUP, G., 1961, *Trans. I.R.E., AP-9,* 22.

BRACEWELL, R.N., SWARUP, G. and SEEGER, C.L., 1962, *Nature, 193,* 412.

BRACEWELL, R.N. 1965, *The Fourier transform and its applications.* New York: McGraw-Hill Inc.

BRACEWELL, R.N. and RIDDLE, A.C., 1967, *Astrophys. J., 150,* 427.

BROWN, F.W., 1961, *Trans. I.R.E., AP-9,* 113.

BROWN, J.S. and McKEE, K.E., 1964, *Microwave J., 7,* 41.

CARTER, A.W.L. and WILD, J.P., 1964, *Proc. R. Soc., A 282,* 252.

CHENG, D.K., 1955, *Trans. I.R.E., AP-3,* 145.

CHRISTIANSEN, W.N. and WARBURTON, J.A., 1953a, *Aust. J. Phys., 6,* 190.

CHRISTIANSEN, W.N. and WARBURTON, J.A., 1953b, *Aust. J. Phys., 6,* 262.

CHRISTIANSEN, W.M. and WARBURTON, J.A., 1955, *Aust. J. Phys., 8,* 474.

CHRISTIANSEN, W.N., MATHEWSON, D.S. and PAWSEY, J.L., 1957, *Nature, 180,* 944.

CHRISTIANSEN, W.N. and MATHEWSON, D.S., 1958, *Proc. I.R.E., 46,* 127.

CHRISTIANSEN, W.N., 1959, *Proc. Instn. Radio Engrs. Aust. 20,* 519.

CHRISTIANSEN, W.N., LABRUM, N.R., McALISTER, K.R. and MATHEWSON, D.S., 1961, *Proc. Instn. elect. Engrs., 108,* 48.

CHRISTIANSEN, W.N., 1963, *A. Rev. Astron. Astrophys. 1,* 1.

CHRISTIANSEN, W.N., ERICKSON, W.C. and HÖGBOM, J.A., 1963, *Proc. Instn. Radio Engrs. Aust., 24,* 219.

CHRISTIANSEN, W.N. and WELLINGTON, K.J., 1966, *Nature, 209,* 1173.

CHRISTIANSEN, W.N. and HÖGBOM, J.A., 1968, (Book in preparation.)

CONWAY, R.G., KELLERMANN, K.I. and LONG, R.J., 1963, *Mon. Not. R. astr. Soc., 125,* 261.

COVINGTON, A.E. and BROTEN, N.W., 1957, *Trans I.R.E., AP-5,* 247.

COVINGTON, A.E., 1959, *Inter. Astron. Union. Pub.* 'Paris Symposium on Radio Astronomy', 159.

COVINGTON, A.E., and HARVEY, GLADYS A., 1959, *Can. J. Phys., 37,* 1216.

COVINGTON, A.E., 1960, *Jl. R. astr. Soc. Can., 54,* (2 parts) 17, 58.

COVINGTON, A.E., LEGG, T.H., BELL, M.B., 1967, *Solar Phys., 1,* 465.

DICKE, R.H., 1946, *Rev. scient. Instrum., 17,* 268.

DRAKE, F.D., 1964, *Proc. IEEE, 52,* 108.

ELSMORE, B., KENDERDINE, S. and RYLE, M., 1966, *Mon. Not. R. astr. Soc., 134,* 87.

ERICKSON, W.C. and HÖGBOM, J.A., 1962. Benelux Cross Antenna Project, Memo 20A (unpublished).

ERICKSON, W.C. and WATKINSON, A., 1962, Benelux Cross Antenna Project, Memo 24 (unpublished).

FINDLAY, J.W., 1964, 'Antennas & Receivers for Radio Astronomy', in *Advances in Radio Research,* Saxton, J.A. (Ed.), Academic Press.

FRATER, R.H., 1964, *Rev. scient. Instrum., 35,* 810.

FRATER, R.H., 1965, *Rev. scient. Instrum., 36,* 634.

FRATER, R.H., 1966a, Ph.D. Thesis, (unpublished).

FRATER, R.H., 1966, *Trans IEEE, IM-15,* 9.

FRATER, R.H. and MACKAY, N.A., 1967, *Proc. Astron. Soc. Aust., 1,* 55.

GODDARD, B.R., 1961, M.E. Thesis, Univ. of Sydney, (unpublished)

HANBURY BROWN, R., PALMER, H.P. and THOMPSON, A.R. 1955 *Phil.Mag.,46,*857.

HANSEN, R.C., (Ed.), 1966, *Microwave Scanning Antennae: Vol 2,* Array theory and practice. New York: Academic Press.

HASLAM, C., DAVIES, J.G., and LARGE, M.I., 1962, *Mon. Not. R. astr. Soc., 124,* 169.

HATANAKA, T., 1963, *Proc. Instn. Radio Engrs. Aust., 24,* 243.

HAZARD, C., MACKEY, M.B., and SHIMMINS, A.J., 1963, *Nature, 197,* 1037.

HELMS, H.D., 1967, *Trans. IEEE, AU-15,* 85.

HÖGBOM, J.A., 1960, Ph.D. Dissertation, Cambridge (unpublished).

HÖGBOM, J.A., 1963, ITR No. 22-63, (Preliminary Report Benelux Antenna Project), (unpublished).

HÖGBOM, J.A., 1963, Private communication.

HOOGHOUDT, B.G., SCHOR, R.J. and SCHIERBEEK, B.B., 1957, *De Ingenieur, 69*, 1.

HOYLE, F. and ELLIOT, J., 1963, London: Transworld Publishers.

JAHNKE, E., EMDE, F. and LÖSCH, F., 1960, *Tables of higher functions.* 6th Ed., New York: McGraw-Hill Book Co.

JASIK, H. (Ed.), 1961, *Antenna Engineering Handbook*, New York: McGraw-Hill Book Co.

KAKINUMA, T. and TANAKA, H., 1963, *Proc. Res. Inst. Atmos.* Nagoya Univ., *10*, 25.

KALACHOV, P.D. and SALOMONOVICH, A.E., 1961, *Radiotekhnika i Elektronika, 6*, 438.

LABRUM, N.R., HARTING, E., KRISHNAN, T. and PAYTEN, W.J., 1963, *Proc. Instn. Radio Engrs. Aust., 24*, 148.

LABRUM, N.R., KRISHNAN, T., PAYTEN, W.J. and HARTING, E., 1964, *Aust. J. Phys., 17*, 323.

LAMPARD, D.G., 1956, *Trans. I.R.E., IT-2*, 4.

LECHTRECK, L.W., 1958, *Electronics*, 104.

LEQUEUX, J., 1962a, *Notes et Informations*, Publ. Obs. Paris, Fasc. IX Radioastronomie N° 1.

LEQUEUX, J., 1962b, *Annls. Astrophys., 25*, 221.

LITTLE, A.G., and PAYNE-SCOTT, R., 1951, *Aust. J. scient. Res., A4*, 489.

LITTLE, A.G., 1958, *Aust. J. Phys., 11*, 70.

LINNES, K.W., MERRICK, W.D. and STEVENS, R., 1960, *Trans I.R.E., SET-6*, 45.

LOVELL, A.C.B., 1963, *New Scientist, 19*, 174.

McALISTER, K.R. and LABRUM, N.R., 1967, *Proc. Instn. Radio elect. Engrs. Aust., 28*, 291.

McCREADY, L.L., PAWSEY, J.L. and PAYNE-SCOTT, R., 1947, *Proc. R. Soc., A, 190*, 357.

MacDONALD, G.H., NEVILLE, A.C. and RYLE, M., 1966, *Nature, 211,* 1241.

McLEAN, D.J. and WILD, J.P., 1961, *Aust. J. Phys., 14,* 489.

McLEAN, D.J., LAMBERT, L.B., ARM, M. and STARK, H., 1967, *Proc. Instn. Radio elect. Engrs. Aust., 28,* 375.

MACKAY, N.A., 1966, Private communication.

MILLS, B.Y. LITTLE, A.G., SHERIDAN, K.V., and SLEE, O.B., 1958, *Proc. Instn. Radio Engrs., 46,* 67.

MILLS, B.Y., 1963, *Proc. Instn. Radio Engrs. Aust., 24,* 132.

MILLS, B.Y. AITCHISON, R.E., LITTLE, A.G., and McADAM, W.B., 1963, *Proc. Instn. Radio Engrs. Aust., 24,* 156.

NATIONAL BUREAU OF STANDARDS, 1954. Tables of functions and zeros of functions. *Appl. Math. Ser. No. 37.*

O'BRIEN, P.A., 1953, *Mon. Not. R. astr. Soc., 113,* 597.

O'BRIEN, P.A. and TANDBERG-HANSSEN, E., 1955, *Observatory, 75,* 11.

PALMER, H.P., ROWSON, B., ANDERSON, B., DONALDSON, W., MILEY, G.K., and GENT, H., ADGIE, R.L., SLEE, O.B., CROWTHER, J.H., 1967, *Nature, 213,* 789.

PAULINY-TOTH, I.I.K., SHAKESHAFT, J.R. and WIELEBINSKI, R., 1962, *Proc. Instn. Radio Engrs., 50,* 2483.

PAWSEY, J.L. and BRACEWELL, R.N., 1955, *Radio astronomy.* Oxford: Clarendon Press.

PAYTEN, W.J., 1967, *Proc. Instn. Radio elect. Engrs. Aust., 28,* 367.

RAMSAY, J.F., 1967, *Microwaves, 6,* 69.

READ, R.B., 1961, *Trans I.R.E., AP-9,* 31.

READ, B.R., 1963, *Astrophys. J., 138,* 1.

ROBINSON, B.J., 1964, *A. Rev. astron. Astrophys., 2,* 401.

ROWSON, B., 1962, *Mon. Not. R. astr. Soc., 125,* 177.

ROWSON, B., 1963, 'Source brightness distribution', in *Radio astronomy today,* Eds. Palmer, H.P., Davies, R.D., and Large, M.I., Manchester: The University Press.

RUZE, J., 1952, *Nuovo Cimento, 9,* suppl. 3, 364.

RYLE, M. and VONBERG, D.D., 1948, *Proc. R. Soc., A293,* 98.

RYLE, M., 1952, *Proc. R. Soc., A211,* 351.

RYLE, M. and HEWISH, A., 1960, *Mon. Not. R. astr. Soc., 120,* 220.

RYLE, M., 1962, *Nature, 194,* 517.

RYLE, M. and NEVILLE, ANN C., 1962, *Mon. Not. R. astr. Soc., 125,* 39.

RYLE, M., ELSMORE, B. and NEVILLE, ANN C., 1965, *Nature, 205,* 1259.

SCHEUER, P.A.G., SLEE, O.B. and FRYAR, C.F., 1963, *Proc. Instn. Radio Engrs. Aust., 24,* 185.

SCOTT, P.F., RYLE, M. and HEWISH, A., 1961, *Mon. Not. R. astr. Soc., 122,* 95.

SHERIDAN, K.V. and SPARKS, J.B., 1967, *Proc. Instn. Radio elect. Engrs. Aust., 28,* 311.

SHKLOVSKY, I.S., 1960, *Cosmic radio waves.* Cambridge: Harvard Univ. Press

SILVER, S., 1949, *Microwave antenna theory and design.* M.I.T. Radiation Lab. Series, 12, New York: McGraw-Hill Book Co.

SMART, W.M., 1962, *Text-book on spherical astronomy.* Cambridge: University Press.

SMERD, S.F. and WILD, J.P., 1957a, *I.A.U. Symposium No. 4 on Radio Astronomy,* (Ed.) van de Hulst, 290.

SMERD, S.F. and WILD, J.P., 1957b, *Phil. Mag., 2,* 119.

SNEDDON, I.N., 1951, *Fourier Transforms.* New York: McGraw-Hill Book Co.

SPENCER, R.C., 1955, *Proc. nat. Electron. Conf., 11,* 506.

STANIER, H.M., 1950, *Nature, 165,* 354.

SUTTON, J., 1967, Ph.D. Thesis, Univ. of Sydney (unpublished)

SWARUP, G. and YANG, K.S., 1961, *Trans I.R.E., AP-9,* 75.

SWARUP, G., THOMPSON, A.R. and BRACEWELL, R.N., 1963, *Astrophys. J, 138,* 305.

SWARUP, G., 1967, Private communication.

SWENSON, G.W. and MATHUR, N.C., 1967, *Proc. Instn. Radio elect. Engrs. Aust., 28,* 370.

TANAKA, H., KAKINUMA, T. and ENOME, S., 1967, *Proc. Res. Inst. Atmospherics, Nagoya Univ., 14,* 23.

THOMPSON, A.R. and KRISHNAN, T., 1965, *Astrophys. J., 141,* 19.

TWISS, R.Q., CARTER, A.W.L. and LITTLE, A.G., 1962, *Aust. J. Phys., 15,* 378.

WADE, C.M., CLARK, B.G., and HOGG, D.E., 1965, *Astrophys. J., 142,* 406.

WATKINSON, A., 1963, ITR No. 17-63 (Status report, Benelux Antenna Project) (unpublished).

WATSON, G.N., 1944, *A treatise on the theory of Bessel functions.* Cambridge University Press.

WESSELING, K.H., 1967, *Trans. IEEE, AP-15,* 332.

WILD, J.P., 1959, *Rendiconti S.I.F., 12,* 281.

WILD, J.P., 1961, *Proc. R. Soc., A262,* 84.

WILD, J.P., 1965, *Proc. R. Soc., A286,* 499.

WILD, J.P., 1967, *Proc. Instn. Radio elect. Engrs. Aust., 28,* 279.

WILLIAMS, D.A., 1963, ITR No. 13-63 (Status report, Benelux Antenna Project) (unpublished).

YATES, K.W., 1967, Ph.D. Thesis, Univ. of Sydney (unpublished).

YATES, K.W., WIELEBINSKI, R. and LANDECKER, T.L., 1967, *Aust. J. Phys. 20,* 595.

' FLO '

The fast, modern, all-weather
on-site transport system.

A 'very modified' 1929 Bullnose (?)
Morris.

APPENDICES

APPENDIX A

A New Radiotelescope of 40-sec-of-arc Resolving Power for Southern Sky Observations.

W.N. Christiansen and K.J. Wellington

(Reprint from Nature, 1966, 209, 1173-1176.)

(Reprinted from Nature, Vol. 209, No. 5029, pp. 1173–1176, March 19, 1966)

A NEW RADIOTELESCOPE OF 40-SEC-OF-ARC RESOLVING POWER FOR SOUTHERN SKY OBSERVATIONS

By Prof. W. N. CHRISTIANSEN and K. J. WELLINGTON
School of Electrical Engineering, University of Sydney

IN 1950–52 the first radio-frequency grating interferometer[1] was constructed at the Commonwealth Scientific and Industrial Research Organization's field station at Potts Hill near Sydney. This consisted of an east–west line of steerable paraboloids, about 1,000 wave-lengths long—analogous to an optical diffraction grating with a variable 'blaze' angle. This antenna produced a system of multiple responses or 'fan beams' about 3 min of arc wide; the spacing between these multiple responses was sufficiently wide so that only one response fell on the Sun at any one time. The Sun could be scanned repeatedly over a period of many hours, during which time the scanning angle changed appreciably, with respect to the north point on the Sun.

At the time that this antenna was being constructed, the first use[2] of 'aperture synthesis' was being made at Cambridge by Ryle and his colleagues. They extracted, serially, the angular components of the radio brightness distribution of various radio sources using movable elements in two-antenna interferometry. These measurements were soon extended to two dimensions[3]. The difficulties associated with the coupling of the movable elements to a receiver prevented a full Fourier synthesis from being attempted at first, since the amplitudes of the components could be measured but not their relative phases. Consequently, it had to be assumed that all sources were symmetrical. Later this technical problem of phase measurements in variable spacing interferometry[4–6] was overcome.

With the grating interferometer, on the other hand, both the amplitudes and phases of all necessary Fourier components of the one-dimensional brightness distribution are obtained simultaneously. To extend the observations to two dimensions, use was made at Potts Hill of the change of scanning angle of the antenna beams with respect to the Sun during the day. The original east–west grating did not provide a sufficient range of scanning angles, and it was necessary to add a second grating in a north–south line. The changes during the day of the co-ordinates of this antenna with respect to the Sun are illustrated in Fig. 1*a*. In Fig. 1*b* radii have been drawn to show the range of directions and apparent lengths taken up by an east–west interferometer 4,000 wave-lengths long when seen from outer space during 0800 h–1600 h measured in local time at the radiotelescope. Similar information for the north–south interferometer is shown in Fig. 1*c*. The actual process of converting a number of strip scans of the Sun to a two-dimensional brightness map is shown diagrammatically in Fig. 2. A map of the 'quiet' sun at a wave-length of 21 cm was produced[7] by these means in 1954.

Recently, the Fleurs radio-astronomy field station and a large Grating Cross[8] were given to the University of Sydney by the Radiophysics Division of the Commonwealth Scientific and Industrial Research Organization. This made possible a plan to use a pair of gratings for two-dimensional, high-sensitivity mapping of small radio sources. To make the instrument generally useful, it was necessary to eliminate the multiple responses of the grating and to improve the sensitivity by several orders of magnitude. The new instrument is in course of construction; the first stage has been completed. The telescope has a resolving power of about 40 sec of arc at a

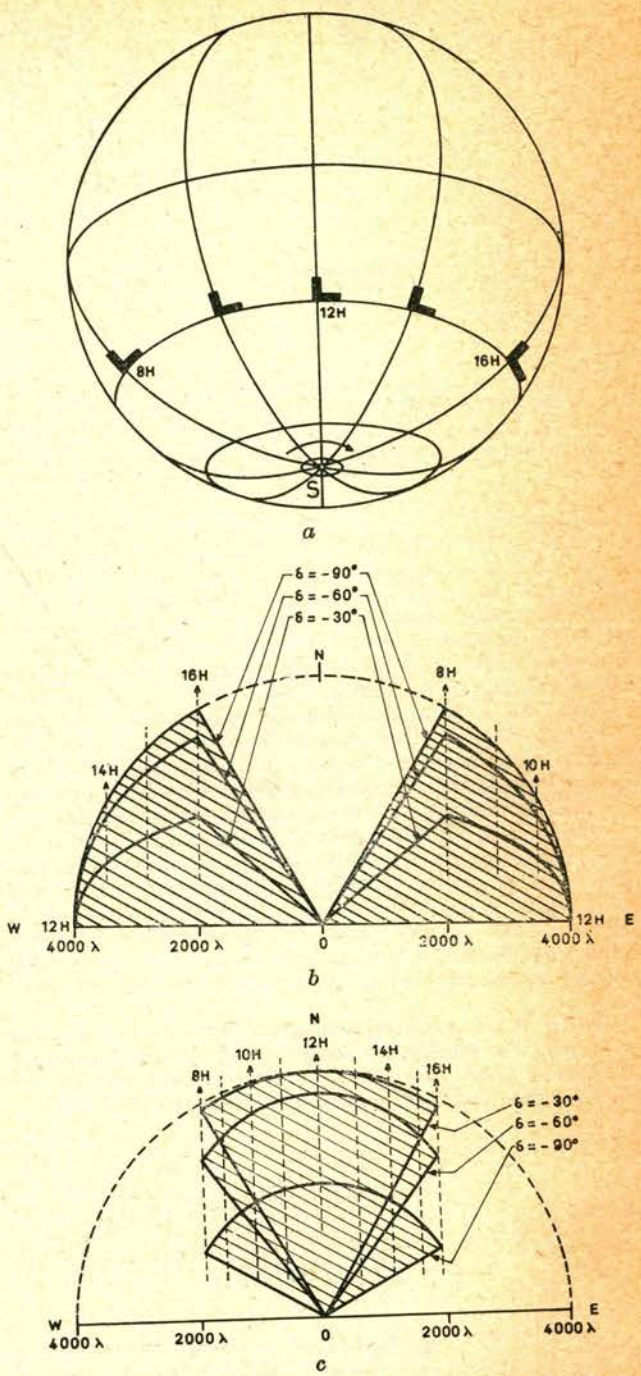

Fig. 1. *a*, The variations in appearance during the day of an *L*-shaped antenna when viewed from outer space (declination about 30° S.). *b* and *c*, Radii drawn from the centre 0 to the edge of the shaded region represent, in length and direction, the appearance of antennae of length 4,000 wave-lengths lying geographically (*b*) in an east–west direction and (*c*) in a north–south direction when seen from outer space during 0800 h–1600 h local time. In the diagrams the antennae are viewed from declinations 90°, 60° and 30° S

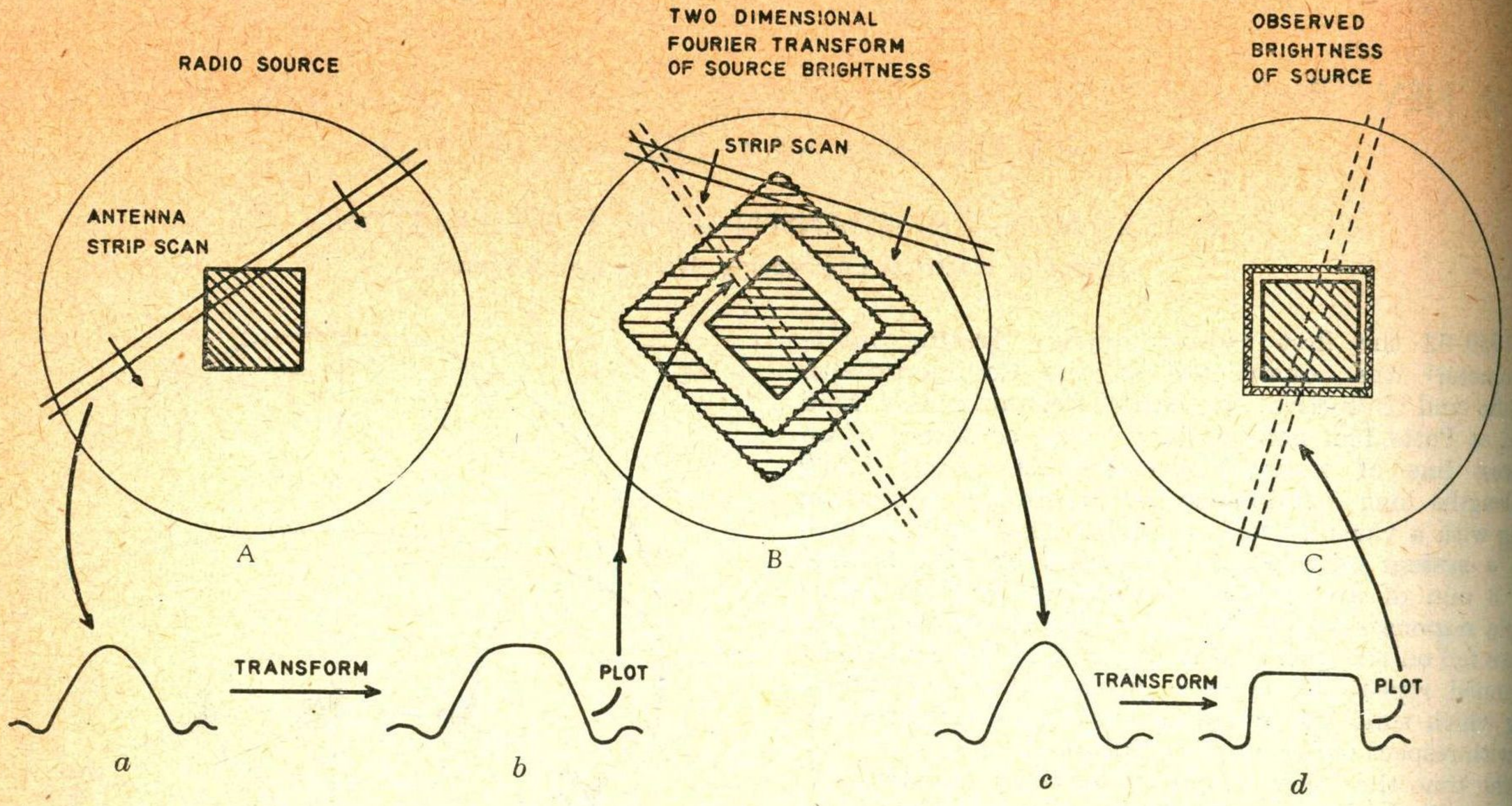

Fig. 2. The process of deriving the brightness distribution over a celestial region from one-dimensional scans in many different directions. The source is scanned by a 'fan-beam' antenna response *A* and a typical record (*a*) is obtained. The Fourier transform (*b*) of this is obtained and plotted along a line in the Fourier transform diagram *B*. After scanning in all directions, the Fourier transform *B* is completed in two dimensions. This diagram is line-scanned in all directions, and (*c*) is a typical record of one scan. These records are Fourier transformed (*d*) and the results plotted along lines in *C*. When the process is complete and contours drawn, the diagram *C* is a representation of the brightness distribution *A*. In the new radiotelescope, stage (*a*) is eliminated and we commence with (*b*)

wave-length of 21 cm and when completed will have a sensitivity of 2 or 3×10^{-28} W m^{-2} Hz^{-1}. This high sensitivity and resolving power will be obtained by making full use of the image-forming potentialities of the multi-antenna system and will of necessity involve a considerable amount of electronic equipment. The compensation for this complexity is the cheapness of the system which, including electronics, is estimated to cost less than a single 30-m diameter steerable parabola of moderate surface accuracy. The reason for the low cost of the system is that a large number of small antennae is used. With the cost of a steerable parabolic antenna increasing roughly as the cube of its linear dimensions, it is obvious, for example, that 64 antennae would cost only an eighth of the amount required to build a single antenna which had the same total area. Moreover, the amount of sky from which energy would be received at any moment would be 64 times greater with the multi-antenna system than with the single large antenna, since the beam-width of the small antenna is eight times that of the larger one.

In Fig. 3 the essential arrangement of the new system is shown. The telescope is composed of a pair of compound interferometers[9], one in the east–west and one in the north–south direction. Each member of the pair consists of 32 steerable paraboloids 5·7 m in diameter combined with two widely spaced paraboloids each 13·6 m in diameter. Shown in broken outline are two additional 13·6-m antennae to be added later. The declination and hour-angle axes of the large antennae are in line with those of the small antennae. The length of the system is 800 m and the operating frequency is 1,415 MHz. Each antenna has its own frequency changer and intermediate-frequency amplifier. Signals are conveyed to a central receiving room by equal lengths of co-axial cable. Here, after suitable time delays have been applied, the output from each of the two large antennae is combined separately with each of the outputs from the 32 small antennae, both with equal length connexions and connexions differing in length by ninety electrical degrees. Thus 128 separate interference patterns are obtained. Half these are cosine and half sine components of a Fourier series which represents the one-dimensional brightness distribution over the region of the sky which is in the field of view of the antennae (about one square degree). Alternatively, these components provide a line of complex numbers in the Fourier plane (Fig. 2*b*). When the source has been scanned from all directions, the Fourier plane is filled and the two-dimensional brightness distribution can be determined as shown in Fig. 2*c*.

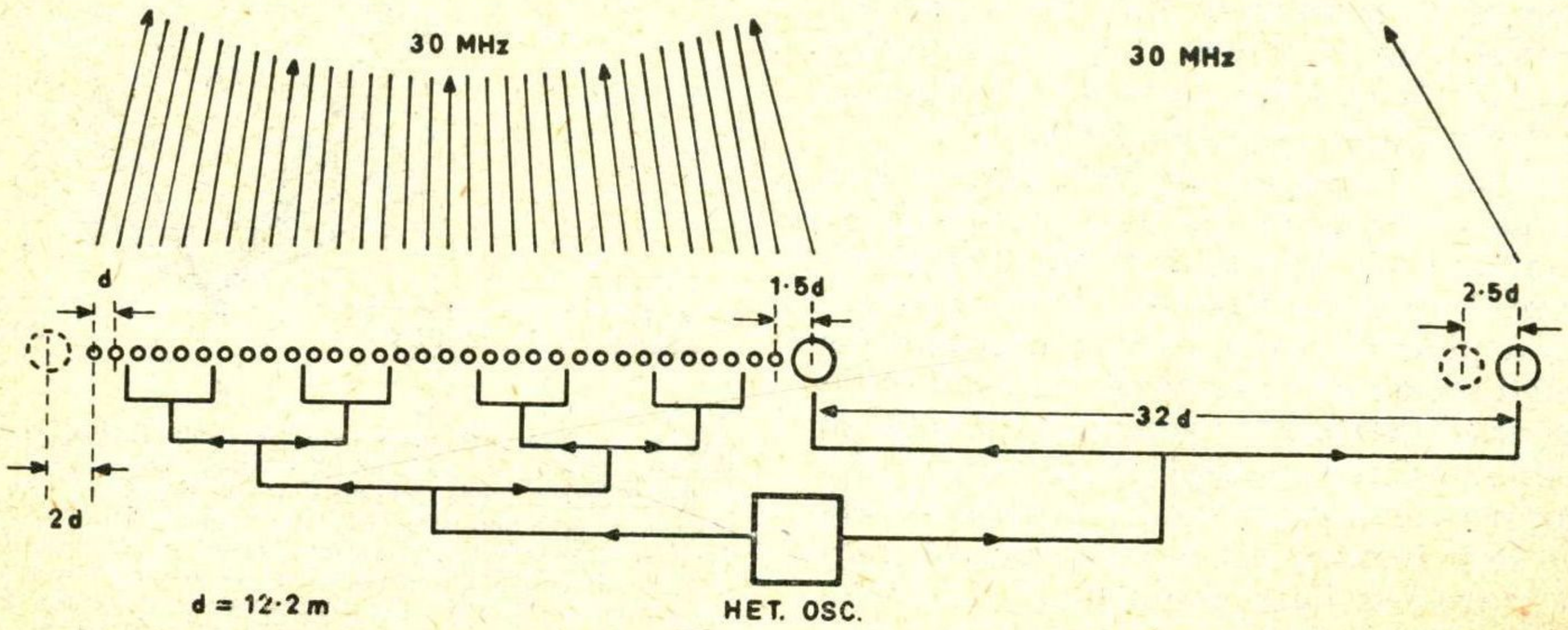

Fig. 3. Diagrams of the east–west interferometer. The antennae drawn in heavy lines are those actually in use. The antenna is designedto operate at 1,415 MHz and 722·5 MHz

In the preceding paragraph it was implied that the Fourier series, which consists of 64 components (given as amplitude and phase, or sine and cosine), will provide all the necessary information to enable the one-dimensional brightness distribution to be derived. This, of course, is an over-simplification. (*a*) The finiteness of the series means that the resolution is limited; (*b*) the missing components near zero angular frequency mean that additional information is required on the coarse structure of the sky before absolute measurements of brightness can be made (this is true of most antennae with unfilled apertures); (*c*) the existence of gaps in the spectrum, that is between the elements of the Fourier series, means that the derived distribution will be periodic with an angular period of about 1°. The last limitation implies the presence of multiple superimposed images with their resultant ambiguities. It is to reduce these that the 13·6-m antennae have been used. To be completely successful they should have no response to any source more than 0·5° from the centre of the field of observation.

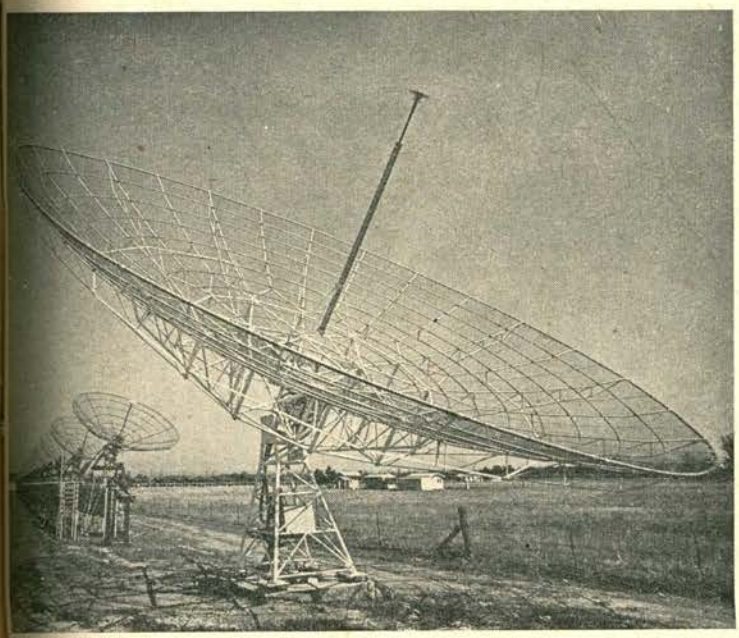

Fig. 4. The East–west interferometer

In fact, they will not eliminate all unwanted responses at angular distances in the range 0·5°–1·0° from the centre. As a result of this, strong spurious responses may sometimes appear near the edge of the field and weak ones near the centre. These spurious responses can be detected easily by making observations at intervals of 0·5°. In the early stages of the work, on relatively isolated strong sources, no difficulties from spurious responses are expected. Nevertheless, provision has been made, as shown in Fig. 3, to add two more 13·6-m antennae to halve the interval between adjacent Fourier components and thus increase the angular frequency of image repetition from 1° to 2°. This will practically eliminate all unwanted responses.

In order to simplify the data handling, all the interference patterns will be brought to rest by a coupled system of phase rotators. Each Fourier component is then represented by two amplitudes (sine and cosine) which change very slowly as the source rotates in the antenna response regions. In practice, new information will be obtained approximately every minute. The compound interferometer will operate for a total time of about 12 h, and during the whole time every point in the response region will be under continuous observation. This very long integration time increases the sensitivity about 100 times over what it would be if the source simply passed once through a 40 sec-of-arc antenna beam. At the end of 12 h of observing, a one square degree region, that is several thousand beam-widths, will have been mapped. This will make the antenna comparable in sensitivity with the largest existing radiotelescope, not only for observations of small regions, but also in terms of the area of sky (square beam-widths) that it surveys in a given time. The antenna uses synthesis methods, but has no elements to be moved along the surface of the Earth. Thus, for a given surface area it is cheaper than a variable-spacing interferometer. It uses its receiving area just as efficiently as the latter.

One may, without difficulty, improve the resolving power of the instrument to 20 sec of arc by adding two or four antennae.

With increasing reliability of electronic equipment associated with the disappearance of the thermionic valve, it would seem that the new antenna may be the first of a new generation of radiotelescopes in which numerous antennae, each of moderate size, are used.

The construction of this new telescope has been made possible by grants from the University of Sydney research vote, the Australian Research Grants Committee, the Nuffield Foundation and the Australian Electrical Research Board.

One of the authors was for some time a member of the design team at Leiden associated with the Benelux Cross Antenna Project; the design of the Sydney antenna was influenced by discussions at Leiden, particularly those with Dr. J. A. Högbom.

[1] Christiansen, W. N., and Warburton, J. A., *Austral. J. Phys.*, **6**, 190 (1953).

[2] Stanier, H. M., *Nature*, **165**, 354 (1950).

[3] O'Brien, P. A., *Mon. Not. Roy. Astro. Soc.*, **113**, 597 (1953).

[4] Ryle, M., and Hewish, A., *Mon. Not. Roy. Astro. Soc.*, **120**, 220 (1960).

[5] Read, R. B., *Observations Cal. Inst. Tech. Radio Obs.* (1960).

[6] Ryle, M., *Nature*, **194**, 517 (1962).

[7] Christiansen, W. N., and Warburton, J. A., *Austral. J. Phys.*, **8**, 474 (1955).

[8] Christiansen, W. N., Mathewson, D. S., and Pawsey, J. L., *Nature*, **180**, 944 (1957).

[9] Covington, A. E., and Broten, N. W., *Inst. Rad. Eng. Trans. AP5*, 247 (1957).

Printed in Great Britain by Fisher, Knight & Co., Ltd., St. Albans.

Appendix B Derivation of the Geometric Relationships involved in Earth Rotation Synthesis

Chapter 3 considers the basic concepts by which a linear array can use the rotation of the earth about its axis to synthesize a two-dimensional aperture. In this Appendix, the relevant equations are derived for a baseline with arbitrary direction and location. These are evaluated for the specific cases of an east-west and a north-south linear array at a latitude of -34°. (The actual latitude at Fleurs is $-33^{\circ}51'.5$.) Some of the resulting equations have also been determined by Rowson (1963), Read (1963), Högbom (1960) and Ryle and Neville (1962).

Equations describing the conic projections

In the method used here, the array baseline is first defined in the (hour-angle, declination) earth coordinates which are then related to a coincident Cartesian system, (x,y,z). This (x,y,z) system then undergoes a rotational transformation to a system, (u,v,w), aligned in the source direction. By this means, the projections of the array are obtained relative to the source. An alternative approach, used by Read (1963) and Rowson (1963), employs spherical trigonometry.

Initially let the array be normalized to unit length and the array line direction, when produced, intersect the celestial sphere at an hour-angle $\underline{h}$ and make an angle σ with the north-south earth axis. This defines the array.

Normally the array will be known in terms of the angle it makes with the north-south meridian, θ_A, and the latitude of the antenna on the earth, ϕ.

These are related to (h,σ) by

$$\left.\begin{aligned} \cos\sigma &= \cos\theta_A.\cos\phi \qquad \text{and} \\ \tan h &= \tan\theta_A.\sec\phi \end{aligned}\right\} \qquad (B.1)$$

Set up a coordinate system (x,y,z) as in Fig. B.1 with the Z axis in the zero hour angle plane and the Y axis as the north-south axis. The direction cosines of the array become:

$$\left.\begin{aligned} x &= -\sin\sigma.\sin h \\ y &= \cos\sigma \\ z &= +\cos h.\sin\sigma \end{aligned}\right\} \qquad (B.2)$$

(i) Let the (u,v,w) coordinate system have the same origin as the (x,y,z) system.

(ii) Let the source lie in the W axis direction. The source coordinates are (α,δ).

The U axis always lies in the earth's equatorial plane and the V axis in the northerly direction. These are then parallel to the right-ascension and declination coordinates across the source.

From Fig. B.2, the matrix relating the two coordinate systems becomes:

	X	Y	Z
U	$+\cos\alpha$	0	$\sin\alpha$
V	$+\sin\alpha.\sin\delta$	$\cos\delta$	$-\cos\alpha.\sin\delta$
W	$-\cos\delta.\sin\alpha$	$\sin\delta$	$\cos\delta.\cos\alpha$

(B.3)

Thus the normalized projections of the array on the source (Fig. B.3) are:

$$\left.\begin{aligned} u &= \sin\sigma.\sin(\alpha-h) \\ v &= \cos\sigma.\cos\delta - \sin\sigma.\sin\delta.\cos(\alpha-h) \\ w &= \cos\sigma.\sin\delta + \sin\sigma.\cos\delta.\cos(\alpha-h) \end{aligned}\right\} \qquad (B.4)$$

These projections are multiplied by the element separations, expressed in wavelengths, to give the actual projected components. At any instant (u, gives the spatial component or line of spatial components being sampled by the system.

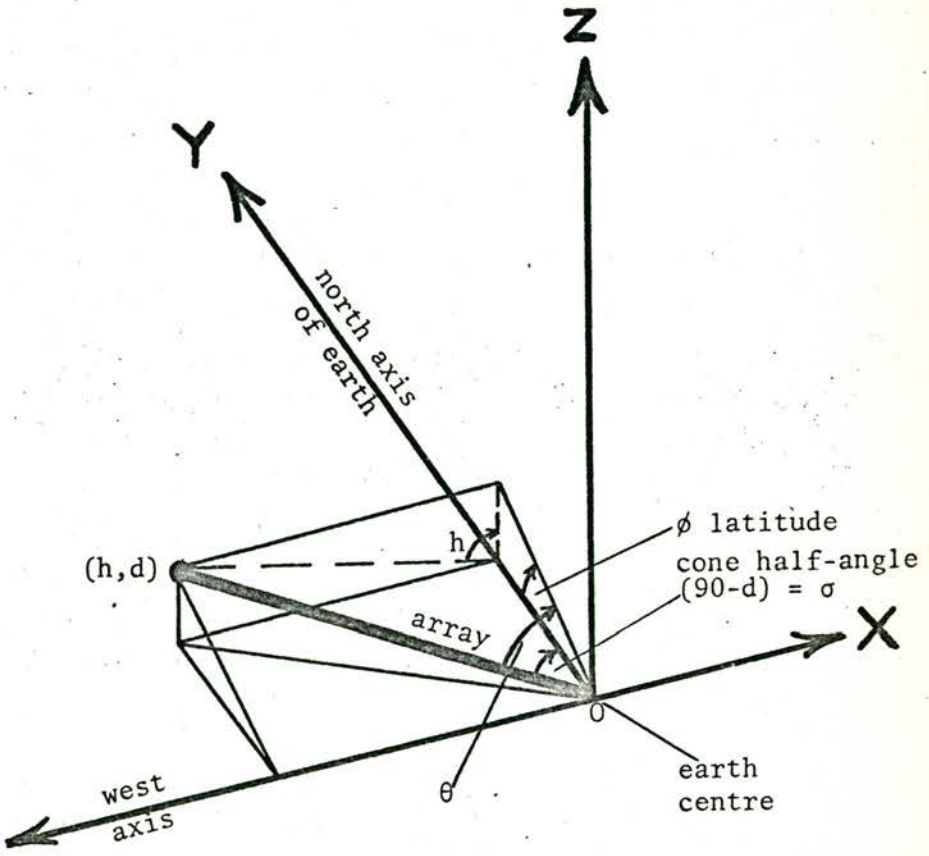

FIGURE B.1 Arbitrary array relative to the earth coordinate system (X,Y,Z).

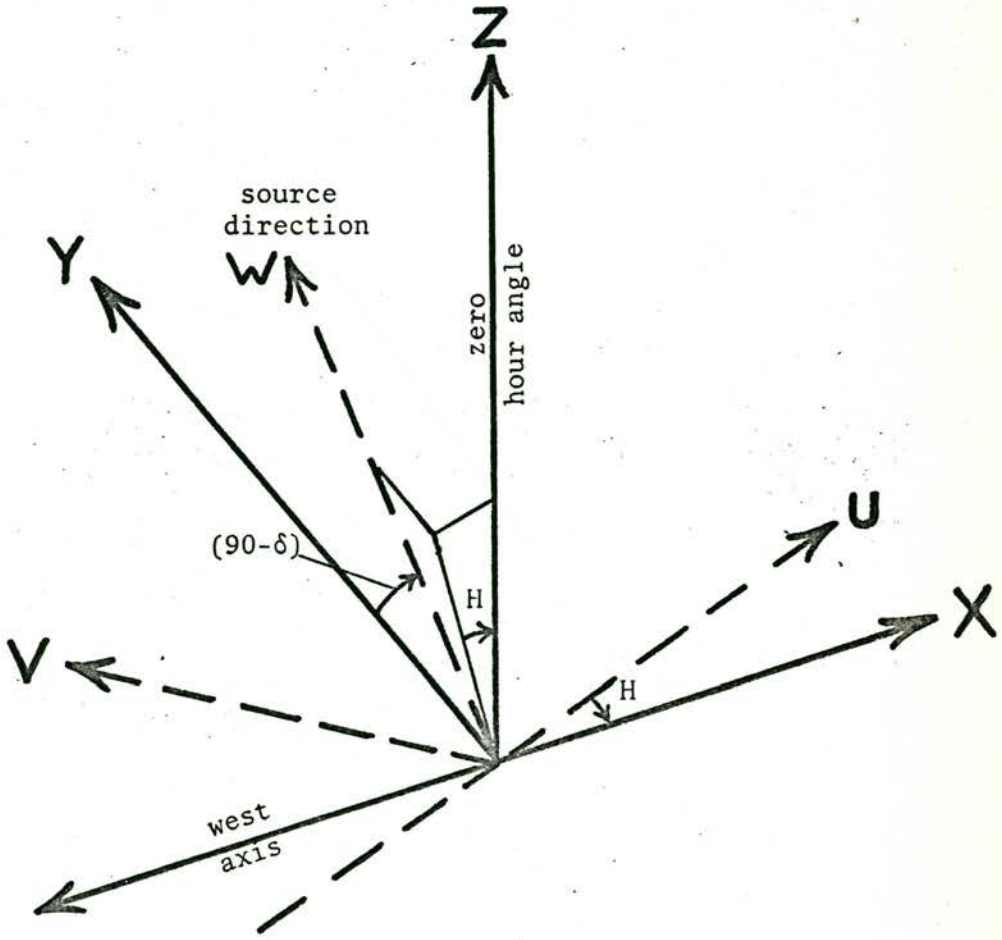

FIGURE B.2 Relation between the earth coordinate system (X,Y,Z) and the source coordinate system (U,V,W).

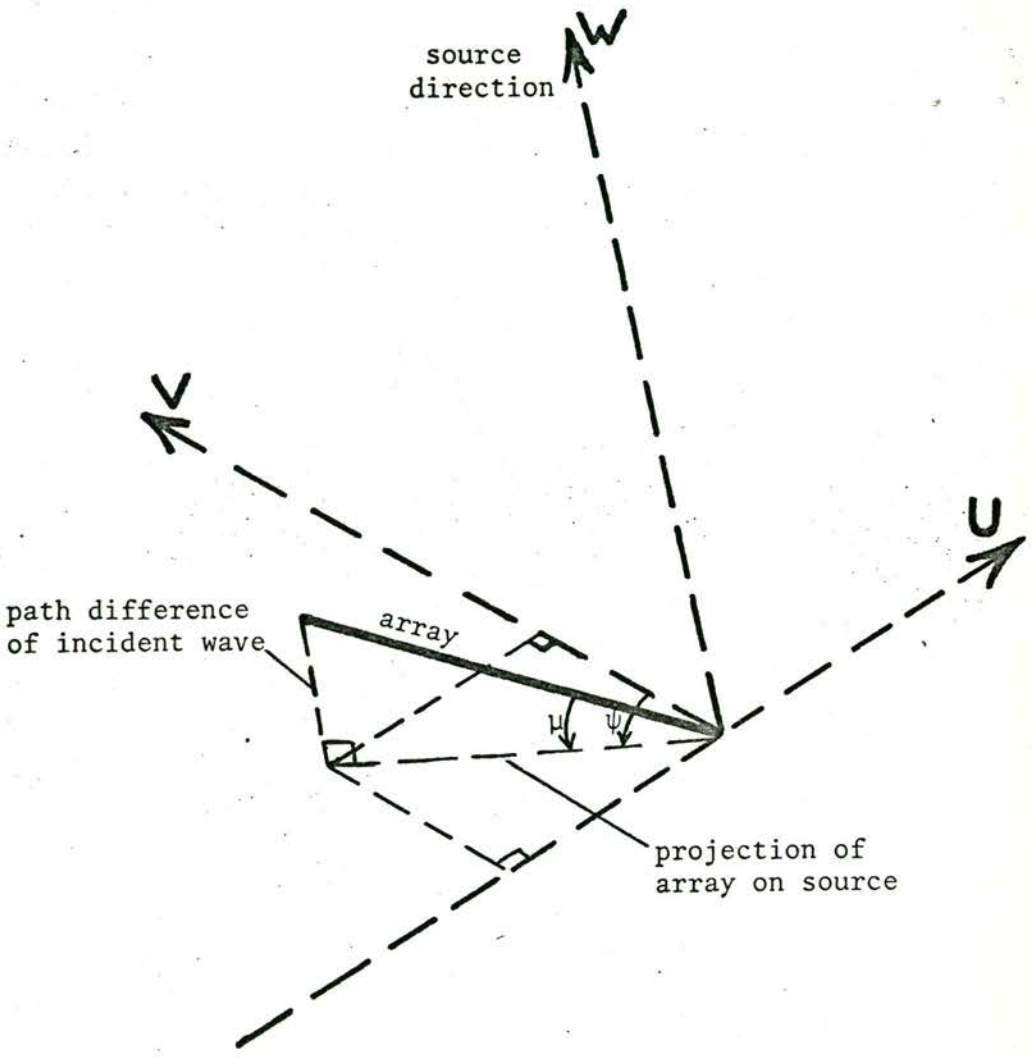

FIGURE B.3 Array relative to the source coordinate system (U,V,W).

The B.4 equations suggest another method of defining the base line direction of each element pair. Instead of using the angle σ, the base line of length $\underline{L}$ wavelengths is resolved parallel and perpendicular to the north-south earth axis. Let the components be

$$\left.\begin{aligned} L_1 &= L.\cos\sigma \\ L_2 &= L.\sin\sigma \\ \text{where} \quad L^2 &= (L_1^2 + L_2^2) \end{aligned}\right\} \qquad (B.5)$$

Then the normalized projected lengths are

$$\left.\begin{aligned} u &= \frac{L_2}{L}.\sin(\alpha-h) \\ v &= \frac{L_1}{L}.\cos\delta - \frac{L_2}{L}.\sin\delta.\cos(\alpha-h) \\ w &= \frac{L_1}{L}.\sin\delta + \frac{L_2}{L}.\cos\delta.\cos(\alpha-h) \end{aligned}\right\} \qquad (B.6)$$

These B.6 equations essentially represent a transformation from the cylindrical (α,δ) earth coordinate system to the Cartesian (u,v,w) source coordinate system.

Evaluation

In order to evaluate these equations, the author wrote a computer program for the arbitrary array with orientation on the earth's surface of θ and at a latitude of ϕ, looking in the direction of δ. The program determines values of ℓ, ψ, μ and $\sin\mu$ as in equation 3.13; and also $\frac{\partial}{\partial\alpha}(\sin\mu)$ and $\frac{\partial\psi}{\partial\alpha}$ (where α is the hour-angle), all as a function of α.

The specific results used to construct the following figures are for an EW and a NS array at a latitude of -34° (Fleurs). The individual antenna sky coverage limits are ignored here (except that coverage is assumed to be 12 hours or less) but are considered, where relevant, in Section 3.3.

For an east-west array

$$\left.\begin{aligned} \frac{\ell}{L} &= (1 - \sin^2\alpha.\cos^2\delta)^{\frac{1}{2}} \\ \psi &= \cot^{-1}(\tan\alpha.\sin\delta) \\ \mu &= \sin^{-1}(-\cos\delta.\sin\alpha) \\ \sin\mu &= -\cos\delta.\sin\alpha \\ \frac{\partial}{\partial\alpha}(\sin\mu) &= -\cos\delta.\cos\alpha \\ \frac{\partial\psi}{\partial\alpha} &= -\sin\delta.\sec^2\alpha.\mathrm{cosec}^2\psi \end{aligned}\right\} \quad (B.7)$$

For a north-south array at -34° latitude

$$\begin{aligned} \frac{\ell}{L} &= \{(\cos\delta.\cos34^\circ - \sin\delta.\sin34^\circ.\cos\alpha) + (\sin34^\circ.\sin\alpha)^2\}^{\frac{1}{2}} \\ \psi &= \cot^{-1}(\cos\delta.\cot34^\circ.\mathrm{cosec}\,\alpha - \sin\delta.\cot\alpha) \\ \mu &= \sin^{-1}\{\sin(\delta+34^\circ) - \sin34^\circ.\cos\delta(1-\cos\alpha)\} \\ \sin\mu &= \{\sin(\delta+34^\circ) - \sin34^\circ.\cos\delta(1-\cos\alpha)\} \qquad (B.8) \\ \frac{\partial}{\partial\alpha}(\sin\mu) &= -\sin34^\circ.\cos\delta.\sin\alpha \\ \frac{\partial\psi}{\partial\alpha} &= \mathrm{cosec}^2\psi.\mathrm{cosec}^2\alpha(\cos\delta.\cot34^\circ.\cos\alpha-\sin\delta) \end{aligned}$$

Figs. B.4 and B.5 plot the normalized values for (u,v) (and (ℓ,ψ)) coverage for the ES and the NS array. For the present array lengths at Fleurs, unit length here is equivalent to 3709 wavelengths at 1415 MHz, and 1815 wavelengths at 692.5 MHz (second observing frequency). Note that lines of constant hour-angle are parallel to the declination axis (V axis). These curves have also been used in Section 4.5 and Appendix C.2 to determine the cone of exclusion inside which aerial shadowing occurs. The limits represent a minimum allowable projected array length (in the present case: 0.53).

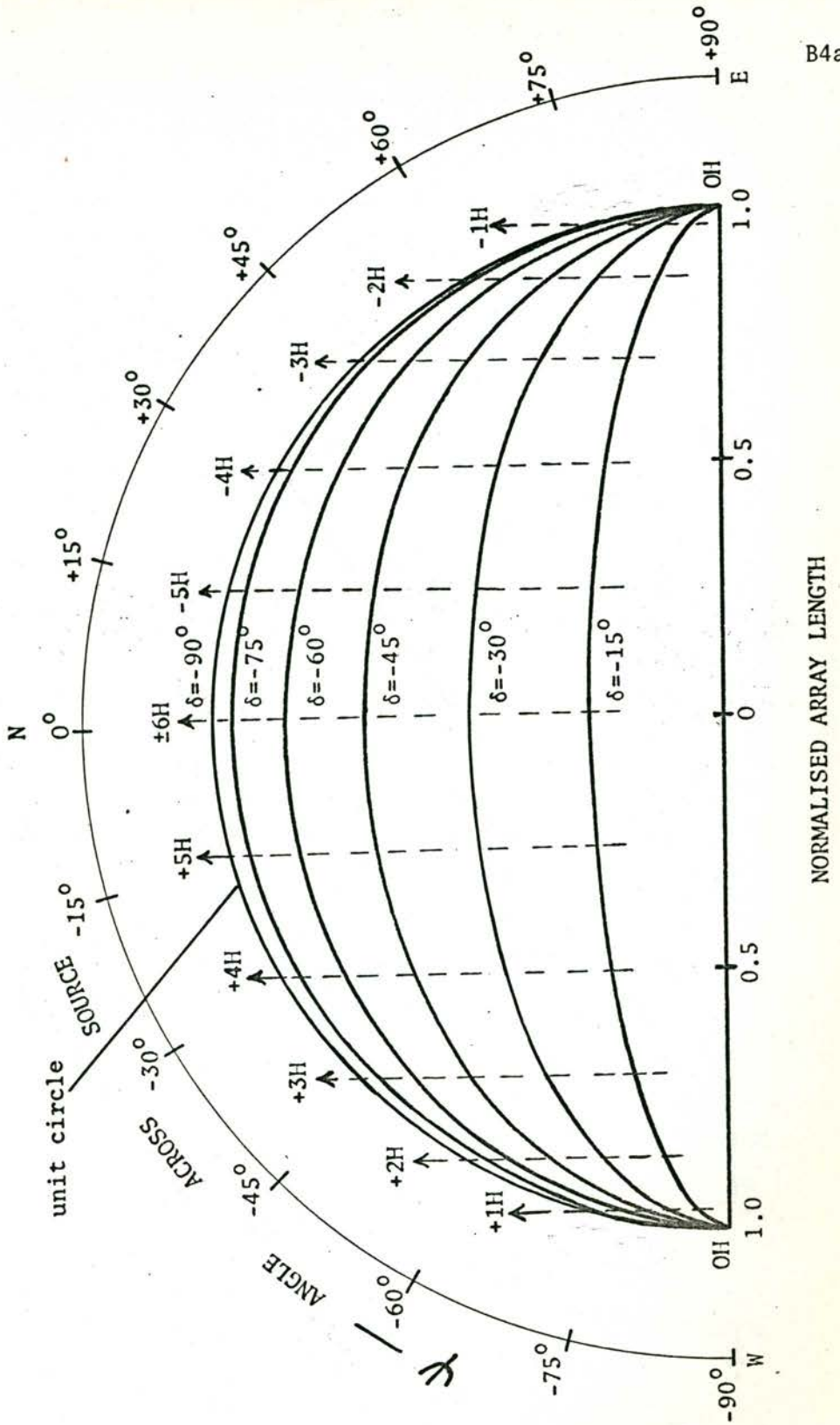

FIGURE B.4 The variation with hour-angle of the projection of an east-west array as seen from different source declinations. Any radius drawn from the centre O to the required ellipse represents the projection in length and direction at a particular hour-angle.

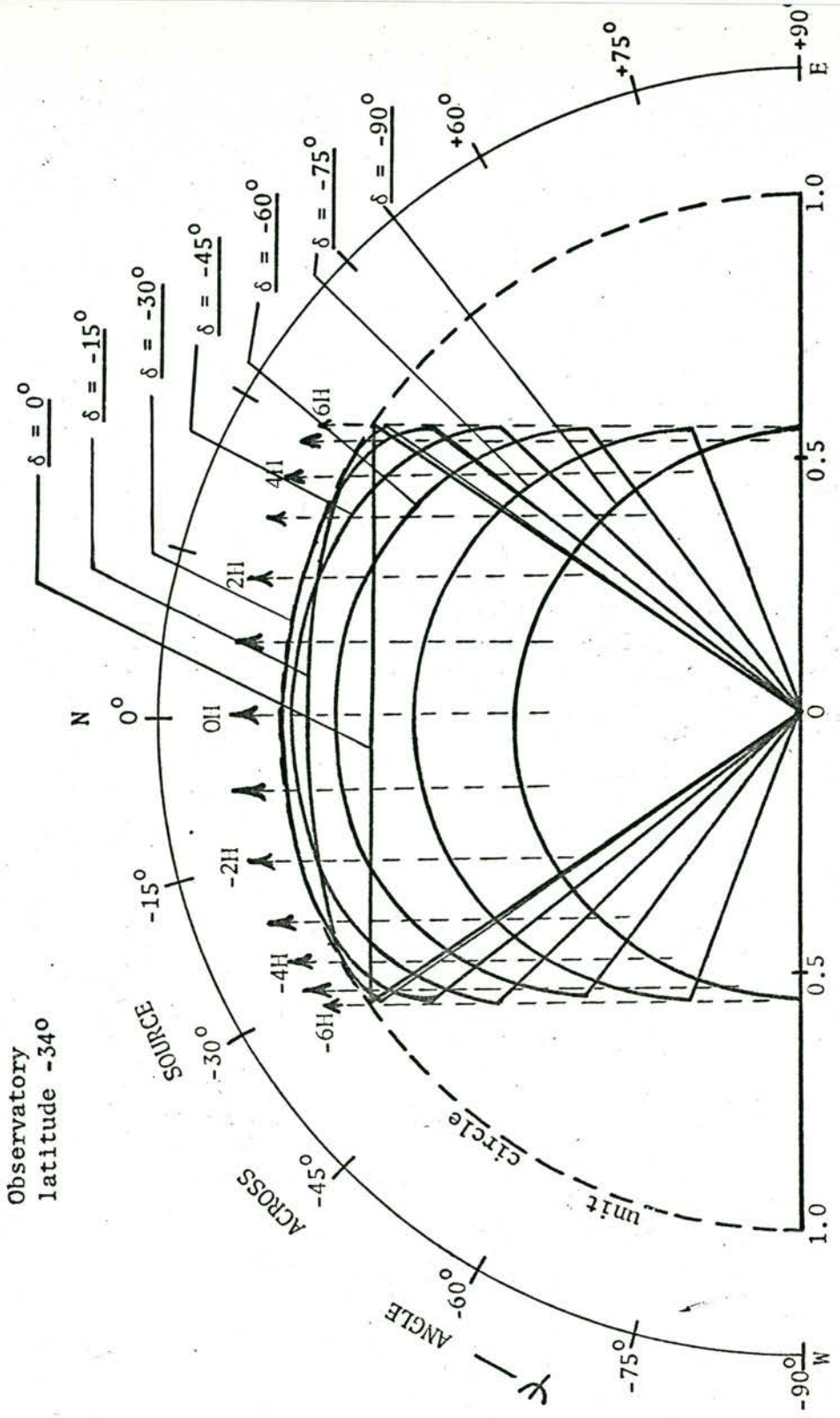

FIGURE B.5 The variation with hour-angle of the projection of a north-south array at latitude -34° as seen from different source declinations. Any radius drawn from the centre O to the required ellipse represents the projection in length and direction at a particular hour-angle.

The Figs. B.4 and B.5 are combined in Fig. 3.4. At the same time the aerial sky coverage (curve A of Fig.5.2) has been applied and the resultant diagram indicates the effective apertures to be expected at various declinations.

The rotational coverage, ψ, on a particular source for a given hour-angle coverage is plotted in Figs. B.6 and B.7 and combined in Figs. B.8 and B.9. The aerial hour-angle coverage required at a particular declination to achieve full rotational coverage is apparent from the points of intersection of the curve in these last two figures.

When the aerial coverage differs from the required value, the effective aperture has either four angular gaps or four angular overlaps. The size of overlap (or gap) is given by $(\psi_{NS} - \psi_{EW})$ for a given (α,δ). This is plotted in Fig 3.5 together with the actual aerial sky coverage, the horizon limits and the 15^{o} altitude limits (ionospheric).

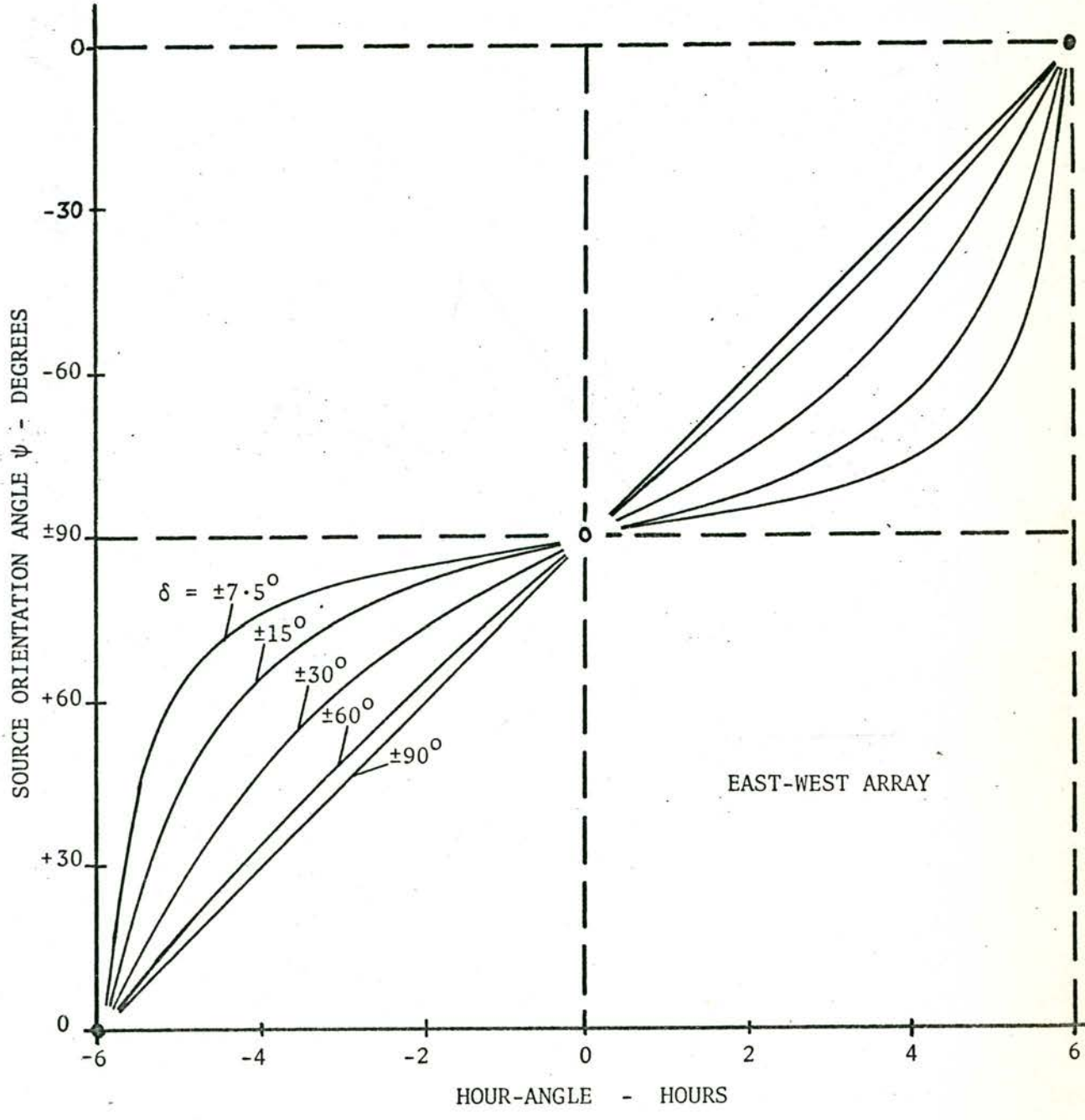

FIGURE B.6 Orientation vs. hour-angle for sources of various declinations.

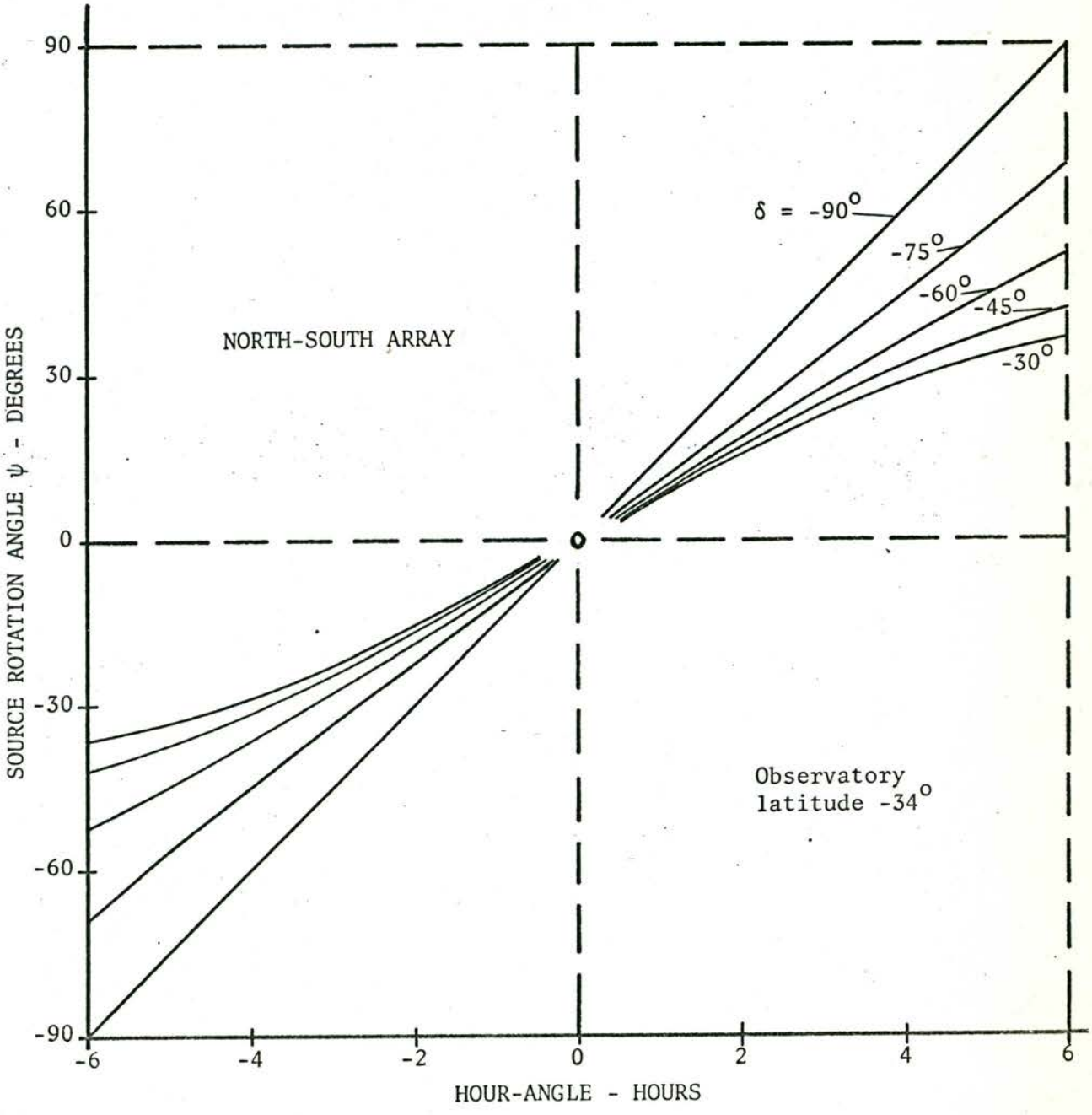

FIGURE B.7 Orientation vs. hour-angle for sources of various declinations.

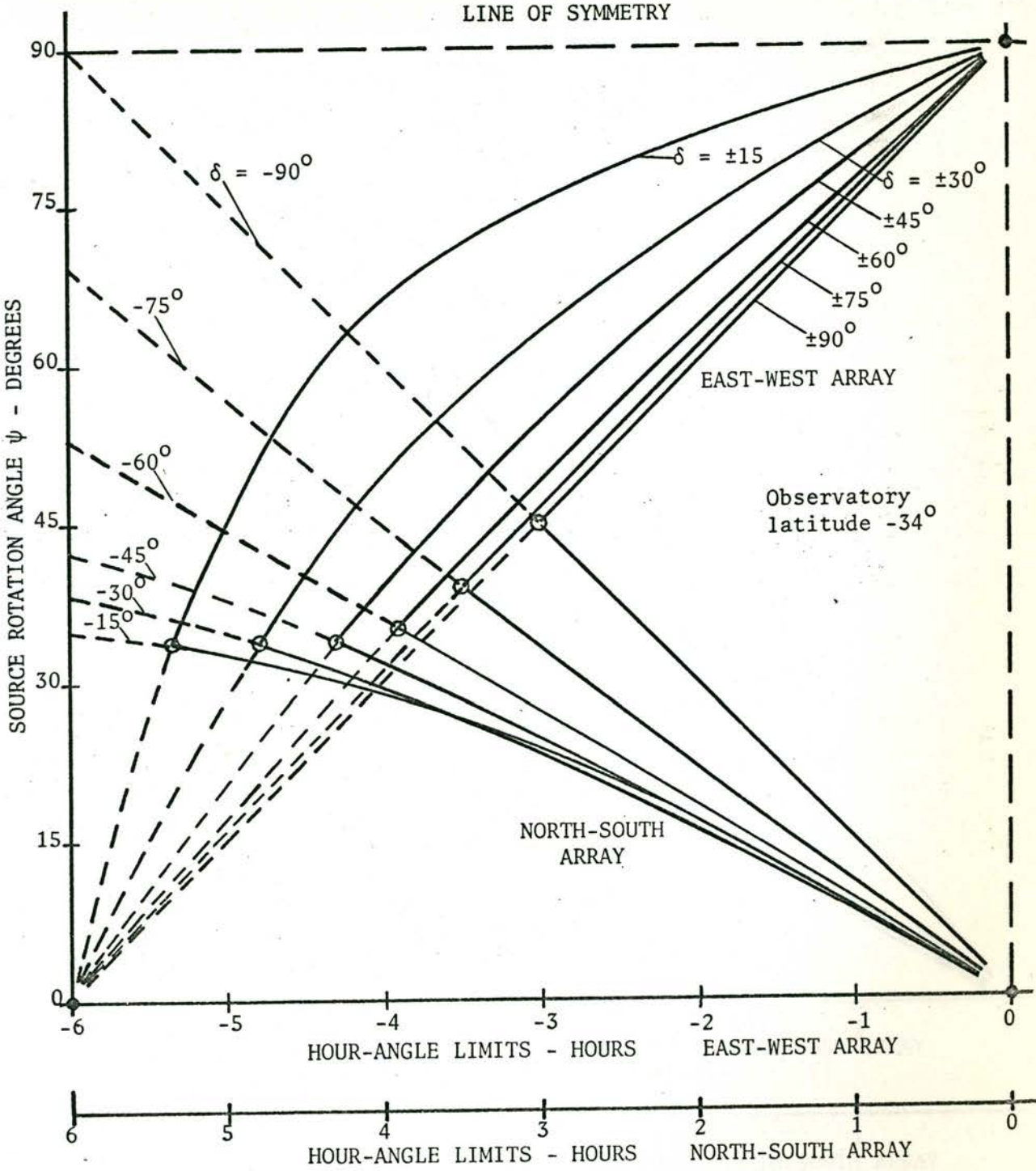

FIGURE B.8 Combines a NS and an EW linear array to give the rotational coverage (ψ) vs. hour-angle limits for sources at declinations between -15^{o} and -90^{o}. Symmetrical hour-angle coverage is assumed. (ψ coverage for 90^{o} to 180^{o} is the same as for 90^{o} to 0^{o}).

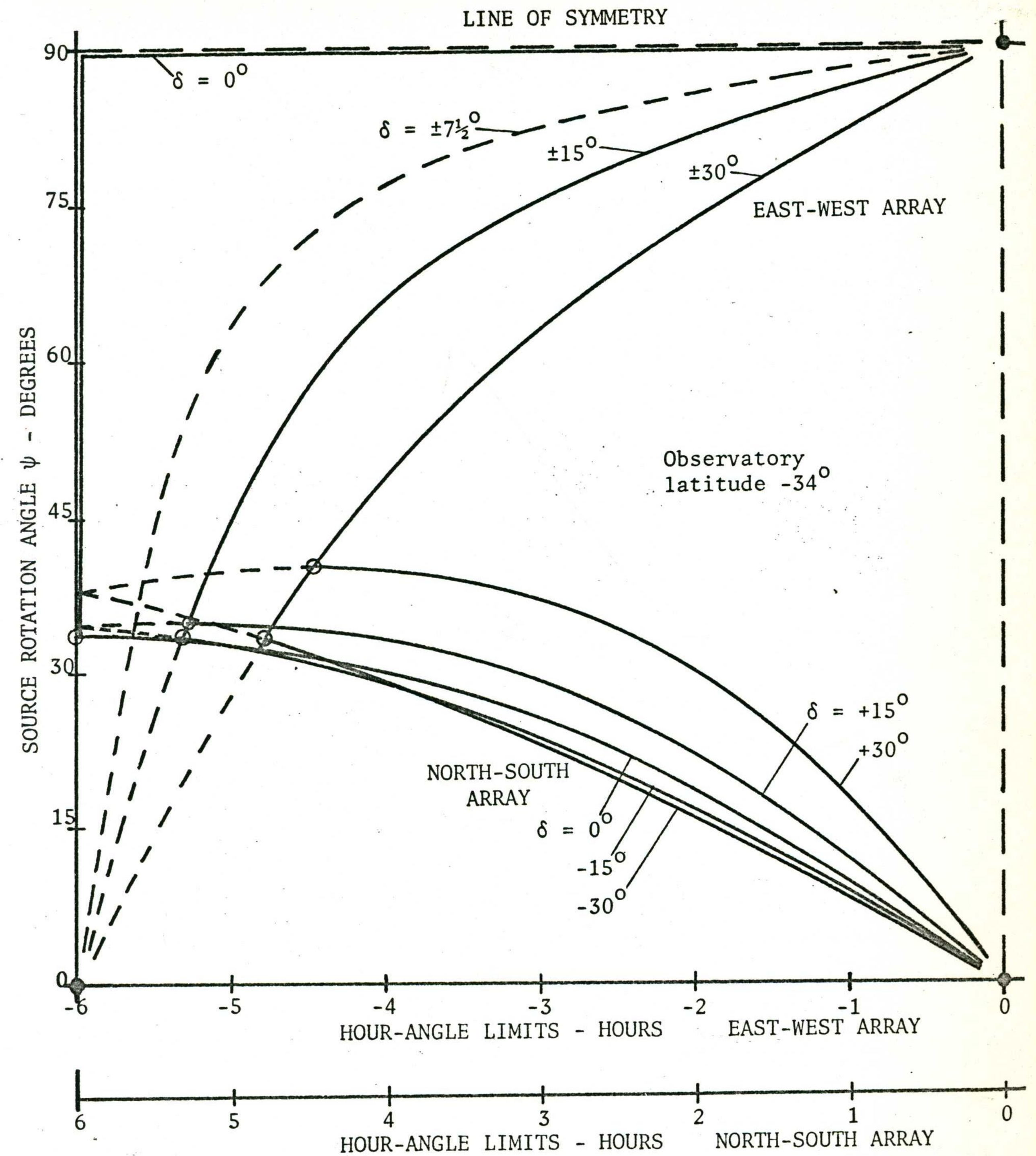

FIGURE B.9 Combines a NS and an EW linear array to give the rotational coverage (ψ) vs. hour-angle limits for sources at declinations between -30^{o} and $+30^{o}$. Symmetrical hour-angle coverage is assumed. (ψ coverage for 90^{o} to 180^{o} is the same as for 90^{o} to 0^{o}).

Appendix C.1 Delineation of the Array Baseline

Positioning of the additional antennae requires the definition of points on each of these aerials which are representative of their positions. This is complicated by:

(i) the combination of large and small aerials of differing designs and

(ii) the separation of the declination and hour-angle axes by 15½ inches on the existing small aerials.

An aperture plane can be defined for each aerial. Its only restriction is perpendicularity with the paraboloid axial line; i.e. it can be placed in any position along this axial line. For signals incident normal to this plane, the path length travelled to the focus from the plane is a constant.

To keep the grating responses stationary relative to the earth throughout the period of observation, it is necessary to maintain the aperture planes of the different aerials in a constant relationship to one another. To do this for all observing directions they should pivot about points which are collinear (Fig. C.1.1). This avoids the difficulties experienced in an earlier compound interferometer system at Fleurs (Labrum et al, 1963).

The collinearity requirement can be relaxed for the image synthesis system provided special phase corrections are made either during reception of the signals or before recombination in the computer. As this entails an extra operation upon the signals, a configuration in which the aerials are all collinear is to be preferred.

In the antennae of some systems (McAlister and Labrum, 1967 and Read, 1963) the declination and hour-angle axes intersect. This then becomes the obvious pivot point.* Since the pivot point is fixed relative to the ground, its position does not vary with the direction of pointing.

---

*The aperture plane of each element may be 'moved' down the axis to coincide with this pivot point by inserting time delays.

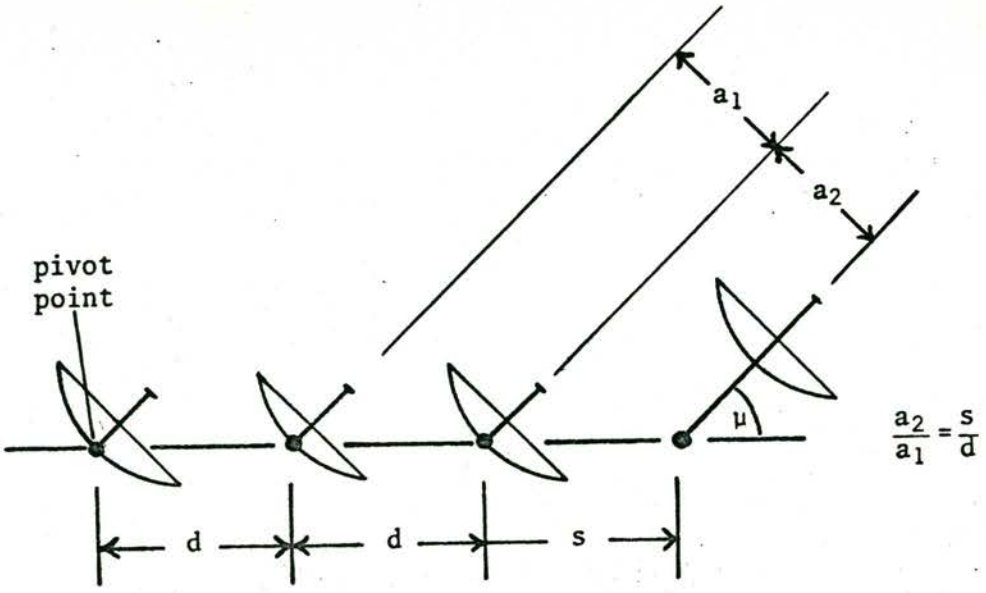

$$\frac{a_2}{a_1} = \frac{s}{d}$$

PIVOT POINTS COLLINEAR

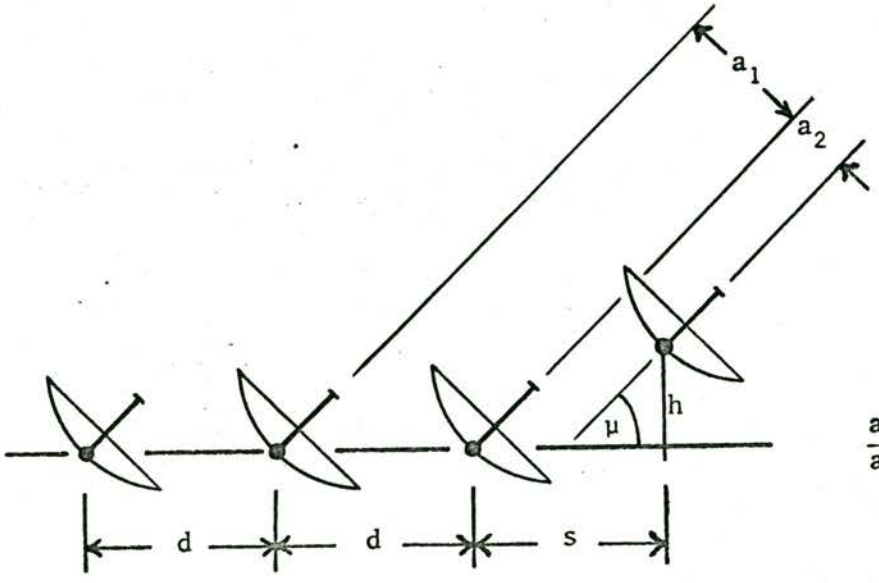

$$\frac{a_2}{a_1} = \frac{s}{d} - \frac{h}{d}\cot\mu$$

$$= \begin{Bmatrix} \text{function of} \\ \text{array angle } \mu \end{Bmatrix}$$

PIVOT POINTS NOT COLLINEAR

FIGURE C.1.1 Illustrating the requirement of collinear pivot points for fan beam operation of an array. For satisfactory operation $\frac{a_2}{a_1}$ should be independent of the direction of observation, μ. This requires collinear pivot points (h=0).

When the axes do not intersect the situation is slightly different (Fig. C.3.2). Phasing can move the aperture plane down the focal axis to the point where it intersects the hour-angle axis. However as the declination is changed, the point of intersection of the aperture plane and the hour-angle axis also varies. This point can be 'termed' the pivot point. Provided the declination and hour-angle axes have the same separation on all dishes, these pivot points will remain collinear and there will be no differential movement.

The following conclusions are reached:

1. The type of mounting, equatorial in this case, must be the same for all aerials.
2. The separation of declination and hour-angle axes must be the same for all aerials (15½ inches in the present system).
3. Focal length differences can be compensated by cable delays (Appendix C.4).
4. With the aerials pointing along the meridian plane the declination axes should be collinear (for fan beam operation).
5. The base line length can be measured as the separation of the hour-angle axes of the aerials for an east-west array and the separation of the declination axes for a north-south array.*

---

*For any other orientation, the baseline should be resolved in north-south and east-west components measured to the declination hour-angle axes respectively. The baseline separation is then the square-root of the sum of the squares of these values.

Appendix C.2 Inter-element Shadowing in a Compound Grating Interferometer

The shadowing of any of the aerials has two effects, both dependent upon the degree of shadowing:

1. The Fourier components associated with the affected aerials experience a reduction in signal proportionate to the size and illumination of the antenna area shadowed.
2. The image plane size and weighting change for these Fourier components.

The shadowing, when it occurs, will always be in the direction of highest resolution of the array.

The degree of shadowing depends upon the diameter and spacing of the aerials concerned and upon μ, the angle between the direction of the source and the direction of the baseline of the array (Fig. C.2.1). ($\sin\mu$ gives the normalized array length.) Equations B.7 and B.8 Appendix B. (on the geometry of earth rotation synthesis) relates μ to the (α, δ) coordinate system.

$$\mu_{EW} = \sin^{-1}\left(-\cos\delta.\sin\alpha\right) \qquad (C.2.1)$$

$$\mu_{NS} = \sin^{-1}\left(\sin(\delta+34^{o}) - \sin 34^{o}.\cos\delta(1 - \cos\alpha)\right) \qquad (C.2.2)$$

Consider only the geometrical shadowing for two aerials of diameters ($2r_1$) and ($2r_2$) and spacing d. Fig. C.2.1 gives the area shadowed, (Λ), as:

$$\Lambda = (r_1)^2(\theta_1 - \tfrac{1}{2}\sin 2\theta_1)+(r_2)^2(\theta_2 - \tfrac{1}{2}\sin 2\theta_2) \qquad (C.2.3)$$

where $d\sin\mu = r_1\cos\theta_1 + r_2\cos\theta_2$

$$r_1\sin\theta_1 = r_2\sin\theta_2$$

and θ_1, θ_2 as indicated in Fig. C.2.1.

If the illumination of each aerial is uniform, then the percentages of effective area shadowed would be $\frac{\Lambda.100}{\pi.(r_1)^2}$ for the small

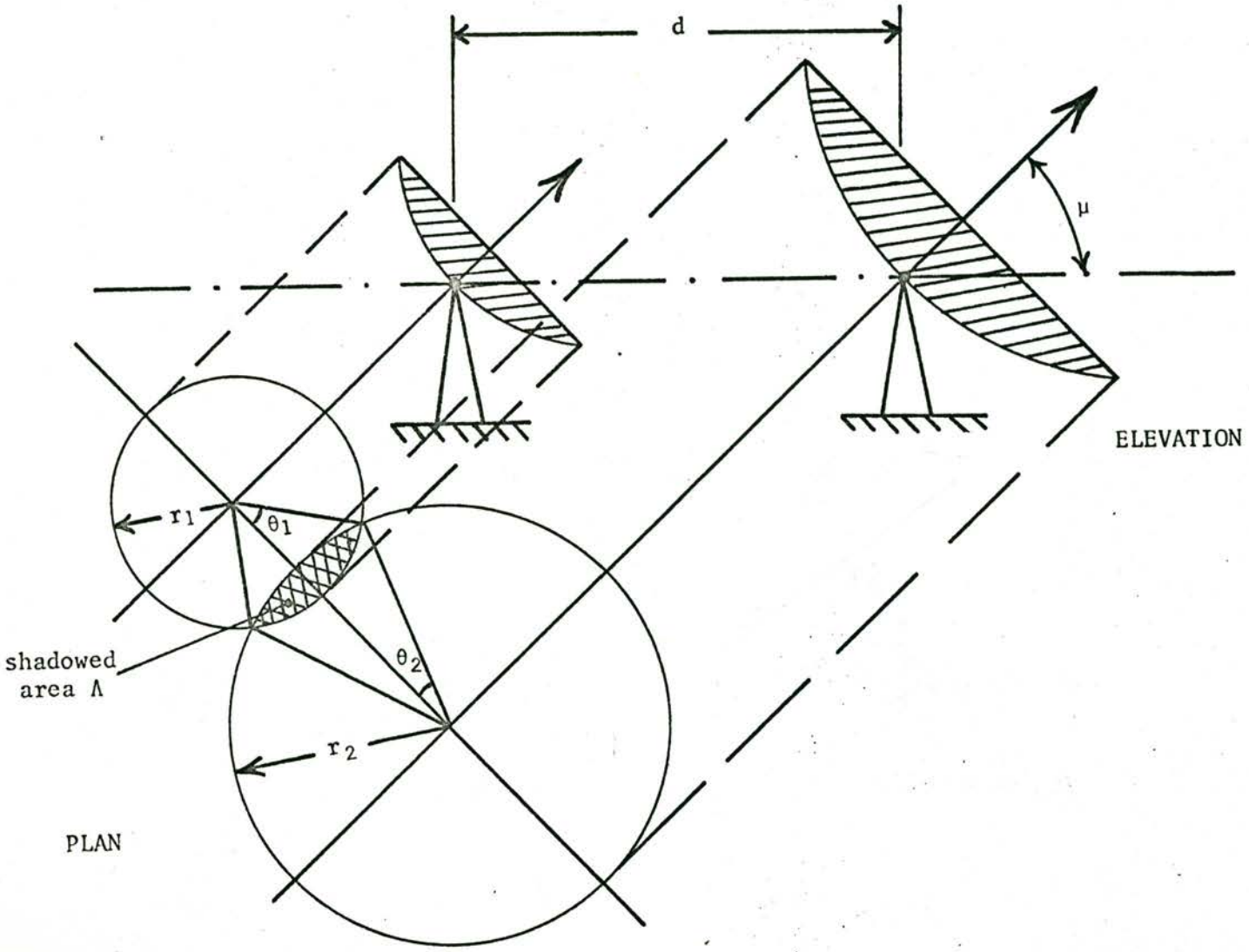

FIGURE C.2.1 Inter Element Shadowing.

aerial and $\frac{\Lambda.100}{\pi.(r_2)^2}$ for the large aerial.

However, the illumination is not uniform but generally tapered severely at the edges. If this aerial illumination is line-integrated, and the shape of the shadowed portion assumed to be a segment of the aerial, then the gain loss or signal variation can be derived accurately as the ratio of areas under the line-integrated curve.

The envelope directivity in a particular direction across the source is dependent upon the maximum dimension and the illumination in the corresponding orientation across the element. Again, shadowing effects can be determined by considering the line integrated illumination pattern. The shadowed edge is removed and either (i) the directivity pattern recomputed or (ii) the change in radius of gyration of the illumination curve calculated (Bracewell, 1965). However a close estimate is obtained by considering the fractional reduction in maximum dimension as a fractional increase in envelope width.

These approximations of gain-loss and envelope width-increase err on the high side (which is desirable) due to the assumptions which have been made.

Shadowing of three types occurs:

(i) The small aerials of the closely spaced grating shadow one another. This causes nearly all the Fourier components to be affected. The degree of shadowing is symmetrical on either side of the zenith direction.

(ii) One small aerial is shadowed by a large aerial. This effects only the lowest spatial frequency and will be very noticeable with broad sources such as the sun. It will only be present on one side of the zenith unless a balanced configuration is used.

(iii) The large aerial closest to the grating is shadowed by a small aerial. This reduces the signal level of a large number of the lower order Fourier components which changes the effective beam

shape of the picture point. Again this is only symmetrical about the zenith with a balanced configuration.

Once a tolerance is set for the Fourier component levels and for picture point gain at the image plane edge, then the aerial spacing and size determines the minimum observable value of μ. This forms a cone of exclusion around the array line direction inside which excessive shadowing occurs.

$\sin\mu$ is given by the normalized array length projection (Figs. B.4 and B.5). Provided this array length projection remains greater than a certain value over the required sky coverage, shadowing will not be excessive.

In practice several parameters must be balanced. These are aerial spacings, aerial sizes, the required sky coverage and the allowable signal level variations. If the system is used as an image synthesis telescope where a whole day's observations are combined, then the effects of shadowing which occur at the extremes of the observing period are less marked, although still important.

For the system at Fleurs, the inter-element shadowing determined the positions of the additional 45 foot diameter antennae. The approximate size of the additional antennae was determined by other factors. The coverage requirement was dictated by rotational synthesis and the existing dish structures. These details of the array configuration are treated in Chapter 4.

Evaluation of the onset of geometrical shadowing

1. Shadowing between two small aerials of the grating

   The aerial diameters are both 19 feet. The separation is 40 feet. Thus the angle of onset of geometrical shadowing, μ_0, is given by:

$$\sin\mu_0 = \frac{19}{40} = 0.475$$

   i.e., the normalised array length should not fall below 0.475 to avoid geometrical shadowing.

2. Shadowing between a small aerial and a large aerial for various separations

The aerial diameters are 19 feet and 45 feet.

Consider separations of 40 feet, 60 feet and 80 feet.

$$\text{40 feet:} \quad \sin(\mu_0) = \frac{32}{40} = 0.80$$

$$\text{60 feet:} \quad \sin(\mu_0) = \frac{32}{60} = 0.53$$

$$\text{80 feet:} \quad \sin(\mu_0) = \frac{32}{80} = 0.40$$

Figs. B.4 and B.5 show that, within the sky coverage requirements, the normalized array length projection often falls below 0.8 but never below 0.53. Thus provided a forty foot spacing is not used for the closest large aerials (giving $\sin\mu_0 = 0.8$), no shadowing occurs at all. (A forty foot initial spacing would cause excessive shadowing over a large portion of the intended sky coverage.)

The percentages of obscured area for both the 40 foot and 60 foot spacing between a 19 foot and a 45 foot diameter aerial are evaluated in Fig. C.2.2 for a range of exclusion-cone half angles.

A 60 foot spacing was adopted as the minimum spatial component.

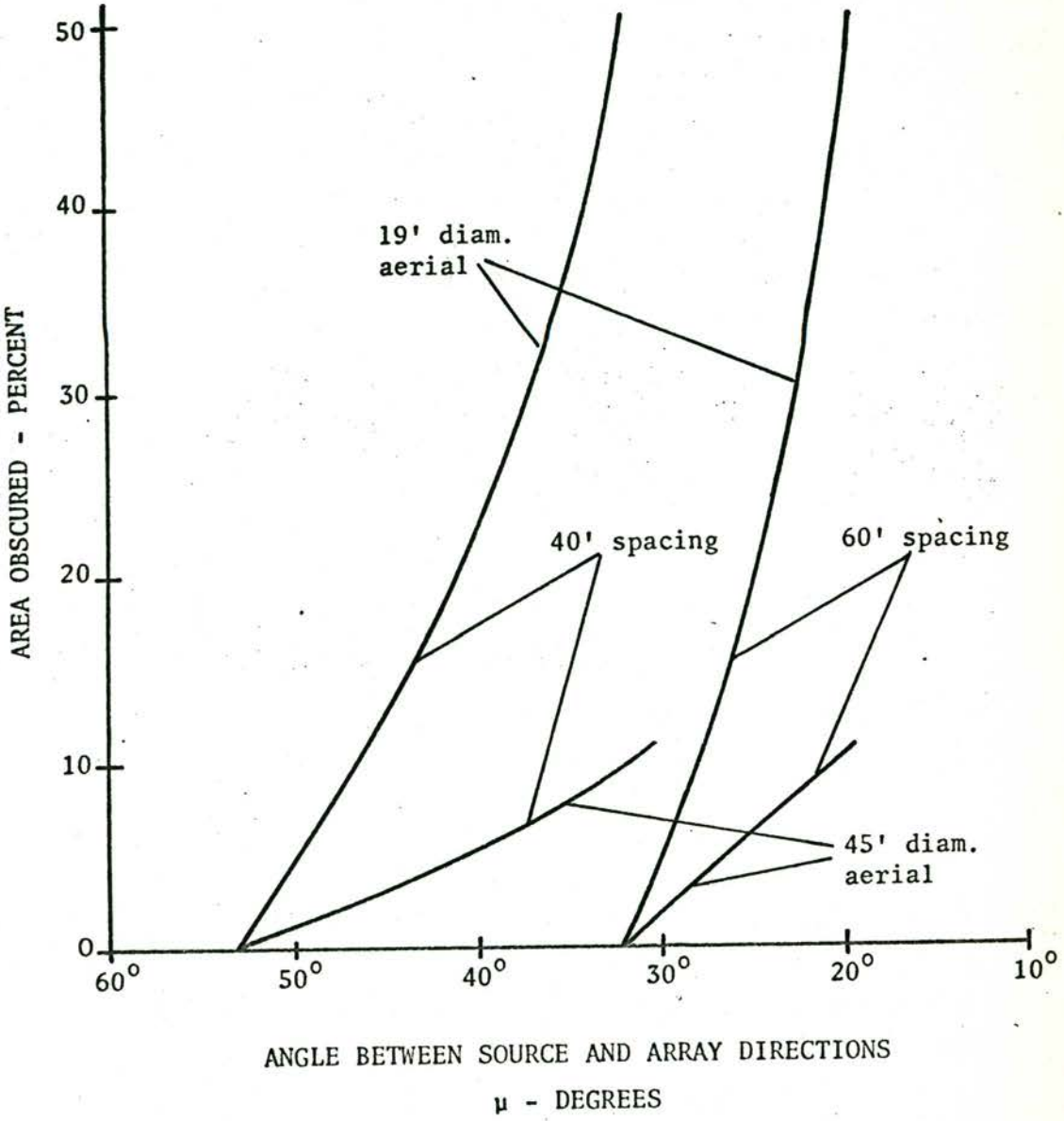

FIGURE C.2.2 The shadowing between a 45 foot diameter aerial and a 19 foot diameter aerial for both 40 foot and 60 foot aerial spacings.

Appendix C.3 Ground Clearance

The small ground-to-axis height of 12½ feet in two of the four new antenna locations proved to be a severe restriction in the design of these large aerials.

The minimum requirements of sky coverage and of aerial diameter, d, were obtained from consideration of source rotation and grating side-lobe levels. A compromise was necessary in maximizing these requirements since they conflict with one another when ground clearance is considered.

Three design factors can be used to give additional ground clearance:

(i) A trench can be dug at those positions where the edge of the aerial strikes the ground. (In the following derivation this is indicated by a negative clearance.) This is permissible within certain limits influenced by the shadowing of the reflector edge by the ground.

(ii) The f/d ratio can be varied. A low f/d 'lifts' the outer edge. However the f/d ratio is determined as 0.41 by the primary feed illumination.

(iii) The vertex-to-declination-axis distance can be increased (compared with the diameter) as illustrated in Fig. C.3.1. This places the whole reflector structure further out along the pointing axis giving more ground clearance but complicating the structural design.

$$\text{Let } K_2 = \frac{\text{vertex-to-declination-axis distance}}{\text{aerial diameter}}$$

$$= \frac{(DV)}{(AB)} \text{ in Fig. C.3.2.} \qquad (C.3.1)$$

This will have a minimum value (with this type of design) of $K_2 \simeq 0.05$, set by the aspect ratio of the rib structure.

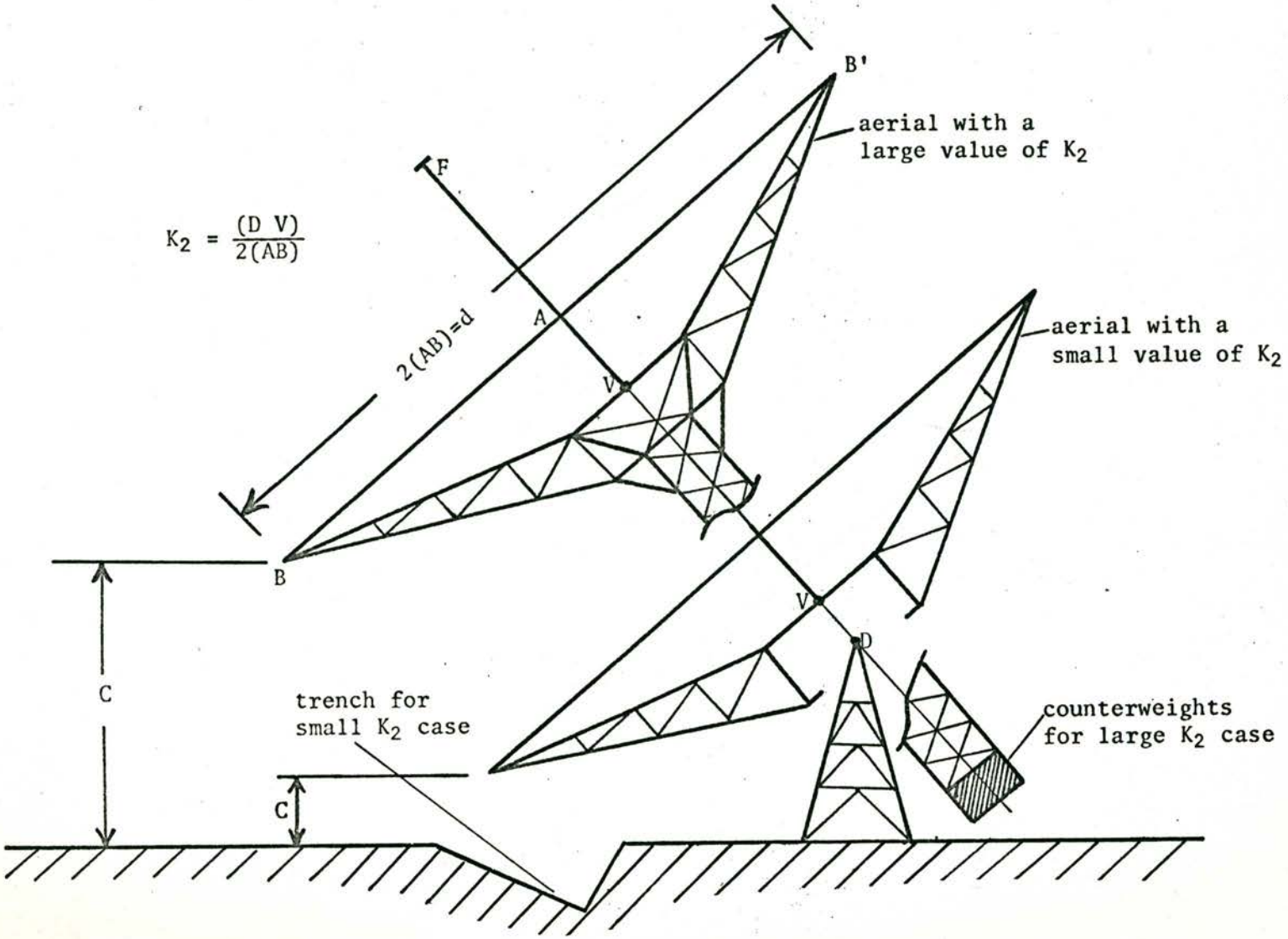

FIGURE C.3.1 Illustrating the clearance difficulties on aerials having the same pivot point height but different values for K_2.

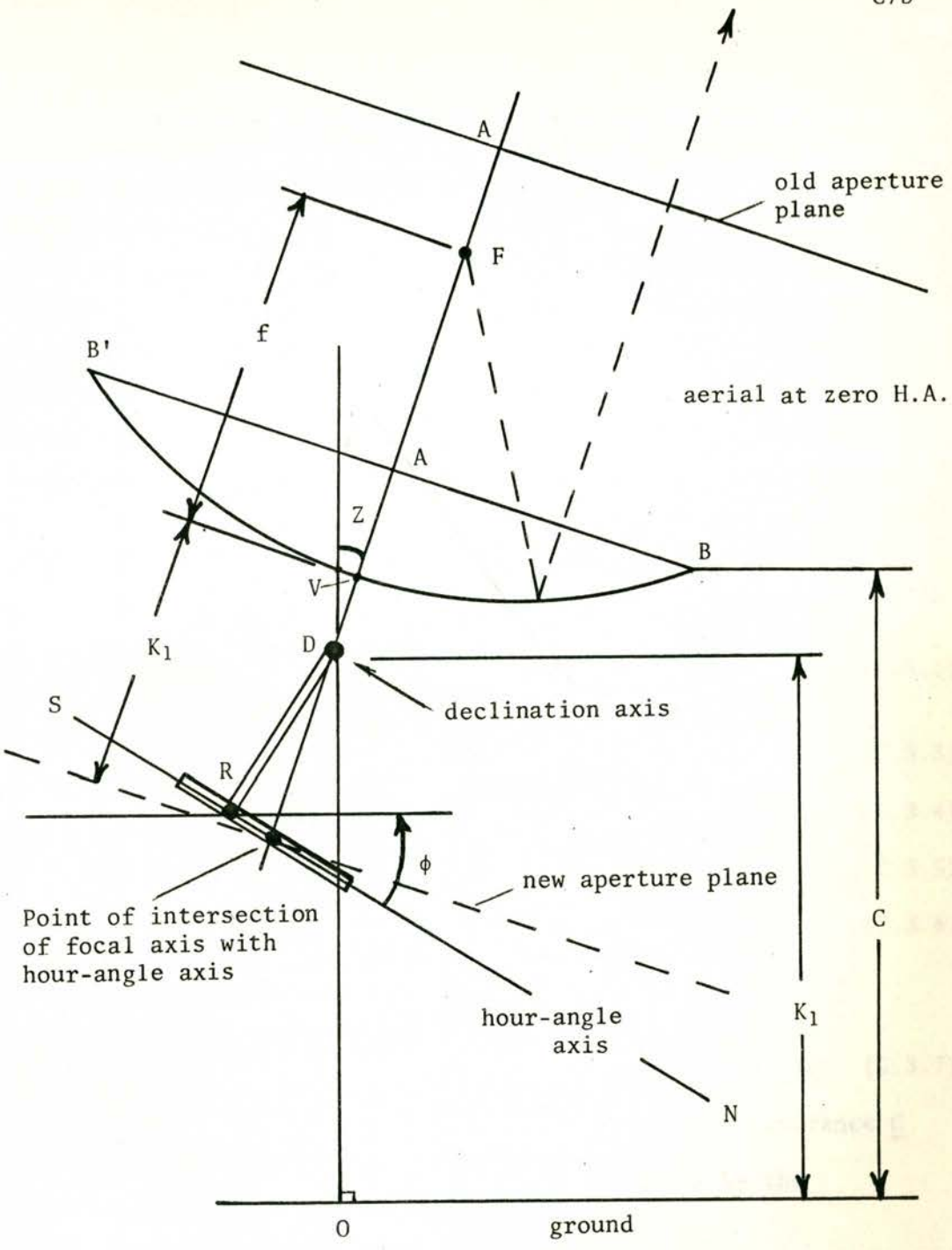

FIGURE C.3.2 Relationship of parameters for computation of the antenna ground clearances.

The antenna axial direction is (α,δ) in equatorial coordinates. This corresponds to (θ,Z) in alt.-az. coordinates. Let the height of the declination axis at zero hour-angle be K_1. We wish to determine the clearance C between the aerial edge and the ground.

Referring to Fig. C.3.2, the vertical height of R is fixed independently of hour-angle. Thus

$$(R'O) = K_1 - K_3 \cos\phi$$

where ϕ is the observatory latitude.

From Fig. C.3.3 the vertical projected length of $(DR=K_3)$ at an hour-angle α is given by:

$$K_3.\cos\alpha.\cos\phi$$

Thus the ground height of D (the intersection of declination and focal axes) is given by:

$$(OD) = K_1 - K_3 \cos\phi(1-\cos\alpha) \qquad (C.3.2)$$

From Fig. C.3.2,

$$C = (OD) + (DV).\cos Z + (BV).\cos(Z+\beta) \qquad (C.3.3)$$

where

$$(DV) = K_2.d \quad \text{(from C.3.1)} \qquad (C.3.4)$$

$$\tan\beta = \frac{AB}{AV} = 8\left(\frac{f}{d}\right) \qquad (C.3.5)$$

and

$$\frac{(BV)}{d} = \left[\frac{1}{4} + \left(\frac{1}{16\left(\frac{f}{d}\right)}\right)^2\right]^{\frac{1}{2}} = K_4 \qquad (C.3.6)$$

Thus combining equations (C.3.2), (C.3.3) and (C.3.4):

$$C = K_1 - K_3.\cos\phi.(1-\cos\alpha) + K_2.d.\cos Z + K_4.d.\cos(Z+\beta) \qquad (C.3.7)$$

To apply this equation in order to determine the clearance C

(i) K_1 and K_3 are fixed at 12½ feet and 15½ inches by the requirements of Appendix C.1,

(ii) the latitude ϕ is -34°, and

(iii) K_4 and β are determined by the $\left(\frac{f}{d}\right)$ ratio of the aerial and computed for the present aerial, using equations (C.3.5) and (C.3.6), as $K_4 = 0.525$ and $\beta = 72\frac{1}{2}^{\circ}$.

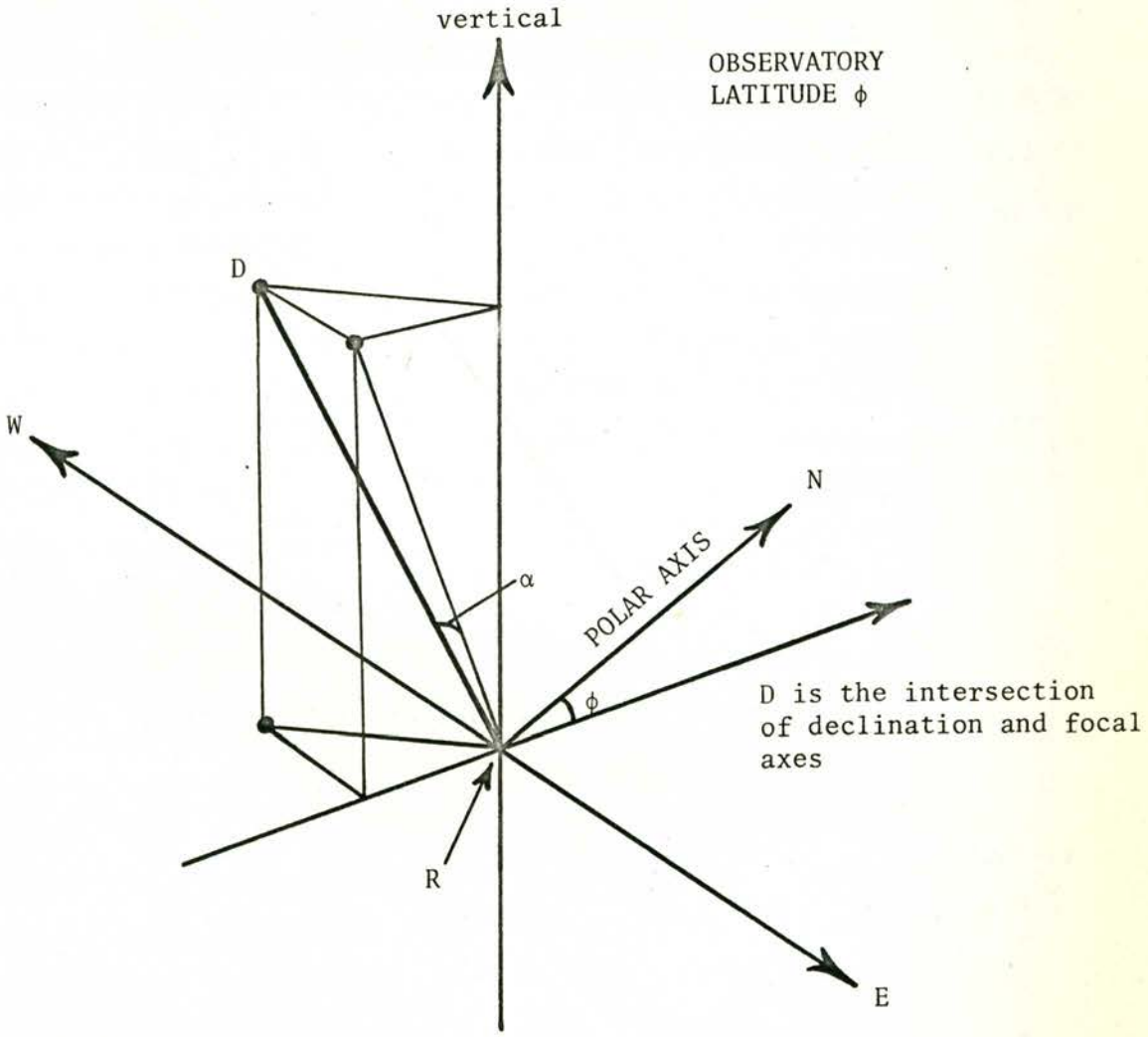

FIGURE C.3.3 Axes relationship of fig. C.3.2 when the aerial is at an hour angle α.

The formulae relating (θ,Z) to (α,δ) are given by Smart (1962, p.35) as

$$\cos Z = \sin \phi . \sin \delta + \cos \phi . \cos \delta . \cos \alpha \qquad (C.3.8)$$

$$\sin \theta = \operatorname{cosec} Z . \cos \delta . \sin \alpha \qquad (C.3.9)$$

Thus the ground clearance C can be determined for a range of the structural variables d and K_1, and for critical values of (α,δ).

Evaluation of the ground clearances

1. As mentioned in Section 4.3, the minimum sky coverage requirements are:

   Declination: -80° to $+23^{\circ}$

   Hour-angle : $\pm 3\frac{1}{3}$ hrs @ $-80^{\circ}\delta$ to $\pm 4\frac{2}{3}$ hrs @ $-30^{\circ}\delta$
   with reduced hour-angle coverage to $+23^{\circ}\delta$.

2. Attenuation of the grating sidelobes requires an aerial diameter of 40 to 60 feet.

3. The constant K_1, ground to axis height, is fixed at 12½ feet by the existing aerials. K_1 could have been increased by raising all 64 small aerials. However this was considered impracticable.

4. A trench is used to accommodate the edge of the large aerial, but it was necessary to limit it in depth to four feet (plus clearance). To avoid shadowing the antenna, the trench needs to be tapered radially at approximately 30° slope. This gives a trench width in the region of ten feet.

5. The constant K_2 is kept close to 0.075 primarily to enable a lightweight structure to be built without using counterweights.

In evaluating the clearance C, a graphical plot of (α,δ) vs. (θ,Z) was used. In terms of ground clearance, the declination requirements were not hard to achieve. A 50 foot diameter aerial with $K_2 = 0.1$ would have required only a two foot deep trench.

For the point ($4\frac{2}{3}$ hrs, -30^{o}) the clearance was computed for aerial diameters 40, 45 and 50 feet and for $K_2 = 0.05$, 0.1, 0.2 and 0.5. For example a 50 foot diameter aerial clears the ground provided $K_2 = 0.2$. (This would put a large loading on the drive gears unless counterweights were used.)

The final values decided upon were a diameter of 45 feet and $K_2 = 0.07$ (3.1 feet). This aerial also clears the ground at ($4\frac{2}{3}$ hrs, -30^{o}).

Appendix C.4 The Aerial Differential Signal Path Length

The two different sizes of antennae in the array have diameters of 13.70 m and 5.55 m. Since f/d = 0.41 for both, their focal lengths, f_1 and f_2, are 5.63 m and 2.28 m respectively. The distances $(K_2)_1$ (0.84 m) and $(K_2)_2$ (0.48 m) from the vertex to the declination axis (Fig. C.3.2) need to be different for structural reasons.

These differences mean the incident wave travels further in the large aerial before reaching the focus. Consider an aperture plane at a distance K in front of the δ axis. This is $(K-f-K_2)$ in front of the focus. A plane wave travels $\left(2f + (K-f-K_2)\right)$ from the aperture plane to the focus. Thus the differential air path length between two aerials with collinear axes is given by

$$\left(f_1 - f_2 - (K_2)_1 + (K_2)_2\right)$$

For the above mentioned aerials this length is 2.99 m.

There will also exist another differential length in the signal feeder line from the focus to the preamplifier-mixer. Neither of these differentials varies with viewing angle. They are compensated for by inserting extra delay in the intermediate frequency signal path of the smaller aerial. (A delay is preferred to a phase shift so that the white fringe is initially in the zenith direction.)

Appendix D.1 A Conic Approximation of a Cylindrical Paraboloid Antenna.

Cylindrical paraboloid antennae are commonly constructed with a lightweight wire mesh as the reflecting surface. This mesh is usually not self supporting and as such, it cannot be constrained to follow the ideal doubly-curved surface of a paraboloid of revolution. Some approximation to the desired shape is necessary.

A convenient form of construction is to have the support points in the form of rings suitably placed so that the mesh, when stretched taut, takes on the form of a series of coaxial conic surfaces. This is the construction that has been applied to the design described in Chapter 5. The problem is to choose the support point positions so that the deviation of these conic surfaces from the ideal reflector shape does not exceed some error criterion.

As an initial error criterion assume a maximum allowable displacement from the paraboloid of $\pm\gamma$ wavelengths in the axial direction. This axial tolerance is a measurement convenient for use during assembly. It is not the path length error. This latter fact and its implications, including the possibility of allowing a radial variation of the axial tolerance, are discussed in Section 5.7 and Appendix D.2.

Brown (1961) used this axial tolerance criterion when he considered the optimum solution for only two conic surfaces. This Appendix derives the optimum solution for an arbitrary number of conic surfaces and applies it to the design of Chapter 5.

As in the main text, all measurements of length are in units of one wavelength, except where indicated otherwise. The wavelength implied herein is 21 cm.

Since both the paraboloid and the conic approximation are circularly symmetrical, the problem can be reduced to one in only two dimensions. The paraboloid is represented by $y^2 = 4fx$ and the cones by straight lines. The ith cone is given by:

$$y = m_i x + a_i \qquad (D.1.1)$$

where m_i is the tangent of the cone half-angle and

a_i is the radius of the circle of intersection of the cone with the plane through the vertex, perpendicular to the axial direction.

Suppose the i^{th} cone intersects with the $(i+1)^{th}$ cone at some point, $(x_i y_i)$. The above error criterion places $(x_i y_i)$ on the parabola $y^2 = 4f(x+\gamma)$ and causes the cone, $y = m_i x + a_i$ to be tangential to the parabola $y^2 = 4f(x-\gamma)$.

At $(x_i y_i)$:

$$\gamma = \frac{y_i}{4f} - \frac{y_i - a_i}{m_i} \qquad (D.1.2)$$

and solving this equation to give the radius of the circle of intersection of two cones:

$$y_{i,i-1} = \frac{2f}{m_i} \pm 2\left[\left(\frac{f}{m_i}\right)^2 - \left(\frac{f}{m_i}\right)a_i + f.\gamma\right]^{\frac{1}{2}} \qquad (D.1.3)$$

The <u>radial</u> panel width (Δy_i) is given by:

$$\begin{aligned} \Delta y_i &= y_i - y_{i-1} \\ &= 4\left[\left(\frac{f}{m_i}\right)^2 - \left(\frac{f}{m_i}\right)a_i + f.\gamma\right]^{\frac{1}{2}} \end{aligned} \qquad (D.1.4)$$

The axial error, <u>e</u>, at any point is given by:

$$e = \frac{y - a_i}{m_i} - \frac{y^2}{4f} \qquad (D.1.5)$$

At some point, $e = +\gamma$ and $\frac{de}{dy} = 0$ and from equation (D.1.5) this occurs at $y = \frac{2f}{m_i}$. Hence:

$$f.\gamma = \left(\frac{f}{m_i}\right)^2 - \left(\frac{f}{m_i}\right)a_i \qquad (D.1.6)$$

Substituting in equation D.1.4,

$$(\Delta y_i) = 4\left(2.\frac{f}{D}.\gamma.D\right)^{\frac{1}{2}} \qquad (D.1.7)$$

where D is the aperture diameter.

The points y_i form a series with a constant increment of $4\left(2.\frac{f}{D}.\gamma.D\right)^{\frac{1}{2}}$ provided γ, the maximum error criterion, is constant over the whole reflector. Therefore

$$y_i = y_0 \pm 4.i\left(2f\gamma\right)^{\frac{1}{2}} \qquad (D.1.8)$$

where (x_0y_0) is the first intersection, not the parabola vertex.

Now (x_iy_i) satisfies the equation $y^2 = 4f(x+\gamma)$,

$$y^2 = 4f(x+\gamma) \qquad (D.1.9)$$

hence,

$$x_i = \frac{y_i^2}{4f} - \gamma \qquad (D.1.10)$$

and

$$x_i = x_0+8.i^2.\gamma+4.i.\left(2\gamma(x_0+\gamma)\right)^{\frac{1}{2}} \qquad (D.1.11)$$

As in equation D.1.8, the points x_i form a series. In this case the increments increase in size and are independent of the focal length.

At the vertex two conditions are possible. There is either (1) a cone, or (2) a frustrum of a cone, the latter being more common.

Case 1	Case 2
$(x_0,y_0) \equiv (-\gamma,0)$	$(x_0,y_0) \equiv \left((\gamma,(8.f.\gamma)^{\frac{1}{2}}\right)$
$x_i = \gamma(8i^2-1)$	$x_i = \gamma(8i^2+8i+1)$
$y_i = \pm 4i(2f\gamma)^{\frac{1}{2}}$	$y_i = (1\pm 2i)(8.f.\gamma)^{\frac{1}{2}}$

(D.1.12)

Width of unsupported mesh

If $\Delta\ell_i$ is the width of panel i, then for case 2 above, since $\Delta x_i = 16i\gamma$ and $\Delta y_i = 4(2f\gamma)^{\frac{1}{2}}$,

$$\Delta\ell_i = \gamma\left(256i^2 + 32\left(\frac{f}{\gamma}\right)\right)^{\frac{1}{2}} \qquad (D.1.13)$$

For a paraboloid of diameter D and focal length f constructed from an integral number of rings, n:

$$n = \frac{D-2y_0}{8(2f\gamma)^{\frac{1}{2}}} \qquad (D.1.14)$$

and if n is large (>10 say), then $D >> 2y_0$, and hence

$$n \simeq \frac{D}{8(2f\gamma)^{\frac{1}{2}}} \qquad (D.1.15)$$

and the maximum unsupported panel width becomes

$$(\Delta\ell_n) \simeq (\gamma D)^{\frac{1}{2}}\left(2\left(\frac{D}{f}\right) + 32\left(\frac{f}{D}\right)\right)^{\frac{1}{2}}$$

Hence

$$(\Delta\ell_n) \simeq K_5(\gamma D)^{\frac{1}{2}} \qquad (D.1.16)$$

where $K_5 = \left(2\left(\frac{D}{f}\right) + 32\left(\frac{f}{D}\right)\right)^{\frac{1}{2}}$, depending only on the choice of $\frac{f}{D}$.

K_5 ranges from 4 at $\frac{f}{D} = 0.25$, through 4.22 at $\frac{f}{D} = 0.4$, to 12.6 at $\frac{f}{D} = 5$, and γ generally ranges from $\frac{1}{64}$ to $\frac{1}{8}$ wavelengths.

Number of support rings

Equation D.1.15 above gives the number of support rings necessary for a given diameter

$$n \simeq \left(\frac{D}{128\left(\frac{f}{D}\right)\gamma}\right)^{\frac{1}{2}} \qquad (D.1.17)$$

For a lightweight structure it is advisable to keep n as small as possible.

Evaluation

For the design described in Chapter 5, the diameter D is 66 wavelengths and $\frac{f}{D}$ = 0.41. The maximum error of the conic approximation, γ, is set at $\pm\frac{1}{16}$ inches over the full diameter. Equations D.1.16 and D.1.17 give the resulting maximum panel width and number of rings as three wavelengths and thirteen respectively.

Case 2 of equation D.1.12 was used to compute the intersection points of the conic surfaces. Graphical methods were applied to translate these coordinates to the coordinates of the support tube centres. These centre values are used in assembling the reflector surface and are tabulated in Appendix E.1.

Appendix D.2 Radial Variation of the Allowable Surface Error of a Paraboloid

In Appendix D.1 a maximum design error, $\pm\gamma$, was chosen to be constant over the whole surface. This gave a constant radial increment between support rings. As mentioned previously in the discussion of surface errors, axial tolerances can be varied radially according to equation 5.4 and to the feed illumination weighting factor.

Application of this radial variation to the structural design creates a reduction in the number, and hence weight, of the support rings towards the outer edge of the paraboloid. A reduction in both the gravitational deflections of the reflector and the drive torques on the gears is the final result.

In the antenna design in Chapter 5, this radial variation of support ring positions was not applied since the resultant panel width at the edge would have allowed excessive mesh sag. Mesh sag can only be reduced by using a high mesh tension. This was not possible with the particular mesh available. Instead, the radial weighting factor was used in the determination of the reflector surface flexure tolerances and also as a criterion applied during assembly and during computation of the rms surface error.

An exact radial tolerance is computed by expressing the illumination pattern in radial terms, compensating for distance and hence deriving a power weighting factor. This is combined with equation 5.4 to derive a function for $\gamma(y)$. $\gamma(y)$ is the allowable rms error in the axial direction. To compute the possible variation in radial separation of the support rings, this error is inserted in the appropriate parts of Appendix D.1.

A simplification to this exact approach combines graphical and iterative techniques and is described below.

Initially, it is necessary to have either the radiation pattern of the feed or some close approximation to it. Unless it is a special case, the pattern will be similar to one or two dipoles in front of a reflector giving a $\sin(90^{o}\cos\theta)$ factor for the field. This pattern is multiplied by $\cos^{2}\frac{\theta}{2}$ to correct for the distance from the focus to the paraboloid. The coordinate, linear in θ, is then changed to be linear in r' where $r' = \frac{r}{r_0} = 4(\frac{f}{D})\tan\frac{\theta}{2}$. All of these computations are done by graphical methods and begin with the primary pattern. The resultant curve is now the normalised radial field illumination of the circular aperture. The ordinate is then squared to give normalised power density, I(r').

Consider an annulus of radius r' and width dr'. The power falling on this is proportional to $I(r').2\pi r'.dr'$, assuming that the illumination is symmetrical. The total power, I_t, falling on the aperture is given by:

$$I_t = \int_0^{r_0} I(r').2\pi r'.dr' \qquad (D.2.1)$$

Suppose ε_0 is the overall allowable rms path error and $\varepsilon(r')$ is the annulus path error, then the contribution of $\varepsilon(r')$ to ε_0 is chosen or weighted, as the case may be, in proportion to the contribution of the annulus to the total aperture power:

$$\varepsilon(r') = \varepsilon_0\left(\frac{I_t}{r_0.I(r').r'}\right)^{\frac{1}{2}} \qquad (D.2.2)$$

To compute this, the normalised illumination curve, I(r'), is multiplied by r' to give the curve I(r').r'. Measurement of the area under this curve will give (I_t/r_0) and computation gives W(r'), where

$$W(r') = \left(\frac{I_t}{r_0.I(r').r'}\right)^{\frac{1}{2}} \qquad (D.2.3)$$

Fig. D.2.1 is the plot of this radial weighting factor used in the design described in Chapter 5. It was established using the experimental primary feed pattern.

To find the allowable radial rms axial tolerance, $\gamma(r')$, equation 5.4 is applied in the form:

$$\gamma(r') = \frac{\varepsilon(r')}{2}\left[1 + \{\frac{r'}{4f/D}\}^2\right] \qquad (D.2.4)$$

Radial variation of panel width

Equation D.2.2 can be applied to equation D.1.7 in Appendix D.1 giving the maximum allowable panel widths at different radial positions. These widths will not increase the overall rms path error due to the conic approximation.

$$\Delta r'_i = \{32f/D.\gamma(r')\}^{\frac{1}{2}} \qquad (D.2.5)$$

The assumption here is that $\gamma(r')$ is constant over the panel width. Using the curve for $\gamma(r)$, $(\Delta r'_i)$ can be drawn as a function of r'. An iterative process is then applied in which $(\Delta r'_0)$ is read from the curve and used to determine the abscissa at which $(\Delta r'_1)$ is read, and so on until the paraboloid outer edge is reached. In the process, the coordinates of the conic intersection points are determined using equation D.1.9.

As mentioned previously, the panel widths were not varied radially due to mesh sag.

Equations D.2.2 and D.2.4 were applied during calculation of the allowable flexure tolerances and also during construction and the consequent evaluation of the rms error of the actual reflector.

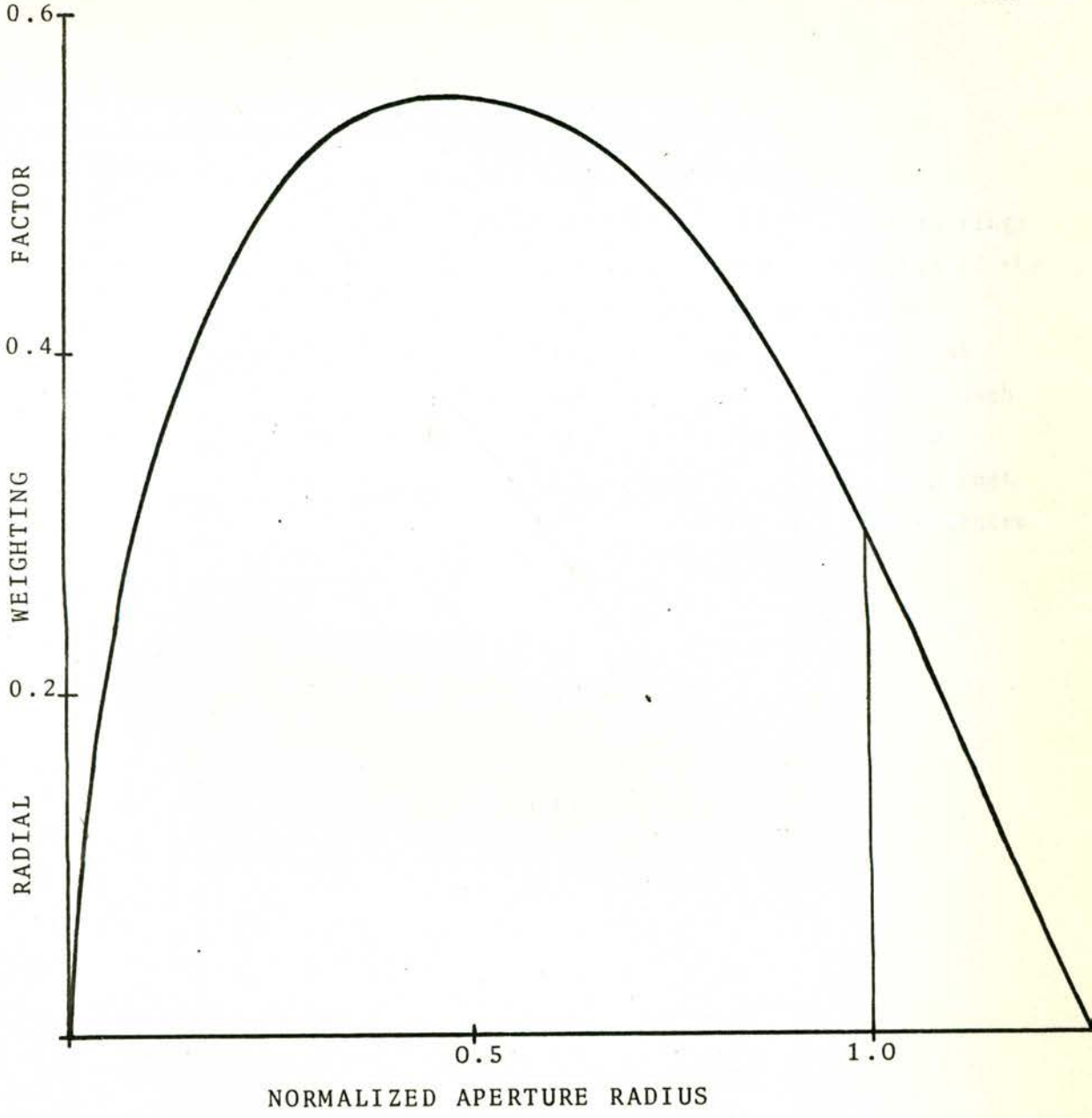

FIGURE D.2.1 The Radial Weighting Factor used in Chapter 5 for computations concerning the surface accuracy of the paraboloid antennae.

Appendix E.1 Reflector Surface Shape of the 45 foot Diameter Antennae

The mesh surface of the antenna is attached to concentric rings of aluminium tube. The following table sets out the coordinates of the tube centres necessary to form this mesh surface to the required paraboloid shape. This shape is actually a conic approximation as derived in Appendix D.1. The heights are relative to a plane through the vertex, perpendicular to the paraboloid axis. The radii are measured out from this axis. Ring 13 is 1½" in diameter and the rest are 1" in diameter. Ring 2 is actually the inner hexagon of the centre section.

Ring No.	Ht(ft)	Radius(ft)
1	No ring	No ring
2	0.051	2.703
3	0.227	4.415
4	0.490	6.307
5	0.840	8.109
6	1.279	9.911
7	1.805	11.712
8	2.418	13.514
9	3.119	15.316
10	3.908	17.117
11	4.784	18.919
12	5.749	20.720
13	6.782	22.531

To adjust the mesh surface to shape accurately and quickly, a rotating convex pattern is 'set-up' inside the reflector. (Kalachov and Salomonovich (1961) used this method on the 22 m Russian radiotelescope.) The pattern is a thin tubular-framed 'rib' about 24 feet long and 4 feet

deep supported in bearings above the dish vertex. Its lower side approximates the reflector shape. Vertical 'fingers' at the ring radii are accurately set to the desired ring heights. The pattern is counterbalanced so that it rotates easily and without distortion about the paraboloid axis. At each reflector rib the aluminium ring positions are adjusted, after which the pattern is lifted out of the reflector.

Appendix E.2 Structural Details of the 45 foot Diameter Antennae

This appendix consists of the plans used in the design and construction of the 45 foot diameter antennae. Originally drawn to scale, they were reduced approximately four times during photographic reproduction.

Drawings B-F45-00, -52 and -53 have been included in Chapter 5.

Of the 54 separate plans, 46 were drawn by the author and the remainder by the Electrical Engineering Workshop.

FLEURS 45 FT RADIO TELESCOPE

ASSEMBLY OF DISH B-F45-00

COMPONENT PARTS LIST (1)

DESCRIPTION	MATERIAL	PART No.	DWG. No.	ASSY DWG Num No.	SCHEMATIC DIAG REF	No. REQ PER UNIT
MAIN RIB			B-F45-01			12
SMALL RIB			B-F45-02			12
CROSS BRACE			D-F45-03			12
RING PLATE/1			P-F45-04		D-F45-05	144
JOINT 'A' - RINGS to RIB & RING JOINT		—	D-F45-06			-
STUB BOLTS - for holding down Rings			P-F45-06			
JOINT 'B' - OUTER RING to RIBS & RING JOINT		—	D-F45-07			-
OUTER RIVET - 9-1P			P-F45-08		D-F45-07	24
U BRACKET - CROSS BRACE to SMALL RIB			P-F45-10		D-F45-11	12
JOINT 'D' - CROSS BRACE to SMALL RIB		—	D-F45-11			
JOINT BRACKET - for joining on SMALL RIB BRACES			D-F45-12			
JOINT 'E' - CROSS BRACE to MAIN RIB		—	D-F45-13			
TUBE PLUG			P-F45-14			72+24
DIAGONAL BRACE - MAIN to small rib			C-F45-15			12
L BRACKET - for diag brace			D-F45-16		D-F45-17	12
JOINT 'F' - SMALL RIB → DIAG BRACE		—	D-F45-17			
JOINT 'G' - DIAG BRACE → MAIN RIB → centre Sec"		—	D-F45-18			
JOINT 'H' - MAIN RIB - centre Sec"		—	D-F45-19			
OUTER RING			D-F45-20		D-F45-07	9½
RINGS			D-F45-21		D-F45-05	x
OUTER RING SLEEVE			P-F45-22		D-F45-07	10
SMALL RING SLEEVE			P-F45-23		D-F45-05	60
CENTRE SECTION			B-F45-25			1
C/S JOINT DETAILS			C-F45-26			
BEARING SUPPORT-DETAIL 'E' - C/S			B-F45-27			2
SPACER			P-F45-28		B-F45-27	8
C/S TYPE CAP			P-F45-29 (-24)		B-F45-28	24
C/S DETAIL 1			P-F45-30 (-24)		B-F45-25	12
C/S DETAIL 2			P-F45-31 (-24)		B-F45-25	12
BRACKET			P-F45-32 (-26)		B-F45-25	12
RING PLATE/2			P-F45-33		B-F45-25	48
RING PLATE/3			P-F45-34		B-F45-25	6
DECLINATION GEAR SEGMENT			C-F45-36			2
DEC. 1ST PINION & 2ND GEAR			D-F45-37			
HOUR ANGLE GEAR SEGMENT			C-F45-38			1
HOUR ANGLE 1ST PINION & 2ND GEAR			D-F45-39			

Kelvin Wellington

COMPILED	JOB No.	No. REQD.	ASSY. DWG. No.	LIST No.
APPROVED				SHEET OF SHEETS
DATE				A

FLEURS 45FT RADIO TELESCOPE

COMPONENT PARTS LIST (2)

DESCRIPTION	MATERIAL	PART No.	DWG. No.	ASSY DWG Num No.	SCHEMATIC DIAG REF	No. REQ PER UNIT
TOWER - TYPE A			B-F45-40			
TOWER - TYPE B			B-F45-41			
ADJUSTABLE BASE PLATE			D-F45-42			
FOUNDATIONS			C-F45-43			
SHAFT			B-F45-44			1
DECLINATION GEAR STUB SHAFT			D-F45-45			2
STUB SHAFT RETAINING CAP			P-F45-46			2
HOUR ANGLE GEAR SHAFT			D-F45-47			1
H.A. PINION 2ND BEARING SUPPORT			P-F45-48			1
MAIN G/B ASSEMBLY			B-F45-49			
H.A. MOUNTING BRACKET			D-F45-51			
DISH CONTROL CIRCUIT			B-F45-52			
SURVEY OF ARRAY			B-F45-53			
MAST BRACKET			D-F45-54			
MAST SUPPORT			D-F45-55			
MAST BOLT			P-F45-57			
MAST FOOTING			D-F45-58			
FEED POLE HOOD			P-F45-59			
BRACKET FOR LOWERING GX DRIVE		—	D-F45-60			
DEMAG MOTOR BRAKE RELEASE			D-F45-61			
MAGNETIC CLUTCH MOUNTING			D-F45-62			
DEC. DRIVE MOTOR MOUNT			D-F45-63			
CONTROL BOX LAYOUT			C-F45-64			
DISH CONTROL PANEL			D-F45-65			
POWER CONTROL PANEL			D-F45-66			

Kelvin Wellington

COMPILED	JOB No.	No. REQD.	ASSY. DWG. No.	LIST No.
APPROVED				SHEET OF SHEETS
DATE				A

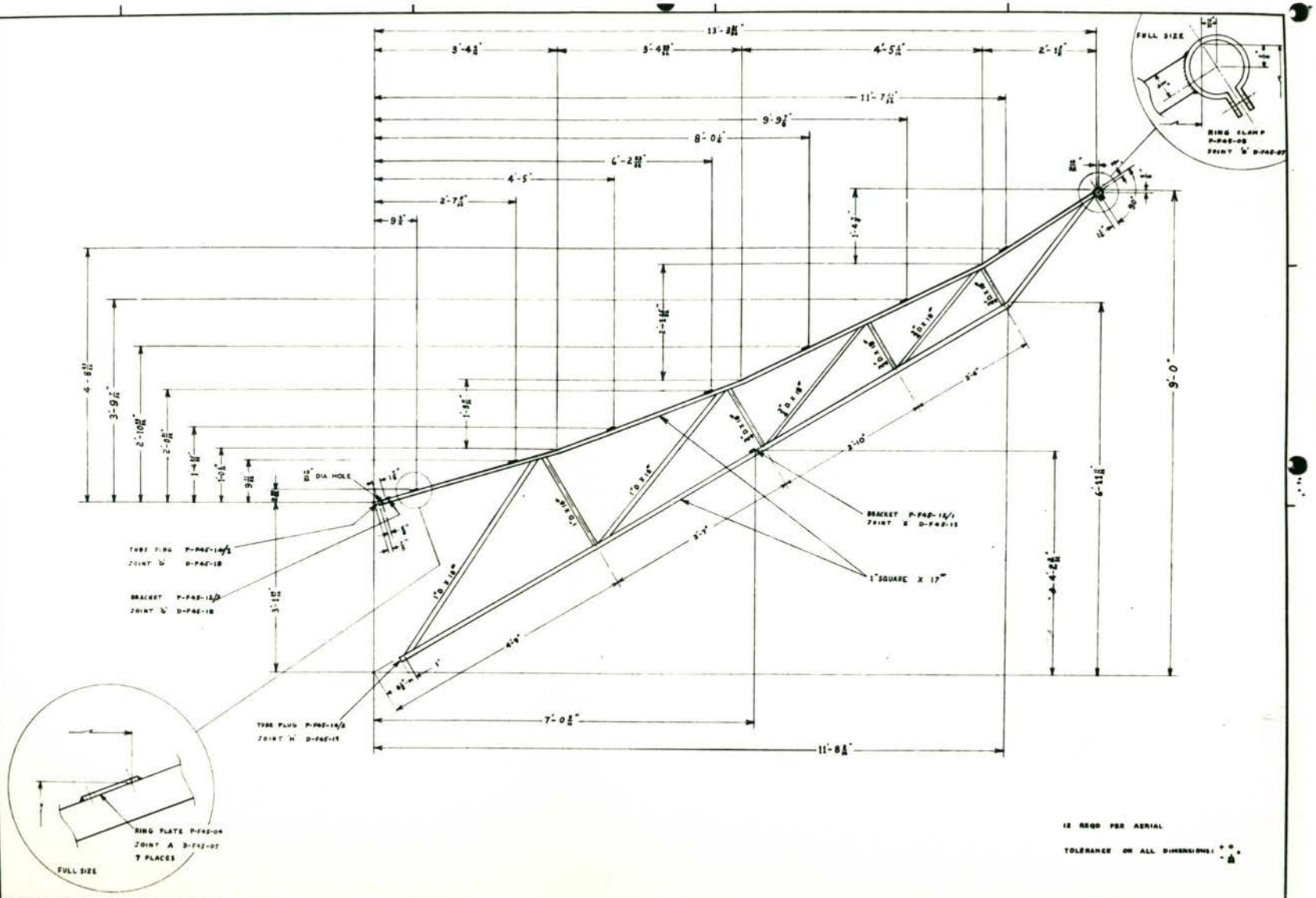

MATERIAL: ELECTRICALLY WELDED M.S. TUBE

FINISH: SEE SPECIFICATION

MAIN RIB - 45 FT DIA. AERIAL

SCALE 1½ = 1 foot

UNIT	DRAWN	DATE
ASSY.	TRACED	8-2-54
C.P.L.	CHECKED	
	PASSED	
	APPROVED	

B-F45-01

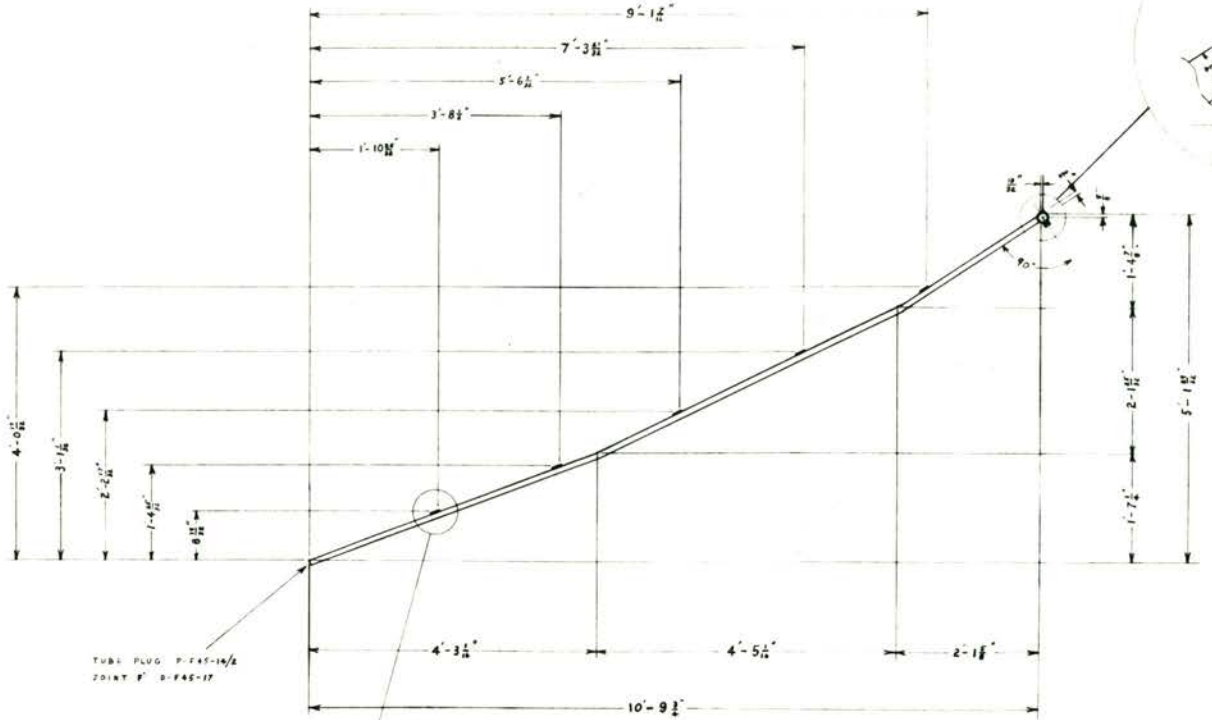

12 REQD PER AERIAL

TOLERANCE ON ALL DIMENSIONS ± 1/2

MATERIAL 1" SQUARE x 12"
ELECTRICALLY WELDED MITRE
FINISH SEE SPECIFICATION

SMALL RIB - 45 FT DIA. AERIAL

SCALE 12" = 1 unit

UNIT
ASSY
C.P.L.

DRAWN
TRACED
CHECKED
PASSED
APPROVED

B-F45-02

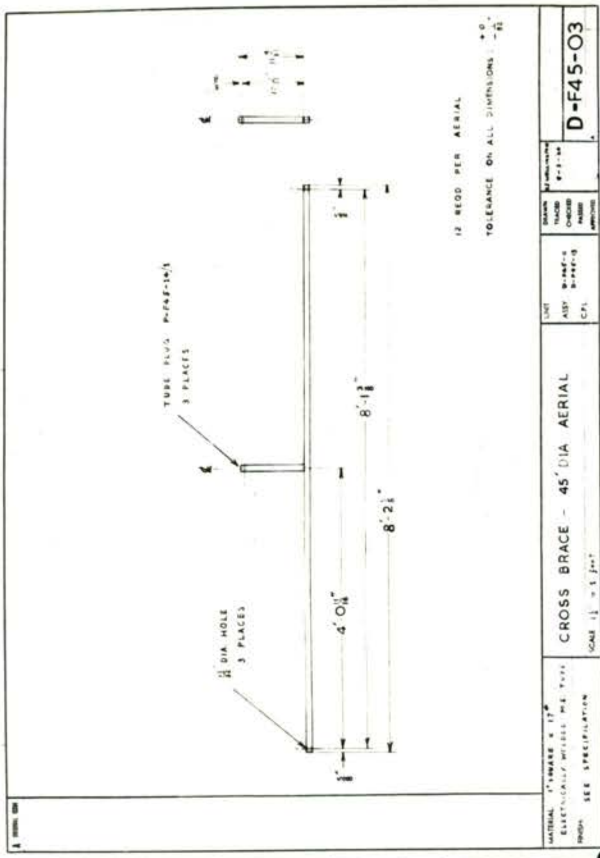
TUBE PLUG P-F42-16/1
3 PLACES
11/32 DIA HOLE
3 PLACES
4'-0 11/16"
8'-1 3/8"
8'-2 1/4"
12 REQD PER AERIAL
TOLERANCE ON ALL DIMENSIONS
CROSS BRACE - 45' DIA AERIAL
SEE SPECIFICATION
D-F45-03

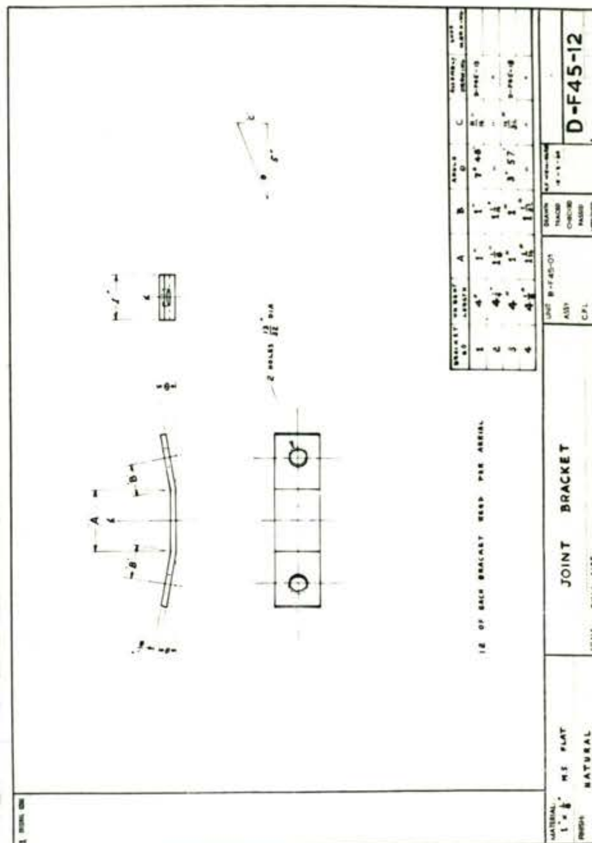
2 HOLES 13/32 DIA
JOINT BRACKET
M.S. FLAT
NATURAL
FULL SIZE
D-F45-12

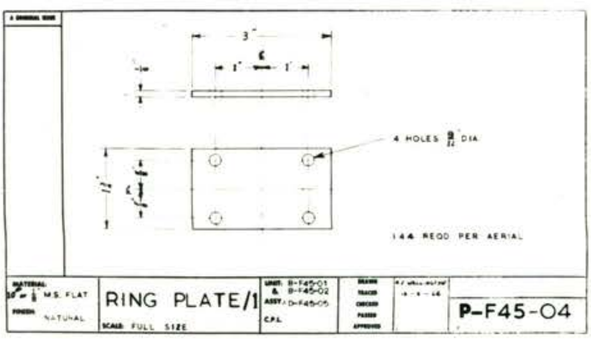
3"
1"
1"
4 HOLES 13/32 DIA
1 1/2"
144 REQD PER AERIAL
M.S. FLAT
NATURAL
RING PLATE/1
SCALE FULL SIZE
UNIT B-F45-01 & B-F45-02
ASSY D-F45-05
C.P.L.
P-F45-04

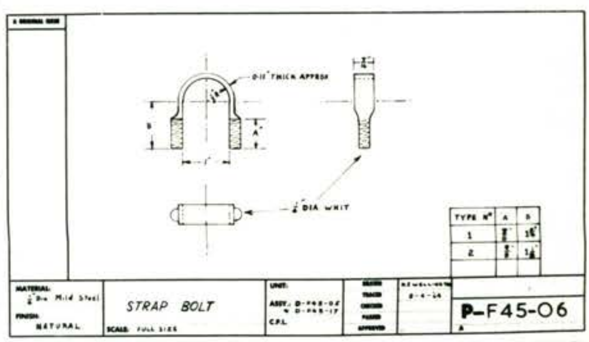
0·11" THICK APPROX
1/4" DIA WHIT
TYPE Nº
A
B
1
2
1/4" Dia Mild Steel
NATURAL
STRAP BOLT
SCALE FULL SIZE
C.P.L.
P-F45-06

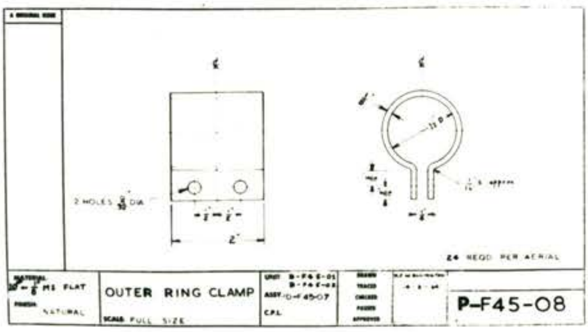
2 HOLES 9/32 DIA
2"
24 REQD PER AERIAL
M.S. FLAT
NATURAL
OUTER RING CLAMP
SCALE FULL SIZE
ASSY D-F45-07
C.P.L.
P-F45-08

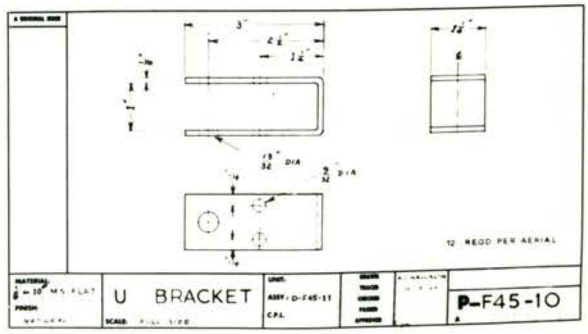
3"
2 1/4"
1 1/2"
1"
13/32 DIA
9/32 DIA
12 REQD PER AERIAL
M.S. FLAT
NATURAL
U BRACKET
ASSY D-F45-11
C.P.L.
P-F45-10

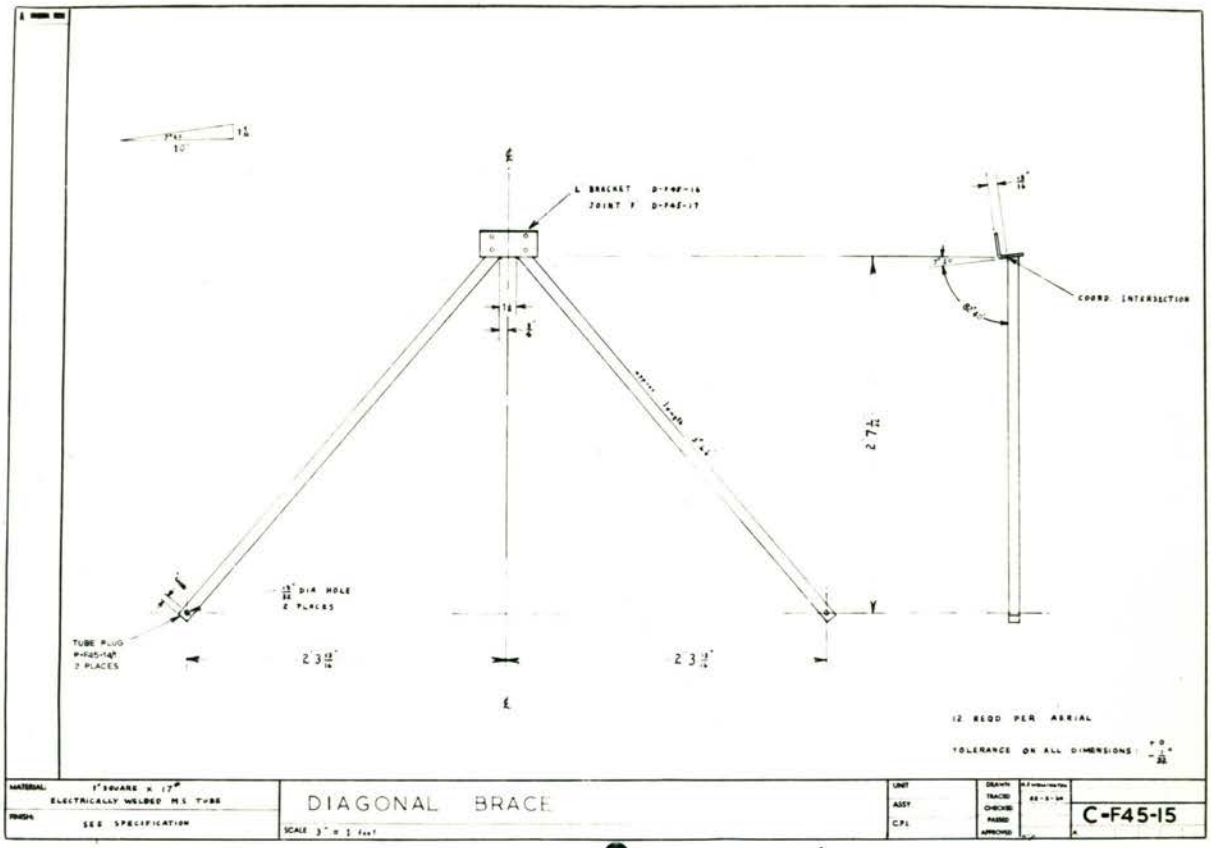

MATERIAL: 1" SQUARE x 17" ELECTRICALLY WELDED M.S. TUBE
FINISH: SEE SPECIFICATION

DIAGONAL BRACE

SCALE 3" = 1 foot

UNIT
ASSY
C.F.L.

DRAWN
TRACED
CHECKED
PASSED
APPROVED

C-F45-15

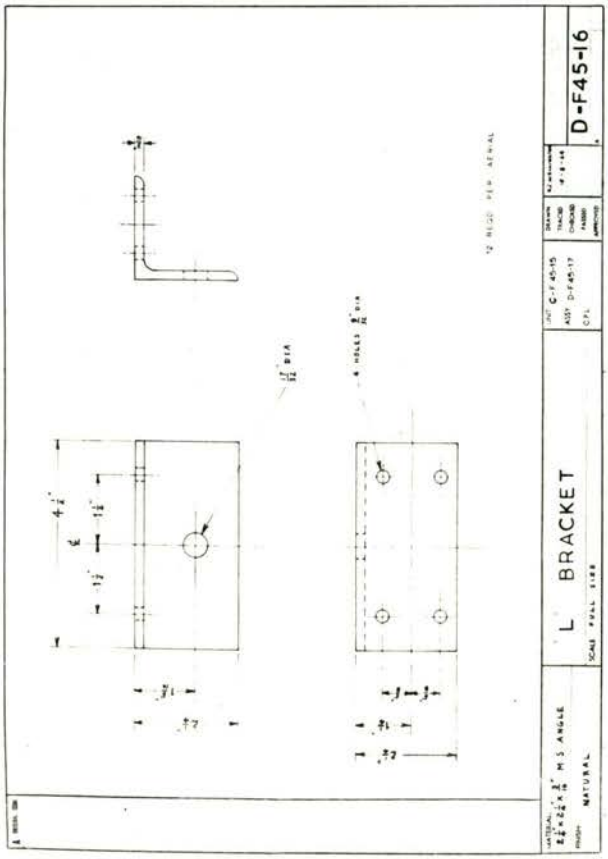

L BRACKET

SCALE FULL SIZE

MATERIAL: 4½" x 2½" x ⅜" M.S. ANGLE
FINISH: NATURAL

D-F45-16

ASSY C-F45-15
C.F.L. D-F45-17

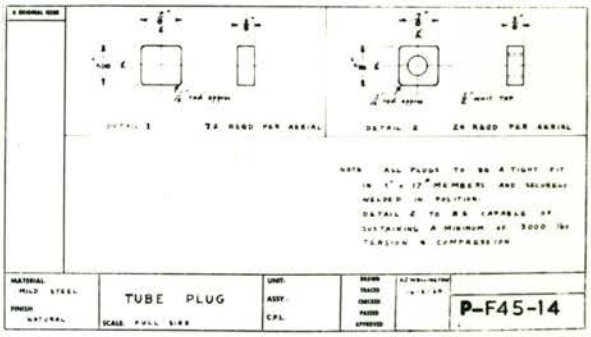

MATERIAL: MILD STEEL
FINISH: NATURAL

TUBE PLUG

SCALE FULL SIZE

UNIT
ASSY
C.F.L.

DRAWN
TRACED
CHECKED
PASSED
APPROVED

P-F45-14

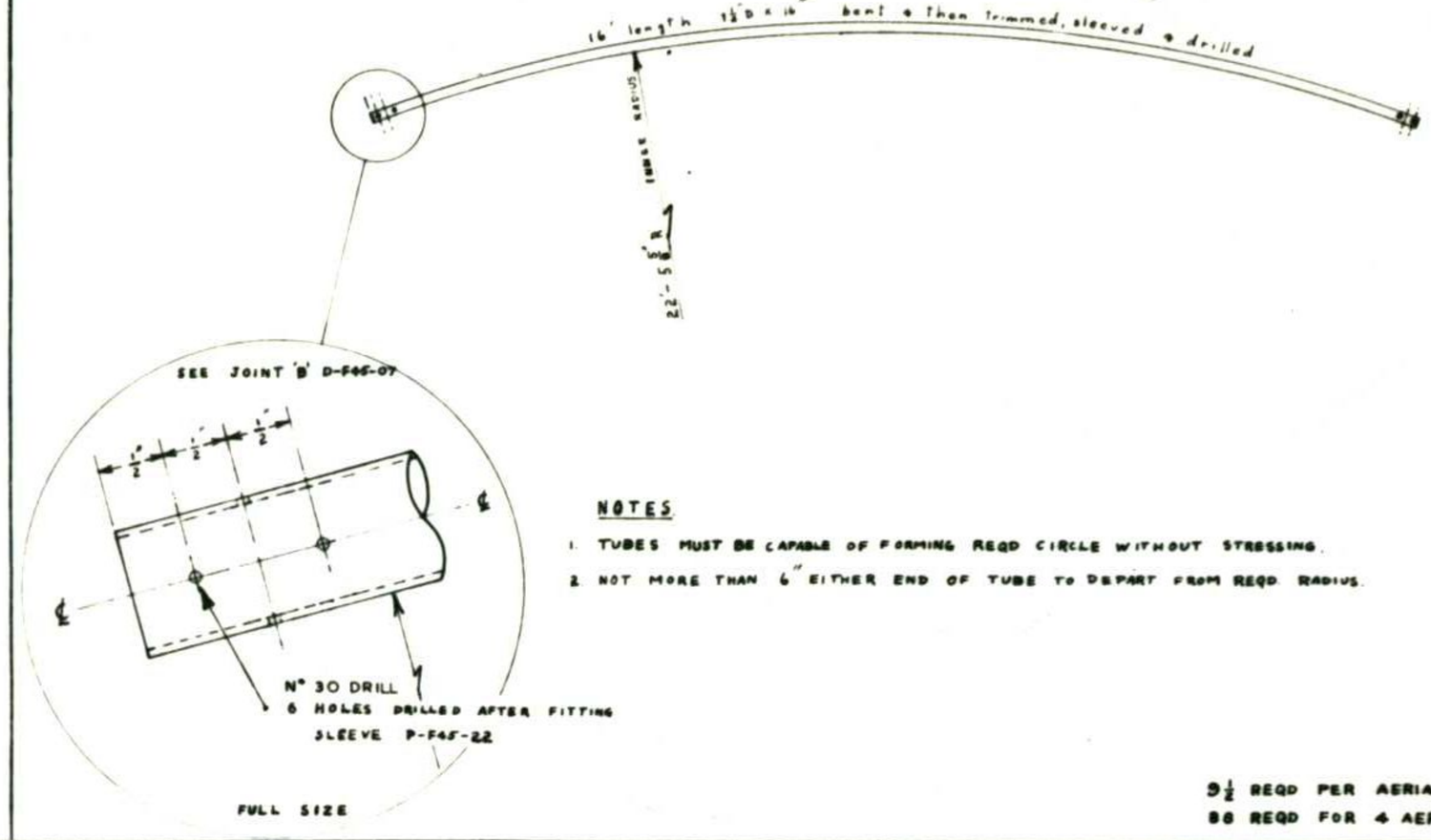

NOTES

1. TUBES MUST BE CAPABLE OF FORMING REQD CIRCLE WITHOUT STRESSING.
2. NOT MORE THAN 6" EITHER END OF TUBE TO DEPART FROM REQD RADIUS.

9½ REQD PER AERIAL
88 REQD FOR 4 AERIALS

MATERIAL: 1½ D x 16" Al ALLOY TUBE	OUTER RING	UNIT	DRAWN	
FINISH: NATURAL	SCALE ¾" = 1 foot	ASSY. D-F45-07	TRACED	2-4-60
		C.P.L.	CHECKED	D-F45-20
			PASSED	
			APPROVED	

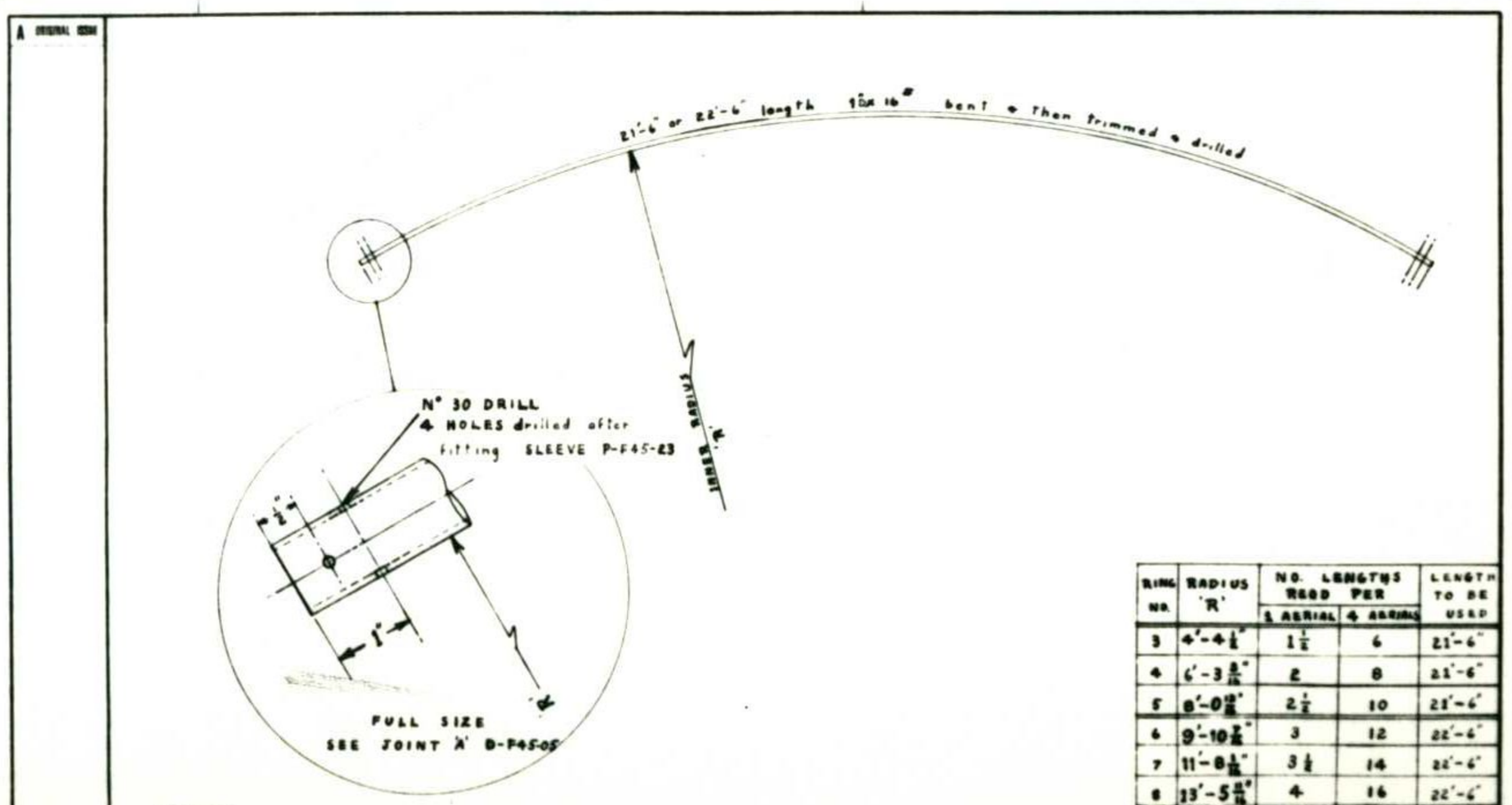

NOTES.

1. TUBES MUST BE CAPABLE OF FORMING REQD CIRCLE WITHOUT STRESSING
2. NOT MORE THAN 6" EITHER END OF TUBE TO DEPART FROM REQD RADIUS

RING NO.	RADIUS 'R'	NO. LENGTHS REQD PER 1 AERIAL	NO. LENGTHS REQD PER 4 AERIALS	LENGTH TO BE USED
3	4'-4½"	1½	6	21'-6"
4	6'-3⅝"	2	8	21'-6"
5	8'-0⅞"	2½	10	21'-6"
6	9'-10⅛"	3	12	22'-6"
7	11'-8⅛"	3½	14	22'-6"
8	13'-5⅜"	4	16	22'-6"
9	15'-3⅜"	4½	18	22'-6"
10	17'-0⅝"	5	20	22'-6"
11	18'-10⅝"	6	24	22'-6"
12	20'-8¾"	6½	26	21'-6"

MATERIAL: 1½"D x 16" Al Alloy Tube 2006/T6	RINGS	UNIT	DRAWN	
FINISH: NATURAL	SCALE ¾" = 1 foot	ASSY. D-F45-05	TRACED	23-3-60
		C.P.L.	CHECKED	D-F45-21
			PASSED	
			APPROVED	

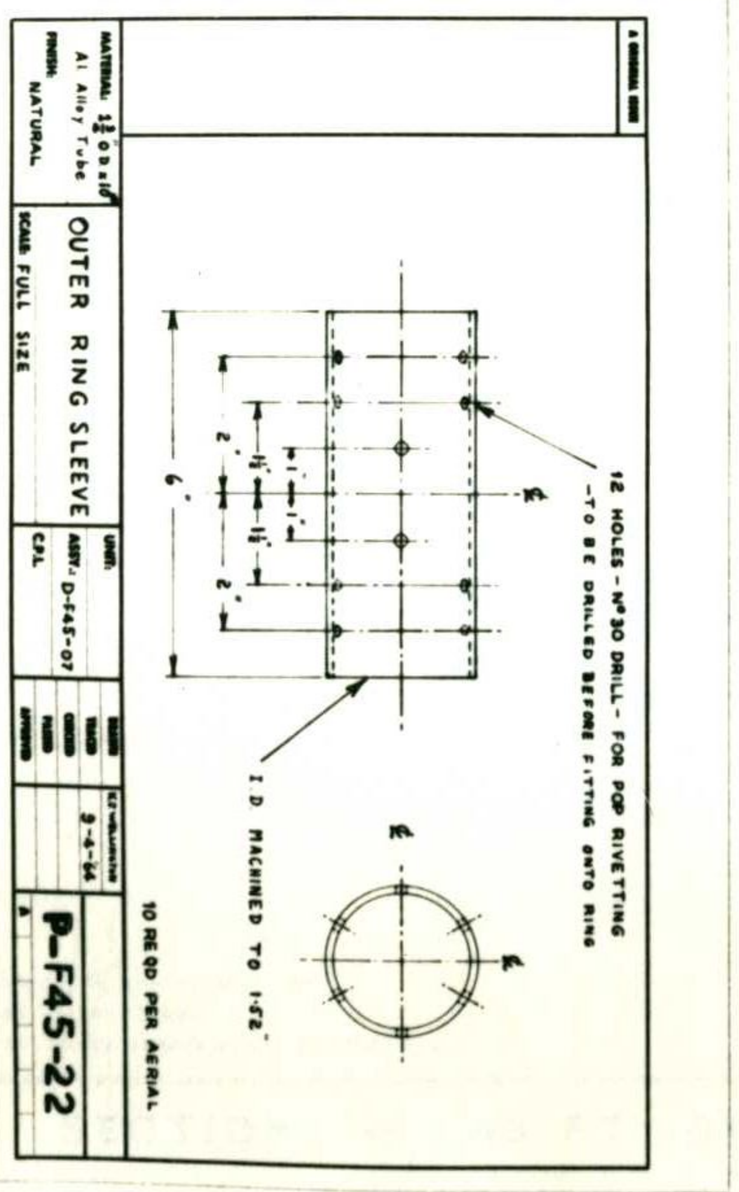

MATERIAL: 1½ OD x 1.0" Al Alloy Tube	OUTER RING SLEEVE	UNIT	DRAWN	
FINISH: NATURAL	SCALE FULL SIZE	ASSY. D-F45-07	TRACED	9-6-60
		C.P.L.	CHECKED	P-F45-22
			PASSED	
			APPROVED	

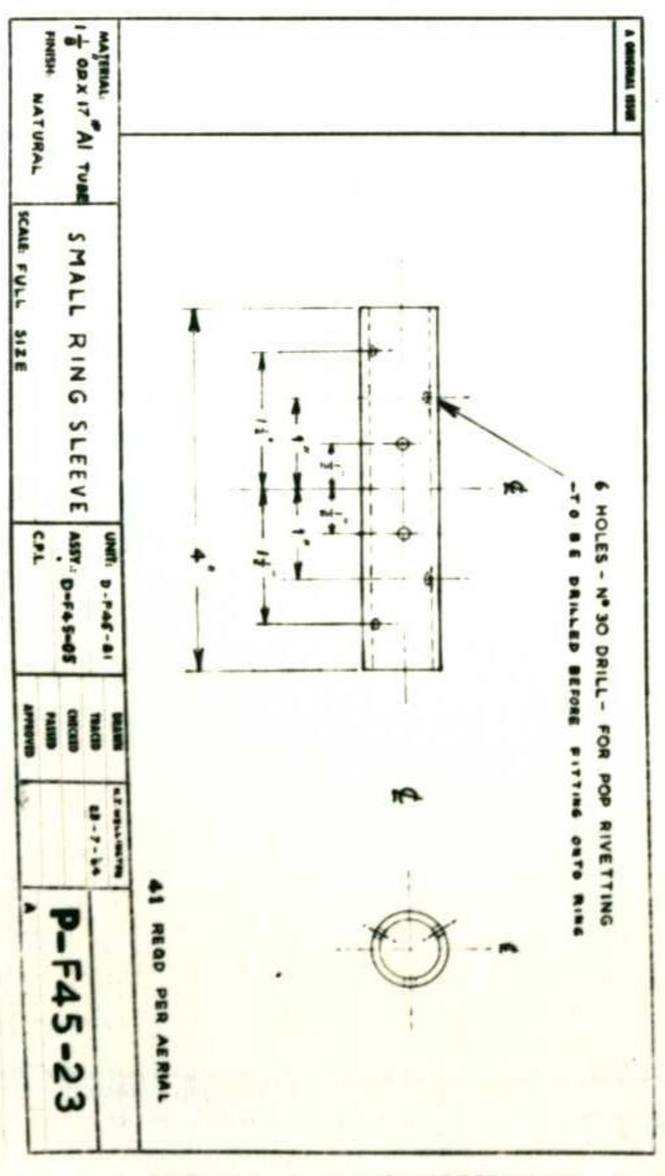

MATERIAL: 1½ OD x 1.0" Al TUBE	SMALL RING SLEEVE	UNIT: D-F45-01	DRAWN	
FINISH: NATURAL	SCALE FULL SIZE	ASSY. D-F45-05	TRACED	23-3-60
		C.P.L.	CHECKED	P-F45-23
			PASSED	
			APPROVED	

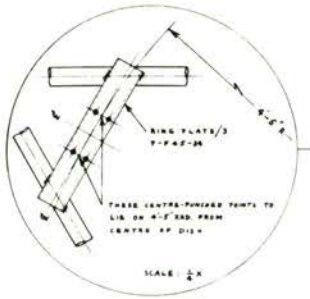

NB RING PLATES HAVE BEEN OMITTED FROM BOTH SECTION XX & SECTION YY FOR SAKE OF CLARITY

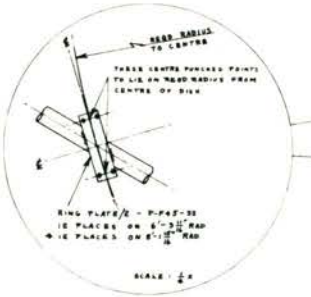

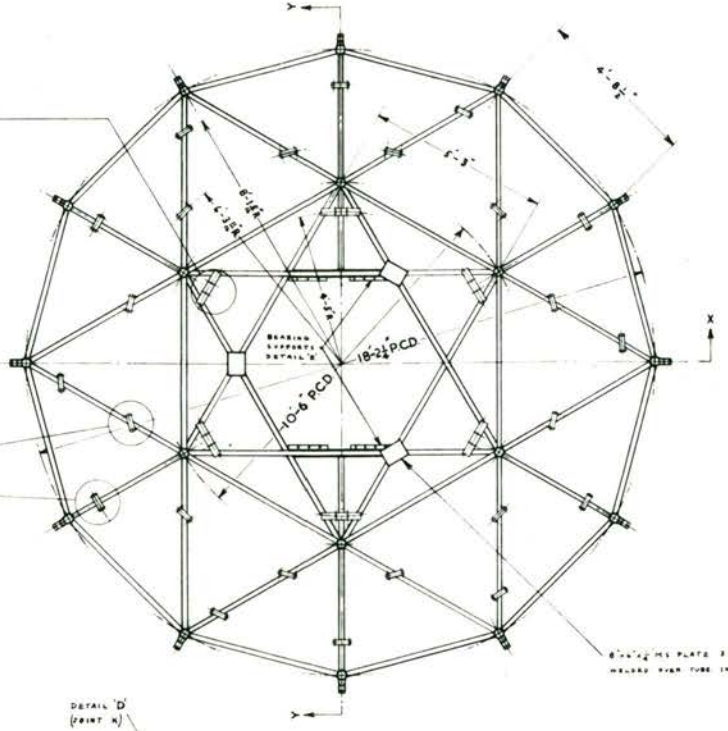

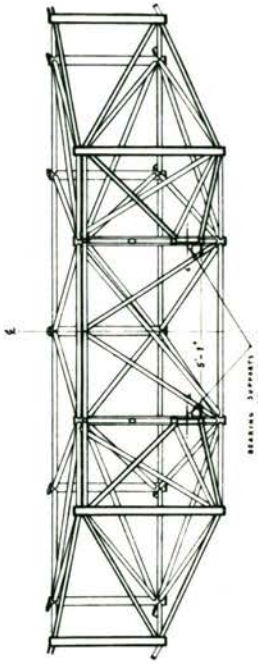

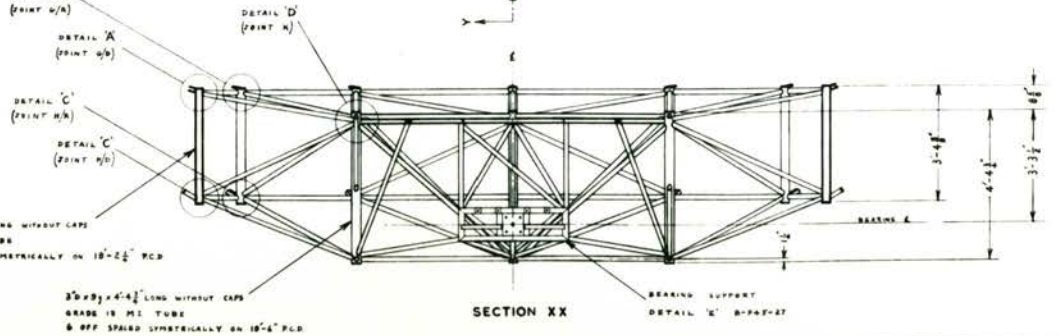

SECTION XX

MATERIAL: ALL MEMBERS TUBE X 18 GRADE 13 M.S. TUBE H.F.W. UNLESS OTHERWISE INDICATED
FINISH: SEE SPECIFICATION NO 4

CENTRE SECTION — 45 FT DIA AERIAL

SCALE 3/4" = 1 Foot

UNIT
ASSY.
C.F.L.

DRAWN
TRACED
CHECKED
PASSED
APPROVED

B-F45-25

DETAIL 'A'
(JOINT A/B)
c/s DETAIL 1
P-F45-30
c/s DETAIL 2
P-F45-31
DETAIL 'B'
(JOINT C/K)
c/s DETAIL 1
P-F45-80
INTERSECTION OF CENTRE LINES
c/s DETAIL 2
P-F45-31
DETAIL 'C'
(JOINT H/D)
NB JOINT H/K DIFFERS FROM THIS JOINT (H/D) ONLY IN THAT THESE 4 DIAGONAL MEMBERS ARE REPLACED BY 2 RADIAL MEMBERS. (DOTTED)
BRACKET T-F45-82
c/s TITE CAP T-F45-89
DETAIL 'D'
(JOINT K)
BEARING SUPPORT
RADIAL MEMBERS
c/s PIPE CAP P-F45-89
RADIAL MEMBER
TANGENTIAL SUPPORT
UNIT B-F45-25
ASSY.
C.P.L.
DRAWN
TRACED
CHECKED
PASSED
APPROVED
DATE 20-2-56
C-F45-26
CENTRE SECTION JOINT DETAILS
SCALE : HALF SIZE
MATERIAL
FINISH

NOTES :- 1. TWO BEARING SUPPORTS PER AERIAL.
2. WELDED CONSTRUCTION THROUGHOUT - $\frac{1}{4}$" FILLETS

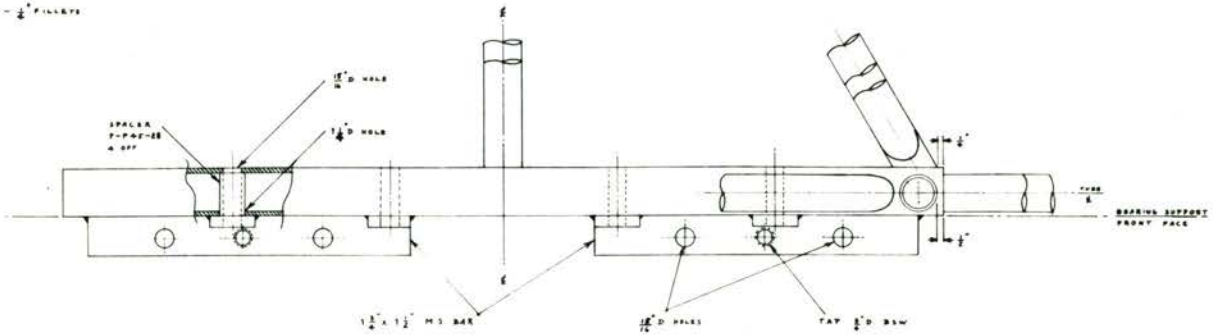

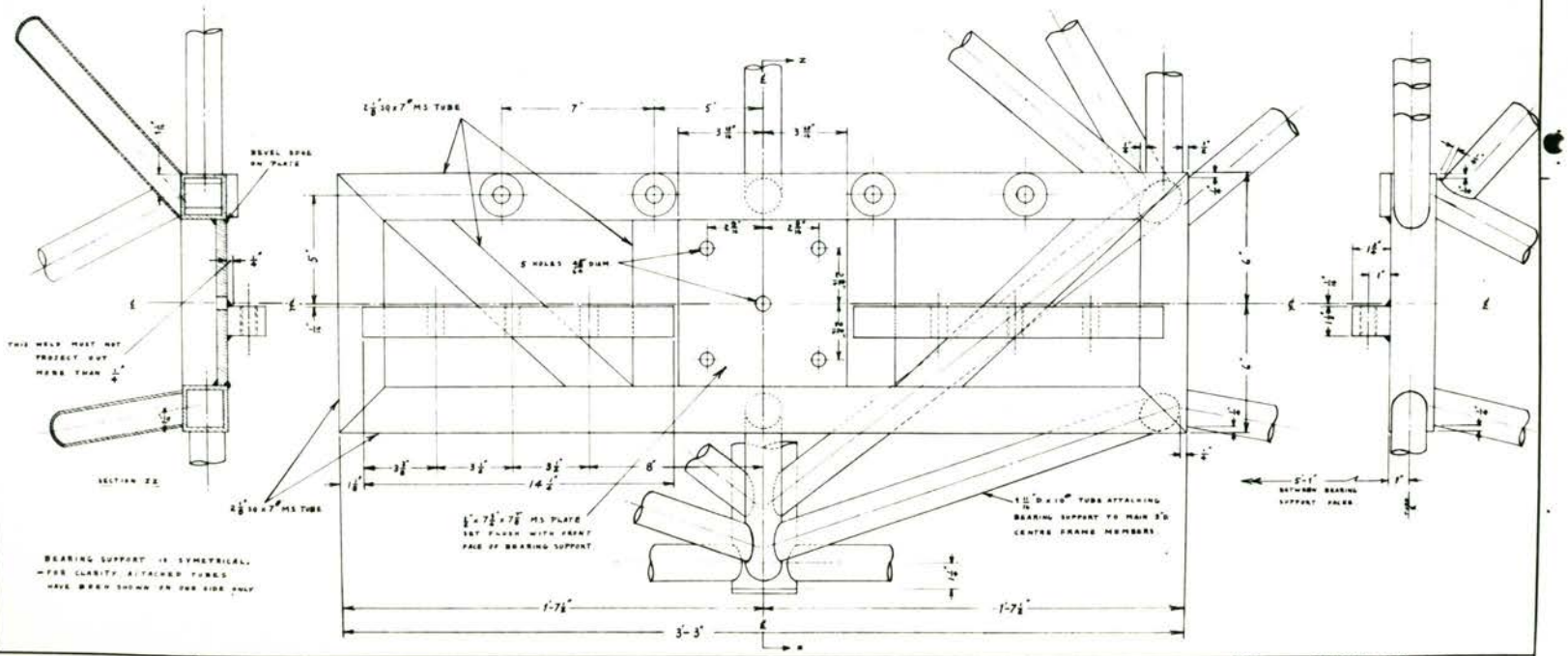

MATERIAL	GRADE 43 MS TUBE HFW	BEARING SUPPORT-DETAIL 'E'-CENTRE SECTION	B-F45-27
FINISH		SCALE HALF SIZE	

A ORIGINAL ISSUE

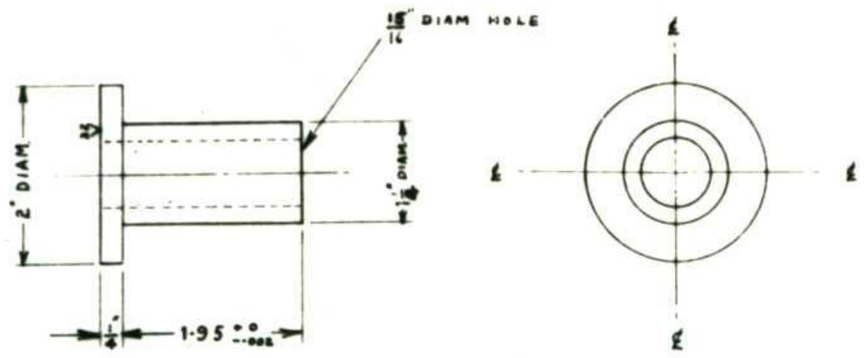

8 REQD PER AERIAL

MATERIAL: MILD STEEL FINISH: NATURAL	SPACER SCALE: FULL SIZE	UNIT: B-F45-27 ASSY.: C.P.L.	DRAWN TRACED CHECKED PASSED APPROVED	N.Z. WELLINGTON 13-5-44	P-F45-28

A ORIGINAL ISSUE

24 REQD PER AERIAL

MATERIAL: 3/16" M.S. FLAT FINISH: NATURAL	C/S PIPE CAP SCALE: FULL SIZE	UNIT: B-F45-25 ASSY.: C-F45-26 C.P.L.	DRAWN TRACED CHECKED PASSED APPROVED	N.Z. WELLINGTON 22-6-44	P-F45-29

A ORIGINAL ISSUE

B 24/6
Holes 7/16" D in lieu of 13/32" D

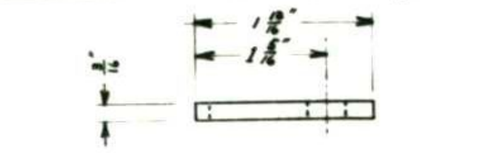

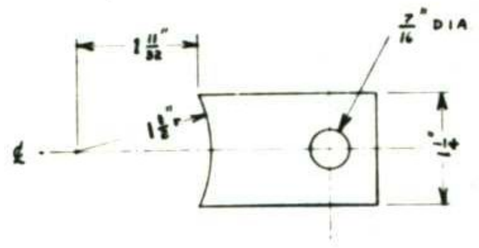

12 REQD PER AERIAL

MATERIAL: 3/16" M.S. FLAT FINISH: NATURAL	C/S DETAIL 1 SCALE: FULL SIZE	UNIT: B-F45-25 ASSY.: C-F45-26 C.P.L.	DRAWN TRACED CHECKED PASSED APPROVED	N.Z. WELLINGTON 22-6-44	P-F45-30 B

A ORIGINAL ISSUE

B 24/6
Holes 7/16" D in lieu of 13/32" D

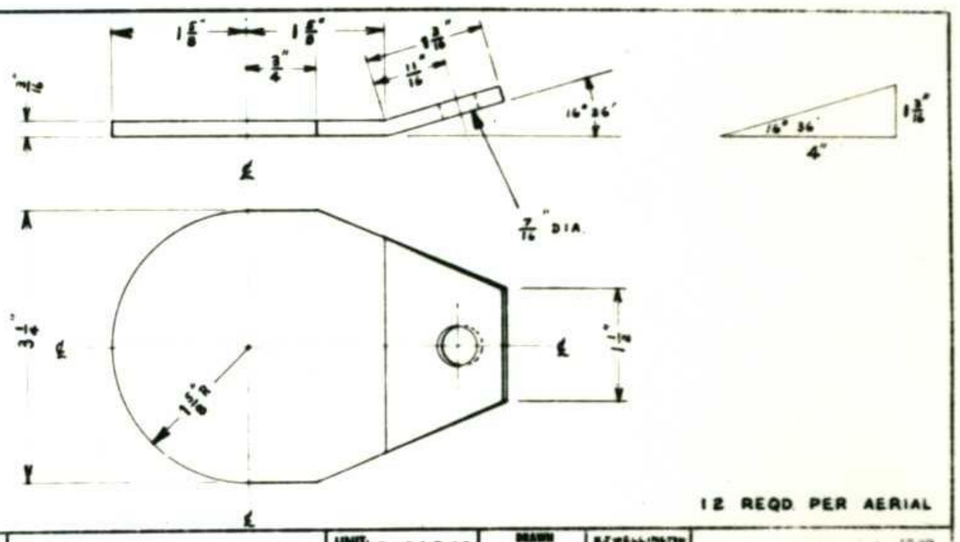

12 REQD PER AERIAL

MATERIAL: 3/16" M.S FLAT FINISH: NATURAL	C/S DETAIL 2 SCALE: FULL SIZE	UNIT: B-F45-25 ASSY.: C-F45-26 C.P.L.	DRAWN TRACED CHECKED PASSED APPROVED	N.Z. WELLINGTON 22-6-44	P-F45-31 B

A ORIGINAL ISSUE

B 24/6
Holes 7/16" D in lieu of 9/32" D

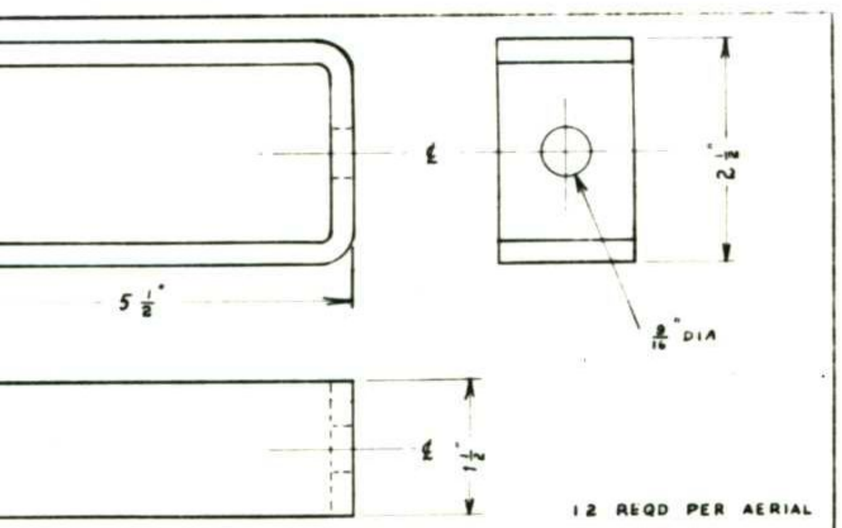

12 REQD PER AERIAL

MATERIAL: 1 1/2" x 1/4" MILD STEEL FINISH: NATURAL	BRACKET SCALE: FULL SIZE	UNIT: B-F45-25 ASSY.: C-F45-26 C.P.L.	DRAWN TRACED CHECKED PASSED APPROVED	N.Z. WELLINGTON 22-6-44	P-F45-32 B

A ORIGINAL ISSUE

B 24/6
Holes 7/16" D in lieu of 9/32" D

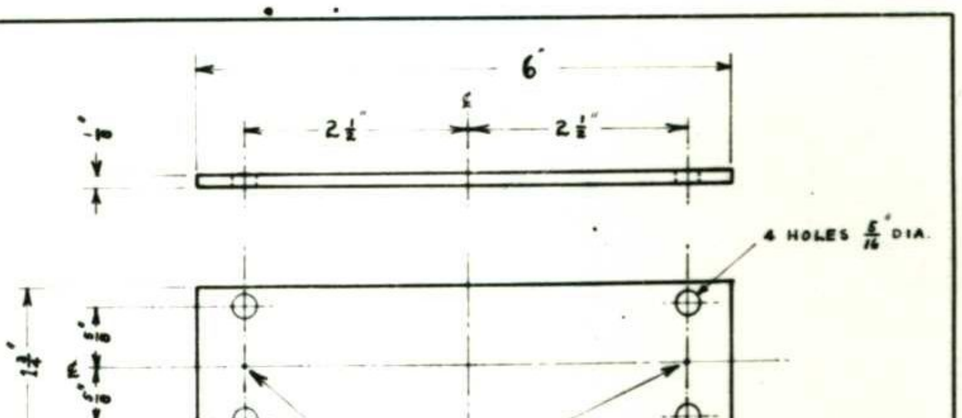

48 REQD PER AERIAL
24 WELDED INTO POSITION
& 24 USED IN ASSEMBLY

MATERIAL: 10 or 1/8" M.S. FLAT FINISH: NATURAL	RING PLATE/2 SCALE: FULL SIZE	UNIT: B-F45-25 ASSY.: C.P.L.	DRAWN TRACED CHECKED PASSED APPROVED	N.Z. WELLINGTON 1-8-44	P-F45-33 B

A ORIGINAL ISSUE

B 24/6
Holes 7/16" D in lieu of 3/32" D

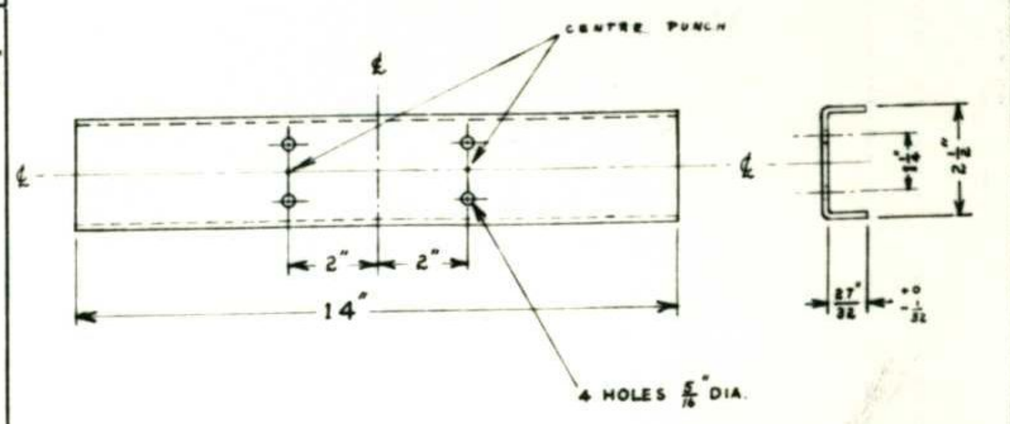

6 REQD PER AERIAL

MATERIAL: 10 or 1/8" M.S. FLAT FINISH: NATURAL	RING PLATE/3 SCALE: HALF SIZE	UNIT: B-F45-25 ASSY.: C.P.L.	DRAWN TRACED CHECKED PASSED APPROVED	N.Z. WELLINGTON 1-8-44	P-F45-34 B

NO OF TEETH IN FULL CIRCLE	150
NO OF TEETH CUT	74 (min)
DIAMETRAL PITCH	4
PITCH CIRCLE DIAMETER	37·500"
OUTSIDE DIAMETER	38·000"
TOOTH FORM	20° INVOLUTE
MATING PINION	D-F45-37

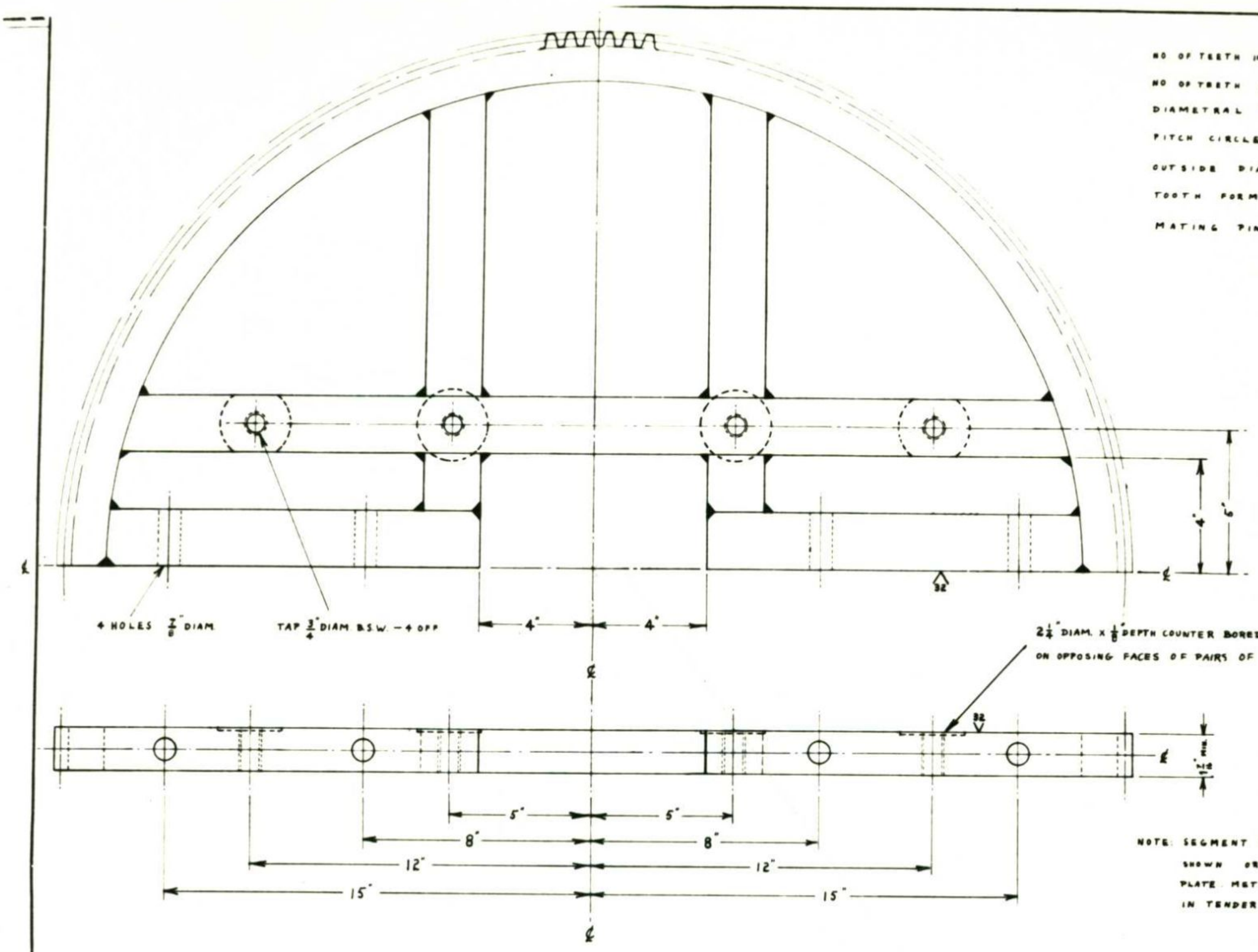

NOTE: SEGMENT MAY BE FABRICATED AS SHOWN OR FLAME CUT FROM SOLID PLATE. METHOD SHOULD BE STATED IN TENDER.

2 REQD PER AERIAL

MATERIAL: SEE SPECIFICATION	DECLINATION GEAR SEGMENT	UNIT	DRAWN		C-F45-36
FINISH: SEE SPECIFICATION	SCALE HALF SIZE	ASSY.	TRACED	15-5-59	
		C.P.L.	CHECKED		
			PASSED		
			APPROVED		A

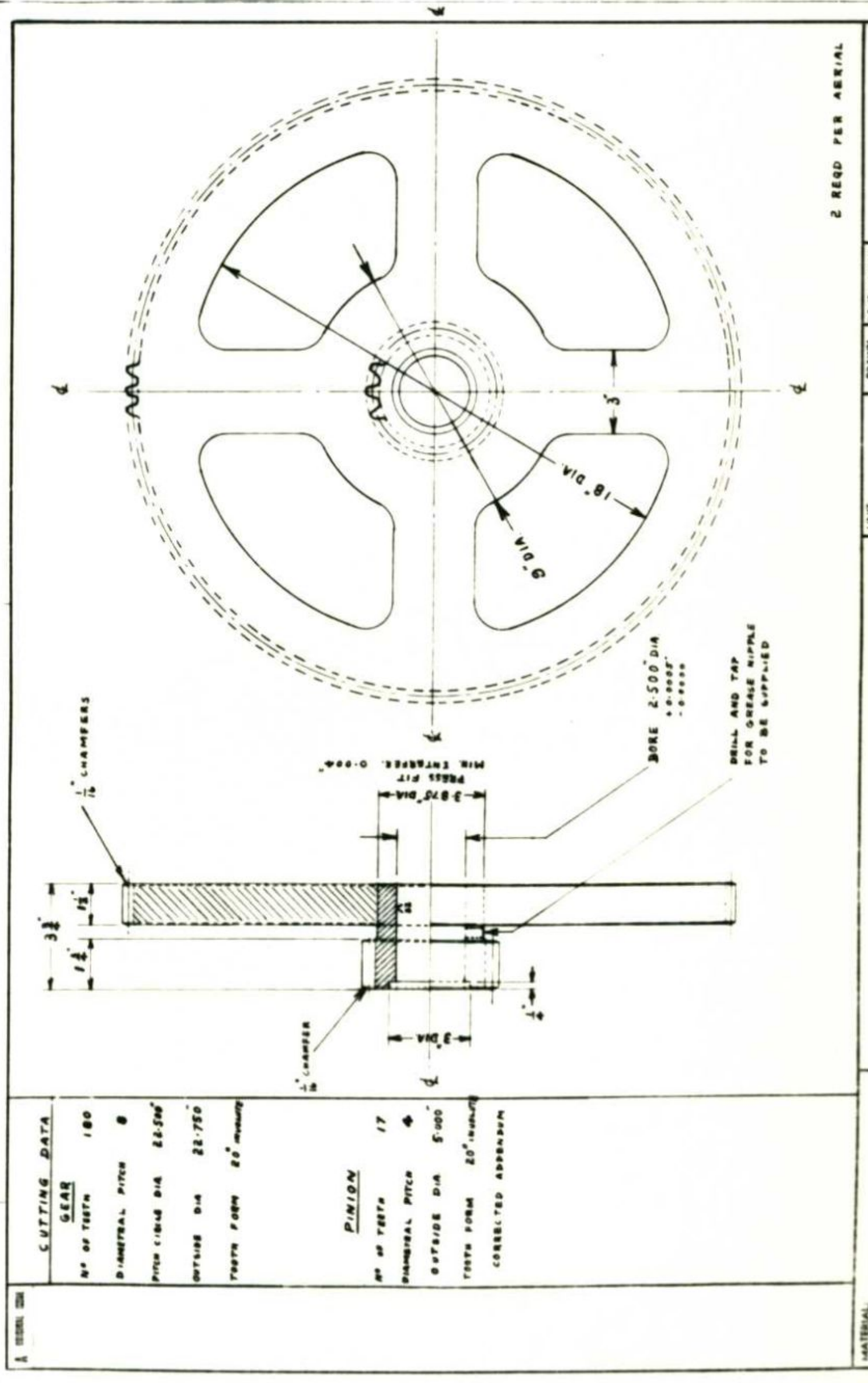

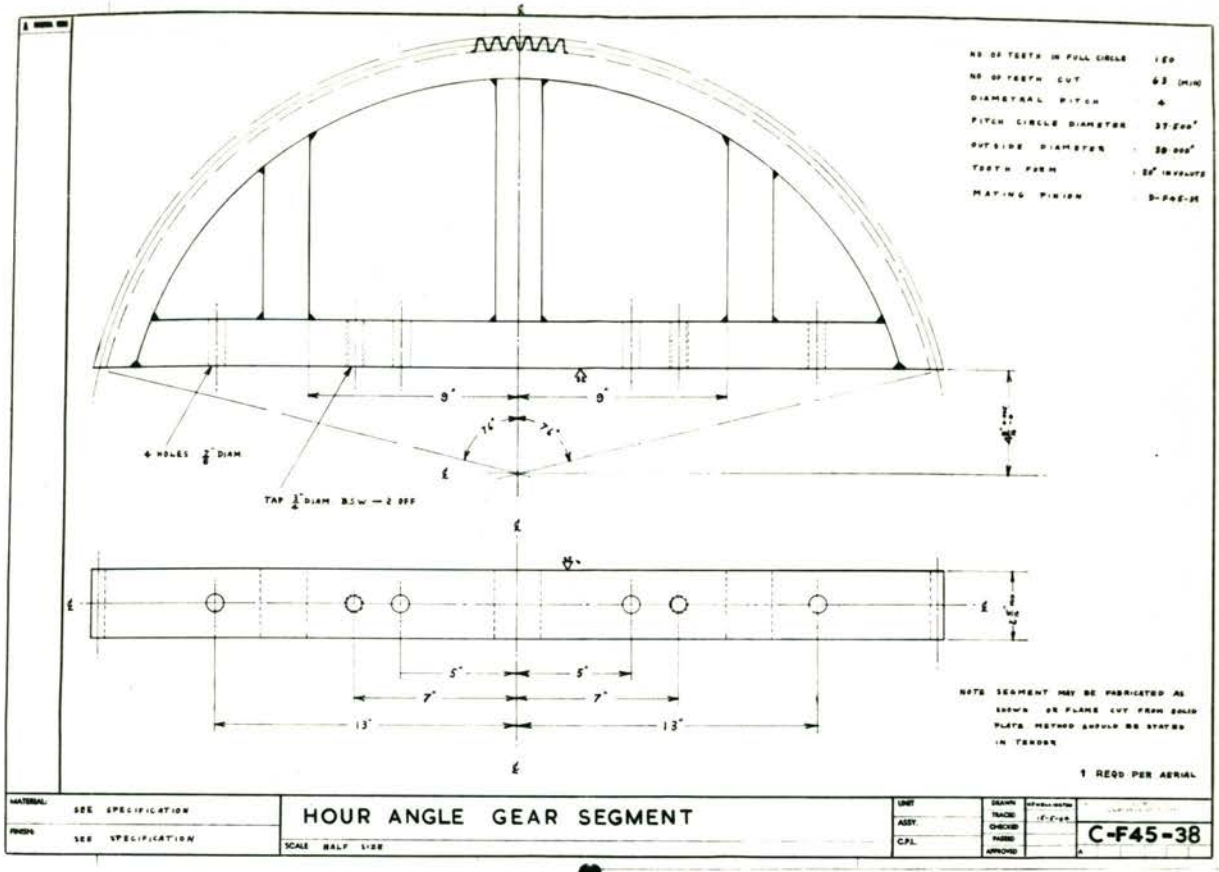
NO OF TEETH IN FULL CIRCLE 160
NO OF TEETH CUT 63 (MIN)
DIAMETRAL PITCH 4
PITCH CIRCLE DIAMETER 37.500"
OUTSIDE DIAMETER 39.000"
TOOTH FORM 20° INVOLUTE
MATING PINION D-F45-39
9"
9"
4 HOLES 7/8" DIAM
TAP 1" DIAM B.S.W — 2 OFF
5"
5"
7"
7"
13"
13"
NOTE SEGMENT MAY BE FABRICATED AS SHOWN OR FLAME CUT FROM SOLID PLATE METHOD SHOULD BE STATED IN TENDER
1 REQD PER AERIAL
MATERIAL SEE SPECIFICATION
FINISH SEE SPECIFICATION
HOUR ANGLE GEAR SEGMENT
SCALE HALF SIZE
UNIT
ASSY.
C.F.L.
DRAWN
TRACED
CHECKED
PASSED
APPROVED
C-F45-38

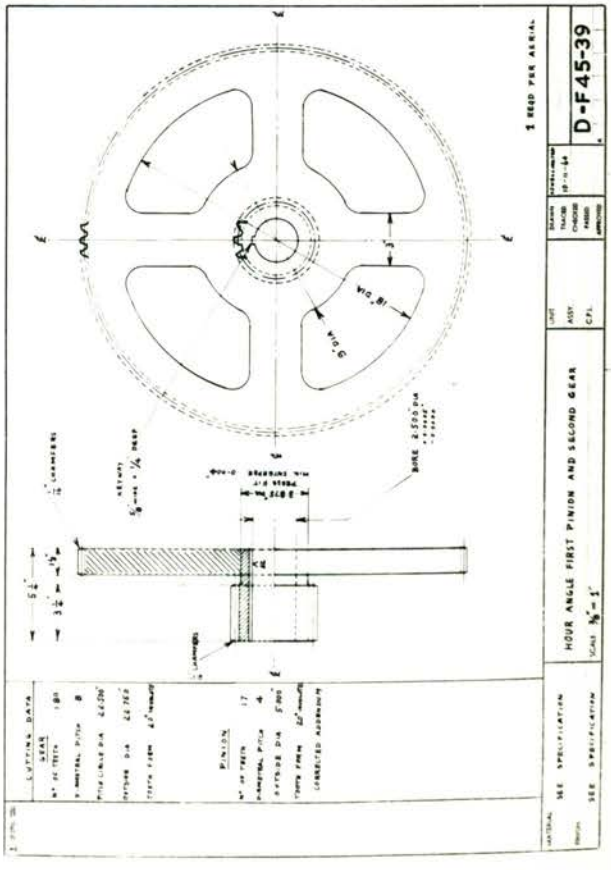
1 REQD PER AERIAL
D-F45-39
HOUR ANGLE FIRST PINION AND SECOND GEAR
SCALE 1/2 - 1"
UNIT
ASSY.
C.F.L.
MATERIAL SEE SPECIFICATION
FINISH SEE SPECIFICATION

DETAIL OF THIS SECTION SHOWN BELOW IN 1½"=1 foot SCALE

THESE MEMBERS ON OTHER SIDE

INTERSECTIONS UNDERSIDE OF BASE PLATES

UNLESS OTHERWISE INDICATED ALL BRACES $1\frac{11}{16}$" O.D. x 8 g

4 BOLTS - $\frac{5}{8}$" D x 4½" WHIT WELD HEADS TO UNDERSIDE OF 2½" x 1½" BAR

GEAR MOUNTING 2⅜" x ½" MS BAR

½" M.S. PLATE

BEARING CENTRE LINE

SECTION X X

SECTION Y Y

SPACER - 2 off 1⅝" OD x 8 g x 2⅜" TACK WELD TO ONE SIDE

5 HOLES $\frac{29}{32}$" DIA + PLACED SYMETRICALLY AROUND CENTRE HOLE

SPACER - 6" x 2⅜" x ½" M.S. PLATE . TACK WELD TO ONE SIDE

SPACER - 2 off 3.08 x 8 g x 2⅜" TACK WELD TO ONE SIDE

4 HOLES $\frac{13}{16}$" D

BASE PLATE - 4 OFF 8"x8"x½" M.S. PLATE

ACCURACY ±⅛" UNLESS OTHERWISE INDICATED

MATERIAL:	GRADE 13 M.S. TUBE	UNIT	
FINISH:	ASS SPECIFICATION	ASSY.	
		C.P.L.	

SUPPORT TOWER - TYPE A — 45 FT DIA. AERIAL

SCALE ⅜" = 1 foot & 1½" = 1 foot

DRAWN		B-F45-40
TRACED	22-2-56	
CHECKED		
PASSED		
APPROVED		

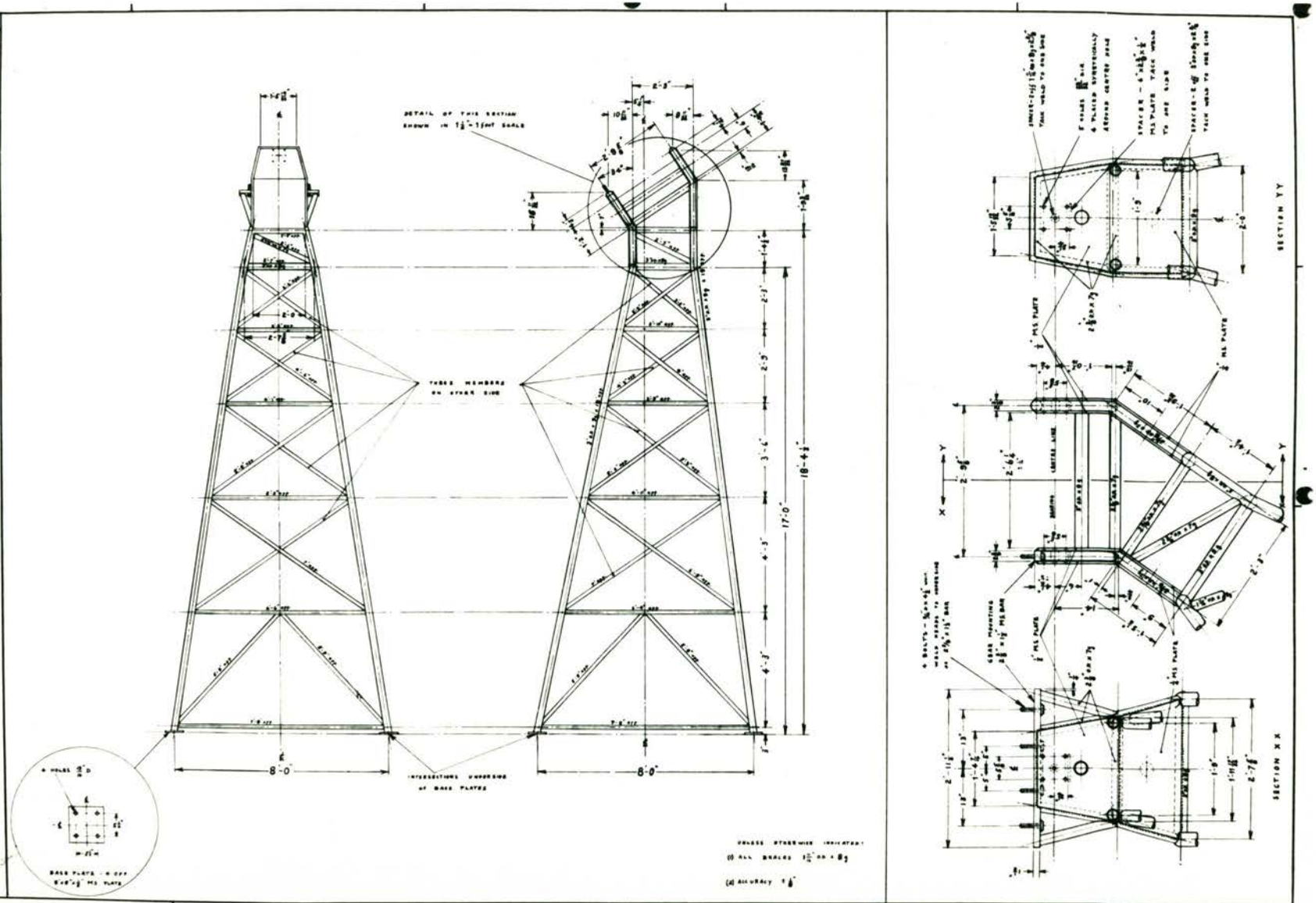

MATERIAL: GRADE 15 M.S. TUBE

FINISH: SEE SPECIFICATION

SUPPORT TOWER - TYPE B — 45 FT DIA. AERIAL

SCALE ½" = 1 foot ⊕ 1½" = 1 foot

UNIT

ASSY.

C.P.L.

DRAWN

TRACED

CHECKED

PASSED

APPROVED

B-F45-41

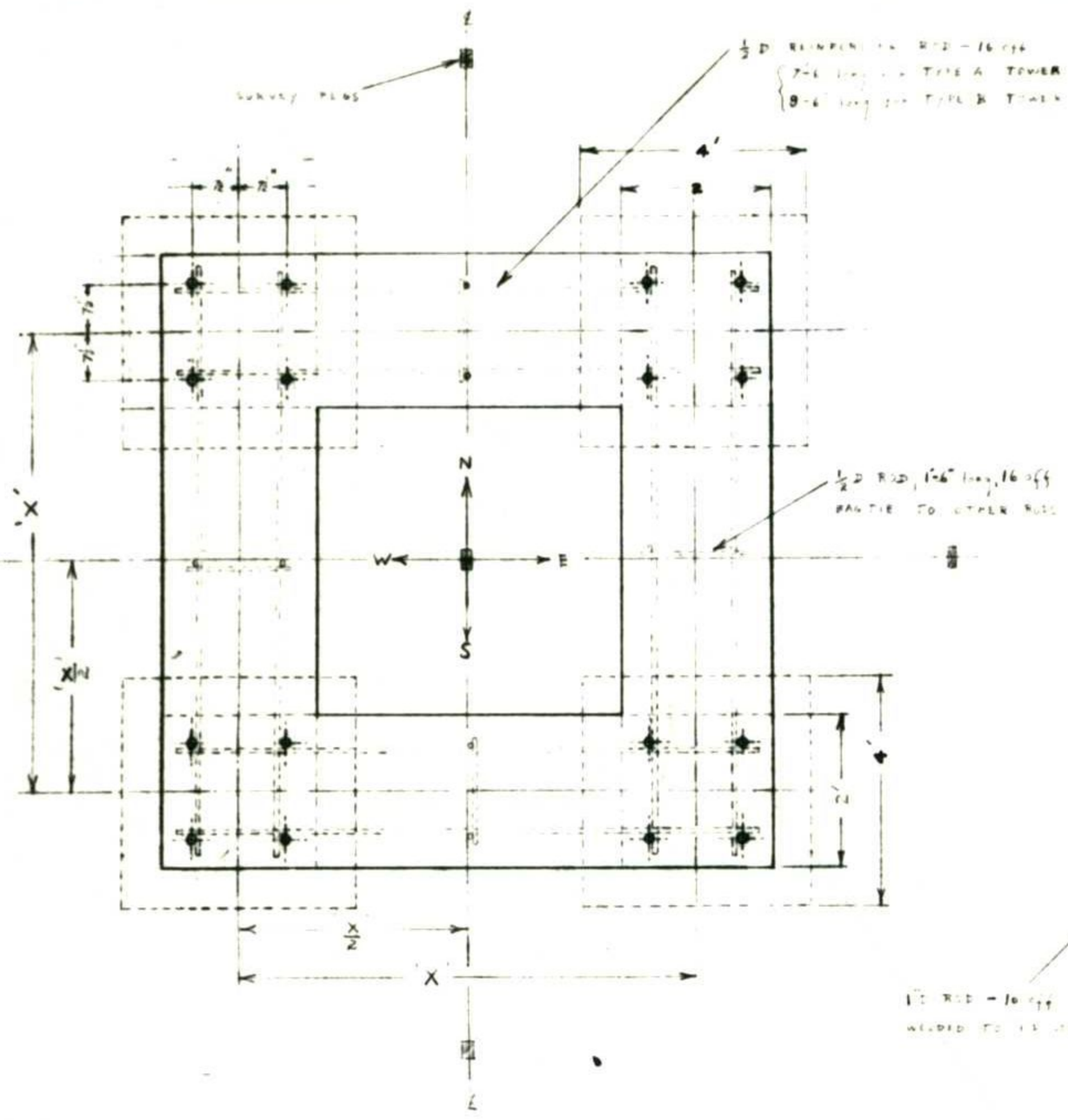

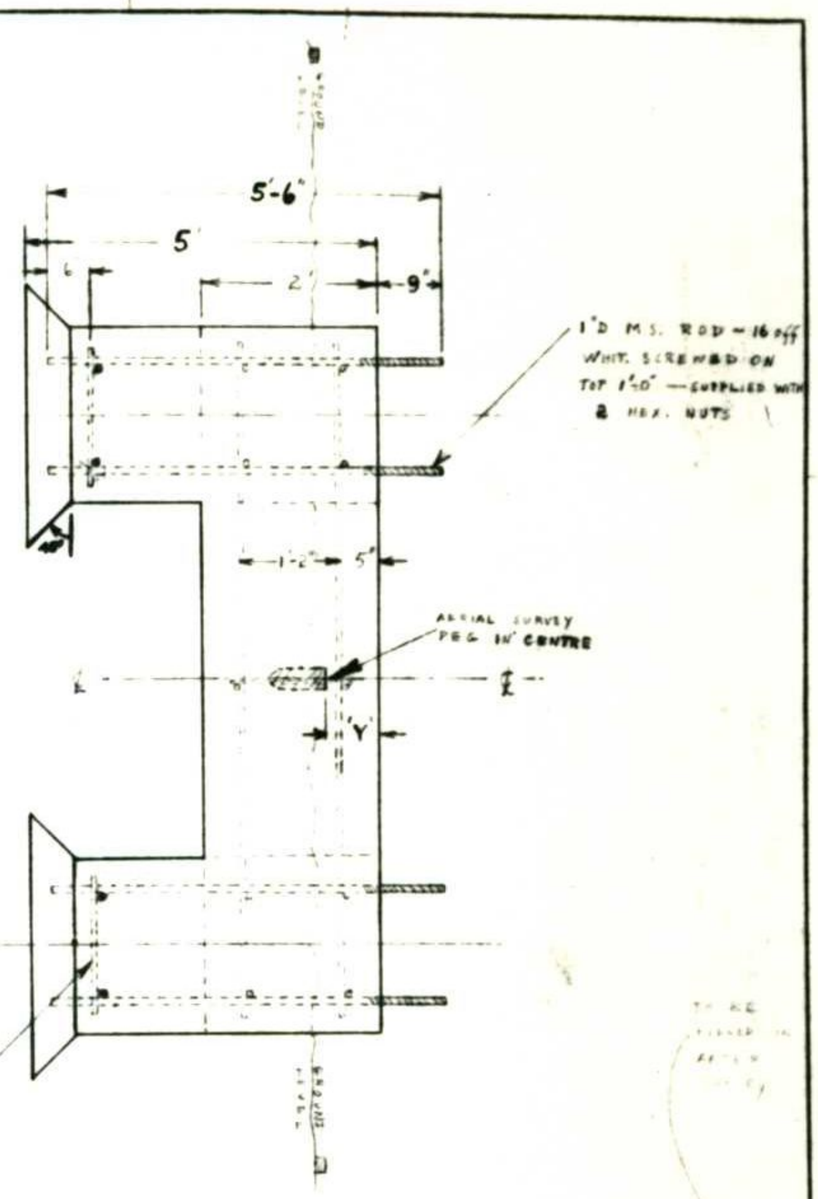

AERIAL	TOWER TYPE	'X'	'Y'
E 17	A	6'-0"	
W 17	B	8'-0"	
N 17	A	6'-0"	
N 18	B	8'-0"	

MATERIAL: CONCRETE
FINISH:

FOUNDATIONS - 45 FT DIA. AERIAL

SCALE —

UNIT
ASSY.
C.P.L.

DRAWN
TRACED
CHECKED
PASSED
APPROVED

SCHOOL OF ELECTRICAL ENGINEERING
UNIVERSITY OF SYDNEY

C-F45-43 A

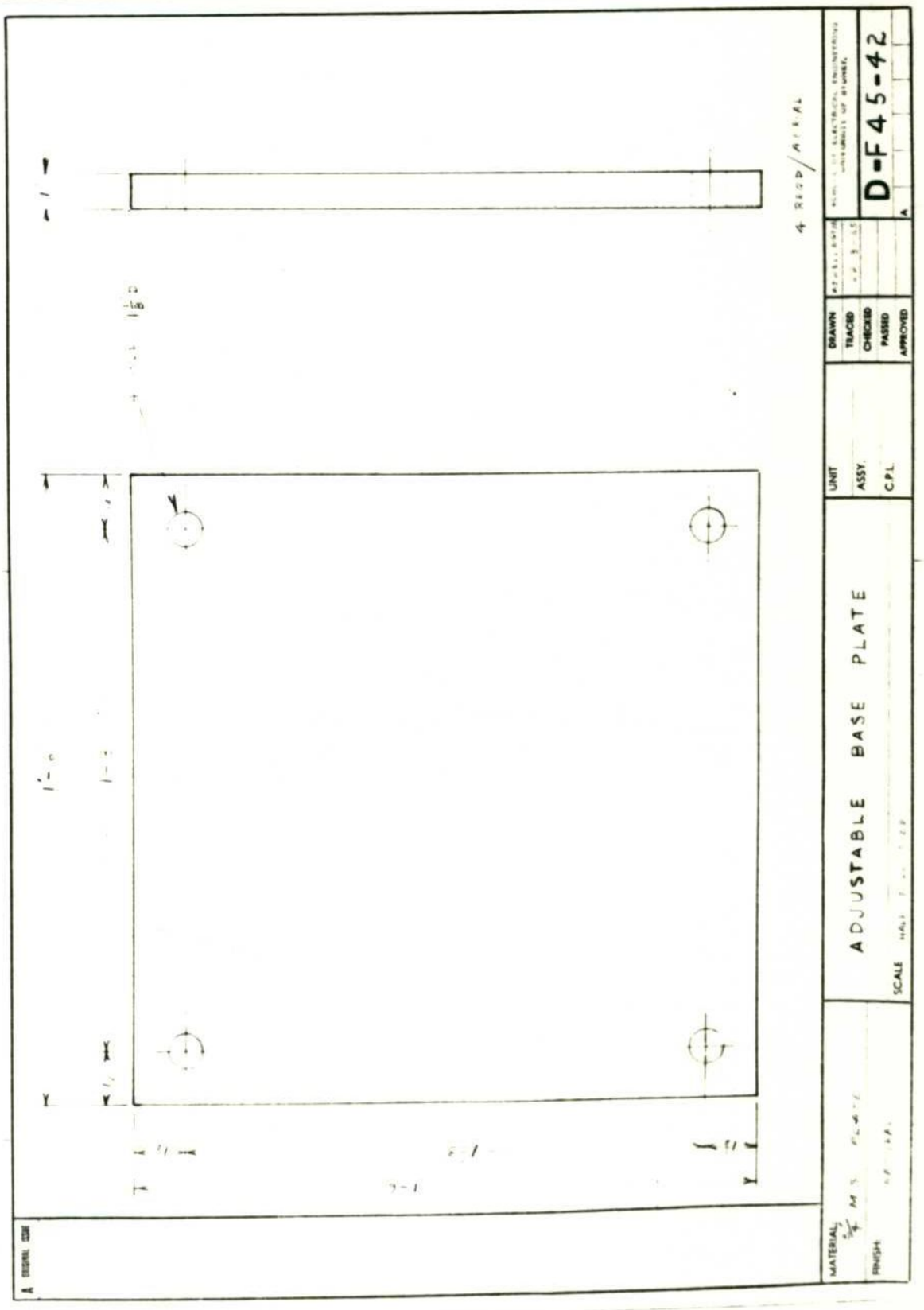

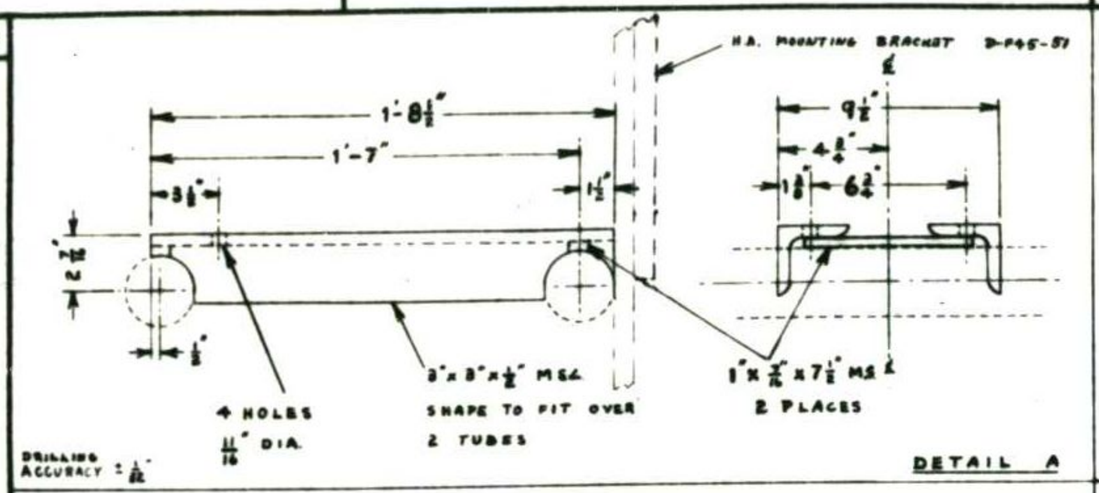

DETAIL A

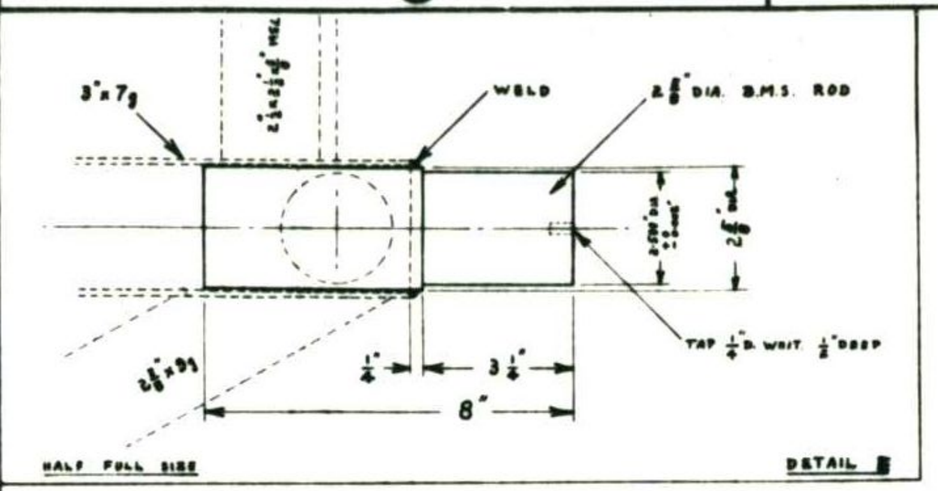

DETAIL B

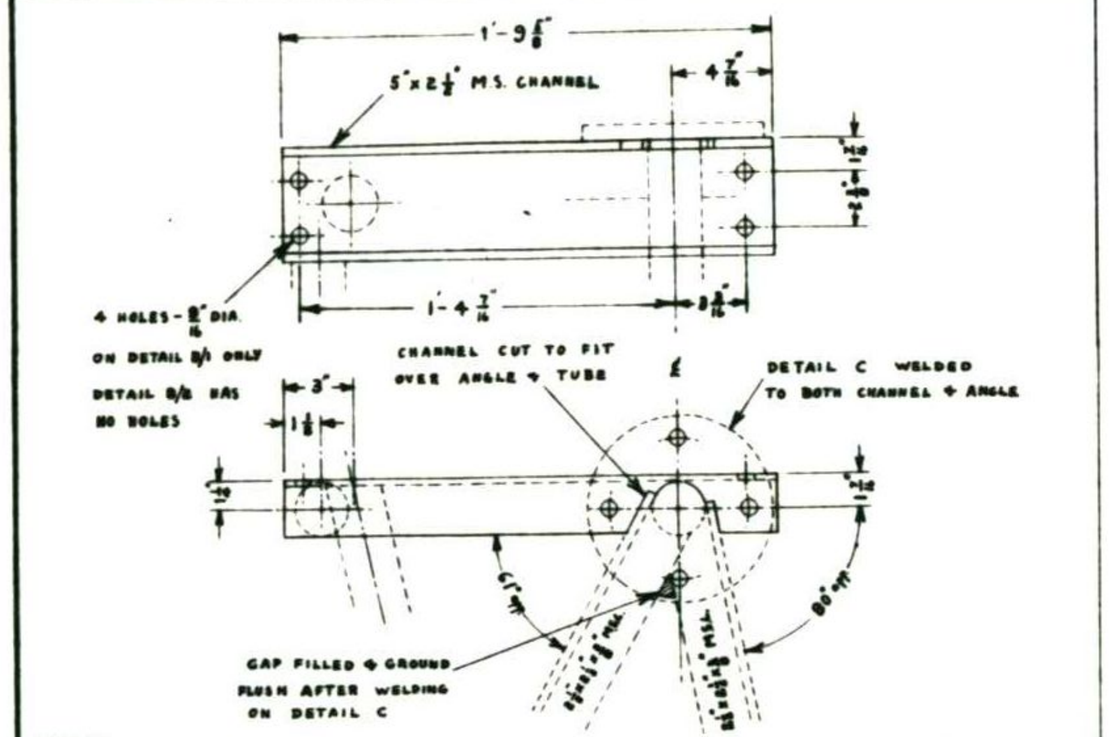

DETAIL B

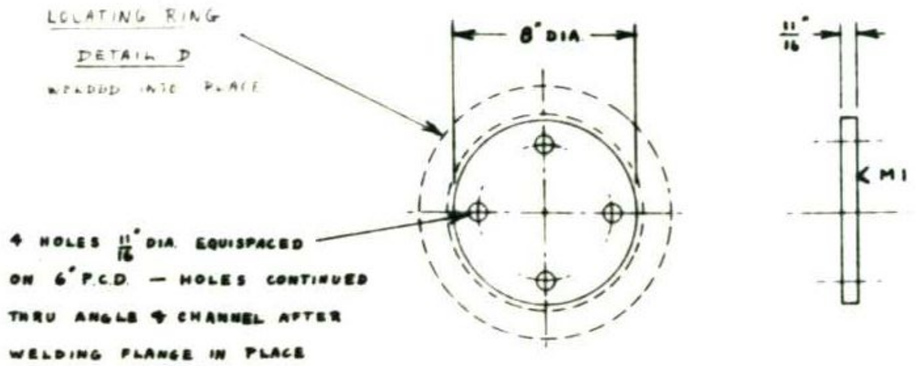

GEAR FLANGE (2 OFF)

DETAIL C

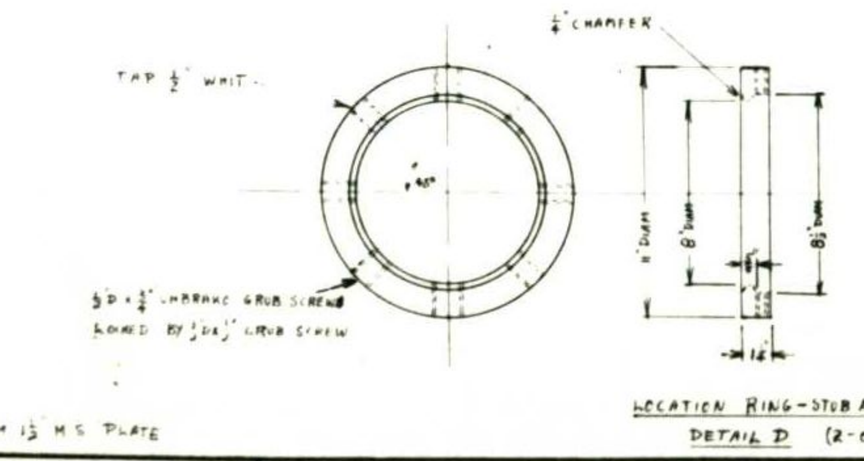

LOCATION RING-STUB AXLES

DETAIL D (2-OFF)

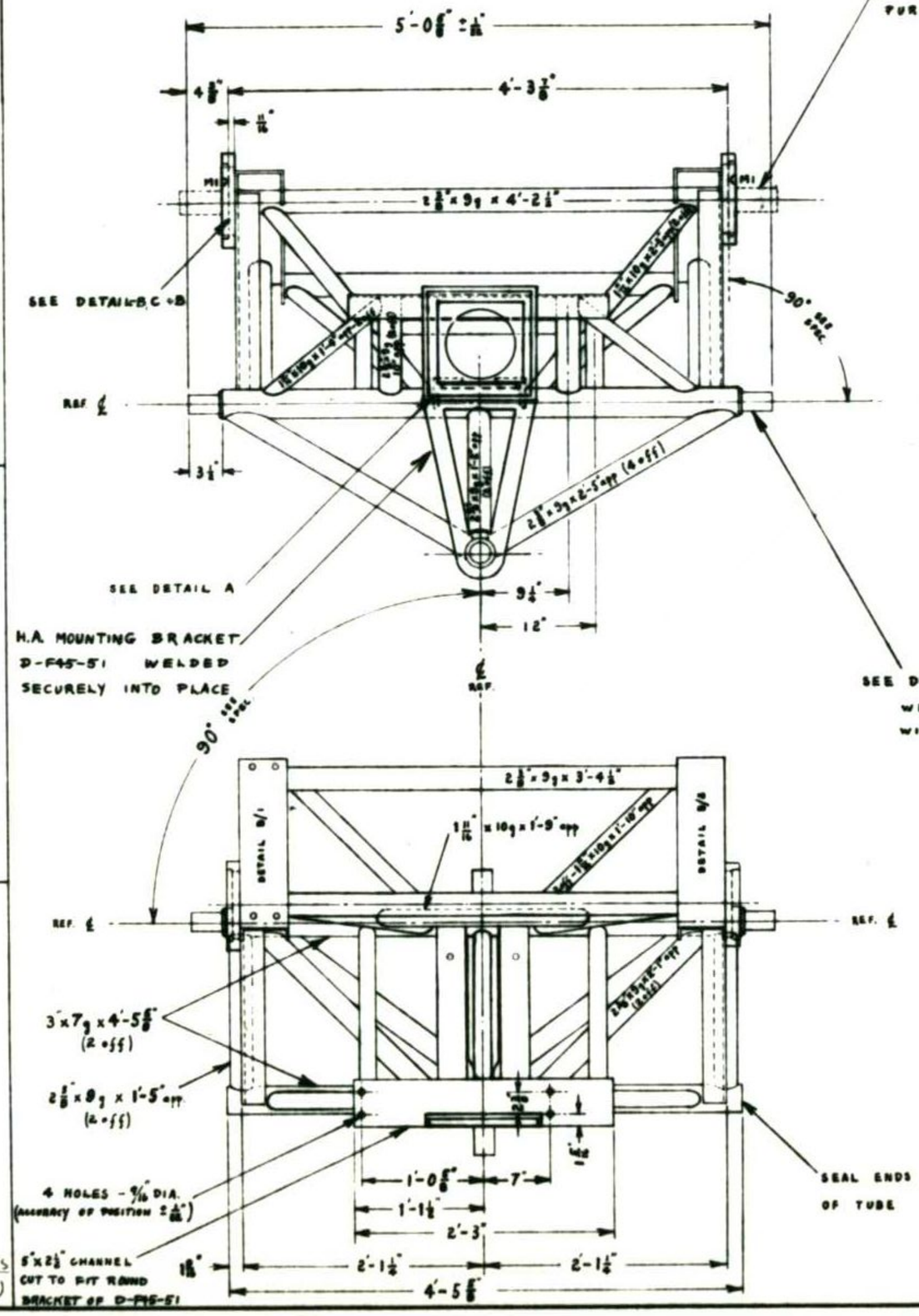

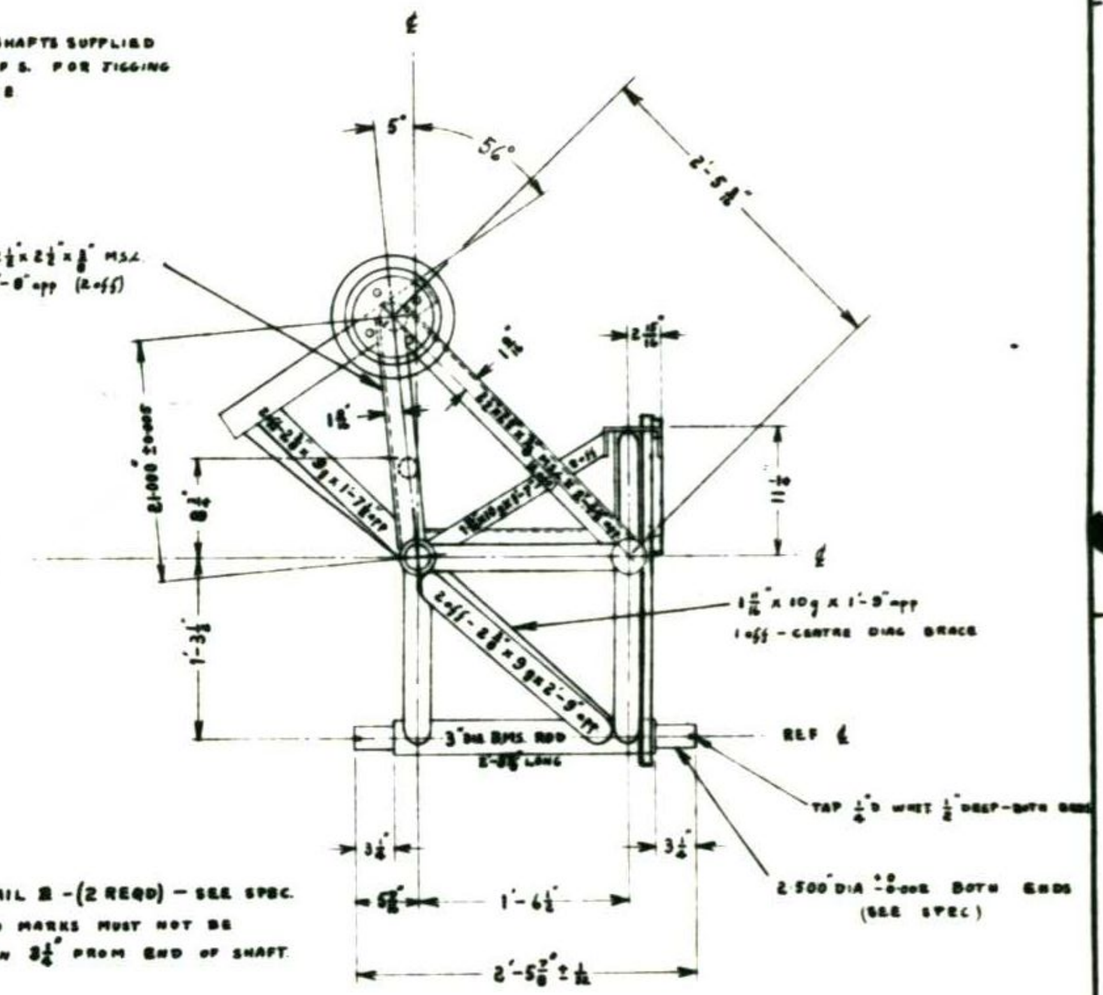

NOTE: 1. WELDED CONSTRUCTION THROUGHOUT — ⅜" FILLETS

2. SHAFT IS STRUCTURALLY SYMETRICAL

3. ACCURACY ± 1/16" UNLESS OTHERWISE NOTED

MATERIAL: GRADE 13 M.S. TUBE M.S. SECTIONS AS SHOWN	REFLECTOR SHAFT — 45 FT DIA. AERIAL	UNIT B-F45-00	DRAWN	R.J. WELLINGTON	B-F45-44
FINISH: SEE SPECIFICATION	SCALE 1½" = 1 foot & 3" = 1 foot	ASSY.	TRACED	21-8-56	
		C.P.L.	CHECKED		
			PASSED		
			APPROVED		A

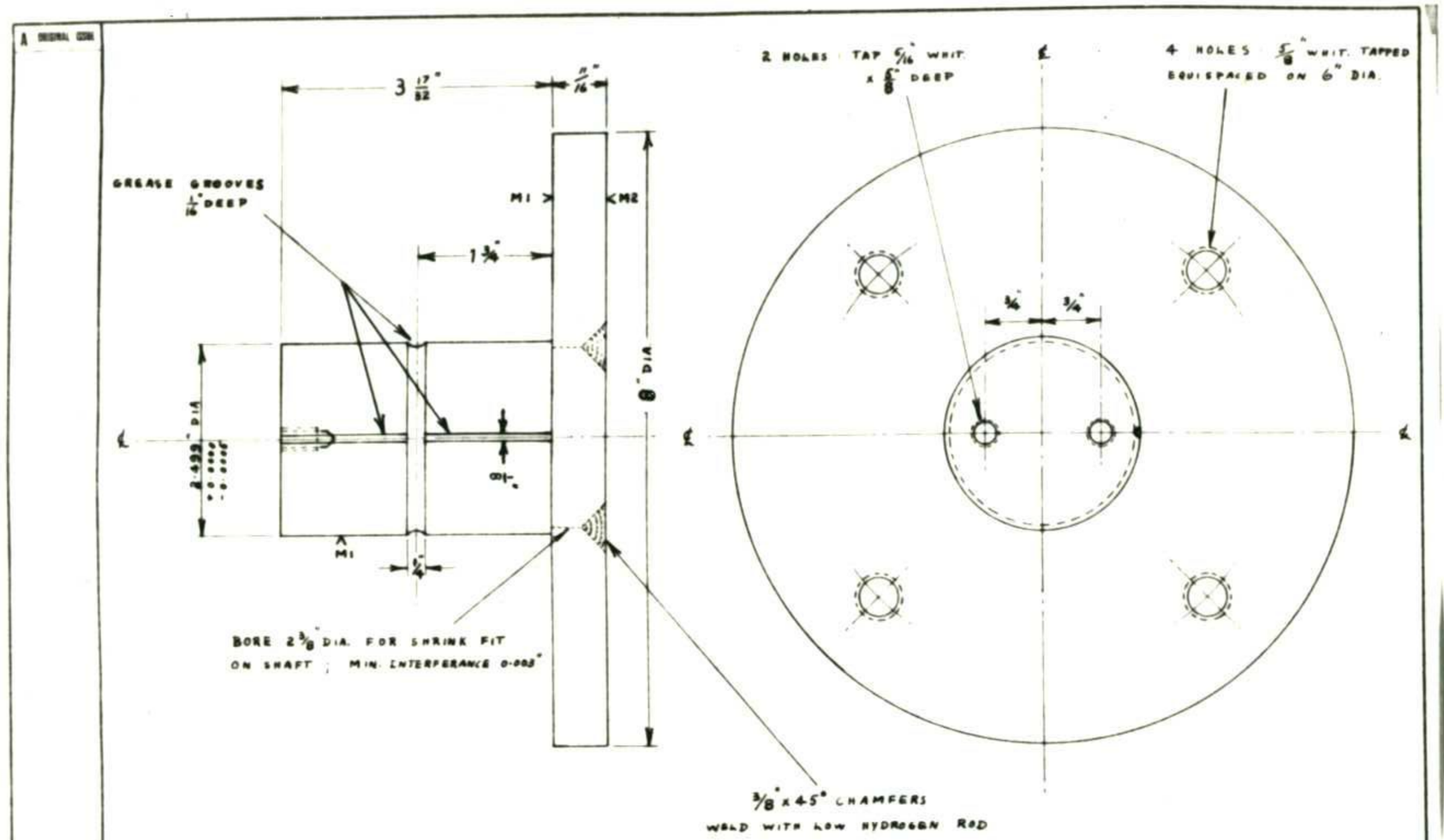

MATERIAL: 2 1/8" BMS ROD; 3/4 MS PLATE	DECLINATION GEAR STUB SHAFT	UNIT	DRAWN	D-F45-45
FINISH: NATURAL	SCALE FULL SIZE	ASSY.	TRACED 8-11-44	
		C.P.L.	CHECKED	
			PASSED	
			APPROVED	A

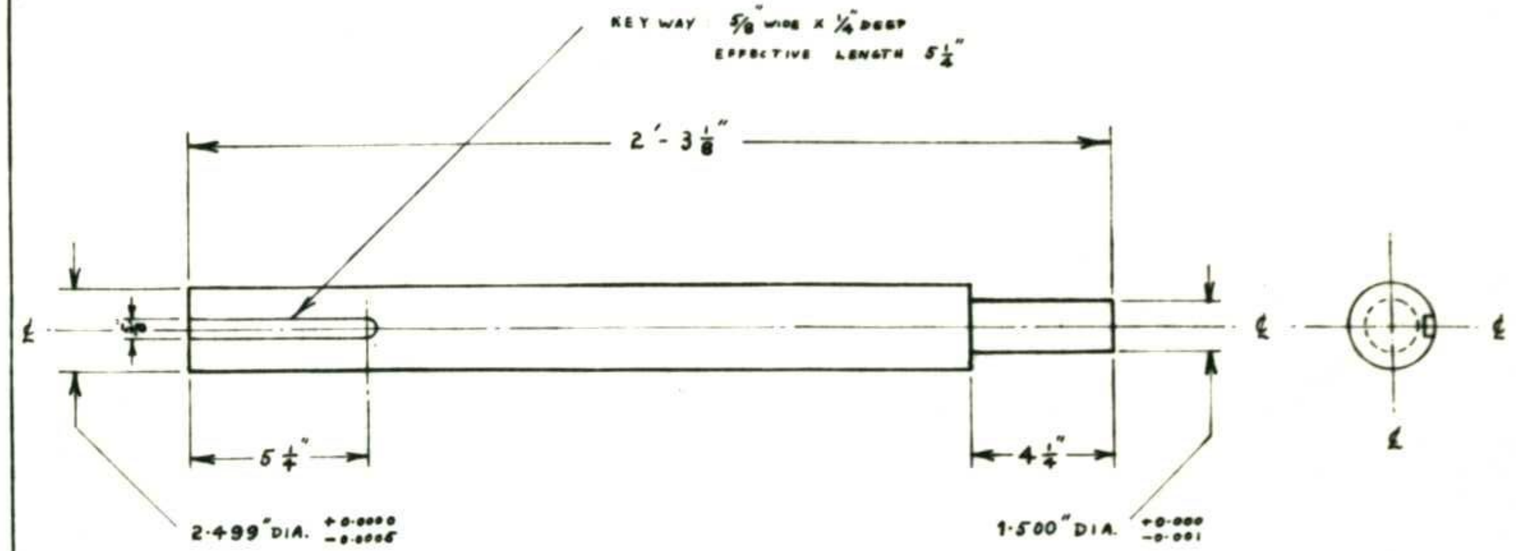

ALSO TO BE SUPPLIED :
1 GIB-HEAD KEY PER SHAFT
5/8" WIDE x 1/2" DEEP x 5" EFFECTIVE LENGTH ; TAPER OF 1 IN 100

1 REQD PER AERIAL

MATERIAL: SD19 STEEL OR EQUIV. 55 to 65 Ton U.T.S. ; 44 Ton Yield Stress	HOUR ANGLE GEAR SHAFT	UNIT	DRAWN	D-F45-47
FINISH: NATURAL	SCALE 3/8" = 1"	ASSY.	TRACED 11-11-44	
		C.P.L.	CHECKED	
			PASSED	
			APPROVED	A

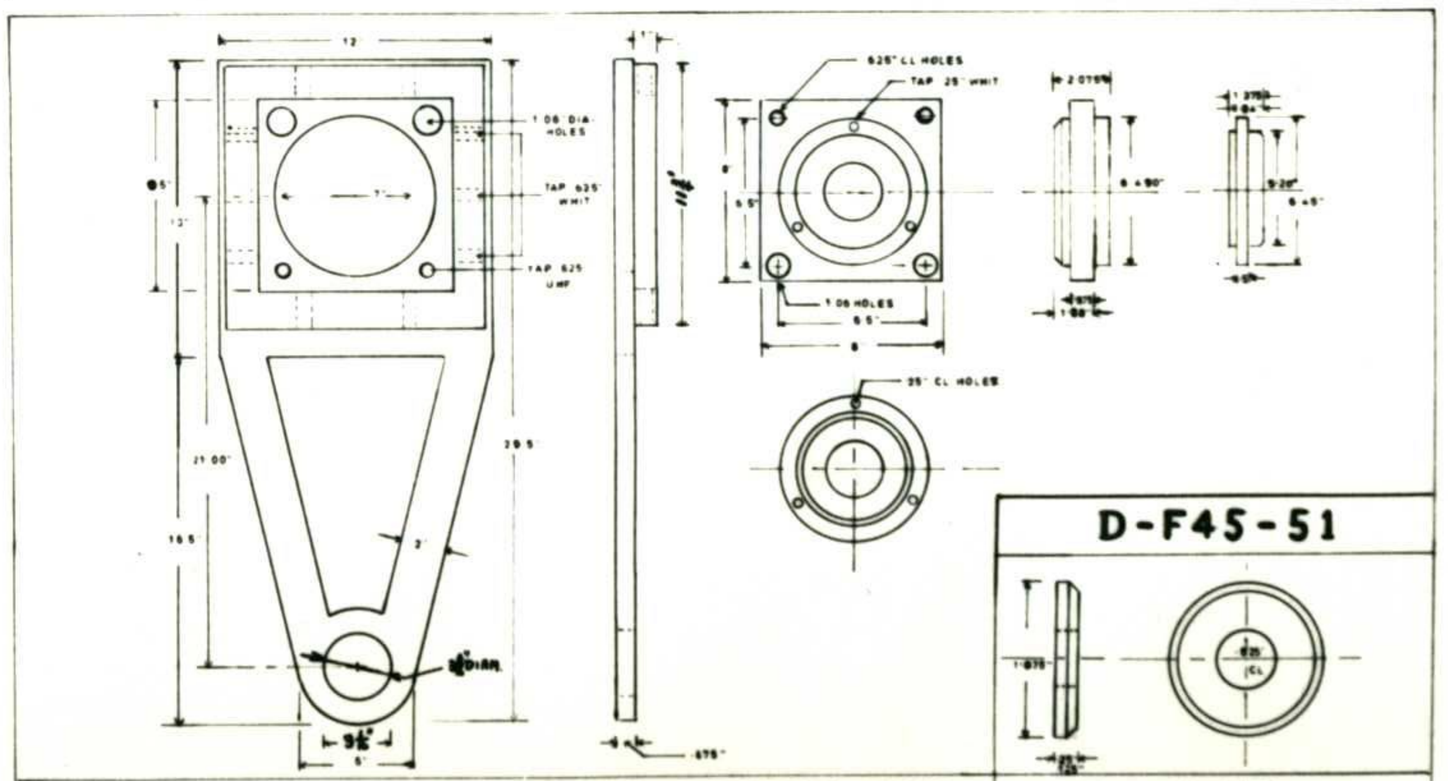

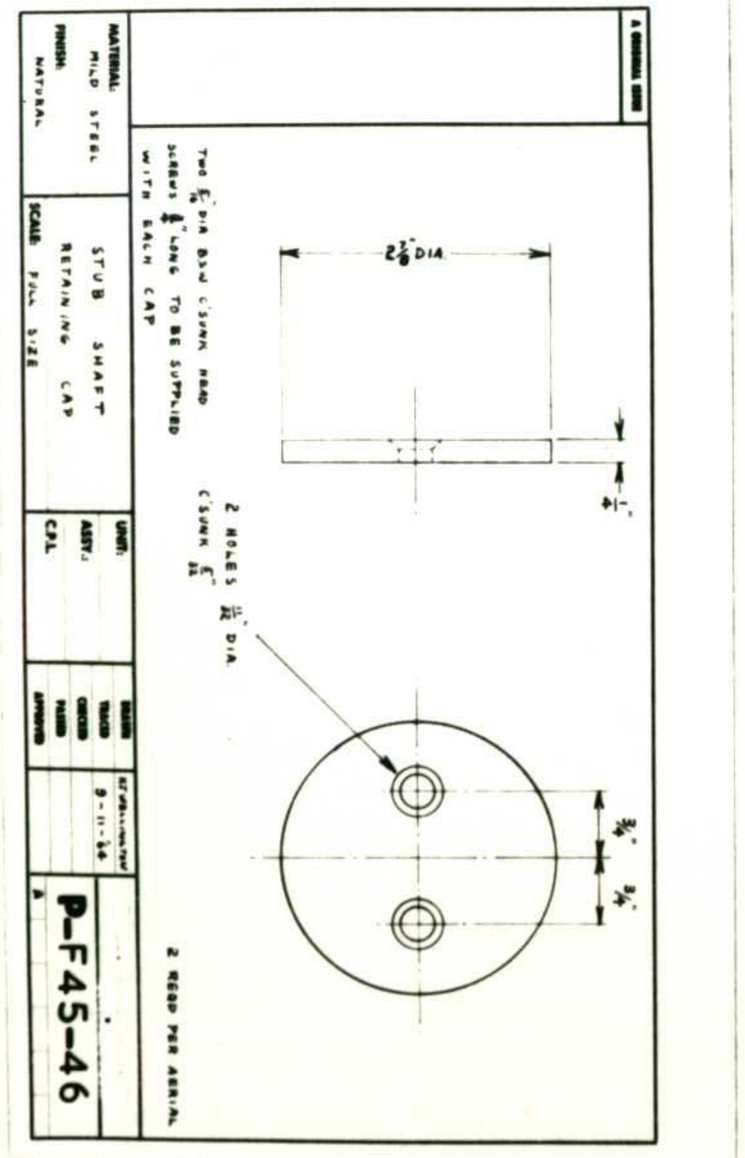

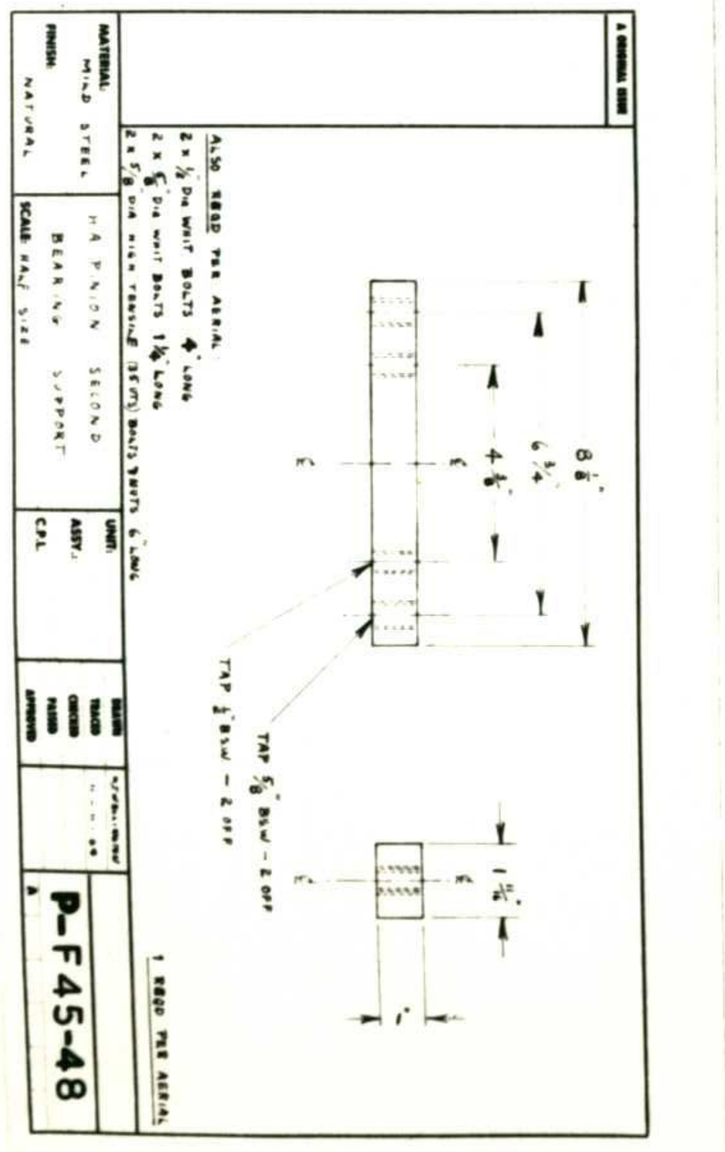

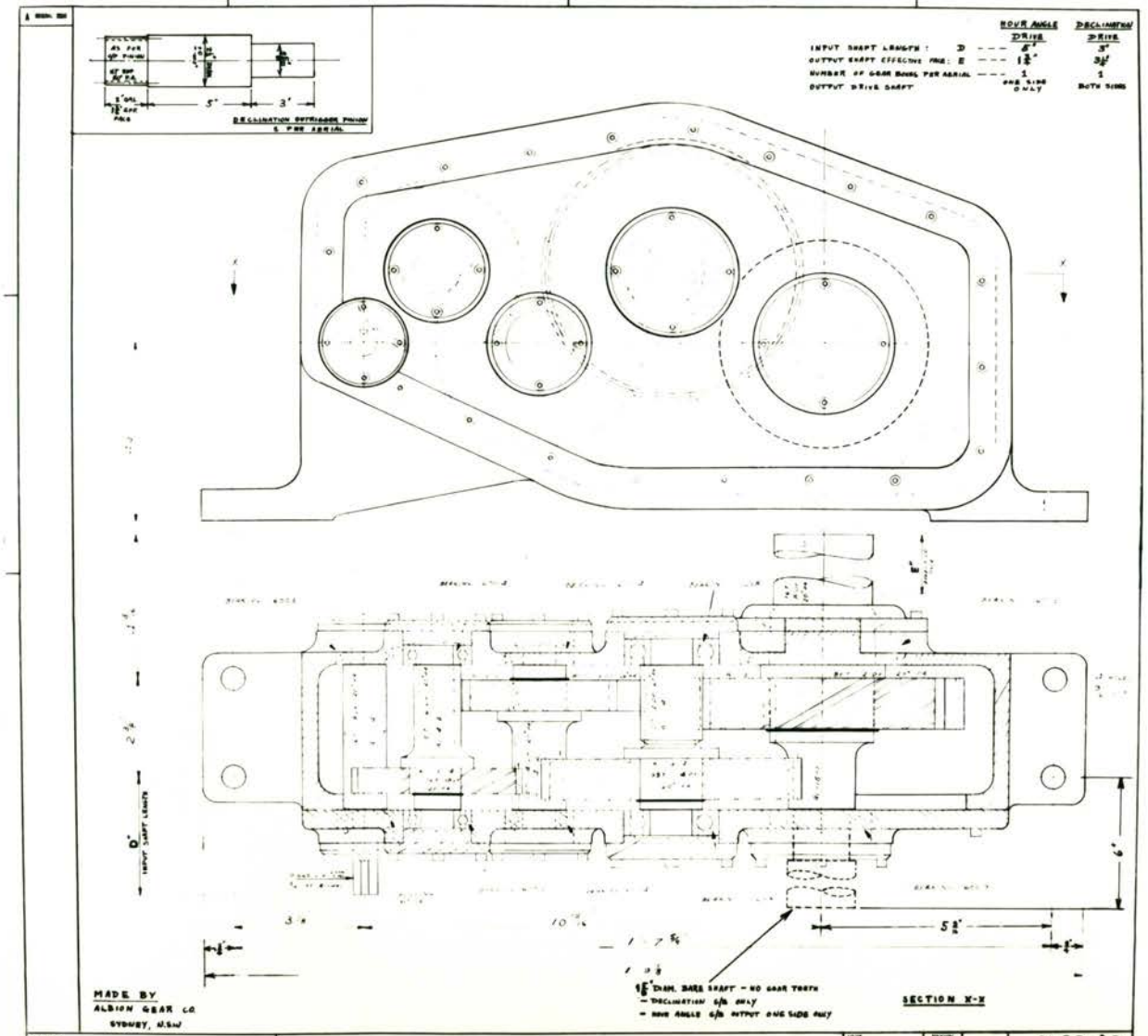
HOUR ANGLE DRIVE
DECLINATION DRIVE
INPUT SHAFT LENGTH : D --- 4"
OUTPUT SHAFT EFFECTIVE PAGE : E --- 12"
NUMBER OF GEAR BOXES PER AERIAL --- 1
OUTPUT DRIVE SHAFT ONE SIDE ONLY
DECLINATION OUTPUT PINION 1 PER AERIAL
5"
3"
INPUT SHAFT LENGTH
10 3/4
5 1/2"
6"
1 5/8" DIAM. BARE SHAFT - NO GEAR TEETH
- DECLINATION S/B ONLY
- HOUR ANGLE S/B OUTPUT ONE SIDE ONLY
SECTION X-X
MADE BY
ALBION GEAR CO
SYDNEY, N.S.W.
MATERIAL
FINISH
MAIN GEAR BOX - ASSEMBLY
SCALE FULL SIZE
UNIT
ASSY.
C.P.L.
DRAWN
TRACED
CHECKED
PASSED
APPROVED
S.H.E.E.-38
B-F45-49

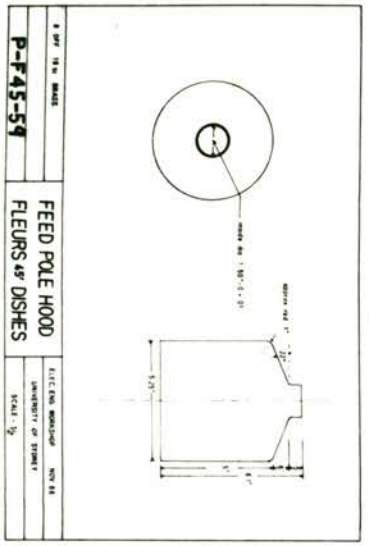
P-F45-54
FEED POLE HOOD
FLEURS 45' DISHES
ELECTRONIC WORKSHOP
UNIVERSITY OF SYDNEY
NOV 83
SCALE - ½

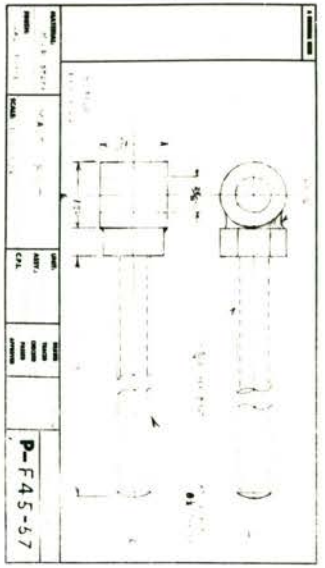
P-F45-57

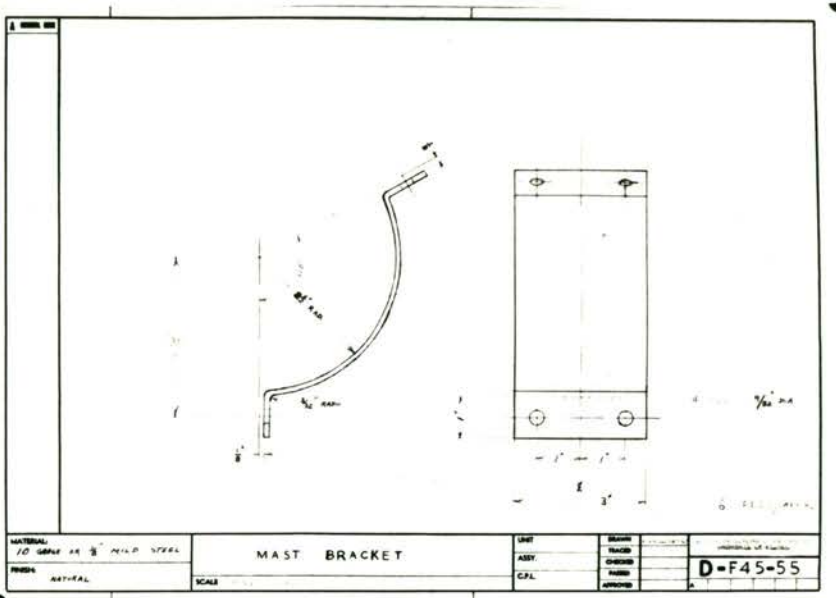
MAST BRACKET
D-F45-55

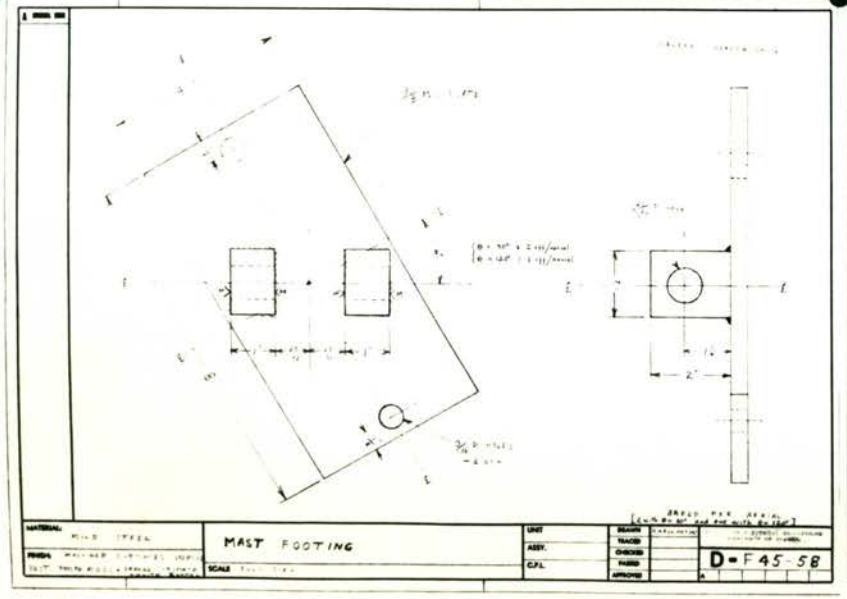
MAST FOOTING
D-F45-58

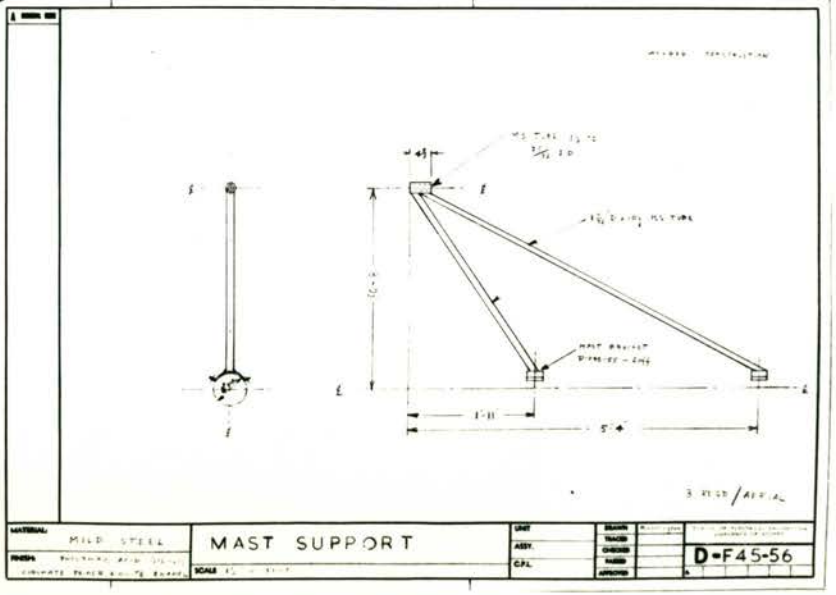
MILD STEEL
MAST SUPPORT
D-F45-56

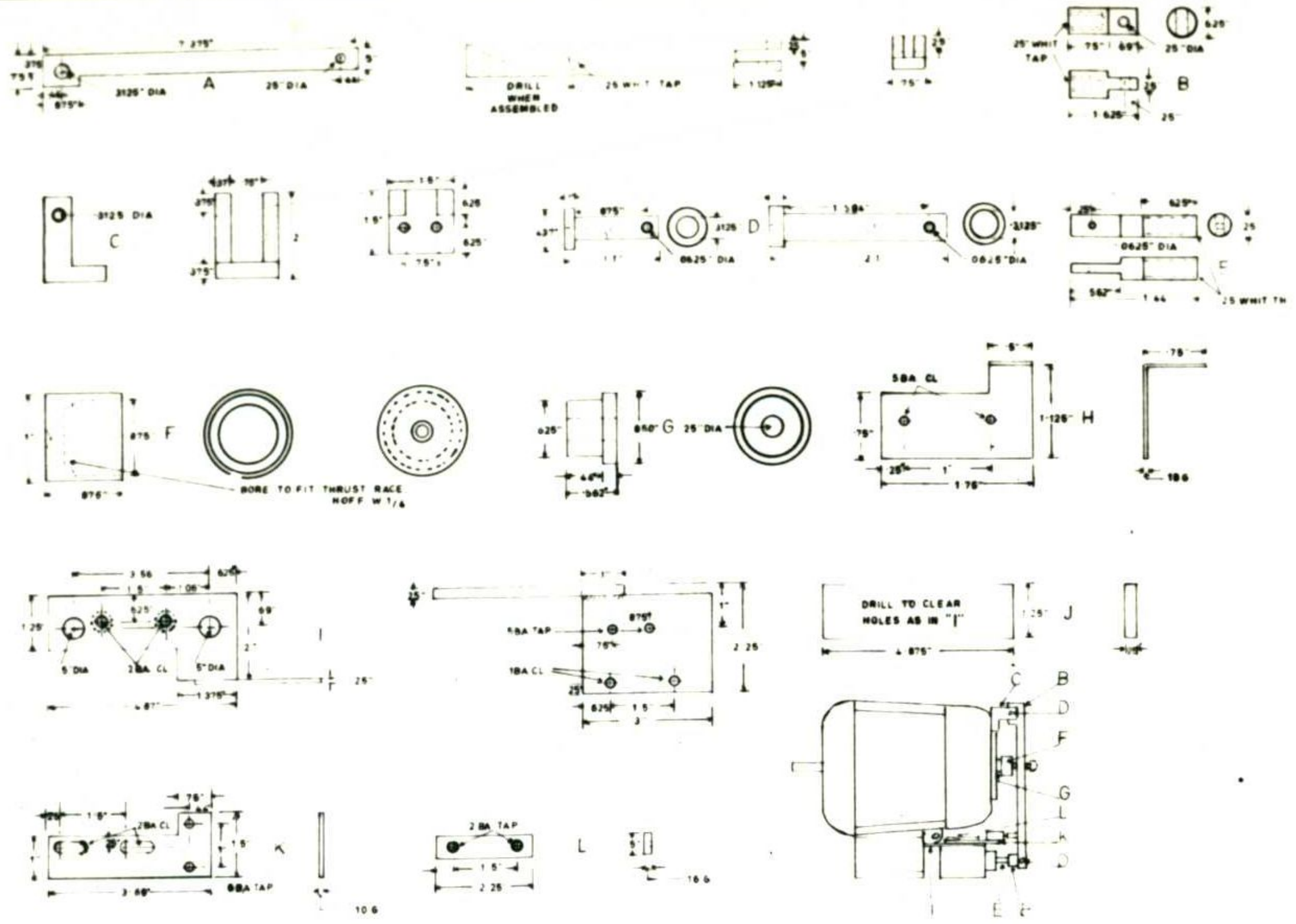

A&B 1-OFF BRASS C.D.E.F.G.H.J.K.L. M STEEL GAL PLATE 1-OFF EACH PER UNIT	COMPONENTS FOR DEMAG MOTOR BRAKE RELEASE	SUEE WORKSHOP **D-F45-61**

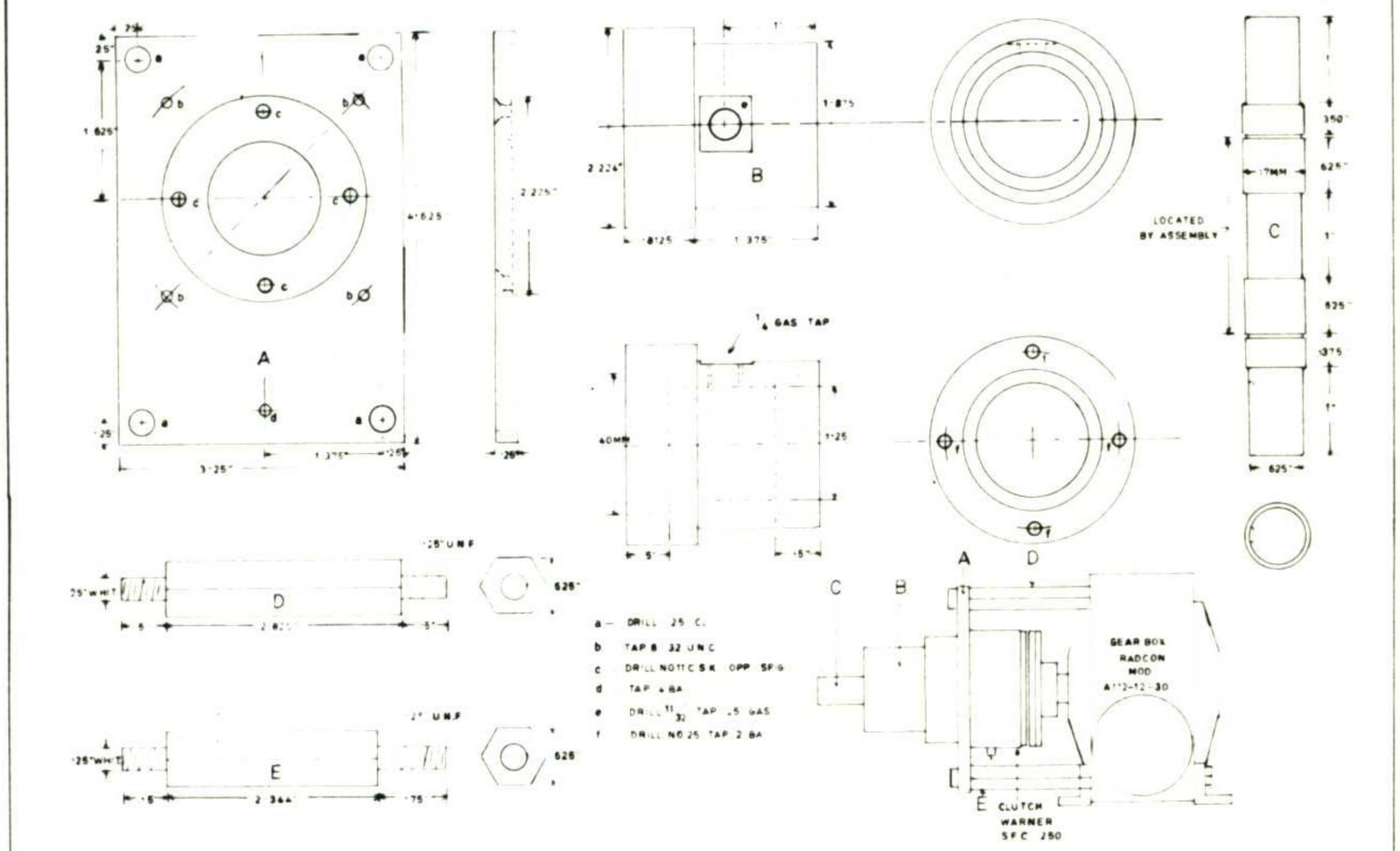

A B C D E BM STEEL	MAGNETIC CLUTCH MOUNTING ON GEAR BOX 45' DISH HOUR ANGLE DRIVE	SUEE WORKSHOP **D-F45-62**

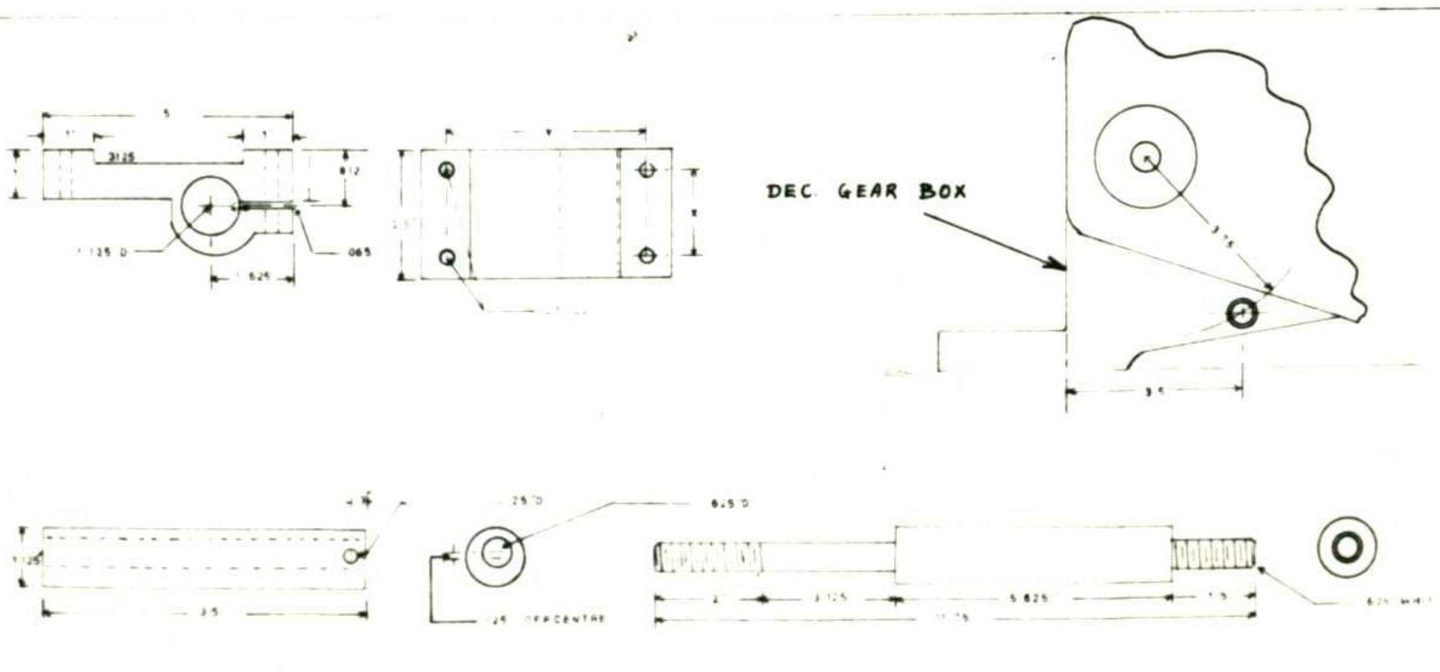

X&Y FROM MOTOR FEET	DEMAG MOTOR MOUNTING DEC. DRIVE GEAR BOX	SUEE WORKSHOP 4 OFF M. STEEL ELECTRO-GAL. **D-F45-63**

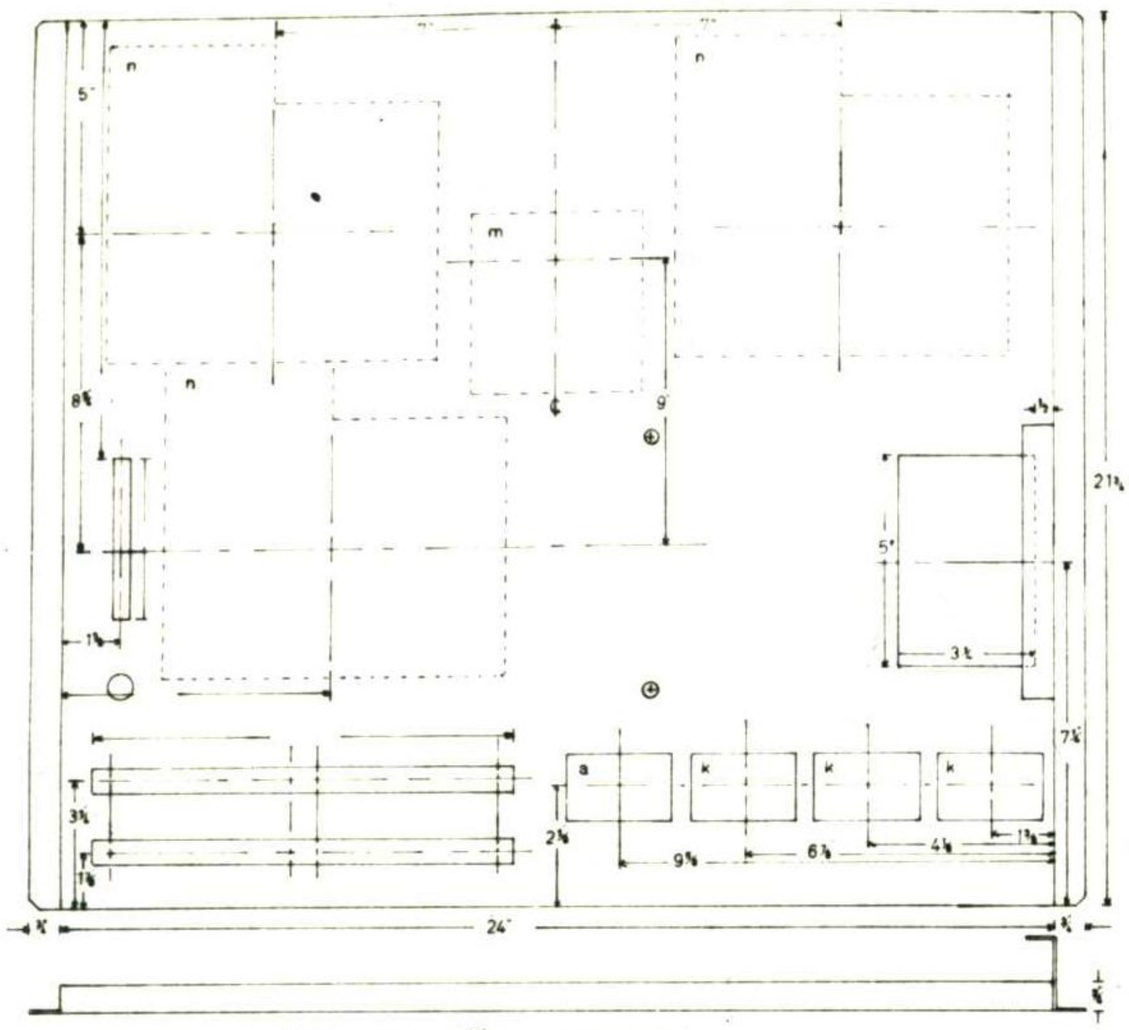

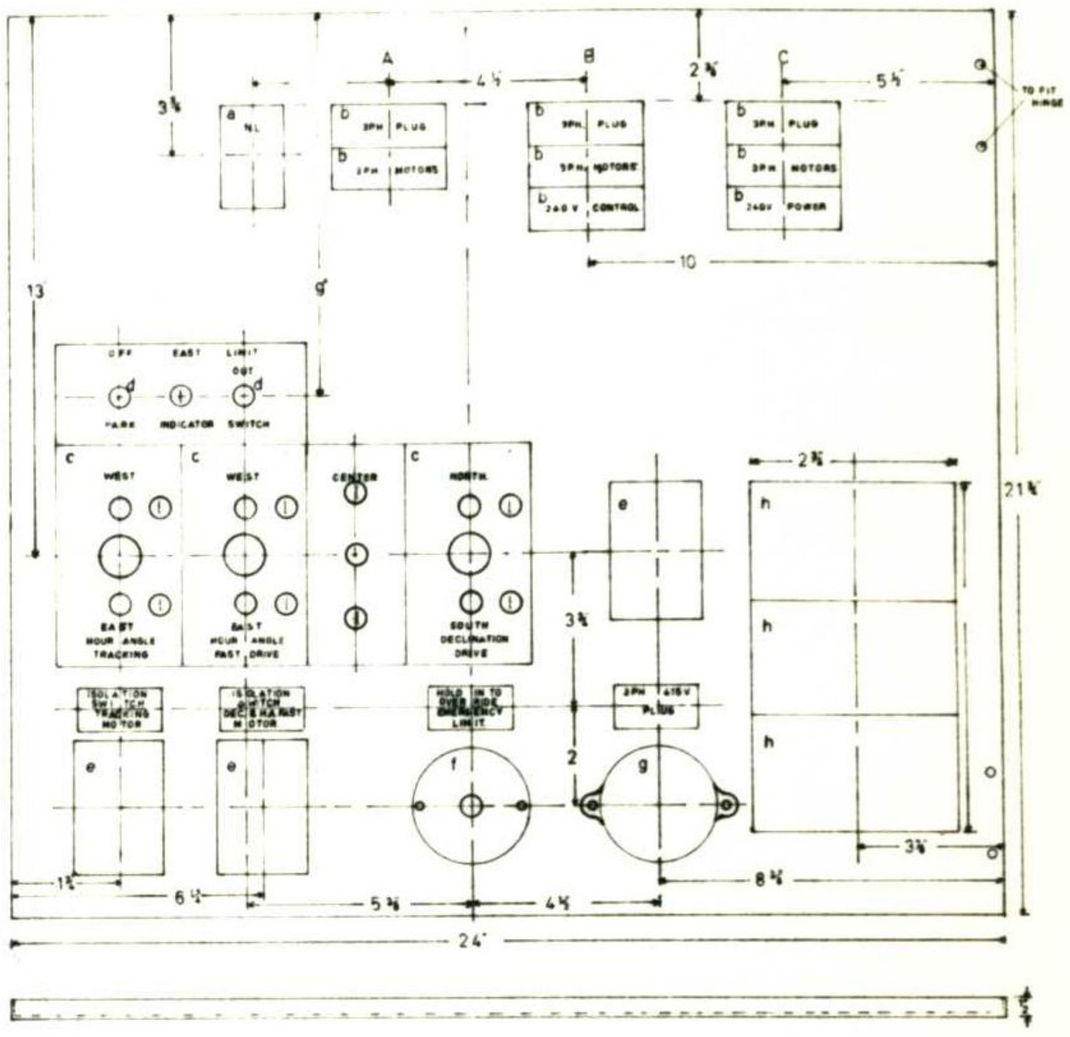

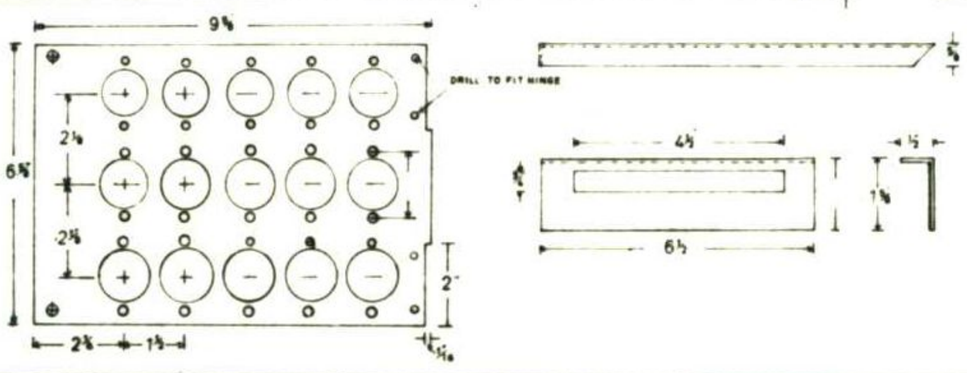

a – FEDERAL 15A 440V LINKS
b – " 20A " ACS HRC FUSES
c – NILSEN PB3 AF STATION
d – CUTLER-HAMMER 3A D.P.D.T. SWITCH
e – FEDERAL 3 PH T20 SWITCHS
f – NILSEN PB1 BF PUSH BUTTON
g – WILCO 3 PH. PLUG
h – CLIPSAL 240 V FLUSH COMBINATION
k – FEDERAL 60A 240 V LINKS.
l – LUMALITE FP1 CL NR 60V DC.
m – OJ15ER REVESING CONTACTORS
n – OJ15 " CONTACTOR.

4 OFF 18 M.S. SHEET SILVER HAMMERGLOW	CONTROL BOXES FLEURS 45' DISHES LAYOUT	S.U.E.E. WORKSHOP SEPT. 1966. C-F45-64

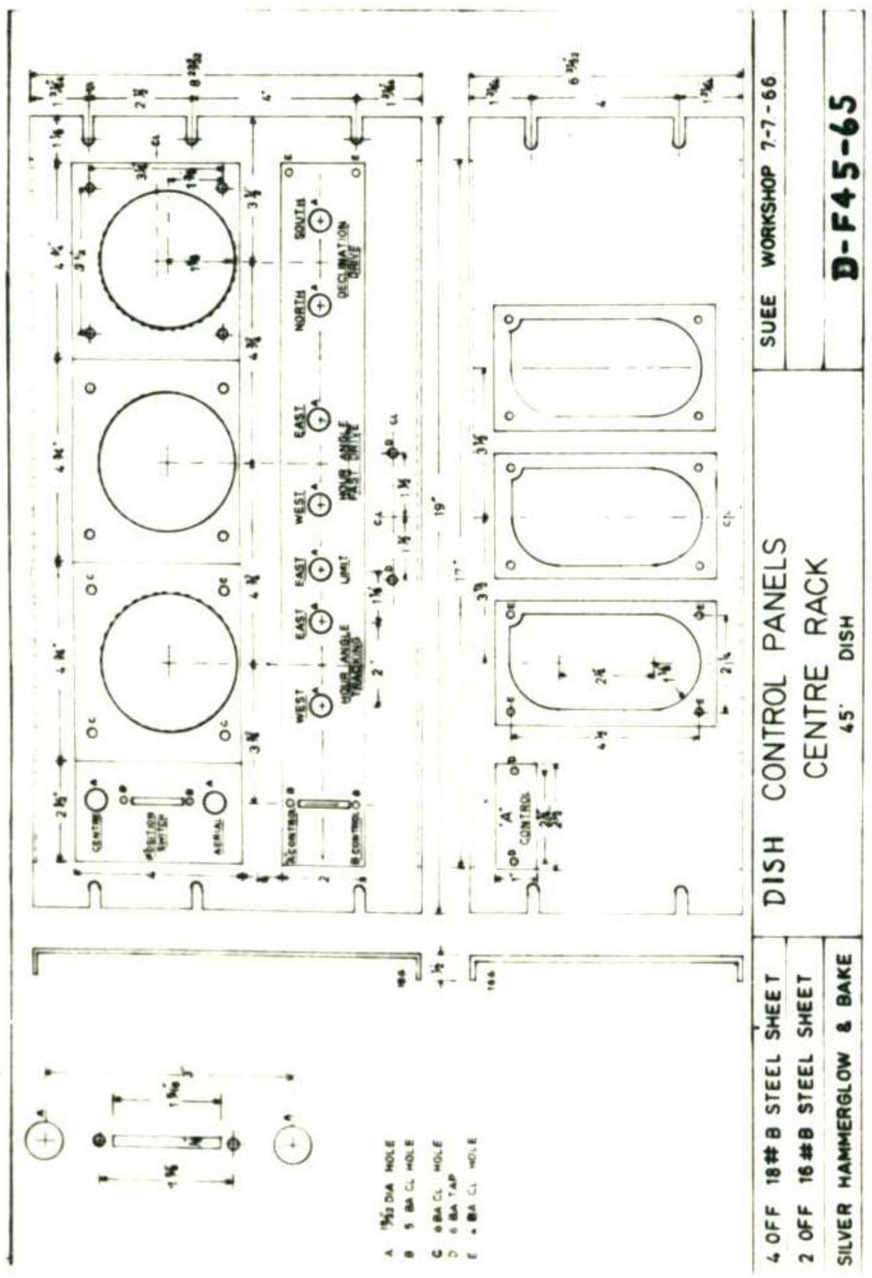

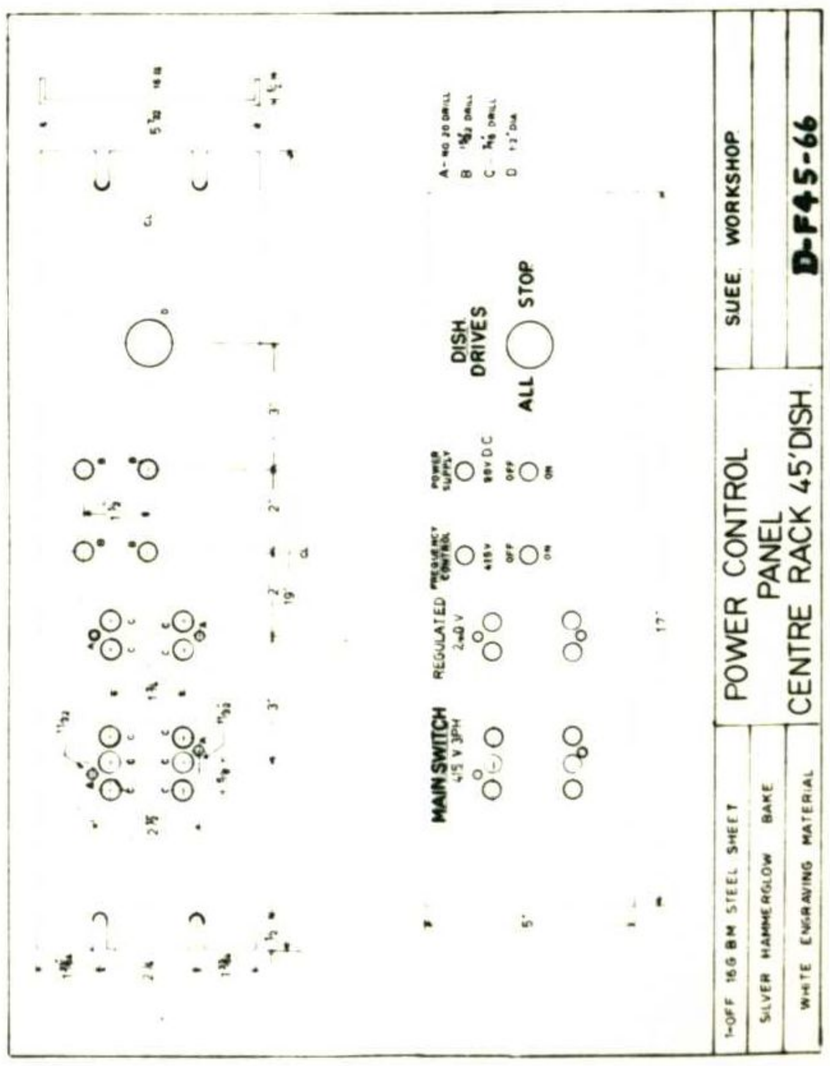

APPENDIX F The Fringe Rate Converter System

F.1 Design and Construction of the Switching Unit

Section 9.4 outlines the method of operation of the receiver system using the fringe rate converter. The aim is to measure the relative phase of signals reaching two widely separated aerials. To do this it is necessary to observe the phase of the intereference fringes from a small diameter radio source (3C273). As the source is also weak in intensity, it is necessary to raise the receiver sensitivity by slowing the output fringe rate and greatly lengthen the receiver time constant.

The fringe rate converter unit generates a switching wave of accurately known frequency and phase. This switching wave is used in such a way as to enable the phase of the source fringes to be determined with precision.

The complete unit, designed and constructed by the writer, is shown in Fig. F.1. A block diagram appears in Fig. 9.3 while the complete circuit logic is set out in Fig. F.2.

A precision sidereal digital clock supplies both a 10 Hz and a 50 Hz square wave as an input to the switching unit. One of these square waves is used to drive a decade counter which is reset after a certain number of counts. The number of counts, and hence the period between resetting, is determined by an adjustable decoder, preset by switches on the front panel. The reset pulse from the decoder generates the required switching wave.

Counter and Decoder

When decoding is necessary, the most convenient form of decade counter is a shift register with negative feedback, (Fig. F.3). The pulses to be counted are used to clock the shift register to the next state. The shift register uses five J-K flip-flops. From the time diagram, Fig. F.4, it is apparent that at each input pulse only one flip-flop changes state, so that no transient error state is created.

FIGURE F.1

The Fringe Rate Converter Unit; dimensions approx.

9" x 6" x 2"

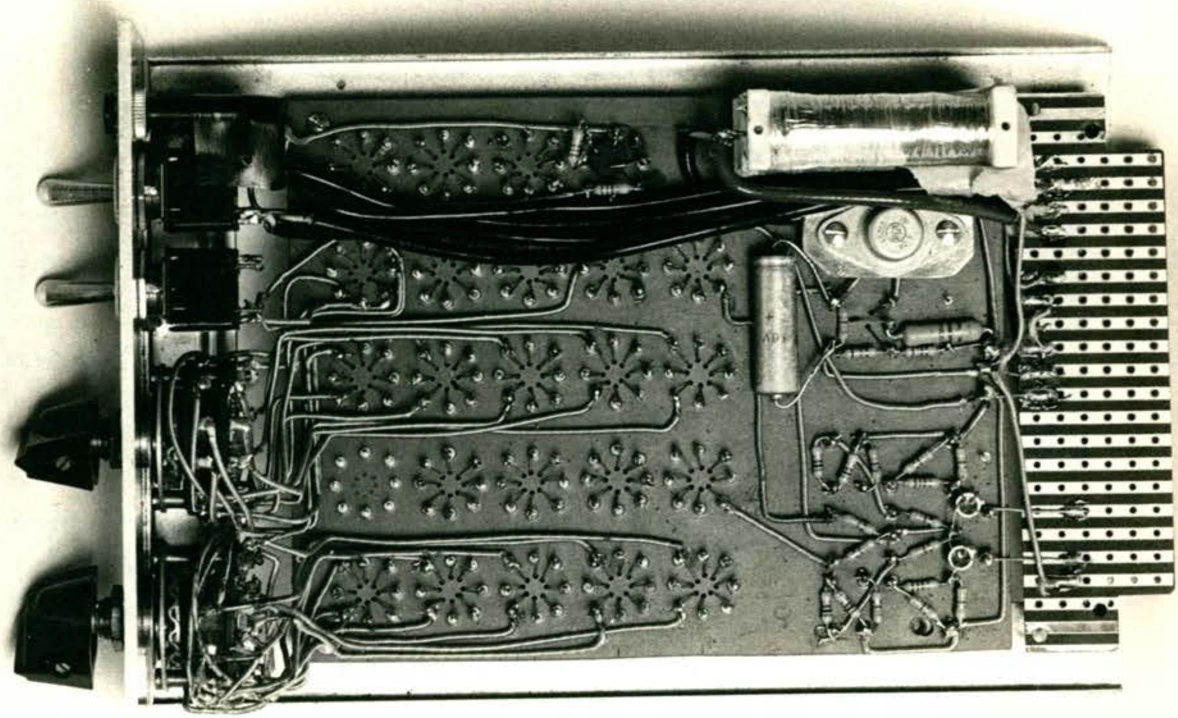

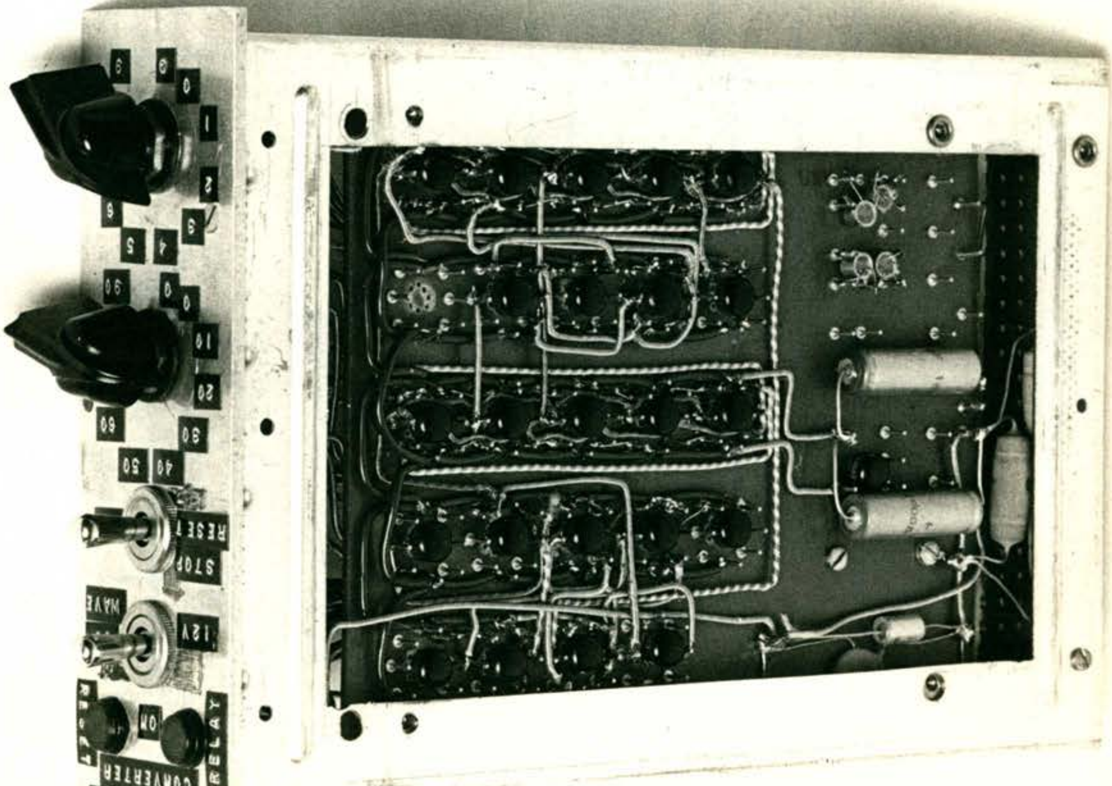

FRINGE RATE
CONVERTER
RELAY
ON
WAVE
12V
STOP
RESET

(a)

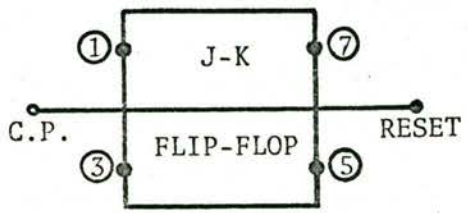

[Fairchild integrated circuit 9923]

TRUTH TABLE

I/P		O/P	
①	③	⑦	⑤
H	H	X^n	$\bar{X}^n$
H	L	H	L
L	H	L	H
L	L	$\bar{X}^n$	X^n

H = high state
L = low state
X = previous output state

H on reset pin gives L on pin 7

(b)

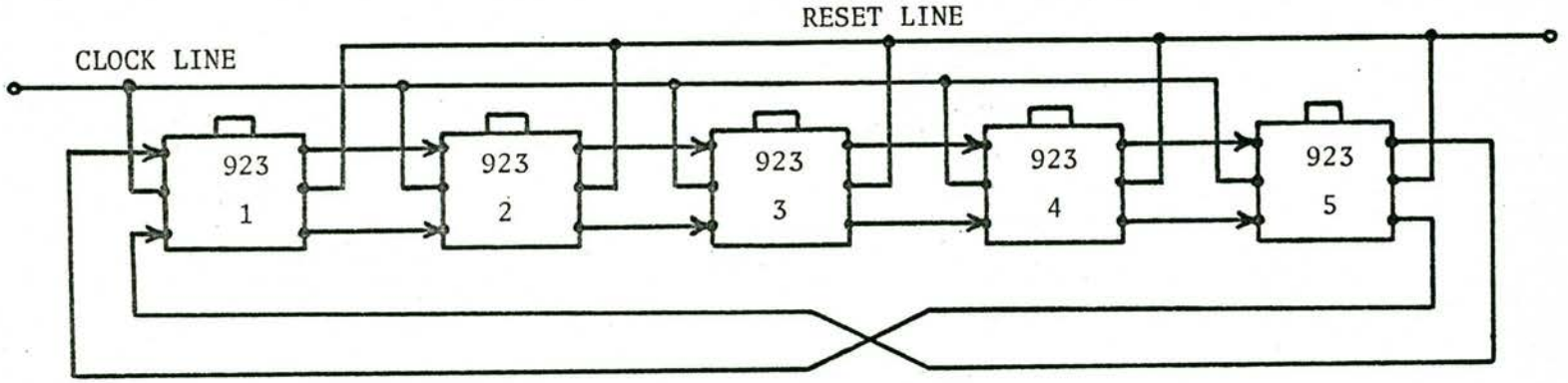

FIGURE F.3 The Decade Counter:
(a) The integrated circuit J-K flip-flop and its truth table.
(b) Block diagram of the counter. This is a shift register with negative feedback.

F1c

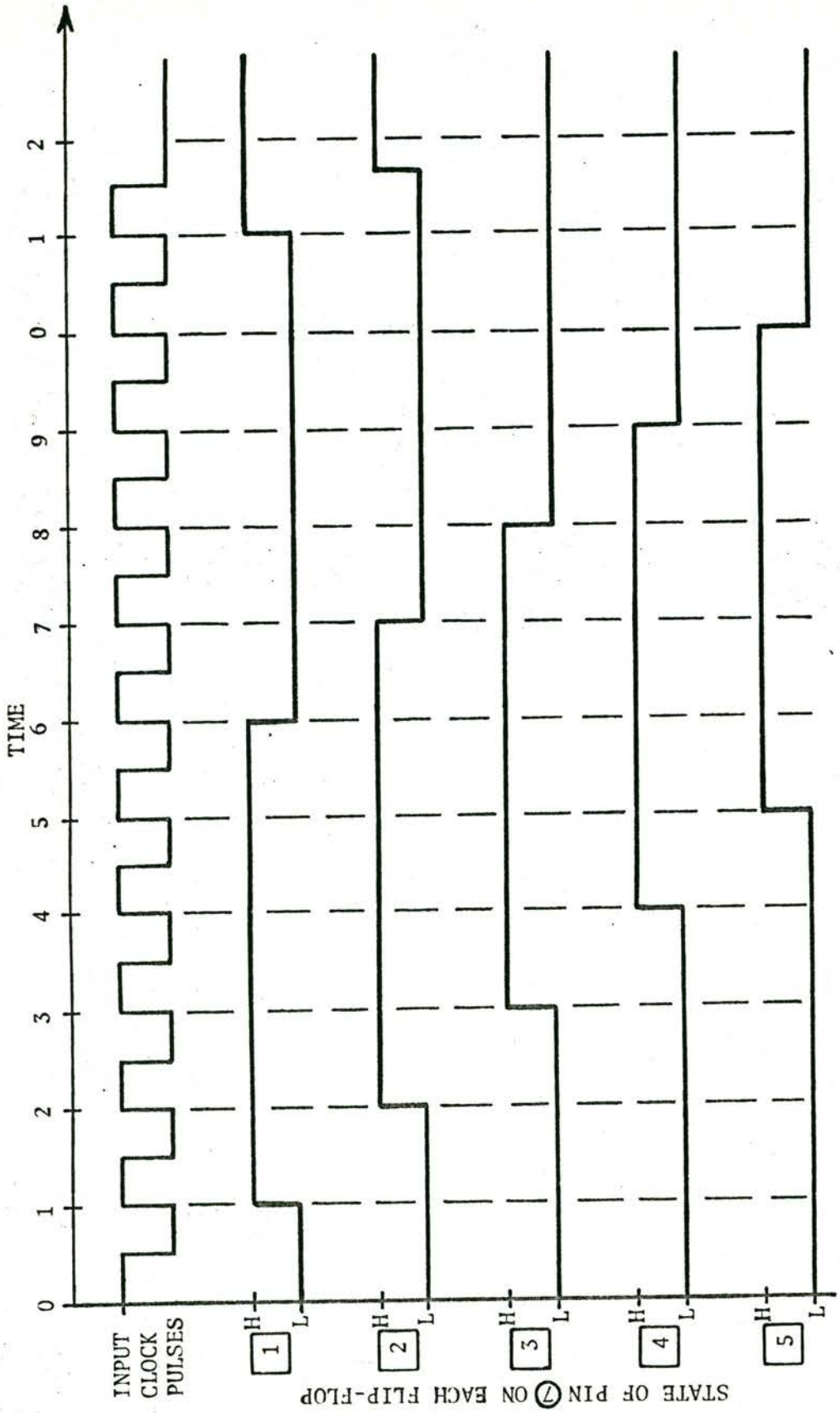

FIGURE F.4 The time diagram of the decade counter illustrated in fig. F.3(b).

Decoding for a particular state can be accomplished by sensing the polarity of signal on two lines only. The decoder for each counter consists of a ten-position two-pole rotary switch driving a coincidence gate. Each switch position senses the two relevant outputs which define the required state.

A second shift register counter serves as a 'tens' counter. In this case the clock pulse is gated with the nine-state sensing lines from the 'units' counter. The 'tens' counter advances one count every time the units counter goes from the nine to zero state.

Reset and Start

When both counters reach the states indicated on the rotary switch, the decoding coincidence gates are activated causing the reset flip-flop to change state and reset all the counter flip-flops. The trailing edge of the last clock pulse is used to remove the reset signal leaving the counters in the zero state ready to receive the next clock pulse.

In order to start at an accurately known time, the one minute markers from the digital clock are used to change the state of the start flip-flop. This start flip-flop is preset by a front panel switch so that it stops the counter reset signal from being removed. The one minute marker allows its removal and thus initiates the count.

Output

A single pole two position reed relay is used as the output element. The reed switches the phase of the 400 Hz drive to the second local oscillator. It is controlled by the output flip-flop which changes state every time a reset pulse occurs.

Front panel lights indicate the state of the reed relay and the reset signal. A switch is also provided to choose the signal to be controlled, either (i) the 400 Hz square wave or (ii) ± 12 volts. This controlled signal determines the state (0^{o} or 180^{o}) of the phase switch in the second local oscillator line.

The fringe rate converter unit contains three types of Fairchild RTμL integrated circuit logic blocks, the 923 J-K flip-flop, the 914 dual two-input gate and the 900 buffer unit. Two transistor Schmitt trigger circuits are used to sharpen the clock input rise times and to set them at the correct driving level for the integrated circuits. A special 3.6 volt regulated power supply drives the integrated circuits and isolates them from any transient pulses in the system.

F.2 Computation of Fringe Rates and Phases

The required switching rate

During observations it is necessary to compute the expected source fringe frequency. This is used to set the frequency of the generated switching wave so that an optimum output fringe frequency is attained.

For an east-west interferometer with baseline length L wavelengths and source direction (α,δ), the fringefrequency F is given (Chapter 3) by:

$$F = \pm \frac{d\alpha}{dt} \cdot L.\cos\delta.\cos\alpha \qquad (F.1)$$

$$= F_{mx}\cos\alpha \qquad (F.2)$$

where F_{mx} is the maximum fringe frequency of the source.

If ΔF is the maximum difference (or output) frequency which can be tolerated, then the fringe rate converter frequency setting, F_n (n^{th} setting from the source transit), and the hour-angle, α_n, at which this frequency must be set can be calculated from the following:

$$\left.\begin{aligned} F_n &= F_{mx} - \Delta F(2n-1) \\ \text{and} \\ \alpha_n &= \cos^{-1}\left(1-\frac{2n.\Delta F}{F_{mx}}\right) \end{aligned}\right\} \qquad (F.3)$$

Fig. F.5 illustrates the procedure required to keep F_n close to the fringe frequency.

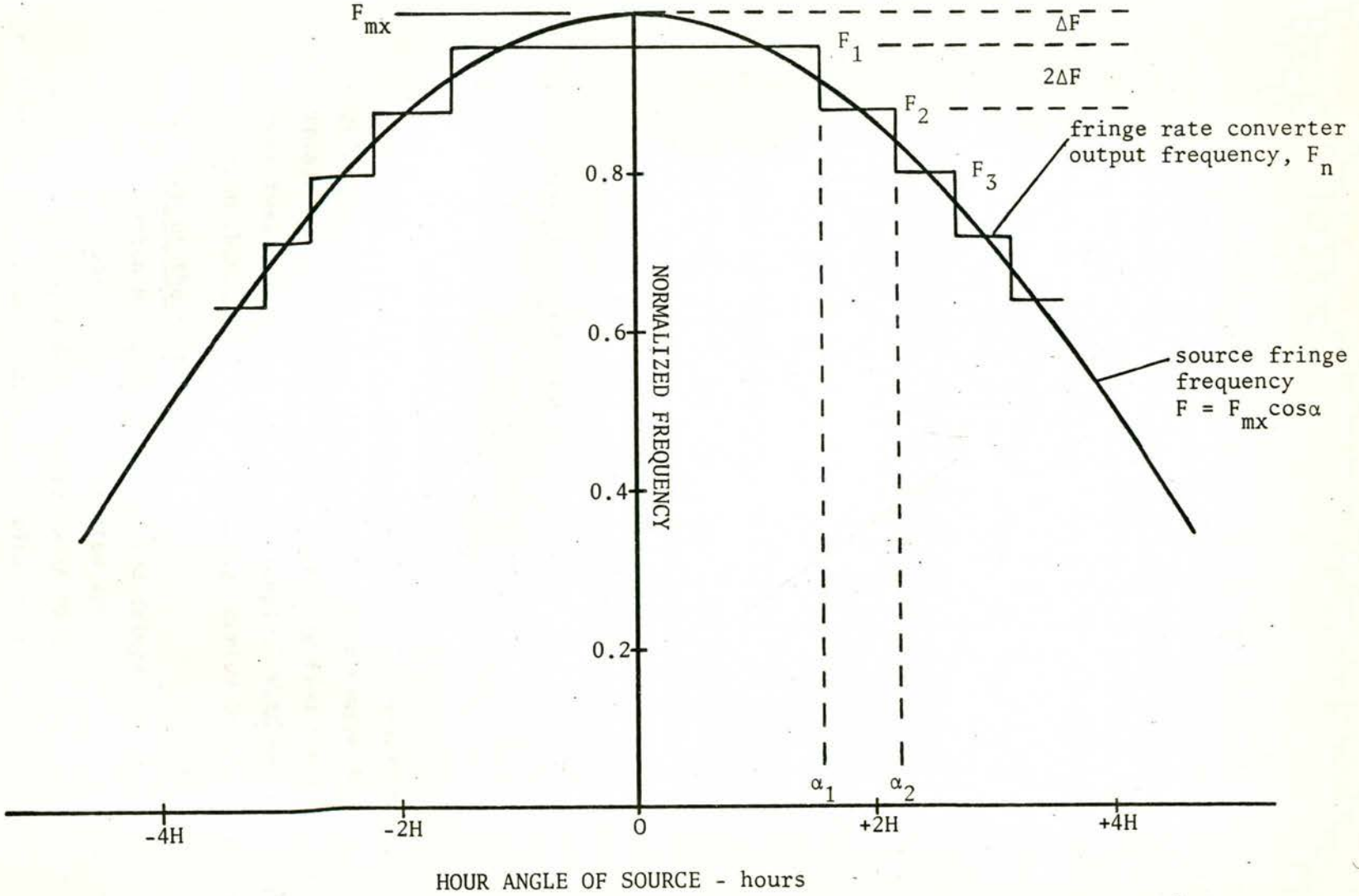

FIGURE F.5 Illustrates the method of maintaining the output fringe frequency $\leq |\Delta F|$

Equalization with the fringe frequency is not desirable since it would then be difficult to determine the phase of the output wave-form. (This is not so if both sine and cosine receivers can be used simultaneously.) In practice the zero crossover times are measured and the phase of the source fringes computed for these points.

The generated frequency F_n is derived in the switching unit by dividing a constant frequency squarewave (F_{c1} = 10 Hz or 50 Hz) from the clock by a variable integer K_n (0 to 99).

$$F_n = \frac{F_{c1}}{2K_n} \quad \text{and} \quad F_{n+1} = \frac{F_{c1}}{2(K_n+x)} \tag{F.4}$$

where $\underline{x}$ is an incremental integer.

During observations, F_n is changed to F_{n+1} when

$$F_n > (F_{mx}\cos\alpha + \Delta F) \tag{F.5}$$

and $\underline{x}$ is chosen such that

$$F_{n+1} \leq (F_{mx}\cos\alpha - \Delta F) \tag{F.6}$$

Provided K_n is high there is no difficulty in choosing a suitable value of $\underline{x}$. When K_n is low (<20), with F_{c1} = 10 Hz, F_{c1} is changed to the higher frequency (50 Hz). This allows use of a high value of K_n.

Each time the generated square wave is changed in frequency, the fringe rate converter is restarted. For the source 3C273, observations can remain uninterrupted for periods ranging from two hours near transit to about twelve minutes at ± 60° hour-angle. With observing periods longer than these, the difference fringe period drops below four minutes.

Computation of the relative phase

Equation F.1 gives the expected fringe frequency, F_{mx}, of the source whose coordinates are corrected for precession and nutation. In the case of 3C273, a double source with 19 sec. of arc separation, the assumed position was that of the radio centroid.

The time, t_p, of each peak of the output fringes and the starting time, t_s, of the fringe rate converter (frequency F_n) are calculated with respect to the source transit time.

If the receiver time constant is τ, then the resultant receiver phase error, ϕ, (excess path in eastern aerial channel) is given by:

$$\phi = (2m+1)\frac{\pi}{2} - 2\pi F_n(t_p - t_s) + \tan^{-1} 2\pi\tau \left| F_n - F_{mx}.\cos\left(\frac{\pi t_p}{720}\right) \right| + 1440.F_{mx}.\sin\left(\frac{\pi t_p}{720}\right) \qquad (F.7)$$

where $\underline{m}$ is an integer,
the time is in minutes,
the phase is in radians, and
the frequency is in cycles per minute.

The major source of error in this absolute measurement of the receiver phase is in the determination of the station longitude. This appears in the above calculations as an error in adjustment of the sidereal clock.

F.3 Choice of the Optimum Receiver Time Constant for the Fringe Rate Converter System.

The synchronous demodulator in the receiver has a normal RC time constant (τ). If this is fed with a sine wave interference pattern of period $\underline{T}$ then the gain $|G|$ is given by:

$$|G| = \left(\frac{1}{1 + \left(\frac{2\pi R.C}{T}\right)^2}\right)^{\frac{1}{2}} \qquad (F.8)$$

If $\tau = R.C.$ then,

$$|G| = \left(\frac{1}{1 + (2\pi r)^2}\right)^{\frac{1}{2}} \qquad (F.9)$$

where $r = \frac{\tau}{T}$.

Thus the gain falls off as the time constant becomes a significant part of the signal period (Fig. F.6). However the signal-to-noise ratio improves as $(\tau)^{\frac{1}{2}}$. For a given fringe period, T, the signal-to-noise ratio will be greatest if τ is chosen such that $\left(\frac{r}{1 + (2\pi r)^2}\right)^{\frac{1}{2}}$ is a maximum. This occurs at about r = 0.16.

APPENDIX G

Preliminary Results from a 35"-arc Compound Interferometer.

K.J. Wellington and A. Watkinson

(Reprint from Proc. A.S.A., 1967, 1, 44-45.)

(Reprinted from the Proceedings of the Astronomical Society of Australia, Vol. 1, No. 2, pp. 44-45, November, 1967)

Preliminary Results from a 35″-arc Compound Interferometer

K. J. WELLINGTON AND A. WATKINSON

School of Electrical Engineering, University of Sydney

This year the School of Electrical Engineering began observations with the new Fleurs compound interferometer[1]. This instrument operates at 21 cm and has a fan-beam response 35″ arc wide in an east-west direction.

Figure 1 shows the arrangement of antennae and receiver units. This is the high-resolution low-sensitivity 'stage 1' of the system, originally planned for solar work. The beam is formed by multiplying the output of two basic interferometer systems. One of these is the original 32-element E-W grating interferometer[2] and the other the newly added two-element interferometer. The two large elements have approximately twice the maximum spacing of the 32-dish grating.

This arrangement provides fan-beam responses across the sky at intervals of approximately 1°. However the primary beams of the 45 ft diameter elements are sufficiently narrow so that only one of these responses is enhanced at any one time. All dishes track the source for up to 9 h. The result is a sequence of fan-beam scans of the source which can be used to build up a picture.

As in all large arrays phase adjustment has presented a problem. The large separation of the 45 ft dishes and difference in focal lengths of the 45 ft and 18 ft dishes were the major difficulties. The small dishes of the array were first phased by applying the Swarup technique[3]. This was checked by measuring the positions of interference fringes produced when the Sun was observed with adjacent pairs of dishes. The nearest 45 ft dish was phased to the array in the same manner.

The two large dishes have a separation of 3820 wavelengths giving interference fringes of period 54″ arc. The quasar 3C273 was used to adjust their relative phase so that there was a fringe maximum at transit. As this source is only 40 f.u. it was necessary to increase the sensitivity by using a large integrating time. Consequently it was necessary to slow down the fringe rate using the synchronous rectification technique first suggested by le Roux at Nançay. Fringe phase is still preserved and can be measured with precision.

To check the phase of the lower spacings Taurus A was observed with only eight of the small dishes multiplied by the output of X1. Figure 2 shows the result of a scan with this system. Taurus A with a half-width of 3′.6 is smaller than the 5′.3 beam. A Fourier analysis of this scan

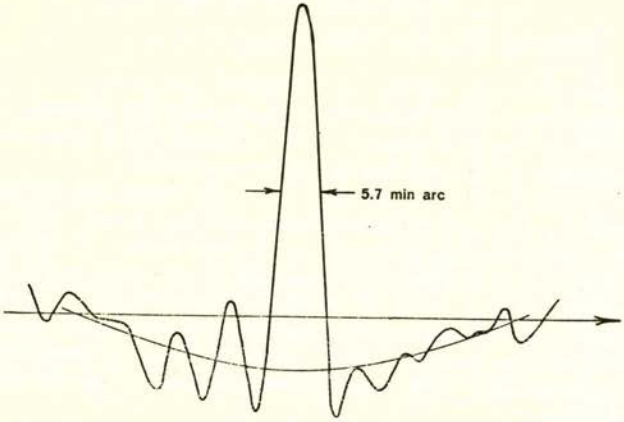

Figure 2. Scan of Taurus A with a 5′.3 fan beam. Fourier analysis is used to indicate phase errors present. The curved baseline is due to the missing 20 ft spacing. Taurus A has a half-power width of 3′.6.

showed which of the spacings were in error. These have since been corrected. It is proposed to repeat the procedure with the full array on 3C273.

The broad negative curved baseline, evident in Figure 2, is due to the missing 20 ft spacing. This spacing is smaller than the dish diameter and the deficiency must obviously be corrected by other means. At present the baseline is straightened during reduction of the records.

Several conclusions can be drawn from the observations to date.

(1) The undisturbed Sun and its slowly varying or 'S' component almost invariably contain some fine structure of low intensity (i.e. less than 1′ arc and less than 1 solar flux unit). These regions are usually but not necessarily associated with the more intense regions previously observed.

(2) Most of the S component features in this part of the solar cycle are resolved at some 1′.5 (range 5-40 s.f.u.).

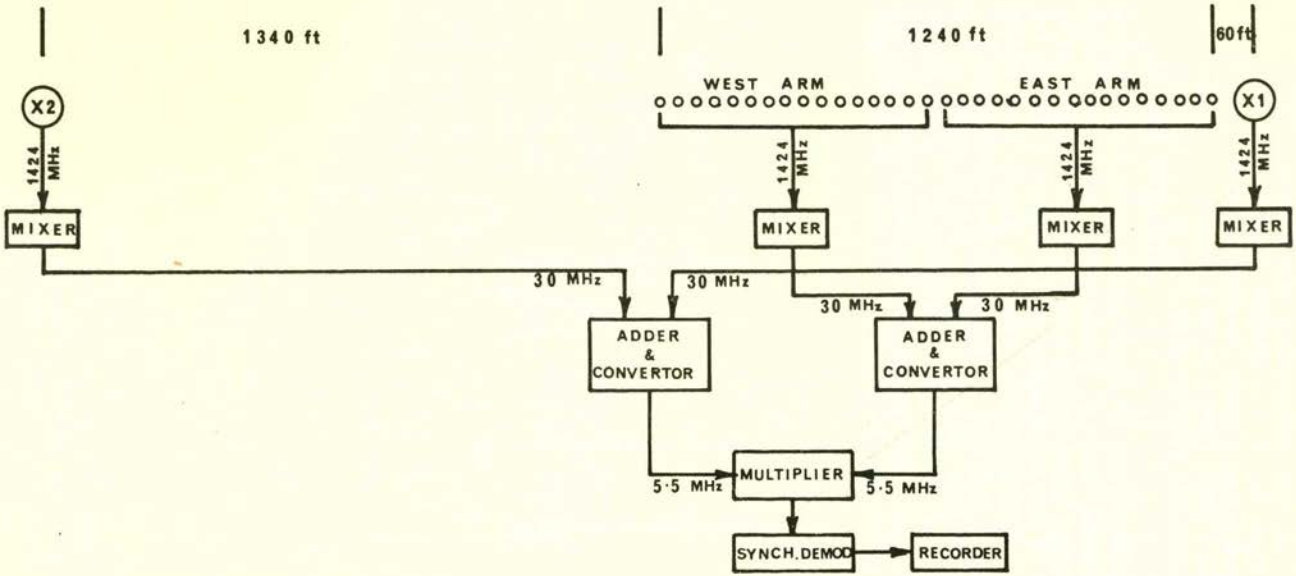

Figure 1. A schematic diagram of the 'stage 1' compound interferometer. X1 and X2 are two fully steerable 45 ft diameter paraboloids. East arm and west arm are two groups of 16 steerable paraboloids 18 ft in diameter.

(3) With a sample of three bursts there was in every case some fine structure associated with the plage. The intensity of this component increased greatly during the burst but diminished to its former value before the burst ended. In one case it reached a maximum before the peak of the burst.

Definite conclusions at this stage are not possible. The higher resolution measurements however indicate that earlier estimates of temperature of these larger regions were not greatly in error[4]. These temperatures will be slightly higher for previously unresolved discrete sources.

The regions of small angular size in Figure 3 are rarely seen as clearly as this. Usually they are confused in with other regions. To detect their presence the array is used with the lower spatial components missing. This arrangement effectively operates as a spatial band pass filter which

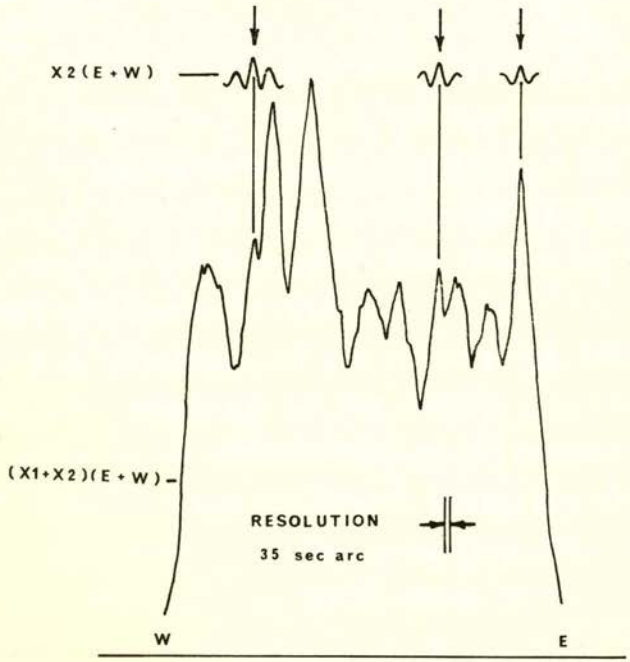

Figure 3. Scan of the Sun on 1967 June 28 with a 35′ arc fan-beam. Superimposed is a filtering scan using X2 multiplied by the array of small dishes.

ignores all the larger features and yet gives accurate positions of the small features. The output of such a system has been superimposed on the compound interferometer scan in Figure 3. The use of a consecutive series of observations will make it possible to follow these regions from day to day across the disk. This is necessary to establish their lifetime, stability and association with optical features.

Our observation that these small features appear in the central portion of a larger region before a burst may lead to a new method of predicting solar activity.

This work was carried out under the direction of Professor W. N. Christiansen at the Fleurs Radio Astronomy Field Station. The project has been made possible by grants from the Australian Research Grants Committee, the University of Sydney research vote, the Nuffield Foundation and the Australian Electrical Research Board. One of the authors (K.J.W.) is a Price Foundation fellow.

[1] Christiansen, W. N., and Wellington, K. J., *Nature*, **209**, 1173 (1966).
[2] Christiansen, W. N., Mathewson, D. S., and Pawsey, J. L., *Nature*, **180**, 944 (1957).
[3] Swarup, G., and Yang, K. S., *Trans. IRE*, **AP-9**, 75 (1961).
[4] Christiansen, W. N., and Mathewson, D. S., 'Paris Symposium on Radio Astronomy', ed. R. N. Bracewell, p. 108, Stanford University Press, 1959.

Appendix H Correlation Telescopes

Introduction

The compound grating antenna described in this thesis is one of the basic types of correlation telescope. As such it has certain properties which are outlined in this Appendix and used in Chapter 2. These properties are investigated in greater detail by Christiansen and Högbom (1968).

The correlation telescope is usually also an unfilled aperture telescope. Unfilled aperture telescopes (in particular, two element interferometers) were initially operated with receivers monitoring total-power. However receiver stability requirements were severe. In the correlation telescope the 'square-law' detector in the receiver is replaced by a correlating (or multiplying) device which compares two signals arriving, generally, from two separate antennae.

The output of the correlating device is proportional to the product of the separate signals. The time average of this output responds only to signals coming from the same source. The time average of uncorrelated voltages is zero and ideally this removes the effects of receiver noise. In practice the averaging time cannot be infinitely long so that some receiver noise still exists.

The main advantage of the correlating device lies in the absence of any 'constant' component in the output. In total-power systems, this component is due to the autocorrelation of receiver noise and of unwanted sky background. These make the output sensitive to gain fluctuations and to changes in orientation of the antenna . The correlation telescope is insensitive to any signal or noise which is not injected into both antennae (or channels) simultaneously.

The effective area of a correlation telescope

The correlation telescope comprises two separate antennae whose outputs are connected through equal lengths of transmission line to a correlating device. The signals arriving at these antennae will have a phase difference ϕ depending upon the direction of arrival of the signal.

If $A_1(\ell,m)$ and $A_2(\ell,m)$ are the separate effective areas then the combined output will be proportional to $(A_1.A_2)^{\frac{1}{2}}\cos\phi$. Thus an effective area, called a cosine effective area $A_c(\ell,m)$, can be defined for this correlation telescope.

$$A_c(\ell,m) = 2(A_1.A_2)^{\frac{1}{2}}\cos\phi \qquad \text{(H.1)}$$

If the transmission lines differ by $\frac{\pi}{2}$ radians phase length then the telescope will respond to signals in directions where $\phi = n\pi + \frac{\pi}{2}$. The cosine receiver then becomes a sine receiver and the telescope has a sine effective area $A_s(\ell,m)$.

$$A_s(\ell,m) = 2(A_1.A_2)^{\frac{1}{2}}\sin\phi \qquad \text{(H.2)}$$

These effective areas can be vastly different in magnitude and direction. For example, in the two element interferometer, the difference between A_c and A_s is principally one of direction. In the case of a balanced interferometer, where the centre element of three equally spaced elements is correlated with the outer two combined, A_s drops to zero.

These two effective areas can be combined to give the complex effective area of a correlation telescope $\underset{\sim}{A}(\ell,m)$ in which the cosine and sine effective areas form the real and imaginary parts.

$$\left.\begin{aligned} \underset{\sim}{A}(\ell,m) &= A_c(\ell,m) + jA_s(\ell,m) \\ &= A_{mx}.F_1(\ell,m).F_2^*(\ell,m) \end{aligned}\right\} \qquad \text{(H.3)}$$

where $A_{mx} = 2(A_{1_{mx}}.A_{2_{mx}})^{\frac{1}{2}}$

Most correlation telescopes to date operate with only a cosine receiver. The exceptions are the synthesis instruments, including the earth rotation synthesis telescope at Fleurs, which require both sine and cosine receivers.

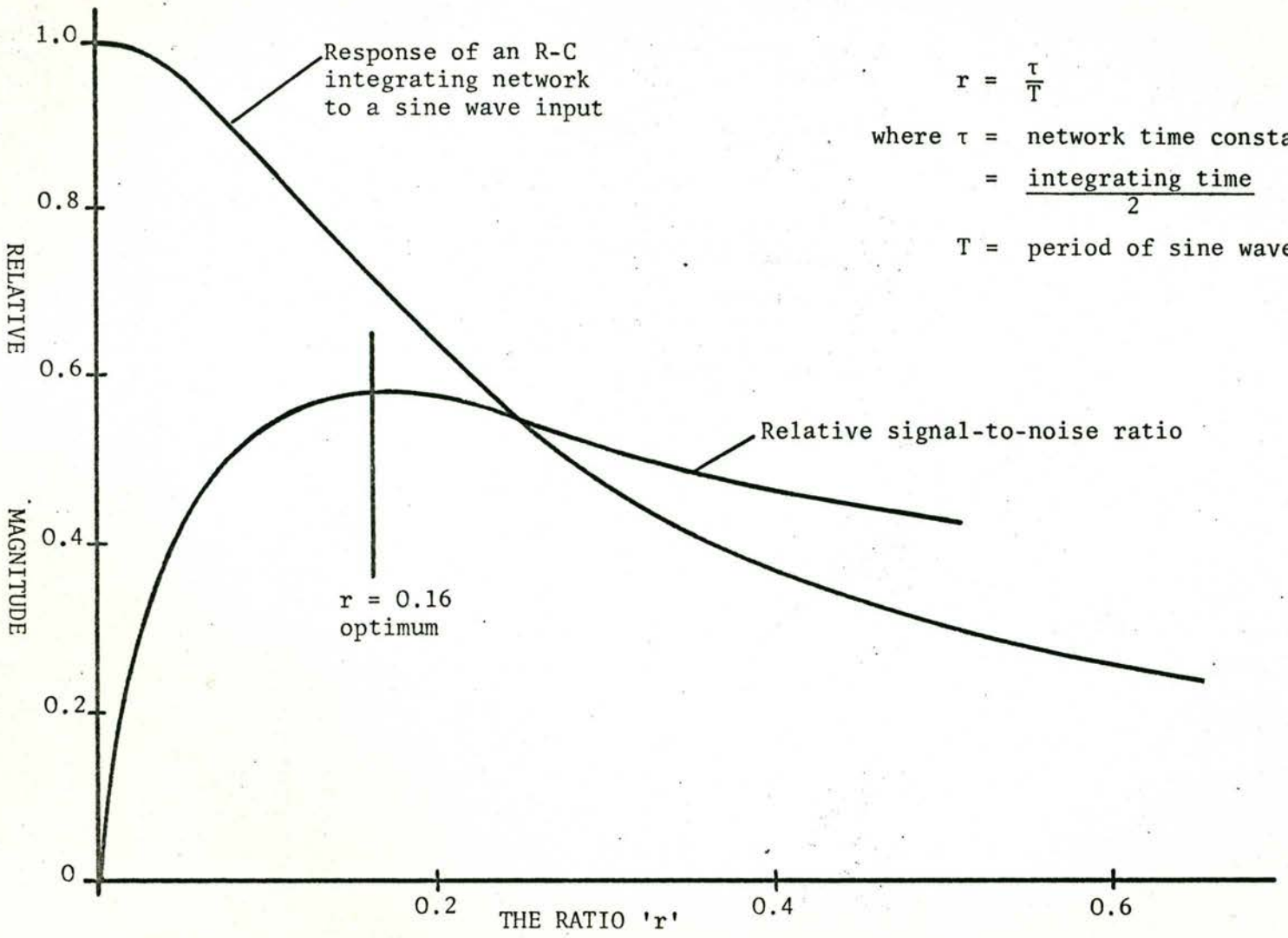

FIGURE F.6 Choice of the Optimum Receiver Time Constant for the Fringe Rate Converter System.

The spectral sensitivity function of the correlation telescope

The grading function $g(x,y)$ of a single antenna is related to the field pattern $F(\ell,m)$ by the Fourier transformation. In a similar way the complex effective area of a correlation telescope can be related to the separate grading functions of the component antennae (Fig. H.1).

If $\quad F_1(\ell,m) \rightleftharpoons (\text{constant}).g_1(x,y)$,

$\quad F_2(\ell,m) \rightleftharpoons (\text{constant}).g_2(x,y)$ and

$\quad \underset{\sim}{A}(\ell,m) = A_{mx}.F_1(\ell,m).F_2^*(\ell,m)$

then $\quad \underset{\sim}{A}(\ell,m) \rightleftharpoons (\text{constant}).g_1(x,y) \otimes g_2^*(x,y)$

using the convolution theorem.

Thus a spectral sensitivity function, $\underset{\sim}{C}(x,y)$, can be defined such that

$$\underset{\sim}{A}(\ell,m) \rightleftharpoons \underset{\sim}{C}(x,y) \qquad \text{(H.4)}$$

where $$\underset{\sim}{C}(x,y) = (\text{constant}).g_1(x,y) \otimes g_2^*(x,y) \qquad \text{(H.5)}$$

The shape of $\underset{\sim}{C}(x,y)$ determines the shape of $\underset{\sim}{A}(\ell,m)$ and hence the response of the telescope. $\underset{\sim}{C}(x,y)$ describes the spatial Fourier components that can be measured by the telescope, in terms of their relative amplitudes and phases. In a three dimensional plot this function becomes the island diagram of Bracewell (1961b).

Since A_c and A_s are the real and imaginary parts of $\underset{\sim}{A}(\ell,m)$, they can also be expressed in terms of the even and odd parts of $\underset{\sim}{C}(x,y)$.

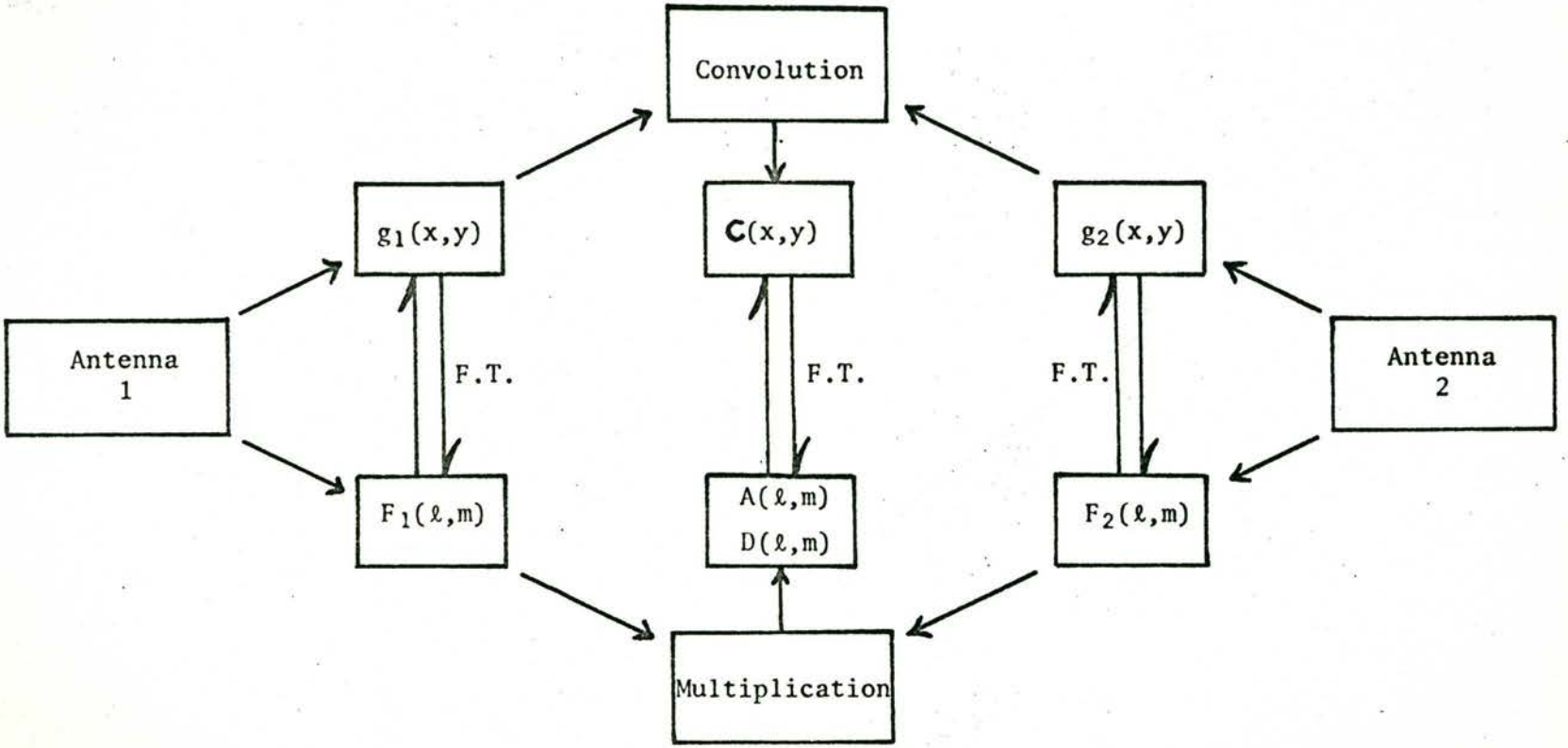

FIGURE H.1 Illustrating the interrelation between the functions describing a correlation telescope.

$$A_c(\ell,m) \rightleftharpoons \text{Even part } \underset{\sim}{C}(x,y) = \underset{\sim}{C}_e(x,y) \quad \text{and}$$
$$jA_s(\ell,m) \rightleftharpoons \text{Odd part } \underset{\sim}{C}(x,y) = \underset{\sim}{C}_o(x,y) \qquad \text{(H.6)}$$

Thus,

$$\begin{array}{ccccc} \underset{\sim}{C}(x,y) & = & \underset{\sim}{C}_o(x,y) + \underset{\sim}{C}_e(x,y) & = & \mathrm{Re}(C_o) + j\mathrm{Im}(C_o) + \mathrm{Re}(C_e) + j\mathrm{Im}(C_e) \\ \uparrow & & & \times & \uparrow \quad \uparrow \\ \underset{\sim}{A}(\ell,m) & = & \underset{\sim}{A}_o(\ell,m) + \underset{\sim}{A}_e(\ell,m) & = & \mathrm{Re}(A_o) + j\mathrm{Im}(A_o) + \mathrm{Re}(A_e) + j\mathrm{Im}(A_e) \end{array} \qquad \text{(H.7)}$$

Hence,

$$A_c(\ell,m) = \mathrm{Re}\{\underset{\sim}{A}(\ell,m)\} = \mathrm{Re}(A_o) + \mathrm{Re}(A_e) \rightleftharpoons \mathrm{Re}(C_e) + j\mathrm{Im}(C_o)$$

and

$$A_s(\ell,m) = \mathrm{Im}\{\underset{\sim}{A}(\ell,m)\} = \mathrm{Im}(A_o) + \mathrm{Im}(A_e) \rightleftharpoons \mathrm{Im}(C_e) - j\mathrm{Re}(C_o) \qquad \text{(H.8)}$$

This separation of the functions is very useful. Like the convolution theorem, it enables a complex function $\underset{\sim}{C}(x,y)$ to be considered as the combination of several simpler functions.

Appendix J — Response of the 'd/4' Compound Grating Antenna Configuration

Fig.J.1a shows this compound grating antenna arrangement. The lowest spatial component is $\frac{d}{4}$ and the harmonic increment is $\underline{d}$. (This is not to be confused with the quasi-symmetrical configuration considered in Chapter 2.)

The response of this arrangement is given by

$$\underset{\sim}{A}(\ell) = A_{mx} \cdot \left(\frac{\sin(N\pi\ell d)}{N \sin(\pi\ell d)}\right) \cdot \exp(j2\pi\ell d')$$

where

$$d' = (N-1)\frac{d}{2} + \frac{d}{4}$$

Now,

$$\exp(j2\pi\ell d') = \cos(2\pi\ell d') + j\sin(2\pi\ell d')$$

$$= \cos(N\pi\ell d) \cdot \cos(\tfrac{\pi\ell d}{2}) + \sin(N\pi\ell d) \cdot \sin(\tfrac{\pi\ell d}{2}) + j\left[\sin(N\pi\ell d) \cdot \cos(\tfrac{\pi\ell d}{2}) - \cos(N\pi\ell d) \cdot \sin(\tfrac{\pi\ell d}{2})\right]$$

Thus, $$A_c = A_{mx}\left[\frac{\sin(2N\pi\ell d)}{2N \sin(\pi\ell d)} \cdot \cos(\tfrac{\pi\ell d}{2}) + \frac{\sin^2(N\pi\ell d)}{N \sin(\pi\ell d)} \cdot \sin(\tfrac{\pi\ell d}{2})\right]$$

and

$$A_s = A_{mx}\left[\frac{\sin^2(N\pi\ell d)}{N \sin(\pi\ell d)} \cdot \cos(\tfrac{\pi\ell d}{2}) - \frac{\sin(2N\pi\ell d)}{2N \sin(\pi\ell d)} \cdot \sin(\tfrac{\pi\ell d}{2})\right]$$

For both a cosine and a sine receiver, responses occur whenever $\underline{\ell d}$ is an integer. With the present spacings this would be every 1^o near the zenith direction. However adjacent responses are entirely different and the lobe pattern has a 'period' of 2^o (when $\underline{2\ell d}$ is an integer).

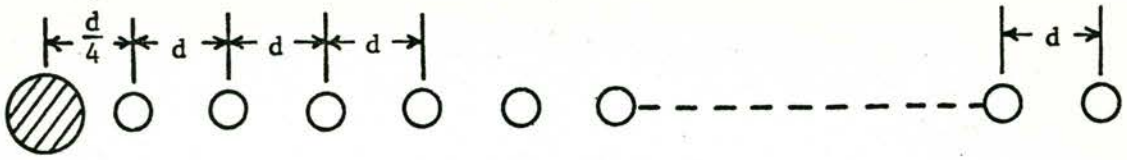

16 small grating aerials

(a)

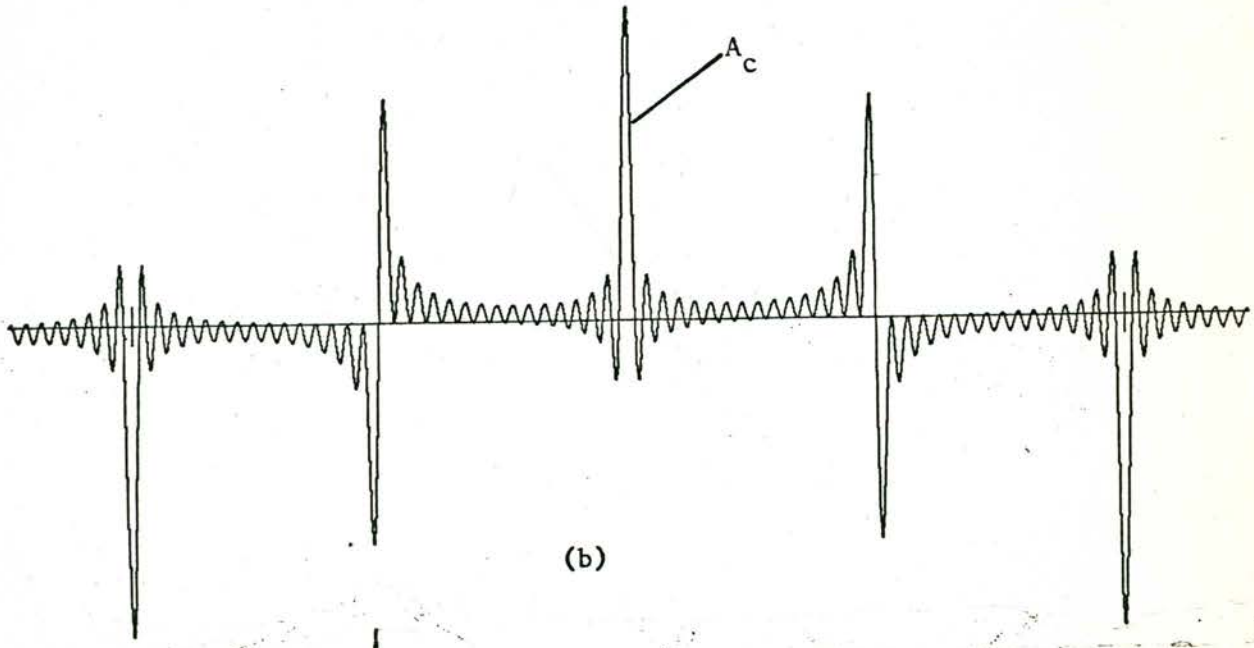

(b)

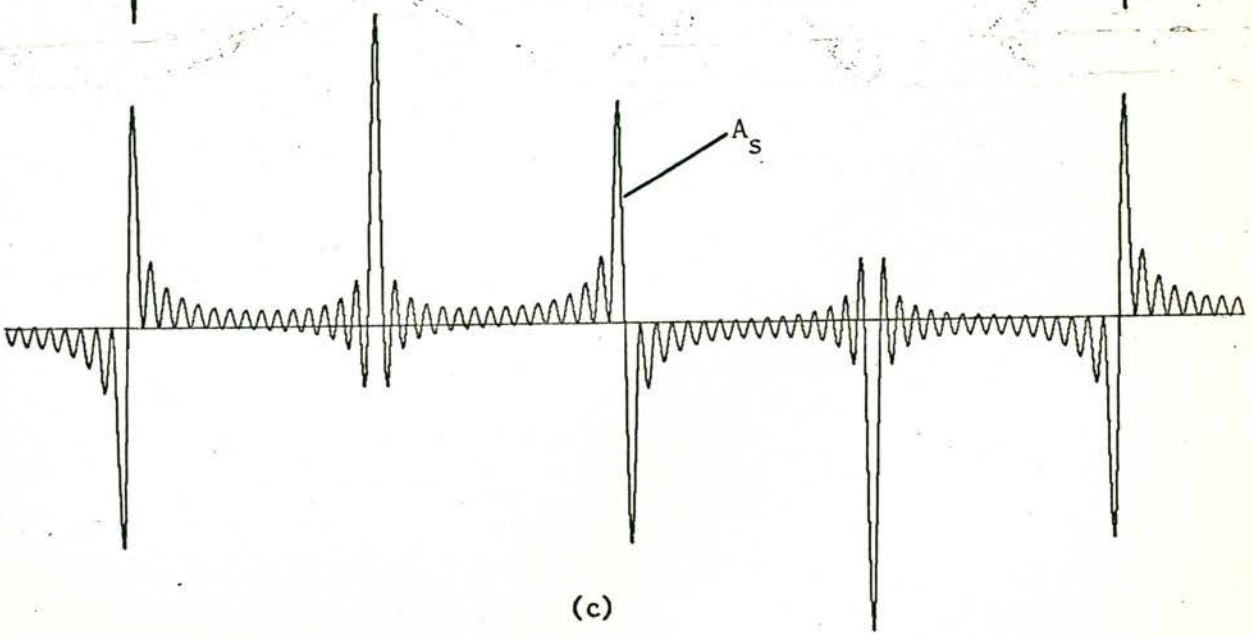

(c)

FIGURE J.1 The basic $\frac{'d'}{4}$ compound grating interferometer:

(a) Configuration

(b) Cosine response

(c) Sine response

Now the response of the basic configuration when $x = \frac{d}{2}$ is given by:

$$A_c = A_{mx} \cdot \frac{\sin(2N\pi\ell d)}{2N \sin(\pi\ell d)}$$

$$A_s = A_{mx} \cdot \frac{\sin^2(N\pi\ell d)}{N \sin(\pi\ell d)}$$

If these effective areas (of the $\frac{d}{2}$ configuration) are compared with those above (of the $\frac{d}{4}$ configuration) it can be seen that the cosine and sine responses of the $\frac{d}{4}$ compound grating antenna are identical but shifted half a period relative to one another (Fig.J.1b&c). (The initial spacing can be $\frac{3d}{4}$ without missing any spacings. The A_c and A_s responses are merely shifted half a period in the opposite direction.)

The value of this system as an observing instrument is uncertain. The 'sine' response (every second response) is such that it will only respond to small sources. As a grating sidelobe on a following system it might be expected to have less effect in general observations. However its odd shape may make it difficult to recognise. For this reason and the fact that as a fixed fan beam instrument every second scan would be useless, this arrangement was not considered further.

Appendix K Increasing the Survey Sensitivity of the Compound Grating Antenna

The three basic types of compound grating antennae are illustrated in Fig. K.1.

In types (1) and (2), the image plane size is defined primarily by the beamwidth of the larger elements. Information of the sky distribution surrounding this region is collected by the small grating elements but because of grating sidelobe considerations, must necessarily be rejected during correlation with the large elements. If this incident energy can be utilized then the survey sensitivity, and hence the efficiency of the instrument, is increased (Section 2.2.7).

A simple method of increasing the survey sensitivity is to place additional off-axis feeds on only the larger elements. The responses from these additional feeds are correlated separately with the responses from the small elements.

These feeds act exactly as the main feeds but point in a slightly different direction. Provided the elements are equatorially mounted, this pointing direction and the polarization vector of the feed remain constant relative to the sky distribution during the entire observing period. The effect is almost the same as observing adjacent areas of sky at the same time instead of on successive days. The only difference is that the amplitude taper on the sky distribution (not the Fourier components) will be different since the area will be under the sloping edge of the small element beamshape.

The added expense of this system is principally in the increased receiver complexity. However the receiver system does not have to be duplicated completely for each additional large-element feed, i.e., each additional image plane. There are two possible alternatives:

(i) A separate receiver channel is applied to each additional feed and a complete set of correlators (proportional to the number of

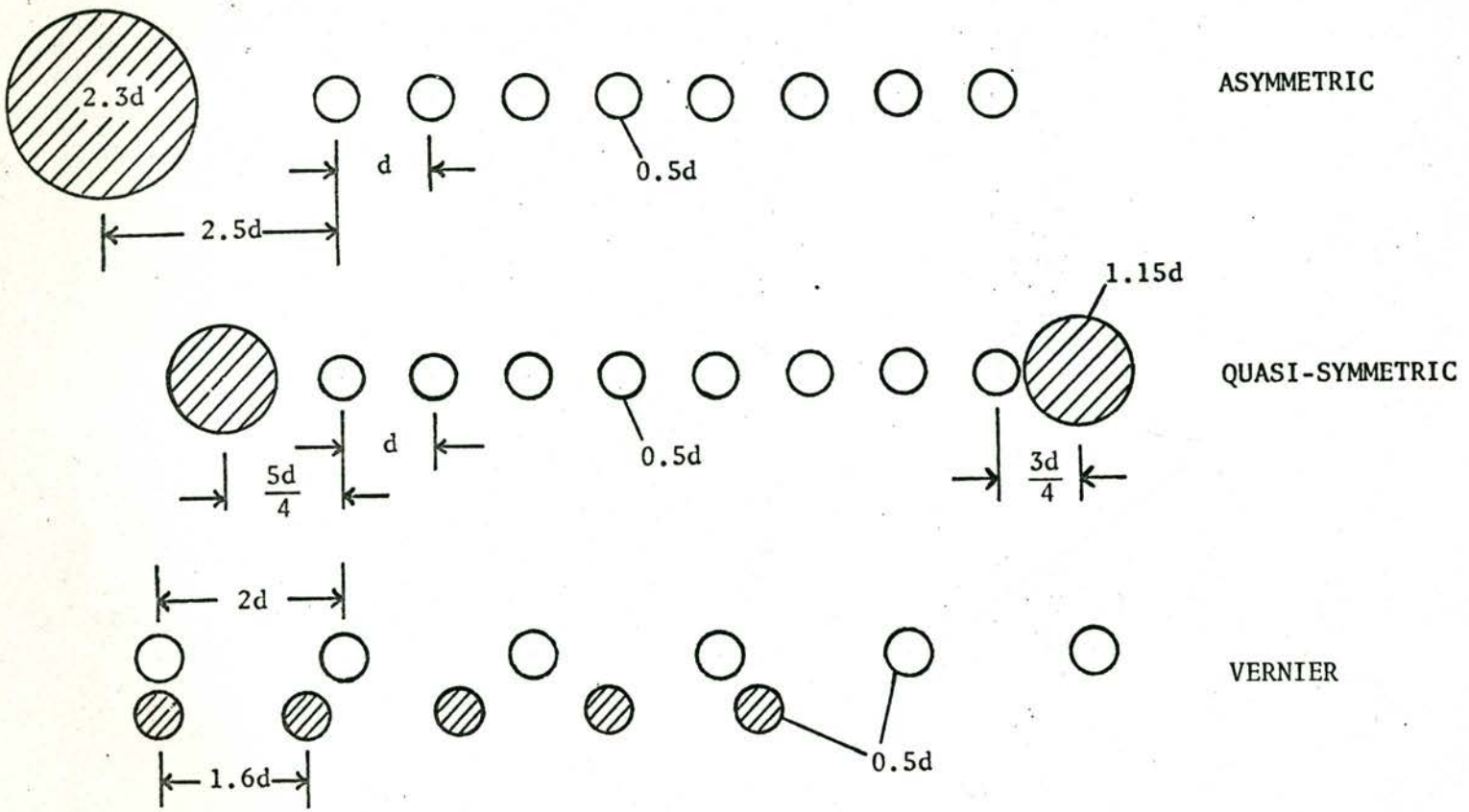

FIGURE K.1 Examples of the three basic types of compound grating antennae.

Fourier components measured) are provided for each image plane.

(ii) The signals from each image plane are coded (phase switched at differing rates) and are added into the one receiver system. After delays, lobestopping and correlation, these image plane responses can be reseparated using synchronous demodulators running at the different synchronizing rates. The disadvantage of this second alternative is the drop in signal-to-noise ratio due to the additional system noise from each channel (even though it is coded at a different rate).

The same delay lengths and lobestopping rates can be applied for all image planes provided: (a) the bandwidth or 'fringe-washing' envelope is not too narrow ($\frac{\sin\pi x}{\pi x}$ factors causing correlation loss of the high spatial components), and (b) the sampling interval of each component is not too long (source rotation rates are higher in these image planes).

The off-axis image planes differ from the central image plane in that they lie under the sloping edge of the small element beamshape. This creates an amplitude taper across the image plane. However this will be advantageous if the responses from these adjacent image planes are used in correction of the central image plane for grating sidelobe effects and/or for the 'centre' problem (Högbom, 1963).